

**Elektrisch aktive, von hiPSC abgeleitete
neurale *in vitro* Modelle – Etablierung,
Charakterisierung und Anwendung in der
Neurotoxizitätstestung**

Inaugural-Dissertation

zur Erlangung des Doktorgrades
der Mathematisch-Naturwissenschaftlichen Fakultät
der Heinrich-Heine-Universität Düsseldorf

vorgelegt von

Julia Hartmann
aus Stolberg (Rhld.)

Düsseldorf, November 2024

angefertigt am IUF – Leibniz-Institut für umweltmedizinische Forschung GmbH
der Heinrich-Heine-Universität Düsseldorf

Gedruckt mit der Genehmigung der Mathematisch-Naturwissenschaftlichen Fakultät
der Heinrich-Heine-Universität Düsseldorf

Berichtersteller:

1. Prof. Dr. Ellen Fritsche

2. Prof. Dr. Christine R. Rose

Tag der mündlichen Prüfung: 18.06.2025

„[...] on the shoulders of Giants“

Isaac Newton, 1675

Inhaltsverzeichnis

1	Einleitung.....	1
1.1	Das menschliche Gehirn	1
1.2	Neurotoxizität (NT).....	2
1.2.1	Paradigmenwechsel in der Neurotoxizitätstestung	3
1.3	Humane induzierte pluripotente Stammzellen (hiPSCs)	6
1.4	Neurale Induktion von pluripotenten Stammzellen	7
1.5	Neurale Entwicklung von Stammzell-basierten <i>in vitro</i> Modellen	9
1.5.1	Neurale Differenzierung durch neurotrophe Substanzen <i>in vitro</i>	9
1.5.2	Beeinflussung der neuronalen Entwicklung durch Laminin-Integrin-Bindung <i>in vitro</i>	10
1.5.3	Unterschiedliche Kultivierungstechniken von Zellen für die neurale Entwicklung <i>in vitro</i>	11
1.6	Neuronale Signalweiterleitung	14
1.7	Ermittlung der neuronalen Aktivität <i>in vitro</i> mittels Mikroelektroden Arrays (MEAs)	17
1.8	Ziel dieser Arbeit	19
2	Publikationen	20
2.1	Neural In Vitro Models for Studying Substances Acting on the Central Nervous System	22
2.2	Stem Cells for Next Level Toxicity Testing in the 21st Century	55
2.3	Characterization and application of electrically active neuronal networks established from human induced pluripotent stem cell-derived neural progenitor cells for neurotoxicity evaluation.....	88

2.4	Measurement of Electrical Activity of differentiated Human iPSC-Derived Neurospheres recorded by Microelectrode Arrays (MEA)	117
2.5	Alginate-laminin hydrogel supports long-term neuronal activity in three-dimensional human induced pluripotent stem cell-derived neuronal networks.....	135
2.6	Molecular and functional characterization of different BrainSphere models for use in neurotoxicity testing on microelectrode arrays.....	161
3	Diskussion	224
3.1	Alternativmethoden – von der Notwendigkeit bis zur derzeitigen Anwendung	224
3.2	Die Eignung verschiedener Kultivierungstechniken für den Einsatz in der Neurotoxizitätstestung	226
3.3	Zusammensetzung des neuronalen <i>in vitro</i> Netzwerks im Kontext der toxikologischen Aussagekraft.....	232
3.4	Auswertung von Mikroelektrodenarrays (MEAs) in der Neurotoxizitätstestung (NT)	236
4	Zusammenfassung.....	240
5	Summary	242
	Abkürzungsverzeichnis	I
	Literaturverzeichnis.....	V
	Danksagung	XXXVIII
	Eidesstattliche Erklärung.....	XXXIX

1 Einleitung

1.1 Das menschliche Gehirn

Das menschliche Gehirn ist ein sehr komplexes Organ, welches aus etwa 200 Milliarden Zellen besteht. Diese sind innerhalb spezifischer Regionen in einzigartiger Architektur angeordnet und lassen sich in die zwei Hauptgruppen Neurone und Gliazellen einteilen (Azevedo et al. 2009; von Bartheld et al. 2016). Neurone dienen dabei hauptsächlich der Signalübertragung und besitzen eine polarisierte Zellmorphologie bestehend aus Dendriten, Zellkörper (Soma) und Axon (Deiters and Schultze 1865; Budday et al. 2015). Die neuronale Kommunikation erfolgt über eine Kombination aus elektrischen und chemischen Signalen und wird in Abschnitt 1.6 ausführlich beschrieben. Abhängig vom Neurotransmitter werden Neurone beispielsweise als glutamaterg, GABAerg, dopaminerg, serotonerg oder cholinerg bezeichnet (Hyman 2005; Rowley et al. 2012). Zusätzlich werden neuronale Subtypen anhand ihrer Funktion, Position, Zellgröße und Morphologie unterschieden und klassifiziert (Lake et al. 2016; Zeng and Sanes 2017; Peng et al. 2021). Aufgrund ethischer und historischer Gründe stammen die meisten dieser Daten aus Nagetieren. Während morphologische Charakteristika weitestgehend zwischen den Spezies konserviert sind, wurden jedoch Unterschiede in der Genexpression zwischen dem murinen und dem menschlichen Gehirn entdeckt, die sich nicht nur auf die Gehirnentwicklung beziehen, sondern auch Rezeptoren, Ionenkanäle und Adhäsionsmoleküle einschließen (Hodge et al. 2019). Ebenso wurden anhand von Gehirnorganoiden Unterschiede in der Genexpression von Primaten und Menschen nachgewiesen (Kanton et al. 2019). Diese nicht zu vernachlässigbaren Speziesunterschiede verdeutlichen die Wichtigkeit von Studien direkt an humanen Modellen wie Zellkulturen oder Gewebeschnitten.

Die zweite große Zellpopulation im Gehirn wird mit dem Begriff Gliazellen bezeichnet und umfasst Astrozyten, Oligodendrozyten und Mikroglia. Das Verhältnis von Neuronen zu Gliazellen im menschlichen Gehirn liegt bei 1:1 und hat einen großen Einfluss auf die Entwicklung und Funktionalität des Gehirns (Weigert 1895; von Bartheld et al. 2016). Astrozyten interagieren mit Neuronen und initiieren die

Synaptogenese. Durch die Freisetzung und Aufnahme von Neurotransmittern wie Glutamate, γ -Aminobuttersäure (GABA) und Noradrenalin aus dem synaptischen Spalt, nehmen sie Einfluss auf die synaptische Übertragung und die synaptische Plastizität. Astrozyten erhalten das homöostatische Gleichgewicht aufrecht und leisten metabolische Unterstützung durch Nährstoffaufnahme aus den Blutgefäßen und Bereitstellung von Ausgangsmolekülen für den Stoffwechsel oder die Neurotransmittersynthese (Allen and Lyons 2018; Verkhratsky and Rose 2020). Die Hauptaufgabe von Oligodendrozyten ist die Bildung von Myelin, welches neuronale Axone im zentralen Nervensystem (ZNS) umgibt und für die saltatorische Erregungsleitung benötigt wird (Stadelmann et al. 2019). Mikroglia sind aus der Peripherie in das sich entwickelnde Gehirn immigrierte Makrophagen-ähnliche Zellen, welche das Immunsystem des Gehirns bilden und Überreste von abgestorbenen Zellen beseitigen. Zudem wirken sie bei mehreren Prozessen der Gehirnentwicklung mit (Arcuri et al. 2017; Wright-Jin and Gutmann 2019).

1.2 Neurotoxizität (NT)

Neurotoxizität (NT) beschreibt adverse Effekte von Substanzen, die die Struktur oder Funktion des Nervensystems beeinträchtigen. Diese Veränderungen können entweder sofort auftreten oder sich unter chronischer Belastung langsam entwickeln. Nach Beendigung der Exposition schreitet die NT in der Regel nicht weiter fort und kann sich zurückbilden, sofern keine bleibenden Schäden verursacht worden sind (Spencer and Lein 2014). Die Substanzen, welche Neurotoxizität auslösen, werden Neurotoxine genannt und kommen in Form von natürlichen Substanzen, Pestiziden, organischen Lösungsmitteln, Metallen oder synthetisch hergestellten Chemikalien vor. In der Datenbank für Gefahrstoffe der US-Nationalbibliothek der Medizin sind über 200 industrielle Chemikalien gelistet, welche neurotoxisch auf den Menschen wirken. Darüber hinaus haben Studien an Tieren zusätzliche 1000 Neurotoxine aufgedeckt (Grandjean and Landrigan 2006). Es wird davon ausgegangen, dass etwa 30% aller kommerziell verwendeten Chemikalien ein neurotoxisches Potential besitzen

(Legradi et al. 2018).

Aufgrund der Komplexität des Gehirns, kann die Exposition gegenüber einem Neurotoxin verschiedenste Auswirkungen haben. Neben der Interaktion mit Neurotransmitterrezeptoren sind die häufigsten Endphänotypen, die im Rahmen von NT beobachtet werden, Schädigung oder Tod von Neuronen (Neuropathie), Degeneration von Axonen (Axonopathie), Veränderung oder Schädigung der Myelinschichten (Myelinopathie), veränderte Funktion der Astrozyten und Störung der interzellulären Kommunikation (neurotransmissionsassoziierte NT) (Costa 2017; Weis and Büttner 2018). Ausgelöst werden diese Schädigungen durch bestimmte molekulare Ereignisse (*mode of action*, MOA), wie zum Beispiel einer veränderten Struktur des Zytoskeletts, welche den axonalen Transport beeinflusst, einer gestörten Proteinhomöostase, der Beeinträchtigung des Energiehaushalts oder der Produktion von reaktiven Sauerstoffspezies (*reactive oxygen species*, ROS) (Spencer and Lein 2014; Masjosthusmann et al. 2018; Crofton et al. 2022). Neurotransmissionsassoziierte NT verhindert die neuronale Kommunikation, indem sie die Synthese oder den Abbau von Neurotransmittern hemmt, deren Transport und Freisetzung erhöhen oder vermindern, Neurotransmitterrezeptoren aktivieren oder inhibieren oder Ionenkanäle blockieren (Spencer and Lein 2014; Costa 2017). Ein Beispiel hierfür ist das Neurotoxin Domainsäure. Das Gift bindet als Agonist spezifisch an den α -Amino-3-Hydroxy-5-Methyl-4-Isoxazol-Propionsäure (AMPA)-Rezeptor und bewirkt dadurch eine erhöhte neuronale Aktivität. Dies führt zu einem Anstieg an ROS und infolgedessen konzentrationsabhängig entweder zu Nekrose oder Apoptose von Neuronen, die den AMPA-Rezeptor exprimieren (exzitatorischer Zelltod) (Giordano et al. 2007).

1.2.1 Paradigmenwechsel in der Neurotoxizitätstestung

Die derzeit anerkannten Prüfrichtlinien (test guidelines, TG) der Organisation für wirtschaftliche Zusammenarbeit und Entwicklung (*Organisation for Economic Co-operation and Development*, OECD) zur Beurteilung der akuten und verzögerten

Neurotoxizität basieren ausschließlich auf *in vivo* Studien (TG418, TG419 und TG424) (OECD 1995a, b, 1997). Diese konzentrieren sich hauptsächlich auf Verhaltens- und neurologische Auffälligkeiten ohne Einblicke in die mechanistische Wirkungsweise der Chemikalien zu geben, weisen eine hohe Variabilität auf und lassen sich aufgrund der Speziesunterschiede nur bedingt auf den menschlichen Organismus übertragen (Bal-Price et al. 2010; Buschmann 2013). Zusätzlich sind sie sehr ressourcenintensiv in Bezug auf Zeit, Geld und Tierverbrauch. Für die Untersuchung einer einzigen Substanz nach der Prüfrichtlinie TG 424 werden mindestens 80 Tiere (vorzugsweise Ratten) benötigt und die Testung nimmt bis zu einem Jahr in Anspruch (OECD 1997). Diese hohen Anforderungen an Ressourcen (Zeit, Geld, Tiere) und der damit verbundene geringe Testdurchsatz führen zu einer großen Menge an noch nicht getesteten Chemikalien. Um diese zu verkleinern, hat die Europäische Kommission im Jahr 2003 eine Verordnung bezüglich der Registrierung, Evaluierung und Autorisierung von Chemikalien (*Registration, Evaluation and Authorization of CHemicals*, REACH) veröffentlicht, die die Untersuchung von rund 30.000 Chemikalien vorgesehen hat. Allein für die Untersuchung auf Neurotoxizität der Chemikalien, welche eine Produktionsrate von mehr als 10 Tonnen/Jahr aufweisen, wurden die benötigten Ressourcen damals auf 3,9 Millionen Tiere und 1,2 - 2,4 Milliarden € geschätzt. Diese Annahmen wurden jedoch weit übertroffen (Pedersen et al. 2003; van der Jagt et al. 2004; Coecke et al. 2006; Taylor 2018; Rovida et al. 2023). Aufgrund der enormen Kosten und der Unsicherheiten von *in vivo* Studien, hat dies zu einem Paradigmenwechsel in der chemischen Gefahren- und Risikobewertung geführt. Dieser beinhaltet die Entwicklung und Anwendung von Alternativmethoden (*new approach methods*, NAMs), wie beispielsweise biochemisch- und zellbasierten *in vitro* Assays, alternativen Tiermodellen (Zebrafisch, *Drosophila melanogaster*, *Caenorhabditis elegans*) und *in silico* Ansätzen (Collins et al. 2008; Magurany et al. 2023). Jede einzelne Methode für sich stellt zwar keinen gesamten (humanen) Organismus dar, aber in Kombination liefern sie einen großen Beitrag zur Vorhersage von Toxizitäten und bilden gemeinsam die Basis für die „Risikobewertung der nächsten Generation“ (*Next generation risk assessment*, NGRA; **Abbildung 1**) (Krewski et al. 2020). Dieser Ansatz unterscheidet sich maßgeblich von der „klassischen“ Risikobewertung mit Hilfe des Tierversuchs, da er NAM-basiert und

Expositions-, sowie Hypothesengesteuert ist (National Research Council 2007; Dent et al. 2021; Pallocca et al. 2022). Diese NAM-basierten Ansätze sollten sowohl allgemeine zelluläre Zielstrukturen wie z.B. Mitochondrien, als auch Organspezifische zelluläre Funktionen abdecken. Aus diesem Grund muss jede NAM sorgfältig auf Vorhandensein und Fehlen biologischer Prozesse untersucht werden, um eine geeignete Anwendungsdomäne (*fit-for-purpose-Modelle*) zu definieren. Diese wird am besten durch die Verwendung von Modellsubstanzen oder die Durchführung von Fallstudien charakterisiert (Kavlock et al. 2018; Mahony et al. 2020; van der Stel et al. 2021).

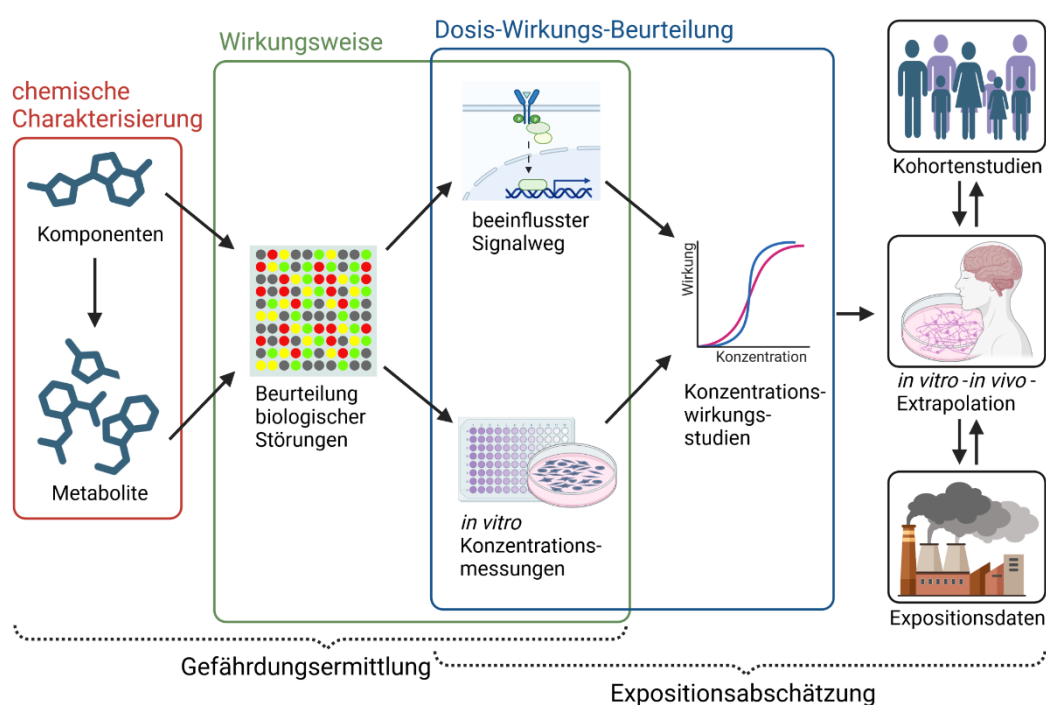


Abbildung 1: Paradigmenwechsel in der Toxikologie. Die Kombination aus chemischer Charakterisierung, biochemisch- und zellbasierten *in vitro* Methoden, *in silico* Methoden und humanen Expositionsdaten ermöglicht die Aufklärung der mechanischen Wirkungsweise eines Toxins. Adaptiert von Krewski et al. 2020; erstellt mit Biorender.com.

1.3 Humane induzierte pluripotente Stammzellen (hiPSCs)

Stammzellen sind undifferenzierte Zellen, die abhängig von intrinsischen und extrinsischen Faktoren zu spezifischen Zellen aller (pluripotent) oder nur bestimmter (multipotent, unipotent) Gewebe differenzieren können (Zakrzewski et al. 2019). Pluripotente Stammzellen können aus der inneren Zellmasse einer befruchteten Eizelle im Blastozysten-Stadium gewonnen (Embryonale Stammzellen, ESC) oder durch genetische Reprogrammierung aus somatischen Zellen hergestellt werden (induzierte pluripotente Stammzellen, iPSC) (Thomson et al. 1998; Takahashi and Yamanaka 2006). Die erste Generierung von iPSCs erfolgte aus murinen Fibroblasten unter Verwendung der vier Transkriptionsfaktoren (TF) Oktamer-bindender TF 3/4 (*octamer-binding transcription factor-3/4*, OCT3/4), geschlechtsbestimmende Region Y-Box 2 (*sex determining region Y-box 2*, SOX2), zelluläres Myelozytomatose-Onkogen (*cellular myelocytomatosis oncogene*, C-MYC) und Krüppel-ähnlicher Faktor 4 (*krüppel-like factor 4*, KLF4), welche als Yamanaka-Faktoren bekannt sind (Takahashi and Yamanaka 2006). Ein Jahr später gelang solch eine auf den Yamanaka-Faktoren sowie mit einer Kombination aus zwei weiteren TF (OCT3/4, SOX2, Homöoboxprotein Nanog (*Nanog homeobox*, NANOG) und abnormale Zellabstammung-28 (*cell lineage abnormal 28*, LIN28)) basierte Reprogrammierung auch mit humanen Fibroblasten (Takahashi et al. 2007; Yu et al. 2007). Während die ersten Reprogrammierungen somatischer Zellen zu humanen iPSCs (hiPSCs) auf retro- und lentiviralen Methoden basieren, welche in die DNA integrieren, wurden inzwischen verschiedene nicht-integrierende Methoden entwickelt, um die genetischen Veränderungen im Zusammenhang mit der genomischen Integration zu umgehen. Die Entwicklung von hiPSCs stellt einen Meilenstein in der Stammzellforschung dar, die eine breitgefächerte und ethisch unbedenkliche Anwendung von humanem Zellmaterial in der Toxikologie, der Medizin und der Grundlagenforschung ermöglicht (Shi et al. 2017). Aus hiPSC differenzierte neurale Vorläuferzellen (hiNPCs) oder daraus entwickelte Neurone und Gliazellen können beispielsweise *in vitro* für physiologische Studien, Medikamenten- oder Substanztestungen oder als Krankheitsmodelle verwendet werden (**Abbildung 2**).

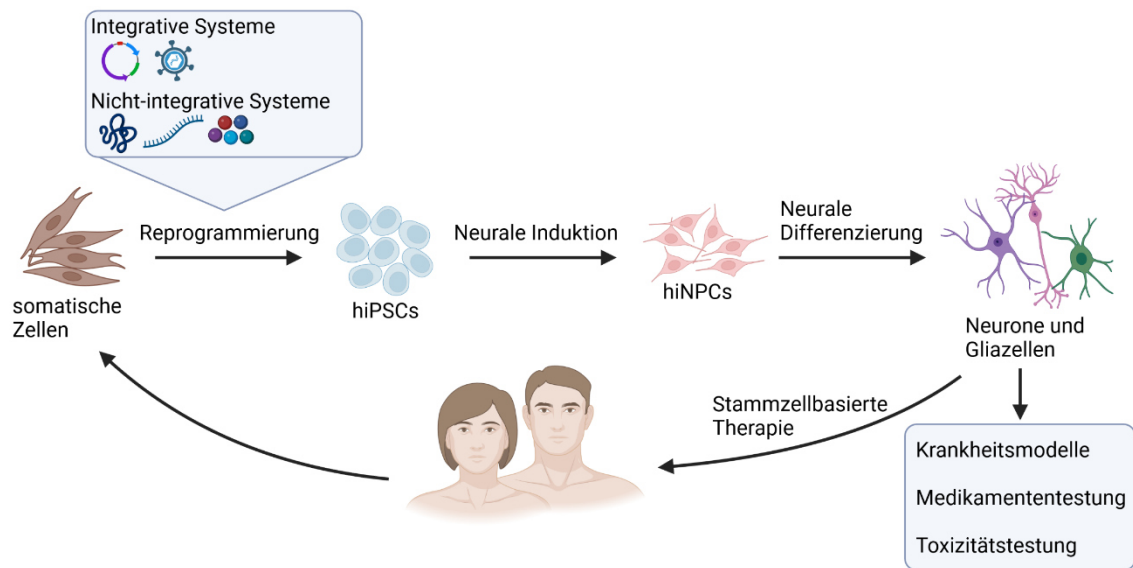


Abbildung 2: Erzeugung und Anwendung von humanen induzierten pluripotenten Stammzellen (hiPSCs). Somatische Zellen werden durch integrative oder nicht-integrative Systeme zu hiPSC reprogrammiert. Anschließend werden sie in neurale Progenitorzellen (hiNPCs) induziert und in Neurone und Gliazellen differenziert, welche daraufhin als Krankheitsmodell oder in der Medikamenten- oder Substanztestung eingesetzt werden. Adaptiert von Csobonyeiova et al. 2019; erstellt mit Biorender.com.

1.4 Neurale Induktion von pluripotenten Stammzellen

Das ZNS entwickelt sich nach der Gastrulation aus dem ektodermalen Keimblatt durch die Bildung des Neuralrohrs. Dieser Vorgang wird Neurulation genannt und kann *in vitro* durch Zugabe spezifischer Morphogene nachgeahmt werden. Das zugrunde liegende Prinzip hierbei ist zum einen die Unterdrückung der meso-endodermalen Differenzierung und zum anderen die Spezialisierung der neuronalen Progenitorzellen (*neural progenitor cells*, NPCs) entlang der anterior-posterior oder der dorsal-ventral Achse (Suzuki and Vanderhaeghen 2015; Tao and Zhang 2016). Die erste erfolgreiche neurale Induktion *in vitro* wurde bereits 1995 mit murinen ESCs durchgeführt und basierte auf der Wirkung des Leukämiehemmenden Faktors (*leukemia inhibitory factor*, LIF) und der Retinsäure (RA) (Bain et al. 1995). Seither wurden viele verschiedene Protokolle für die neurale Induktion entwickelt, die sich sowohl in der Medienzusammensetzung als auch in der Kultivierungstechnik (adhärente

Kultivierung, Neurosphären, Rosettenbildung) unterscheiden (Pistollato et al. 2014; Wen et al. 2014; Galiakberova and Dashinimaev 2020). Ein wichtiger Fortschritt war die Entdeckung der dualen SMAD-Inhibierung, welche auf der Wirkung von Noggin und SB431542 basiert (Chambers et al. 2009). SMAD-Proteine sind intrazelluläre Transkriptionsfaktoren, die extrazelluläre Signale der transformierenden Wachstumsfaktor β (*transforming growth factor β* , TGF- β) Superfamilie weiterleiten. Sie werden durch Phosphorylierung aktiviert, in den Zellkern transportiert und steuern dort die Expression spezifischer Gene (Derynck and Zhang 2003). Das Protein Noggin verhindert durch die Bindung an das Knochenmorphogenetische Protein 4 (*bone morphogenetic protein 4*, BMP4) die Aktivierung von SMAD 1/5/8 (Zimmerman et al. 1996; Itsykson et al. 2005). SB431542 blockiert durch die Inhibition der TGF- β Typ I Rezeptoren Aktivin Rezeptor-ähnlichen Kinasen (*activin receptor-like kinases*, ALK) - 4, ALK-5 und ALK-7 die Phosphorylierung von SMAD 2/3 (Inman et al. 2002; Park 2011). In Kombination führt dies zu einer hoch effizienten Differenzierung in die neuroektodermale Richtung (Chambers et al. 2009). In neueren Studien konnte das rekombinant hergestellte Protein Noggin erfolgreich durch die kleinen Moleküle LDN193189 oder Dorsomorphin ersetzt werden (Surmacz et al. 2012; Horbelt et al. 2015). Sogenannte kleine Moleküle haben den Vorteil, dass sie preiswerter und in größeren Mengen hergestellt werden können, stabil sind und xenofreie Kulturbedingungen ermöglichen (Neely et al. 2012). Das Prinzip der dualen SMAD-Inhibierung wurde in den letzten Jahren sowohl in adhärenenten Zellkulturen als auch in Neurosphärenkulturen erfolgreich eingesetzt (Neely et al. 2012; Shi et al. 2012; Chandrasekaran et al. 2017; Qi et al. 2017; Hofrichter et al. 2017; Nadadhur et al. 2018; Pauly et al. 2018; Hyvärinen et al. 2019). Um eine erfolgreiche neurale Induktion sicherzustellen, sollten die Zellen auf die Expression spezifischer Marker für NPCs untersucht werden, wie zum Beispiel NESTIN, gepaartes Box-Protein 6 (*paired box protein 6*, PAX6), Proliferationsmarker KI-67, Geschlechtsbestimmende Region des Y-Proteins-Transkriptionsfaktor 1 (Sex determining region of Y-Gen (*SRY*)-box *transcription factor 1*, SOX1) oder SOX2 (Chandrasekaran et al. 2017; Liu et al. 2021).

1.5 Neurale Entwicklung von Stammzell-basierten *in vitro* Modellen

1.5.1 Neurale Differenzierung durch neurotrophe Substanzen *in vitro*

Aus hiPSC-generierte NPCs (hiNPCs) können entweder in Proliferationskultur gehalten oder mit spezialisierten Differenzierungsmedien in Neurone und Gliazellen differenziert werden. Abhängig vom gewählten Differenzierungsziel werden dem Medium unterschiedliche neurotrophe Substanzen beigesetzt, wobei das Basismedium meist auf der Supplementierung von B27 und N2 sowie dem Entzug von Wachstumsfaktoren beruht (Gunhanlar et al. 2017; Pistollato et al. 2017; Paavilainen et al. 2018; Hyvärinen et al. 2019; Izsak et al. 2019; Schenke et al. 2020; de Leeuw et al. 2022). B27 und N2 sind komplexe, chemisch definierte Mischungen aus antioxidativen Enzymen, Proteinen, Vitaminen, Fettsäuren und Hormonen, welche das Überleben von Neuronen in einer serum-freien Kultur ermöglichen (Bottenstein et al. 1980; Brewer et al. 1993; Brewer 1995). Der epidermale Wachstumsfaktor (*epidermal growth factor*, EGF) und der Fibroblasten Wachstumsfaktor 2 (*fibroblast growth factor 2*, FGF-2) begünstigen die Zellproliferation (Kuhn et al. 1997). Die in dieser Arbeit verwendeten neuralen Differenzierungsmedien wurden mit zyklischem Adenosinmonophosphat (*cyclic adenosine monophosphate*, cAMP), Interferon- γ , Neurotrophin-3 (NT-3), Gehirn-abstammenden neurotrophen Faktor (*brain-derived neurotrophic factor*, BDNF), Gliazellen abstammenden neurotrophen Faktor (*glial cell line-derived neurotrophic factor*, GDNF), Ascorbinsäure und Kreatin vervollständigt. Der sekundäre Botenstoff cAMP unterstützt die Axonbildung, Gliogenese, Differenzierung zu dopaminergen Neuronen und inhibiert die Zellproliferation (Mark and Storm 1997; Cebolla et al. 2008; Shelly et al. 2010; Belinsky et al. 2013). Eine Kombination mit dem pro-inflammatorischen Zytokin Interferon- γ verstärkt die *in vitro* Differenzierung in Neurone und Astrozyten zusätzlich (Zahir et al. 2009). Es wird vermutet, dass der positive Effekt des Interferon- γ über die Aktivierung von c-Jun N-terminale Kinasen (JNK) oder des Transkriptionsfaktors Signalüberträger und Aktivator der Transkription 1 (*signal transducer and activator of transcription 1*, STAT1) erfolgt (Wong et al. 2004; Kim et al. 2007; Leipzig et al. 2010; Pereira et al. 2015). Die Neurotrophine BDNF und NT-3 regulieren die synaptische Plastizität durch Aktivierung

der Tropomyosinrezeptorkinasen (TrK) B beziehungsweise C (Park and Poo 2013; Shinoda et al. 2019; Hernández-Echeagaray 2020). GDNF bindet an den GDNF Familienrezeptor α 1 (*GDNF family receptor α 1*, GFRA1) sowie an das neurale Zelladhäsionsmolekül (*neural cell adhesion molecule*, NCAM) und steuert auf diesem Weg das Axonwachstum, den Neuritenauswuchs, die Ausbildung von Dornenfortsätzen (*dendritic spines*) und die Differenzierung und Funktion von dopaminergen Neuronen (Irala et al. 2016; Barak et al. 2019; Ibáñez et al. 2020). Zudem regulieren GDNF und BDNF die serotonerge Differenzierung (Popova et al. 2017). Ascorbinsäure ist ein Neuromodulator, der die neurale Differenzierung und Reifung beeinflusst, und die Zellen vor oxidativem Stress schützt (Dutta et al. 2015; Moretti et al. 2017). Kreatin wird für die schnelle Bereitstellung von Energie benötigt, um den stark fluktuierenden Energiebedarf von Neuronen zu decken (Andres et al. 2008).

1.5.2 Beeinflussung der neuralen Entwicklung durch Laminin-Integrin-Bindung *in vitro*

Die extrazelluläre Matrix (*extracellular matrix*, ECM) des Gehirns ist ein dynamisches, dreidimensionales (3D) Netzwerk bestehend aus fibrillären Proteinen, Glykoproteinen, Proteoglykanen und Zytokinen. Es dient den Zellen nicht nur als Stütz- und Verbundgewebe, sondern wird auch für die Migration, Differenzierung und synaptische Plastizität benötigt (Flanagan et al. 2006; Ma et al. 2020). Von besonderer Bedeutung ist das Glykoprotein Laminin. Das Heterotrimer besteht aus drei verschiedenen, umeinander gewobenen Polypeptidketten, die abhängig von Entwicklungszustand und Organ variieren und für die Namensgebung verantwortlich sind: Laminin 111 (L111) besteht beispielsweise aus der α 1, β 1 und γ 1-Kette (Aumailley 2013). Die Steuerung von Signalwegen über Proteine der ECM, wie Laminin, wird über die Bindung an Integrine vermittelt (Yamada and Sekiguchi 2015). Integrine sind transmembrane Moleküle mit einer großen extrazellulären Domäne, welche aus einer α und einer β Untereinheit zusammengesetzt sind. Die Integrin-

Untereinheiten $\alpha 1$, $\alpha 3$, $\alpha 6$, $\alpha 7$, $\alpha 10$, $\beta 1$ und $\beta 4$ sind dabei für die Lamininbindung verantwortlich (Humphries et al. 2006; Nishiuchi et al. 2006). Es konnte gezeigt werden, dass insbesondere die Integrin $\beta 1$ -L111-Bindung für die Adhäsion und Migration von radialen Gliazellen verantwortlich ist (Barenys et al. 2017; Klose et al. 2022a). Zusätzlich sind weitere Integrin-Laminin-Bindungen für die Führung des Axonwachstums, strukturelle Stabilität von Synapsen, synaptische Transmission, neurale Differenzierung und neuronale Elongation von Bedeutung (Flanagan et al. 2006; Ma et al. 2008; Ortinau et al. 2010; Stabenfeldt et al. 2010; Hyysalo et al. 2017; Hellwig et al. 2018; Lilja and Ivaska 2018).

1.5.3 Unterschiedliche Kultivierungstechniken von Zellen für die neurale Entwicklung *in vitro*

Die Kultivierungsmethoden für die neurale Entwicklung *in vitro* sind vielfältig. Neurone und Gliazellen können adhärent, als Neurosphären, als Organoide oder in 3D Konstrukten in Hydrogelen kultiviert werden (**Abbildung 3**). Die Wahl der Methode sollte jedoch sorgfältig getroffen werden, da jeder dieser Methoden seine eigenen Vor- und Nachteile besitzt. Adhärente, zweidimensionale (2D) Kulturen werden als einschichtige Zellen, auch *Monolayer* genannt, auf Kulturoberflächen aus Plastik oder Glas kultiviert, die mit Molekülen der ECM beschichtet sind. Dies ist die älteste Kultivierungstechnik, die das erste Mal 1885 von Wilhelm Roux durchgeführt wurde und seitdem kontinuierlich verbessert wurde (Abbas et al. 2021). Die Zellen weisen jedoch häufig eine unphysiologische und abgeflachte Zellmorphologie auf, da gewebespezifische Strukturen, sowie mechanische und biochemische Stimuli fehlen. Zusätzlich können nur begrenzt Zell-Zell-Kontakte ausgebildet werden (Murphy et al. 2017; Duval et al. 2017).

Sphären- und Organoidmodelle werden in Suspensionskultur gehalten und entstehen durch spontane Selbstaggregation einzelner Zellen oder Zellklumpen. Dies führt zu einer komplexeren Zytoarchitektur als in 2D Kulturen und somit zu mehr Zell-Zell-Kontakten (Zhuang et al. 2018). Die kompakte sphärische Struktur führt

jedoch zu einer ungleichen Versorgung mit Nährstoffen und Sauerstoff sowie einem erschwerten Abtransport von Abfallprodukten aus dem Sphärenkern. Um die Bildung eines nekrotischen Kerns zu verhindern, wird die Sphärengröße üblicherweise auf 350-500 µm begrenzt (Ou and Hosseinkhani 2014; Smirnova et al. 2016). Durch Kultivierung auf einer mit Laminin-beschichteten Kulturoberfläche migrieren die Zellen aus dem Sphärenkern heraus und ermöglichen die Analyse von Migrations- und Differenzierungsprozessen in sogenannten „sekundären 3D Strukturen“ (Moors et al. 2009; Alépée 2014; Barenys et al. 2017; Hofrichter et al. 2017; Chen et al. 2019; Koch et al. 2022). Sphärenkulturen aus neuronalen Vorläuferzellen verschiedener Spezies existieren bereits seit Jahrzehnten (Gritti et al. 1996; Reynolds and Weiss 1996; Brannen and Sugaya 2000; Piper et al. 2000). Diese können in 3D zu sogenannten BrainSpheres differenziert werden, die Neurone, Astrozyten und auch Oligodendrozyten enthalten (Pamies et al. 2017b; Leite et al. 2019). Solche BrainSpheres sind multizellulär und die Zellen haben die Möglichkeit zur Selbstorganisation durch Zell-Zell-Kontakte in allen drei Ebenen. Sie besitzen jedoch keine anatomischen Strukturen wie kortikale Zonen oder verschiedene Gehirnregionen. Solch eine komplexere Morphologie *in vitro* erreicht man durch die Kultivierung von Gehirnorganoiden, welche hochgradig organisiert sind (Paşca et al. 2015; Qian et al. 2016; Bagley et al. 2017; Lancaster et al. 2017). Die dafür erforderliche Größe von bis zu 6 mm kann durch Kultivierung in Schüttel- und Drehinkubatoren erreicht werden, welche das Diffusionslimit erhöhen (Lancaster et al. 2013; Qian et al. 2016, 2018; Benito-Kwiecinski and Lancaster 2020).

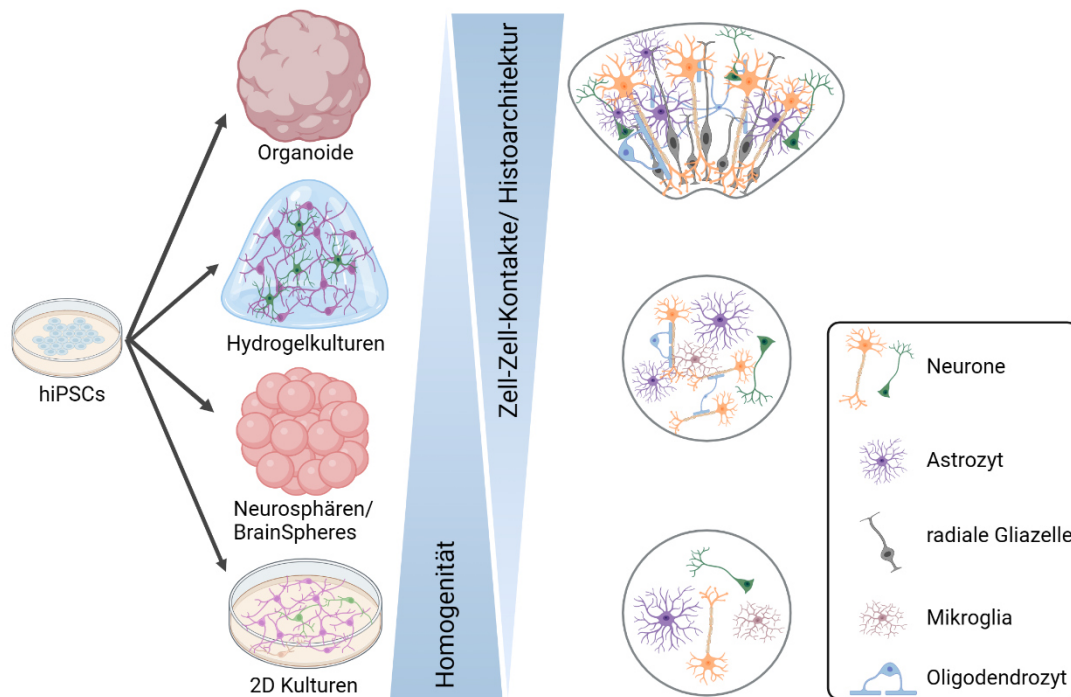


Abbildung 3: Vergleich verschiedener Kultivierungstechniken von neuronalen Netzwerken *in vitro*.
 Adaptiert von Pelkonen et al. 2021; erstellt mit Biorender.com.

Hydrogelkulturen bieten eine weitere Möglichkeit der 3D Kultivierung von Zellen *in vitro*. Die Herstellung erfolgt meist durch die Mischung von Zellen mit dem Hydrogel und einer anschließenden Vernetzung (engl. *crosslinking*) durch z.B. Ionen oder ultraviolette Strahlung (Ou and Hosseinkhani 2014). Für die Kultivierung von neuronalen Zellen eignen sich besonders weiche Materialien, die die mechanischen Eigenschaften des Gehirns nachahmen. Die natürliche Porosität der vernetzten Hydrogele erlaubt zudem eine ausreichende Nähr- und Sauerstoffversorgung der eingebetteten Zellen, so dass es keinen limitierenden Diffusionsgradienten gibt (Hopkins et al. 2015; Murphy et al. 2017). Damit die Zellen im Hydrogel haften, migrieren und differenzieren können, sind Zell-Matrix-Kontakte von entscheidender Bedeutung. Aus diesem Grund werden Hydrogele wie Alginat häufig mit Komponenten der ECM funktionalisiert (Stabenfeldt et al. 2010; Zhuang et al. 2018).

1.6 Neuronale Signalweiterleitung

Die Hauptaufgabe von Neuronen besteht in der Aufnahme, Verarbeitung und Weiterleitung von Informationen. Diese werden zunächst über eines der Dendriten aufgenommen, in der Zelle weitergeleitet und über das Axon an die Nachbarzelle übertragen (Adrian 1936; Budday et al. 2015). Die Signalübertragung erfolgt an hochspezialisierten Kontaktstellen, den Synapsen, wobei zwischen elektrischen und chemischen Synapsen unterschieden wird. Elektrische Synapsen sind *gap junctions* und ermöglichen einen bidirektionalen und passiven Ionentransfer (Curti and O'Brien 2016). Wohingegen chemische Synapsen aus Präsynapse, synaptischen Spalt und Postsynapse bestehen und Neurotransmitter für die Signalübertragung verwenden. Sie ermöglichen die Weiterleitung von exzitatorischen, inhibitorischen und biochemischen Signalen (Hyman 2005; O'Rourke et al. 2012). Im Fall einer Signalweiterleitung setzt die Präsynapse Neurotransmitter frei, die über den synaptischen Spalt diffundieren und reversibel an spezifische postsynaptische Rezeptoren binden. Wenn es sich um einen metabotropen Rezeptor handelt, dann werden „*second messenger*“-Systeme aktiviert, die funktionelle und strukturelle Änderungen bewirken. Bindet der Neurotransmitter allerdings an einen ionotropen Rezeptor, dann wird die Information durch Änderung des Membranpotentials in elektrische Signale umgewandelt (Goudet et al. 2009; Goodwani et al. 2017). Ionotrope Rezeptoren können inhibitorisch oder exzitatorisch wirken. Im Fall eines inhibitorischen Rezeptors strömen durch die Bindung des Neurotransmitters negativ geladene Ionen (z.B. Cl^-) in die Zelle und verursachen ein inhibitorisches postsynaptisches Potential (*inhibitory postsynaptic potential*, IPSP). Durch die einströmenden Ionen entsteht eine temporäre Hyperpolarisation der postsynaptischen Membran, die zum Axonhügel weitergeleitet wird. Bei der Bindung eines Neurotransmitters an einen exzitatorischen Rezeptor strömen Kationen (z.B. Na^+ und Ca^{2+}) in die Zelle und es entsteht ein exzitatorisches postsynaptisches Potential (*excitatory postsynaptic potential*, EPSP), wodurch die postsynaptische Membran temporär depolarisiert wird (Bourin 2018; Cantor 2018; Hansen et al. 2018). Das EPSP wird ebenfalls zum Axonhügel weitergeleitet, wo alle ankommenden IPSPs und EPSPs aufsummiert werden. Überwiegen die inhibierenden Signale, dann wird kein

Aktionspotential (AP) ausgelöst. Überwiegen die depolarisierenden EPSPs, so dass der Schwellenwert erreicht wird, wird ein AP ausgelöst. Spannungsgesteuerte Na^+ -Kanäle öffnen sich entlang des Axons nacheinander und die Zelle wird durch die einströmenden Natriumkationen depolarisiert. In der Präsynapse sorgt das AP dafür, dass spannungsgesteuerte Ca^{2+} -Kanäle geöffnet werden. Die einströmenden Ca^{2+} -Ionen initiieren die Fusion von Vesikeln mit der präsynaptischen Membran. Dies führt zur Freisetzung von Neurotransmittern in den synaptischen Spalt und somit zur Signalweiterleitung an das nächste Neuron. Die spannungsgesteuerten Natriumkanäle entlang des Axons schließen sich und Kaliumkanäle öffnen sich. Durch das Ausströmen der Kaliumkationen (K^+) wird die Zelle wieder negativ geladen (Repolarisation) und bei Erreichen des Ruhepotentials schließen die Kaliumkanäle. Während des Schließvorgangs fließen weitere Kaliumkationen aus der Zelle, so dass die Zelle hyperpolarisiert und für kurze Zeit nicht mehr erregbar ist. Die Natrium-Kalium-Pumpe stellt das Ruhepotential unter ATP-Verbrauch wieder her, in dem sie gleichzeitig drei Na^+ aus der Zelle und zwei K^+ in die Zelle schleust (**Abbildung 4**) (Hodgkin and Huxley 1939; Hyman 2005; Barnett and Larkman 2007; Ganguly and Chakrabarti 2020). Die zu vermittelnde Information wird dabei über die Anzahl, die Frequenz und die Form der APs übertragen (Bean 2007).

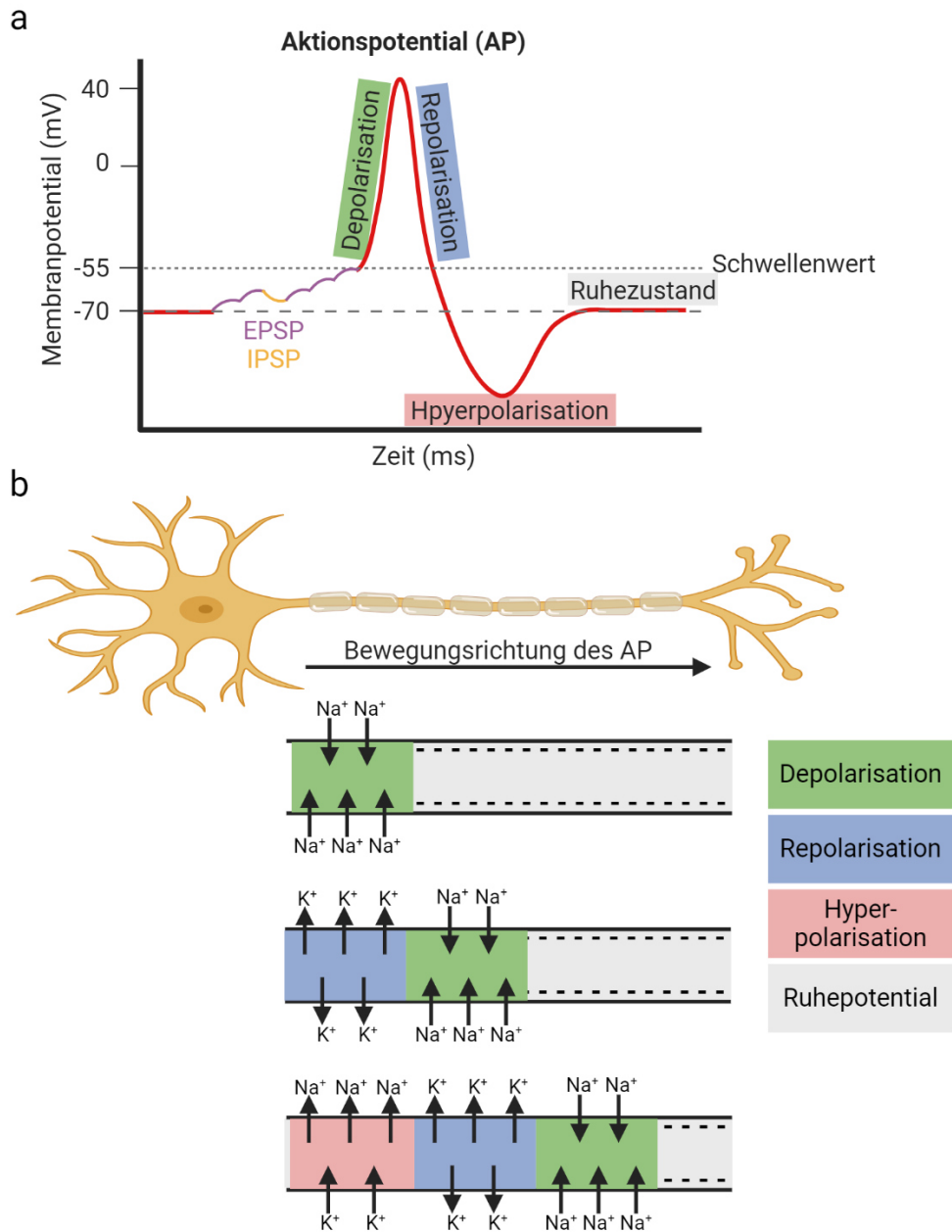


Abbildung 4: Die verschiedenen Phasen des Aktionspotentials. **a.** Zeitlicher Verlauf eines Aktionspotentials und die Änderung des Membranpotentials. **b.** Vereinfachte Darstellung der Ionenströme während eines Aktionspotentials. Erstellt mit Biorender.com.

1.7 Ermittlung der neuronalen Aktivität *in vitro* mittels Mikroelektroden Arrays (MEAs)

Die elektrische Aktivität von Neuronen lässt sich *in vitro* unter anderem mittels Mikroelektroden Arrays (MEAs) messen. Die Technologie gibt es seit 1972 und wurde zunächst für Kardiomyozyten verwendet, bevor ein paar Jahre später die ersten neuronalen Aktivitäten damit vermessen wurden (Thomas et al. 1972; Gross et al. 1977, 1982). MEAs sind (meist planare) Kulturoberflächen aus Glas oder Plastik in die Elektroden eingesetzt werden, welche mit leitenden Materialien wie Gold, Platin oder Indium-Zinnoxid beschichtet werden. Die Elektroden besitzen einen Durchmesser von 10 bis 50 μm und sind meist in der Form eines Gitters angeordnet. Dies ermöglicht die simultane Messung des extrazellulären Aktionspotentials (EAP), auch Spike genannt, an mehreren Stellen eines neuronalen Netzwerks. Die Messung ist nicht invasiv, so dass die Zellen über mehrere Wochen bis Monate auf den MEAs kultiviert und regelmäßig gemessen werden können (Johnstone et al. 2010; Shafer 2019). Die Analyse der gemessenen EAPs liefert wichtige Informationen über die allgemeine elektrische Aktivität, die Differenzierung und die Netzwerkaktivität. Dargestellt werden die Signale meist als Spikerasterplot (SRP), auf dem einzelne Spikes und Gruppierungen von Spikes, so genannte Bursts, unterschieden werden können (**Abbildung 5a**). Die Länge und die Frequenz von Bursts variiert dabei je nach Zelltyp und Entwicklungszustand (Kapucu et al. 2012; Cotterill and Eglen 2019). Jede Zeile eines SRPs wird einer bestimmten Elektrode zugeordnet. Detektieren mehrere Elektroden zur gleichen Zeit einen Burst, wird dies als Netzwerkburst (engl. *network burst*) definiert. Sie sind ein Zeichen für die Reife eines Netzwerks, in dem die Neurone miteinander kommunizieren und synchron verschaltet sind (Bradford and McNutt 2015). Der Entwicklungsstand des neuronalen Netzwerks spielt dabei eine entscheidende Rolle. Die frühesten Aktivitätsmuster sind unregelmäßige und einzelne Spikes, da die Neuronen zu dem Zeitpunkt noch nicht miteinander verschaltet sind. Während der fötalen Entwicklung weisen zunächst kleine Gruppen von Neuronen ein synchrones Verhalten auf und etwa zum Zeitpunkt der Geburt zeigt sich bereits eine umfassendere und multilineuronale Synchronität. Diese zunächst noch heterogene

Aktivität reift weiter zu einer starken Synchronität mit zeitlich aufeinander abgestimmten Aktivierungen von Neuronen. Reife neuronale Netzwerke enthalten schließlich hochspezifische Neuronenanordnungen mit hemmenden oder erregenden synaptischen Kopplungen, die jeweils spezifische Aufgaben bei der Signalverarbeitung und -weiterleitung erfüllen (Egorov and Draguhn 2013). Weitere wichtige Informationen liefert die Wellenform des Aktionspotentials, da diese unter anderem je nach Zelltyp, Zellmorphologie und Anzahl der Ionenkanäle variieren kann. Eine einzelne Elektrode detektiert üblicherweise die Signale von mehreren Neuronen und durch Sortierung der verschiedenen Spikeformen (engl. *Spike Sorting*) können diese voneinander getrennt und einzeln analysiert werden (**Abbildung 5b**) (Bean 2007; Rey et al. 2015).

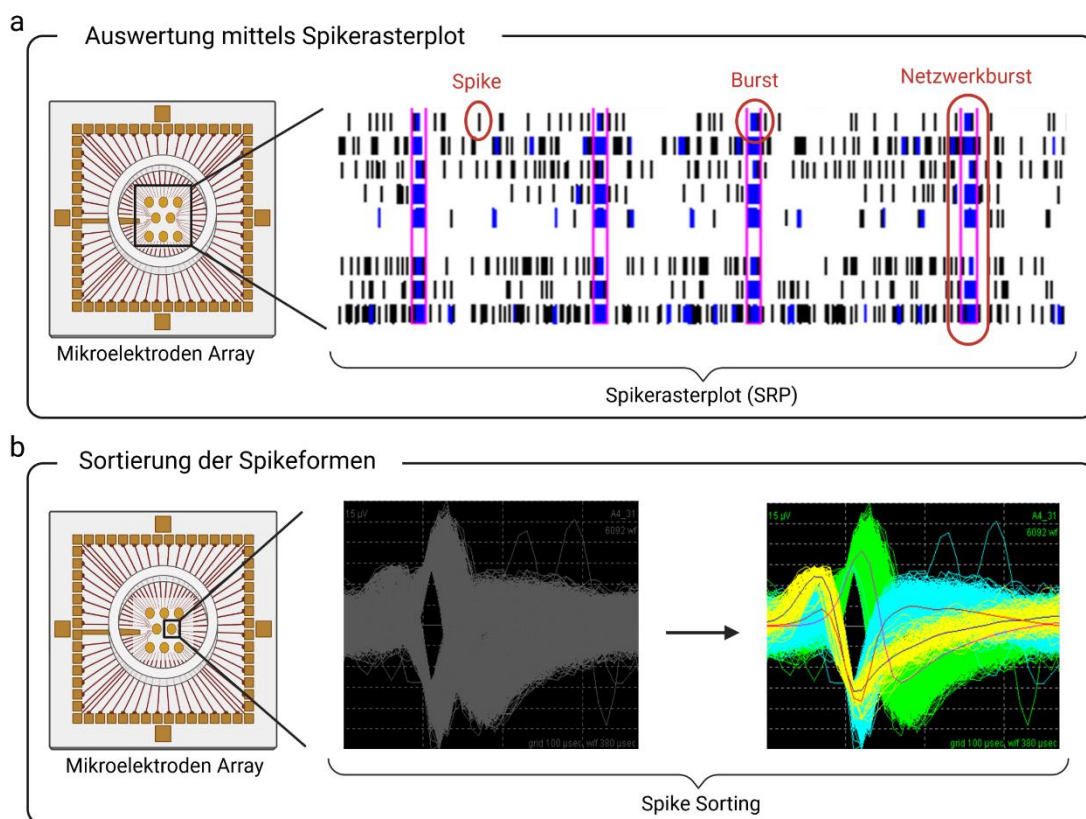


Abbildung 5: Von Mikroelektroden Arrays (MEAs) erzeugte Daten. **a.** Gezeigt ist ein repräsentativer Spikerasterplot (SRP). Die schwarzen Linien repräsentieren Spikes und die blauen Balken stellen Bursts dar. Treten die Bursts auf mehreren Elektroden gleichzeitig auf, handelt es sich um einen Netzwerkburst. **b.** Visuelle Darstellung des *Spike Sortings*. Eine einzelne Elektrode detektiert die Aktivität von mehreren Neuronen und durch Sortierung der Spikeformen können diese einzeln analysiert werden. Erstellt mit biorender.com.

1.8 Ziel dieser Arbeit

Tierversuche sind derzeit der Goldstandard in der Testung auf NT. Hohe Kosten und ein geringer Testdurchsatz erschweren jedoch ihre Anwendung für eine große Anzahl an Chemikalien. Darüber hinaus stellen verschiedene speziesspezifische Unterschiede ihre Vorhersagbarkeit für den Menschen in Frage. Um die Datenlücke zu schließen, die durch den geringen Testdurchsatz von Tierversuchen entstehen, müssen alternative, humanrelevante *in vitro*-Methoden entwickelt werden, die zum Beispiel auf menschlichen Stammzellen basieren. Voraussetzung für die Anwendbarkeit von NAMs ist eine gute Reproduzierbarkeit, sowie eine sorgfältige und auf ihren Anwendungsbereich bezogene Charakterisierung (Kavlock et al. 2018; Krewski et al. 2020).

Aufgrund dieses übergeordneten Ziels, befasst sich die vorliegende Dissertation mit den folgenden Zielen:

- I. Etablierung eines reproduzierbaren Protokolls zur adhärennten neuronalen Induktion von hiPSCs zu hiNPCs.
- II. Generierung und Charakterisierung von elektrisch aktiven neuronalen Netzwerken in 3D.
- III. Entwicklung einer neuen MEA-basierten Testmethode für die Testung auf akute Neurotoxizität *in vitro*.

2 Publikationen

Diese Dissertation beinhaltet folgende sechs Publikationen:

Die erste Publikation 2.1. “Neural In Vitro Models for Studying Substances Acting on the Central Nervous System” (Fritsche et al. 2020b) ist ein Buchkapitel welches den Einsatz von hiPSC-abstammenden neuronalen *in vitro* Kulturen in der Substanztestung sowie als Krankheitsmodell behandelt. Der Fokus wurde dabei auf zweidimensionale (2D) Zellkulturen bestehend aus Neuronen und Gliazellen, die *in vitro* Differenzierung in Mikroglia, sowie dreidimensionale (3D) Organoid – und Hydrogelkulturen gelegt.

Die zweite Publikation 2.2 “Stem Cells for Next Level Toxicity Testing in the 21st Century” (Fritsche et al. 2020a) diskutiert die Verwendung von Stammzellen in der heutigen und zukünftigen Toxizitätstestung und fokussiert die neusten Kultivierungstechniken, Organ-on-a-chip und Genome Editing. Alternativmodelle für die Organe Haut, Gehirn, Schilddrüse, Lunge, Herz, Leber, Niere und Darm werden behandelt.

In der dritten Publikation 2.3 “Characterization and application of electrically active neuronal networks established from human induced pluripotent stem cell-derived neural progenitor cells for neurotoxicity evaluation” (Nimtz et al. 2020) wurden humane induzierte pluripotente Stammzellen (hiPSCs) als Neurosphären zu neuronalen Progenitorzellen (hiNPCs) induziert und die Differenzierung in elektrisch aktive humane neurale Netzwerke (hNN) mit (CINDA) und ohne (NDM) reifungsfördernde Faktoren untersucht. Die in CINDA-differenzierten hNN weisen eine stärkere elektrische Aktivität auf und zeigen eine starke inhibitorische Wirkung auf den Neurotransmitter GABA.

In der vierten Publikation 2.4 “Measurement of Electrical Activity of differentiated Human iPSC-Derived Neurospheres recorded by Microelectrode Arrays (MEA)” (Bartmann et al. 2021) wird die 3D neurale Induktion von hiPSCs in hiNPCs und die anschließende neurale Differenzierung auf Multielektroden Arrays (MEAs) detailliert beschreiben. Die Messung und Datenauswertung der neuronalen elektrischen Aktivität werden ebenfalls geschildert.

Die fünfte Publikation 2.5 “Alginate-laminin hydrogel supports long-term neuronal activity in three-dimensional human induced pluripotent stem cell-derived neuronal networks” (Hartmann et al. 2022) untersucht den Einfluss von Laminin 111 (L111) auf 3D neurale Netzwerke (3D-NN), welche in Alginathydrogelen kultiviert werden. Es zeigte sich, dass L111 einen positiven Einfluss auf die neuronale Migration, die Differenzierung in Neurone und Astrozyten, die Synaptogenese und die Reifung der 3D-NN hat.

In der sechsten Publikation 2.6 “Molecular and functional characterization of different BrainSphere models for use in neurotoxicity testing on microelectrode arrays” (Hartmann et al. 2023) wurden drei verschiedene 2D neurale Induktionsprotokolle und zwei Differenzierungsmedien molekularbiologisch und elektrophysiologisch verglichen. Die Sortierung der Spikeformen ermöglichte die Entwicklung des humanen Multineurotransmitterrezeptor Assays (*human multi-neurotransmitter receptor assay*, hMNR) für die Verwendung in der Neurotoxizitätstestung (NT).

2.1 Neural In Vitro Models for Studying Substances Acting on the Central Nervous System

Ellen Fritsche, Julia Tigges, **Julia Hartmann**, Julia Kapr, Melania Maria Serafini, and Barbara Viviani

Handbook of Experimental Pharmacology

Die Arbeit mit Tiermodellen hat uns viele Einblicke in die Physiologie und die Mechanismen bestimmter Krankheiten sowie die Toxizität bestimmter Chemikalien gegeben. Jedoch lassen sich die Unterschiede zwischen den Spezies Ratte und Mensch nicht verleugnen und führen zu einer hohen Rate an Medikamenten, die in der klinischen Phase am Menschen durchfallen. Dies betrifft insbesondere Medikamente zur Behandlung von Krankheiten des zentralen Nervensystems (ZNS). Aus diesem Grund sollten Untersuchungen hinsichtlich der Sicherheit und der Wirkung dieser Chemikalien an human-basierten neuronalen *in vitro*-Modellen durchgeführt werden. hiPSCs eignen sich hierfür sehr gut, da sie den genetischen und molekularen Phänotyp des (kranken) Spenders behalten und den einzigartigen Vorteil besitzen, dies im menschlichen Kontext *in vitro* zu reproduzieren. Die gezielte Differenzierung von hiPSCs in neurale Zellen in einem 2D oder 3D Kontext ermöglicht die Bildung von komplexen Modellen, die für die Untersuchung von Neurotoxizität oder das ZNS-betreffende Krankheiten geeignet sind. Dieses Buchkapitel gibt einen Überblick über hiPSC-basierte humane 2D Neuronenkulturen und Neuronen-Glia-Mischkulturen, *in vitro*-Kulturen von Mikroglia und ZNS-Krankheitsmodelle. Hierbei liegt der Fokus auf neuen Entwicklungen in diesem Bereich, Gehirnorganoiden und 3D-gedruckten Hydrogelmodellen sowie ihre Anwendung in der Sicherheits- und Wirksamkeitsbewertung.



Neural In Vitro Models for Studying Substances Acting on the Central Nervous System

Ellen Fritsche, Julia Tigges, Julia Hartmann, Julia Kapr, Melania Maria Serafini, and Barbara Viviani

Contents

- 1 Introduction into In Vitro Neurotoxicity Evaluation
 - 1.1 Stem Cell-Based Human 2D Neuronal and Mixed Neuronal/Astrocyte Models
 - 1.2 In Vitro Cultures of Microglia
 - 1.3 Moving In Vitro Cultures into the Third Dimension with Brain Organoids
 - 1.4 3D Bioprinted In Vitro Neural Models
 - 1.5 CNS Disease Models
- 2 Summary and Conclusion
- References

Abstract

Animal models have been greatly contributing to our understanding of physiology, mechanisms of diseases, and toxicity. Yet, their limitations due to, e.g., interspecies variation are reflected in the high number of drug attrition rates, especially in central nervous system (CNS) diseases. Therefore, human-based neural in vitro models for studying safety and efficacy of substances acting on the CNS are needed. Human iPSC-derived cells offer such a platform with the unique advantage of reproducing the “human context” in vitro by preserving the genetic

Ellen Fritsche, Julia Tigges, Julia Hartmann, Julia Kapr, Melania Maria Serafini, and Barbara Viviani contributed equally to this work.

E. Fritsche (✉) · J. Tigges · J. Hartmann · J. Kapr
IUF-Leibniz Research Institute for Environmental Medicine at the Heinrich-Heine-University
Dusseldorf gGmbH, Dusseldorf, Germany
e-mail: ellen.fritsche@iuf-duesseldorf.de; julia.tigges@iuf-duesseldorf.de;
julia.hartmann@iuf-duesseldorf.de; julia.kapr@iuf-duesseldorf.de

M. M. Serafini · B. Viviani (✉)
Department of Pharmacological and Biomolecular Sciences, University of Milan, Milan, Italy
e-mail: melania.serafini@unimi.it; barbara.viviani@unimi.it

and molecular phenotype of their donors. Guiding the differentiation of hiPSC into cells of the nervous system and combining them in a 2D or 3D format allows to obtain complex models suitable for investigating neurotoxicity or brain-related diseases with patient-derived cells. This chapter will give an overview over stem cell-based human 2D neuronal and mixed neuronal/astrocyte models, in vitro cultures of microglia, as well as CNS disease models and considers new developments in the field, more specifically the use of brain organoids and 3D bioprinted in vitro models for safety and efficacy evaluation.

Keywords

Bioprinted neuronal models · Brain organoids · CNS disease models · Developmental neurotoxicity (DNT) · Human induced pluripotent stem cells (hiPSCs) · Microglia culture · Neurotoxicity (NT)

1 Introduction into In Vitro Neurotoxicity Evaluation

Adult *neurotoxicity* occurs when exposure to natural or human-made toxic substances (*neurotoxicants*) alters the normal activity of the nervous system. It can eventually disrupt or even kill *neurons* or the surrounding *glial* cells, influencing the transmission and processing of signals in the brain and other parts of the *nervous system*. Neurotoxicity can result from exposure to substances used in radiation treatment, chemotherapy, other drug therapies, and organ transplants, as well as exposure to heavy metals such as lead and mercury; certain foods and food additives; pesticides; industrial and/or cleaning solvents; cosmetics, i.e., mercury for skin bleaching or new actives with unknown systemic effects; and some naturally occurring substances (Massaro 2002). Symptoms may appear immediately after exposure or be delayed. They may include limb weakness or numbness; loss of memory or vision; headache; intellect, cognitive, and behavioral problems; and visceral, including sexual dysfunction. Individuals with certain disorders may be especially vulnerable to neurotoxicants (National Institute of Health Neurotoxicity Information 2019).

The recognized test method for evaluating the neurotoxic potential of chemicals is the OECD Guideline 424 (Neurotoxicity studies in rodents). This method uses complex in vivo tests which are often labor-intensive and expensive (Crofton et al. 2012) and might also not well reflect the human situation because of interspecies variation (Leist and Hartung 2013). Such interspecies variation is also thought to be one of the reasons for the high attrition rates in drug development. Before a drug candidate can be taken into human clinical trials, it must be tested for safety and efficacy in animals that display relevant disease characteristics. This poses unique challenges in *central nervous system* (CNS) research, because of the difficulties to induce or quantify, e.g., depression, anxiety, or impairment of social interaction. In addition, pharmacokinetics and pharmacodynamics might differ between species

and thus cause poor prediction for beneficial or adverse effects in humans (Toutain et al. 2010). It stands to reason that diseases with the most complex and least understood etiologies are typically the ones that are the hardest to develop treatments for, which is reflected in the translation failure of CNS drug discovery (Danon et al. 2019; Gribkoff and Kaczmarek 2017).

Understanding compounds' modes of action (*MoA*) and pathophysiology of disease in the human context is of high importance for correct safety and efficacy predictions. This is exemplified by the activation of peroxisome proliferator-activated receptor alpha (PPAR α) via PPAR α agonists inducing liver tumors in rodents, yet not in humans, probably due to lower PPAR α and/or co-activators/co-repressors expression in the latter (Klaunig et al. 2003). Here, animal models overestimate PPAR α agonists' hazard for human health. In the case of searching for drugs curing Alzheimer's disease, animal models, which are genetically predisposed to generate A β plaques or neurofibrillary tangles of Tau protein, have been used. Yet no results have translated from these animal disease models into effective human medication, probably because they do not represent human AD pathophysiology sufficiently (Danon et al. 2019).

These two examples nicely pin down the issue of model predictivity in compound safety and efficacy evaluation and their translation to human health. One strategy to overcome such translational shortcomings lies in the use of test systems of human origin. Therefore, the biomedical achievement of producing human induced pluripotent stem cells (*hiPSC*) from somatic cells (Takahashi et al. 2007) opened up a whole new arena in the ethically sound production of an unlimited number of human cells, including neurons and glia. In addition, the recent surge in tissue modeling, by culturing such cells in three dimensions (3D), is producing a paradigm shift in disease modeling and in pharmacological as well as toxicological testing strategies (Lancaster and Knoblich 2014; Lancaster et al. 2017; Pasca 2018). In vitro cultures are currently also taken to the next level by their growth in bioreactors, which, when connected, can be assembled as organs-on-the-chip and designed to mimic in vivo environments (Park et al. 2019).

Such *new approach methods* (NAMs) cannot be used in an isolated manner, as a cell culture does not represent a whole organism, even if cells grow in 3D. Therefore, frameworks are needed that allow the interpretation of data generated with human 2D or 3D in vitro methods (Fig. 1). One general deficiency of in vitro methods is the lack of picturing pharmacokinetics that is crucial for toxicity and efficacy evaluation. Here, physiology-based pharmacokinetics modeling can be of great help (Paini et al. 2019; Zhuang and Lu 2016) as it provides wet-lab researchers with target tissue concentrations as rationales for their in vitro studies. Finding that human exposure-relevant concentrations is fundamental, yet how to choose and proceed with the readouts of in vitro studies? Here, the "Adverse Outcome Pathway" (AOP) concept is of tremendous help. The AOP is an organizational model that identifies a sequence of biochemical and cellular events (*molecular initiating event*, MIE; *key events*, KE) required to produce a toxic effect (*adverse outcome*, AO) when an organism is exposed to a substance (Fig. 1). Construction of an AOP can (1) organize information about biological interactions and toxicity mechanisms into models that describe

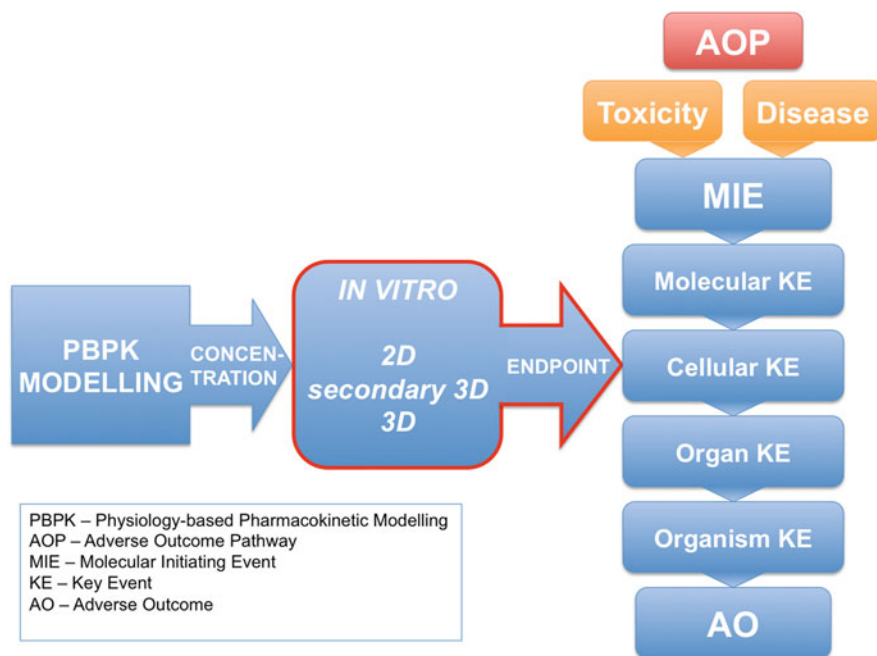


Fig. 1 Framing of data from in vitro models with pharmacokinetics information from PBPK modeling and endpoint judgment according to the AOP concept

how exposure to a substance might cause illness or injury, (2) suggest cell- or biochemical-based tests for pathway elements that could be used to develop testing strategies for targeted toxicity, and (3) identify data gaps in a pathway of toxicity that need more information with the final goal of using fewer resources and experimental animals (Ankley et al. 2010). This concept was soon also applied to neurotoxicity (Bal-Price et al. 2015). Recently it was suggested that the AOP framework is also applicable to understanding disease pathways for prevention, diagnosis, and treatment and in biomedical and clinical research for drug discovery, efficacy, and safety testing (Carusi et al. 2018). Studying cellular effects with in vitro methods in a conceptual framework for toxicity or disease provides drug developers and basic or regulatory scientists with greater confidence in the meaningfulness and thus applicability of generated in vitro data (Fig. 1). In the end, higher human relevance of scientific outcomes will protect society and the individual and also reduce health-care costs.

Neurotoxicity can be triggered by a multitude of MoA (Masjosthusmann et al. 2018). In vitro, this MoA can either be measured as specific changes in endpoints, like effects on ion currents, specific receptor activation, or loss in myelin. In addition, MoA can cause neuronal cell death, an endpoint relevant for in vitro and in vivo neurotoxicology. For example, excitatory cell death can occur through stimulation of glutamatergic neurotransmission, or dopaminergic cell death can be

induced via mitochondrial dysfunction. Although neural cell death is indeed a relevant endpoint, it does not inform on the underlying MIE. Moreover, a compound not inducing neural cell death cannot be excluded as a neurotoxicant. When studying neurotoxicity in vitro, knowledge about molecular equipment of cells is crucial for defining the application domain of the respective model.

This chapter now intends to fill the red box in Fig. 1 by summarizing the current state of the art on hiPSC/ESC-based 2D or secondary 3D neuronal and mixed neuronal/glia as well as microglial models, neural organoids, bioprinted neural models, and 2D or 3D neurological disease models. Such find their application in pharma- and toxicological studies by investigating endpoints in vitro that lead to AOs or possibly represent relevant therapeutic targets. A summary of the main toxicological targets is given in Table 1. Although historically most brain-related in vitro data has been derived from rodents (Masjosthusmann et al. 2018), this chapter will focus on published human test systems due to the species specificities discussed above.

1.1 Stem Cell-Based Human 2D Neuronal and Mixed Neuronal/Astrocyte Models

Stem cells (SC) are divided into adult stem cells and *embryonic stem cells* (ESC), depending on their origin and potency (Singh et al. 2015). ESCs are derived from the inner cell mass of the blastocyst and have the ability to self-renew and to generate all cell types of the body except extraembryonic cells (placenta) and are therefore termed pluripotent (Guenther 2011). In 1998 the first human ESC line was isolated from human embryos initially produced for in vitro fertilization (Thomson et al. 1998).

Yamanaka and co-workers created the basis for a new generation of neural in vitro models by developing the Nobel Prize-winning cell system of *human induced pluripotent stem cells* (hiPSC). These cells can be derived from human mature somatic cells by different reprogramming methods (Janabi et al. 1995; Lowry and Plath 2008; Warren et al. 2010; Zhang et al. 2013; Victor et al. 2014) and thus avoid the ethical issues of human ESC (Takahashi et al. 2007; Yu et al. 2007). Human iPSC can be differentiated into cells from all three germ layers (Takahashi et al. 2007; Shi et al. 2017).

Using hiPSC, it is possible to induce a variety of neural cell types. *Neural stem cells* (NSCs) and *neuronal progenitor cells* (NPCs) can be differentiated from hiPSC in large quantities with high reproducibility (Farkhondeh et al. 2019). Cheng and co-workers describe a method to generate NPC from hiPSC using a multistep protocol including embryoid body formation and formation of neural rosettes, followed by multidimensional fluorescence-activated cell sorting (FACS) to purify NPCs by using a set of cell surface markers (Cheng et al. 2017). The authors claim that these cells are suitable for probing human neuroplasticity and mechanisms underlying CNS disorders using high-content, single-cell level automated microscopy assays. Still, a proof-of-concept study remains to be published.

Table 1 Mode of action (MoA) relevant for human neurotoxicity identified within a systematic review investigating 248 individual chemical compounds, 23 compound classes, and 212 natural neurotoxins (Masjosthusmann et al. 2018; modified from Appendix D)

#	Mode of action	MoA related to
1	Stimulation of cholinergic neurotransmission	Neurotransmission
2	Inhibition of cholinergic neurotransmission	
3	Stimulation of GABAergic neurotransmission	
5	Inhibition of glycinergic neurotransmission	
6	Stimulation of glutamatergic neurotransmission	
7	Inhibition of glutamatergic neurotransmission	
8	Stimulation of adrenergic neurotransmission	
9	Inhibition of adrenergic neurotransmission	
10	Stimulation of serotonergic neurotransmission	
11	Inhibition of serotonergic neurotransmission	
12	Inhibition of dopaminergic neurotransmission	
13	Neurotransmission in general	
14	Activation of sodium channels	Ion channels/receptors
15	Inhibition of sodium channels	
16	Inhibition of potassium channels	
17	Inhibition of calcium channels	
18	Activation of chloride channels	
19	Inhibition of chloride channels	
20	Effects on other neuronal receptors	
21	Mitochondrial dysfunction/oxidative stress/apoptosis	Cell biology
22	Redox cycling	
23	Altered calcium signaling	
24	Cytoskeletal alterations	
25	Neuroinflammation	
26	Axonopathies	
27	Myelin toxicity	
28	Delayed neuropathy	
29	Enzyme inhibition	
30	Other	Other

Human iPSC-derived neurons can be generated directly from hiPSC or with NSCs/NPCs as an intermediate step (Yu et al. 2014; Ghaffari et al. 2018). The latter protocol takes about 2 weeks and can be used for the evaluation of drug efficacy, although purity and maturity of the cells are in question and need further characterization (Farkhondeh et al. 2019; Dai et al. 2016).

Numerous protocols have been published describing the generation of specific neuronal subtypes as well as glial cells from hiPSC such as *cortical neurons* (Shi et al. 2014; Eiraku et al. 2008; Boissart et al. 2013), *glutamatergic neurons* (Boissart et al. 2013; Cheng et al. 2017; Wang et al. 2017; D'Aiuto et al. 2014; Sanchez-Danes et al. 2012; Yu et al. 2009; Nehme et al. 2018), *GABAergic neurons* (Yang et al. 2017; Liu et al. 2013; Flames et al. 2007; Manabe et al. 2005), *serotonergic and*

dopaminergic neurons (Chambers et al. 2009; Cooper et al. 2012; Kriks et al. 2011; Sanchez-Danes et al. 2012; Li et al. 2017), *motor neurons* (Corti et al. 2012; Sareen et al. 2012, 2013; Kiskinis et al. 2014; Maury et al. 2015), *sensory neurons* (Boisvert et al. 2015; Stacey et al. 2018), *astrocytes* (Lundin et al. 2018; Suga et al. 2019), *oligodendrocytes* (Osaki et al. 2018; Ehrlich et al. 2017; García-León et al. 2018b), and *microglia* (McQuade et al. 2018), just to name a few. In this chapter, we will focus on published in vitro systems that have already been used for screening approaches or are at a state of assay development that will allow substance screening in the near future.

Malik and co-workers established a high-throughput screening platform using hiPSC-derived NSCs and rat cortical cells to screen a compound library of 2,000 chemicals including known drugs (50%), natural products (30%), and bioactive compounds (20%) for their cytotoxic potential (Malik et al. 2014; Efthymiou et al. 2014). In a follow-up study, a subset of 100 compounds was screened in hiPSC, NSC-derived neurons (Efthymiou et al. 2014), and fetal astrocytes. This approach enabled the authors to identify species- and cell type-specific differences in responses to compounds. Specifically, they found that human NSCs were more sensitive to the screened compounds than rodent cultures. In addition, they identified compounds with cell type-specific toxicities. A limitation of the study is the assessment of cytotoxicity as the sole endpoint, which might not be the most sensitive one. Another restriction of this approach is the lack of co-culture of neuronal and glial cells. Moreover, in the species comparison, cells from different maturation stages and single (human) versus co-cultures (rat) were related, making data interpretation difficult.

Another study used small molecule-based NPCs differentiated from three different hiPSC lines, which were then differentiated into neurons and astrocytes within 15 days, using a highly standardized protocol (Seidel et al. 2017). The authors used *multi-microelectrode arrays* (MMEA) for monitoring neuronal network activities via field potential measurements. Such recordings assess multiple endpoints stipulating that different neuronal receptors are expressed by the cells (Table 1). Here, they show reactivity towards dopamine, GABA, serotonin, acetylcholine, and glutamic acid, but not norepinephrine. To date, there are no general guidelines for the analysis and quantification of MMEA measurements. Seidel et al. use single electrodes as the statistical unit, but using different chips or experiments as an individual “n” number would be preferable to assess the reproducibility and standardization between experiments (Masjosthusmann et al. 2018).

In recent years, more and more companies have been offering commercially available hiPSC-based neuronal cells. One study compared different commercially available hiPSC-derived mature neurons (excitatory and inhibitory) from different suppliers, with and without astrocyte co-culture, again utilizing MMEA activity as a functional readout, this time in combination with measurements of calcium signaling (Tukker et al. 2016). Treatment with glutamate and GABA strongly reduced the mean spike rate of the analyzed cultures. Calcium transients of individual neurons were generated upon treatment with glutamate, GABA, and acetylcholine. Here, astrocytes seem to be crucial for *neuronal network* generation because pure neuronal

cultures in the absence of astrocytes lack bursting, a sign for neuronal network maturity. In this study, the statistical unit was chosen as one well of a 48-well plate, not allowing assessment of reproducibility and standardization between experiments (Masjosthusmann et al. 2018). A follow-up study in 2018 also used commercially available hiPSC-derived neurons and astrocytes, this time exploring the effect of the ratio of mixed neurons and astrocytes (Tukker et al. 2018). This study strongly supports the previous observation that the addition of astrocytes to the model in near-physiological proportions of 50% (glia/neuron ratio 1:1; von Bartheld et al. 2017) and a ratio of 1:5 for GABAergic inhibitory neurons and excitatory neurons (Hendry et al. 1987; Sahara et al. 2012) indeed promotes neuronal network formation and maturation best. This study primarily indicates that hiPSC-derived neuronal models must be carefully designed and characterized before their large-scale use in neurotoxicity screenings, as each model exerts different responses to compounds, depending on the composition of the networks. The importance of the presence of astrocytes was also assessed by another study using commercially available cortical neurons on MMEAs (Kayama et al. 2018).

For controlled plating of neuron/astrocyte ratios, cells must be differentiated separately. A recent protocol instructs how to differentiate hiPSC into astroglia (NES-Astro) within 28 days (Lundin et al. 2018). These cells were extensively characterized using transcriptomics, proteomics, glutamate uptake, inflammatory competence, calcium signaling response, and APOE secretion and were compared to primary astrocytes, commercially available hiPSC-derived astrocytes, and an astrocytoma cell line. The data show large diversity among the different analyzed astrocytic models and strongly suggest to take the cellular context into account when studying astrocyte biology. Taking this to the next level, it indicates the importance of choosing the right astrocytic model to combine with hiPSC-derived neurons for the testing of substances acting on the CNS.

One major challenge in the field is the availability of a sufficient number of cells for large-scale screening approaches. Stacey et al. (2018) describe the concept of cryopreserved “near-assay-ready” cells, which decouples complex cell production from assay development and screening. Using this approach, the authors developed a 384-well veratridine-evoked calcium flux assay which assesses neuronal excitability and screened 2,700 compounds to profile the range of target-based mechanisms able to inhibit veratridine-evoked excitability using hiPSC-derived sensory neurons. In order to be able to use this approach for the identification of active compounds with unknown MoA, further secondary assays (e.g., using MMEA-technology) need to be developed to characterize the hits on a mechanistic level (Stacey et al. 2018). In addition, experiments were performed using pure neuronal cultures without the addition of astrocytes, probably leading to different neuronal responses than with astrocytes present.

Along those lines another high-throughput screening using 11 different compound libraries with a total of 4,421 unique substances, all bioactive small molecules, which include approved drugs, well-characterized tool compounds, natural products, and human metabolites, has been described lately (Sherman and Bang 2018). The authors use high-content image analysis, focusing on neurite outgrowth

of commercially available hiPSC-derived neurons, consisting primarily of GABAergic and glutamatergic neurons, but no astrocytes. They identified 108 hit compounds containing 38 approved drugs (outgrowth: erlotinib, clomiphene, tamoxifen, 17 β -estradiol, dehydroepiandrosterone-3-acetate (DHEA), alfacalcidol, lynestrenol, benzotropine, dibucaine, fluphenazine, perphenazine, prochlorperazine, trifluoperazine, sertindole, quetiapine, ifenprodil, meclizine, alverine, econazole, oxiconazole, letrozole, SAHA (Vorinostat); inhibition: methyltestosterone, thioridazine, methotrimeprazine, colchicine, docetaxel, vincristine, mebendazole, emetine, daunorubicin, doxorubicin, mitoxantrone, topotecan, hexachlorophene, ouabain, digoxin, suramin) which fall into the following categories: kinase inhibitors, steroid hormone receptor modulators, and channel and neurotransmitter system modulators (Sherman and Bang 2018). Inhibition of neurite outgrowth is one key characteristic in developmental neurotoxicity (Fritsche et al. 2018a, b), yet its implication in adult neurotoxicity is not clear.

Using a similar readout, hiPSC-derived peripheral-like neurons were applied to study the effect of chemotherapeutic agents on neuronal cytotoxicity and neurite length, again using high-content image analysis (Rana et al. 2017). This approach identified compounds that cause interference in microtubule dynamics but failed to depict the adverse effects of platinum and anti-angiogenic chemotherapeutics, which are compounds that do not act directly on neuronal processes. Here the addition of astrocytes to the model might lead to a higher predictivity, as the administration of fluorocitrate, an astrocyte-specific metabolic inhibitor, increased the pain tolerance of the animals in a rat model of oxaliplatin-induced neuropathic pain (Di Cesare et al. 2014; Kanat et al. 2017), indicating the role of astrocytes in sustaining platinum-mediated neurotoxicity.

One important cell type for neurotoxicological assessment of substances is myelin-producing oligodendrocytes. Yet publications on hiPSC-derived oligodendrocyte are scarce, and the protocols that are available are very time-consuming and of limited efficiency (Wang et al. 2013; Douvaras et al. 2014; Djelloul et al. 2015). Therefore, they are not suitable for medium- to high-throughput screening approaches. In contrast, the three transcription factors SOX10, OLIG2, and NKX6.2 produced 80% O4⁺ oligodendrocytes from hiPSC within 28 days and might thus be a promising approach for future neurotoxicological applications (Ehrlich et al. 2017). Another recent study even reports that the overexpression of the transcription factor SOX10 alone is sufficient to generate 60% O4⁺ and 10% MBP⁺ cells in only 22 days (García-León et al. 2018b).

Although this part of the chapter primarily covers the use of hiPSC for the generation of neural in vitro models for studying substances acting on the CNS, the method of direct reprogramming of neuronal cells from somatic cells should not be disregarded. Lee et al. (2015) directly reprogrammed human blood to NPC without the intermediate step of hiPSC generation. These induced neurons (iNs) can be generated by overexpression of a set of transcription factors (Ichida and Kiskinis 2015; Vierbuchen et al. 2010; Ambasudhan et al. 2011; Hu et al. 2015; Wapinski et al. 2017) or miRNAs (Victor et al. 2014; Yoo et al. 2011; Abernathy et al. 2017) that promote chromatin remodeling and drive direct neural lineage

differentiation (Silva and Haggarty 2019). Especially for research regarding age-associated neurodegenerative diseases, like Alzheimer's disease (AD) or Parkinson's disease (PD), this method is of high interest, as bypassing the hiPSC reprogramming process reduces the disruption of epigenetic markers associated with the age of the somatic cell, therefore allowing to create neuronal models at "pathogenic ages" (Mertens et al. 2018). This method preserves multiple age-associated markers, including DNA methylation patterns, transcriptomic and microRNA profiles, oxidative stress, DNA damage (loss of heterochromatin and nuclear organization), and telomere length (Mertens et al. 2018; Silva and Haggarty 2019), and is therefore a promising approach to study substances acting on the aged CNS or screening for pharmaceuticals as a treatment for these conditions.

When working with either of these models, it is of utmost importance to have a well-characterized cell system, which suits the research question in case of basic research or contains a defined application domain for neurotoxic MoA (Table 1) when used for screening applications. Lack of characterization or definition of the application domain might result in false-negative data due to a lack of cellular targets. In addition, as with other *in vitro* approaches, the multicellular context of cultures seems to be crucial, possibly resulting in false predictions of chemicals when pure neuronal cultures lacking glia are used.

1.2 In Vitro Cultures of Microglia

Microglia constitute 5–10% of total brain cells and represent the resident innate immune cells of the CNS (Arcuri et al. 2017). Microglia discovery dates back to the end of the nineteenth century, but the name was coined in the 1920s by del Rio Hortega who phenotypically characterized the only immune cells resident in the brain parenchyma (Pérez-Cerdá et al. 2015). The function of microglia was for a long time underestimated because of the misconception that the brain is an immune-privileged site; moreover it was initially wrongly thought that this cell type originates from the neuroectoderm. To date, it is known that microglia arise from embryonic yolk sac (YS) precursors (Ginhoux et al. 2010) which give rise to YS macrophages that colonize the embryo, including the brain, to generate all types of tissue-resident macrophages (Li and Barres 2018). In the CNS, microglia maintain their population by self-renewal (Ajami et al. 2007) and by recruiting monocytes from the bloodstream (Hashimoto et al. 2013). The presence of microglia in the brain parenchyma is fundamental because of the variety of functions they perform from early brain development throughout the entire life of the organism, both in brain homeostasis and disease (for an extensive review, see Li and Barres 2018).

Considering the pivotal contribution of microglia to brain functions, it is important to have *in vitro* models containing microglia when studying the influence of drugs and toxicants on the brain. The majority of published *in vitro* studies mainly used primary microglia cultures from embryonic/neonatal rodent brain (mouse or rat). Still, fetal microglia seem to be quite different from adult ones. Due to ethical reasons, it is challenging to obtain brain-derived microglia from humans. The few

human microglia cell lines generated, such as HMO6 (Nagai et al. 2005) and HMC3 (Janabi et al. 1995), are not considered as an optimal model because long-term culture and genetic manipulation altered their functions and morphology. Finally, the low number of cells collected from humans does not allow large-scale neurotoxicity in vitro studies.

Starting from these premises, Leone and colleagues set up a monocyte-derived microglia-like cell model by culturing human monocytes with astrocyte-conditioned medium (Leone et al. 2006). This protocol was successively standardized using human peripheral blood mononuclear cells (PBMCs) stimulated with four recombinant human cytokines. The microglia cells obtained display a ramified morphology after 2 weeks in culture and express surface markers typical for the known pattern of microglia (Etemad et al. 2012).

More recently, human microglia-like cells were obtained from hESC and hiPSC. As previously stated, microglia derive from non-monocytic primitive myeloid cells, unlike adult bone marrow-derived macrophages. Thus microglia-like cells derived from PBMCs do not mirror this ontogeny. Muffat and co-workers established a robust protocol that allows the derivation of microglia-like cells from hiPSC, obtained from reprogrammed fibroblasts, using a serum-free medium that mimics the environment of the CNS interstitial milieu and adding interleukin 34 (IL-34), an alternative ligand for colony-stimulating factor 1 receptor. The microglia-like cells obtained with this protocol are highly phagocytic, and their gene expression profile resembles human primary microglia. They progressively adopt a ramified morphology when cultured in isolation, while when co-cultured in the presence of hiPSC-derived neurons, microglia-like cells refine their molecular signature. In terms of activity and response to stressors, unstimulated microglia-like cells secrete detectable levels of various cytokines and chemokines, which were enhanced after stimulation with lipopolysaccharide (Muffat et al. 2016) (Fig. 2).

Similar protocols were published a few months later reprogramming fibroblasts or PBMCs. In the paper of Pandya et al. (2017), hiPSCs were sequentially differentiated into myeloid progenitor-like intermediate cells and then into cells with the phenotypic, transcriptional, and in vitro functional signatures of brain-derived microglia. Abud and co-workers demonstrated that microglia-like cells obtained from hiPSC secrete cytokines in response to inflammatory stimuli, migrate, undergo calcium transients, and phagocytose (Abud et al. 2017). All those protocols require from 30 to about 70 days of time to obtain mature glia (McComish and Caldwell 2018). Taken together, those data suggest that microglia obtained from reprogrammed hiPSC better mirror the developmental stages of microglia maturation and ontogeny, in comparison to microglia-like cells derived from PBMCs stimulated with a cocktail of factors.

The potential applications of hiPSC-derived microglia include drug discovery studies, neurotoxicity screening assays, and use in disease modeling. Microglia-mediated inflammation can negatively impact the brain, and much evidence shows that microglial activation plays a role in neurodegeneration, contributing to the etiology of neurodegenerative disorders (Ransohoff and El Khoury 2016). The availability of robust protocols to generate and maintain microglia from patients with different brain dysfunctions in culture would facilitate the study of the

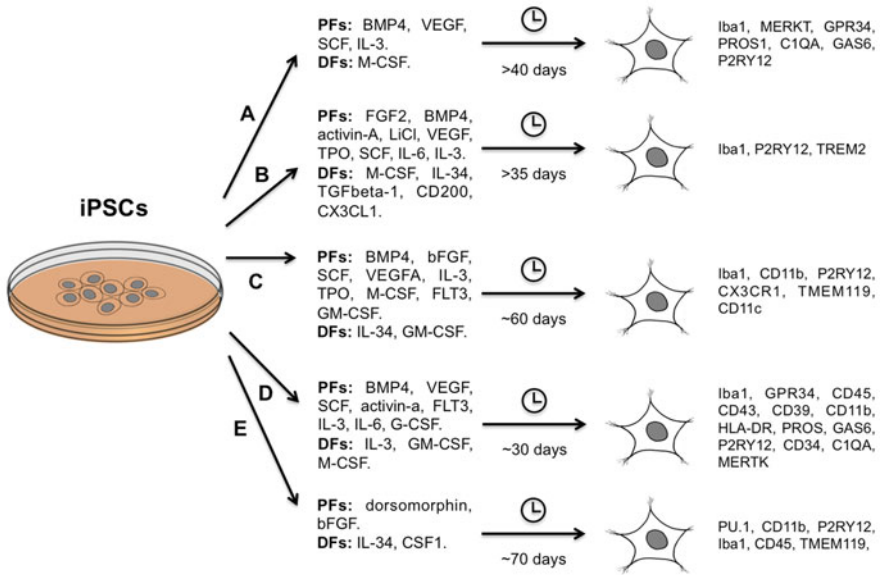


Fig. 2 Human iPSC-derived microglia protocols. (a) Haenseler et al. (2017), (b) Abud et al. (2017), (c) Douvaras et al. (2017), (d) Pandya et al. (2017), (e) Muffat et al. (2016). *PFs* patterning factors, *DFs* differentiation factors, *BMP4* brain morphogenetic protein 4, *VEGF* vascular endothelial growth factor, *SCF* stem cell factor, *IL-3* interleukin 3, *M-CSF* macrophage colony-stimulating factor, *FGF2* or *bFGF* fibroblast growth factor 2, *TPO* thrombopoietin, *IL-6* interleukin 6, *IL-34* interleukin 34, *TGFbeta-1* transforming growth factor beta 1, *CD200* cluster of differentiation 200, *CX3CL1* fractalkine, *VEGF-A* vascular endothelial growth factor A, *FLT-3* fm-like tyrosine kinase 3, *GM-CSF* granulocyte-macrophage colony-stimulating factor, *G-CSF* granulocyte colony-stimulating factor, *CSF1* colony-stimulating factor 1, *Iba1* ionized calcium-binding adapter molecule 1, *MERTK* tyrosine kinase phagocytic receptor, *GPR34* G protein-coupled receptor 34, *PROS1* protein S1, *C1QA* complement C1q subcomponent subunit A, *GAS6* growth arrest-specific 6, *P2RY12* purinergic receptor P2Y, *TREM2* triggering receptor expressed on myeloid cells 2, *CD11b* cluster of differentiation 11b, *CX3CR1* CX3C chemokine receptor 1, *TMEM119* transmembrane protein 119, *CD11c* cluster of differentiation 11c, *CD45* cluster of differentiation 45, *CD43* cluster of differentiation 43, *CD39* cluster of differentiation 39, *HLA-DR* human leukocyte antigen – DR isotype, *CD34* cluster of differentiation 34

pathology and the discovery of new pharmacological approaches. The first evidence of in vitro culturing disease-related microglia cells from patients was in 2012, when Almeida and colleagues generated multiple induced hiPSC lines from subjects with frontotemporal dementia (Almeida et al. 2012). More recently, Ryan and co-workers performed, on human monocyte-derived microglia-like cells, a quantitative expression trait locus study to examine the effects of common genetic variation on the expression of genes found in susceptibility loci for Alzheimer's disease, Parkinson's disease, and multiple sclerosis (Ryan et al. 2017). Microglia-like cells obtained by reprogramming PBMCs were also combined with neural progenitor cells and synaptosomes from hiPSC-derived neurons to create patient-specific cellular models useful to model CNS diseases facilitating high-throughput drug screening and neurotoxicity assays based on microglia function in the future (Sellgren et al. 2017).

In conclusion, different protocols for the derivation of human microglia are available that enable experiments in authentic human in vitro systems. Unlike methods for the derivation of neurons and astrocytes, protocols for microglia lack regionality and do not reflect microglia subtypes found within the brain (Grabert et al. 2016), which is a true challenge for the future.

1.3 Moving In Vitro Cultures into the Third Dimension with Brain Organoids

For investigating possible CNS disease mechanisms or screening drugs or toxins for safety and efficacy, it is thought to be advantageous to use complex 3D systems such as *brain organoids*. The benefits of organoids compared to “conventional” cultures lie in their composition of multiple cell types, which are functional in an in vivo-like manner and display morphological features of the organ to be modeled (Lancaster and Knoblich 2014). Yet, one has to be aware that there are major differences between in vivo embryogenesis or organogenesis and in vitro organoid formation, since even extremely well-controlled in vitro conditions strongly differ from real, regionally defined, physiological in vivo conditions (Bayir et al. 2019).

Different protocols for generating brain organoids have been established. Lancaster et al. (2017) used a floating scaffold out of poly(lactide-co-glycolide) copolymer (PLGA) fiber microfilaments to generate elongated embryoid bodies, called microfilament-engineered cerebral organoids (enCORGs). Other groups used shaking platforms (Matsui et al. 2018), self-made spinning bioreactors (Qian et al. 2016), or soft matrices for embedding the cells (Lindborg et al. 2016; Bian et al. 2018) to let them form self-organized brain organoids. While neural organoids mostly mimic the early phases of embryonic development of the human brain, Matsui et al. (2018) cultivated their organoids up to 6 months and showed cell differentiation into functional neurons and myelin basic protein (MBP)-positive oligodendrocytes. The cerebral organoids fabricated by Quadrato et al. (2017) contained mature neurons including dendritic spine-like structures that generated spontaneously active neuronal networks as well as photosensitive cells after 8–9 months. These CNS models that display a later developmental status can now be used for safety and efficacy evaluations in medium to high throughput. One has to note that integration of microglia into organoids will be necessary in the future to better model toxicity and disease. This advanced technology is currently evolving (Ormel et al. 2018). In addition, although seemingly much more complex than 2D models, organoids also need definition of their applicability domains, with regard to the presence of cellular targets mediating neurotoxicity or drug efficacy (Table 1). Because reproducibility of organoid formation is still an issue with high variation making well-to-well comparison difficult, this neurotoxicity/efficacy target characterization has to be performed with great caution focusing on reproducibility of results.

As an example, hiPSC-derived brain organoids were recently employed for drug efficacy screening against ZIKA virus infection (Zhou et al. 2017) indicating that it is

possible to use such complex in vitro systems for medium- to high-throughput applications. The authors' high-content imaging approach identified a compound prohibiting organoid ZIKA virus infection and eliminating virus from infected organoids (Zhou et al. 2017). Other ZIKA virus-infected organoids were also published recently (Cugola et al. 2016; Garcez et al. 2016; Dang et al. 2016; Qian et al. 2016). Two groups (Watanabe et al. 2017; Xu et al. 2016) used these organoids similar to Zhou et al. (2017), for drug screening against ZIKA virus. Since the declaration of a public health emergency of international concern by the World Health Organization in 2016, a lot of drug candidates against ZIKA virus were tested in in vitro as well as in in vivo systems, but only few of them with anti-ZIKA virus activity in animal models made it to clinical trials (Bernatchez et al. 2019).

Due to the higher throughput of such models, they are logistically superior over the low-throughput mouse models and can thus screen a large number of compounds. Moreover, their translational success to the human in vivo situation might be higher due to the human nature of cells. However, as already pointed out in Fig. 1, kinetic modeling is crucial for correct predictions that has to go hand in hand with the in vitro work.

While brain organoids are good models to examine the effects of disease and genetic aberrances on brain development, they lack to model the blood-brain barrier (BBB) of the adult human cortex. Many drugs for neurologic diseases and disorders fail to pass the BBB; therefore, there is a need for a BBB model that enables the examination of the permeability of these drugs. BBB organoid models can be derived from three (Cho et al. 2017; Bergmann et al. 2018) or from six (Nzou et al. 2018) different cell types that include astrocytes, pericytes, and endothelial cells. Both models are able to reproduce the properties and functions of the BBB through the exhibition of tight/adherent junctions, efflux pumps, and transporters. Nzou et al. (2018) showed in their organoids also the impenetrability of the BBB for specific molecules: by adding MPTP, MPP+, and mercury chloride to the medium they proofed that their models indeed have a charge-selective barrier. Data from such models might also be useful for feeding PBPK models.

In conclusion, there are currently several different organoid models in development, both normal and disease models. However, these are still in the process of establishment and characterization and are not yet in use for substance screenings.

1.4 3D Bioprinted In Vitro Neural Models

The next generation of in vitro models already arising is fabricated by 3D *bioprinting*. The state of the art of 3D bioprinting of brain cells was recently comprehensively reviewed by Antill-O'Brien et al. (2019). 3D bioprinting of brain cells is faced with a variety of challenges needing sophisticated solutions. The first is the choice of biomaterial biomimicking brain tissue from extracellular matrix components as well as the mechanical, structural, biochemical, and diffusive properties of the brain with high cellular biocompatibility. Here, especially, the tremendous softness of brain tissue poses a great challenge for bioengineers.

Biomaterials currently used for neural cell culture are *hydrogels*. These hydrophilic polymers can be reversibly or irreversibly cross-linked via chemical or physical triggers to maintain their structure over a long period of time. Hydrogels are an attractive material for culturing cells in 3D due to their biocompatibility, high water content, and tuneable physical and chemical properties. For neuronal cultures, the pore structure of the hydrogel must be able to support neural cell bodies, which are 10–50 μm in diameter, and allow neurite extension (Antill-O'Brien et al. 2019). Once a suitable biomaterial is identified, the biofabrication strategy has to be defined. Prior to printing, 3D neural tissue can be manufactured via layering. Cell embedding in gels and manual layering thereby allow studying cytocompatibility of hydrogels. Printing of soft materials is often challenging. A major hurdle to 3D biofabrication of such soft structures is their shaping into 3D structures with high spatial resolution to achieve an anisotropically accurate mimic of the brain microstructure. Sacrificial scaffolds, e.g., from gelatine, have previously been used to support soft gels like 0.5% alginate, which otherwise fall below the printable viscosity range. Usage of this sacrificial scaffold improved cell survival in the hydrogel (Naghieh et al. 2019). For scaffold-free 3D bioprinting, extrusion-based printing has mainly been employed due to its economy, ease of use, and capability to print with high cell density with a wide range of materials. Despite a small number of studies using rat or hiPSC-derived neurons for extrusion-based bioprinting, one study should be highlighted. Joung et al. (2018) developed a bioengineered spinal cord combining bioprinting with 3D printed scaffolds in the only example of functional neurons with extensive axon propagation from bioprinted neural precursor cells. Pre-differentiated spinal NPC and oligodendrocyte progenitor cells from hiPSC were bioprinted in precise alternating points in silicon channels. After 4 days, β -III tubulin-positive axons spread throughout the channel, and after 14 days the cells were found to have differentiated into mature glutamate-responsive neurons with synchronous responses to K^+ and glutamate (Joung et al. 2018). This method of a spinal cord model could be applied to CNS neural tissue engineering.

This paragraph is not supposed to give a comprehensive overview of 3D bioprinting of neural structures, yet should touch on the challenges of this rising technique. 3D bioprinting of neural models is still in the early stages of development and offers great potential for exquisite spatial bioink patterning to recapitulate the microarchitecture of brain tissue. Although 3D bioprinted neural disease models have not yet been developed, the potential advantages over animal models include species- and patient-specific disease modeling. For more detailed information on cells, materials, techniques, and readouts, the reader is referred to Antill-O'Brien et al. (Antill-O'Brien et al. 2019).

1.5 CNS Disease Models

Improvement of the hiPSC technology allows to obtain and culture neurological patient-specific hiPSC lines, which recapitulate molecular and cellular phenotypic aspects of the respective disease. These offer a unique opportunity to generate

physiologically relevant in vitro models to understand disease etiology and progression, as well as to support preclinical drug discovery. Genomically unaltered human iPSC-derived neurons and astrocytes have been derived from Alzheimer's disease (AD), Parkinson's disease (PD), *Huntington's disease* (HD), *amyotrophic lateral sclerosis* (ALS), and *idiopathic autistic spectrum disorder* (ASD) patients (Table 2), to provide 2D and, most recently, 3D cultures reproducing features of these neurological diseases. In addition to patient-derived iPSCs, inserting genetic changes manually into iPSCs can also generate disease models. Manipulating gene expression of *LIS1*, the most common gene mutated in patients with *lissencephaly*, and using an on-chip organoid approach as an exciting example, allowed studying the emergence of folding during in vitro development and the physical mechanisms of folding reproducing pathogenesis of lissencephaly using organoids (Karzbrun et al. 2018).

In 2D cultures, patient-derived iPSCs are generally committed to differentiate into neuronal monoculture representative of the affected cell type: in PD research iPSCs are differentiated into dopaminergic neurons (TH-positive) functionally characterized by dopamine decarboxylase and the dopamine transporter (Hartfield et al. 2014), while cortical glutamatergic neuron or motor neurons are derived to best represent AD or ALS features, respectively.

More recently, greater attention has been dedicated to both microglia (Haenseler et al. 2017) and patient-derived astrocytes (Kondo et al. 2013; Qian et al. 2017; Hsiao et al. 2015), due to the recognition of the relevance of glial cells in contributing to disease initiation and progression. Similar to toxicity evaluation described above, the aim here is to develop co-cultures, which take the complexity of neuron-glia interactions into account, hence also considering inflammatory responses, which have a high impact on the course of pathology (Haenseler et al. 2017). In addition, the presence of multiple cell type allows to address neuron-glia cross-talk in drug discovery. The diversity of cell types in a single culture is also retained in organoid models, which add a further step of complexity by respecting brain cytoarchitecture.

A clarifying example on the potentiality of patient-derived stem cell models comes from AD patients (for extensive review, see Arber et al. 2017). Extracellular amyloid plaques composed of amyloid beta peptide ($A\beta$) and Tau protein intracellular neurofibrillary tangles are considered hallmarks of AD. $A\beta$ is the product of β - and γ -secretase processing of amyloid precursor protein (APP). Autosomal dominant mutations in APP and alternative subunits of γ -secretase presenilin 1 and 2 (PSEN1 and PSEN2) have been detected in AD patients, implicating an altered APP processing and $A\beta$ imbalance in AD pathogenesis. Reprogramming cells derived from patients with genetic predisposition to AD into cortical glutamatergic neurons, cortical interneurons, and cholinergic neurons (Table 2) allowed to reproduce AD features like increased $A\beta_{42:40}$ ratio and enhanced Tau phosphorylation (Table 2). These models were then used to gain insight into biochemical pathomechanisms of AD (Kondo et al. 2013), contribution of neurons and astrocytes to pathophysiology (Kondo et al. 2013; Oksanen et al. 2017) and identify drug targets potentially relevant in the progression of the disease. In these studies, also

Table 2 Patients' iPSC-derived neurons as disease models for investigating neurological disorders

	Mutations investigated	Cell type	Pathological hallmarks	Reference
<i>Alzheimer's disease</i>				
fAD	PSEN1 A246E PSEN1 N141I	Neurons	Increased A β Increased A β 42:40 ratio	Yagi et al. (2011)
fAD sAD	APP duplication	Neurons Glutamatergic GABAergic Cholinergic	Increased A β 40 Increased pTau Activated GSK3b	Israel et al. (2012)
fAD sAD	APP E693 Δ APP V717L	Cortical neurons ¹ or astrocytes ²	Increased A β 42:40 ratio ¹ Extracellular A β oligomers ^{1,2}	Kondo et al. (2013)
fAD	PSEN1 Δ E9	Neurons	Increased A β 42:40 ratio	Woodruff et al. (2013)
sAD	ApoE3/E4 (AD-E3/E4)	Cholinergic neurons	Increased A β 42:40 ratio	Duan et al. (2014)
fAD	APPV717I	Neurons	Increased A β 42:40 ratio Increased A β 38:40 ratio Increased total and phosphorylated Tau	Muratore et al. (2014)
fAD	PSEN1 Δ E9	Astrocytes	Accumulation of full-length PS-1 Increased A β 42:40 ratio Disturbance in ER calcium signaling Development of a pro-inflammatory profile	Oksanen et al. (2017)
fAD sAD	PSEN1 M146L <i>ApoE4</i> ^{+/+}	Astrocytes		Jones et al. (2017)
fAD	APP duplication PSEN1 M146I PSEN1 A264E	3D organoids	Amyloid aggregation Hyperphosphorylated tau protein Endosome abnormalities	Raja et al. (2016)
Down syndrome		Cortical glutamatergic neurons	Increased A β 40 Increased A β 42 A β aggregates	Shi et al. (2012)
Down syndrome		Neurons with forebrain characteristics	A β aggregates Tau protein hyperphosphorylation Tau intracellular redistribution	Chang et al. (2015)

(continued)

Table 2 (continued)

	Mutations investigated	Cell type	Pathological hallmarks	Reference
<i>Parkinson's disease</i>				
	PARK2/Parkin V324A PINK1 Q456X	Midbrain DA neurons	Increased α -synuclein expression	Chung et al. (2016)
	SNCA gene triplication	DA neurons	Increased α -synuclein expression	Oliveira et al. (2015)
	a-synuclein A53T	Cortical neurons and glia	α -Synuclein expression	Chung et al. (2013)
<i>Amyotrophic lateral sclerosis</i>				
sALS	Patients' presented symptoms relating to motor-neurons degeneration of the spinal cord (not in brainstem or cortex) in the absence of C9ORF72 gene mutations	Astrocytes	Increased GFAP immunofluorescence	Qian et al. (2017)
	GGGGCC repeat expansions in C9ORF72	Motor neurons	Aging increased DNA damage	Lopez-Gonzalez et al. (2016)
	VCP mutations R191Q or R155C	Enriched cultures of motor neurons and astrocytes	Increased percentage of cytosolic TDP-43	Hall et al. (2017)
	SOD1 E100G	Spinal motor neurons	Significant decline in survival compared with the healthy control MNs	Bhinge et al. (2017)
fALS	TDP-43	Motor neurons	Cytosolic aggregates Shorter neurites	Egawa et al. (2012)
<i>Huntington's disease</i>				
HD	43 CAG repeats	Astrocytes	Increased vascular endothelial growth factor A	Hsiao et al. (2015)
HD Juvenile HD	109 CAG repeats		Contain both normal and mutant huntingtin	Szlachcic et al. (2015)
Juvenile HD	60 and 109 CAG repeats	Mixed culture: Neurons, glia, and progenitor cells	Alterations in genes and gene pathways that are associated with a pathological CAG repeat length	Consortium TH iPSC (2017)
HD	180 CAG repeats	Striatal-like cultures	Significantly lower ATP levels than control	Rindt et al. (2017)
<i>fAD</i> familial AD, <i>sAD</i> sporadic AD, <i>sALS</i> sporadic ALS, <i>DA</i> dopaminergic				

novel mechanisms like endoplasmic reticulum and oxidative stress were identified (Kondo et al. 2013; Muratore et al. 2014). In addition, iPSCs derived from patients carrying multiple genetic variants allow investigations of AD risk factors, i.e., linking mutations to increased risk of late onset AD (Duan et al. 2014; Young et al. 2015; Huang et al. 2017; Schröter et al. 2016). The organization of genomically unaltered iPSC-derived neurons in a 3D structure, thereby reproducing brain cytoarchitecture, favors the retention of proteins secreted by cells that are lost in a 2D culture, like A β peptides. In 3D their local concentration is increased and pathology better recapitulated (Raja et al. 2016). 2D and 3D models obtained from iPSCs derived from AD patients have been used to investigate drug efficacy and toxicity, so far targeting β - and γ -secretase with specific inhibitors (Yagi et al. 2011; Shi et al. 2012; Kondo et al. 2013; Duan et al. 2014; Raja et al. 2016; Woodruff et al. 2013) and inflammation with nonsteroidal anti-inflammatory drugs (Yahata et al. 2011).

Although the models obtained from patients' hiPSCs exhibit clear advantages, their use to model aging and neurodegenerative diseases poses a relevant challenge due to the fact that differentiation protocols mimic neurodevelopmental processes. Indeed, derived cells retain molecular characteristics closer to the fetal than the adult stage (Patani et al. 2012; Camp et al. 2015), which might limit the full development of an AD model. For example, Tau isoform expression is tightly regulated during development (Bunker et al. 2004), and the lack of formation of aggregated Tau in non-manipulated patients' hiPSCs might reflect the absence of the adult isoforms. In general, this implicates that any disease phenotype has to be discriminated from phenotypes of earlier developmental stages. So far this issue that represents a possible limit in drug discovery has been solved by generating footprint-free triple MAPT-mutant human iPSCs (García-León et al. 2018a), overexpressing mutant PSEN1 (DE9) and APP (K670N/M671L plus V7171; Choi et al. 2014), or could be overcome by direct reprogramming, thus skipping the intermediate step of hiPSC (for details on this, see second to last paragraph of Sect. 1.1 of this chapter).

In the context of CNS pathologies recapitulated by an hiPSC approach, neurodevelopmental and psychiatric diseases are worth a note. CNS cells derived from patients by reprogramming allow to capture a complex genetic architecture of diseases that are highly polygenic in nature, overcoming the difficulty to generate genetically accurate animal models of psychiatric disorders. Patient hiPSC-derived neural cells allow to dissect the gene network associated with features of altered neurodevelopment that controls the phenotypic trait and the signaling pathways involved (Mariani et al. 2015; Haggarty et al. 2016).

As listed in Table 2, patients' hiPSCs replicate disease phenotypes to an extent to represent clinically relevant features of the illness, thus providing human cellular assays that may improve drug preclinical evaluation and translation of the results to clinical trial in the process of drug discovery (Silva and Haggarty 2019). Clinically relevant targets and phenotypes displayed in hiPSC-derived disease models may drive the testing of candidate drugs selected on a hypothesis-driven screening or the screening of large compound libraries for identification of novel molecules for their ability to rescue disease phenotypes. In addition, the generation of large numbers of

patients' cell models representative of the heterogeneity of each disorder may represent a strategy to identify patient subpopulations with specific responsiveness to therapeutic agents. Finally, by interlinking a patient's genetic background with specific disease characteristics, hiPSCs apply to the concept of personalized medicine, possibly allowing the development of personalized drug evaluation in the future (Engle and Puppala 2013).

2 Summary and Conclusion

Animal models have been greatly contributing to our understanding of physiology, mechanisms of diseases, and toxicity. Yet, they have limitations due to interspecies variation, which determines the lack of information of the "human context," and deficiency in pathophysiologically relevant disease models. This deficiency has a tremendous negative impact on the understanding of basic physiology, human disease, mechanisms of toxicity, and the process of successful drug discovery.

Human iPSC-derived cells offer a platform with the unique advantage of reproducing the "human context" missing in animal models, by preserving the genetic and the molecular phenotype of donors. Forcing the differentiation of hiPSC into cells of the nervous system and combining them in a 2D or 3D format allows obtaining complex models suitable to investigate neurodevelopmental processes and to reproduce neurodegenerative diseases with patient-derived cells. This has the potentiality to drive the identification of molecular targets that may be predictive for the evolution of specific human diseases as well as for beneficial and/or adverse drug responses. Thus, with such cell platforms, screening assays can be set up that are based on human-relevant targets and thus are useful for drug testing and discovery with the hope of overcoming the low success rate of CNS drug development due to poor clinical efficacy or elevated toxicity. Cell culture standardization is mandatory in this process. Well-characterized and overall reproducible cell systems that contain neural and immune cells of the CNS, are based on standardized protocols and procedures to generate differentiated and mature cells representative of different brain areas, and are able to address the fundamental unanswered questions of drug discovery and toxicity are urgently needed.

References

- Abermathy DG, Kim WK, McCoy MJ, Lake AM, Ouwenga R, Lee SW, Xing X, Li D, Lee HJ, Heuckeroth RO, Dougherty JD, Wang T, Yoo AS (2017) MicroRNAs induce a permissive chromatin environment that enables neuronal subtype-specific reprogramming of adult human fibroblasts. *Cell Stem Cell* 21:332–348.e9. <https://doi.org/10.1016/j.stem.2017.08.002>
- Abud EM, Ramirez RN, Martinez ES, Healy LM, Nguyen CHH, Newman SA, Yeromin AV, Scarfone VM, Marsh SE, Fimbres C, Caraway CA, Fote GM, Madany AM, Agrawal A, Kayed R, Gyls KH, Cahalan MD, Cummings BJ, Antel JP, Mortazavi A et al (2017) iPSC-derived human microglia-like cells to study neurological diseases. *Neuron* 94:278–293.e9. <https://doi.org/10.1016/j.neuron.2017.03.042>

- Ajami B, Bennett JL, Krieger C, Tetzlaff W, Rossi FMV (2007) Local self-renewal can sustain CNS microglia maintenance and function throughout adult life. *Nat Neurosci* 10:1538–1543
- Almeida S, Zhang Z, Coppola G, Mao W, Futai K, Karydas A, Geschwind MD, Tartaglia MC, Gao F, Gianni D, Sena-Esteves M, Geschwind DH, Miller BL, Farese RV, Gao FB (2012) Induced pluripotent stem cell models of progranulin-deficient frontotemporal dementia uncover specific reversible neuronal defects. *Cell Rep* 2:789–798
- Ambasudhan R, Talantova M, Coleman R, Yuan X, Zhu S, Lipton SA (2011) Brief report direct reprogramming of adult human fibroblasts to functional neurons under defined conditions. *Stem Cell* 9:113–118. <https://doi.org/10.1016/j.stem.2011.07.002>
- Ankley GT, Bennett RS, Erickson RJ, Hoff DJ, Hornung MW, Johnson RD, Mount DR, Nichols JW, Russom CL, Schmieder PK, Serrano JA, Tietge JE, Villeneuve DL (2010) Adverse outcome pathways: a conceptual framework to support ecotoxicology research and risk assessment. *Environ Toxicol Chem* 29:730–741
- Antill-O'Brien N, Bourke J, O'Connell CD (2019) Layer-by-layer: the case for 3D bioprinting neurons to create patient-specific epilepsy models. *Materials (Basel)* 12:3218
- Arber C, Lovejoy C, Wray S (2017) Stem cell models of Alzheimer's disease: progress and challenges. *Alzheimers Res Ther* 9:1–17
- Arcuri C, Mecca C, Bianchi R, Giambanco I, Donato R (2017) The pathophysiological role of microglia in dynamic surveillance, phagocytosis and structural remodeling of the developing CNS. *Front Mol Neurosci* 10:1–22
- Bal-Price A, Crofton KM, Sachana M, Shafer TJ, Behl M, Forsby A, Hargreaves A, Landesmann B, Lein PJ, Louise J, Monnet-Tschudi F, Paini A, Rolaki A, Schrattenholz A, Suñol C, van Thriel C, Whelan M, Fritsche E (2015) Putative adverse outcome pathways relevant to neurotoxicity. *Crit Rev Toxicol* 45:83–91
- Bayir E, Sendemir A, Missirlis YF (2019) Mechanobiology of cells and cell systems, such as organoids. *Biophys Rev* 11:721–728
- Bergmann S, Lawler SE, Qu Y, Fadzen CM, Wolfe JM, Regan MS, Pentelute BL, Agar NYR, Cho CF (2018) Blood–brain-barrier organoids for investigating the permeability of CNS therapeutics. *Nat Protoc* 13:2827–2843
- Bernatchez JA, Tran LT, Li J, Luan Y, Siqueira-Neto JL, Li R (2019) Drugs for the treatment of Zika virus infection. *J Med Chem*
- Bhingre A, Namboori SC, Zhang X, VanDongen AMJ, Stanton LW (2017) Genetic correction of SOD1 mutant iPSCs reveals ERK and JNK activated API as a driver of neurodegeneration in amyotrophic lateral sclerosis. *Stem Cell Rep* 8:856–869. <https://doi.org/10.1016/j.stemcr.2017.02.019>
- Bian S, Repic M, Guo Z, Kavirayani A, Burkard T, Bagley JA, Krauditsch C, Knoblich JA (2018) Genetically engineered cerebral organoids model brain tumor formation. *Nat Methods* 15:748–748. <http://www.nature.com/articles/s41592-018-0118-8>
- Boissart C, Poulet A, Georges P, Darville H, Julita E, Delorme R, Bourgeron T, Peschanski M, Benchoua A (2013) Differentiation from human pluripotent stem cells of cortical neurons of the superficial layers amenable to psychiatric disease modeling and high-throughput drug screening. *Transl Psychiatry* 3:e294–e211. <https://doi.org/10.1038/tp.2013.71>
- Boisvert EM, Engle SJ, Hollowell SE, Liu P, Wang Z (2015) The specification and maturation of nociceptive neurons from human embryonic stem cells. *Nat Publ Gr*:1–12. <https://doi.org/10.1038/srep16821>
- Bunker JM, Leslie W, Jordan MA, Feinstein SC (2004) Modulation of microtubule dynamics by tau in living cells: implications for development and neurodegeneration. *Mol Biol Cell* 15:2720–2728
- Camp JG, Badsha F, Florio M, Kanton S, Gerber T, Wilsch-Bräuninger M, Lewitus E, Sykes A, Hevers W, Lancaster M, Knoblich JA, Lachmann R, Pääbo S, Huttner WB, Treutlein B (2015) Human cerebral organoids recapitulate gene expression programs of fetal neocortex development. *Proc Natl Acad Sci U S A* 112:15672–15677

- Carusi A, Davies MR, de Grandis G, Escher BI, Hodges G, KMY L, Whelan M, Willett C, Ankley GT (2018) Science of the total environment harvesting the promise of AOPs: an assessment and recommendations. *Sci Total Environ* 628–629:1542–1556. <https://doi.org/10.1016/j.scitotenv.2018.02.015>
- Chambers SM, Fasano CA, Papapetrou EP, Tomishima M, Sadelain M, Studer L (2009) Highly efficient neural conversion of human ES and iPS cells by dual inhibition of SMAD signaling. *Nat Biotechnol* 27:275–280. <http://www.nature.com/nbt/journal/v27/n3/abs/nbt.1529.html>
- Chang CY, Chen SM, Lu HE, Lai SM, Lai PS, Shen PW, Chen PY, Shen CI, Harn HJ, Lin SZ, Hwang SM, Su HL (2015) N-butylidenephthalide attenuates Alzheimer's disease-like cytopathy in down syndrome induced pluripotent stem cell-derived neurons. *Sci Rep* 5:1–7
- Cheng C, Fass DM, Folz-Donahue K, MacDonald ME, Haggarty SJ (2017) Highly expandable human iPS cell-derived neural progenitor cells (NPC) and neurons for central nervous system disease modeling and high-throughput screening. *Curr Protoc Hum Genet* 93:21.8.1–21.8.21
- Cho CF, Wolfe JM, Fadzen CM, Calligaris D, Hornburg K, Chiocca EA, Agar NYR, Pentelute BL, Lawler SE (2017) Blood-brain-barrier spheroids as an in vitro screening platform for brain-penetrating agents. *Nat Commun* 8:1–14. <https://doi.org/10.1038/ncomms15623>
- Choi SH, Kim YH, Hebisch M, Sliwinski C, Lee S, D'Avanzo C, Chen H, Hooli B, Asselin C, Muffat J, Klee JB, Zhang C, Wainger BJ, Peitz M, Kovacs DM, Woolf CJ, Wagner SL, Tanzi RE, Kim DY (2014) A three-dimensional human neural cell culture model of Alzheimer's disease. *Nature* 515:274. <https://doi.org/10.1038/nature13800>
- Chung CY, Khurana V, Auluck PK, Tardiff DF, Mazzulli JR, Soldner F, Baru V, Lou Y, Freyzen Y, Cho S, Mungenast AE, Muffat J, Mitalipova M, Pluth MD, Jui NT, Schulze B, Lippard SJ, Tsai LH, Krainc D, Buchwald SL et al (2013) Identification and rescue of α -synuclein toxicity in Parkinson patient-derived neurons. *Science* 342:983–987
- Chung SY, Kishinevsky S, Mazzulli JR, Graziotto J, Mrejeru A, Mosharov EV, Puspita L, Valiulahi P, Sulzer D, Milner TA, Taldone T, Krainc D, Studer L, won Shim J (2016) Parkinson and PINK1 patient iPSC-derived midbrain dopamine neurons exhibit mitochondrial dysfunction and α -synuclein accumulation. *Stem Cell Reports* 7:664–677. <https://doi.org/10.1016/j.stemcr.2016.08.012>
- Consortium TH iPSC (2017) Developmental alterations in Huntington's disease neural cells and pharmacological rescue in cells and mice. *Nat Neurosci* 20:648–660
- Cooper O, Seo H, Andrabi S, Guardia-Laguarta C, Graziotto J, Sundberg M, McLean JR, Carrillo-Reid L, Xie Z, Osborn T, Hargus G, Deleidi M, Lawson T, Bogetoft H, Perez-Torres E, Clark L, Moskowitz C, Mazzulli J, Chen L, Volpicelli-Daley L et al (2012) Pharmacological rescue of mitochondrial deficits in iPSC-derived neural cells from patients with familial Parkinson's disease. *Sci Transl Med* 4:141ra90
- Corti S, Nizzardo M, Simone C, Falcone M, Nardini M, Ronchi D, Donadoni C, Salani S, Riboldi G, Magri F, Menozzi G, Bonaglia C, Rizzo F, Bresolin N, Comi GP (2012) Genetic correction of human induced pluripotent stem cells from patients with spinal muscular atrophy. *Sci Transl Med* 4:1–32
- Crofton KM, Mundy WR, Shafer TJ (2012) Developmental neurotoxicity testing: a path forward. *Congenit Anom* 52:140–146
- Cugola FR, Fernandes IR, Russo FB, Freitas BC, Dias JLM, Guimarães KP, Benazzato C, Almeida N, Pignatari GC, Romero S, Polonio CM, Cunha I, Freitas CL, Brandaõ WN, Rossato C, Andrade DG, Faria DDP, Garcez AT, Buchpiguel CA, Braconi CT et al (2016) The Brazilian Zika virus strain causes birth defects in experimental models. *Nature* 534:267–271
- D'Aiuto L, Zhi Y, Kumar Das D, Wilcox MR, Johnson JW, Mc Clain L, Macdonald ML, Di Maio R, Schurdak ME, Piazza P, Viggiano L, Sweet R, Kinchington PR, Bhattacharjee AG, Yolken R, Nimgaonka VL (2014) Large-scale generation of human ipsc-derived neural stem cells/early neural progenitor cells and their neuronal differentiation. *Organogenesis* 10:365–377
- Dai S, Li R, Long Y, Titus S, Zhao J, Huang R, Xia M, Zheng W (2016) One-step seeding of neural stem cells with vitronectin- supplemented medium for high throughput screening assays. *J Biomol Screen* 21:1112–1124

- Dang J, Tiwari SK, Lichinchi G, Qin Y, Patil VS, Eroshkin AM, Rana TM (2016) Zika virus depletes neural progenitors in human cerebral organoids through activation of the innate immune receptor TLR3. *Cell Stem Cell* 19:258–265
- Danon JJ, Reekie TA, Kassiou M (2019) Challenges and opportunities in central nervous system drug discovery. *Trends Chem* 1:612–624. <https://doi.org/10.1016/j.trechm.2019.04.009>
- Di Cesare ML, Pacini A, Micheli L, Tani A, Zanardelli M, Ghelardini C (2014) Glial role in oxaliplatin-induced neuropathic pain. *Exp Neurol* 261. <https://doi.org/10.1016/j.expneurol.2014.06.016>
- Djelloul M, Holmqvist S, Boza-Serrano A, Azevedo C, Yeung MS, Goldwurm S, Frisé J, Deierborg T, Roybon L (2015) Alpha-synuclein expression in the oligodendrocyte lineage: an in vitro and in vivo study using rodent and human models. *Stem Cell Rep* 5:174–184
- Douvaras P, Wang J, Zimmer M, Hanchuk S, O’Bara MA, Sadiq S, Sim FJ, Goldman J, Fossati V (2014) Efficient generation of myelinating oligodendrocytes from primary progressive multiple sclerosis patients by induced pluripotent stem cells. *Stem Cell Rep* 3:250–259. <https://doi.org/10.1016/j.stemcr.2014.06.012>
- Douvaras P, Sun B, Wang M, Kruglikov I, Lallo G, Zimmer M, Terrenoire C, Zhang B, Gandy S, Schadt E, Freytes DO, Noggle S, Fossati V (2017) Directed differentiation of human pluripotent stem cells to microglia. *Stem Cell Rep* 8:1516–1524. <https://doi.org/10.1016/j.stemcr.2017.04.023>
- Duan L, Bhattacharyya BJ, Belmadani A, Pan L, Miller RJ, Kessler JA (2014) Stem cell derived basal forebrain cholinergic neurons from Alzheimer’s disease patients are more susceptible to cell death. *Mol Neurodegener* 9:1–14
- Efthymiou A, Shaltouki A, Steiner JP, Jha B, Heman-Ackah SM, Swistowski A, Zeng X, Rao MS, Malik N (2014) Functional screening assays with neurons generated from pluripotent stem cell-derived neural stem cells. *J Biomol Screen* 19:32–43
- Egawa N, Kitaoka S, Tsukita K, Naitoh M, Takahashi K, Yamamoto T, Adachi F, Kondo T, Okita K, Asaka I, Aoi T, Watanabe A, Yamada Y, Morizane A, Takahashi J, Ayaki T, Ito H, Yoshikawa K, Yamawaki S, Suzuki S et al (2012) Drug screening for ALS using patient-specific induced pluripotent stem cells. *Sci Transl Med* 4:145ra104
- Ehrlich M, Mozafari S, Glatza M, Starost L, Velychko S, Hallmann AL, Cui QL, Schambach A, Kim KP, Bachelin C, Marteyn A, Hargus G, Johnson RM, Antel J, Sternecker J, Zaehres H, Schöler HR, Baron-Van Evercooren A, Kuhlmann T (2017) Rapid and efficient generation of oligodendrocytes from human induced pluripotent stem cells using transcription factors. *Proc Natl Acad Sci U S A* 114:E2243–E2252
- Eiraku M, Watanabe K, Matsuo-takasaki M, Kawada M, Yonemura S, Matsumura M, Wataya T, Nishiyama A, Muguruma K, Sasai Y (2008) Article self-organized formation of polarized cortical tissues from ESCs and its active manipulation by extrinsic signals. *Stem Cell* 3:519–532. <https://doi.org/10.1016/j.stem.2008.09.002>
- Engle SJ, Puppala D (2013) Integrating human pluripotent stem cells into drug development. *Cell Stem Cell* 12:669–677. <https://doi.org/10.1016/j.stem.2013.05.011>
- Etemad S, Zamin RM, Ruitenberg MJ, Filgueira L (2012) A novel in vitro human microglia model: characterization of human monocyte-derived microglia. *J Neurosci Methods* 209:79–89
- Farkhondeh A, Li R, Gorshkov K, Chen KG, Might M, Rodems S, Lo DC, Zheng W (2019) Induced pluripotent stem cells for neural drug discovery. *Drug Discov Today* 24:992–999. <https://doi.org/10.1016/j.drudis.2019.01.007>
- Flames N, Gelman DM, Rubenstein JLR, Puelles L, Mari O, Herna UM, Joan S (2007) Delineation of multiple subpallial progenitor domains by the combinatorial expression of transcriptional codes. *J Neurosci* 27:9682–9695
- Fritsche E, Barenys M, Klose J, Masjosthusmann S, Nimtz L, Schmuck M, Wuttke S, Tigges J (2018a) Current availability of stem cell-based in vitro methods for developmental neurotoxicity (DNT) testing. *Toxicol Sci* 165:21–30

- Fritsche E, Barenys M, Klose J, Masjosthusmann S, Nimtz L, Schmuck M, Wuttke S, Tigges J (2018b) Development of the concept for stem cell-based developmental neurotoxicity evaluation. *Toxicol Sci* 165:14–20. <https://academic.oup.com/toxsci/article/165/1/14/5046970>
- Garcez P, Loiola E, Madeiro da Costa R, Higa L, Trindade P, Delvecchio R, Nascimento J, Brindeiro R, Tanuri A, Rehen S (2016) Zika virus impairs growth in human neurospheres and brain organoids. *Science* 13:816–818
- García-León JA, Cabrera-Socorro A, Eggermont K, Swijssen A, Terryn J, Fazal R, Nami FA, Ordovás L, Quiles A, Lluís F, Serneels L, Wierda K, Sierksma A, Kreir M, Pestana F, Van Damme P, De Strooper B, Thorrez L, Ebner A, Verfaillie CM (2018a) Generation of a human induced pluripotent stem cell-based model for tauopathies combining three microtubule-associated protein TAU mutations which displays several phenotypes linked to neurodegeneration. *Alzheimers Dement* 14:1261–1280
- García-León JA, Kumar M, Boon R, Chau D, One J, Wolfs E, Eggermont K, Berckmans P, Gunhanlar N, de Vrij F, Lendemeijer B, Pavie B, Corthout N, Kushner SA, Dávila JC, Lambrichts I, Hu WS, Verfaillie CM (2018b) SOX10 single transcription factor-based fast and efficient generation of oligodendrocytes from human pluripotent stem cells. *Stem Cell Rep* 10:655–672
- Ghaffari LT, Starr A, Nelson AT, Sattler R (2018) Representing diversity in the dish: using patient-derived in vitro models to recreate the heterogeneity of neurological disease. *Front Neurosci* 12:1–18
- Ginhoux F, Greter M, Leboeuf M, Nandi S, See P, Gokhan S, Mehler MF, Conway SJ, Ng LG, Stanley ER, Samokhvalov IM, Merad M (2010) Fate mapping analysis reveals that adult microglia derive from primitive macrophages. *Science* 330:841–845
- Grabert K, Michael T, Karavolos MH, Clohisey S, Kenneth Baillie J, Stevens MP, Freeman TC, Summers KM, McColl BW (2016) Microglial brain regionâ dependent diversity and selective regional sensitivities to aging. *Nat Neurosci* 19:504–516
- Gribkoff VK, Kaczmarek LK (2017) The need for new approaches in CNS drug discovery: why drugs have failed, and what can be done to improve outcomes. *Neuropharmacology* 120:11–19. <https://doi.org/10.1016/j.neuropharm.2016.03.021>
- Guenther MG (2011) Transcriptional control of embryonic and induced pluripotent stem cells. *Epigenomics* 3:323–343
- Haenseler W, Sansom SN, Buchrieser J, Newey SE, Moore CS, Nicholls FJ, Chintawar S, Schnell C, Antel JP, Allen ND, Cader MZ, Wade-Martins R, James WS, Cowley SA (2017) A highly efficient human pluripotent stem cell microglia model displays a neuronal-co-culture-specific expression profile and inflammatory response. *Stem Cell Rep* 8:1727–1742. <https://doi.org/10.1016/j.stemcr.2017.05.017>
- Haggarty SJ, Silva MC, Cross A, Brandon NJ, Perlis RH (2016) Advancing drug discovery for neuropsychiatric disorders using patient-specific stem cell models. *Mol Cell Neurosci* 73:104–115. <https://doi.org/10.1016/j.mcn.2016.01.011>
- Hall CE, Yao Z, Choi M, Tyzack GE, Serio A, Luisier R, Harley J, Preza E, Arber C, Crisp SJ, Watson PMD, Kullmann DM, Abramov AY, Wray S, Burley R, Loh SHY, Martins LM, Stevens MM, Luscombe NM, Sibley CR et al (2017) Progressive motor neuron pathology and the role of astrocytes in a human stem cell model of VCP-related ALS. *Cell Rep* 19:1739–1749. <https://doi.org/10.1016/j.celrep.2017.05.024>
- Hartfield EM, Yamasaki-Mann M, Ribeiro Fernandes HJ, Vowles J, James WS, Cowley SA, Wade-Martins R (2014) Physiological characterisation of human iPS-derived dopaminergic neurons. *PLoS One* 9:e87388
- Hashimoto D, Chow A, Noizat C, Teo P, Beasley MB, Leboeuf M, Becker CD, See P, Price J, Lucas D, Greter M, Mortha A, Boyer SW, Forsberg EC, Tanaka M, van Rooijen N, García-Sastre A, Stanley ER, Ginhoux F, Frenette PS et al (2013) Tissue-resident macrophages self-maintain locally throughout adult life with minimal contribution from circulating monocytes. *Immunity* 38:792–804

- Hendry SH, Schwark HD, Jones EG, Yan J (1987) Numbers and proportions of GABA-immunoreactive neurons in different areas of monkey cerebral cortex. *J Neurosci* 7:1503–1519
- Hsiao HY, Chen YC, Huang CH, Chen CC, Hsu YH, Chen HM, Chiu FL, Kuo HC, Chang C, Chern Y (2015) Aberrant astrocytes impair vascular reactivity in Huntington disease. *Ann Neurol* 78:178–192
- Hu W, Qiu B, Guan W, Wang Q, Wang M, Li W, Gao L, Shen L (2015) Short article direct conversion of normal and Alzheimer's disease human fibroblasts into neuronal cells by small molecules short article direct conversion of normal and Alzheimer's disease human fibroblasts into neuronal cells by small molecules. *Stem Cell* 17:204–212. <https://doi.org/10.1016/j.stem.2015.07.006>
- Huang YWA, Zhou B, Wernig M, Südhof TC (2017) ApoE2, ApoE3, and ApoE4 differentially stimulate APP transcription and A β secretion. *Cell* 168:427–441.e21
- Ichida JK, Kiskinis E (2015) Probing disorders of the nervous system using reprogramming approaches. *EMBO J* 34:1456–1477
- Israel MA, Yuan SH, Bardy C, Reyna SM, Mu Y, Herrera C, Hefferan MP, Van Gorp S, Nazor KL, Boscolo FS, Carson CT, Laurent LC, Marsala M, Gage FH, Remes AM, Koo EH, Goldstein LSB (2012) Probing sporadic and familial Alzheimer's disease using induced pluripotent stem cells. *Nature* 482:216–220. <https://doi.org/10.1038/nature10821>
- Janabi N, Peudenier S, Héron B, Ng KH, Tardieu M (1995) Establishment of human microglial cell lines after transfection of primary cultures of embryonic microglial cells with the SV40 large T antigen. *Neurosci Lett* 195:105–108
- Jones VC, Atkinson-Dell R, Verkhatsky A, Mohamet L (2017) Aberrant iPSC-derived human astrocytes in Alzheimer's disease. *Cell Death Dis* 8:1–11. <https://doi.org/10.1038/cddis.2017.89>
- Joung D, Truong V, Neitzke CC, Guo SZ, Walsh PJ, Monat JR, Meng F, Park SH, Dutton JR, Parr AM, McAlpine MC (2018) 3D printed stem-cell derived neural progenitors generate spinal cord scaffolds. *Adv Funct Mater* 28:1–10
- Kanat O, Ertas H, Caner B (2017) Platinum-induced neurotoxicity: a review of possible mechanisms. *World J Clin Oncol* 8:329–336
- Karzbrun E, Kshirsagar A, Cohen SR, Hanna JH, Reiner O (2018) Human brain organoids on a chip reveal the physics of folding. *Nat Phys* 14:515–522
- Kayama T, Suzuki I, Odawara A, Sasaki T, Ikegaya Y (2018) Temporally coordinated spiking activity of human induced pluripotent stem cell-derived neurons co-cultured with astrocytes. *Biochem Biophys Res Commun* 495:1028–1033. <https://doi.org/10.1016/j.bbrc.2017.11.115>
- Kiskinis E, Sandoe J, Williams LA, Boulting GL, Moccia R, Wainger BJ, Han S, Peng T, Thams S, Mikkilineni S, Mellin C, Merkle FT, Davis-dusenbery BN, Ziller M, Oakley D, Ichida J, Dicostanza S, Atwater N, Maeder ML, Goodwin MJ et al (2014) Article pathways disrupted in human ALS motor neurons identified through genetic correction of mutant SOD1. *Stem Cell* 43:1–15. <https://doi.org/10.1016/j.stem.2014.03.004>
- Klaunig JE, Babich MA, Baetcke KP, Cook JC, Corton JC, David RM, DeLuca JG, Lai DY, McKee RH, Peters JM, Roberts RA, Fenner-Crisp PA (2003) PPAR α agonist-induced rodent tumors: modes of action and human relevance. *Crit Rev Toxicol* 33:655–780
- Kondo T, Asai M, Tsukita K, Kutoku Y, Ohsawa Y, Sunada Y, Imamura K, Egawa N, Yahata N, Okita K, Takahashi K, Asaka I, Aoi T, Watanabe A, Watanabe K, Kadoya C, Nakano R, Watanabe D, Maruyama K, Hori O et al (2013) Modeling Alzheimer's disease with iPSCs reveals stress phenotypes associated with intracellular A β and differential drug responsiveness. *Cell Stem Cell* 12:487–496. <https://doi.org/10.1016/j.stem.2013.01.009>
- Kriks S, Shim J, Piao J, Ganat YM, Wakeman DR, Xie Z, Carrillo-reid L (2011) Dopamine neurons derived from human ES cells efficiently engraft in animal models of Parkinson's disease. *Nature* 480:547–551. <https://doi.org/10.1038/nature10648>
- Lancaster MA, Knoblich JA (2014) Organogenesis in a dish: modeling development and disease using organoid technologies. *Science* 345:1247125

- Lancaster MA, Corsini NS, Wolfinger S, Gustafson EH, Phillips AW, Burkard TR, Otani T, Livesey FJ, Knoblich JA (2017) Guided self-organization and cortical plate formation in human brain organoids. *Nat Biotechnol* 35:659–666
- Lee JH, Mitchell RR, McNicol JD, Shapovalova Z, Laronde S, Tanasijevic B, Milsom C, Casado F, Fiebig-Comyn A, Collins TJ, Singh KK, Bhatia M (2015) Single transcription factor conversion of human blood fate to NPCs with CNS and PNS developmental capacity. *Cell Rep* 11:1367–1376. <https://doi.org/10.1016/j.celrep.2015.04.056>
- Leist M, Hartung T (2013) Reprint: inflammatory findings on species extrapolations: humans are definitely no 70-kg mice. *ALTEX* 30:227–230
- Leone C, Le Pavec G, Mème W, Porcheray F, Samah B, Dormont D, Gras G (2006) Characterization of human monocyte-derived microglia-like cells. *Glia* 54:183–192
- Li Q, Barres BA (2018) Microglia and macrophages in brain homeostasis and disease. *Nat Rev Immunol* 18:225–242. <https://doi.org/10.1038/nri.2017.125>
- Li Y, Muffat J, Omer A, Bosch I, Lancaster MA, Sur M, Gehrke L, Knoblich JA, Jaenisch R (2017) Induction of expansion and folding in human cerebral organoids. *Cell Stem Cell* 20:385–396.e3. <https://doi.org/10.1016/j.stem.2016.11.017>
- Lindborg BA, Brekke JH, Vegoe AL, Ulrich CB, Haider KT, Subramaniam S, Venhuizen SL, Eide CR, Orchard PJ, Chen W, Wang Q, Pelaez F, Scott CM, Kokkoli E, Keirstead SA, Dutton JR, Tolar J, O'Brien TD (2016) Rapid induction of cerebral organoids from human induced pluripotent stem cells using a chemically defined hydrogel and defined cell culture medium. *Stem Cells Transl Med* 5:970–979. <https://doi.org/10.5966/sctm.2015-0305>
- Liu Y, Liu H, Sauvey C, Yao L, Zarnowska ED, Zhang S (2013) Directed differentiation of forebrain GABA interneurons from human pluripotent stem cells. *Nat Protoc* 8:1670–1679. <https://doi.org/10.1038/nprot.2013.106>
- Lopez-Gonzalez R, Lu Y, Gendron TF, Karydas A, Tran H, Yang D, Petrucelli L, Miller BL, Almeida S, Gao FB (2016) Poly(GR) in C9ORF72-related ALS/FTD compromises mitochondrial function and increases oxidative stress and DNA damage in iPSC-derived motor neurons. *Neuron* 92:383–391. <https://doi.org/10.1016/j.neuron.2016.09.015>
- Lowry WE, Plath K (2008) The many ways to make an iPS cell. *Nat Biotechnol* 26:1246–1248
- Lundin A, Delsing L, Clausen M, Ricchiuto P, Sanchez J, Sabirsh A, Ding M, Synnergren J, Zetterberg H, Brolén G, Hicks R, Herland A, Falk A (2018) Human iPS-derived astroglia from a stable neural precursor state show improved functionality compared with conventional astrocytic models. *Stem Cell Rep* 10:1030–1045. <https://linkinghub.elsevier.com/retrieve/pii/S221367111830047X>
- Malik N, Efthymiou AG, Mather K, Chester N, Wang X, Nath A, Rao MS, Steiner JP (2014) Compounds with species and cell type specific toxicity identified in a 2000 compound drug screen of neural stem cells and rat mixed cortical neurons. *Neurotoxicology* 45:192–200
- Manabe T, Tatsumi K, Inoue M, Matsuyoshi H, Makinodan M, Yokoyama S, Wanaka A (2005) L3/Lhx8 is involved in the determination of cholinergic or GABAergic cell fate. *J Neurochem* 94:723–730
- Mariani J, Coppola G, Zhang P, Abyzov A, Provini L, Tomasini L, Amenduni M, Szekely A, Palejev D, Wilson M, Gerstein M, Grigorenko EL, Chawarska K, Pelphrey KA, Howe JR, Vaccarino FM (2015) FOXG1-dependent dysregulation of GABA/glutamate neuron differentiation in autism spectrum disorders. *Cell* 162:375–390
- Masjosthusmann S, Barenys M, El-Gamal M, Geerts L, Gerosa L, Gorreja A, Kühne B, Marchetti N, Tigges J, Viviani B, Witters H, Fritsche E (2018) Literature review and appraisal on alternative neurotoxicity testing methods. *EFSA Support Publ* 15:1–108
- Massaro EJ (2002) *Handbook of neurotoxicology*. Springer Science + Business Media, New York
- Matsui TK, Matsubayashi M, Sakaguchi YM, Hayashi RK, Zheng C, Sugie K, Hasegawa M, Nakagawa T, Mori E (2018) Six-month cultured cerebral organoids from human ES cells contain matured neural cells. *Neurosci Lett* 670:75–82. <https://doi.org/10.1016/j.neulet.2018.01.040>

- Maury Y, Côme J, Piskorowski RA, Salah-Mohellibi N, Chevalere V, Peschanski M, Martinat C, Nedelec S (2015) Combinatorial analysis of developmental cues efficiently converts human pluripotent stem cells into multiple neuronal subtypes. *Nat Biotechnol* 33:89–96
- McComish SF, Caldwell MA (2018) Generation of defined neural populations from pluripotent stem cells. *Philos Trans R Soc B Biol Sci* 373:20170214
- McQuade A, Coburn M, Tu CH, Hasselmann J, Davtyan H, Blurton-Jones M (2018) Development and validation of a simplified method to generate human microglia from pluripotent stem cells. *Mol Neurodegener* 13:1–13
- Mertens J, Reid D, Lau S, Kim Y, Gage FH (2018) Aging in a dish: iPSC-derived and directly induced neurons for studying brain aging and age-related neurodegenerative diseases. *Annu Rev Genet* 52:271–293
- Muffat J, Li Y, Yuan B, Mitalipova M, Omer A, Corcoran S, Bakiasi G, Tsai LH, Aubourg P, Ransohoff RM, Jaenisch R (2016) Efficient derivation of microglia-like cells from human pluripotent stem cells. *Nat Med* 22:1358–1367
- Muratore CR, Rice HC, Srikanth P, Callahan DG, Shin T, Benjamin LNP, Walsh DM, Selkoe DJ, Young-Pearse TL (2014) The familial alzheimer’s disease APPV717I mutation alters APP processing and Tau expression in iPSC-derived neurons. *Hum Mol Genet* 23:3523–3536
- Nagai A, Mishima S, Ishida Y, Ishikura H, Harada T, Kobayashi S, Kim SU (2005) Immortalized human microglial cell line: phenotypic expression. *J Neurosci Res* 81:342–348
- Naghieh S, Sarker MD, Abelseh E, Chen X (2019) Indirect 3D bioprinting and characterization of alginate scaffolds for potential nerve tissue engineering applications. *J Mech Behav Biomed Mater* 93:183–193
- National Institute of Health Neurotoxicity Information (2019). <https://www.ninds.nih.gov/disorders/all-disorders/neurotoxicity-information-page#disorders-r1>
- Nehme R, Zuccaro E, Ghosh SD, Fu Z, Ghosh SD, Li C, Sherwood JL, Pietilainen O (2018) Combining NGN2 programming with developmental patterning generates human excitatory neurons with NMDAR-mediated synaptic transmission resource combining NGN2 programming with developmental patterning generates human excitatory neurons with NMDAR-mediated. *Cell Rep* 23:2509–2523. <https://doi.org/10.1016/j.celrep.2018.04.066>
- Nzou G, Wicks RT, Wicks EE, Seale SA, Sane CH, Chen A, Murphy SV, Jackson JD, Atala AJ (2018) Human cortex spheroid with a functional blood brain barrier for high-throughput neurotoxicity screening and disease modeling. *Sci Rep* 8:1–10. <https://doi.org/10.1038/s41598-018-25603-5>
- Oksanen M, Petersen AJ, Naumenko N, Puttonen K, Lehtonen Š, Gubert Olivé M, Shakirzyanova A, Leskelä S, Sarajärvi T, Viitanen M, Rinne JO, Hiltunen M, Haapasalo A, Giniatullin R, Tavi P, Zhang SC, Kanninen KM, Hämäläinen RH, Koistinaho J (2017) PSEN1 mutant iPSC-derived model reveals severe astrocyte pathology in Alzheimer’s disease. *Stem Cell Rep* 9:1885–1897
- Oliveira LMA, Falomir-Lockhart LJ, Botelho MG, Lin KH, Wales P, Koch JC, Gerhardt E, Taschenberger H, Outeiro TF, Lingor P, Schüle B, Arndt-Jovin DJ, Jovin TM (2015) Elevated α -synuclein caused by SNCA gene triplication impairs neuronal differentiation and maturation in Parkinson’s patient-derived induced pluripotent stem cells. *Cell Death Dis* 6:1–13
- Ormel PR, Vieira de Sá R, van Bodegraven EJ, Karst H, Harschnitz O, Sneeboer MAM, Johansen LE, van Dijk RE, Scheefhals N, Berdenis van Berlekom A, Ribes Martínez E, Kling S, MacGillavry HD, van den Berg LH, Kahn RS, Hol EM, de Witte LD, Pasterkamp RJ (2018) Microglia innately develop within cerebral organoids. *Nat Commun* 9:4167. <https://doi.org/10.1038/s41467-018-06684-2>
- Osaki T, Shin Y, Sivathanu V, Campisi M, Kamm RD (2018) In vitro microfluidic models for neurodegenerative disorders. *Adv Healthc Mater* 7
- Paini A, Leonard JA, Joossens E, Bessens JGM, Desalegn A, Dorne JL, Gosling JP, Heringa MB, Klaric M, Kliment T, Kramer NI, Loizou G, Louisse J, Lumen A, Madden JC, Patterson EA, Proenca S, Punt A, Setzer RW, Suciu N et al (2019) Next generation physiologically based

- kinetic (NG-PBK) models in support of regulatory decision making. *Comput Toxicol* (Amsterdam, Netherlands) 9:61–72
- Pandya H, Shen MJ, Ichikawa DM, Sedlock AB, Choi Y, Johnson KR, Kim G, Brown MA, Elkahloun AG, Maric D, Sweeney CL, Gossa S, Malech HL, McGavern DB, Park JK (2017) Differentiation of human and murine induced pluripotent stem cells to microglia-like cells. *Nat Neurosci* 20:753–759
- Park DY, Lee J, Chung JJ, Jung Y, Kim SH (2019) Integrating organs-on-chips: multiplexing, scaling, vascularization, and innervation. *Trends Biotechnol* 38:99–112. <https://doi.org/10.1016/j.tibtech.2019.06.006>
- Pasca SP (2018) The rise of three-dimensional human brain cultures. *Nature* 553:437–445. <https://doi.org/10.1038/nature25032>
- Patani R, Lewis PA, Trabzuni D, Puddifoot CA, Wyllie DJA, Walker R, Smith C, Hardingham GE, Weale M, Hardy J, Chandran S, Rytten M (2012) Investigating the utility of human embryonic stem cell-derived neurons to model ageing and neurodegenerative disease using whole-genome gene expression and splicing analysis. *J Neurochem* 122:738–751
- Pérez-Cerdá F, Sánchez-Gómez MV, Matute C (2015) Pío del Río horteiga and the discovery of the oligodendrocytes. *Front Neuroanat* 9:7–12
- Qian X, Nguyen HN, Song MM, Hadiono C, Ogden SC, Hammack C, Yao B, Hamersky GR, Jacob F, Zhong C, Yoon KJ, Jeang W, Lin L, Li Y, Thakor J, Berg DA, Zhang C, Kang E, Chickering M, Nauen D et al (2016) Brain-region-specific organoids using mini-bioreactors for modeling ZIKV exposure. *Cell* 165:1238–1254. <https://doi.org/10.1016/j.cell.2016.04.032>
- Qian X, Nguyen HN, Jacob F, Song H, Ming GL (2017) Using brain organoids to understand Zika virus-induced microcephaly. *Dev* 144:952–957
- Quadrato G, Nguyen T, Macosko EZ, Sherwood JL, Min Yang S, Berger DR, Maria N, Scholvin J, Goldman M, Kinney JP, Boyden ES, Lichtman JW, Williams ZM, McCarroll SA, Arlotta P (2017) Cell diversity and network dynamics in photosensitive human brain organoids. *Nature* 545:48–53. <http://www.nature.com/articles/nature22047>
- Raja WK, Mungenast AE, Lin YT, Ko T, Abdurrob F, Seo J, Tsai LH (2016) Self-organizing 3D human neural tissue derived from induced pluripotent stem cells recapitulate Alzheimer's disease phenotypes. *PLoS One* 11:1–18
- Rana P, Luerman G, Hess D, Rubitski E, Adkins K, Somps C (2017) Toxicology in vitro utilization of iPSC-derived human neurons for high-throughput drug- induced peripheral neuropathy screening. *Toxicol Vitro* 45:111–118. <https://doi.org/10.1016/j.tiv.2017.08.014>
- Ransohoff RM, El Khoury J (2016) Microglia in health and disease. *Cold Spring Harb Perspect Biol* 8:a020560. <http://cshperspectives.cshlp.org/lookup/doi/10.1101/cshperspect.a020560>
- Rindt H, Tom CM, Lorson CL, Mattis VB (2017) Optimization of trans-splicing for Huntington's disease RNA therapy. *Front Neurosci* 11:1–13
- Ryan KJ, White CC, Patel K, Xu J, Olah M, Replogle JM, Frangieh M, Cimpean M, Winn P, McHenry A, Kaskow BJ, Chan G, Cuerdon N, Bennett DA, Boyd JD, Imitola J, Elyaman W, De Jager PL, Bradshaw EM (2017) A human microglia-like cellular model for assessing the effects of neurodegenerative disease gene variants. *Sci Transl Med* 9:1–13
- Sahara S, Yanagawa Y, O'Leary DDM, Stevens CF (2012) The fraction of cortical GABAergic neurons is constant from near the start of cortical neurogenesis to adulthood. *J Neurosci* 32:4755–4761
- Sanchez-Danes A, Richaud-patin Y, Carballo-carbajal I, Sa A, Caig C, Mora S, Di Guglielmo C, Ezquerro M, Vila M, Cuervo AM, Tolosa E, Consiglio A, Raya A (2012) Disease-specific phenotypes in dopamine neurons from human iPS-based models of genetic and sporadic Parkinson's disease. *EMBO Mol Med* 4:380–395
- Sareen D, Ebert AD, Heins BM, McGivern JV, Ornelas L, Svendsen CN (2012) Inhibition of apoptosis blocks human motor neuron cell death in a stem cell model of spinal muscular atrophy. *PLoS One* 7:e39113
- Sareen D, O'Rourke JG, Meera P, Muhammad AKMG, Grant S, Simpkinson M, Bell S, Carmona S, Ornelas L, Sahabian A, Gendron T, Petrucelli L, Baughn M, Ravits J, Harms

- MB, Rigo F, Bennett CF, Otis TS, Svendsen CN, Baloh RH (2013) Targeting RNA foci in iPSC-derived motor neurons from ALS patients with C9ORF72 repeat expansion. *Sci Transl Med* 5:1–57
- Schröter F, Slegers K, Van Cauwenberghe C, Bohndorf M, Wruck W, Van Broeckhoven C, Adjaye J (2016) Lymphoblast-derived integration-free iPSC lines from a female and male Alzheimer's disease patient expressing different copy numbers of a coding CNV in the Alzheimer risk gene CR1. *Stem Cell Res* 17:560–563. <https://doi.org/10.1016/j.scr.2016.10.003>
- Seidel D, Jahnke H, Englich B, Girard M, Robitzki AA (2017) In vitro field potential monitoring on a multi-microelectrode array for the electrophysiological long-term screening of neural stem cell maturation. *Analyst* 142:1929–1937. <http://xlink.rsc.org/?DOI=C6AN02713J>
- Sellgren CM, Sheridan SD, Gracias J, Xuan D, Fu T, Perlis RH (2017) Patient-specific models of microglia-mediated engulfment of synapses and neural progenitors. *Mol Psychiatry* 22:170–177
- Sherman SP, Bang AG (2018) High-throughput screen for compounds that modulate neurite growth of human induced pluripotent stem cell-derived neurons. *DMM Dis Model Mech* 11: dmm031906
- Shi Y, Kirwan P, Smith J, MacLean G, Orkin SH, Livesey FJ (2012) A human stem cell model of early Alzheimer's disease pathology in down syndrome. *Sci Transl Med* 4:124ra29. <https://doi.org/10.1016/j.jalz.2012.05.1946>
- Shi Y, Kirwan P, Smith J, Robinson HPC, Livesey FJ (2014) Human cerebral cortex development from pluripotent stem cells to functional excitatory synapses. *Nat Neurosci* 15:1–25. <http://www.pubmedcentral.nih.gov/articlerender.fcgi?artid=3882590&tool=pmcentrez&rendertype=abstract>
- Shi Y, Inoue H, Wu JC, Yamanaka S (2017) Induced pluripotent stem cell technology: a decade of progress. *Nat Rev Drug Discov* 16:115–130
- Silva MC, Haggarty SJ (2019) Human pluripotent stem cell-derived models and drug screening in CNS precision medicine. *Ann N Y Acad Sci*
- Singh VK, Kalsan M, Kumar N, Saini A, Chandra R (2015) Induced pluripotent stem cells: applications in regenerative medicine, disease modeling, and drug discovery. *Front Cell Dev Biol* 3:1–18
- Stacey P, Wassermann AM, Kammonen L, Impey E, Wilbrey A, Cawkill D (2018) Plate-based phenotypic screening for pain using human iPSC-derived sensory neurons. *SLAS Disc* 23:585–596
- Suga M, Kondo T, Inoue H (2019) Modeling neurological disorders with human pluripotent stem cell-derived astrocytes. *Int J Mol Sci* 20:9–14
- Szlachcic WJ, Switonski PM, Krzyzosiak WJ, Figlerowicz M, Figiel M (2015) Huntington disease iPSCs show early molecular changes in intracellular signaling, the expression of oxidative stress proteins and the p53 pathway. *Dis Model Mech* 8:1047–1057
- Takahashi K, Tanabe K, Ohnuki M, Narita M, Ichisaka T, Tomoda K, Yamanaka S (2007) Induction of pluripotent stem cells from adult human fibroblasts by defined factors. *Cell* 131:861–872. <http://www.ncbi.nlm.nih.gov/pubmed/18035408>
- Thomson JA, Itskovitz-eldor J, Shapiro SS, Waknitz MA, Swiergiel JJ, Marshall VS, Jones JM (1998) Embryonic stem cell lines derived from human blastocysts. *Science* 282:1145–1148
- Toutain P-L, Ferran A, Bousquet-Melou A (2010) Species differences in pharmacokinetics and pharmacodynamics. *Handb Exp Pharmacol*:19–48
- Tukker AM, De Groot MWGDM, Wijnolts FMJ, Kasteel EEJ, Hondebrink L, Westerink RHS (2016) Research article is the time right for in vitro neurotoxicity testing using human iPSC-derived neurons? *ALTEX* 33:261–271
- Tukker AM, Wijnolts FMJ, de Groot A, Westerink RHS (2018) Neurotoxicology human iPSC-derived neuronal models for in vitro neurotoxicity assessment. *Neurotoxicology* 67:215–225. <https://doi.org/10.1016/j.neuro.2018.06.007>
- Victor MB, Richner M, Hermansteyne TO, Ransdell JL, Sobieski C, Deng P, Klyachko VA, Nerbonne JM, Yoo AS (2014) NeuroResource generation of human striatal neurons by

- MicroRNA-dependent direct conversion of fibroblasts. *Neuron* 84:311–323. <https://doi.org/10.1016/j.neuron.2014.10.016>
- Vierbuchen T, Ostermeier A, Pang ZP, Kokubu Y, Südhof TC, Wernig M (2010) Direct conversion of fibroblasts to functional neurons by defined factors. *Nature* 463:1035–1041
- von Bartheld CS, Bahney J, Herculano-houzel S (2017) The search for true numbers of neurons and glial cells in the human brain: a review of 150 years of cell counting. *J Comp Neurol* 524:3865–3895
- Wang S, Bates J, Li X, Schanz S, Chandler-militello D, Levine C, Maherali N, Studer L, Hochedlinger K, Windrem M, Goldman SA (2013) Clinical progress progenitor cells can myelinate and rescue a mouse model of congenital hypomyelination. *Stem Cell* 12:252–264. <https://doi.org/10.1016/j.stem.2012.12.002>
- Wang C, Ward ME, Chen R, Liu K, Tracy TE, Chen X, Xie M, Sohn PD, Ludwig C, Meyer-Franke A, Karch CM, Ding S, Gan L (2017) Scalable production of iPSC-derived human neurons to identify Tau-Lowering compounds by high-content screening. *Stem Cell Rep* 9:1221–1233. <https://doi.org/10.1016/j.stemcr.2017.08.019>
- Wapinski OL, Lee QY, Chen AC, Li R, Corces MR, Ang CE, Treutlein B, Xiang C, Baubet V, Suchy FP, Sankar V, Sim S, Quake SR, Dahmane N, Wernig M, Chang HY (2017) Rapid chromatin switch in the direct reprogramming of fibroblasts to neurons. *Cell Rep* 20:3236–3247
- Warren L, Manos PD, Ahfeldt T, Loh YH, Li H, Lau F, Ebina W, Mandal PK, Smith ZD, Meissner A, Daley GQ, Brack AS, Collins JJ, Cowan C, Schlaeger TM, Rossi DJ (2010) Highly efficient reprogramming to pluripotency and directed differentiation of human cells with synthetic modified mRNA. *Cell Stem Cell* 7:618–630
- Watanabe M, Buth JE, Vishlaghi N, de la Torre-Ubieta L, Taxis J, Khakh BS, Coppola G, Pearson CA, Yamauchi K, Gong D, Dai X, Damoiseaux R, Aliyari R, Liebscher S, Schenke-Layland K, Caneda C, Huang EJ, Zhang Y, Cheng G, Geschwind DH et al (2017) Self-organized cerebral organoids with human-specific features predict effective drugs to combat Zika virus infection. *Cell Rep* 21:517–532. <https://doi.org/10.1016/j.celrep.2017.09.047>
- Woodruff G, Young JE, Martinez FJ, Buen F, Gore A, Kinaga J, Li Z, Yuan SH, Zhang K, Goldstein LSB (2013) The Presenilin-1 δ E9 mutation results in reduced γ -secretase activity, but not total loss of PS1 function, in isogenic human stem cells. *Cell Rep* 5:974–985. <https://doi.org/10.1016/j.celrep.2013.10.018>
- Xu M, Lee EM, Wen Z, Cheng Y, Huang WK, Qian X, Tcw J, Kouznetsova J, Ogden SC, Hammack C, Jacob F, Nguyen HN, Itkin M, Hanna C, Shinn P, Allen C, Michael SG, Simeonov A, Huang W, Christian KM et al (2016) Identification of small-molecule inhibitors of Zika virus infection and induced neural cell death via a drug repurposing screen. *Nat Med* 22:1101–1107
- Yagi T, Ito D, Okada Y, Akamatsu W, Nihei Y, Yoshizaki T, Yamanaka S, Okano H, Suzuki N (2011) Modeling familial Alzheimer's disease with induced pluripotent stem cells. *Hum Mol Genet* 20:4530–4539
- Yahata N, Asai M, Kitaoka S, Takahashi K, Asaka I, Hioki H, Kaneko T, Maruyama K, Saido TC, Nakahata T, Asada T, Yamanaka S, Iwata N, Inoue H (2011) Anti-A β drug screening platform using human iPS cell-derived neurons for the treatment of Alzheimer's disease. *PLoS One* 6:e25788
- Yang N, Chanda S, Marro S, Ng YH, Janas JA, Haag D, Ang CE, Tang Y, Flores Q, Mall M, Wapinski O, Li M, Ahlenius H, Rubenstein JL, Chang HY, Buyla AA, Südhof TC, Wernig M (2017) Generation of pure GABAergic neurons by transcription factor programming. *Nat Methods* 14:621–628. <https://doi.org/10.1038/nmeth.4291>
- Yoo AS, Sun AX, Li L, Shcheglovitov A, Portmann T, Li Y, Lee-Messer C, Dometsch RE, Tsien RW, Crabtree GR (2011) MicroRNA-mediated conversion of human fibroblasts to neurons. *Nature* 476:228–231. <https://www.ncbi.nlm.nih.gov/pmc/articles/PMC3624763/pdf/nihms412728.pdf>
- Young JE, Boulanger-Weill J, Williams DA, Woodruff G, Buen F, Revilla AC, Herrera C, Israel MA, Yuan SH, Edland SD, Goldstein LSB (2015) Elucidating molecular phenotypes caused by

- the SORL1 Alzheimer's disease genetic risk factor using human induced pluripotent stem cells. *Cell Stem Cell* 16:373–385. <https://doi.org/10.1016/j.stem.2015.02.004>
- Yu J, Vodyanik MA, Smuga-Otto K, Antosiewicz-Bourget J, Frane JL, Tian S, Nie J, Jonsdottir GA, Ruotti V, Stewart R, Slukvin II, Thomson JA (2007) Induced pluripotent stem cell lines derived from human somatic cells. *Science* 318:1917–1920
- Yu J, Hu K, Smuga-otto K, Tian S, Stewart R, Igor I, Thomson JA (2009) Human induced pluripotent stem cells free of vector and transgene sequences. *Science* 324:797–801
- Yu D, Swaroop M, Wang M, Baxa U, Yang R, Yan Y, Coksaygan T, DeTolla L, Marugan JJ, Austin CP, Mckew JC, Gong D-W, Zheng W (2014) Niemann-Pick disease type C: induced pluripotent stem cell- derived neuronal cells for modeling neural disease and evaluating drug efficacy. *J Biomol Screen* 19:1164–1173
- Zhang Y, Pak CH, Han Y, Ahlenius H, Zhang Z, Chanda S, Marro S, Patzke C, Acuna C, Covy J, Xu W, Yang N, Danko T, Chen L, Wernig M, Südhof TC (2013) Rapid single-step induction of functional neurons from human pluripotent stem cells. *Neuron* 78:785–798
- Zhou T, Tan L, Cederquist GY, Fan Y, Hartley BJ, Mukherjee S, Tomishima M, Brennand KJ, Zhang Q, Schwartz RE, Evans T, Studer L, Chen S (2017) High-content screening in hPSC-neural progenitors identifies drug candidates that inhibit Zika virus infection in fetal-like organoids and adult brain. *Cell Stem Cell* 21:274–283.e5. <https://doi.org/10.1016/j.stem.2017.06.017>
- Zhuang X, Lu C (2016) PBPK modeling and simulation in drug research and development. *Acta Pharm Sin B* 6:430–440

Neural In Vitro Models for Studying Substances Acting on the Central Nervous System

Ellen Fritsche, Julia Tigges, **Julia Hartmann**, Julia Kapr, Melania Maria Serafini, and Barbara Viviani

Fachzeitschrift/Buch: *Handbook of Experimental Pharmacology*

Impact Factor: wird für Buchkapitel nicht berechnet

Beteiligung an der Publikation: 17 %

Schreiben des Kapitels „Moving *In Vitro* Cultures into the Third Dimension with Brain Organoids”

Typ der Autorenschaft: Erstautorenschaft

Status der Publikation: veröffentlicht am 28.Juni 2020

2.2 Stem Cells for Next Level Toxicity Testing in the 21st Century

Ellen Fritsche, Thomas Haarmann-Stemmann, Julia Kapr, Saskia Galanjuk, **Julia Hartmann**, Peter R. Mertens, Angela A. M. Kämpfer, Roel P. F. Schins, Julia Tigges, and Katharina Koch

Small

Die Forderung nach einem Paradigmenwechsel in der Toxikologie des nationalen Forschungsrats der Vereinigten Staaten (engl. *United States National Research Council*) im Jahr 2007 initiierte die Entwicklung und Nutzung von humanrelevanten Alternativmethoden in der toxikologischen Gefahrenbewertung. Während einfache 2D *in vitro* Modelle für ein erstes Screening eingesetzt werden können, deuten neuere Entwicklungen auf die Notwendigkeit von komplexeren, organotypischen Modellen hin, die die Komplexität menschlicher Organe besser nachahmen. Die vielfältigen Wirkungsweisen, mit denen eine Substanz mit den Organen wechselwirken und dabei toxische Reaktionen auslösen kann, unterstreicht diese Notwendigkeit. In diesem Übersichtsartikel werden die kritischsten Organe für die Toxizitätsbewertung, das heißt Haut, Gehirn, Schilddrüse, Lunge, Herz, Leber, Niere und Darm, im Hinblick auf ihre Funktionen bei Gesundheit und Krankheit diskutiert. *In vitro* Modelle, die bereits für toxikologische Untersuchungen verwendet werden und solche, die sich derzeit noch in der Entwicklung befinden, werden betrachtet. Der Fokus liegt dabei auf Modellen, die auf humanen embryonalen Stammzellen (hESCs) oder hiPSCs basieren. Zusätzlich wird die Anwendung innovativer Technologien wie Organ-on-a-chip und Genome Editing in Bezug auf den toxikologischen Paradigmenwechsel diskutiert.

Stem Cells for Next Level Toxicity Testing in the 21st Century

Ellen Fritsche,* Thomas Haarmann-Stemmann, Julia Kapr, Saskia Galanjuk, Julia Hartmann, Peter R. Mertens, Angela A. M. Kämpfer, Roel P. F. Schins, Julia Tigges, and Katharina Koch

The call for a paradigm change in toxicology from the United States National Research Council in 2007 initiates awareness for the invention and use of human-relevant alternative methods for toxicological hazard assessment. Simple 2D in vitro systems may serve as first screening tools, however, recent developments infer the need for more complex, multicellular organotypic models, which are superior in mimicking the complexity of human organs. In this review article most critical organs for toxicity assessment, i.e., skin, brain, thyroid system, lung, heart, liver, kidney, and intestine are discussed with regards to their functions in health and disease. Embracing the manifold modes-of-action how xenobiotic compounds can interfere with physiological organ functions and cause toxicity, the need for translation of such multifaceted organ features into the dish seems obvious. Currently used in vitro methods for toxicological applications and ongoing developments not yet arrived in toxicity testing are discussed, especially highlighting the potential of models based on embryonic stem cells and induced pluripotent stem cells of human origin. Finally, the application of innovative technologies like organs-on-a-chip and genome editing point toward a toxicological paradigm change moves into action.


1. Introduction

Toxicology integrates biology, chemistry, pharmacology, and medicine to study adverse effects of exogenous noxae (e.g., chemicals, drugs, particles, radiation) on living organisms with the final goal of human and environmental health protection.

Prof. E. Fritsche, Dr. T. Haarmann-Stemmann, J. Kapr, S. Galanjuk, J. Hartmann, Dr. A. A. M. Kämpfer, Dr. R. P. F. Schins, Dr. J. Tigges, Dr. K. Koch
IUF – Leibniz Research Institute for Environmental Medicine
Düsseldorf 40225, Germany
E-mail: Ellen.Fritsche@iuf-duesseldorf.de

Prof. E. Fritsche
Medical Faculty
Heinrich-Heine University Düsseldorf
Düsseldorf 40225, Germany

Prof. P. Mertens
Department of Nephrology and Hypertension
Diabetes and Endocrinology
Otto-von-Guericke-University Magdeburg
Magdeburg 39106, Germany

 The ORCID identification number(s) for the author(s) of this article can be found under <https://doi.org/10.1002/sml.202006252>.

© 2020 The Authors. Small published by Wiley-VCH GmbH. This is an open access article under the terms of the Creative Commons Attribution License, which permits use, distribution and reproduction in any medium, provided the original work is properly cited.

DOI: 10.1002/sml.202006252

For the last decades, human health risk assessment has been mainly based on results from animal experiments. These are stipulated, e.g., for chemicals in Organization for Economic Co-operation and Development (OECD) guidelines including acute toxicity (oral, inhalation, dermal), irritation (skin and eye), sensitization (skin and respiratory), repeated dose toxicity (28-day, 90-day, and chronic), mutagenicity and genotoxicity, reproductive and developmental toxicity, as well as carcinogenicity. Such animal experiments have been useful for hazard identification in the past and still guide the current risk assessment process. However, there are several drawbacks in this procedure that provoked a call for a paradigm change in toxicity testing by the United States National Research Council in the beginning of the century.^[1,2] These drawbacks include the issues that animal experiments i) are extremely time- and cost-intensive, hence not suited for testing the

wealth (in the ten-thousands) of chemicals that need hazard characterization,^[3–5] ii) might produce results that are questionable in their translation to humans due to interspecies differences in pharmac/toxico-kinetics and -dynamics,^[6–10] best studied for the drug development process,^[11–14] iii) are not designed for generating mechanistic understanding,^[15,16] iv) do not cover the complexity of human diseases like immunotoxicity, developmental neurotoxicity, chronic neurological disorders, neuropsychological diseases, or endocrine disorders,^[15] v) do not consider coexposures,^[15] and vi) are ethically not in concordance with the 3R (replacement, reduction, and refinement of animal studies) principle.^[5,17] Therefore, the new approach envisions a transformation from apical endpoint assessments in animals to mechanistically relevant studies that primarily rely on in vitro assays and computational (in silico) methods based on human biology, thereby circumventing species differences and increasing hazard prediction.^[12,18,19] In particular, this strategy aims at i) covering a broad range of chemicals, chemical mixtures, endpoints, and life stages, ii) reducing the cost and increasing the throughput of testing, iii) using fewer animals and causing minimal suffering of the animals used, and iv) developing a robust scientific basis for assessing health effects of environmental agents.^[2]

A promising tool for bridging between species or from health to disease are in vitro cell cultures and accordingly the field of in vitro toxicology has been emerging over the last decades. Mainly primary animal cells, tissue specimens, and immortalized

as well as tumor cell lines have been used. However, similar to Garbage In, Garbage Out in informatics,^[20] data produced with in vitro test systems that do not contain high extrapolative power for physiology, might lead to unsatisfactory toxicity predictions.^[21] For example, this might be the study of physiologic, tissue-specific cell proliferation in a tumor cell line.^[22,23] Therefore, the emergence of stem cell systems in the early 21st century—as exemplified for the field of neurotoxicity^[24–26]—was a big gain for in vitro science. Especially the development of the human-induced pluripotent stem cell (hiPSC) technology^[27] was a significant milestone for many research areas including toxicology. Due to their pluripotent nature these reprogrammed cells provide an ethically innocuous, standardized and reproducible^[28] human cell source with high similarity to blastocyst-derived human embryonic stem cells (hESCs).^[29–31] Furthermore, hiPSCs and their differentiated progeny closely resemble their human in vivo counterparts in health and disease which is a prerequisite for successful translational research, with brain and liver providing examples.^[32–35] However, since the ground-breaking publication of brain organoids by Lancaster et al. in 2013,^[36] a variety of hiPSC-derived in vitro models have been taken to the next, 3D level by assembling organ-specific cell clusters containing secondary anatomical structures.^[37–39] These are promising for application in basic research, disease modeling, drug development, personalized treatment, and regenerative medicine. However, they are also understood as promising tools for species-specific in vitro toxicological studies.^[40]

This review will provide a state-of-the-art summary on advanced in vitro methods using stem cells for drug and chemical evaluation. Here, primary target organs, i.e., skin, lung, and intestine that come in direct contact with potentially hazardous substances, as well as secondary exposure organs, i.e., cardiovascular system, liver, kidney, thyroid gland, and brain are highlighted. Structural and/or functional units of each organ that are necessary for its function and thus need modeling for comprehensive toxicity assessment are depicted in respective figures. Benefits of overarching technologies like genome editing and “organ-on-a-chip (OOAC)” methods for toxicological applications are discussed and achievements and challenges in the field are pointed out.

2. Human Organ Structure and Functions and Their Modeling In Vitro

2.1. Skin

With $\approx 2\text{ m}^2$ and around 15% of total body mass, the skin is one of the largest organs of the human body.^[41] Its multilayered architecture consists of epidermis, dermis, and hypodermis (subcutaneous fat) and combines crucial functions such as thermoregulation, energy storage, water homeostasis, removal of waste metabolites through sweat, and production of pigments protecting against sunlight.^[42,43] In addition, the skin is capable of xenobiotic metabolism (reviewed by Oesch et al.^[44]) and is one of the major endocrine sites of peripheral vitamin D synthesis.^[45] The skin is also a sensory organ equipped with specialized sensory nerve endings for perception of touch, pain, heat, cold, acid, and pressure.^[42] From a toxicological point of view, it is a primary target organ for toxicant exposure^[46] since it

constitutes an important barrier to the outside environment,^[47] protecting the body from penetrating pathogens and chemical exposure. The skin barrier is a complex interaction of different barrier compartments: i) the physical barrier consisting of the stratum corneum (SC) corneocytes, the cornified envelope, and the tight junctions of keratinocytes within the stratum granulosum (SG), ii) the chemical barrier formed by antimicrobial peptides, which are produced by keratinocytes, and to a lesser extent by immune cells, and protect against bacterial infections together with reactive oxygen species (ROS)-scavenging molecules secreted by keratinocytes, iii) the immunological barrier consisting of T-cells and Langerhans cells in the lower epidermal layers as well as pattern recognition receptors expressed and immunomodulatory factors secreted by keratinocytes in the SG, and iv) the microbial barrier formed by the commensal skin microbiome preventing infections by pathogenic microbes (Figure 1).^[48] All these factors contributing to the barrier function of human skin together with the multitude of cell types involved (keratinocytes, melanocytes, fibroblasts, adipocytes, immune, and endothelial cells, not to mention the different sensory cells and skin appendages) make the reconstruction of human skin in vitro challenging, yet important for future toxicological testing of cosmetics and topical drugs as well as for hazard assessment of chemicals.

The development of human-based in vitro skin models for toxicological hazard assessment is probably more advanced compared to the other organs described in this review,^[49,50] due to the ban of animal tests for cosmetic products by the European Union (EU) in 2004, followed by an in vivo test ban for cosmetic ingredients in 2013.^[51] An exception is the current in vitro test battery for mutagenicity/genotoxicity consisting of i) a bacterial reverse mutation assay (Ames; TG 471),^[52] ii) an in vitro mammalian cell gene mutation test (TG 476),^[53] and iii) an in vitro micronucleus or in vitro mammalian chromosome aberration test (TG 473).^[54] Due to its low specificity^[55,56,57–65] this battery needs validated in vitro follow up tests which are currently not available.^[66] Therefore, efforts are made to improve the specificity of the existing in vitro test battery^[55,67–72] and to develop new in vitro assays.^[71,73–75]

Those in vitro models accepted by the OECD include ex vivo human skin (TG 428),^[76] an immortalized keratinocyte reporter cell line (TG 442D),^[77] and a human monocytic leukemia cell line (TG 442E),^[78] as well as reconstructed human epidermis (RhE) models (TG 431, 439).^[79,80] So far four RhE models are accepted by the regulatory authorities for studies on skin irritation^[79] and skin corrosion:^[80] EpiSkin, EpiDerm, SkinEthic, and epiCS.^[81] They consist of human primary epidermal keratinocytes which are cultured in cell culture inserts and then lifted to the air-liquid-interphase (ALI) to induce differentiation, epithelial stratification, and cornification. These RhEs then closely resemble a normal human epidermis with a basement membrane, proliferating keratinocytes, and an SC with an intact physical barrier function and xenobiotic metabolizing capacity similar to human skin,^[46,82] thereby overcoming the limitations of classical cell monolayers^[83] and making them suitable for topical applications of test compounds.^[81] As a drawback, these models consisting of a single cell type (epidermal keratinocytes) resemble only the physical skin barrier and disregard other barrier components and cell types. A variety of full thickness skin models (FTM) exist, which are composed of

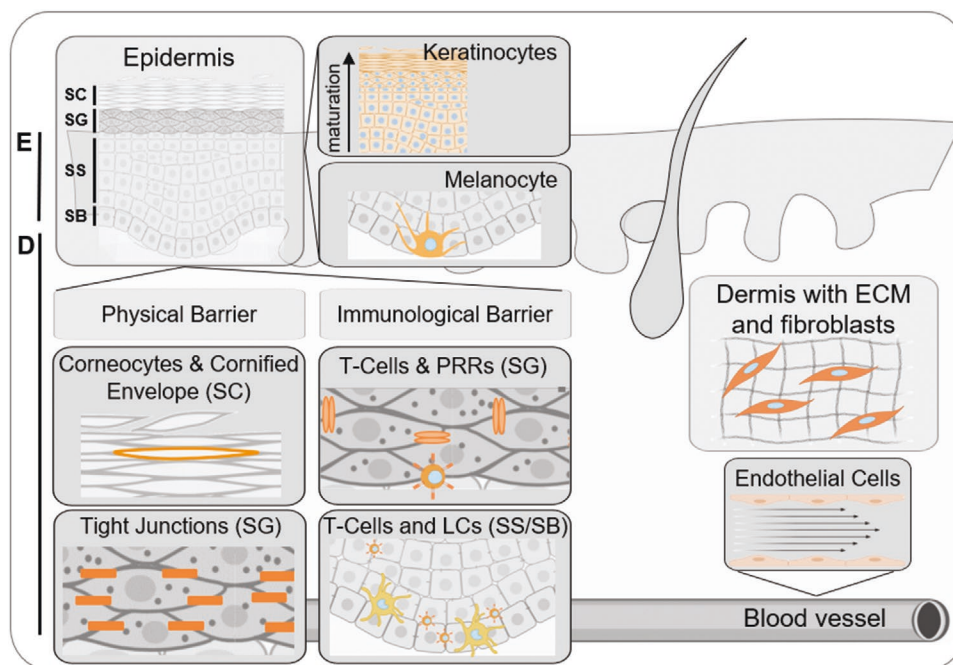


Figure 1. Schematic overview of important cell types and functional units of the skin. Abbreviations: E, epidermis; D, dermis; SC, stratum corneum; SG, stratum granulosum; SS, stratum spinosum; SB, stratum basale; PRR, pattern recognition receptors; LC, Langerhans cell; ECM, extracellular matrix. Figure created with BioRender.com.

an epidermal layer comparable to RhEs and a dermal layer of human dermal fibroblasts embedded in a collagen matrix.^[50,84] Basic research studies investigated the inclusion of other cell types like melanocytes,^[85] Langerhans cells,^[86] or dendritic cells,^[87] resulting in improved modeling of skin sensitization, while others included endothelial cells,^[88–90] sweat glands,^[91] or hair follicles.^[92]

A key challenge in the development of more sophisticated skin in vitro models is to use a combination of cells that best mimic the in vivo responses.^[46] Although human skin derived from plastic surgeries undisputedly is the best starting material for 3D skin models, the supply of material is limited and subjected to donor variation.^[47,93] Human iPSCs provide a solution for overcoming the obstacle of restricted supply,^[46] since hiPSC-derived RhE exhibits differentiation and barrier properties similar to in vivo epidermis.^[94] Recently, the combination of hiPSC and 3D bioprinting technologies led to more physiological in vitro skin models, containing vasculature, appendages, pigment, innervation, and adipose tissue, which could be used for pharmaceutical screening (reviewed by Abaci et al.^[95]). The group of Christiano^[96–99] and others^[100] reported on FTM build from hiPSC-derived fibroblasts, keratinocytes, and/or melanocytes containing a functional hiPSC-derived epidermal-melanin unit and hiPSC-derived keratinocytes participating in melanin uptake and transfer.^[99] The same group incorporated functional hiPSC-derived endothelial cells into FTMs using a sacrificial layer of alginate microchannels in 3D-printed molds as basis for the dermal and epidermal compartment, which was dissolved by sodium citrate treatment followed by endothelial cell seeding. This system allows in vitro perfusion of skin vasculature and evaluation of endothelial barrier function, and therefore the study of systemic delivery

of therapeutics or toxicants, making it a promising model for future toxicological testing.^[101] Interestingly, while hiPSC-derived dendritic cells are used for clinical applications and have the potential of large-scale production,^[102,103] to date none of the developed hiPSC-based RhEs or FTMs have incorporated immune cells.^[104,105] Recently, the generation of hESC-derived skin organoids was achieved by coinducing cranial epithelial cells and neural crest cells within a spherical cell aggregate. After long-time cultivation (4–5 month) this resulted in a cyst-like skin organoid composed of stratified epidermis, dermis, and pigmented hair follicles with sebaceous glands. Together with a network of sensory neurons and Schwann cells from nerve-like bundles that target Merkel cells in organoid hair follicles, the authors report that their model resembles facial skin of human fetuses in the second trimester of development, making it suitable to investigate cellular dynamics of developing human skin and its appendages,^[106] but not relevant for toxicological testing in the near future due to its complexity and maturation status.

A known limitation of in vitro models for human skin is the altered barrier formation and resulting impaired functionality compared to native human skin (NHS).^[48,107–109] One issue contributing to this is that these models, independent of their cell origin, are traditionally maintained at atmospheric oxygen levels of 160 mmHg (21%).^[110] However, with ≈ 26.6 mmHg or 3.5% O₂^[111] oxygen concentration in vivo (physioxia of the skin) is significantly lower, with oxygen levels increasing from apical to basal throughout different skin layers: ≈ 8.5 mmHg ($\approx 1\%$) in the superficial region at 5–10 μm depth, ≈ 25 mmHg ($\approx 3\%$) in dermal papillae at 45–64 μm , and ≈ 37 mmHg ($\approx 5\%$) in the subpapillary plexus at 100–120 μm skin depth.^[112,113] Comparative studies of organotypic skin cultures under normoxia

(21% oxygen) and hypoxia/physioxia (1–3% oxygen) revealed that epidermal structure, SC barrier formation, and epidermal proliferation index better mimics NHS when models are cultured under hypoxic/physioxic conditions.^[110,114]

With regard to skin models, the squamous oral epithelium and the superficial mucus layer of the oral mucosa play a special role. They are the first line of protection against toxicants derived from food, oral care products, and tobacco smoke.^[115] Since mucositis and ulceration are frequent causes of toxicants,^[116] chemicals are evaluated for acute (TG 420, 423, 425),^[117–119] subacute (TG 407),^[120] and subchronic (TG 408)^[121] oral toxicity according to OECD guidelines in rodent animal studies.^[122] Multiple in vitro 3D models of the human oral epithelium were designed as partial thickness oral mucosa or full-thickness oral mucosa (FTOM) models either from primary,^[123–126] immortalized,^[127] or malignant oral epithelial cells.^[128] The majority of these models are grown in ALI-cultures to ensure partial stratification of the epithelial layer.^[124,127] Incorporation of artificial lamina propria composed of collagen-embedded fibroblasts in the FTOM models promotes the differentiation of the epithelial layer, thus increasing the in vivo resemblance.^[129] Although several models have been applied in toxicological studies evaluating oral consumers products,^[123,124] dental composite resins,^[128] or tobacco heating systems,^[125] none of these approaches uses stem cell-derived cell sources, instead relying on primary cells and immortalized or malignant cell lines, the first representing a very restricted cell source and the latter two cells which do not resemble the physiology

of primary cells, respectively. Moreover, no medium- or high-throughput approaches were developed. Therefore, the in vitro oral mucosa models are far away from application in toxicological screening approaches.

While basic research is making huge progress in the development of hiPSC-based 3D skin models, it is yet a long way to a standardized toxicological application. Future efforts should focus on the development of standardized models with high tissue complexity and an adequate representation of the in vivo situation (e.g., by addition of immune cells). Moreover, testing throughput can be increased by the use of multiwell plates. Finally, such complex systems need validation for application in toxicology and disease modeling.^[130]

2.2. Brain

The brain is the most complex organ of the human body, composed of billions of cells and subdivided in multiple regions each containing a specific cytoarchitecture necessary for its particular function. It is mainly composed of two superordinate cell types, neurons and glial cells. In the fully developed brain, neurons transmit information via electrical and chemical stimuli and, depending on the brain region, differ tremendously in size, morphology, neurotransmitters expression pattern, and overall function (Figure 2).^[131] Although there is a certain amount of neurogenesis in adulthood due to residual neural progenitor cells (NPCs), e.g., in hippocampus,^[132,133]

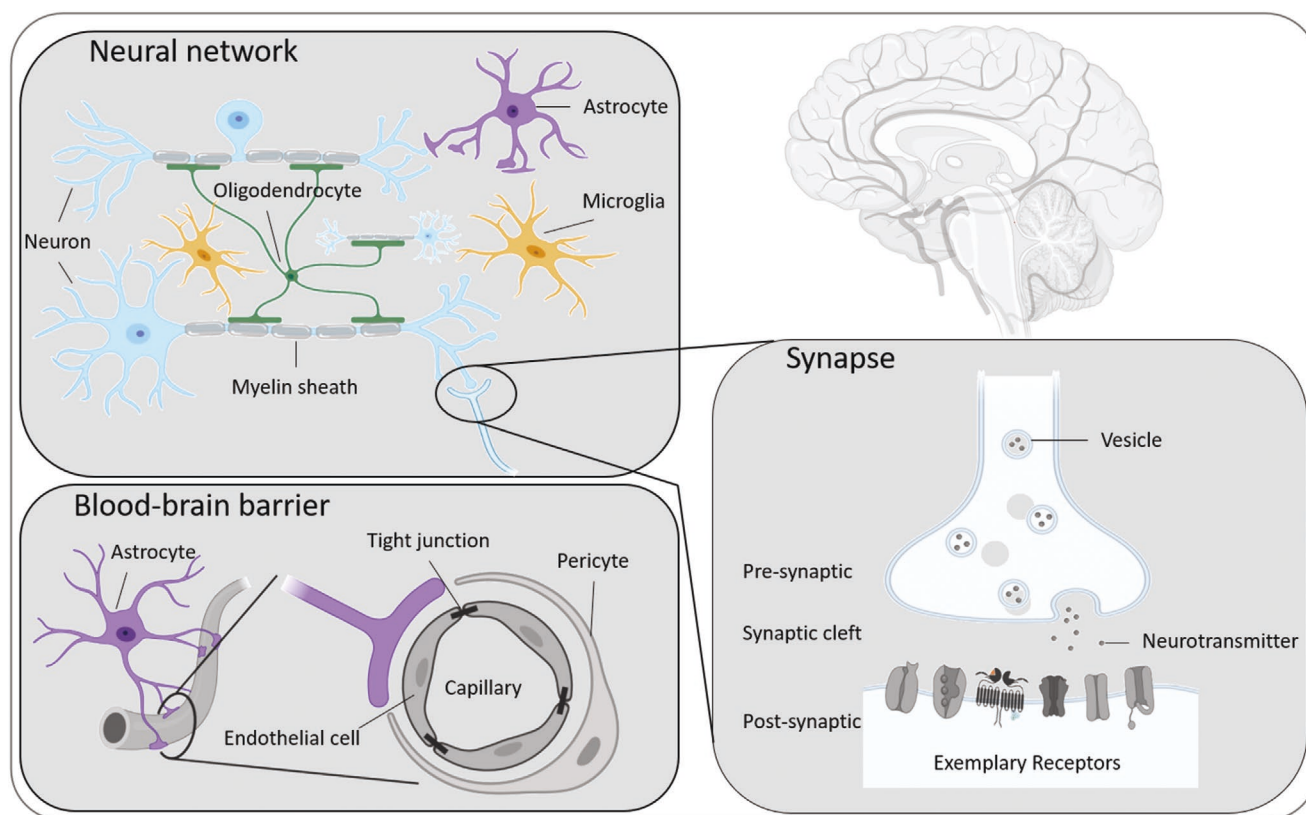


Figure 2. Schematic overview of important cell types and functional units of the brain. Figure created with BioRender.com.

neurons are terminally differentiated post-mitotic cells, which cannot divide to compensate for the neuronal loss after neurotoxic exposure.^[134] Glia cells constitute about half of the cells within the developed central nervous system (CNS)^[135] and can be divided into oligodendrocytes, astrocytes, microglia, and ependymal cells. Oligodendrocytes facilitate rapid saltatory conduction by insulating neuronal axons with myelin sheaths to guarantee adequate motor, sensory, and cognitive function.^[136] Astrocytes exhibit a variety of morphological and physiological properties reflecting their diverse functions in the CNS: They i) regulate synaptogenesis and synaptic transmission, ii) provide neurons with nutrients and neurotransmitters, iii) maintain the blood-brain barrier (BBB), iv) build scar tissue in case of injury, and v) form structural scaffolds.^[137] Microglia are the resident immune cells of the brain which orchestrate the inflammatory response and guide neuronal expansion and maturation.^[138] The brain is protected from most environmental chemicals by the BBB and the blood-cerebrospinal fluid barrier. Although both provide highly selective permeability, several substances can penetrate or disrupt the barrier structures to eventually reach the brain (Figure 2).^[139]

Due to the brain's complexity, neurotoxicity summarizes various modes-of-action (MoA) including i) neuronal injury or death (neuronopathies), ii) axon degeneration and secondary myelin degeneration (axonopathies), iii) separation of myelin sheets or selective myelin loss (myelinopathies), iv) altered astrocyte function (astrocyte neurotoxicity), v) disturbance of intercellular communication (neurotransmission-associated neurotoxicity) as well as vi) changes in cognitive function, level of consciousness and vigilance (toxic encephalopathy) including compromised adult neurogenesis.^[140] According to the OECD guidelines, neurotoxicity testing is performed in rodent animal studies, however species differences between rodent and human brains including astrocyte morphology,^[141] neuronal subtype ratios,^[142] and receptor affinities^[143–145] questions the predictivity of rodent models for human health. Therefore, the development of *in vitro* assays based on hiPSC or NPCs has led to promising alternative approaches.

Zhang et al. first described the differentiation of hESCs into a mixed culture of neurons, astrocytes, and oligodendrocytes.^[146] Moreover, targeted differentiation of hESCs and hiPSCs into neuronal subtypes including dopaminergic neurons, spinal motoneurons, and electrically active glutamatergic and GABAergic neurons can be either performed directly^[147–151] or following neural induction into NPCs.^[152–154] Of note, direct comparison of the neural-differentiation capacity of hiPSCs and hESCs revealed that both cell types produce neuronal cell types over the same developmental time course, however, hiPSCs exhibited a reduced differentiation potency and increased variability.^[155] Several 2D *in vitro* models based on neurally induced human pluripotent SCs^[156–160] or primary hNPCs^[144,161–163] have been used in neurotoxicity testing, predominantly in a developmental context focusing on i) neural progenitor proliferation, ii) neuronal differentiation, outgrowth, and network formation, iii) oligodendrocyte differentiation and maturation, iv) ROS accumulation, and v) epigenetic and transcriptional reprogramming. However, in a multiparametric high content approach, 36 chemicals were analyzed according to their potential to

induce acute neurotoxicity in hESC-derived neurons with cell viability, cytotoxicity, neurite length, and mitochondrial area as readouts.^[164]

Since cerebral 2D cultures cannot depict the complex *in vivo* cytoarchitecture of the brain, self-assembling 3D multicellular brain organoids emerged as an alternative especially in developmental research.^[36,165,166] Several approaches successfully generated brain-region-specific organoids recapitulating the specific cytoarchitecture, epigenome, and transcriptome of the forebrain, midbrain or hypothalamus.^[167–169] Fusions of different region-specific organoids demonstrated interneuron migration between fused parts, highlighting their applicability to model complex interactions between brain regions *in vitro*.^[170] To study the inflammatory response and increase the physiological relevance, functional, cytokine-secreting microglia have been cultured as immortalized cell lines or differentiated from hPSCs and incorporated into cerebral organoids.^[171–173] Since their early developmental stage limits the applicability of organoids for nondevelopmental testing, efforts have been made to increase the maturity, thereby generating stem cell-derived organoids including dendritic spines, active neuronal networks, mature oligodendrocytes, and myelinated axons.^[174–177] Another limitation for toxicity testing using organoids is their high variability.^[178] A compromise for staying in 3D yet with reduced variability are brain spheres, multicellular 3D brain aggregates that can be derived from ESCs or hiPSC, but lack higher anatomical structures.^[171,176,179–181] Such brain spheres have already been used for toxicity evaluation and proved useful to identify neurotoxins causing mitochondrial dysfunction, ROS accumulation, and metabolic disruption.^[180–182] Moreover, Sandström et al. tested the effect of non-neurotoxic and neurotoxic compounds in hESC-derived brain spheres exhibiting myelinated axons and functional neuronal networks and confirmed their usefulness for *in vitro* neurotoxicity testing.^[183] Schwartz et al. showed that self-assembled hESC-derived neural constructs composed of multiple neuronal and glial cell types, microglia, and interconnected vascular networks respond to toxic compounds as measured by RNA sequencing and confirmed in a cross-validation experiment that machine learning techniques can be used to correctly predict chemical effects. However, chemical effects on viability or cytotoxicity were not assessed.^[184]

Since the BBB is crucial for neuroprotection, lack of blood vessels is one of the major shortcomings of most *in vitro* models. Implementing such an interorgan crosstalk was realized by incorporating vasculature to cerebral organoids. This was achieved by either adding ETV2 variant 2 (ETV2)-expressing hESCs during organoid formation or by re-embedding organoids in Matrigel droplets containing hiPSC-derived endothelial cells.^[185,186] Of note, vasculature-like structures enhanced organoid maturity and induced BBB-like characteristics.^[185] Moreover, several functional BBB models have been developed as spheroids^[187,188] or in microfluidics devices.^[189–191] Since they show comparable permeabilities to *in vivo* measurements, promising candidates for drug-permeability screenings and neurotoxicity testing have been identified. However, these BBB models not only consist of stem cell-derived cells, but also contain human and rodent primary cells as well as immortalized cell lines.

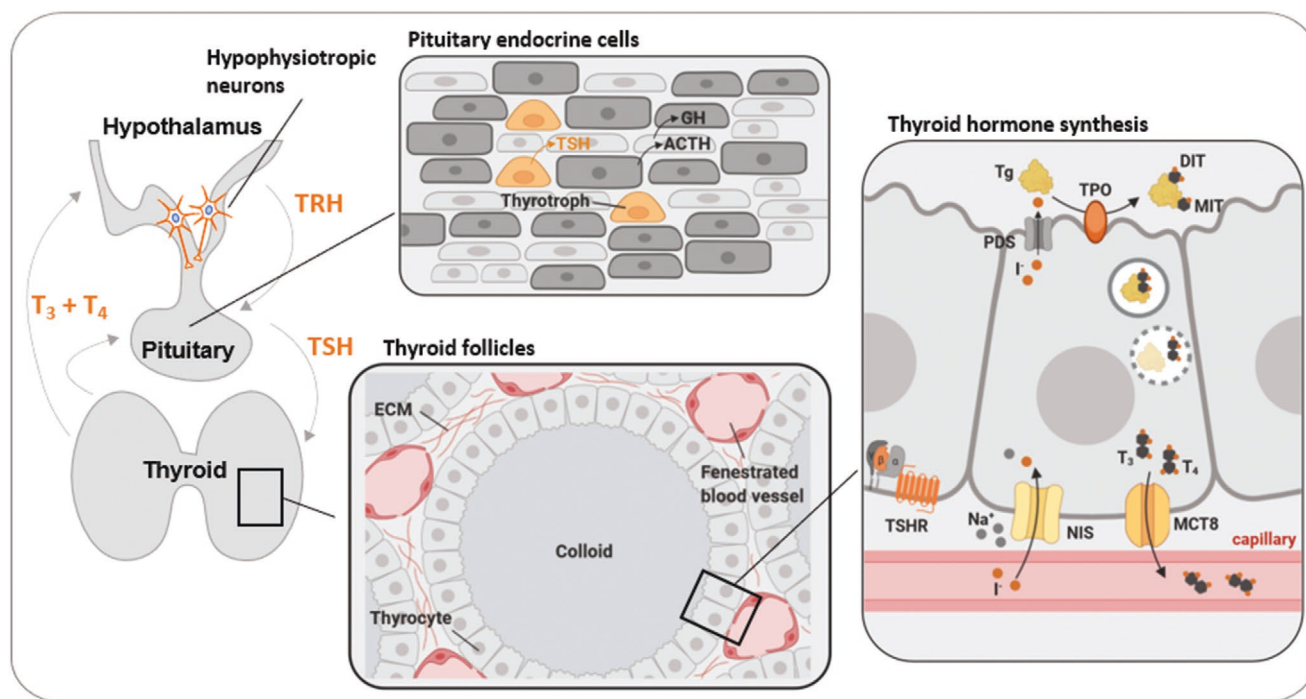


Figure 3. Cell types and functional units of the HPT axis necessary for TH production. Abbreviations: ACTH, adrenocorticotrophic hormone; DIT, diiodotyrosine; ECM, extracellular matrix; GH, growth hormone; MCT8, monocarboxylate transporter 8; MIT, monoiodotyrosines; NIS, sodium-iodide symporter; PDS, pendrin; T₃, triiodothyronine; T₄, thyroxine; Tg, thyroglobulin; TPO, thyroperoxidase; TRH, thyrotropin-releasing hormone; TSH, thyroid-stimulating hormone/thyrotropin; TSHR, thyroid-stimulating hormone receptor. Figure created with BioRender.com.

Vascularization would not only increase the resemblance to the native *in vivo* situation, but further eliminate the gradient of nutrients and oxygen from the outer spherical shell to the spheroid core. This gradient results in zonation of the spheroid, the formation of a hypoxic core, and an uneven distribution of the test substance.^[192,193]

Cultures of different hiPSC-derived neuronal subtypes, astrocytes and microglia (iCell, Cellular Dynamics; CNS.4U, Ncardia; SynFire, ReproCELL) as well as multicellular brain organoids (microBrain 3D, StemoniX) are commercially available and already applied in neurotoxicity testing in high-throughput, high-content approaches in 384 multiwell plates.^[179,194] Moreover, comparative electrophysiological analysis and neurotoxic exposure of neuronal models revealed differences in sensitivity and the degree of chemical-induced effects, but the models performed reproducibly and even outperformed primary rat cortical neurons in terms of sensitivity to detect seizurogenicity.^[195]

2.3. Thyroid System

The thyroid system is a neuroendocrine axis which regulates the production of the thyroid hormones (THs) thyroxine (T₄), and triiodothyronine (T₃). THs control a variety of physiological processes including energy metabolism,^[196] nervous system development,^[197] and thermoregulation,^[198] and are particularly important during perinatal development. Thyroid function is regulated by a fine-tuned interplay between the hypothalamus, the pituitary gland, and the thyroid (HPT axis) and is initiated by the secretion of thyrotropin-releasing hormone (TRH)

from hypophysiotropic neurons within the hypothalamus (Figure 3). TRH enters the pituitary portal circulation and binds to receptors on the plasma membrane of thyrotropes within the anterior pituitary.^[199] Binding causes the acute release of thyroid-stimulating hormone (TSH) from secretory granules, an essential regulator of thyroid function, differentiation, and growth.^[200] The thyroid's task is the production of THs, which involves uptake of iodide and its utilization during TH synthesis. Iodide absorption from the plasma is mediated by the sodium-iodide symporter (NIS) located within the basal membrane of polarized follicular thyrocytes.^[201] Thyrocyte follicles are vascularized spherical secretory units filled with a protein-rich substance called the colloid. Within the colloid, iodide is oxidized and bound to tyrosine residues of the colloid-protein thyroglobulin (Tg) in an organification reaction catalyzed by the enzyme thyroperoxidase (TPO) generating both monoiodotyrosines (MIT) and diiodotyrosines (DIT) within the Tg protein. Subsequent coupling of two neighboring DIT molecules generates T₄ whereas the coupling of one MIT and one DIT molecule yields T₃.^[202,203] Endocytosis of Tg and lysosomal proteolysis releases T₄ and T₃ from Tg and the transporter MCT8 within the basolateral membrane releases the THs into the circulation.^[204] The amount of TSH secreted by the anterior pituitary substantially determines the TH production rate since TSH receptor (TSHR) activation positively regulates iodide uptake by NIS, Tg expression, and TH synthesis. Moreover, THs exert a negative feedback on the secretion of TSH and TRH by the pituitary and hypothalamus, respectively (Figure 3).^[200]

Environmental chemicals deregulate the thyroid system by various routes of interference (e.g., TH synthesis, metabolism,

transport, elimination, or TH receptor activation).^[205] However, the ability to influence circulating levels of TH or TSH in vivo is the only readout used to identify thyroid disruptors in toxicity testing. TH levels are mandatorily assessed in OECD in vivo toxicity guideline studies (i.e., TG 408, 414, 421, 422, and 443),^[121,206–209] however, they do not provide information about the mechanism of TH disruption complicating the extrapolation of study results across species. Moreover, high costs, ethical concerns, and the low-throughput of animal-based assays in contrast to the numerous chemicals which need to be tested have driven efforts to develop and validate in vitro assays based on key molecular initiating events (MIEs) in thyroid disruption.^[198,210–212] To facilitate their regulatory application, a thyroid-related adverse outcome pathway (AOP) network has been established linking the MIEs to toxicity-mediated thyroid dysgenesis and downstream adverse outcomes.^[213] Several high-throughput screening (HTS) assays have been developed,^[198] however, the uncertainty of these assays to predict functional effects on the tissue-level questions their physiological relevance and elucidates the need for organotypic cell culture models. The use of a tiered screening approach in which positive hits from HTS assays (Tier 1) are further verified in organotypic medium-throughput models (Tier 2) as a preselection for final Tier 3 in vivo testing significantly reduces costs, the testing throughput and guarantees the predictivity of the risk assessment.^[198,214] Since the HPT axis comprises several organs, the establishment of a single organotypic Tier 2 model is insufficient. By contrast, models depicting interim steps within the thyroid system including TRH and TSH secretion, iodide uptake, and TH production are needed.

Already in the 1980s, thyroid tissue was reconstructed in collagen gels from primary human thyrocytes.^[215,216] The cells formed follicles secreting Tg into the colloid in response to TSH stimulation. Moreover, they proved functional in vitro concentration-dependently responding to TSH exposure with iodide uptake and T₃ secretion. Exposure to the TPO inhibitor methimazole further confirmed response to chemical interference.^[216] Studies on thyroid models derived from primary mouse thyrocytes further confirmed in vivo functionality and yielded follicles capable of TSH-dependent iodide uptake and TH secretion after transplantation into hypothyroid mice.^[217,218] In order to increase the applicability for toxicological screenings, Deisenroth et al. developed a medium-throughput organotypic screening assay in a 96-well plate format.^[219] Functional follicular structures expressing genes of mature thyrocytes (NIS, TPO, TSHR, Tg), capable of iodide uptake and TH production, were derived from human thyrocyte tissue. Of note, screening of reference compounds identified in established HTS assays for thyroid disruption (i.e., NIS and TPO enzyme activity) revealed both similar effects and potencies in the microtissue model, highly indicating its applicability for a tiered screening approach. However, the use of primary thyrocytes for toxicological testing is challenging. Their low turnover rate (five renewals per lifetime) and general impurities in primary cultures limit their application in a regulatory context.^[220] Therefore, the development of 3D models based on ESCs or iPSCs is more promising. Two different approaches successfully generated functional thyroid follicles from ESCs and iPSCs in 3D Matrigel cultures: i) the enrichment of cells

expressing the transcription factors Pax6 and Nkx2.1 by genetic modification or FACS sorting and ii) the induction of anterior foregut endoderm (AFE) by treatment with Activin A, Noggin, SB431542 followed by cultivation in thyroid differentiation medium supplemented with insulin, IGF-1, FGF2, FGF10, and bone-morphogenic 4 (BMP4). Both protocols generated follicular thyroid tissue expressing NIS, TSHR, and TPO from human and mouse ESCs^[221–224] and iPSCs.^[223,225,226] The follicles increased iodide uptake upon TSH stimulation and secreted Tg into the colloid. Furthermore, TH production was observed both in vitro^[223–225] and in vivo^[222,223] after transplantation into hypothyroid mice. Direct comparison of 2D and 3D cultivation approaches revealed increased expression of TSHR, TPO, and Tg in 3D cultures. Moreover, NIS expression and TH secretion was completely limited to Matrigel-embedded follicular 3D cultures, highlighting the increased functionality of organoid compared to monolayer models.^[219] The stem cell-based thyroid models seem promising in identifying chemical interference with iodide uptake, Tg production, and TH synthesis and thus represent interesting candidates for application in tiered approaches in toxicity testing. Bioprinting of primary thyroid and allantoic spheroids as sources of thyroid and endothelial cells, respectively, resulted in follicles containing microvascular networks which proved functional in vivo after grafting into mice. Since folliculogenesis is guided by angiogenesis and iodide is taken up from the bloodstream, vascularization could increase the functionality of the thyroid 3D model and the technique could be adapted to stem cell-derived thyroid and endothelial cells.^[217] Additional optimization of the culture parameters could further promote the differentiation into thyroid tissues, since hypoxia (2% O₂) was reported to increase the expression of thyroid transcription factors (Pax8 and Nkx2.1), the expression of NIS and TSHR, and the uptake of iodide.^[227]

Fewer efforts have been directed at developing 3D models for the initiating steps of the HPT axis within the hypothalamus and the pituitary. However, coinduction of hypothalamic and oral ectoderm from ESCs^[228,229] and hiPSCs^[230] facilitated the formation of 3D organoids with different hormone-producing pituitary cells adjacent to functional hypothalamic tissue. The protocol is based on the formation of large cell aggregates in suspension culture and the concurrent activation of BMP4 and sonic hedgehog signaling pathways. Of note, interactions between the two juxtaposed tissues were critical for the development of hormone-producing pituitary cells, elucidating the importance of the hypothalamus for pituitary maturation.^[228] Although the model gave rise to high amounts of adrenocorticotrophic hormone (ACTH)- and growth hormone (GH)-producing pituitary cells both in vitro and after transplantation into hypopituitary mice in vivo, only few TSH-producing thyrotropes were observed. Therefore, additional optimization of the protocol is needed to make it suitable for the screening of chemicals interfering with TSH synthesis and secretion.

2.4. Lung

The respiratory tract is one of the principle barrier organs of the human body. Its main function is to facilitate the exchange of oxygen and carbon dioxide between the air and the blood. An

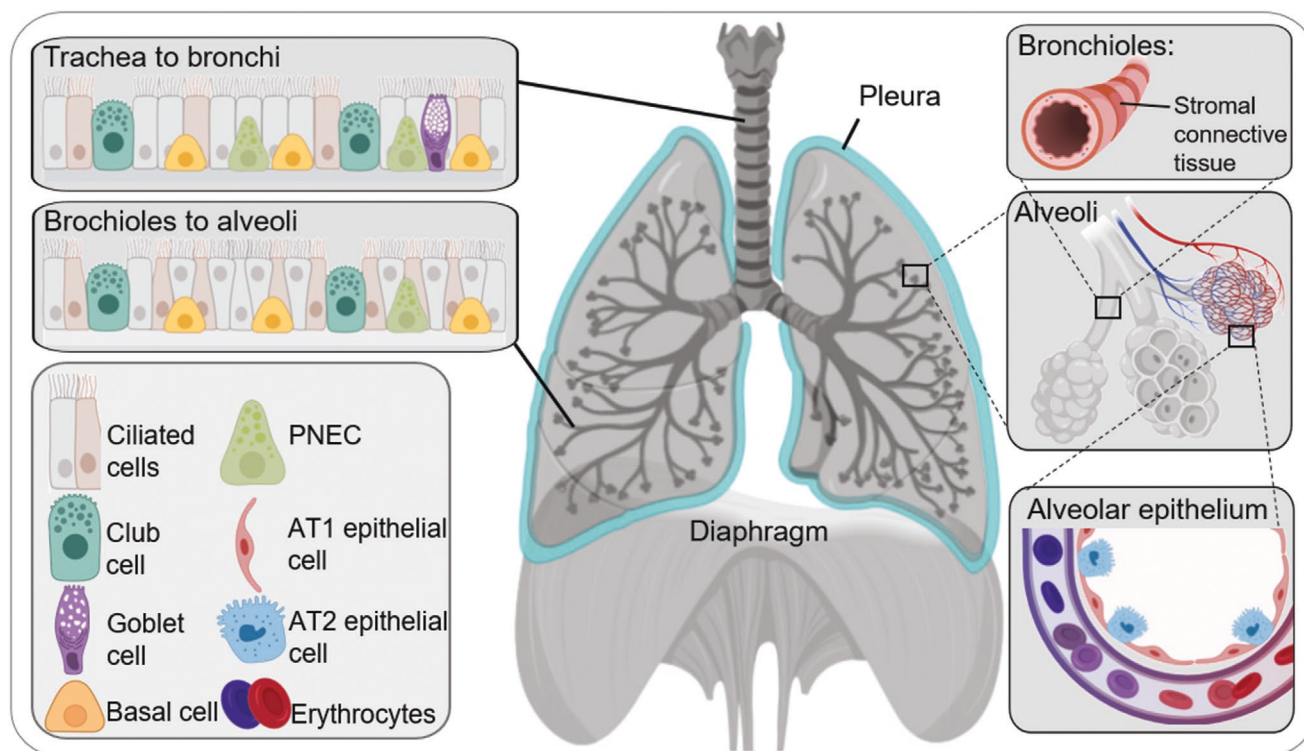


Figure 4. Schematic overview of important cell types and functional units of the respiratory tract. Abbreviations: PNEC, pulmonary neuroendocrine cell; AT, alveolar type. Figure created with BioRender.com.

adult human inhales ≈ 15 to 20 m^3 of air per day and as such the lung epithelium, with an estimated surface area of $30\text{--}130 \text{ m}^2$,^[231,232] can be directly exposed to gaseous and particulate contaminants of chemical and biological origin. Apart from being a target for occupational and environmental airborne toxicants, the respiratory tract represents a dominant uptake route for noxious agents affecting other organs. In turn, the lung can be affected by toxicants that reach this organ via other uptake pathways. Considering the multitude of resident cell types (over 40),^[233] architectural and physiological particularities in terms of airflow dynamics, and stretch as well as shear stress effects (Figure 4), the development of robust and realistic *in vitro* models to replace *in vivo* inhalation studies is a major challenge. Risk assessment of inhalable toxicants traditionally relies on the in-depth (histo-)pathological and clinical/biochemical investigation of experimental animals, predominantly rodents, following acute or long-term repeated inhalation exposures.^[234] Such studies often include analysis of further endpoints, such as inflammation (by bronchoalveolar lavage), genotoxicity, or even lung function.^[235] Inhalation studies are laborious, expensive, and complex, not only regarding the evaluation of effects, but also in view of the requirements for the controlled, reproducible, and safe generation and monitoring of the exposure cloud.^[236]

In vitro methods have been used since long in inhalation toxicology research and major developments in the last decades yielded innovative approaches that aim for high throughput analysis and models that better mimic specific aspects of the complex anatomy and physiology of the human respiratory tract. Model developments have mostly focused on the selection

of epithelial cells as they represent the first target for inhaled toxicants.^[237] Anatomically and functionally, the respiratory tract can be subdivided into two principle regions. i) The conducting airways are represented by mucus producing goblet cells, ciliated cells, club cells, and neuroendocrine cells as well as basal cells, the progenitor cells for the airway epithelium.^[238–240] ii) The epithelium of the alveolar region, where the gas exchange takes place, is composed of alveolar type I epithelial (AT1) cells and type II (AT2) cells. The surfactant producing AT2 cells serve as progenitors to replace damaged alveolar epithelial cells.^[238,241] When designing or selecting the type(s) of epithelial cells for an *in vitro* model the target site specificity of a toxicant must be taken into account. Its airborne concentration and its physicochemical properties (e.g., water-solubility and reactivity of gases, aerodynamic size and shape of particles) as well as host factors (e.g., breathing pattern, activity) determine the predominant region of interaction.^[242–244]

For decades, *in vitro* studies addressing effects on epithelial cells have used primary cells, explant cultures or immortalized cell lines from (fetal) lungs of rodents or human origin.^[245–248] The adenocarcinoma cell line A549 represents by far the most investigated human AT2-like epithelial cell model.^[249] Effects on AT1 cells can be modeled by the immortalized human alveolar type-I-like epithelial cell line TT1.^[250] Novel methods have been developed in recent years to improve the collection of human primary bronchial epithelial cells, e.g., to investigate disease susceptibility.^[251,252]

Besides epithelial cells, various other cell types of the lung have been used, or included in coculture with epithelial cells, for *in vitro* inhalation toxicology research purposes. This

includes mesenchymal cells to study fibrosis hazards and mechanisms,^[253,254] primary alveolar macrophages obtained from experimental animals or humans by lung lavage to study host defense and particle clearance,^[255–258] monocytes/macrophages, neutrophils, dendritic cells, and mast cells to simulate lung inflammation processes,^[259–261] and pleural cells to study mechanisms and hazards of pleural disease and malignant pleural mesothelioma.^[262–265] Vascular and capillary endothelial cells have been introduced in coculture models together with lung epithelial cells to explore epithelial–endothelial crosstalk mechanisms, airway or alveolar barrier impairments and systemic uptake of inhaled chemicals and particles.^[266–268]

Specific model developments for lung research have focused on the recreation of physiological aspects of this organ. Herein, major milestones have been achieved through the ongoing development of ALI systems, using monocultures,^[269,270] multiple cell types,^[260,271] or commercially available human lung tissue.^[272] ALI approaches allow for the controlled testing of gases, particles or their mixtures in immediate contact with epithelial cells, unlike models in which cells are submerged in (testing) medium. Combined with advanced exposure systems ALI cultures enable *in vitro* testing scenarios that better mimic inhalation exposure. This is particularly the case for inhalable particles in terms of their complex kinetics of particle deposition and initial interaction with the epithelial lining fluid. Mechanical stretch models mimicking breathing movements have been introduced to study its role in lung development,^[273] repair of damaged lung epithelium,^[274] and possible modulation of toxicant effects.^[275] Sophisticated human lung-on-a-chip models have been developed using microfluidic devices that mimic both architectural and physiological aspects of the alveolar-capillary region, by combining breathing–mimicking mechanical strain with respective air and blood-flow characteristics in epithelial and endothelial compartments.^[276]

Stem-cell based technologies brought major innovations into lung research. The developments and methodological advancements of stem cell-based tissue engineering focused on elaboration of mechanisms of lung development, damage repair, regeneration, and the pathogenesis of lung diseases.^[277,278] Principal approaches to generate mature adult lung cells from ESCs or iPSCs include coculture approaches with mesenchymal cells or successive treatment and selection protocols that mimic lung development. Early developments include the generation of AT2 and club cells from murine ESCs. When cultivated under ALI conditions, these ESCs can grow into a differentiated airway epithelium comprising basal, ciliated, intermediate, and club cells.^[279] Lung progenitor cells can also be derived from the circulation^[280] and used to generate AT2-like cells from CD34⁽⁺⁾ cells.^[281] Major progress in the field was achieved with the generation of human epithelial cells from AFE-derived from hESC and hiPSC, whereby caudal region of the AFE gives rise to the tracheal and lung.^[282] Along these lines, bronchial and alveolar progenitors can be derived for the generation of both airway and alveolar epithelial cells from iPSCs.^[283,284] Of note, hypoxia of 1% O₂ enhanced both the spontaneous and activin A-dependent formation of definitive endoderm from mouse ESCs and the subsequent differentiation into AT2 and club cells in a hypoxia-inducible factor 1 alpha (HIF1 α)-dependent manner. This indicates, that a careful timing of hypoxia may

increase the efficiency of *in vitro* differentiation processes into the lung lineage.^[285] Scaffold-based methods have been used to generate alveolar-like structures, characterized by AT1 and AT2-like epithelial cells from murine lung stem/progenitor cells using 3D-gelatin microbubbles.^[286] Also human alveolar organoids, composed of a pool of self-renewable AT2-like cells and AT1-like cells have been successfully created from hiPSCs.^[287] These and various further protocols to develop lung organoids and AT2 cells from hiPSCs are nowadays at hand, offering great potential for *in vitro* inhalation toxicology testing.^[288–290] However, also concern has been expressed especially regarding the generation of mature, differentiated AT2 cells.^[291] Chen et al. described the construction of lung bud organoids from hPSCs containing pulmonary endoderm and mesoderm which, following xenotransplantation or in Matrigel 3D cultures, develop into branching airway and alveolar like structures.^[292] They also showed the potential of their model to study molecular and morphological hallmarks of diseases, like fibrosis. In combination with gene editing approaches innovative lung organoid developments are envisaged to benefit research on susceptibility toward idiopathic or toxicant-induced lung diseases.^[293,294]

In the future, stem cell-based technologies in combination with the latest developments in tools that reliably mimic the specific physiology of the respiratory tract are anticipated to bring major advancements to the field. However, the complexity of the respiratory tract needs to be critically considered here. Promising advancements can be achieved by combining stem-cell and lung-on-a-chip approaches (reviewed by Nawroth et al.^[295]). However, the authors also promote the inclusion of lung physiology aspects in such models, especially concerning toxicological or drug safety testing. Moreover, while elegant systems are available for controlled exposure of epithelial cells or tissues at the ALI interface,^[296] they do not yet allow for a straightforward incorporation of complex (scaffold-based) lung organoid models. Toxicological hazard assessment analysis calls for reliable, robust, and reproducible models to generate valid concentration-response data. And it is precisely this dosimetry aspect that fuels the complexity of inhalation toxicology research, on gases, vapors, and especially particles.

2.5. Cardiovascular System

Together with the circulatory system the heart orchestrates an unidirectional continuous blood flow to provide all organs with oxygen, nutrients, and hormones.^[297] It is composed of four chambers that are divided into two blood receiving atria and two pumping ventricles. The ability to beat requires a thick wall robust enough to withstand the continuous movement and the associated shear forces. The inner wall of the heart is lined with the endocardium, followed by the thick myocardium containing cardiomyocytes (CMs) embedded in extracellular matrix and the electrical conduction system composed of specialized muscle fibers capable of signal conduction. The outer epicardium consists of elastic fibers, which protect the heart and reduce friction (**Figure 5**; reviewed by Bauer^[298]). The complex structure of the heart with its multiple cell types, the permanent blood flow, the shear forces caused by the contraction, and the electrical stimulation are all factors complicating

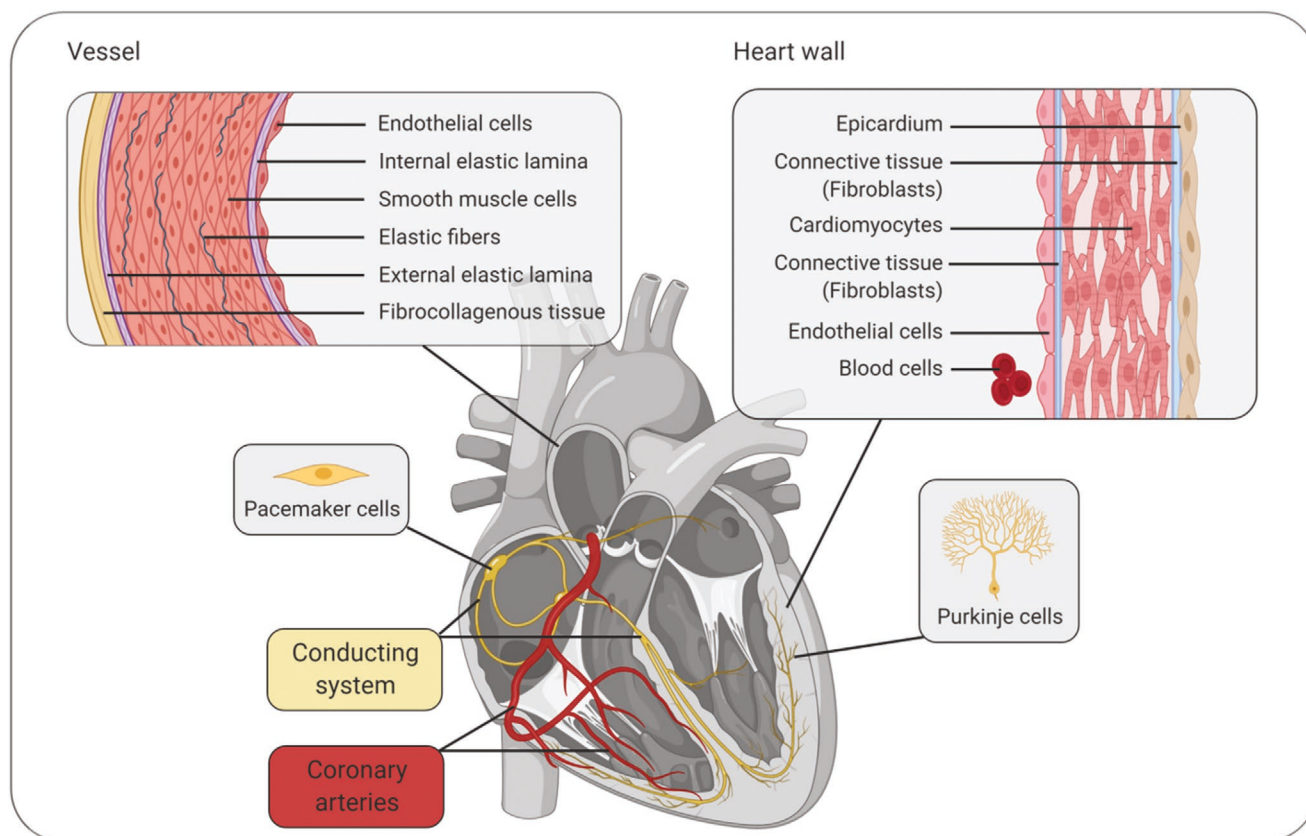


Figure 5. Schematic overview of important cell types, tissues and functional units of the heart. Figure created with BioRender.com.

the development of predictive *in vitro* systems for cardiotoxicity testing. Nevertheless, cardiotoxicity is the most crucial adverse event in drug development, making cardiovascular safety issues the number one reason why drug candidates fail in preclinical trials or have to be withdrawn from the market.^[299] Therefore, arrhythmia, altered QT intervals, channelopathies in general, decreased cell viability, and structural cell damage are possible heart-related effects of substances which have to be ruled out prior to drug release.

Typically, first line drug testing includes the hERG *in vitro* assay detecting inhibitors of potassium channels essential for the repolarization phase of action potentials.^[300] The human ether-a-go-go related gene (hERG) encodes for a channel subunit whose blockage results in QT interval prolongation potentially followed by Torsade de Pointe (TdP), a drug-induced lethal arrhythmia.^[301] The QT interval represents the time from the Q wave (first depolarization of the ventricles) to the T wave (total repolarization) and abnormalities in interval lengths are associated with tremendous adverse effects making QT prolongation one of the most common reasons for drug withdrawal.^[302,303] The classic hERG assay utilizes patch clamp recording in immortalized human embryonic kidney (HEK) 293 cells heterologously expressing hERG channels.^[301] This setup in noncardiac cells exhibits limited predictive power and thus is inferior to novel approaches with hiPSC-derived CM cultures.^[300] In addition to the hERG assay, the proarrhythmic potential of chemicals is further tested in nonclinical *in vivo* animal studies according to ICH S7B and E14 guidelines.^[304,305] However, species

differences, especially in terms of ion channel expression and phenotypic causes of channel inhibition, question the predictivity of rodent experiments for human health.^[297,306]

Stem cell research revolutionized the development of alternative *in vitro* methods for cardiotoxicity testing, generating spontaneously contracting CMs from pluripotent stem cells which express most of the ion channels and sarcomeric proteins found *in vivo*. For the induction of functional CMs from hESCs or hiPSCs, numerous 2D and 3D culture protocols exist which slightly differ in factors like cell source, culture media, days of preculture, and days of toxicant exposure.^[307–309] The *in vitro* cardiotoxicity assessment can be divided according to the functional readout into models evaluating electrophysiology, cardiac cellular contractility, and cytotoxicity. Electrophysiological cardiotoxicity is either measured by i) microelectrode arrays (MEAs),^[310,311] ii) by patch clamp techniques which are extremely sensitive but exhibit reduced throughput^[312] or iii) by optical imaging of voltage sensitive dyes.^[313] In order to implement a next-generation, mechanism-based standard for preclinical risk assessment of proarrhythmic chemicals, the comprehensive *in vitro* proarrhythmia assay initiative combines *in vitro* assays with *in silico* reconstructions of cardiac electrophysiological activity, thereby encouraging a paradigm change in cardiotoxicity testing beyond the hERG assay to better understand and predict TdP risk.^[314,315] As part of that ongoing movement, drugs linked to low, intermediate, and high TdP risk are tested with respect to their proarrhythmic potential in hiPSC-CMs using MEAs or voltage-sensing optical approaches.

Besides proarrhythmic effects, the impact on cardiac cellular contractility is a key element of cardiotoxicity risk assessment, therefore, altered contractility of CMs is addressed in several *in vitro* assays. Since the direct measurement of the force component of contractility in cell culture is technically challenging, indirect readouts like sarcomere shortening, Ca^{2+} flux or mitochondrial membrane potential changes are used.^[316,317] Moreover, hiPSC-derived CMs are responsive to ionotropic drugs like norepinephrine and their beating frequency can be modulated via electrical stimulation.^[318] Sharma et al. recently established the cardiac safety index (CSI) as a measure to evaluate cardiotoxic chemicals in a HTS format in 384 multiwells.^[319] The CSI is based on several *in vitro* readouts for measuring chemical effects on contractility and cytotoxicity in hiPSC-derived CMs.

Although CM-based models are functional and widely applied in cardiotoxicity testing, the impact of multiple cardiac cell types like fibroblasts, epithelial cells (epicardium), and endothelial cells (endocardium) on cardiotoxicity is neglected. Kurokawa et al. showed that the cardiotoxic effects of the ErbB2 (HER2) inhibitor Trastuzumab can only be recapitulated *in vitro* within a coculture model of hiPSC-CMs and endothelial cells, highlighting the relevance of organotypic, preferably 3D models containing multiple cardiac cell types.^[320] Challenges in recapitulating the cellular complexity of the heart *in vitro* with its continuous movement and perfusion by the cardiovascular system impedes the development of functional cardiac organoids.^[321] However, multicellular spheroids have been constructed from hiPSC-CMs, coronary artery endothelial cells, and cardiac fibroblasts using the hanging drop method.^[322] Doxorubicin exposure evoked responses comparable to primary cardiac cultures, however, this system is not yet ready for high throughput cardiotoxicity testing. Within a high throughput approach, human 3D cardiac microtissues were assembled from the same cell types in 384 multiwell plates, exposed to known cardiotoxins and the mitochondrial membrane potential, endoplasmic reticulum integrity, and cell viability were used as readouts to evaluate the risk for cardiotoxicity.^[323] Although the model could detect cardiotoxicity at clinically relevant concentrations, it is still lacking toxicological relevant cell types like smooth muscle fibers and the influence of shear stress caused by the continuous blood flow is neglected.

TdP can be modeled in human 3D cardiac tissue sheets (CTSs) which are constructed from hiPSC-CMs and non-myocytes.^[324] The arrhythmias are detected by simultaneous measurement of the extracellular field potential on MEAs and evaluation of the contractile movement by a high-precision live cell imaging system capturing the beating motion. Of note, TdP could predominantly be detected in multilayered 3D CTSs composed of cell mixtures, highlighting the superiority of multicellular 3D models for *in vitro* cardiotoxicity testing compared to pure CM 2D cultures.

Although stem cell-based *in vitro* assays have been successfully applied in cardiotoxicity testing, the available systems do not live up to the cellular and structural complexity of the heart and do not model the blood flow. A limitation of the widely used hiPSC-CMs is their insufficient maturity rather representing fetal CMs.^[321] The choice of *in vitro* culture parameters like media supplementation or oxygen content significantly affect

CM maturation. Glucose rich media promote anaerobic glycolysis in CM cultures, a metabolic phenotype observed in fetal hearts *in vivo* or under hypoxic condition. By contrast, glucose deprivation or HIF1 α inhibition increase oxidative phosphorylation in CM cultures which is an indicator of metabolic maturation observed in adult hearts *in vivo*.^[325] Efforts have been made to accelerate hiPSC-CMs maturation but so far, no mature CMs have been established *in vitro*. However, the use of a testing battery of *in vitro* assays detecting specific cardiotoxic events like ion channel blockage, altered electrophysiology or contractility and cardio cytotoxicity could be a promising approach to circumvent the limitations of the individual assays.

2.6. Liver

Connecting the gastrointestinal tract with the systemic circulation, the liver is of tremendous importance for the metabolism and elimination of first pass doses of drugs, food contaminants, microbial metabolites, and other xenobiotics. The structural unit of the liver is the hepatic lobule, which consists of hexagonally arranged hepatocytes infused by a network of liver sinusoids. Nutrient- and oxygen-rich blood coming from the portal vein and the hepatic artery, respectively, enters the lobule via the interlobular portal triad (i.e., hepatic arteriole, portal venule, and bile duct), passes the sinusoid network and drains into the central vein of the lobule. The resulting oxygen gradient, ranging from normoxic to hypoxic conditions, and the associated activation of signal transduction pathways, i.e., β -catenin and hedgehog signaling, contribute to the zonation of the liver, which critically determines spatial enzyme expression and corresponding metabolic activity.^[326] In addition, hepatic blood flow through the liver sinusoids causes shear stress not only in the endothelial cells but also in the lining hepatocytes, which shapes various hepatic functions, including xenobiotic metabolism and hepatocyte maturation.^[327] Liver zonation, shear stress, and other parameters, such as the crosstalk between hepatocytes and nonparenchymal cells, in particular sinusoidal endothelial cells, Kupffer cells, stellate cells, and lymphocytes, have a critical impact on hepatic functions and thus challenge the development and implementation of appropriate *in vitro* test systems for predictive hepatotoxicity testing (Figure 6).

In fact, hepatotoxicity is a major safety concern for the pharmaceutical industry. Adverse drug reactions are responsible for a remarkable high attrition rate of new chemical entities of up to 90%,^[328] with hepatotoxic effects being causative second to cardiovascular safety issues.^[329] Moreover, drug-induced liver injury, which in severe cases may cause life-threatening acute liver failure, is the most frequent cause of postmarketing warnings and withdrawals.^[330,331] Thus, existing (preclinical) testing strategies, combining *in vivo* and *in vitro* studies as well as *in silico* predictions, are of obvious limited success.

Besides ethical considerations, animal studies face the challenge of considerable interspecies differences in the toxicopharmacokinetics and -dynamics of a chemical or drug and thus often fail to predict human hepatotoxicity.^[332,333] The current gold standard for *in vitro* hepatotoxicity testing during drug development are human primary hepatocytes grown in monolayer culture. Obvious limitations of these cells are their

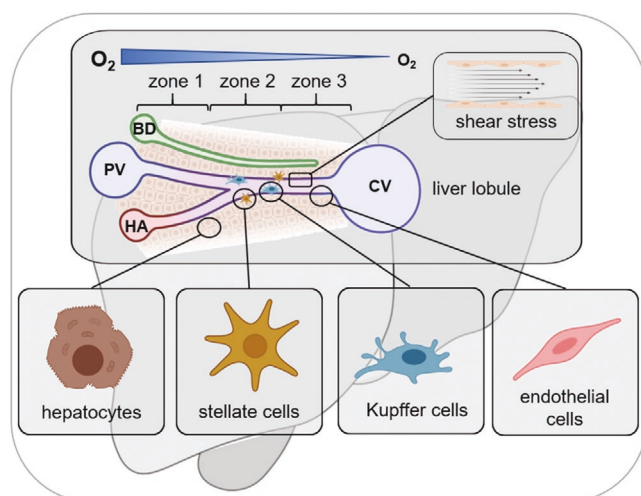


Figure 6. Structural and functional aspects and cell-types of the liver. Abbreviations: BD, bile duct; CV, central vein; HA, hepatic arteriole; PV, portal venule. Figure created with BioRender.com.

scarce availability, short life span, and tendency to rapidly dedifferentiate in culture, which is associated with a substantial downregulation of phase I and phase II enzymes.^[334] Other cell models that are widely employed to assess potential hepatotoxicity are human hepatoma cell-lines, such as HepG2, Hep3B, and HepaRG. However, these cell-lines have a tumor background, rendering them less sensitive toward chemical threats, and lack the expression of major xenobiotic-metabolizing enzymes.^[334]

The use of 3D *in vitro* models for hepatotoxicity testing is superior to monolayer cultures of hepatocytes or hepatoma cells, as these models, at least to some extent, resemble liver architecture and cellular diversity and thus are closer to liver physiology. In fact, 3D culture maintains the viability and hepatic functionality of incorporated primary human hepatocytes or hepatoma cells for up to several weeks.^[335] As thoroughly summarized in various recent overview articles,^[333,335,336] there is an ever-growing list of novel 3D liver models with each having its individual advantages and drawbacks. Today, several 3D liver models are on the market, an up-to-date list of commercially available models can be found here.^[290] Liver spheroids, e.g., derived by the hanging drop technique, consisting of primary human hepatocytes or hepatoma cells are relatively easy to handle and are already more sensitive and specific in predicting hepatotoxicity and drug-induced liver injury than the corresponding plain monolayer cultures.^[333,337,338] Spheroid and higher organized organoid models allow the incorporation of nonparenchymal cell-types, which is of particular importance for the screening of complex adverse effects, such as inflammation and fibrosis. The complex liver architecture and cellular complexity, including endothelial cells, can also be reconstituted by means of 3D bioprinting^[339] and usage of organ-on-a-chip-platforms, such as microfluidic biochips or microfluidic multiorgan chips, enabling a more physiologically relevant supply with nutrients, oxygen, and test compounds.^[333,337] For instance, different approaches, including the generation of 3D hepatic zonal channels and biochips, enabling the mounting of an oxygen gradient (from normoxia to hypoxia) across

hepatocytes, exists that mimic hepatic zonation and spatially distributed metabolic activities.^[340–342]

However, most of these models depend on primary human hepatocytes with all their limitations. Hepatocyte-like cells have been successfully differentiated from pluripotent stem cells including iPSCs, and used for hepatotoxicity testing.^[343,344] However, when cultured in 2D monolayers these cells lose morphology, proper cell–cell contact (tight junctions), and metabolic capacity.^[345] Self-organizing 3D hepatic organoid systems derived from PSCs or iPSCs may overcome these limitations by closely mimicking the hepatic microenvironment and physiology.^[336] Stem cell-derived 3D liver models can be cultured for month or years without losing their metabolic capacity or other hepatic functions. Several methodological approaches exist, including scaffold-free (decellularized liver matrices, spheroids, and organoids) and scaffold-based (nanofiber- and hydrogel-based, nanoscaffolds) setups.^[333] Moreover, PSC/iPSC-derived 3D liver organoids can be generated by starting either with a coculture of cell-types, for instance, iPSC-derived endodermal, endothelial, and mesenchymal cells,^[346] or with a homogeneous cell population that during the culture protocol differentiates into the different hepatic cell-lineages.^[347,348] The use of PSCs/iPSCs allows to generate multicellular 3D models with all hepatic cell lineages incorporated being genetically identical.^[336,347] Human iPSCs derived from fibroblasts, blood cells or any other cell-type of a donor, can be differentiated in all hepatic cell-types and thus present an unlimited pool of cellular material for diagnostic purposes or toxicity testing. The simultaneous generation of 3D liver organoids from hiPSCs of different donors in combination with high-throughput hepatotoxicity testing enables comparative compound testing, and thus tackles the issue of population diversity/interindividual susceptibility. In fact, a high-throughput approach with hiPSC-derived hepatocytes grown in 2D and 3D cultures assessing the impact of 48 substances on cell number, viability, nuclear integrity, mitochondrial membrane potential, apoptosis, and other parameters, demonstrated that hiPSC-derived 3D liver models are suitable for high-throughput testing.^[349] Powerful gene engineering techniques, such as transcription activator-like effector nucleases (TALENs) and the CRISPR/Cas system, allow the introduction of point mutations, smaller deletions, etc. and thus the creation of hiPSC cultures, which in a 3D context may phenocopy functionally relevant single nucleotide polymorphisms (SNP) and rare mutations that frequently occur in genes coding for xenobiotic-metabolizing enzymes.^[350] Stem cell-derived 3D liver organoids can also be used to model complex hepatic diseases. Ouchi et al., for instance, successfully simulated the sequential pathogenesis of steatohepatitis, consisting of steatosis, inflammation, and fibrosis, by treating PSC-derived 3D models made of hepatocyte-, macrophage-, cholangiocyte-, and stellate-like cells with free fatty acids.^[347] By incorporating human fetal liver mesenchymal cells into human ESC-derived expandable hepatic organoids, Wang and co-workers generated another intriguing test model, which is suitable to investigate the pathophysiology of alcoholic liver injury. Specifically, under ethanol treatment, the model allows to assess the generation of oxidative stress, steatosis, the secretion of inflammatory mediators, and fibrosis.^[351]

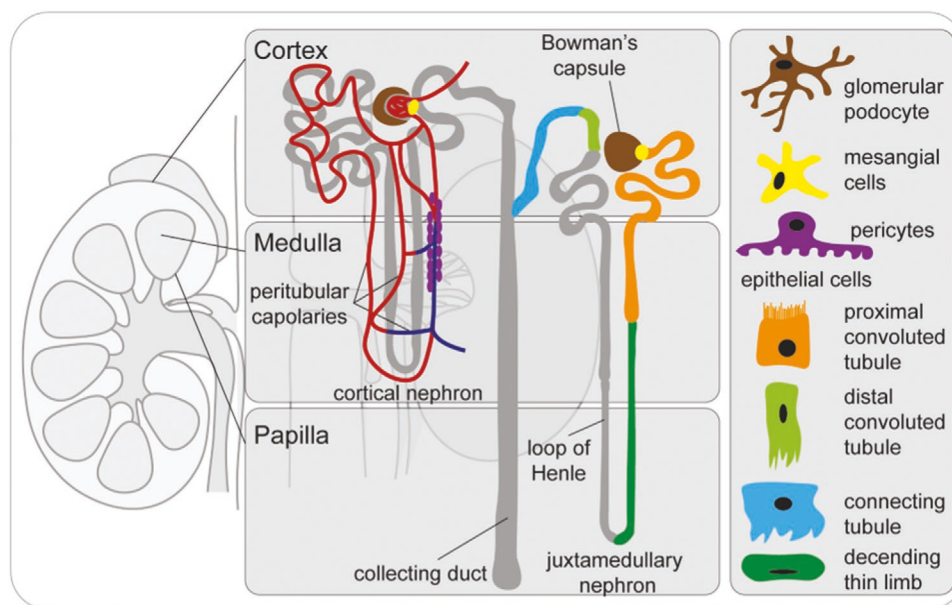


Figure 7. Schematic overview of important cell types and functional units of the kidney. Adapted under the terms of the Creative Commons Attribution license.^[531] Copyright 2013, The Author(s). Published by Wiley (<https://staging.onlinelibrary.wiley.com/page/journal/20011326/open-access-license-and-copyright.html>). Figure created with BioRender.com.

Even though there is an urgent need for the development, characterization, and validation of new in vitro models suitable for a solid prediction of the hepatotoxic properties of chemicals and drugs, the use of stem cell-derived 3D models still remains a challenging task. Besides improving the model systems toward hepatic functionality, for instance, by optimizing hepatocyte polarization, oxygen and nutrient gradients and cell–cell interactions, it is also important to consider how simple or complex, for instance, in terms of the number of incorporated cell-types, a model should be to adequately predict a certain toxicological/pharmacological readout or address a specific scientific question. In order to get PSC-derived 3D liver models employed, i.e., accepted by industry and regulatory authorities, in the current test battery for hepatotoxicity, a proper standardization of the protocols and a comparison of the different protocols and models assessing the same adverse outcome across laboratories is urgently needed.

2.7. Kidney

Kidney functions are closely linked with homeostasis of the inner body milieu, electrolyte and fluid balance, acid base handling, and retention of amino acids. Furthermore, kidneys are major players in the excretion of water-soluble waste products and xenobiotics, toxins, and “end-products” such as uric acid. At the same time kidneys achieve retainment of serum proteins and glucose within the body, a process that requires numerous active transport processes.^[352] This plethora of functions is achieved through the interplay of different kidney cell types, i.e., podocytes, parietal epithelial, mesangial, glomerular endothelial, juxtaglomerular, specialized epithelial cells (proximal and distal tubules, loops of Henle, collecting ducts),

interstitial, endothelial, stromal, dendritic and stem cells, that are organized in structural units, denoted nephrons (**Figure 7**). At the one end of the nephron a filtration barrier, the glomerulus, produces a primary urine volume of 180 l per day into the Bowman’s capsule. This urine is further concentrated and processed within the renal tubular structures. The anatomy and transporter/ion channel distribution allows to distinguish five different nephron sections with individual functions, i.e., the proximal tubule, the thick part of Henle’s loop, the distal convolute, and the collecting ducts.^[353] The tubules are lined by at least 20 different epithelial cell types that are highly differentiated, linked through tight junctions and have a high oxygen consumption rate due to their metabolic activities, which demands constant high nutrition, oxygen, and energy supply. Which kidney structures transport renal malfunctions can be specified by shedding light on acute or chronic kidney injury, which are due to multiple causes with hypocirculatory, immune, and direct toxic effects being most frequent.^[354] Transient interruptions of adequate blood supply in the course of blood volume contractions or vasoconstriction are common reasons for acute kidney injury. These can originate from severe bleeding episodes or nonsteroidal anti-inflammatory drug applications, the latter inhibiting prostaglandin synthesis and abrogating the vasodilatory effects of endogenous prostaglandins thereby reducing glomerular blood flow.^[355] Some drugs are notorious for increasing the vascular tone with similar effects on blood flow especially on the afferent capillaries that enter the glomerular structures, e.g. calcineurin inhibitors often prescribed as immunosuppressive drugs in organ transplanted patients.^[356] These “hypocirculatory” events result in regional or complete kidney ischemia with cellular damage incited in those cells that are most dependent on energy and oxygen supply, the tubular cells, which respond with necrosis and apoptosis.

At the cellular level the kidneys have the potential to recover from such acute kidney injuries by tubular cell proliferation and endocycle-related tubular cell hypertrophy.^[357] Direct toxic effects of pharmaceutical compounds and environmental toxins are common phenomena and drug-induced kidney toxicity accounts for about 25% of the reported severe adverse drug reactions.^[358] Drug- or toxin-induced kidney damage might occur in different nephron sections. For example, the heavy metal mercury induces proximal tubule dysfunction due to its uptake by the organic anion transporters OAT1 and OAT3, which are preferably expressed in the proximal tubule.^[359] Fluoride yet acts on the ascending limb of the loop of Henle by interfering with chloride transport.^[360] On the contrary, kidney toxicity induced by amphotericin B mainly targets the distal tubule. This seems to be due to the impaired cellular repair mechanism at low urine pH values that counteracts toxicity in the proximal tubule due to a higher urine pH at this part of the nephron.^[361] Another phenomena in the kidney following tubular cell injury is an immunological response, such as tubulointerstitial cell infiltration. The infiltrating immune cells release inflammatory cytokines that propagate fibrosis on the one side, and are thought to coordinate tissue reparative processes on the other side.^[362]

Keeping the aforementioned mechanisms of acute kidney injury in mind with a large cellular repertoire at risk, toxicological studies have to address the aspects of cell-specific drug levels and adverse effects including phenotypic and functional alterations. The number of different cell types within the glomerulus, the tubular structures and tubulointerstitial compartment are even growing with the advent of single cell sequencing.^[363–365] Homogenous cell cultures of the respective cells have been established earlier. One success story in the early 2000s was the establishment of immortalized podocyte cells that grow or differentiate in dependence of environmental temperature.^[366] However, economics should balance testing efforts and therefore compound testing across the at least 26 individual renal cell types identified so far^[367] does not seem feasible – or physiological, as they are devoid of cell–cell interactions and higher complex organization. Modeling different functional nephron sections with their complex architectures including cell–cell interactions, presence of capillaries, differences in oxygen tensions and shear fluid stress in vitro remains challenging. To cover especially these complex context-dependent changes in cellular compartments, fibrogenic niches, capillaries, pericapillary cells, mesangium or due to differing oxygen tensions, most studies dealing with kidney toxicity combine in vitro with in vivo approaches. In vivo studies concerning kidney using rodents bear the drawback of interspecies differences^[368] when extrapolating to humans, and most former in vitro models do not picture the architectural complexity of the kidney. Here, stem cell technology has been offering a sky-rocketing development toward organotypic cultures including hiPSC-derived kidney organoids and adult stem cell-derived tubuloids bridging the gap between traditional 2D cultures and animal models.^[369] Although organoids contain a large variety of renal cells, they are still largely devoid of mesangial cells, immune cells, glomerular endothelium, principal and intercalated cells and their functionality has hardly been studied.^[369] One example of a valuable

development in the kidney organoid field is the establishment of reporter human pluripotent stem cell lines that encompass all kidney cell types of the glomerulus, proximal and distal tubule as well as an extensive endothelial network, and renal interstitium. These “whole kidney organoids” enable live assessment of kidney cell differentiation and organoid development in a toolbox format.^[370] For phenotypic screening including toxicity testing, renal organoid production was also brought to the next level by setting up a robotic platform for miniaturizing and speeding up kidney organoid formation in microwell formats for high-throughput screening.^[371] Some kidney organoids even produce renin,^[372] an endopeptidase synthesized by juxtaglomerular cells, which is crucial for blood pressure regulation. Such functional aspects are valuable additions to the descriptive nature of organoid cellular composition and structure. Protocols for kidney organoids derived from human inducible progenitor stem cells have proven successful to mimic late capillary loop stage nephrons on day 14 of cultures. Later on, some cells are not sufficiently supplied by oxygen and nutrients resulting in cell damage with ensuing fibrosis.^[373] Despite these achievements in cellular differentiation and organizational features at the nephron level, significant challenges remain. i) Kidney organoids represent a very immature, i.e., fetal kidney system.^[363] ii) Current protocols do not embrace the whole array of renal cells, especially heterogeneous stromal cell populations and the minimal requirement for kidney toxicity assessment is uncertain. iii) Functional vasculature and a common urinary collecting system are currently not depicted even in complex in vitro systems.^[374] iv) More “physiological” culture conditions, e.g., with varying fluid shear stress or oscillating pressure^[375] will be of paramount relevance to mimic the milieu of the kidney. Given the low oxygen tension in most parts of kidney tissue cell culture protocols with organoids also need to address the issue of reduced oxygen supply. Drug nephrotoxicity testing by kidney-on-a-chip testing has been adopted by some groups with experimental setups that also include fluid shear stress. Such test systems will likely revolutionize toxicity testing when they succeed to be standardized.^[376–379]

2.8. Intestine

The intestine is comprised of subsections with substantial anatomical and physiological heterogeneity in luminal pH, presence or abundance of cell types, and presence and composition of the microbiome. The intestine is an organ of superlatives: its epithelium is one of the fastest renewing tissues within the human body with a maximum cellular life span of 5 days.^[380] It harbors the largest pool of microbial communities, which is contained by a semipermeable epithelial barrier forming one of the largest interfaces between the endogenous and exogenous environment. To safeguard the uptake of exogenous compounds and to govern the host–microbiome interactions, vast numbers of immune cells reside along the gut, resulting in a major compartment of the immune system.^[381] Apart from its most commonly known tasks, the regulation of water balance, digestion of food and nutrient absorption, the intestine is recognized for its impact on overall physical and mental health with endocrine activity, immune regulatory functions, and

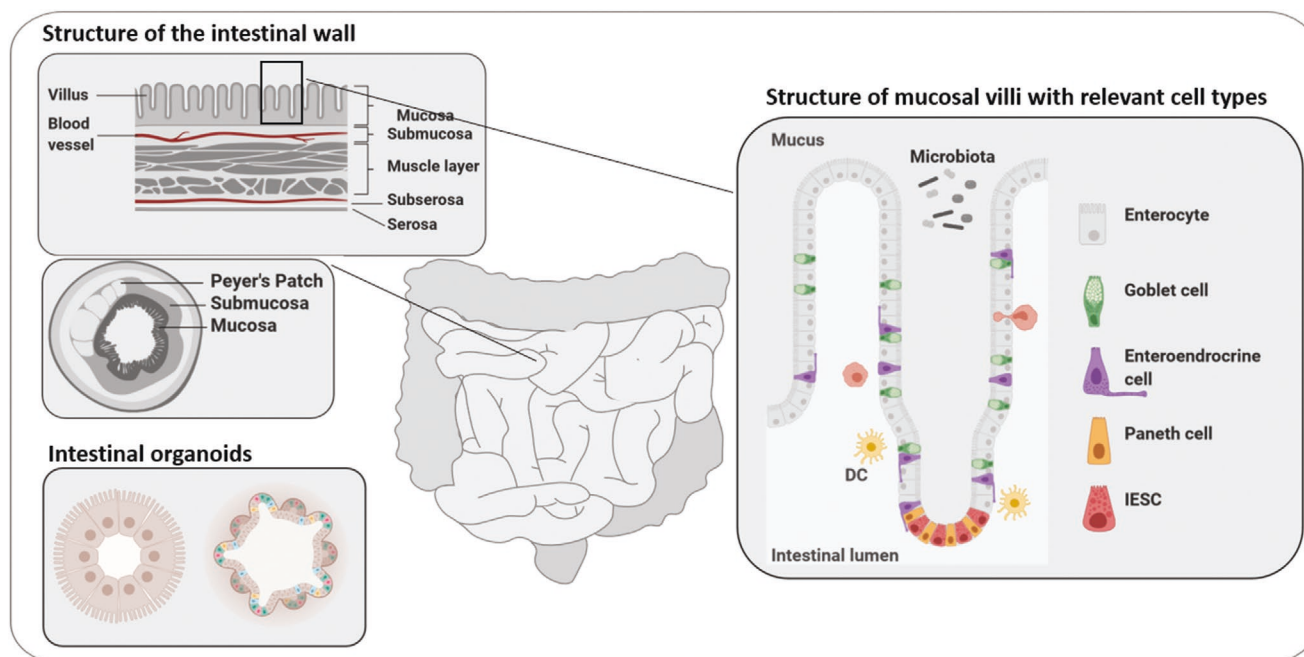


Figure 8. Structural and functional units of the intestine. Abbreviations: DC, dendritic cell; Mφ, macrophage; IESC, intestinal epithelial stem cell. Figure created with BioRender.com.

extensive neuronal network (reviewed in refs. [382,383]). Its basic structure folds into villi and crypts and is lined with a single layer of intestinal epithelial cells (IECs) of which enterocytes and goblet cells make up the majority, while Paneth cells, endocrine cells and Microfold cells account for the rest (**Figure 8**). All IECs develop from intestinal stem cell (ISC)-derived progenitors and differentiate while traveling along the crypt-villus axis.

This complexity of the intestine is challenging to mimic experimentally, as summarized by Costa and Ahluwalia.^[384] However, the availability of relevant intestinal models is indispensable. Intestinal disorders, e.g., intestinal cancer, inflammatory bowel disease and infections, affect millions of people worldwide and present a substantial economic and societal burden.^[385,386] Furthermore, oral toxicity testing is a requirement for pharmaceutical and chemical development.^[387,388] The oral route is preferred for the application of pharmaceuticals, but gastrointestinal adverse events (GI AE), e.g., diarrhea, abdominal pain, and nausea, are common side effects. Though hardly ever the reason for market removal or clinical attrition, AE can significantly affect treatment compliance.^[389–391] To facilitate and standardize noxae investigations, the OECD has specified test guidelines for rodent (e.g., TG 408)^[121] and non-rodent species (e.g., TG 409).^[392] Models of larger vertebrate species (e.g., dog and pig) as well as invertebrate organisms (e.g., zebrafish and *C. elegans*) are available, but the majority of studies is conducted in rodents. The most suitable way of exposure is based on the intended application and physicochemical properties of the test substance. To address questions in non-regulatory context, e.g., on intestinal inflammation, digestion, and the microbiome, specialized *in vivo* models are available (reviewed in refs. [393–395]). However, the predictive quality of animal models for intestinal effects in humans is increasingly disputed as substantial anatomical, biochemical, and

microbiological differences prevail.^[396–398] Especially the role of the microbiome has been neglected with regard to preclinical reproducibility and clinical translation efficacy, which might be a factor in the low congruence in drug toxicity testing between humans and other animals.^[9,399–401]

In context of the 3Rs, a variety of intestinal *in vitro* models has been developed in the last three decades, of which cancer-derived cell lines are the most commonly applied system.^[402–404] Although these cell lines are inherently diseased and do not fully match healthy tissue biochemically and genetically,^[404,405] good correlations to human tissue were found.^[406,407] Since then, highly sophisticated models have been developed by combining multiple cell types, mimicking the intestinal architecture, luminal flow or peristalsis, and even incorporating the microbiota.^[408–410] In this context, hypoxia has emerged as potentially important factor for intestinal systems. Unlike other organs, the intestine is characterized by a substantial heterogeneity in oxygen levels to a nearly anaerobic environment in the lumen (reviewed by Zeitouni et al.^[411]). Chen et al.^[412] have developed a scaffold-based 3D coculture model, where the oxygen tension can be adapted to create micro- to anaerobic conditions within the lumen. As the group demonstrated, the consideration of oxygen levels in intestinal models may affect their applicability especially for studies on host–microbial interactions.^[412–414] But also the toxicity of nanomaterials may change depending on the availability of oxygen.^[415] However, many of these elaborate models stagnate at a proof of concept stage with little or no routine application in toxicity testing. Whereas strong agreement exists on the suitability of transwell cultures over undifferentiated monocultures, studies failed to demonstrate a clear advantage of more complex models.^[416,417]

As GI AE still commonly occur at clinical stages and are frequent side effects of marketed drugs, the suitability and

adequacy of existing models needs to be considered. The use of stem cells is investigated to improve the predictive quality of *in vitro* models for toxicity testing. Different approaches are available: i) the use of ISCs of isolated intestinal crypts, and ii) ESCs or iPSCs, which result in the formation of self-organized 3D spheroids. The studies by Sato et al.^[418,419] are regarded as game changer in the field, as they enabled the long-term culture of primary intestinal cells in absence of mesenchymal tissue—until then the bottleneck for primary intestinal cultures.^[420] Methods for the targeted differentiation of human iPSC^[421] or murine ESCs^[422] into intestinal tissue further expanded the stem cell toolbox. It is noteworthy that the differentiation protocols for ESC and iPSC cultures are generally more complex and time intensive—requiring at least 28–34 days.^[421,423] They span three differentiation stages: i) to definitive endoderm, ii) to hindgut-like tissue, and iii) toward organoids resembling intestine-like tissue.^[421,423,424] In stem cell-derived organoids, all major IEC types are detectable, including enterocytes, goblet cells, Paneth cells, and endocrine cells. In iPSC-based models, ISC markers are only present after an extensive differentiation time.^[421] The resulting organoids were found to resemble fetal rather than mature adult tissue,^[425] which might be a critical limitation.^[426] To improve maturation, different approaches were reported, e.g., using interleukin 2,^[427] cell sorting,^[423,428] or *in vivo* engraftment.^[424,425]

Notwithstanding these limitations, stem cell-derived intestinal cultures have been applied for a range of research questions, including biological processes of intestinal tissue,^[429] organ development,^[430,431] intestinal pathologies,^[423] and to lesser extent the toxicity of xenobiotics.^[432,433] They appear to be a promising tool for the study of host–microbiome or host–pathogen interactions, using passive colonization^[434] or active microinjection into the lumen.^[435] Although these models were found to be suitable to investigate drug transport and metabolism, only few reports are available to date.^[436–439] Their limited application in exposure studies may be due to the organoids' physiology and morphology—a polarized status with the apical side facing inward. This restricts their suitability as the absorption of nutrients and drugs as well as the interaction with noxae and the microbiota are initiated from the apical side. Studies aimed to push these boundaries by luminal injection of organoids,^[435] establishment of flow through the lumen^[440] or development of “apical-out” organoids.^[441] Others have turned to approaches that break up the organoid structure to seed 2D barriers on transwells or microchips using the whole organoid^[442–444] or selected cell types.^[445,446]

Altogether, stem cells have the potential to greatly advance the field of intestinal research, including toxicity testing. Apart from the use of physiologically healthy tissue, patient-specific organoids may be developed to investigate intestinal disease development and treatment strategies.^[447] However, questions remain on the regional identity as well the maturity status of the stem cell-derived organoids.^[425,448] Undoubtedly, the intestine is important in itself, but its full impact only emerges in the interplay with other organs, e.g., the liver, the CNS, and the microbiome, which remains a shortcoming in these models.^[447] Although the protocols are described as “highly efficient” and “robust,”^[421,449] they greatly exceed the intricacy of most *in vitro*

systems. Their superiority over these established, less complex models for toxicity and safety evaluations remains to be demonstrated, and will likely determine their implementation rate and application range.

3. Genome Editing

Genome manipulation using zinc finger nucleases and TALENs^[450,451] realized insertion of genetic elements into specific sites of the genome. The CRISPR revolution^[452,453] substantially improved this procedure by making genome editing fairly easy to achieve. A comprehensive overview about the rapidly evolving field of applications and protocols of CRISPR/Cas and related genome editing tools is provided by the following review articles.^[454–456] Toxicology benefits from such genome editing approaches in several ways. Reporter lines with fluorescent or luminescent reporters under endogenous promoter control can be used for following stem cell differentiation and target cell toxicity, e.g., for neurons,^[457] kidney cells^[370] or CMs.^[458] Also, genetically encoded indicators, e.g., for calcium signaling, are useful tools for assessing calcium transients. These can be combined with other functional indicators as, e.g., for voltage. Such lines offer the possibility for functional studies in target cells without the use of dyes like Fura-2 and thus offer a great possibility for functional toxicity testing in high throughput formats using high content imaging.^[459,460]

Besides value in generation of stem cell reporter lines, genome editing techniques can also be used for disease modeling, in toxicology particularly relevant for studying gene–environmental interactions. Human PSC knockout lines or the targeted integration of specific mutations for the establishment of isogenic disease models is definitely of great significance for such applications with the combined effort of CRISPR in hiPSC-derived organoids representing cutting-edge toolsets.^[461–464]

Also, in mechanistic toxicology the CRISPR/Cas system has already proven its great value. CRISPR/Cas-based approaches identified genes critically involved in determining the toxicity of various chemicals, including arsenic trioxide, formaldehyde, and paraquat.^[465–467] For example, a CRISPR-based positive-selection screen identified the genes coding for CYP oxidoreductase, copper transporter ATP7A, and sucrose transporter SLC45A4, as critical mediators of paraquat-induced cell-death.^[466] Moreover, the study revealed CYP oxidoreductase as a major source for paraquat-induced oxidative stress. In another study, CRISPR/Cas technology was used to identify targets of anticancer small molecules by a mutagenesis scanning of essential genes.^[468] Hence, CRISPR/Cas-based functional genomic screening approaches are suitable to provide unprecedented mechanistic insight in modern toxicology and pharmacology.^[469]

Finally, combining genome editing with iPSC technology enables the integration of genetic variation, which may determine the interindividual susceptibility toward a given drug or xenobiotic, into modern toxicity testing. In fact, genome-wide association studies have contributed to the identification of a large number of SNPs and rare genetic variants in genes, amongst others encoding xenobiotic-metabolizing,

antioxidative, and DNA repair enzymes, which critically shape the adverse and/or beneficial outcome of a certain chemical or drug.^[470,471] A well-known example is the human cytochrome P450 (CYP) 2D6 monooxygenase, which accounts for the metabolism of ~15% of clinically used drugs, including opioids, beta-blockers, antiarrhythmics, and antidepressants.^[472] More than 110 SNPs, some of them displaying allele frequencies of up to 32%, have been identified in the CYP2D6 gene to either enhance, attenuate or completely abolish its catalytic activity.^[472] By generating iPSC-derived hepatocyte-like cells from hepatocytes of CYP2D6 polymorphic donors and subsequent analyses of the metabolism of CYP2D6 substrates, i.e., desipramine and tamoxifen, Takayama et al. demonstrated that the application of iPSC-derived cells with different SNPs is suitable to predict the interindividual differences in the metabolism of drugs and associated biological effects.^[473] In general, the use of donor cells with well-defined polymorphic genes for iPSC generation or the integration of mutations that resemble a certain SNP directly in the iPSC genome, would for sure improve the prediction of drug-induced cardiotoxicity, liver injury, neurotoxicity, and other frequent adverse drug reactions.^[474,475] Besides CYP2D6, potential candidates for such a screening approach are genetic variants of glutathione S-transferases T1 and M1, N-acetyltransferase 2, and mitochondrial DNA polymerase- γ . In fact, the mentioned gene variants are not only associated with a reduced catalytic activity of the respective enzyme, but also increase the individual's susceptibility to idiosyncratic drug-induced liver injury.^[476–478] Along the same line, missense variants of genes encoding retinoic acid receptor- γ , CYP2C19, and multidrug resistance protein-2 have been identified to enhance the risk for anthracycline-induced cardiotoxicity.^[479–481] Recent studies reporting the generation of genome-edited hiPSC-derived hepatocyte-like cells resembling CYP2C19 poor metabolizers,^[482] and CMs carrying the retinoic acid receptor- γ missense variant S427L and exhibiting the associated enhanced sensitivity toward doxorubicin treatment,^[481] illustrated the outstanding potential of genome-edited iPSC cells and organotypic models derived thereof for future compound testing in toxicology and pharmacology.

4. Biofabrication

4.1. Organ-on-a-Chip/Microphysiological Systems

Advances in material engineering and biofabrication enabled the development of highly adaptable microphysiological systems. Such systems integrate the biological complexity of 2D and 3D cell cultures with a defined spatial organization and a controlled microenvironment to closely mimic the in vivo situation, including naturalistic stimuli.^[483] Microphysiological systems, such as OOAC systems, aim at reconstructing the complex mechanical and biochemical cellular environment of the human body. By complementing and enhancing standard cell culture models, these systems have the potential to improve toxicity testing, accelerate drug discovery, improve diseases modeling, and reduce the use of animal models. The high adaptability of OOACs allows their application in many different cell, tissue, and organ models.^[483–487]

OOACs are extremely divers and customizable, thriving toward the reproducible generation of single cell cultures, cocultures or even complex 3D scaffolds. The option for the compartmentalized cultivation of different cell types and their supplementation with distinct media, massively extends the possible applications for such systems including organ cross-talk. At the same time, OOACs require a very little amount of cell material, media, and test substances, thereby reducing cultivation costs.

OOACs have already been adapted to fit a diversity of applications, such as modeling the BBB,^[191,488] assessing and driving cellular maturation,^[489,490] (patient-specific) modeling of diseases,^[491,492] mimicking the capillary formation,^[493] and the capillary flow,^[494] assessing the effect of stretch and strain on tissues^[495,496] and showing the applicability of OOACs for drug and substance exposures and development.^[378,490,495,497] OOACs have even been applied to study nanoparticles, which are currently of great public concern^[498] thus allowing to study indirect adverse effects. No large-scale toxicity testing has been done with OOACs, yet. However, smaller scale applications that aim at the establishment of testing platforms have been developed, mainly with human, but nonstem cell-based cell systems.^[376,498–500] Some toxicity biomarkers that have already been utilized with OOACs are summarized by Cong et al.^[376]

Even though the development of the OOACs for the field of toxicology is still heavily under construction, strong beneficial aspects can already be anticipated. The system will add complexity to the conventional cell culture models by recapitulating the physiological forces, increasing the reproducibility due to the controllable environment and improving long-term viability by enhancing the nutrient and waste flux within the samples. By implementing human-based stem cell systems, the OOACs could help reduce animal experiments by providing relevant indication of substance MoA and their impact on toxicity in humans, prior to animal experiments or clinical testing. Mechanistic questions concerning MoAs can be investigated with OOACs by including molecular and cellular readout methods. Coexposures and cocultures are also easily implementable due to the modularity of most OOAC systems. This increases the predictivity for example in drug design and substance testing. Maoz et al. developed a multichip system to model the BBB, which could be used to test the efficiency of drug flux across the BBB.^[488]

The evaluation of organ crosstalk in vitro was long thought to be beyond the bounds of possibility, but these fast-developing OOAC systems and the option to combine them to form integrated body-on-a-chip (BOC) systems have opened up the unique opportunity to make the impossible possible. In BOC systems, organ chips can be connected to transfer flow-through from one chip to another, thereby not only transferring nutrients, but also metabolites as well as waste- and by-products. BOCs could therefore give valuable insights into substance metabolism and toxicological effects across tissues.^[377,501] Tsamandouras et al. developed a fluidic platform that allows for the study of pharmacokinetics in a multiorgan setting.^[502] They successfully tested their platform using gut and liver interconnected chips. Another impressive study was performed by Oleaga et al.,^[503] who generated a functional model to evaluate human multiorgan toxicity under continuous flow conditions.

The group tested their four integrated modules, namely cardiac, muscle, neuronal and liver modules, for their pharmacological relevance, by evaluating their response to five drugs with known side effects. Their culture model exhibited a multiorgan toxicity response and the results were in general agreement with published toxicity data.

Besides the relatively high manufacturing costs and the usually medium to low scalability, one of the greater challenges with OOAC systems is the design of biocompatible materials that support cell survival and growth, and at the same time allow for the appropriate readouts. Although ready-to-use chips can be purchased from commercial manufacturers such as TissueUse GmbH, Mimetas, and EmulateBio, the majority of the research community working in this field produce their own chips. Many OOACs so far rely on imaging methods to assess the culture, which requires a clear and thin imaging surface. Silicon-based and polydimethylsiloxane are currently used in the field,^[504] however, the development is still striving forward. Additional points of consideration for substance testing in OOACs are the resistance of the material toward the uptake of the tested substances to avoid unintended postexposures, and the integration of endpoint-specific readouts needed for each specific model type. The material of the chip has to be biocompatible, meaning that it has to be resistant to leaching and must not interfere with the test compound thereby altering exposure concentrations. Moreover, most OOAC models are unsuitable for screening applications that require parallelization (96- and 384-well plates). However, high-throughput modules that hold up to 96 microfluidic structures have been established and are commercially available (OrganoPlate, Mimetas). These modules are compatible with automation and HTS instruments and have already been tested using SCs as cell source.^[505,506] In summary, OOAC and BOC models still need to be validated against established toxicity assays using a library of compounds with known toxicological effects. The biological functionalities of the chips must be highly reproducible and reliable to gain acceptance in toxicity studies. Moreover, they have to be user-friendly, cost-effective, and should be compatible with the standard cell culture equipment and HTS devices. Keeping this in mind, there are promising developments in the field of OOAC and BOC, that will very likely lead to a leap forward in toxicological testing, disease modeling and fundamental research.

4.2. Bioprinting

Bioprinting is a biofabrication technique to generate organotypic tissue or organ models. Goal of this strategy is to augment the complexity of the models to recapitulate the *in vivo* 3D physiology in more detail than manually generated 3D models. There are a variety of printing technologies available, the most popular of which are inkjet-based, extrusion-based, and laser-assisted.^[507] Each technology has its own advantages and disadvantages, e.g., concerning the bioink property requirements, printing resolution, possible cell densities, and shear stress effecting cell viability.^[507] The printing process itself is influenced by three main variables: i) the material (bioink), ii) the cell source, and iii) biomechanical factors, such as viscosity, elasticity, and stress relaxation.^[508–510] The right choice of

bioink is crucial to adequately mimic the cellular microenvironment.^[511] Widely used materials are natural hydrogels (gellan gum, alginate, chitosan) and synthetic hydrogels poly(ethylene oxide), poly(vinyl alcohol), poly(pro-pylene fumarate)). Their high water content and tunable properties render them ideal for 3D models.^[512–515] The choice of material heavily depends on the cell type and the intended 3D differentiation or growth process. Studies looking at bioprinted models often focus on basic cellular processes within the printed gels (i.e., cell survival, cell growth, and differentiation), or aim at the highest possible accuracy in recapitulating the physiological *in vivo* situation.^[516] Additionally, bioprinting rises great hopes to fabricate vascularized tissues, thereby diminishing the dead core effect. Bioprinting of ES- and hiPSC-based models has been intensively reviewed in Romanazzo et al.^[517] and Ong et al.,^[518] discussing advantages, limitations, and future perspectives. In brief, ESCs and iPSCs are ideal cell sources for bioprinting applications. They are available in virtually unlimited quantity and can proliferate and differentiate into various cell types within the bioink. Among others, SCs have been used for bioprinting of cardiac,^[519] neural,^[520] and hepatic^[521] tissues. An advanced printing strategy using a triculture of hiPSC-derived hepatic progenitors, human umbilical vein endothelial cells, and adipose-derived stem cells, developed an organotypic 3D liver model which recapitulates the native *in vivo* structure and is able to secrete products of liver metabolism.^[339] Challenges of SC bioprinting include the search for suitable bioinks supporting cell growth and differentiation, the need for printing parameters that the cells can withstand, and the optimization of long-term cultivation parameters allowing adequate *in- and efflux* of nutrients and oxygen. However, these challenges also apply for other cell sources like primary cells and immortalized cell lines. Regarding a toxicological application, bioprinted organotypic models are very rarely intended to work in a high-throughput context, which is mandatory for screening approaches. Moreover, the influx and efflux of the test substance within the hydrogel as well as interactions with hydrogel components are difficult to predict. Nevertheless, the automated printing process provides a higher degree of consistency and decreased batch-to-batch variations compared to manual 3D fabrication techniques, thereby increasing the reproducibility and reliability.

5. Challenges and Opportunities

With toxicology moving from apical endpoint testing in *vitro* to human cell-based *in vitro* assays, comprehensive cellular models are needed that cover the organ- and cell type-specific MoA for a large variety of toxicants. In this review article we discussed which structural and functional units of the skin, brain, thyroid system, lung, heart, liver, kidney, and intestine are targets of or mediate toxicity and disease and thus have to be modeled *in vitro* for human health prediction without using animals. Moreover, we summarized which preferably stem cell-based *in vitro* models have been developed for modeling the respective organs and evaluate their coverage of all necessary functional and structural criteria discussed above. Additionally, we highlighted organotypic models can be taken

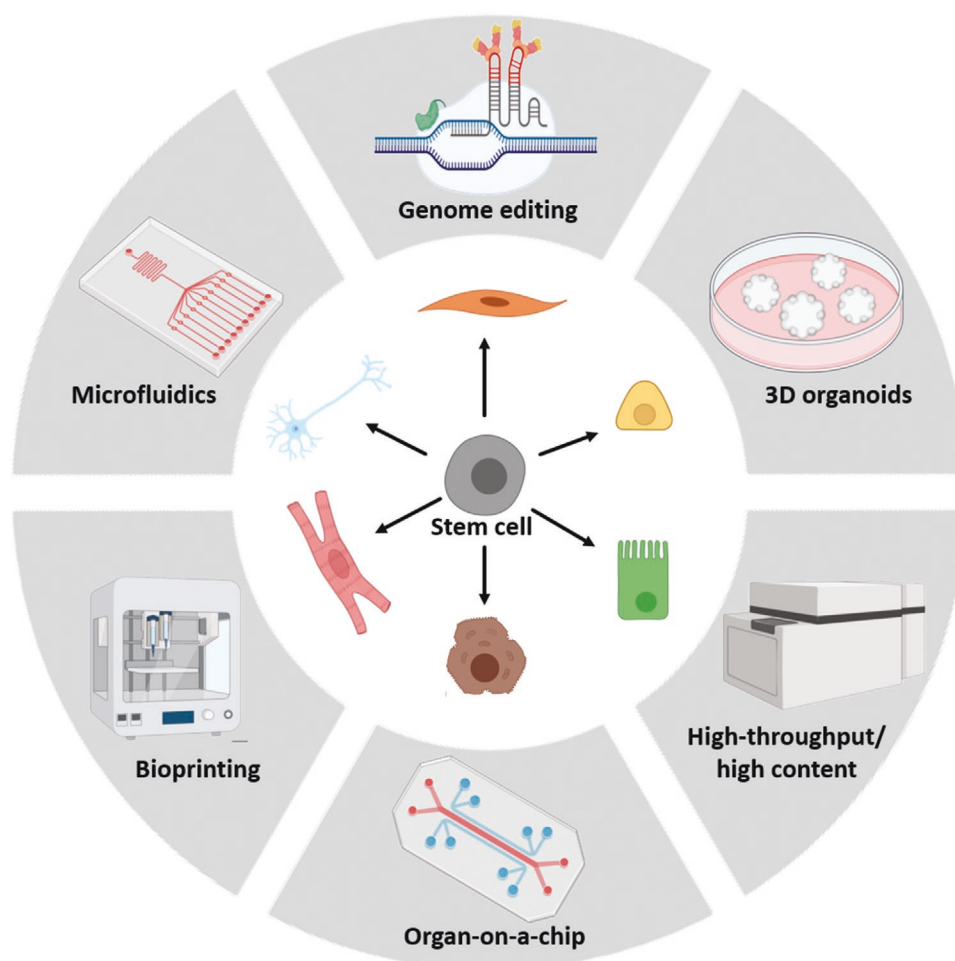


Figure 9. Opportunities of stem-cell based models for future toxicological testing. Figure created with BioRender.com.

to the next level using cutting edge technologies like genome editing and bioprinting in combination with sophisticated culturing methods (e.g., microfluidic systems and OOAC) with the final goal to facilitate high throughput/high content screening in the near future (**Figure 9**). Through targeted differentiation into multiple cell types, stem cell-based in vitro models can be accurate representations of human cell physiology and widely applied to study adversity on the cellular level in toxicity and disease without the necessity to rely on primary cells, tumor cell models or immortalized cell lines. They can even model functional properties of the organ like hormone production^[223,224] or generate complex 3D structures including multiple tissues and several functional units in one model.^[170,372] The use of human instead of rodent cell cultures substantially decreased the uncertainties arising from species differences concerning cellular functions, cytoarchitecture, hormonal regulation, and sensitivity to internal/external stimuli or toxicants.^[8,10,142,297,368] Moreover, hiPSCs-based techniques in combination with targeted genome editing enable the development of patient-specific disease models and the generation of cell type-specific transgenes in a human genetic background.^[226,453,457,458] However, human iPSC technology still struggles from issues such as variability among iPSC lines,^[522] genomic instability,^[523] low

reprogramming efficiency,^[524] which might be improved by keeping the cells under hypoxic conditions for a limited time span after reprogramming,^[525] preservation of an epigenetic memory of the parental cell,^[526] and difficulties in achieving a mature phenotype of iPSC-derived cells.^[46] Cultivation techniques have evolved quickly in the last decade with 2D monolayer models representing the classical approach which is well established and documented by broad literature. 2D cultivation is rather inexpensive, highly reproducible, and advantageous to study specific effects of factors on the individual cell. Coculturing of different cell types increases the complexity and predictivity of the model and enables the elucidation of cell-cell interactions. However, the still limited complexity, lack of cell-ECM interactions and the insufficient representation of the complex in vivo cytoarchitecture of the respective organ, suggests limitations of the predictivity of 2D models for toxicity testing. The development of 3D organoid techniques led to models exhibiting highly complex organotypic cytoarchitectures including cell-cell and cell-ECM interactions. Organoids enable the analysis of not only molecular but also functional readouts which strengthen the methods' clinical and toxicological relevance. However, increasing complexity comes with increased batch-to-batch variability, reduced reproducibility and

decreased testing throughput. Moreover, organoid culture is technically challenging and more expensive than 2D monolayer culture. Although organoids comprise a complex organotypic cytoarchitecture, they still represent immature developmental stages of the respective organ (reviewed by Logan et al.^[527]). Lack of complexity common to all organs reviewed comprises missing immune cells and blood vessels. First steps for the incorporation of microvascular structures^[101,185,186] and immune cells^[171,172,188,268,408] have been made. However, the complex crosstalk between organs, the involvement of the nervous, endocrine, and immunological system, as well as the impact of the blood flow and serum components are barely covered. Recent approaches are moving to the multiorgan level by tissue-on-a-chip methods enabling the evaluation of organ crosstalk in vitro.^[410,444,494,498,500]

6. Conclusion

From a toxicological point of view, making systemic predictions based on cellular effects is challenging. Therefore, the AOP concept was developed that helps placing cellular hazards into a systemic context.^[528,529] Advanced pharmac- and toxicokinetics including computational modeling are also needed to predict internal exposure as well as in vitro kinetics combining both by IVIVE (in vitro–in vivo extrapolation).^[530] Another obstacle is the necessary willingness to consider innovative methods in the field. Although it is known that the predictivity of animal studies is limited, the year-long experience conveys a feeling of security in contrast to the use of alternative approaches, which are perceived as bearing higher uncertainties due to their novelty.

Acknowledgements

J.T. and K.K. contributed equally to this work. The authors thank Thomas Nentwich and Jakob Fritsche for the biography pictures of Ellen Fritsche and Katharina Koch, respectively. This work was supported by the project CERST (Center for Alternatives to Animal Testing) of the Ministry for culture and science of the State of North-Rhine Westphalia, Germany (File No. 233-1.08.03.03-121972/131–1.08.03.03–121972), and the European Union's Horizon 2020 Research and Innovation Program, under the Grant Agreement No. 825759 of the ENDpoiNTs project. P.R.M. was supported by the German Research Foundation (funding code 97850925, SFB 854 project A1; GRK 2408 project 8, Grant Nos. ME-1365/7-2 and ME-1365/9-2).

Open access funding enabled and organized by Projekt DEAL.

Conflict of Interest

The authors declare no conflict of interest.

Keywords

3R, alternative methods, high throughput, human-induced pluripotent stem cells, organoids, risk assessment

Received: October 8, 2020
Revised: November 13, 2020
Published online:

- [1] F. S. Collins, G. M. Gray, J. R. Bucher, *Science* **2008**, 319, 906.
- [2] National Research Council (2007), *Toxicity Testing in the 21st Century: A Vision and a Strategy*, The National Academies Press, Washington, DC **2007**.
- [3] D. Krewski, M. E. Andersen, M. G. Tyshenko, K. Krishnan, T. Hartung, K. Boekelheide, J. F. Wambaugh, D. Jones, M. Whelan, R. Thomas, C. Yauk, T. Barton-Maclaren, I. Cote, *Arch. Toxicol.* **2020**, 94, 1.
- [4] L. Meigs, L. Smirnova, C. Rovida, M. Leist, T. Hartung, *ALTEX* **2018**, 35, 275.
- [5] T. Höfer, I. Gerner, U. Gundert-Remy, M. Liebsch, A. Schulte, H. Spielmann, R. Vogel, K. Wettig, *Arch. Toxicol.* **2004**, 78, 549.
- [6] K. Gassmann, J. Abel, H. Bothe, T. Haarmann-Stemmann, H. F. Merk, K. N. Quasthoff, T. D. Rockel, T. Schreiber, E. Fritsche, *Environ. Health Perspect.* **2010**, 118, 1571.
- [7] A. R. Green, M. V. King, S. E. Shortall, K. C. F. Fone, *Br. J. Pharmacol.* **2012**, 166, 1523.
- [8] A. Strasser, H. J. Wittmann, A. Buschauer, E. H. Schneider, R. Seifert, *Trends Pharmacol. Sci.* **2013**, 34, 13.
- [9] M. Clark, T. Steger-Hartmann, *Regul. Toxicol. Pharmacol.* **2018**, 96, 94.
- [10] S. Herculano-Houzel, *Brain. Behav. Evol.* **2011**, 78, 22.
- [11] A. Knight, *ALTEX* **2007**, 24, 320.
- [12] M. J. Waring, J. Arrowsmith, A. R. Leach, P. D. Leeson, S. Mandrell, R. M. Owen, G. Pairaudau, W. D. Pennie, S. D. Pickett, J. Wang, O. Wallace, A. Weir, *Nat. Rev. Drug Discovery* **2015**, 14, 475.
- [13] I. W. Y. Mak, N. Evaniew, M. Ghert, *Am. J. Transl. Res.* **2014**, 6, 114.
- [14] M. Leist, T. Hartung, *Arch. Toxicol.* **2013**, 87, 563.
- [15] S. H. Bennekou, *EFSA J.* **2019**, 17, e170711.
- [16] A. Lanzoni, A. F. Castoldi, G. E. Kass, A. Terron, G. De Seze, A. Bal-Price, F. Y. Bois, K. B. Deldcos, D. R. Doerge, E. Fritsche, T. Halldorsson, M. Kolossa-Gehring, S. Hougaard Bennekou, F. Koning, A. Lampen, M. Leist, E. Mantus, C. Rousselle, M. Siegrist, P. Steinberg, A. Tritscher, B. Van de Water, P. Vineis, N. Walker, H. Wallace, M. Whelan, M. Younes, *EFSA J.* **2019**, 17, e170712.
- [17] T. Hartung, *J. Toxicol. Environ. Health, Part B* **2010**, 13, 277.
- [18] National Academies of Sciences Engineering and Medicine, *Using 21st Century Science to Improve Risk-Related Evaluations*, National Academies Press, Washington, DC **2017**.
- [19] E. Fritsche, H. T. Hogberg, *Front. Toxicol.* **2020**, 2, 3.
- [20] J. D. Clark, *Ignition! An Informal History of Liquid Rocket Propellants*, Rutgers University Press, New Brunswick, NJ **1972**.
- [21] R. S. Thomas, M. B. Black, L. Li, E. Healy, T. M. Chu, W. Bao, M. E. Andersen, R. D. Wolfinger, *Toxicol. Sci.* **2012**, 128, 398.
- [22] W. Oehlert, *Cell Proliferation* **1973**, 6, 325.
- [23] D. Hanahan, R. A. Weinberg, *Cell* **2011**, 144, 646.
- [24] E. Fritsche, H. Alm, J. Baumann, L. Geerts, H. Hakansson, S. Masjosthusmann, H. Witters, *EFSA Support. Publ.* **2015**, 12, 186.
- [25] S. Masjosthusmann, M. Barenys, M. El-Gamal, L. Geerts, L. Gerosa, A. Gorreja, B. Kühne, N. Marchetti, J. Tigges, B. Viviani, H. Witters, E. Fritsche, *EFSA Support. Publ.* **2018**, 15, 125.
- [26] M. Barenys, E. Fritsche, *Toxicol. Sci.* **2018**, 165, 10.
- [27] K. Takahashi, K. Tanabe, M. Ohnuki, M. Narita, T. Ichisaka, K. Tomoda, S. Yamanaka, *Cell* **2007**, 131, 861.
- [28] G. N. Stacey, *Stem Cell Rev. Rep.* **2009**, 5, 301.
- [29] J. Munoz, T. Y. Low, Y. J. Kok, A. Chin, C. K. Frese, V. Ding, A. Choo, A. J. R. Heck, *Mol. Syst. Biol.* **2011**, 7, 550.
- [30] D. H. Phanstiel, J. Brumbaugh, C. D. Wenger, S. Tian, M. D. Probasco, D. J. Bailey, D. L. Swaney, M. A. Tervo, J. M. Bolin, V. Ruotti, R. Stewart, J. A. Thomson, J. J. Coon, *Nat. Methods* **2011**, 8, 821.
- [31] R. S. Lindoso, T. H. Kasai-Brunswick, G. Monnerat Cahli, F. Collino, A. Bastos Carvalho, A. C. Campos de Carvalho, A. Vieyra, *Cells* **2019**, 8, 703.
- [32] Y. Du, J. Wang, J. Jia, N. Song, C. Xiang, J. Xu, Z. Hou, X. Su, B. Liu, T. Jiang, D. Zhao, Y. Sun, J. Shu, Q. Guo, M. Yin, D. Sun, S. Lu, Y. Shi, H. Deng, *Cell Stem Cell* **2014**, 14, 394.

- [33] B. Hanger, A. Couch, L. Rajendran, D. P. Srivastava, A. C. Vernon, *Front. Psychiatry* **2020**, 11, 789.
- [34] T. A. Juopperi, W. R. Kim, C. H. Chiang, H. Yu, R. L. Margolis, C. A. Ross, G. L. Ming, H. Song, *Mol. Brain* **2012**, 5, 17.
- [35] M. A. Cayo, J. Cai, A. Delaforest, F. K. Noto, M. Nagaoka, B. S. Clark, R. F. Coltery, K. Si-Tayeb, S. A. Duncan, *Hepatology* **2012**, 56, 2163.
- [36] M. A. Lancaster, M. Renner, C. A. Martin, D. Wenzel, L. S. Bicknell, M. E. Hurler, T. Homfray, J. M. Penninger, A. P. Jackson, J. A. Knoblich, *Nature* **2013**, 501, 373.
- [37] T. Takahashi, *Annu. Rev. Pharmacol. Toxicol.* **2019**, 59, 447.
- [38] C. Olgasi, A. Cucci, A. Follenzi, *Int. J. Mol. Sci.* **2020**, 21, 6215.
- [39] P. de Carvalho Ribeiro, L. F. Oliveira, M. A. Filho, H. C. Caldas, *Stem Cells Int.* **2020**, 2020, 8894590.
- [40] J. Augustyniak, A. Bertero, T. Coccini, D. Baderna, L. Buzanska, F. Caloni, *J. Appl. Toxicol.* **2019**, 39, 1610.
- [41] M. Rauma, A. Boman, G. Johanson, *Adv. Drug Delivery Rev.* **2013**, 65, 306.
- [42] K. M. Albers, B. M. Davis, *Neuroscientist* **2007**, 13, 371.
- [43] A. A. H. Deniz, E. A. Abdik, H. Abdik, S. Aydın, F. Şahin, P. N. Taşlı, *Adv. Exp. Med. Biol.* **2020**, 1247, 157.
- [44] F. Oesch, E. Fabian, R. Landsiedel, *Arch. Toxicol.* **2018**, 92, 2411.
- [45] M. Gaur, M. Dobke, V. V. Lunyak, *Int. J. Mol. Sci.* **2017**, 18, 208.
- [46] N. Alépée, A. Bahinski, M. Daneshian, B. De Wever, E. Fritsche, A. Goldberg, J. Hansmann, T. Hartung, J. Haycock, H. T. Hogberg, L. Hoelting, J. M. Kelm, S. Kadereit, E. McVey, R. Landsiedel, M. Leist, M. Lübberstedt, F. Noor, C. Pellevoisin, D. Petersohn, U. Pfannenbecker, K. Reisinger, T. Ramirez, B. Rothen-Rutishauser, M. Schäfer-Korting, K. Zeilinger, M. G. Zurich, *ALTEX* **2014**, 31, 441.
- [47] C. Riebeling, A. Luch, T. Tralau, *Exp. Dermatol.* **2018**, 27, 526.
- [48] H. Niehues, J. A. Bouwstra, A. El Ghalbzouri, J. M. Brandner, P. L. J. M. Zeeuwen, E. H. van den Bogaard, *Exp. Dermatol.* **2018**, 27, 501.
- [49] S. H. Mathes, H. Ruffner, U. Graf-Hausner, *Adv. Drug Delivery Rev.* **2014**, 69–70, 81.
- [50] C. S. Pridgeon, C. Schlott, M. W. Wong, M. B. Heringa, T. Heckel, J. Leedale, L. Launay, V. Gryshkova, S. Przyborski, R. N. Bearon, E. L. Wilkinson, T. Ansari, J. Greenman, D. F. G. Hendriks, S. Gibbs, J. Sidaway, R. L. Sison-Young, P. Walker, M. J. Cross, B. K. Park, C. E. P. Goldring, *Arch. Toxicol.* **2018**, 92, 557.
- [51] Council of the European Union and the European Parliament, Directive 2003/15/EC of the European Parliament and of the Council of 27 February 2003 Amending Council Directive 76/768/EEC on the Approximation of the Laws of the Member States Relating to Cosmetic Products, **2003**.
- [52] OECD (2020), Test No. 471: *Bacterial Reverse Mutation Test*, OECD Publishing, Paris **2020**.
- [53] OECD (1997), Test No. 476: *In Vitro Mammalian Cell Gene Mutation Test*, OECD Publishing, Paris **1997**.
- [54] OECD (2016), Test No. 473: *In Vitro Mammalian Chromosomal Aberration Test*, OECD Publishing, Paris **2016**.
- [55] G. Ates, T. Y. Doktorova, M. Pauwels, V. Rogiers, *Mutagenesis* **2014**, 29, 115.
- [56] D. Kirkland, M. Aardema, L. Henderson, L. Müller, *Mutat. Res., Genet. Toxicol. Environ. Mutagen.* **2005**, 584, 1.
- [57] D. Kirkland, M. Aardema, L. Müller, M. Hayashi, *Mutat. Res., Genet. Toxicol. Environ. Mutagen.* **2006**, 608, 29.
- [58] E. J. Matthews, N. L. Kruhlak, M. C. Cimino, R. D. Benz, J. F. Contrera, *Regul. Toxicol. Pharmacol.* **2006**, 44, 83.
- [59] E. J. Matthews, N. L. Kruhlak, M. C. Cimino, R. D. Benz, J. F. Contrera, *Regul. Toxicol. Pharmacol.* **2006**, 44, 97.
- [60] V. Rogiers, M. Pauwels, *Curr. Probl. Dermatol.* **2008**, 36, 129.
- [61] V. Rogiers, M. Pauwels, *Curr. Probl. Dermatol.* **2008**, 36, XVII.
- [62] V. Rogiers, M. Pauwels, *Curr. Probl. Dermatol.* **2008**, 36, 58.
- [63] V. Rogiers, M. Pauwels, *Curr. Probl. Dermatol.* **2008**, 36, 1.
- [64] V. Rogiers, M. Pauwels, *Curr. Probl. Dermatol.* **2008**, 36, 29.
- [65] G. Speit, *Mutat. Res., Genet. Toxicol. Environ. Mutagen.* **2009**, 678, 108.
- [66] EU SCHER/SCENIHR/SCCP, Risk Assessment Methodologies and Approaches for Genotoxic and Carcinogenic Substances, **2009**.
- [67] P. Fowler, R. Smith, K. Smith, J. Young, L. Jeffrey, D. Kirkland, S. Pfuhler, P. Carmichael, *Mutat. Res., Genet. Toxicol. Environ. Mutagen.* **2012**, 747, 104.
- [68] P. Fowler, R. Smith, K. Smith, J. Young, L. Jeffrey, P. Carmichael, D. Kirkland, S. Pfuhler, *Mutat. Res., Genet. Toxicol. Environ. Mutagen.* **2014**, 767, 28.
- [69] D. Kirkland, S. Pfuhler, D. Tweats, M. Aardema, R. Corvi, F. Darroudi, A. Elhajouji, H. Glatt, P. Hastwell, M. Hayashi, P. Kasper, S. Kirchner, A. Lynch, D. Marzin, D. Maurici, J. R. Meunier, L. Müller, G. Nohynek, J. Parry, E. Parry, V. Thybaud, R. Tice, J. van Benthem, P. Vanparys, P. White, *Mutat. Res., Genet. Toxicol. Environ. Mutagen.* **2007**, 628, 31.
- [70] D. Kirkland, L. Reeve, D. Gatehouse, P. Vanparys, *Mutat. Res., Genet. Toxicol. Environ. Mutagen.* **2011**, 721, 27.
- [71] S. Pfuhler, A. Kirst, M. Aardema, N. Banduhn, C. Goebel, D. Araki, M. Costabel-Farkas, E. Dufour, R. Fautz, J. Harvey, N. J. Hewitt, J. Hibatallah, P. Carmichael, M. Macfarlane, K. Reisinger, J. Rowland, F. Schellau, A. Schepky, J. Scheel, *Regul. Toxicol. Pharmacol.* **2010**, 57, 315.
- [72] S. Pfuhler, M. Fellows, J. Van Benthem, R. Corvi, R. Curren, K. Dearfield, P. Fowler, R. Frötschl, A. Elhajouji, L. L. e Hégarat, T. Kasamatsu, H. Kojima, G. Ouédraogo, A. Scott, G. Speit, *Mutat. Res., Genet. Toxicol. Environ. Mutagen.* **2011**, 723, 101.
- [73] T. Y. Doktorova, M. Pauwels, M. Vinken, T. Vanhaecke, V. Rogiers, *Crit. Rev. Toxicol.* **2012**, 42, 91.
- [74] T. Y. Doktorova, G. Ates, M. Vinken, T. Vanhaecke, V. Rogiers, *T. Vitro*, **2014**, 28, 54.
- [75] P. Vanparys, R. Corvi, M. J. Aardema, L. Gribaldo, M. Hayashi, S. Hoffmann, L. Schechtman, *Mutat. Res., Genet. Toxicol. Environ. Mutagen.* **2012**, 744, 111.
- [76] OECD (2004), Test No. 428: *Skin Absorption: In Vitro Method*, OECD Publishing, Paris **2004**.
- [77] OECD (2018), Test No. 442D: *In Vitro Skin Sensitisation: ARE-Nrf2 Luciferase Test Method*, OECD Publishing, Paris **2018**.
- [78] OECD (2016), Test No. 442E: *In Vitro Skin Sensitisation*, OECD Publishing, Paris **2016**.
- [79] OECD (2013), Test No. 431: *In Vitro Skin Corrosion: Reconstructed Human Epidermis (RHE) Test Method*, OECD Publishing, Paris **2013**.
- [80] OECD (2019), Test No. 439: *In Vitro Skin Irritation: Reconstructed Human Epidermis Test Method*, OECD Guidelines for the Testing of Chemicals, Section 4, OECD Publishing, Paris **2019**.
- [81] A. Almeida, B. Sarmento, F. Rodrigues, *Int. J. Pharm.* **2017**, 519, 178.
- [82] C. Götz, R. Pfeiffer, J. Tigges, V. Blatz, C. Jäckh, E. M. Freytag, E. Fabian, R. Landsiedel, H. F. Merk, J. Krutmann, R. J. Edwards, C. Pease, C. Goebel, N. Hewitt, E. Fritsche, *Exp. Dermatol.* **2012**, 21, 358.
- [83] B. Sarmento, F. Andrade, S. B. Da Silva, F. Rodrigues, J. Das Neves, D. Ferreira, *Expert Opin. Drug Metab. Toxicol.* **2012**, 8, 607.
- [84] S. Gordon, M. Daneshian, J. Bouwstra, F. Caloni, S. Constant, D. E. Davies, G. Dandekar, C. A. Guzman, E. Fabian, E. Haltner, T. Hartung, N. Hasiwa, P. Hayden, H. Kandarova, S. Khare, H. F. Krug, C. Kneuer, M. Leist, G. Lian, U. Marx, M. Metzger, K. Ott, P. Prieto, M. S. Roberts, E. L. Roggen, T. Tralau, C. Van Den Braak, H. Walles, C. M. Lehr, *ALTEX* **2015**, 32, 327.
- [85] C. Duval, C. Chagnoleau, F. Pouradier, P. Sextius, E. Condom, F. Bernerd, *Tissue Eng., Part C* **2012**, 18, 947.
- [86] I. J. Kosten, S. W. Spiekstra, T. D. de Gruij, S. Gibbs, *Toxicol. Appl. Pharmacol.* **2015**, 287, 35.
- [87] D. Y. S. Chau, C. Johnson, S. Macneil, J. W. Haycock, A. M. Ghaemmaghami, *Biofabrication* **2013**, 5, 035011.

- [88] P. L. Tremblay, F. Berthod, L. Germain, F. A. Auger, *J. Pharmacol. Exp. Ther.* **2005**, 315, 510.
- [89] M. Matsusaki, K. Fujimoto, Y. Shirakata, S. Hirakawa, K. Hashimoto, M. Akashi, *J. Biomed. Mater. Res., Part A* **2015**, 103, 3386.
- [90] T. Akagi, M. Nagura, A. Hiura, H. Kojima, M. Akashi, *Tissue Eng., Part A* **2017**, 23, 481.
- [91] S. Huang, Y. Xu, C. Wu, D. Sha, X. Fu, *Biomaterials* **2010**, 31, 5520.
- [92] M. Michel, N. L'Heureux, R. Pouliot, W. Xu, F. A. Auger, L. Germain, *In Vitro Cell. Dev. Biol.: Anim.* **1999**, 35, 318.
- [93] S. Lönnqvist, K. Briheim, G. Kratz, *Toxicol. Mech. Methods* **2016**, 26, 82.
- [94] A. Petrova, A. Celli, L. Jacquet, D. Dafou, D. Crumrine, M. Hupe, M. Arno, C. Hobbs, A. Cvoro, P. Karagiannis, L. Devito, R. Sun, L. C. Adame, R. Vaughan, J. A. McGrath, T. M. Mauro, D. Ilic, *Stem Cell Rep.* **2014**, 2, 675.
- [95] H. E. Abaci, Z. Guo, Y. Doucet, J. Jacków, A. Christiano, *Exp. Biol. Med.* **2017**, 242, 1657.
- [96] M. Itoh, M. Kiuru, M. S. Cairo, A. M. Christiano, *Proc. Natl. Acad. Sci. USA* **2011**, 108, 8797.
- [97] M. Itoh, N. Umegaki-Arao, Z. Guo, L. Liu, C. A. Higgins, A. M. Christiano, *PLoS One* **2013**, 8, 77673.
- [98] N. Umegaki-Arao, A. M. G. Pasmooij, M. Itoh, J. E. Cerise, Z. Guo, B. Levy, A. Gostyrski, L. R. Rothman, M. F. Jonkman, A. M. Christiano, *Sci. Transl. Med.* **2014**, 6, 264ra164.
- [99] K. Gledhill, Z. Guo, N. Umegaki-Arao, C. A. Higgins, M. Itoh, A. M. Christiano, *PLoS One* **2015**, 10, 0136713.
- [100] Y. Kim, N. Park, Y. A. Rim, Y. Nam, H. Jung, K. Lee, J. H. Ju, *Stem Cell Res. Ther.* **2018**, 9, 217.
- [101] H. E. Abaci, Z. Guo, A. Coffman, B. Gillette, W. Lee, S. K. Sia, A. M. Christiano, *Adv. Healthcare Mater.* **2016**, 5, 1800.
- [102] Y. Li, M. Liu, S.-T. Yang, *World J. Stem Cells* **2014**, 6, 1.
- [103] Y. Li, T. Ma, *J. Hematol. Malign.* **2011**, 1, 35.
- [104] A. Pupovac, B. Senturk, C. Griffoni, K. Maniura-Weber, M. Rottmar, S. L. McArthur, *Adv. Healthcare Mater.* **2018**, 7, 1701405.
- [105] A. Thélou, S. Catoire, S. Kerdine-Römer, *Toxicol. In Vitro* **2020**, 62, 104691.
- [106] J. Lee, C. C. Rabbani, H. Gao, M. R. Steinhart, B. M. Woodruff, Z. E. Pflum, A. Kim, S. Heller, Y. Liu, T. Z. Shipchandler, K. R. Koehler, *Nature* **2020**, 582, 399.
- [107] V. S. Thakoersing, G. S. Gooris, A. Mulder, M. Rietveld, A. E. I. Ghalbzouri, J. A. Bouwstra, *Tissue Eng., Part C* **2012**, 18, 1.
- [108] S. Schreiber, A. Mahmoud, A. Vuia, M. K. Rübbecke, E. Schmidt, M. Schaller, H. Kandárová, A. Haberland, U. F. Schäfer, U. Bock, H. C. Korting, M. Liebsch, M. Schäfer-Korting, *Toxicol. In Vitro* **2005**, 19, 813.
- [109] F. P. Schmook, J. G. Meingassner, A. Billich, *Int. J. Pharm.* **2001**, 215, 51.
- [110] R. Koh, I. Szevényi, B. Lee, S. L. I. J. Denil, S. Y. J. Lim, P. A. Benny, N. Grasset, B. K. Tan, E. B. Lane, *J. Invest. Dermatol.* **2020**, 140, 235.
- [111] A. Carreau, B. E. I. Hafny-Rahbi, A. Matejuk, C. Grillon, C. Kieda, *J. Cell. Mol. Med.* **2011**, 15, 1239.
- [112] W. Wang, C. P. Winlove, C. C. Michel, *J. Physiol.* **2003**, 549, 855.
- [113] K. R. Rivera, M. A. Yokus, P. D. Erb, V. A. Pozdin, M. Daniele, *Analyst* **2019**, 144, 3190.
- [114] A. Mieremet, A. Vázquez García, W. Boiten, R. van Dijk, G. Gooris, J. A. Bouwstra, A. El Ghalbzouri, *Sci. Rep.* **2019**, 9, 7811.
- [115] E. Fröhlich, E. Roblegg, *Toxicology* **2012**, 291, 10.
- [116] G. R. Betton, *Cell Biol. Toxicol.* **2013**, 29, 321.
- [117] OECD (2002), *Test No. 420: Acute Oral Toxicity – Fixed Dose Procedure*, OECD Publishing, Paris **2002**.
- [118] OECD (2002), *Test No. 423: Acute Oral Toxicity – Acute Toxic Class Method*, OECD Publishing, Paris **2002**.
- [119] OECD (2008), *Test No. 425: Acute Oral Toxicity: Up-and-Down Procedure*, OECD Publishing, Paris **2008**.
- [120] OECD (2008), *Test No. 407: Repeated Dose 28-Day Oral Toxicity Study in Rodents*, OECD Publishing, Paris **2008**.
- [121] OECD (2018), *Test No. 408: Repeated Dose 90-Day Oral Toxicity Study in Rodents*, OECD Publishing, Paris **2018**.
- [122] A. Rodríguez-Lara, M. D. Mesa, J. Aragón-Vela, R. A. Casuso, C. C. Vázquez, J. M. Zúñiga, J. R. Huertas, *Nutrients* **2019**, 11, 2133.
- [123] J. N. Norton, L. A. Rylander, J. L. Richards, *Toxicol. In Vitro* **1995**, 9, 67.
- [124] M. Klausner, S. Ayehunie, B. A. Breyfogle, P. W. Wertz, L. Bacca, J. Kubilus, *Toxicol. In Vitro* **2007**, 21, 938.
- [125] F. Zanetti, A. Sewer, C. Mathis, A. R. Iskandar, R. Kostadinova, W. K. Schlage, P. Leroy, S. Majeed, E. Guedj, K. Trivedi, F. Martin, A. Elamin, C. Merg, N. V. Ivanov, S. Frentzel, M. C. Peitsch, J. Hoeng, *Chem. Res. Toxicol.* **2016**, 29, 1252.
- [126] L. Pindáková, V. Kašpárková, K. Kejlová, M. Dvořáková, D. Krsek, D. Jírová, L. Kašparová, *Int. J. Pharm.* **2017**, 527, 12.
- [127] A. Dongari-Bagtzoglou, H. Kashleva, *Nat. Protoc.* **2006**, 1, 2012.
- [128] K. Moharamzadeh, I. M. Brook, A. M. Scutt, M. H. Thornhill, R. Van Noort, *J. Dent.* **2008**, 36, 331.
- [129] M. B. Kautsky, P. Fleckman, B. A. Dale, *J. Invest. Dermatol.* **1995**, 104, 224.
- [130] D. G. Nguyen, S. L. Pentoney, *Drug Discovery Today Technol.* **2017**, 23, 37.
- [131] T. Kumamoto, C. Hanashima, *Neurosci. Res.* **2014**, 86, 37.
- [132] S. M. G. Braun, S. Jessberger, *Development* **2014**, 141, 1983.
- [133] P. S. Eriksson, E. Perfilieva, T. Björk-Eriksson, A. M. Alborn, C. Nordborg, D. A. Peterson, F. H. Gage, *Nat. Med.* **1998**, 4, 1313.
- [134] A. Aranda-Anzaldo, *Commun. Integr. Biol.* **2012**, 5, 134.
- [135] C. S. von Bartheld, J. Bahney, S. Herculanu-Houzel, *J. Comp. Neurol.* **2016**, 524, 3865.
- [136] K. A. Nave, H. B. Werner, *Annu. Rev. Cell Dev. Biol.* **2014**, 30, 503.
- [137] L. Ben Haim, D. H. Rowitch, *Nat. Rev. Neurosci.* **2016**, 18, 31.
- [138] D. Nayak, T. L. Roth, D. B. McGavern, *Annu. Rev. Immunol.* **2014**, 32, 367.
- [139] W. Zheng, *J. Toxicol., Clin. Toxicol.* **2001**, 39, 711.
- [140] S. Weis, A. Büttner, in *Handbook of Clinical Neurology*, Elsevier B.V., Amsterdam **2018**, pp. 181–192.
- [141] N. A. Oberheim, T. Takano, X. Han, W. He, J. H. C. Lin, F. Wang, Q. Xu, J. D. Wyatt, W. Pilcher, J. G. Ojemann, B. R. Ransom, S. A. Goldman, M. Nedergaard, *J. Neurosci.* **2009**, 29, 3276.
- [142] J. DeFelipe, L. Alonso-Nanclares, J. I. Arellano, *J. Neurocytol.* **2002**, 31, 299.
- [143] M. Schmidt, B. Raghavan, V. Müller, T. Vogl, G. Fejer, S. Tchaptchet, S. Keck, C. Kalis, P. J. Nielsen, C. Galanos, J. Roth, A. Skerra, S. F. Martin, M. A. Freudenberger, M. Goebeler, *Nat. Immunol.* **2010**, 11, 814.
- [144] K. Dach, F. Bendt, U. Huebenthal, S. Giersiefer, P. J. Lein, H. Heuer, E. Fritsche, *Sci. Rep.* **2017**, 7, 44861.
- [145] J. Klose, J. Tigges, S. Masjosthusmann, K. Schmuck, F. Bendt, U. Huebenthal, P. Petzsch, K. Köhrer, K. Koch, E. Fritsche, *ALTEX* **2020**, DOI 10.14573/altex.2007201.
- [146] S. C. Zhang, M. Wernig, I. D. Duncan, O. Brüstle, J. A. Thomson, *Nat. Biotechnol.* **2001**, 19, 1129.
- [147] H. J. Rhee, A. H. Shaib, K. Rehbach, C. K. Lee, P. Seif, C. Thomas, E. Gideons, A. Guenther, T. Krutenko, M. Heibisch, M. Peitz, N. Brose, O. Brüstle, J. S. Rhee, *Cell Rep.* **2019**, 27, 2212.
- [148] Y. Shi, P. Kirwan, F. J. Livesey, *Nat. Protoc.* **2012**, 7, 1836.
- [149] R. Nehme, E. Zuccaro, S. D. Ghosh, C. Li, J. L. Sherwood, O. Pietilainen, L. E. Barrett, F. Limone, K. A. Worringer, S. Kommineni, Y. Zang, D. Cacchiarelli, A. Meissner, R. Adolfsson, S. Haggarty, J. Madison, M. Muller, P. Arlotta, Z. Fu, G. Feng, K. Eggan, *Cell Rep.* **2018**, 23, 2509.
- [150] M. Frega, S. H. C. Van Gestel, K. Linda, J. Van Der Raadt, J. Keller, J. R. Van Rhijn, D. Schubert, C. A. Albers, N. N. Kasri, *J. Vis. Exp.* **2017**, 8, 54900.

- [151] N. Yang, S. Chanda, S. Marro, Y. H. Ng, J. A. Janas, D. Haag, C. E. Ang, Y. Tang, Q. Flores, M. Mall, O. Wapinski, M. Li, H. Ahlenius, J. L. Rubenstein, H. Y. Chang, A. A. Buylia, T. C. Südhof, M. Wernig, *Nat. Methods* **2017**, *14*, 621.
- [152] S. M. Chambers, C. A. Fasano, E. P. Papapetrou, M. Tomishima, M. Sadelain, L. Studer, *Nat. Biotechnol.* **2009**, *27*, 275.
- [153] L. Nimtz, J. Hartmann, J. Tigges, S. Masjosthusmann, M. Schmuck, E. Keßel, S. Theiss, K. Köhrer, P. Petzsch, J. Adjaye, C. Wigmann, D. Wiczorek, B. Hildebrandt, F. Bendt, U. Hübenthal, G. Brockerhoff, E. Fritsche, *Stem Cell Res.* **2020**, *45*, 101761.
- [154] M. Hofrichter, L. Nimtz, J. Tigges, Y. Kabiri, F. Schröter, B. Royer-Pokora, B. Hildebrandt, M. Schmuck, A. Epanchintsev, S. Theiss, J. Adjaye, J. M. Egly, J. Krutmann, E. Fritsche, *Stem Cell Res.* **2017**, *25*, 72.
- [155] B. Y. Hu, J. P. Weick, J. Yu, L. X. Ma, X. Q. Zhang, J. A. Thomson, S. C. Zhang, *Proc. Natl. Acad. Sci. USA* **2010**, *107*, 4335.
- [156] J. A. Harrill, T. Freudenrich, K. Wallace, K. Ball, T. J. Shafer, W. R. Mundy, *Toxicol. Appl. Pharmacol.* **2018**, *354*, 24.
- [157] E. Rempel, L. Hoelting, T. Waldmann, N. V. Balmer, S. Schildknecht, M. Grinberg, J. A. Das Gaspar, V. Shinde, R. Stöber, R. Marchan, C. van Thriel, J. Liebing, J. Meisig, N. Blüthgen, A. Sachinidis, J. Rahnenführer, J. G. Hengstler, M. Leist, *Arch. Toxicol.* **2015**, *89*, 1599.
- [158] V. Shinde, S. Klima, P. S. Sureshkumar, K. Meganathan, S. Jagtap, E. Rempel, J. Rahnenführer, J. G. Hengstler, T. Waldmann, J. Hescheler, M. Leist, A. Sachinidis, *J. Vis. Exp.* **2015**, 52333.
- [159] N. V. Balmer, M. K. Weng, B. Zimmer, V. N. Ivanova, S. M. Chambers, E. Nikolaeva, S. Jagtap, A. Sachinidis, J. Hescheler, T. Waldmann, M. Leist, *Hum. Mol. Genet.* **2012**, *21*, 4104.
- [160] F. Pistollato, J. Louise, B. Scelfo, M. Mennecozzi, B. Accordi, G. Basso, J. A. Gaspar, D. Zagoura, M. Barilari, T. Palosaari, A. Sachinidis, S. Bremer-Hoffmann, *Toxicol. Appl. Pharmacol.* **2014**, *280*, 378.
- [161] S. Masjosthusmann, C. Siebert, U. Hübenthal, F. Bendt, J. Baumann, E. Fritsche, *Chemosphere* **2019**, *235*, 447.
- [162] M. Barenys, K. Gassmann, C. Baksmeier, S. Heinz, I. Reverte, M. Schmuck, T. Temme, F. Bendt, T. C. Zschauer, T. D. Rockel, K. Unfried, W. Wätjen, S. M. Sundaram, H. Heuer, M. T. Colomina, E. Fritsche, *Arch. Toxicol.* **2017**, *91*, 827.
- [163] K. Gassmann, T. Schreiber, M. M. L. Dingemans, G. Krause, C. Roderigo, S. Giersiefer, J. Schuwald, M. Moors, K. Unfried, Å. Bergman, R. H. S. Westerink, C. R. Rose, E. Fritsche, *Arch. Toxicol.* **2014**, *88*, 1537.
- [164] M. S. Wilson, J. R. Graham, A. J. Ball, *Neurotoxicology* **2014**, *42*, 33.
- [165] M. A. Lancaster, N. S. Corsini, S. Wolfinger, E. H. Gustafson, A. W. Phillips, T. R. Burkard, T. Otani, F. J. Livesey, J. A. Knoblich, *Nat. Biotechnol.* **2017**, *35*, 659.
- [166] A. M. Pasca, S. A. Sloan, L. E. Clarke, Y. Tian, C. D. Makinson, N. Huber, C. H. Kim, J. Y. Park, N. A. O'Rourke, K. D. Nguyen, S. J. Smith, J. R. Huguenard, D. H. Geschwind, B. A. Barres, S. P. Pasca, *Nat. Methods* **2015**, *12*, 671.
- [167] X. Qian, H. N. Nguyen, M. M. Song, C. Hadiono, S. C. Ogden, C. Hammack, B. Yao, G. R. Hamersky, F. Jacob, C. Zhong, K. J. Yoon, W. Jeang, L. Lin, Y. Li, J. Thakor, D. A. Berg, C. Zhang, E. Kang, M. Chickering, D. Nauen, C. Y. Ho, Z. Wen, K. M. Christian, P. Y. Shi, B. J. Maher, H. Wu, P. Jin, H. Tang, H. Song, G. L. Ming, *Cell* **2016**, *165*, 1238.
- [168] C. Luo, M. A. Lancaster, R. Castanon, J. R. Nery, J. A. Knoblich, J. R. Ecker, *Cell Rep.* **2016**, *17*, 3369.
- [169] A. López-Tobón, C. E. Villa, C. Cheroni, S. Trattaro, N. Caporale, P. Conforti, R. Iennaco, M. Lachgar, M. T. Rigoli, B. Marcó de la Cruz, P. Lo Riso, E. Tenderini, F. Troglio, M. De Simone, I. Liste-Noya, G. Macino, M. Pagani, E. Cattaneo, G. Testa, *Stem Cell Rep.* **2019**, *13*, 847.
- [170] J. A. Bagley, D. Reumann, S. Bian, J. Lévi-Strauss, J. A. Knoblich, *Nat. Methods* **2017**, *14*, 743.
- [171] C. M. Abreu, L. Gama, S. Krasemann, M. Chesnut, S. Odwin-Dacosta, H. T. Hogberg, T. Hartung, D. Pamies, *Front. Microbiol.* **2018**, *9*, 2766.
- [172] M. Brüll, A. S. Spreng, S. Gutbier, D. Loser, A. Krebs, M. Reich, U. Kraushaar, M. Britschgi, C. Patsch, M. Leist, *ALTEX* **2020**, *37*, 409.
- [173] J. Muffat, Y. Li, B. Yuan, M. Mitalipova, A. Omer, S. Corcoran, G. Bakiasi, L. H. Tsai, P. Aubourg, R. M. Ransohoff, R. Jaenisch, *Nat. Med.* **2016**, *22*, 1358.
- [174] G. Quadrato, T. Nguyen, E. Z. Macosko, J. L. Sherwood, S. M. Yang, D. R. Berger, N. Maria, J. Scholvin, M. Goldman, J. P. Kinney, E. S. Boyden, J. W. Lichtman, Z. M. Williams, S. A. McCarroll, P. Arlotta, *Nature* **2017**, *545*, 48.
- [175] T. K. Matsui, M. Matsubayashi, Y. M. Sakaguchi, R. K. Hayashi, C. Zheng, K. Sugie, M. Hasegawa, T. Nakagawa, E. Mori, *Neurosci. Lett.* **2018**, *670*, 75.
- [176] D. Pamies, P. Barreras, K. Block, G. Makri, A. Kumar, D. Wiersma, L. Smirnova, C. Zhang, J. Bressler, K. M. Christian, G. Harris, G. L. Ming, C. J. Berlinicke, K. Kyro, H. Song, C. A. Pardo, T. Hartung, H. T. Hogberg, *ALTEX* **2017**, *34*, 362.
- [177] R. M. Marton, Y. Miura, S. A. Sloan, Q. Li, O. Revah, R. J. Levy, J. R. Huguenard, S. P. Pasca, *Nat. Neurosci.* **2019**, *22*, 484.
- [178] G. Quadrato, P. Arlotta, *Curr. Opin. Cell Biol.* **2017**, *49*, 47.
- [179] O. Sirenko, F. Parham, S. Dea, N. Sodhi, S. Biesmans, S. Mora-Castilla, K. Ryan, M. Behl, G. Chandy, C. Crittenden, S. Vargas-Hurlston, O. Guicherit, R. Gordon, F. Zanella, C. Carroumeu, *Toxicol. Sci.* **2019**, *167*, 249.
- [180] L. Hoelting, B. Scheinhardt, O. Bondarenko, S. Schildknecht, M. Kapitza, V. Tanavde, B. Tan, Q. Y. Lee, S. Mecking, M. Leist, S. Kadereit, *Arch. Toxicol.* **2013**, *87*, 721.
- [181] L. Smirnova, G. Harris, J. Delp, M. Valadares, D. Pamies, H. T. Hogberg, T. Waldmann, M. Leist, T. Hartung, *Arch. Toxicol.* **2016**, *90*, 2725.
- [182] D. Pamies, K. Block, P. Lau, L. Gribaldo, C. A. Pardo, P. Barreras, L. Smirnova, D. Wiersma, L. Zhao, G. Harris, T. Hartung, H. T. Hogberg, *Toxicol. Appl. Pharmacol.* **2018**, *354*, 101.
- [183] J. Sandström, E. Eggermann, I. Charvet, A. Roux, N. Toni, C. Greggio, A. Broyer, F. Monnet-Tschudi, L. Stoppini, *Toxicol. In Vitro* **2017**, *38*, 124.
- [184] M. P. Schwartz, Z. Hou, N. E. Propson, J. Zhang, C. J. Engstrom, V. S. Costa, P. Jiang, B. K. Nguyen, J. M. Bolin, W. Daly, Y. Wang, R. Stewart, C. D. Page, W. L. Murphy, J. A. Thomson, *Proc. Natl. Acad. Sci. USA* **2015**, *112*, 12516.
- [185] B. Cakir, Y. Xiang, Y. Tanaka, M. H. Kural, M. Parent, Y. J. Kang, K. Chapeton, B. Patterson, Y. Yuan, C. S. He, M. S. B. Raredon, J. Dengelegi, K. Y. Kim, P. Sun, M. Zhong, S. Lee, P. Patra, F. Hyder, L. E. Niklason, S. H. Lee, Y. S. Yoon, I. H. Park, *Nat. Methods* **2019**, *16*, 1169.
- [186] M. T. Pham, K. M. Pollock, M. D. Rose, W. A. Cary, H. R. Stewart, P. Zhou, J. A. Nolte, B. Waldau, *Neuroreport* **2018**, *29*, 588.
- [187] C. F. Cho, J. M. Wolfe, C. M. Fadzen, D. Calligaris, K. Hornburg, E. A. Chiocca, N. Y. R. Agar, B. L. Pentelute, S. E. Lawler, *Nat. Commun.* **2017**, *8*, 15623.
- [188] G. Nzou, R. T. Wicks, E. E. Wicks, S. A. Seale, C. H. Sane, A. Chen, S. V. Murphy, J. D. Jackson, A. J. Atala, *Sci. Rep.* **2018**, *8*, 7413.
- [189] G. Adriani, D. Ma, A. Pavesi, R. D. Kamm, E. L. K. Goh, *Lab Chip* **2017**, *17*, 448.
- [190] M. Campisi, Y. Shin, T. Osaki, C. Hajal, V. Chiono, R. D. Kamm, *Biomaterials* **2018**, *180*, 117.
- [191] Y. I. Wang, H. E. Abaci, M. L. Shuler, *Biotechnol. Bioeng.* **2017**, *114*, 184.
- [192] S. R. Horman, C. Hogan, K. D. Reyes, F. Lo, C. Antczak, *Future Med. Chem.* **2015**, *7*, 513.

- [193] R. I. Dmitriev, A. V. Zhdanov, Y. M. Nolan, D. B. Papkovsky, *Biomaterials* **2013**, 34, 9307.
- [194] K. R. Ryan, O. Sirenko, F. Parham, J. H. Hsieh, E. F. Cromwell, R. R. Tice, M. Behl, *Neurotoxicology* **2016**, 53, 271.
- [195] A. M. Tukker, R. G. D. M. van Kleef, F. M. J. Wijnolts, A. de Groot, R. H. S. Westerink, *ALTEX* **2020**, 37, 121.
- [196] R. Mullur, Y. Y. Liu, G. A. Brent, *Physiol. Rev.* **2014**, 94, 355.
- [197] S. Horn, H. Heuer, *Mol. Cell. Endocrinol.* **2010**, 315, 19.
- [198] A. T. J. Murk, E. Rijntjes, B. J. Blaauboer, R. Clewell, K. M. Crofton, M. M. L. Dingemans, J. D. Furlow, R. Kavlock, J. Köhrle, R. Opitz, T. Traas, T. J. Visser, M. Xia, A. C. Gutleb, *Toxicol. In Vitro* **2013**, 27, 1320.
- [199] H. J. Steinfeld, P. Hauser, Y. Nakayama, S. Radovick, J. H. McCluskey, T. Taylor, B. D. Weintraub, F. E. Wondisford, *Proc. Natl. Acad. Sci. USA* **1991**, 88, 3130.
- [200] T. M. Ortega-Carvalho, M. I. Chiamolera, C. C. Pazos-Moura, F. E. Wondisford, *Compr. Physiol.* **2016**, 6, 1387.
- [201] G. Dai, O. Levy, N. Carrasco, *Nature* **1996**, 379, 458.
- [202] D. P. Carvalho, C. Dupuy, *Mol. Cell. Endocrinol.* **2017**, 458, 6.
- [203] C. E. Citterio, H. M. Targovnik, P. Arvan, *Nat. Rev. Endocrinol.* **2019**, 15, 323.
- [204] C. Di Cosmo, X. H. Liao, A. M. Dumitrescu, N. J. Philp, R. E. Weiss, S. Refetoff, *J. Clin. Invest.* **2010**, 120, 3377.
- [205] F. Brucker-Davis, *Thyroid* **1998**, 8, 827.
- [206] OECD (2018), *Test No. 414: Prenatal Developmental Toxicity Study*, OECD Publishing, Paris **2018**.
- [207] OECD (1995), *Test No. 421: Reproduction/Developmental Toxicity Screening Test*, OECD Publishing, Paris **1995**.
- [208] OECD (2016), *Test No. 422: Combined Repeated Dose Toxicity Study with the Reproduction/Developmental Toxicity Screening Test*, OECD Publishing, Paris **2016**, p. 2016.
- [209] OECD (2018), *Test No. 443: Extended One-Generation Reproductive Toxicity Study*, OECD Publishing, Paris **2018**.
- [210] N. Andersson, M. Arena, D. Auteri, S. Barmaz, E. Grignard, A. Kienzler, P. Lepper, A. M. Lostia, S. Munn, J. M. Parra Morte, F. Pellizzato, J. Tarazona, A. Terron, S. Van der Linden, *EFSA J.* **2018**, 16, e05311.
- [211] U.S. Environmental Protection Agency, *Endocrine Disruptor Screening Program (EDSP) Comprehensive Management Plans*, Washington, D.C. **2014**.
- [212] OECD (2017), *New Scoping Document on in Vitro and Ex Vivo Assays for the Identification of Modulators of Thyroid Hormone Signalling*, OECD Publishing, Paris **2017**.
- [213] P. D. Noyes, K. P. Friedman, P. Browne, J. T. Haselman, M. E. Gilbert, M. W. Hornung, S. Barone, K. M. Crofton, S. C. Laws, T. E. Stoker, S. O. Simmons, J. E. Tietge, S. J. Degitz, *Environ. Health Perspect.* **2019**, 127, 95001.
- [214] R. S. Thomas, T. Bahadori, T. J. Buckley, J. Cowden, C. Deisenroth, K. L. Dionisio, J. B. Frithsen, C. M. Grulke, M. R. Gwinn, J. A. Harrill, M. Higuchi, K. A. Houck, M. F. Hughes, E. Sidney Hunter, K. K. Isaacs, R. S. Judson, T. B. Knudsen, J. C. Lambert, M. Linnenbrink, T. M. Martin, S. R. Newton, S. Padilla, G. Patlewicz, K. Paul-Friedman, K. A. Phillips, A. M. Richard, R. Sams, T. J. Shafer, R. W. Setzer, I. Shah, J. E. Simmons, S. O. Simmons, A. Singh, J. R. Sobus, M. Strynar, A. Swank, R. Tornero-Valez, E. M. Ulrich, D. L. Villeneuve, J. F. Wambaugh, B. A. Wetmore, A. J. Williams, *Toxicol. Sci.* **2019**, 169, 317.
- [215] C. Thomas-Morvan, B. Caillou, M. Schlumberger, P. Fragu, *Biol. Cell* **1988**, 62, 247.
- [216] C. Massart, B. Hody, D. Condé, G. Leclech, G. Edan, M. Nicol, *Mol. Cell. Endocrinol.* **1988**, 56, 227.
- [217] E. A. Bulanova, E. V. Koudan, J. Degosserie, C. Heymans, F. D. A. S. Pereira, V. A. Parfenov, Y. Sun, Q. Wang, S. A. Akhmedova, I. K. Sviridova, N. S. Sergeeva, G. A. Frank, Y. D. Khesuani, C. E. Pierreux, V. A. Mironov, *Biofabrication* **2017**, 9, 34105.
- [218] Y. Saito, N. Onishi, H. Takami, R. Seishima, H. Inoue, Y. Hirata, K. Kameyama, K. Tsuchihashi, E. Sugihara, S. Uchino, K. Ito, H. Kawakubo, H. Takeuchi, Y. Kitagawa, H. Saya, O. Nagano, *Biochem. Biophys. Res. Commun.* **2018**, 497, 783.
- [219] C. Deisenroth, V. Y. Soldatow, J. Ford, W. Stewart, C. Brinkman, E. L. Lecluyse, D. K. MacMillan, R. S. Thomas, *Toxicol. Sci.* **2020**, 174, 63.
- [220] J. Coclet, F. Foureau, P. Ketelbant, P. Galand, J. E. Dumont, *Clin. Endocrinol.* **1989**, 31, 655.
- [221] R. Ma, R. Latif, T. F. Davies, *Thyroid* **2015**, 25, 455.
- [222] F. Antonica, D. F. Kasprzyk, R. Opitz, M. Iacovino, X. H. Liao, A. M. Dumitrescu, S. Refetoff, K. Peremans, M. Manto, M. Kyba, S. Costagliola, *Nature* **2012**, 491, 66.
- [223] A. A. Kurmann, M. Serra, F. Hawkins, S. A. Rankin, M. Mori, I. Astapova, S. Ullas, S. Lin, M. Bilodeau, J. Rossant, J. C. Jean, L. Ikonou, R. R. Deterding, J. M. Shannon, A. M. Zorn, A. N. Hollenberg, D. N. Kotton, *Cell Stem Cell* **2015**, 17, 527.
- [224] K. Dame, S. Cincotta, A. H. Lang, R. M. Sanghrajka, L. Zhang, J. Choi, L. Kwok, T. Wilson, M. M. Kariduta, S. Monti, A. N. Hollenberg, P. Mehta, D. N. Kotton, L. Ikonou, *Stem Cell Rep.* **2017**, 8, 216.
- [225] A. Arauchi, K. Matsuura, T. Shimizu, T. Okano, *Front. Endocrinol.* **2017**, 8, 22.
- [226] R. Ma, S. A. Morshed, R. Latif, T. F. Davies, *Front. Endocrinol.* **2015**, 6, 56.
- [227] Y. Yang, Y. Lu, T. Chen, S. Zhang, B. Chu, Y. Gong, W. Zhao, J. Zhu, Y. Liu, *Int. J. Dev. Biol.* **2016**, 60, 85.
- [228] H. Suga, T. Kadoshima, M. Minaguchi, M. Ohgushi, M. Soen, T. Nakano, N. Takata, T. Wataya, K. Muguruma, H. Miyoshi, S. Yonemura, Y. Oiso, Y. Sasai, *Nature* **2011**, 480, 57.
- [229] C. Ozone, H. Suga, M. Eiraku, T. Kadoshima, S. Yonemura, N. Takata, Y. Oiso, T. Tsuji, Y. Sasai, *Nat. Commun.* **2016**, 7, 10351.
- [230] T. Kasai, H. Suga, M. Sakakibara, C. Ozone, R. Matsumoto, M. Kano, K. Mitsumoto, K. Ogawa, Y. Kodani, H. Nagasaki, N. Inoshita, M. Sugiyama, T. Onoue, T. Tsunekawa, Y. Ito, H. Takagi, D. Hagiwara, S. Iwama, M. Goto, R. Banno, J. Takahashi, H. Arima, *Cell Rep.* **2020**, 30, 18.
- [231] P. Gehr, M. Bachofen, E. R. Weibel, *Respir. Physiol.* **1978**, 32, 121.
- [232] E. Fröhlich, A. Mercuri, S. Wu, S. Salar-Behzadi, *Front. Pharmacol.* **2016**, 7, 181.
- [233] T. J. Franks, T. V. Colby, W. D. Travis, R. M. Tuder, H. Y. Reynolds, A. R. Brody, W. V. Cardoso, R. G. Crystal, C. J. Drake, J. Engelhardt, M. Frid, E. Herzog, R. Mason, S. H. Phan, S. H. Randell, M. C. Rose, T. Stevens, J. Serge, M. E. Sunday, J. A. Vaynow, B. M. Weinstein, J. Whitsett, M. C. Williams, *Proc. Am. Thorac. Soc.* **2008**, 5, 763.
- [234] OECD (2018), *Guidance Document on Inhalation Toxicity Studies*, OECD Publishing, Paris, **2018**.
- [235] H. G. Hoymann, *J. Pharmacol. Toxicol. Methods* **2007**, 55, 16.
- [236] L. C. Chen, M. Lippmann, *Curr. Protoc. Toxicol.* **2015**, 63, 24.4.1.
- [237] P. S. Hiemstra, G. Grootaers, A. M. van der Does, C. A. M. Krul, I. M. Kooter, *Toxicol. In Vitro* **2018**, 47, 137.
- [238] J. D. Crapo, B. E. Barry, P. Gehr, M. Bachofen, E. R. Weibel, *Am. Rev. Respir. Dis.* **1982**, 126, 332.
- [239] D. E. Johnson, M. K. Georgieff, *Am. Rev. Respir. Dis.* **1989**, 140, 1807.
- [240] K. U. Hong, S. D. Reynolds, S. Watkins, E. Fuchs, B. R. Stripp, *Am. J. Pathol.* **2004**, 164, 577.
- [241] B. D. Uhal, K. M. Flowers, D. E. Rannels, *Am. J. Physiol. Cell. Mol. Physiol.* **1991**, 261, 110.
- [242] M. A. Medinsky, J. A. Bond, *Toxicology* **2001**, 160, 165.
- [243] M. Lippmann, D. B. Yeates, R. E. Albert, *Br. J. Ind. Med.* **1980**, 37, 337.
- [244] B. Asgharian, T. P. Owen, E. D. Kuempel, A. M. Jarabek, *Toxicol. Appl. Pharmacol.* **2018**, 361, 27.

- [245] T. T. Crocker, T. V. O'Donnell, L. L. Nunes, *Cancer Res.* **1973**, 33, 88.
- [246] J. E. Craighead, B. T. Mossman, B. J. Bradley, *Environ. Health Perspect.* **1980**, 34, 37.
- [247] U. Mohr, M. Emura, *Food Chem. Toxicol.* **1985**, 23, 233.
- [248] K. E. Driscoll, J. M. Carter, P. T. Iype, H. L. Kumari, L. L. Crosby, M. J. Aardema, R. J. Isfort, D. Cody, M. H. Chestnut, J. L. Burns, R. A. LeBoeuf, *In Vitro Cell. Dev. Biol.: Anim.* **1995**, 31, 516.
- [249] M. Lieber, G. Todaro, B. Smith, A. Szakal, W. Nelson-Rees, *Int. J. Cancer* **1976**, 17, 62.
- [250] I. W. H. Jarvis, Z. Enlo-Scott, E. Nagy, I. S. Mudway, T. D. Tetley, V. M. Arlt, D. H. Phillips, *Environ. Mol. Mutagen.* **2018**, 59, 290.
- [251] N. Fujino, H. Kubo, C. Ota, T. Suzuki, S. Suzuki, M. Yamada, T. Takahashi, M. He, T. Suzuki, T. Kondo, M. Yamaya, *Am. J. Respir. Cell Mol. Biol.* **2012**, 46, 422.
- [252] P. Khan, K. Fytianos, L. Tamò, M. Roth, M. Tamm, T. Geiser, A. Gazdhar, K. E. Hostettler, *Respir. Res.* **2018**, 19, 204.
- [253] M. A. Shatos, J. M. Doherty, J. P. Marsh, B. T. Mossman, *Environ. Res.* **1987**, 44, 103.
- [254] G. Vietti, S. Ibouaardaten, M. Palmai-Pallag, Y. Yakoub, C. Bailly, I. Fenoglio, E. Marbaix, D. Lison, S. van den Brule, *Part. Fibre Toxicol.* **2013**, 10, 52.
- [255] A. C. Allison, J. S. Harington, M. Birbeck, *J. Exp. Med.* **1966**, 124, 141.
- [256] M. C. Jaurand, J. Bignon, A. Gaudichet, L. Magne, A. Oblin, *Environ. Res.* **1978**, 17, 216.
- [257] P. Gosset, P. Lassalle, D. Vanh  e, B. Wallaert, C. Aerts, C. Voisin, A. B. Tonnel, *Am. J. Respir. Cell Mol. Biol.* **1991**, 5, 431.
- [258] R. P. F. Schins, P. J. A. Borm, *Ann. Occup. Hyg.* **1999**, 43, 7.
- [259] A. M. Knaapen, R. P. F. Schins, P. J. A. Borm, F. J. van Schooten, *Carcinogenesis* **2005**, 26, 1642.
- [260] F. Herzog, M. J. D. Clift, F. Piccapietra, R. Behra, O. Schmid, A. Petri-Fink, B. Rothen-Rutishauser, *Part. Fibre Toxicol.* **2013**, 10, 11.
- [261] S. G. Klein, T. Serchi, L. Hoffmann, B. Bl  meke, A. C. Gutleb, *Part. Fibre Toxicol.* **2013**, 10, 31.
- [262] H. Batra, V. B. Antony, *J. Thorac. Dis.* **2015**, 7, 964.
- [263] C. Blanquart, M. C. Jaurand, D. Jean, *Front. Oncol.* **2020**, 10, 388.
- [264] A. Renier, M. Yegles, A. Buard, H. Dong, L. Kheuang, L. Saint-Etienne, P. Laurent, M. C. Jaurand, *Cell Biol. Toxicol.* **1992**, 8, 133.
- [265] F. A. Murphy, A. Schinwald, C. A. Poland, K. Donaldson, *Part. Fibre Toxicol.* **2012**, 9, 8.
- [266] M. I. Hermanns, R. E. Unger, K. Kehe, K. Peters, C. J. Kirkpatrick, *Lab. Invest.* **2004**, 84, 736.
- [267] K. Luyts, D. Napierska, D. Dinsdale, S. G. Klein, T. Serchi, P. H. M. Hoet, *Toxicol. In Vitro* **2015**, 29, 234.
- [268] A. Costa, C. de Souza Carvalho-Wodarz, V. Seabra, B. Sarmento, C. M. Lehr, *Acta Biomater.* **2019**, 91, 235.
- [269] K. B. Adler, P. W. Cheng, K. C. Kim, *Am. J. Respir. Cell Mol. Biol.* **1990**, 2, 145.
- [270] F. Blank, B. M. Rothen-Rutishauser, S. Schurch, P. Gehr, *J. Aerosol Med.* **2006**, 19, 392.
- [271] G. Lacroix, W. Koch, D. Ritter, A. C. Gutleb, S. T. Larsen, T. Loret, F. Zanetti, S. Constant, S. Chortarea, B. Rothen-Rutishauser, P. S. Hiemstra, E. Frejafon, P. Hubert, L. Gribaldo, P. Kearns, J. M. Aublant, S. Diabat  , C. Weiss, A. De Groot, I. Kooter, *Appl. In Vitro Toxicol.* **2018**, 4, 91.
- [272] S. Huang, B. Boda, J. Vernaz, E. Ferreira, L. Wiszniewski, S. Constant, *Eur. J. Pharm. Biopharm.* **2017**, 118, 68.
- [273] M. Liu, S. J. M. Skinner, J. Xu, R. N. N. Han, A. K. Tanswell, M. Post, *Am. J. Physiol.: Lung Cell. Mol. Physiol.* **1992**, 263, 376.
- [274] U. Savla, C. M. Waters, *Am. J. Physiol.: Lung Cell. Mol. Physiol.* **1998**, 274, 883.
- [275] C. Schmitz, J. Welck, I. Tavernaro, M. Grinberg, J. Rahnenf  hrer, A. K. Kierner, C. van Thriel, J. G. Hengstler, A. Kraegeloh, *Nanotoxicology* **2019**, 13, 1227.
- [276] D. Huh, D. C. Leslie, B. D. Matthews, J. P. Fraser, S. Jurek, G. A. Hamilton, K. S. Thorne  e, M. A. McAlexander, D. E. Ingber, *Sci. Transl. Med.* **2012**, 4, 159ra147.
- [277] S. Gotoh, I. Ito, T. Nagasaki, Y. Yamamoto, S. Konishi, Y. Korogi, H. Matsumoto, S. Muro, T. Hirai, M. Funato, S. I. Mae, T. Toyoda, A. Sato-Otsubo, S. Ogawa, K. Osafune, M. Mishima, *Stem Cell Rep.* **2014**, 3, 394.
- [278] M. C. Basil, J. Katzen, A. E. Engler, M. Guo, M. J. Herriges, J. J. Kathiriyi, R. Windmueller, A. B. Ysasi, W. J. Zacharias, H. A. Chapman, D. N. Kotton, J. R. Rock, H. W. Snoeck, G. Vunjak-Novakovic, J. A. Whitsett, E. E. Morrisey, *Cell Stem Cell* **2020**, 26, 482.
- [279] C. Coraux, B. Nawrocki-Raby, J. Hinnrasky, C. Kileztky, D. Gaillard, C. Dani, E. Puchelle, *Am. J. Respir. Cell Mol. Biol.* **2005**, 32, 87.
- [280] B. Mehrad, M. P. Keane, B. N. Gomperts, R. M. Strieter, *Expert Rev. Respir. Med.* **2007**, 1, 157.
- [281] L. Srikanth, K. Venkatesh, M. M. Sunitha, P. S. Kumar, C. Chandrasekhar, B. Vengamma, P. V. G. K. Sarma, *Biotechnol. Lett.* **2016**, 38, 237.
- [282] M. D. Green, A. Chen, M. C. Nostro, S. L. D'Souza, C. Schaniel, I. R. Lemischka, V. Gouon-Evans, G. Keller, H. W. Snoeck, *Nat. Biotechnol.* **2011**, 29, 267.
- [283] F. Hawkins, D. N. Kotton, *Ann. Am. Thorac. Soc.* **2015**, 12, S50.
- [284] M. Ghaedi, L. E. Niklason, in *Methods in Molecular Biology*, Humana Press Inc., Totowa **2019**, pp. 55–92.
- [285] P. Pimton, S. Lecht, C. T. Stabler, G. Johannes, E. S. Schulman, P. I. Lelkes, *Stem Cells Dev.* **2015**, 24, 663.
- [286] T. Y. Ling, Y. L. Liu, Y. K. Huang, S. Y. Gu, H. K. Chen, C. C. Ho, P. N. Tsao, Y. C. Tung, H. W. Chen, C. H. Cheng, K. H. Lin, F. H. Lin, *Biomaterials* **2014**, 35, 5660.
- [287] Y. Yamamoto, S. Gotoh, Y. Korogi, M. Seki, S. Konishi, S. Ikeo, N. Sone, T. Nagasaki, H. Matsumoto, S. Muro, I. Ito, T. Hirai, T. Kohno, Y. Suzuki, M. Mishima, *Nat. Methods* **2017**, 14, 1097.
- [288] S. X. L. Huang, M. D. Green, A. T. De Carvalho, M. Mumau, Y. W. Chen, S. L. D'souza, H. W. Snoeck, *Nat. Protoc.* **2015**, 10, 413.
- [289] A. J. Miller, B. R. Dye, D. Ferrer-Torres, D. R. Hill, A. W. Overeem, L. D. Shea, J. R. Spence, *Nat. Protoc.* **2019**, 14, 518.
- [290] X. Zhang, T. Jiang, D. Chen, Q. Wang, L. W. Zhang, *Crit. Rev. Toxicol.* **2020**, 50, 279.
- [291] M. F. Beers, Y. Moodley, *Am. J. Respir. Cell Mol. Biol.* **2017**, 57, 18.
- [292] Y. W. Chen, S. X. Huang, A. L. R. T. De Carvalho, S. H. Ho, M. N. Islam, S. Volpi, L. D. Notarangelo, M. Ciancanelli, J. L. Casanova, J. Bhattacharya, A. F. Liang, L. M. Palermo, M. Porotto, A. Moscona, H. W. Snoeck, *Nat. Cell Biol.* **2017**, 19, 542.
- [293] A. Jacob, M. Morley, F. Hawkins, K. B. McCauley, J. C. Jean, H. Heins, C. L. Na, T. E. Weaver, M. Vedaie, K. Hurley, A. Hinds, S. J. Russo, S. Kook, W. Zacharias, M. Ochs, K. Traber, L. J. Quinton, A. Crane, B. R. Davis, F. V. White, J. Wambach, J. A. Whitsett, F. S. Cole, E. E. Morrisey, S. H. Guttentag, M. F. Beers, D. N. Kotton, *Cell Stem Cell* **2017**, 21, 472.
- [294] R. Wang, K. B. McCauley, D. N. Kotton, F. Hawkins, in *Methods Cell Biol.*, Academic Press Inc., Cambridge **2020**, pp. 95–114.
- [295] J. C. Nawroth, R. Barrile, D. Conegliano, S. van Riet, P. S. Hiemstra, R. Villenave, *Adv. Drug Delivery Rev.* **2019**, 140, 12.
- [296] Y. Ding, P. Weindl, A. G. Lenz, P. Mayer, T. Krebs, O. Schmid, *Part. Fibre Toxicol.* **2020**, 17, 44.
- [297] M. R. Tanner, C. Beeton, *Front. Biosci., Landmark* **2018**, 23, 43.
- [298] M. Bauer, in *Basic Science In Anesthesia*, Springer International Publishing, Basel, **2017**, pp. 195–228.
- [299] N. Ferri, P. Siegl, A. Corsini, J. Herrmann, A. Lerman, R. Benghozi, *Pharmacol. Ther.* **2013**, 138, 87.
- [300] M. Takeda, S. Miyagawa, S. Fukushima, A. Saito, E. Ito, A. Harada, R. Matsuura, H. Iseoka, N. Sougawa, N. Mochizuki-Oda, M. Matsusaki, M. Akashi, Y. Sawa, *Tissue Eng., Part C* **2018**, 24, 56.

- [301] T. Jin, B. Hu, S. Chen, Q. Wang, X. Dong, Y. Zhang, Y. Zhu, Z. Zhang, *Front. Pharmacol.* **2018**, 9, 577.
- [302] J. Cuadros, N. Dugarte, S. Wong, P. Vanegas, V. Moroch, R. Medina, *J. Healthcare Eng.* **2019**, 2019, 6371871.
- [303] B. Darpo, *Br. J. Pharmacol.* **2010**, 159, 49.
- [304] B. D. Guth, S. Germeyer, W. Kolb, M. Markert, *J. Pharmacol. Toxicol. Methods* **2004**, 49, 159.
- [305] I. Cavero, W. Crumb, *Expert Opin. Drug Saf.* **2005**, 4, 509.
- [306] C. L. Mummery, *Stem Cell Rep.* **2018**, 11, 1306.
- [307] M. Zhang, J. S. Schulte, A. Heinick, I. Piccini, J. Rao, R. Quaranta, D. Zeuschner, D. Malan, K. P. Kim, A. Röpke, P. Sasse, M. Araújo-Bravo, G. Seeböhm, H. Schöler, L. Fabritz, P. Kirchhof, F. U. Müller, B. Greber, *Stem Cells* **2015**, 33, 1456.
- [308] P. W. Burridge, E. Matsa, P. Shukla, Z. C. Lin, J. M. Churko, A. D. Ebert, F. Lan, S. Diecke, B. Huber, N. M. Mordwinkin, J. R. Plews, O. J. Abilez, B. Cui, J. D. Gold, J. C. Wu, *Nat. Methods* **2014**, 11, 855.
- [309] X. Lian, J. Zhang, S. M. Azarin, K. Zhu, L. B. Hazeltine, X. Bao, C. Hsiao, T. J. Kamp, S. P. Palecek, *Nat. Protoc.* **2013**, 8, 162.
- [310] H. Ando, T. Yoshinaga, W. Yamamoto, K. Asakura, T. Uda, T. Taniguchi, A. Ojima, T. Osada, S. Hayashi, C. Kasai, N. Miyamoto, H. Tashibu, D. Yamazaki, A. Sugiyama, Y. Kanda, K. Sawada, Y. Sekino, H. Ando, T. Yoshinaga, K. Asakura, T. Osada, S. Hayashi, C. Kasai, H. Tashibu, A. Sugiyama, K. Sawada, Y. Sekino, H. Ando, T. Uda, T. Yoshinaga, T. Taniguchi, A. Ojima, R. Shinkyo, K. Kikuchi, N. Miyamoto, K. Sawada, W. Yamamoto, K. Asakura, S. Hayashi, T. Osada, C. Kasai, H. Tashibu, D. Yamazaki, Y. Kanda, Y. Sekino, A. Sugiyama, *J. Pharmacol. Toxicol. Methods* **2017**, 84, 111.
- [311] M. Shi, N. T. Tien, L. de Haan, J. Louisse, I. M. C. M. Rietjens, H. Bouwmeester, *Toxicol. In Vitro* **2020**, 67, 104891.
- [312] S. Stoelzle, A. Haythornthwaite, R. Kettenhofen, E. Kolossov, H. Bohlen, M. George, A. Brüggemann, N. Fertig, *J. Biomol. Screen.* **2011**, 16, 910.
- [313] K. Blinova, J. Stohman, J. Vicente, D. Chan, L. Johannesen, M. P. Hortigon-Vinagre, V. Zamora, G. Smith, W. J. Crumb, L. Pang, B. Lyn-Cook, J. Ross, M. Brock, S. Chvatal, D. Millard, L. Galeotti, N. Stockbridge, D. G. Strauss, *Toxicol. Sci.* **2017**, 155, 234.
- [314] T. Colatsky, B. Fermini, G. Gintant, J. B. Pierson, P. Sager, Y. Sekino, D. G. Strauss, N. Stockbridge, *J. Pharmacol. Toxicol. Methods* **2016**, 81, 15.
- [315] K. Blinova, Q. Dang, D. Millard, G. Smith, J. Pierson, L. Guo, M. Brock, H. R. Lu, U. Kraushaar, H. Zeng, H. Shi, X. Zhang, K. Sawada, T. Osada, Y. Kanda, Y. Sekino, L. Pang, T. K. Feaster, R. Kettenhofen, N. Stockbridge, D. G. Strauss, G. Gintant, *Cell Rep.* **2018**, 24, 3582.
- [316] B. R. Berridge, A. E. Schultze, J. R. Heyen, G. H. Searfoss, R. D. Sarazan, *ILAR J.* **2016**, 57, 120.
- [317] G. Gintant, P. T. Sager, N. Stockbridge, *Nat. Rev. Drug Discovery* **2016**, 15, 457.
- [318] E. G. Navarrete, P. Liang, F. Lan, V. Sanchez-Freire, C. Simmons, T. Gong, A. Sharma, P. W. Burridge, B. Patlolla, A. S. Lee, H. Wu, R. E. Beygui, S. M. Wu, R. C. Robbins, D. M. Bers, J. C. Wu, *Circulation* **2013**, 128.
- [319] A. Sharma, W. L. McKeithan, R. Serrano, T. Kitani, P. W. Burridge, J. C. del Álamo, M. Mercola, J. C. Wu, *Nat. Protoc.* **2018**, 13, 3018.
- [320] Y. K. Kurokawa, M. R. Shang, R. T. Yin, S. C. George, *Toxicol. Lett.* **2018**, 285, 74.
- [321] B. Nugraha, M. F. Buono, L. von Boehmer, S. P. Hoerstrup, M. Y. Emmert, *Clin. Pharmacol. Ther.* **2019**, 105, 79.
- [322] L. Polonchuk, M. Chabria, L. Badi, J. C. Hoflack, G. Figtree, M. J. Davies, C. Gentile, *Sci. Rep.* **2017**, 7, 7005.
- [323] C. R. Archer, R. Sargeant, J. Basak, J. Pilling, J. R. Barnes, A. Pointon, *Sci. Rep.* **2018**, 8, 10160.
- [324] M. Kawatou, H. Masumoto, H. Fukushima, G. Morinaga, R. Sakata, T. Ashihara, J. K. Yamashita, *Nat. Commun.* **2017**, 8, 1078.
- [325] D. Hu, A. Linders, A. Yamak, C. Correia, J. D. Kijlstra, A. Garakani, L. Xiao, D. J. Milan, P. Van Der Meer, M. Serra, P. M. Alves, I. J. Domian, *Circ. Res.* **2018**, 123, 1066.
- [326] T. Kietzmann, *Redox Biol.* **2017**, 11, 622.
- [327] H. Rashidi, S. Alhaque, D. Szkolnicka, O. Flint, D. C. Hay, *Arch. Toxicol.* **2016**, 90, 1757.
- [328] M. Hay, D. W. Thomas, J. L. Craighead, C. Economides, J. Rosenthal, *Nat. Biotechnol.* **2014**, 32, 40.
- [329] M. Z. Sakatis, M. J. Reese, A. W. Harrell, M. A. Taylor, I. A. Baines, L. Chen, J. C. Bloomer, E. Y. Yang, H. M. Ellens, J. L. Ambroso, C. A. Lovatt, A. D. Ayrton, S. E. Clarke, *Chem. Res. Toxicol.* **2012**, 25, 2067.
- [330] J. L. Stevens, T. K. Baker, *Drug Discovery Today* **2009**, 14, 162.
- [331] N. Kaplowitz, *Nat. Rev. Drug Discovery* **2005**, 4, 489.
- [332] T. Hartung, *Nature* **2009**, 460, 208.
- [333] A. Natale, K. Vanmol, A. Arslan, S. Van Vlierberghe, P. Dubruel, J. Van Erps, H. Thienpont, M. Buzgo, J. Boeckmans, J. De Kock, T. Vanhaecke, V. Rogiers, R. M. Rodrigues, *Arch. Toxicol.* **2019**, 93, 1789.
- [334] P. Godoy, N. J. Hewitt, U. Albrecht, M. E. Andersen, N. Ansari, S. Bhattacharya, J. G. Bode, J. Bolleyn, C. Borner, J. Böttger, A. Braeuning, R. A. Budinsky, B. Burkhardt, N. R. Cameron, G. Camussi, C. S. Cho, Y. J. Choi, J. Craig Rowlands, U. Dahmen, G. Damm, O. Dirsch, M. T. Donato, J. Dong, S. Dooley, D. Drasdo, R. Eakins, K. S. Ferreira, V. Fonsato, J. Fraczek, R. Gebhardt, A. Gibson, M. Glanemann, C. E. P. Goldring, M. J. Gómez-Lechón, G. M. M. Groothuis, L. Gustavsson, C. Guyot, D. Hallifax, S. Hammad, A. Hayward, D. Häussinger, C. Hellerbrand, P. Hewitt, S. Hoehme, H. G. Holzhütter, J. B. Houston, J. Hrach, K. Ito, H. Jaeschke, V. Keitel, J. M. Kelm, B. Kevin Park, C. Kordes, G. A. Kullak-Ublick, E. L. Lecluyse, P. Lu, J. Luebke-Wheeler, A. Lutz, D. J. Maltman, M. Matz-Soja, P. McMullen, I. Merfort, S. Messner, C. Meyer, J. Mwinyi, D. J. Naisbitt, A. K. Nussler, P. Olinga, F. Pampaloni, J. Pi, L. Pluta, S. A. Przyborski, A. Ramachandran, V. Rogiers, C. Rowe, C. Schelcher, K. Schmich, M. Schwarz, B. Singh, E. H. K. Stelzer, B. Stieger, R. Stöber, Y. Sugiyama, C. Tetta, W. E. Thasler, T. Vanhaecke, M. Vinken, T. S. Weiss, A. Wiedera, C. G. Woods, J. J. Xu, K. M. Yarborough, J. G. Hengstler, *Arch. Toxicol.* **2013**, 87, 1315.
- [335] V. M. Lauschke, D. F. G. Hendriks, C. C. Bell, T. B. Andersson, M. Ingelman-Sundberg, *Chem. Res. Toxicol.* **2016**, 29, 1936.
- [336] W. L. Thompson, T. Takebe, in *Methods in Cell Biology*, Academic Press Inc., Cambridge **2020**, pp. 47–68.
- [337] C. C. Bell, D. F. G. Hendriks, S. M. L. Moro, E. Ellis, J. Walsh, A. Renblom, L. Fredriksson Puigvert, A. C. A. Dankers, F. Jacobs, J. Snoeys, R. L. Sison-Young, R. E. Jenkins, Å. Nordling, S. Mkrtchian, B. K. Park, N. R. Kitteringham, C. E. P. Goldring, V. M. Lauschke, M. Ingelman-Sundberg, *Sci. Rep.* **2016**, 6, 25187.
- [338] W. R. Proctor, A. J. Foster, J. Vogt, C. Summers, B. Middleton, M. A. Pilling, D. Shienson, M. Kijanska, S. Ströbel, J. M. Kelm, P. Morgan, S. Messner, D. Williams, *Arch. Toxicol.* **2017**, 91, 2849.
- [339] X. Ma, X. Qu, W. Zhu, Y. S. Li, S. Yuan, H. Zhang, J. Liu, P. Wang, C. S. E. Lai, F. Zanella, G. S. Feng, F. Sheikh, S. Chien, S. Chen, *Proc. Natl. Acad. Sci. USA* **2016**, 113, 2206.
- [340] F. Tonon, G. G. Giobbe, A. Zambon, C. Luni, O. Gagliano, A. Floreani, G. Grassi, N. Elvassore, *Sci. Rep.* **2019**, 9, 13557.
- [341] J. Ahn, J. H. Ahn, S. Yoon, Y. S. Nam, M. Y. Son, J. H. Oh, *J. Biol. Eng.* **2019**, 13, 22.
- [342] Y. B. Kang, J. Eo, B. Bulutoglu, M. L. Yarmush, O. B. Usta, *Bio-technol. Bioeng.* **2020**, 117, 763.
- [343] F. A. Grimm, Y. Iwata, O. Sirenko, M. Bittner, I. Rusyn, *Assay Drug Dev. Technol.* **2015**, 13, 529.
- [344] O. Sirenko, J. Hesley, I. Rusyn, E. F. Cromwell, *Assay Drug Dev. Technol.* **2014**, 12, 43.

- [345] P. Horvath, N. Aulner, M. Bickle, A. M. Davies, E. Del Nery, D. Ebner, M. C. Montoya, P. Östling, V. Pietiäinen, L. S. Price, S. L. Shorte, G. Turcatti, C. Von Schantz, N. O. Carragher, *Nat. Rev. Drug Discovery* **2016**, 15, 751.
- [346] T. Takebe, K. Sekine, M. Kimura, E. Yoshizawa, S. Ayano, M. Koido, S. Funayama, N. Nakanishi, T. Hisai, T. Kobayashi, T. Kasai, R. Kitada, A. Mori, H. Ayabe, Y. Ejiri, N. Amimoto, Y. Yamazaki, S. Ogawa, M. Ishikawa, Y. Kiyota, Y. Sato, K. Nozawa, S. Okamoto, Y. Ueno, H. Taniguchi, *Cell Rep.* **2017**, 21, 2661.
- [347] R. Ouchi, S. Togo, M. Kimura, T. Shinozawa, M. Koido, H. Koike, W. Thompson, R. A. Karns, C. N. Mayhew, P. S. McGrath, H. A. McCauley, R. R. Zhang, K. Lewis, S. Hakoziaki, A. Ferguson, N. Saiki, Y. Yoneyama, I. Takeuchi, Y. Mabuchi, C. Akazawa, H. Y. Yoshikawa, J. M. Wells, T. Takebe, *Cell Metab.* **2019**, 30, 374.
- [348] F. Wu, D. Wu, Y. Ren, Y. Huang, B. Feng, N. Zhao, T. Zhang, X. Chen, S. Chen, A. Xu, *J. Hepatol.* **2019**, 70, 1145.
- [349] O. Sirenko, M. K. Hancock, J. Hesley, D. Hong, A. Cohen, J. Gentry, C. B. Carlson, D. A. Mann, *Assay Drug Dev. Technol.* **2016**, 14, 381.
- [350] A. K. Daly, *Nat. Rev. Genet.* **2010**, 11, 241.
- [351] S. Wang, X. Wang, Z. Tan, Y. Su, J. Liu, M. Chang, F. Yan, J. Chen, T. Chen, C. Li, J. Hu, Y. Wang, *Cell Res.* **2019**, 29, 1009.
- [352] J. L. Zhuo, X. C. Li, *Compr. Physiol.* **2013**, 3, 1079.
- [353] N. O. Lindström, M. L. Lawrence, S. F. Burn, J. A. Johansson, E. R. M. Bakker, R. A. Ridgway, C. H. Chang, M. J. Karolak, L. Oxburgh, D. J. Headon, O. J. Sansom, R. Smits, J. A. Davies, P. Hohenstein, *eLife* **2014**, 3, e04000.
- [354] M. A. Perazella, *Clin. J. Am. Soc. Nephrol.* **2018**, 13, 1897.
- [355] M. Carlström, C. S. Wilcox, W. J. Arendshorst, *Physiol. Rev.* **2015**, 95, 405.
- [356] E. J. Hoorn, S. B. Walsh, J. A. McCormick, A. Fürstenberg, C. L. Yang, T. Roeschel, A. Paliege, A. J. Howie, J. Conley, S. Bachmann, R. J. Unwin, D. H. Ellison, *Nat. Med.* **2011**, 17, 1304.
- [357] E. Lazzeri, M. L. Angelotti, A. Peired, C. Conte, J. A. Marschner, L. Maggi, B. Mazzinghi, D. Lombardi, M. E. Melica, S. Nardi, E. Ronconi, A. Sisti, G. Antonelli, F. Becherucci, L. De Chiara, R. R. Guevara, A. Burger, B. Schaefer, F. Annunziato, H. J. Anders, L. Lasagni, P. Romagnani, *Nat. Commun.* **2018**, 9, 1344.
- [358] M. A. Perazella, *Clin. J. Am. Soc. Nephrol.* **2009**, 4, 1275.
- [359] M. H. Hazelhoff, R. P. Bulacio, A. M. Torres, *Int. J. Mol. Sci.* **2012**, 13, 10523.
- [360] R. J. Roman, J. R. Carter, W. C. North, M. L. Kauker, *Anesthesiology* **1977**, 46, 260.
- [361] I. Walev, S. Bhakdi, *Antimicrob. Agents Chemother.* **1996**, 40, 1116.
- [362] A. Bernhardt, A. Fehr, S. Brandt, S. Jerchel, T. M. Ballhause, L. Philipsen, S. Stolze, R. Geffers, H. Weng, K. D. Fischer, B. Isermann, M. C. Brunner-Weinzierl, A. Batra, B. Siegmund, C. Zhu, J. A. Lindquist, P. R. Mertens, *Kidney Int.* **2017**, 92, 1157.
- [363] H. Wu, B. D. Humphreys, *Clin. J. Am. Soc. Nephrol.* **2020**, 15, 550.
- [364] Y. Kiritani, H. Wu, K. Uchimura, P. Wilson, B. Humphreys, *Proc. Natl. Acad. Sci. USA* **2020**, 117, 15874.
- [365] H. Li, B. Humphreys, *Kidney Int.* **2020**, S0085–2538, 30817.
- [366] M. A. Saleem, M. J. O'Hare, J. Reiser, R. J. Coward, C. D. Inward, T. Farren, Y. X. Chang, L. Ni, P. W. Mathieson, P. Mundel, *J. Am. Soc. Nephrol.* **2002**, 13, 630.
- [367] Q. Al-Awqati, J. A. Oliver, *Kidney Int.* **2002**, 61, 387.
- [368] E. Bigaeva, E. Gore, E. Simon, M. Zwick, A. Oldenburger, K. P. de Jong, H. S. Hofker, M. Schlepütz, P. Nicklin, M. Boersema, J. F. Rippmann, P. Olinga, *Arch. Toxicol.* **2019**, 93, 3549.
- [369] F. A. Yousef Yengej, J. Jansen, M. B. Rookmaaker, M. C. Verhaar, H. Clevers, *Cells* **2020**, 9, 1326.
- [370] S. E. Howden, M. H. Little, in *Methods in Molecular Biology*, Humana Press Inc., Totowa **2020**, pp. 183–192.
- [371] S. M. Czerniecki, N. M. Cruz, J. L. Harder, R. Menon, J. Annis, E. A. Otto, R. E. Gulieva, L. V. Islas, Y. K. Kim, L. M. Tran, T. J. Martins, J. W. Pippin, H. Fu, M. Kretzler, S. J. Shankland, J. Himmelfarb, R. T. Moon, N. Paragas, B. S. Freedman, *Cell Stem Cell* **2018**, 22, 929.
- [372] A. S. Shankar, Z. Du, H. T. Mora, T. P. P. van den Bosch, S. S. Korevaar, I. M. Van den Berg – Garrelds, E. Bindels, C. Lopez-Iglesias, M. C. Groningen, J. Gribnau, C. C. Baan, A. H. J. Danser, E. J. Hoorn, M. J. Hoogduijn, *Kidney Int.* **2020**, S0085–2538, 30968.
- [373] A. Przepiorski, V. Sander, T. Tran, J. A. Hollywood, B. Sorrenson, J. H. Shih, E. J. Wolvetang, A. P. McMahon, T. M. Holm, A. J. Davidson, *Stem Cell Rep.* **2018**, 11, 470.
- [374] R. Nishinakamura, *Nat. Rev. Nephrol.* **2019**, 15, 613.
- [375] P. R. Mertens, V. Espenkott, B. Venjakob, B. Heintz, S. Handt, H. G. Sieberth, *Hypertension* **1998**, 32, 945.
- [376] Y. Cong, X. Han, Y. Wang, Z. Chen, Y. Lu, T. Liu, Z. Wu, Y. Jin, Y. Luo, X. Zhang, *Micromachines* **2020**, 11, 381.
- [377] R. Novak, M. Ingram, S. Marquez, D. Das, A. Delahanty, A. Herland, B. M. Maoz, S. S. F. Jeanty, M. R. Somayaji, M. Burt, E. Calamari, A. Chalkiadaki, A. Cho, Y. Choe, D. B. Chou, M. Crouce, S. Dauth, T. Divic, J. Fernandez-Alcon, T. Ferrante, J. Ferrier, E. A. FitzGerald, R. Fleming, S. Jalili-Firoozinezhad, T. Grevesse, J. A. Goss, T. Hamkins-Indik, O. Henry, C. Hinojosa, T. Huffstater, K. J. Jang, V. Kujala, L. Leng, R. Mannix, Y. Milton, J. Nawroth, B. A. Nestor, C. F. Ng, B. O'Connor, T. E. Park, H. Sanchez, J. Sliz, A. Sontheimer-Phelps, B. Swenor, G. Thompson, G. J. Touloumes, Z. Tranchemontagne, N. Wen, M. Yadid, A. Bahinski, G. A. Hamilton, D. Levner, O. Levy, A. Przekwas, R. Prantil-Baun, K. K. Parker, D. E. Ingber, *Nat. Biomed. Eng.* **2020**, 4, 407.
- [378] S. Musah, A. Mammoto, T. C. Ferrante, S. S. F. Jeanty, M. Hirano-Kobayashi, T. Mammoto, K. Roberts, S. Chung, R. Novak, M. Ingram, T. Fatanat-Didar, S. Koshy, J. C. Weaver, G. M. Church, D. E. Ingber, *Nat. Biomed. Eng.* **2017**, 1, 0069.
- [379] F. Schutgens, M. B. Rookmaaker, T. Margaritis, A. Rios, C. Ammerlaan, J. Jansen, L. Gijzen, M. Vormann, A. Vonk, M. Viveen, F. Y. Yengej, S. Derakhshan, K. M. de Winter-de Groot, B. Artergiani, R. van Bortel, E. Cuppen, A. P. A. Hendrickx, M. M. van den Heuvel-Eibrink, E. Heitzer, H. Lanz, J. Beekman, J. L. Murk, R. Masereeuw, F. Holstege, J. Drost, M. C. Verhaar, H. Clevers, *Nat. Biotechnol.* **2019**, 37, 303.
- [380] L. G. Van Der Flier, H. Clevers, *Annu. Rev. Physiol.* **2009**, 71, 241.
- [381] W. W. Agace, K. D. McCoy, *Immunity* **2017**, 46, 532.
- [382] J. König, J. Wells, P. D. Cani, C. L. García-Ródenas, T. MacDonald, A. Mercenier, J. Whyte, F. Troost, R. J. Brummer, *Clin. Transl. Gastroenterol.* **2016**, 7, e196.
- [383] T. C. Fung, C. A. Olson, E. Y. Hsiao, *Nat. Neurosci.* **2017**, 20, 145.
- [384] J. Costa, A. Ahluwalia, *Front. Bioeng. Biotechnol.* **2019**, 7, 144.
- [385] J. Tack, V. Stanghellini, F. Mearin, Y. Yiannakou, P. Laver, B. Coffin, M. Simren, J. Mackinnon, G. Wiseman, A. Marciniak, *BMC Gastroenterol.* **2019**, 19, 69.
- [386] S. J. O'Brien, in *Encyclopedia of Food Safety*, Elsevier, Amsterdam **2014**, pp. 302–311.
- [387] European Medicines Agency, ICH Guideline M3(R2) on Non-Clinical Safety Studies for the Conduct of Human Clinical Trials and Marketing Authorisation for Pharmaceuticals, **2009**.
- [388] Regulation (EC) No 1907/2006, European Parliament, Regulation Concerning the Registration, Evaluation, Authorisation and Restriction of Chemicals (REACH), **2006**.
- [389] C. Federer, M. Yoo, A. C. Tan, *Assay Drug Dev. Technol.* **2016**, 14, 557.
- [390] H. L. Philpott, S. Nandurkar, J. Lubel, P. R. Gibson, *Postgrad. Med. J.* **2014**, 90, 411.
- [391] R. Düsing, K. Lottermoser, T. Mengden, *Nephrol. Dial. Transplant.* **2001**, 16, 1317.
- [392] OECD (1998), *Test No. 409: Repeated Dose 90-Day Oral Toxicity Study in Non-Rodents*, OECD Publishing, Paris **1998**.

- [393] J. A. Jiminez, T. C. Uwiera, G. D. Inglis, R. R. E. Uwiera, *Gut Pathog.* **2015**, 7, 29.
- [394] A. E. Tammariello, J. A. Milner, *J. Nutr. Biochem.* **2010**, 21, 77.
- [395] J. C. Park, S. H. Im, *Exp. Mol. Med.* **2020**, 52, 1383.
- [396] G. B. Hatton, V. Yadav, A. W. Basit, H. A. Merchant, *J. Pharm. Sci.* **2015**, 104, 2747.
- [397] X. Cao, S. T. Gibbs, L. Fang, H. A. Miller, C. P. Landowski, H. C. Shin, H. Lennernas, Y. Zhong, G. L. Amidon, L. X. Yu, D. Sun, *Pharm. Res.* **2006**, 23, 1675.
- [398] R. Nagpal, S. Wang, L. C. Solberg Woods, O. Seshie, S. T. Chung, C. A. Shively, T. C. Register, S. Craft, D. A. McClain, H. Yadav, *Front. Microbiol.* **2018**, 9, 2897.
- [399] B. D. Wallace, H. Wang, K. T. Lane, J. E. Scott, J. Orans, J. S. Koo, M. Venkatesh, C. Jobin, L. A. Yeh, S. Mani, M. R. Redinbo, *Science* **2010**, 330, 831.
- [400] J. Zhan, Y. Liang, D. Liu, X. Ma, P. Li, C. Liu, X. Liu, P. Wang, Z. Zhou, *Microbiome* **2018**, 6, 224.
- [401] A. Vich Vila, V. Collij, S. Sanna, T. Sinha, F. Imhann, A. R. Bourgonje, Z. Mujagic, D. M. A. E. Jonkers, A. A. M. Masclee, J. Fu, A. Kurilshikov, C. Wijmenga, A. Zhernakova, R. K. Weersma, *Nat. Commun.* **2020**, 11, 1.
- [402] A. R. Hilgers, R. A. Conradi, P. S. Burton, *Pharm. Res.* **1990**, 7, 902.
- [403] W. Rubas, N. Jezyk, G. M. Grass, *Pharm. Res.* **1993**, 10, 113.
- [404] T. Lesuffleur, A. Barbat, E. Dussaulx, A. Zweibaum, *Cancer Res.* **1990**, 50, 6334.
- [405] S. Djelloul, M. E. Forgue-Lafitte, B. Hermelin, M. Mareel, E. Bruyneel, A. Baldi, A. Giordano, E. Chastre, C. Gespach, *FEBS Lett.* **1997**, 406, 234.
- [406] A. M. Sääf, J. M. Halbleib, X. Chen, T. Y. Siu, Y. L. Suet, W. J. Nelson, P. O. Brown, *Mol. Biol. Cell* **2007**, 18, 4245.
- [407] K. Lenaerts, F. K. Bouwman, W. H. Lamers, J. Renes, E. C. Mariman, *BMC Genomics* **2007**, 8, 91.
- [408] R. Lehner, W. Wohlleben, D. Septiadi, R. Landsiedel, A. Petri-Fink, B. Rothen-Rutishauser, *Arch. Toxicol.* **2020**, 94, 2463.
- [409] L. Cacopardo, J. Costa, N. Guazzelli, S. Giusti, S. Meucci, A. Corti, G. Mattei, A. Ahluwalia, *Biomed. Sci. Eng.* **2020**, 3, 104.
- [410] H. J. Kim, D. Huh, G. Hamilton, D. E. Ingber, *Lab Chip* **2012**, 12, 2165.
- [411] N. E. Zeitouni, S. Chotikatum, M. von Köckritz-Blickwede, H. Y. Naim, *Mol. Cell. Pediatr.* **2016**, 3, 14.
- [412] Y. Chen, Y. Lin, K. M. Davis, Q. Wang, J. Rnjak-Kovacina, C. Li, R. R. Isberg, C. A. Kumamoto, J. Mecsas, D. L. Kaplan, *Sci. Rep.* **2015**, 5, 13708.
- [413] N. E. Zeitouni, P. Dersch, H. Y. Naim, M. Von Köckritz-Blickwede, *PLoS One* **2016**, 11, 0146103.
- [414] Y. Tazuke, R. A. Drongowski, D. H. Teitelbaum, A. G. Coran, *Pediatr. Surg. Int.* **2003**, 19, 316.
- [415] H. Xu, F. Qu, H. Xu, W. Lai, Y. A. Wang, Z. P. Aguilar, H. Wei, *BioMetals* **2012**, 25, 45.
- [416] J. Susewind, C. De Souza Carvalho-Wodarz, U. Repnik, E. M. Collnot, N. Schneider-Daum, G. W. Griffiths, C. M. Lehr, *Nanotoxicology* **2016**, 10, 53.
- [417] A. A. M. Kämpfer, M. M. Busch, V. Büttner, G. Bredeck, B. Stahlmecke, B. Hellack, I. Masson, A. Sofranko, C. Albrecht, R. P. F. Schins, *Small* **2020**, 66, 402.
- [418] T. Sato, R. G. Vries, H. J. Snippert, M. Van De Wetering, N. Barker, D. E. Stange, J. H. Van Es, A. Abo, P. Kujala, P. J. Peters, H. Clevers, *Nature* **2009**, 459, 262.
- [419] T. Sato, D. E. Stange, M. Ferrante, R. G. J. Vries, J. H. Van Es, S. Van Den Brink, W. J. Van Houdt, A. Pronk, J. Van Gorp, P. D. Siersema, H. Clevers, *Gastroenterology* **2011**, 141, 1762.
- [420] M. Keding, P. M. Simon-Assmann, B. Lacroix, A. Marxer, H. P. Hauri, K. Haffen, *Dev. Biol.* **1986**, 113, 474.
- [421] J. R. Spence, C. N. Mayhew, S. A. Rankin, M. F. Kuhar, J. E. Vallance, K. Tolle, E. E. Hoskins, V. V. Kalinichenko, S. I. Wells, A. M. Zorn, N. F. Shroyer, J. M. Wells, *Nature* **2011**, 470, 105.
- [422] L. Cao, J. D. Gibson, S. Miyamoto, V. Sail, R. Verma, D. W. Rosenberg, C. E. Nelson, C. Giardina, *Differentiation* **2011**, 81, 1.
- [423] A. Mithal, A. Capilla, D. Heinze, A. Berical, C. Villacorta-Martin, M. Vedaie, A. Jacob, K. Abo, A. Szymaniak, M. Peasley, A. Stuffer, J. Mahoney, D. N. Kotton, F. Hawkins, G. Mostoslavsky, *Nat. Commun.* **2020**, 11, 215.
- [424] C. L. Watson, M. M. Mahe, J. Múnera, J. C. Howell, N. Sundaram, H. M. Poling, J. I. Schweitzer, J. E. Vallance, C. N. Mayhew, Y. Sun, G. Grabowski, S. R. Finkbeiner, J. R. Spence, N. F. Shroyer, J. M. Wells, M. A. Helmrath, *Nat. Med.* **2014**, 20, 1310.
- [425] S. R. Finkbeiner, D. R. Hill, C. H. Altheim, P. H. Dedhia, M. J. Taylor, Y. H. Tsai, A. M. Chin, M. M. Mahe, C. L. Watson, J. J. Freeman, R. Nattiv, M. Thomson, O. D. Klein, N. F. Shroyer, M. A. Helmrath, D. H. Teitelbaum, P. J. Dempsey, J. R. Spence, *Stem Cell Rep.* **2015**, 4, 1140.
- [426] Y. S. Son, S. J. Ki, R. Thanavel, J. J. Kim, M. O. Lee, J. Kim, C. R. Jung, T. S. Han, H. S. Cho, C. M. Ryu, S. H. Kim, D. S. Park, M. Y. Son, *FASEB J.* **2020**, 34, 9899.
- [427] K. B. Jung, H. Lee, Y. S. Son, M. O. Lee, Y. D. Kim, S. J. Oh, O. Kwon, S. Cho, H. S. Cho, D. S. Kim, J. H. Oh, M. Zilbauer, J. K. Min, C. R. Jung, J. Kim, M. Y. Son, *Nat. Commun.* **2018**, 9, 3039.
- [428] N. Arora, J. I. Alsous, J. W. Guggenheim, M. Mak, J. Munera, J. M. Wells, R. D. Kamm, H. H. Asada, S. Y. Shvartsman, L. G. Griffith, *Development* **2017**, 144, 1128.
- [429] T. Grabinger, L. Luks, F. Kostadinova, C. Zimmerlin, J. P. Medema, M. Leist, T. Brunner, *Cell Death Dis.* **2014**, 5, 1228.
- [430] M. Navis, T. Martins Garcia, I. B. Renes, J. L. Vermeulen, S. Meisner, M. E. Wildenberg, G. R. van den Brink, R. M. van Elburg, V. Muncan, *EMBO Rep.* **2019**, 20, 46221.
- [431] K. B. Jung, O. Kwon, M.-O. Lee, H. Lee, Y. S. Son, O. Habib, J.-H. Oh, H.-S. Cho, C.-R. Jung, J. Kim, M.-Y. Son, *J. Clin. Med.* **2019**, 8, 976.
- [432] W. Lu, E. Rettenmeier, M. Paszek, M. F. Yueh, R. H. Tukey, J. Trottier, O. Barbier, S. Chen, *Drug Metab. Dispos.* **2017**, 45, 748.
- [433] D. G. Belair, R. J. Visconti, M. Hong, M. Marella, M. F. Peters, C. W. Scott, K. L. Kolaja, *Toxicol. In Vitro* **2020**, 68, 104928.
- [434] Y. G. Zhang, S. Wu, Y. Xia, J. Sun, *Physiol. Rep.* **2014**, 2, 12147.
- [435] J. L. Leslie, S. Huang, J. S. Opp, M. S. Nagy, M. Kobayashi, V. B. Young, J. R. Spence, *Infect. Immun.* **2015**, 83, 138.
- [436] T. Iwao, N. Kodama, Y. Kondo, T. Kabeya, K. Nakamura, T. Horikawa, T. Niwa, K. Kurose, T. Matsunaga, *Drug Metab. Dispos.* **2015**, 43, 603.
- [437] T. Kabeya, S. Mima, Y. Imakura, T. Miyashita, I. Ogura, T. Yamada, T. Yasujima, H. Yuasa, T. Iwao, T. Matsunaga, *Drug Metab. Pharmacokinet.* **2020**, 35, 374.
- [438] T. Akazawa, S. Yoshida, S. Ohnishi, T. Kanazu, M. Kawai, K. Takahashi, *Drug Metab. Dispos.* **2018**, 46, 1497.
- [439] K. Mayumi, T. Akazawa, T. Kanazu, S. Ohnishi, H. Hasegawa, *J. Pharm. Sci.* **2020**, 109, 1605.
- [440] B. Sidar, B. R. Jenkins, S. Huang, J. R. Spence, S. T. Walk, J. N. Wilking, *Lab Chip* **2019**, 19, 3552.
- [441] J. Y. Co, M. Margalef-Català, X. Li, A. T. Mah, C. J. Kuo, D. M. Monack, M. R. Amieva, *Cell Rep.* **2019**, 26, 2509.
- [442] T. Roodsant, M. Navis, I. Aknouch, I. B. Renes, R. M. van Elburg, D. Pakr, K. C. Wolthers, C. Schultsz, K. C. H. van der Ark, A. Sridhar, V. Muncan, *Front. Cell. Infect. Microbiol.* **2020**, 10, 272.
- [443] L. R. Madden, T. V. Nguyen, S. Garcia-Mojica, V. Shah, A. V. Le, A. Peier, R. Visconti, E. M. Parker, S. C. Presnell, D. G. Nguyen, K. N. Retting, *iScience* **2018**, 2, 156.
- [444] M. Kasendra, A. Tovaglieri, A. Sontheimer-Phelps, S. Jalili-Firoozinezhad, A. Bein, A. Chalkiadaki, W. Scholl, C. Zhang,

- H. Rickner, C. A. Richmond, H. Li, D. T. Breault, D. E. Ingber, *Sci. Rep.* **2018**, *8*, 2871.
- [445] S. Yoshida, H. Miwa, T. Kawachi, S. Kume, K. Takahashi, *Sci. Rep.* **2020**, *10*, 5989.
- [446] M. J. Workman, J. P. Gleeson, E. J. Troisi, H. Q. Estrada, S. J. Kerns, C. D. Hinojosa, G. A. Hamilton, S. R. Targan, C. N. Svendsen, R. J. Barrett, *Cell. Mol. Gastroenterol. Hepatol.* **2018**, *5*, 669.
- [447] K. L. Sinagoga, J. M. Wells, *EMBO J.* **2015**, *34*, 1149.
- [448] Y. H. Tsai, R. Nattiv, P. H. Dedhia, M. S. Nagy, A. M. Chin, M. Thomson, O. D. Klein, J. R. Spence, *Development* **2017**, *144*, 1045.
- [449] K. W. McCracken, J. C. Howell, J. M. Wells, J. R. Spence, *Nat. Protoc.* **2011**, *6*, 1920.
- [450] D. Carroll, *Genetics* **2011**, *188*, 773.
- [451] J. Boch, *Nat. Biotechnol.* **2011**, *29*, 135.
- [452] L. Cong, F. A. Ran, D. Cox, S. Lin, R. Barretto, N. Habib, P. D. Hsu, X. Wu, W. Jiang, L. A. Marraffini, F. Zhang, *Science* **2013**, *339*, 819.
- [453] P. Mali, L. Yang, K. M. Esvelt, J. Aach, M. Guell, J. E. DiCarlo, J. E. Norville, G. M. Church, *Science* **2013**, *339*, 823.
- [454] J. A. Doudna, *Nature* **2020**, *578*, 229.
- [455] F. Hille, H. Richter, S. P. Wong, M. Bratovič, S. Ressel, E. Charpentier, *Cell* **2018**, *172*, 1239.
- [456] J. Lee, D. Bayarsaikhan, G. Bayarsaikhan, J. S. Kim, E. Schwarzbach, B. Lee, *Pharmacol. Ther.* **2020**, *209*, 107501.
- [457] G. Vöfely, T. Berecz, E. Szabó, K. Szabó, E. Hathy, T. I. Orbán, B. Sarkadi, L. Homolya, M. C. Marchetto, J. M. Réthelyi, Á. Apáti, *Mol. Cell. Neurosci.* **2018**, *88*, 222.
- [458] R. Shinnawi, I. Huber, L. Maizels, N. Shaheen, A. Gepstein, G. Arbel, A. J. Tijssen, L. Gepstein, *Stem Cell Rep.* **2015**, *5*, 582.
- [459] S. Li, M. Xia, *Arch. Toxicol.* **2019**, *93*, 3387.
- [460] Á. Apáti, N. Varga, T. Berecz, Z. Erdei, L. Homolya, B. Sarkadi, *Expert Opin. Drug Metab. Toxicol.* **2019**, *15*, 61.
- [461] C. Pires, B. Schmid, C. Petráus, A. Poon, N. Nimsanor, T. T. Nielsen, G. Waldemar, L. E. Hjermand, J. E. Nielsen, P. Hyttel, K. K. Freude, *Stem Cell Res.* **2016**, *17*, 285.
- [462] S. Merkert, U. Martin, *Int. J. Mol. Sci.* **2016**, *17*, 1000.
- [463] C. Cheroni, N. Caporale, G. Testa, *Mol. Autism* **2020**, *11*, 69.
- [464] J. W. Lunden, M. Durens, J. Nestor, R. F. Niescier, K. Herold, C. Brandenburg, Y. C. Lin, G. J. Blatt, M. W. Nestor, *Advances in Neurobiology*, Springer, Berlin **2020**, pp. 259–297.
- [465] A. Sobh, A. Loguinov, G. N. Yazici, R. S. Zeidan, A. Tagmount, N. S. Hejazi, A. E. Hubbard, L. Zhang, C. D. Vulpe, *Toxicol. Sci.* **2019**, *169*, 108.
- [466] C. R. Reczek, K. Birsoy, H. Kong, I. Martínez-Reyes, T. Wang, P. Gao, D. M. Sabatini, N. S. Chandel, *Nat. Chem. Biol.* **2017**, *13*, 1274.
- [467] Y. Zhao, L. Wei, A. Tagmount, A. Loguinov, A. Sobh, A. Hubbard, C. M. McHale, C. J. Chang, C. D. Vulpe, L. Zhang, *Chemosphere* **2020**.
- [468] J. E. Neggers, B. Kwanten, T. Dierckx, H. Noguchi, A. Voet, L. Bral, K. Minner, B. Massant, N. Kint, M. Delforge, T. Vercruysse, E. Baloglu, W. Senapedis, M. Jacquemyn, D. Daelemans, *Nat. Commun.* **2018**, *9*, 502.
- [469] H. Shen, C. M. McHale, M. T. Smith, L. Zhang, *Mutat. Res.: Rev. Mutat. Res.* **2015**, *764*, 31.
- [470] S. Ahmed, Z. Zhou, J. Zhou, S. Q. Chen, *Genomics, Proteomics Bioinf.* **2016**, *14*, 298.
- [471] M. Bachtar, B. N. S. Ooi, J. Wang, Y. Jin, T. W. Tan, S. S. Chong, C. G. L. Lee, *Pharmacogenomics J.* **2019**, *19*, 516.
- [472] S. C. Preissner, M. F. Hoffmann, R. Preissner, M. Dunkel, A. Gewiess, S. Preissner, *PLoS One* **2013**, *8*, 82562.
- [473] K. Takayama, Y. Morisaki, S. Kuno, Y. Nagamoto, K. Harada, N. Furukawa, M. Ohtaka, K. Nishimura, K. Imagawa, F. Sakurai, M. Tachibana, R. Sumazaki, E. Noguchi, M. Nakanishi, K. Hirata, K. Kawabata, H. Mizuguchi, *Proc. Natl. Acad. Sci. USA* **2014**, *111*, 16772.
- [474] D. P. Williams, *Philos. Trans. R. Soc., B* **2018**, *373*, 20170228.
- [475] V. Schwach, R. H. Slaats, R. Passier, *Front. Cardiovasc. Med.* **2020**, *7*, 50.
- [476] J. D. Stewart, R. Horvath, E. Baruffini, I. Ferrero, S. Bulst, P. B. Watkins, R. J. Fontana, C. P. Day, P. F. Chinnery, *Hepatology* **2010**, *52*, 1791.
- [477] M. I. Lucena, R. J. Andrade, C. Martínez, E. Ulzurrun, E. García-Martín, Y. Borraz, M. C. Fernández, M. Romero-Gomez, A. Castiella, R. Planas, J. Costa, S. Anzola, J. A. G. Agúndez, *Hepatology* **2008**, *48*, 588.
- [478] C. S. Ng, A. Hasnat, A. Al Maruf, M. U. Ahmed, M. Pirmohamed, C. P. Day, G. P. Aithal, A. K. Daly, *Eur. J. Clin. Pharmacol.* **2014**, *70*, 1079.
- [479] J. L. Mega, S. L. Close, S. D. Wiviott, L. Shen, R. D. Hockett, J. T. Brandt, J. R. Walker, E. M. Antman, W. Macias, E. Braunwald, M. S. Sabatine, *N. Engl. J. Med.* **2009**, *360*, 354.
- [480] L. Wojnowski, B. Kulle, M. Schirmer, G. Schlüter, A. Schmidt, A. Rosenberger, S. Vonhof, H. Bickeböller, M. R. Toliat, E. K. Suk, M. Tzvetkov, A. Kruger, S. Seifert, M. Kloess, H. Hahn, M. Loeffler, P. Nürnberg, M. Pfreundschuh, L. Trümper, J. Brockmüller, G. Hasenfuss, *Circulation* **2005**, *112*, 3754.
- [481] E. Christidi, H. Huang, S. Shafaattalab, A. Maillet, E. Lin, K. Huang, Z. Laksman, M. K. Davis, G. F. Tibbits, L. R. Brunham, *Sci. Rep.* **2020**, *10*, 10363.
- [482] S. Deguchi, T. Yamashita, K. Igai, K. Harada, Y. Toba, K. Hirata, K. Takayama, H. Mizuguchi, *Drug Metab. Dispos.* **2019**, *47*, 632.
- [483] J. Parrish, K. Lim, B. Zhang, M. Radisic, T. B. F. Woodfield, *Trends Biotechnol.* **2019**, *37*, 1327.
- [484] M. Karimi, S. Bahrami, H. Mirshekari, S. M. M. Basri, A. B. Nik, A. R. Aref, M. Akbari, M. R. Hamblin, *Lab Chip* **2016**, *16*, 2551.
- [485] S. Ahadian, R. Civitarese, D. Bannerman, M. H. Mohammadi, R. Lu, E. Wang, L. Davenport-Huyer, B. Lai, B. Zhang, Y. Zhao, S. Mandla, A. Korolj, M. Radisic, *Adv. Healthcare Mater.* **2018**, *7*, 1700506.
- [486] B. Zhang, M. Radisic, *Lab Chip* **2017**, *17*, 2395.
- [487] T. Osaki, Y. Shin, V. Sivathanu, M. Campisi, R. D. Kamm, *Adv. Healthcare Mater.* **2018**, *7*.
- [488] B. M. Maoz, A. Herland, E. A. Fitzgerald, T. Grevesse, C. Vidoudez, A. R. Pacheco, S. P. Sheehy, T. E. Park, S. Dauth, R. Mannix, N. Budnik, K. Shores, A. Cho, J. C. Nawroth, D. Segrè, B. Budnik, D. E. Ingber, K. K. Parker, *Nat. Biotechnol.* **2018**, *36*, 865.
- [489] S. Sances, R. Ho, G. Vatine, D. West, A. Laperle, A. Meyer, M. Godoy, P. S. Kay, B. Mandefro, S. Hatata, C. Hinojosa, N. Wen, D. Sareen, G. A. Hamilton, C. N. Svendsen, *Stem Cell Rep.* **2018**, *10*, 1222.
- [490] Y. Wang, H. Wang, P. Deng, W. Chen, Y. Guo, T. Tao, J. Qin, *Lab Chip* **2018**, *18*, 3606.
- [491] G. Wang, M. L. McCain, L. Yang, A. He, F. S. Pasqualini, A. Agarwal, H. Yuan, D. Jiang, D. Zhang, L. Zangi, J. Geva, A. E. Roberts, Q. Ma, J. Ding, J. Chen, D. Z. Wang, K. Li, J. Wang, R. J. A. Wanders, W. Kulik, F. M. Vaz, M. A. Laflamme, C. E. Murry, K. R. Chien, R. I. Kelley, G. M. Church, K. K. Parker, W. T. Pu, *Nat. Med.* **2014**, *20*, 616.
- [492] T. Tao, Y. Wang, W. Chen, Z. Li, W. Su, Y. Guo, P. Deng, J. Qin, *Lab Chip* **2019**, *19*, 948.
- [493] M. R. Zanotelli, H. Ardalani, J. Zhang, Z. Hou, E. H. Nguyen, S. Swanson, B. K. Nguyen, J. Bolin, A. Elwell, L. L. Bischof, A. W. Xie, R. Stewart, D. J. Beebe, J. A. Thomson, M. P. Schwartz, W. L. Murphy, *Acta Biomater.* **2016**, *35*, 32.
- [494] B. W. Ellis, A. Acun, U. Isik Can, P. Zorlutuna, *Biomicrofluidics* **2017**, *11*, 024105.
- [495] J. Ribas, Y. S. Zhang, P. R. Pitrez, J. Leijten, M. Miscuglio, J. Rouwkema, M. R. Dokmeci, X. Nissan, L. Ferreira, A. Khademhosseini, *Small* **2017**, *13*, 1603737.
- [496] K. K. Lee, H. A. McCauley, T. R. Broda, M. J. Kofron, J. M. Wells, C. I. Hong, *Lab Chip* **2018**, *18*, 3079.

- [497] K. Achberger, C. Probst, J. C. Haderspeck, S. Bolz, J. Rogal, J. Chuchuy, M. Nikolova, V. Cora, L. Antkowiak, W. Haq, N. Shen, K. Schenke-Layland, M. Ueffing, S. Liebau, P. Loskill, *Elife* **2019**, 8, e46188.
- [498] M. Zhang, C. Xu, L. Jiang, J. Qin, *Toxicol. Res.* **2018**, 7, 1048.
- [499] E. M. Materne, A. P. Ramme, A. P. Terrasso, M. Serra, P. M. Alves, C. Brito, D. A. Sakharov, A. G. Tonevitsky, R. Lauster, U. Marx, *J. Biotechnol.* **2015**, 205, 36.
- [500] D. Bovard, A. Sandoz, K. Luettich, S. Frentzel, A. Iskandar, D. Marescotti, K. Trivedi, E. Guedj, Q. Dutertre, M. C. Peitsch, J. Hoeng, *Lab Chip* **2018**, 18, 3814.
- [501] M. B. Esch, T. L. King, M. L. Shuler, *Annu. Rev. Biomed. Eng.* **2011**, 13, 55.
- [502] N. Tsamandouras, W. L. K. Chen, C. D. Edington, C. L. Stokes, L. G. Griffith, M. Cirit, *AAPS J.* **2017**, 19, 1499.
- [503] C. Oleaga, C. Bernabini, A. S. T. Smith, B. Srinivasan, M. Jackson, W. McLamb, V. Platt, R. Bridges, Y. Cai, N. Santhanam, B. Berry, S. Najjar, N. Akanda, X. Guo, C. Martin, G. Ekman, M. B. Esch, J. Langer, G. Ouedraogo, J. Cotovio, L. Breton, M. L. Shuler, J. J. Hickman, *Sci. Rep.* **2016**, 6, 20030.
- [504] A. Sharma, S. Sances, M. J. Workman, C. N. Svendsen, *Cell Stem Cell* **2020**, 26, 309.
- [505] N. R. Wevers, R. Van Vught, K. J. Wilschut, A. Nicolas, C. Chiang, H. L. Lanz, S. J. Trietsch, J. Joore, P. Vulto, *Sci. Rep.* **2016**, 6, 38856.
- [506] E. Naumovska, G. Aalderink, C. W. Valencia, K. Kosim, A. Nicolas, S. Brown, P. Vulto, K. S. Erdmann, D. Kurek, *Int. J. Mol. Sci.* **2020**, 21, 4964.
- [507] F. Salaris, A. Rosa, *Brain Res.* **2019**, 1723, 146393.
- [508] H. Cui, M. Nowicki, J. P. Fisher, L. G. Zhang, *Adv. Healthcare Mater.* **2017**, 6.
- [509] P. Zhuang, J. An, L. P. Tan, C. K. Chua, in *Proc. Int. Conf. Progress in Additive Manufacturing*, ISSN National Centre For Singapore, Singapore **2018**, pp. 183–188.
- [510] Z. Gu, J. Fu, H. Lin, Y. He, *Asian J. Pharm. Sci.* **2020**, 15, 529.
- [511] L. de la Vega, C. Lee, R. Sharma, M. Amereh, S. M. Willerth, *Brain Res. Bull.* **2019**, 150, 240.
- [512] S. Ilkhanizadeh, A. I. Teixeira, O. Hermanson, *Biomaterials* **2007**, 28, 3936.
- [513] J. Sun, H. Tan, *Materials* **2013**, 6, 1285.
- [514] C. Licht, J. C. Rose, A. O. Anarkoli, D. Blondel, M. Roccio, T. Haraszti, D. B. Gehlen, J. A. Hubbell, M. P. Lutolf, L. De Laporte, *Biomacromolecules* **2019**, 20, 4075.
- [515] M. Bahram, N. Mohseni, M. Moghtader, in *Emerging Concepts Anal. Appl. Hydrogels*, IntechOpen Limited, London **2016**.
- [516] N. Noor, A. Shapira, R. Edri, I. Gal, L. Wertheim, T. Dvir, *Adv. Sci.* **2019**, 6, 1900344.
- [517] S. Romanazzo, S. Nemec, I. Roohani, *Materials* **2019**, 12, 2453.
- [518] C. S. Ong, P. Yesantharao, C. Y. Huang, G. Mattson, J. Boktor, T. Fukunishi, H. Zhang, N. Hibino, *Pediatr. Res.* **2018**, 83, 223.
- [519] F. Maiullari, M. Costantini, M. Milan, V. Pace, M. Chirivi, S. Maiullari, A. Rainer, D. Baci, H. E. S. Marei, D. Seliktar, C. Gargioli, C. Bearzi, R. Rizzi, *Sci. Rep.* **2018**, 8, 13532.
- [520] Q. Gu, E. Tomaskovic-Crook, G. G. Wallace, J. M. Crook, in *Methods in Molecular Biology*, Humana Press Inc., Totowa **2018**, pp. 129–138.
- [521] A. Faulkner-Jones, C. Fyfe, D. J. Cornelissen, J. Gardner, J. King, A. Courtney, W. Shu, *Biofabrication* **2015**, 7, 044102.
- [522] R. Lister, M. Pelizzola, Y. S. Kida, R. D. Hawkins, J. R. Nery, G. Hon, J. Antosiewicz-Bourget, R. Ogmalley, R. Castanon, S. Klugman, M. Downes, R. Yu, R. Stewart, B. Ren, J. A. Thomson, R. M. Evans, J. R. Ecker, *Nature* **2011**, 471, 68.
- [523] L. C. Laurent, I. Ulitsky, I. Slavin, H. Tran, A. Schork, R. Morey, C. Lynch, J. V. Harness, S. Lee, M. J. Barrero, S. Ku, M. Martynova, R. Semechkin, V. Galat, J. Gottesfeld, J. C. I. Belmonte, C. Murry, H. S. Keirstead, H. S. Park, U. Schmidt, A. L. Laslett, F. J. Muller, C. M. Nievergelt, R. Shamir, J. F. Loring, *Cell Stem Cell* **2011**, 8, 106.
- [524] T. M. Schlaeger, L. Daheron, T. R. Brickler, S. Entwisle, K. Chan, A. Ciani, A. DeVine, A. Ettenger, K. Fitzgerald, M. Godfrey, D. Gupta, J. McPherson, P. Malwadkar, M. Gupta, B. Bell, A. Doi, N. Jung, X. Li, M. S. Lyles, E. Brookes, A. B. C. Chetty, D. Demirbas, A. M. Tsankov, L. I. Zon, L. L. Rubin, A. P. Feinberg, A. Meissner, C. A. Cowan, G. Q. Daley, *Nat. Biotechnol.* **2015**, 33, 58.
- [525] Y. Yoshida, K. Takahashi, K. Okita, T. Ichisaka, S. Yamanaka, *Cell Stem Cell* **2009**, 5, 237.
- [526] K. Kim, R. Zhao, A. Doi, K. Ng, J. Unternaehrer, P. Cahan, H. Hongguang, Y. H. Loh, M. J. Aryee, M. W. Lensch, H. Li, J. J. Collins, A. P. Feinberg, G. Q. Daley, *Nat. Biotechnol.* **2011**, 29, 1117.
- [527] S. Logan, T. Arzua, S. G. Canfield, E. R. Seminary, S. L. Sison, A. D. Ebert, X. Bai, *Compr. Physiol.* **2019**, 9, 565.
- [528] D. L. Villeneuve, D. Crump, N. Garcia-Reyero, M. Hecker, T. H. Hutchinson, C. A. LaLone, B. Landesmann, T. Lettieri, S. Munn, M. Nepelska, M. A. Ottinger, L. Vergauwen, M. Whelan, *Toxicol. Sci.* **2014**, 142, 312.
- [529] D. L. Villeneuve, D. Crump, N. Garcia-Reyero, M. Hecker, T. H. Hutchinson, C. A. LaLone, B. Landesmann, T. Lettieri, S. Munn, M. Nepelska, M. A. Ottinger, L. Vergauwen, M. Whelan, *Toxicol. Sci.* **2014**, 142, 321.
- [530] S. M. Bell, X. Chang, J. F. Wambaugh, D. G. Allen, M. Bartels, K. L. R. Brouwer, W. M. Casey, N. Choksi, S. S. Ferguson, G. Fraczekiewicz, A. M. Jarabek, A. Ke, A. Lumen, S. G. Lynn, A. Paini, P. S. Price, C. Ring, T. W. Simon, N. S. Sipes, C. S. Sprankle, J. Strickland, J. Troutman, B. A. Wetmore, N. C. Kleinstreuer, *Toxicol. In Vitro* **2018**, 47, 213.
- [531] Y. Li, R. A. Wingert, *Clin. Transl. Med.* **2013**, 2, 11.



Ellen Fritsche is PI at the IUF – Leibniz Research Institute for Environmental Medicine and appointed University Professor for Environmental Toxicology at the Heinrich-Heine University in Duesseldorf, Germany. She did a postdoc at the National Institute for Environmental Health Sciences at Research Triangle Park in North Carolina, USA and habilitated in 2008 on the role of the aryl hydrocarbon receptor in skin. She has been collaborating with international agencies like the European Food Safety Authority and the US-Environmental Protection Agency for many years with the goal of advancing alternative methods for developmental neurotoxicity testing for regulatory application.



Julia Tigges is a postdoctoral researcher in the research group of Prof. Ellen Fritsche at the IUF – Leibniz Research Institute for Environmental Medicine. She received her Ph.D. degree from the Heinrich-Heine University Duesseldorf, Germany in 2011 for her work on the role of the arylhydrocarbon-receptor in the reaction of the skin to exogenous noxae. In addition to her skin expertise, she became specialist on quality control management of human-induced pluripotent stem cells (hiPSC) and the development of hiPSC-based alternative methods to animal tests.



Katharina Koch is a postdoctoral researcher in the research group of Prof. Ellen Fritsche at the IUF. She received her Ph.D. degree in 2018 for her work in the Neurosurgical Clinic of the University Hospital Düsseldorf, Germany focusing on the interference in cellular energy and lipid metabolism to target therapy-resistant cancer stem cells in glioblastoma. During her Ph.D., she was a visiting researcher at the Pathology Department of the Johns Hopkins Hospital, Baltimore, USA. Since 2019, she works at the IUF developing stem cell-based in vitro assays for endocrine disruption-mediated developmental neurotoxicity as part of the Horizon 2020 ENDpoiNTs project.

Stem Cells for Next Level Toxicity Testing in the 21st Century

Ellen Fritsche, Thomas Haarmann-Stemmann, Julia Kapr, Saskia Galanjuk, **Julia Hartmann**, Peter R. Mertens, Angela A. M. Kämpfer, Roel P. F. Schins, Julia Tigges, and Katharina Koch

Fachzeitschrift/Buch: *Small*

Impact Factor: 13,281 (2020)

Beteiligung an der Publikation: 10 %

Schreiben des Kapitels „2.2 Brain“

Typ der Autorenschaft: Co-Autorenschaft

Status der Publikation: veröffentlicht am 23.Dezember 2020

2.3 Characterization and application of electrically active neuronal networks established from human induced pluripotent stem cell-derived neural progenitor cells for neurotoxicity evaluation

Laura Nimtz, **Julia Hartmann**, Julia Tigges, Stefan Masjosthusmann, Martin Schmuck, Eike Keßel, Stephan Theiss, Karl Köhrer, Patrick Petzsch, James Adjaye, Claudia Wigmann, Dagmar Wieczorek, Barbara Hildebrandt, Farina Bendt, Ulrike Hübenthal, Gabriele Brockerhoff, Ellen Fritsche

Stem Cell Research

Neurotoxizität wird durch eine Vielzahl von Wirkmechanismen vermittelt, die zu einer Störung der neuronalen Funktion führen. Funktionelle *in vitro*-basierte neurale Netzwerke können dabei helfen, eine größere Anzahl an Chemikalien bezüglich ihres neurotoxischen Potentials zu untersuchen. In dieser Studie haben wir hiPSCs in einer Sphärenkultur in hiNPCs und anschließend in hNN differenziert. Der Einfluss von zwei Differenzierungsmedien mit (CINDA) oder ohne (NDM) zugesetzte Faktoren, welche eine Netzwerkreifung begünstigen, wurde untersucht und mit Netzwerken, welche aus primären Rattenzellen (rNN) generiert wurden, verglichen. Gen- und Proteinexpression, sowie die elektrische Aktivität, wurden an verschiedenen Zeitpunkten während der Netzbildung untersucht. Das Transkriptom von für 5, 14 oder 28 Tage in CINDA differenzierten hNN wurde mit der Genexpression des sich entwickelnden menschlichen Gehirns verglichen. Molekulare Expressionsanalysen sowie Messung der elektrischen Aktivität zeigen, dass die hiNPCs in unterschiedliche neuronale Subtypen und Astrozyten differenzieren. Im Vergleich zu rNN, sind hNN nach derselben Differenzierungszeit weniger elektrisch aktiv. Allerdings zeigen die in CINDA differenzierten hNN höhere Spikeraten als die in NDM differenzierten hNN.

Durch die Belastung mit Substanzen, die neuronale Rezeptoren stimulieren oder inhibieren, konnten inhibitorische, GABAerge Neurone nachgewiesen werden, während die Reaktion auf Glutamat und seine Antagonisten AP5 und NBQX begrenzt war. In CINDA differenzierte GABAerge hNN könnten eine nützliche Ergänzung in einer *in vitro* Testbatterie zur Ermittlung von Neurotoxizität darstellen.



Characterization and application of electrically active neuronal networks established from human induced pluripotent stem cell-derived neural progenitor cells for neurotoxicity evaluation

Laura Nimtz^a, Julia Hartmann^a, Julia Tigges^a, Stefan Masjosthusmann^a, Martin Schmuck^a, Eike Keßel^{a,b}, Stephan Theiss^c, Karl Köhrer^d, Patrick Petzsch^d, James Adjaye^e, Claudia Wigmann^a, Dagmar Wiczorek^f, Barbara Hildebrandt^f, Farina Bendt^a, Ulrike Hübenthal^a, Gabriele Brockerhoff^a, Ellen Fritsche^{a,g,*}

^a IUF - Leibniz Research Institute for Environmental Medicine, Duesseldorf, Germany

^b Department of Biophysics, Ruhr-University Bochum, Bochum, Germany

^c Medical Faculty, Institute of Clinical Neuroscience and Medical Psychology, Heinrich-Heine-University, Duesseldorf, Germany

^d Biological and Medical Research Centre (BMFZ), Medical Faculty, Heinrich-Heine-University, Universitätsstraße 1, 40225 Duesseldorf, Germany

^e Medical Faculty, Institute for Stem Cell Research & Regenerative Medicine, Heinrich-Heine-University, Duesseldorf, Germany

^f Medical Faculty, Institute of Human Genetics, Heinrich-Heine-University, Duesseldorf, Germany

^g Medical Faculty, Heinrich-Heine-University, Duesseldorf, Germany

ARTICLE INFO

Keywords:

Neurotoxicology

Stem cell

hiPSC-NPC

MEA

Neuronal network

Electrical activity

Transcriptome

Dopaminergic

Cholinergic

In vitro in vivo comparison

ABSTRACT

Neurotoxicity is mediated by a variety of modes-of-actions leading to disturbance of neuronal function. In order to screen larger numbers of compounds for their neurotoxic potential, *in vitro* functional neuronal networks (NN) might be helpful tools. We established and characterized human NN (hNN) from hiPSC-derived neural progenitor cells by comparing hNN formation with two different differentiation media: in presence (CINDA) and absence (neural differentiation medium (NDM)) of maturation-supporting factors. As a NN control we included differentiating rat NN (rNN) in the study. Gene/protein expression and electrical activity from *in vitro* developing NN were assessed at multiple time points. Transcriptomes of 5, 14 and 28 days *in vitro* CINDA-grown hNN were compared to gene expression profiles of *in vivo* human developing brains. Molecular expression analyses as well as measures of electrical activity indicate that NN mature into neurons of different subtypes and astrocytes over time. In contrast to rNN, hNN are less electrically active within the same period of differentiation time, yet hNN grown in CINDA medium develop higher firing rates than hNN without supplements. Challenge of NN with neuronal receptor stimulators and inhibitors demonstrate presence of inhibitory, GABAergic neurons, whereas glutamatergic responses are limited. hiPSC-derived GABAergic hNN grown in CINDA medium might be a useful tool as part of an *in vitro* battery for assessing neurotoxicity.

1. Introduction

For protecting human and environmental health, industrial, agricultural and consumer products must be registered and approved by the European Food Safety Authority (EFSA) or the European Chemical Agency (ECHA) before entering the market. Neurotoxic effects are of major scientific and socio-political concern, because they often result in irreversible adverse outcomes (Costa et al., 2008; Aschner et al., 2017). Neurotoxicity guideline studies (OECD, 1997; EPA, 1998) are currently performed *in vivo*. These are resource-intensive regarding the time and

costs required (Bal-Price et al., 2008) and might not well reflect the human situation because of inter-species variations (Matthews, 2008; Leist and Hartung, 2013). Therefore, alternative *in vitro* testing strategies based on human cells that reduce or replace animal experiments (Russell et al., 1959) are of high interest for neurotoxicity research (Coecke et al., 2006; Zuang et al., 2018). Medium- to high-throughput *in vitro* testing requires a large amount of cell material. In contrast to the use of human embryonic stem cells, which bear ethical concerns (Kao et al., 2008; Singh et al., 2015; Mayer et al., 2018) human induced pluripotent stem cells (hiPSC) are ideal for providing an ethically

* Corresponding author at: IUF - Leibniz Institute for Environmental Medicine, Aufm Hennekamp 50, 40225 Duesseldorf, Germany.

E-mail address: ellen.fritsche@iuf-duesseldorf.de (E. Fritsche).

<https://doi.org/10.1016/j.scr.2020.101761>

Received 25 June 2019; Received in revised form 20 February 2020; Accepted 5 March 2020

Available online 10 March 2020

1873-5061/ © 2020 The Authors. Published by Elsevier B.V. This is an open access article under the CC BY-NC-ND license (<http://creativecommons.org/licenses/by-nc-nd/4.0/>).

inoffensive and unlimited supply of material for *in vitro* neurotoxicological evaluations (Takahashi et al., 2007; Robinton and Daley, 2012; Zagoura et al., 2017). For screening larger numbers of compounds for their neurotoxic potential, *in vitro* functional neuronal networks (NN) derived from hiPSC might be helpful tools. Neural differentiation, NN formation and establishment of functional signal transmissions for neurotoxicity assessment based on hiPSC is thus very auspicious, yet still barely studied (Odawara et al., 2014; Cotterill et al., 2016; Kasteel and Westerink, 2017; Pistollato et al., 2017; Paavilainen et al., 2018; Tukker et al., 2018; Izsak et al., 2019; Hyvärinen et al., 2019), especially in light of the multiple modes-of-actions (MoA) initiating disturbance of neuronal functions (Masjosthusmann et al., 2018a).

One method for studying electrophysiology of neurons and NN is the microelectrode array (MEA) technology. MEAs record extracellular local field potentials at different locations of neurons on a network-level and provide data about their activity properties and patterns (Johnstone et al., 2010). The MEA technology allows assessment of NN electrical activity in real-time and evaluation of the dynamics of network behavior under chemical manipulations (Odawara et al., 2014, 2016; Tukker et al., 2016, 2018). The use of MEAs in toxicological testing is relatively new and has so far been mainly applied for rat NN (rNN) (Hogberg et al., 2011; McConnell et al., 2012; Valdivia et al., 2014; Brown et al., 2016; Cotterill et al., 2016; Frank et al., 2017; Vassallo et al., 2017; Shafer et al., 2019; Wagenaar et al., 2006; Napoli and Obeid, 2016).

In this study, we continue our previous work on neural induction of hiPSC (Hofrichter et al., 2017) by establishing and characterizing human NN (hNN) from hiPSC-derived neural progenitor cells (hiNPC) by comparing hNN formation with two different differentiation media: in presence (CINDA) and absence (NDM) of maturation-supporting factors. As a NN control we included differentiating rNN. Gene and protein expression and electrical activity from *in vitro* developing NN were assessed at multiple time points and in presence and absence of pharmacological compounds. In addition, microarrays were performed for transcriptome analyses of hNN, which were compared to *in vivo* transcriptomes of human developing brains.

2. Material and methods

2.1. Compounds used

γ -Aminobutyric acid (GABA), Glutamate and Domoic acid (DA) were obtained from Sigma Aldrich (Saint Louis, USA). NBQX disodium salt, DL-AP5 sodium salt and Bicuculline were obtained from Santa Cruz Biotechnologies (Texas, USA). CytoToxOne Cytotoxicity Assay Kit was obtained from Promega Corporation (Madison, USA). For detailed information and solvents see Supplementary Material.

2.2. Cell culture and neural induction

The hiPSC lines A4 (Wang and Adjaye, 2011) and IMR-90 (Clone-4, WiCell, USA) were cultured in mTeSR1 medium (Stemcell Technologies, Germany) on Matrigel (BD Bioscience, Germany). Medium was changed every day and cells were passaged chemically in colonies with 0.5 mM EDTA. hiPSC lines were regularly tested for their pluripotency and their chromosomal integrity.

Neural induction of hiPSC lines was performed using the neural induction medium (NIM) protocol according to (Hofrichter et al., 2017). Briefly, hiPSC colonies were cut in $200 \times 200 \mu\text{m}$ squares using a passaging tool (STEMPRO EZPassage, Thermo Fisher Scientific) and cultured on polyhema (Sigma Aldrich) coated dishes with NIM medium (for detailed medium composition see Supplementary Material) for 7 days. Generated free-floating 3D-Spheres were transferred into new polyhema dishes with NIM containing 10 ng/mL bFGF (R&D Systems, Germany) for another 14 days. Afterwards they were referred to as

hiNPC and cultured in polyhema dishes with neural proliferation medium (NPM, see Supplementary Material).

Primary rat NPC (rNPC) were prepared from full brains of Wistar rats on postnatal day 1 as previously described (Baumann et al., 2014). 3D neurospheres were cultured free-floating in NPM and half of the medium was changed every 2–3 days.

Proliferating NPC at a diameter of 400–500 μm were cut into $200 \times 200 \mu\text{m}$ squares using a McIlwaine tissue chopper (Mickle Laboratory, UK) to expand the culture (Fritsche et al., 2011; Baumann et al., 2014). For experimental use, spheres were chopped 2 days before plating.

2.3. Neuronal differentiation and immunocytochemistry

Neuronal differentiation and immunocytochemistry were performed as described previously by Hofrichter et al., 2017, using NDM and CINDA medium, the latter consisting of NDM, creatine monohydrate, interferon- γ , neurotrophin-3, dibutyryl-cAMP and ascorbic acid. For detailed information and medium composition see Supplementary Material.

Quantification of synapses and receptors was performed by analyzing neurite mass in μm^2 and number of synapses (synapses/neurite area (μm^2)) using the Omnisphero software as previously described (Hofrichter et al., 2017). Due to differences in TUBB3 intensities between rat and human cells, different structuring elements were used to eliminate uneven backgrounds. Resulting images were thresholded with the Otsu method (for detailed information see Supplementary Material).

2.4. Quantitative reverse-transcription PCR

RNA was isolated using the RNeasy Mini Kit (Qiagen, Germany) according to manufacturer's protocol. RNA of hiPSC (undifferentiated controls), proliferating hiNPC and rNPC (30 neurospheres of 300 μm diameter each) and human and rat NN after 7, 14, 21 and 28 days *in vitro* (DIV) were prepared. For the latter, cells were chopped to 100 μm aggregates and plated on poly-D-lysine (PDL)/laminin-coated 24-well-plates in NDM or CINDA (hiNPC) or only NDM (rNPC). For reverse transcription, 500 ng RNA was transcribed into cDNA using the QuantiTect Reverse Transcription Kit (Qiagen, Germany). Quantitative polymerase chain reaction (q-RT-PCR) was performed using the QuantiFast SYBR Green PCR Kit (Qiagen, Germany) in the Rotor Gene Q Cycler (Qiagen, Germany) following manufacturer's instructions. Analysis was performed using standards of the gene of interest, allowing to calculate copy numbers, and expression was normalized to β -actin (Dach et al., 2017). Each experiment was performed at least three times with three independent neural inductions. For primer sequences see Supplementary Material.

2.5. NN differentiation on microelectrode arrays (MEA)

Electrical activities of NN were recorded as described in Hofrichter et al., 2017. Briefly, we used 200 hiNPC or rNPC neurospheres (100 μm diameter), seeded onto PDL/laminin pre-coated single-well MEAs (Multichannelsystems (MCS), Germany) either in NDM or CINDA medium. Recordings were performed with the MC-Rack (MCS, Germany) from 2 to 15 weeks *in vitro*. After approximately 5 min of equilibration, each recording consisted of a 5 min baseline recording of spontaneous activity. For data analyses the first minute was cut off and mean values of the mean firing rate (MFR), mean bursting rate (MBR), spikes per burst and active electrodes (AE) of the last 4 min were calculated. For statistical analyses see Supplementary Material.

2.6. NN characterization with pharmaceuticals

To characterize NN regarding their receptor composition MEA chips

were equilibrated in the MEA-headstage 2 min prior to recording. To be regarded as active, NN had to have a minimum of 3 AE. These were defined by the detection of a minimum of 5 spikes/min. For treatment analyses, a baseline measurement of active MEAs for 5 min was recorded. Afterwards, the respective receptor agonist/antagonist was added to the well and allowed to equilibrate for 5 min (wash-in-phase), followed by 5 min recording. Then MEAs were washed twice with medium (wash-out-phase) and further cultivated in fresh medium. Measurements of receptor treatment were performed twice a week starting at day 7. The recordings and data analyses were done as described in 2.5.

2.7. DA treatment on multi-well-MEAs (mwMEAs)

24-well MEA plates (MCS, Germany), each well containing 12 gold electrodes were used. Wells were coated with PDL (0.1 mg/mL, 50 μ L for 48 h at 4 °C; Sigma Aldrich) washed with PBS and coated with Laminin (0.01 mg/mL, 48 h at 4 °C, L2020, Sigma Aldrich). Afterwards, 50 hiNPC or rNPC spheres (100 μ m diameter) were seeded into the wells and incubated with NDM or CINDA medium, respectively. MwMEAs were recorded with the Multiwell-Screen (MCS) and analyzed with Multiwell-Analyzer (MCS, Germany). For details on hardware settings and spike and burst detection parameters see Supplementary Material. Active networks were defined as stated in 2.5. Individual recordings were performed in week 2–6, in the absence (baseline) and presence of the indicated concentrations of DA in NDM or CINDA for 15 min.

2.8. Affymetrix microarrays

For hiPSC and hiNPC (30 neurospheres of 300 μ m diameter each) isolation of RNA was performed using the RNeasy Mini Kit (Qiagen, Germany) according to manufacturer's protocol. Therefore, cells were chopped to 100 μ m aggregates and plated on PDL/laminin-coated 6-well-plates. After 5, 14 and 28 days of cultivation in CINDA medium cells were harvested and RNA was isolated. cDNA synthesis and biotin labeling of cDNA was performed according to the manufacturer's protocol (3' IVT Plus Kit; Affymetrix, Inc.) and as previously described (Masjostusmann et al., 2018b). For detailed information on the gene expression analysis by microarrays see Supplementary Material.

2.9. Data analysis and statistics

Unless otherwise stated all statistical analyses were performed using GraphPad Prism 6.00 for Windows (GraphPad, USA). Immunocytochemical quantification and pharmaceutical data were analyzed using one-way ANOVA, qRT-PCR and DA-treatment data were analyzed using a two-way ANOVA followed by a Bonferroni test to correct for multiple testing. The significance cut-off was set to $p \leq 0.05$.

3. Results

3.1. Molecular characterization of hiNPC-differentiated cultures

Differentiation of hiNPC was performed with NDM and maturation supporting CINDA medium. Before plating, hiNPC stained positive for the markers PAX6, NESTIN and SOX2 (Fig. S1). After 28DIV hiNPC grown in NDM or CINDA medium and rNPC grown in NDM differentiated into TUBB3⁺ neurons and GFAP⁺ astrocytes (Figs. 1 and 2A; Fig. S2). Human neurons express the pre- and postsynaptic proteins SYN1 and PSD95 as well as the receptor-specific proteins GABAAR β , GluR1 and NMDAR1 with no significant differences between the tested medium conditions, i.e. NDM and CINDA (Fig. 2A and B). To further characterize the networks, mRNA expression analyses were performed and gene copy numbers determined by product-specific standards. This procedure enables comparison of gene expression across species and

has the advantage of giving information on magnitude of absolute gene expression rather than relative gene changes as by using the $\Delta\Delta CT$ method (Gassmann et al., 2010; Walter et al., 2019). Gene expression of the NPC marker *NESTIN* was stably expressed in human cultures over time, whereas its expression significantly decreased in rat cultures starting at DIV14 (Fig. 3A). The expression of the mature astrocyte marker *AQP4* was significantly upregulated on DIV28 in CINDA- compared to NDM-cultures, whereas *Aqp4* expression in rat cultures increased early starting at DIV7 (Fig. 3C). Expression of the glial fibrillar astrocytic protein *gfap*/*GFAP* significantly increased from DIV7 in rNN but exhibited only marginal changes in human cells (Fig. 3D). The neuronal marker *MAP2* increased in hNN from DIV7 and low expression values for *map2* were observed in rNN (Fig. 3E). To analyze the time of synapse formation we used the pre- and post-synaptic markers *SYN1* and *DLG4*, respectively, which are expressed after 7DIV in both species (Fig. 3F–G). Expression of *SLC17A7* (glutamate transporter vGLUT1) and *GAD1* (glutamic acid decarboxylase) differ remarkably. While *SLC17A7* copy numbers are extremely low (<1–5 copy numbers/10,000 copies β -ACTIN), *GAD1* is well expressed (>100 copy numbers/10,000 copies β -ACTIN) suggesting predominantly GABAergic neurotransmission (Fig. 3H and I). Concerning neuronal subtypes, hNN show an increasing expression of *ACHE* (acetylcholinesterase), *GRIA1* (AMPA receptor), and *TH* (tyrosine hydroxylase) over time with *TH* expression being significantly induced on 14DIV in CINDA-NN compared to NDM-NN (Fig. 3J), while similar to *SLC17A7*, *GRIN1* (NMDAR, Fig. 3K) and *SLC6A4* (serotonergic neurons, Fig. S3) copy numbers are very low. In contrast, rNN revealed very low expression of *ache* and *th* (<1 copy numbers/10,000 copies β -actin) compared to human cells (Fig. 3J and M).

3.2. Electrical activity of hiNPC–CINDA- and hiNPC–NDM-NN over time

We studied whether differentiation of neural cultures resulted in generation of functional NN. Therefore, we examined multiple electrophysiological parameters on MEA chips for single electrodes as well as the entire network. Human NN exhibited spontaneous electrical activity after 2 weeks in culture. Starting with the same number of MEA-chips for both medium conditions, hNN grown in CINDA medium (CINDA-NN) produced more active chips (Fig. 4; Fig. S4) and higher electrical activities measured as MBR, spikes per burst and the number of AEs than NDM-NN (Fig. 4B–D). In week 3 the mean value of all recorded activities (except for the MFR) was significantly higher in CINDA-NN compared to NDM-NN. NN generated from rNPC serve as positive controls (Mack et al., 2014; Alloisio et al., 2015; Wallace et al., 2015) and displayed higher bursting activity levels than hNN (Fig. 4A–D). Over the entire differentiation time of 15 weeks (Fig. S4), CINDA- and NDM-NN reached highest activity levels of all measured parameters within the first 6 weeks with CINDA-NN exhibiting higher MBR, spikes/burst and number of AEs than NDM-NN. In contrast, rNN reached their maximum activity across all parameters measured within 7 to 11 weeks of differentiation.

3.3. Characterization of NNs with agonists and antagonists of neuronal receptors

To study if differentiated NN contain functional GABAergic and glutamatergic neurons, we treated NN with the GABA receptor (GABAR) agonist GABA or the glutamate receptor agonist glutamate (Fig. 5). NN of both species responded to GABA with a reduction in MFR, MBR and number of spikes/burst (Fig. 5A–C and D) suggesting presence of functional GABARs. Glutamate also decreased these parameters, yet to a lower extent indicating no functional excitatory glutamatergic receptors. Treatment of NN with the GABAR inhibitor bicuculline also reduced MFR and spikes/burst in NN not treated with external GABA (Fig. 5A, C, and E) implying a minimal presence of glutamatergic neurons in the networks. If the NN consisted of a

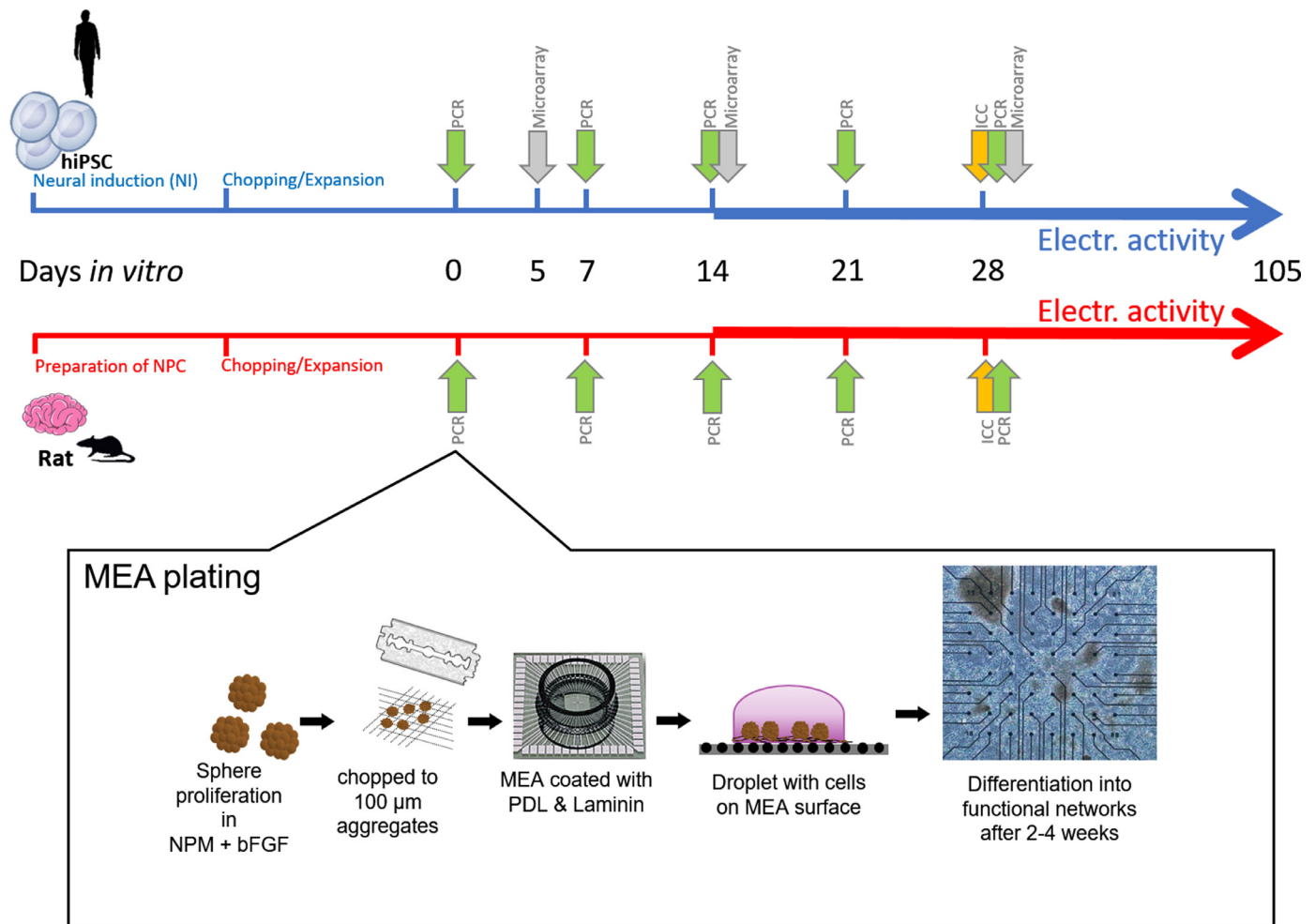


Fig. 1. Experimental set up. hiNPC were neurally induced from hiPSC or generated from rat brain (PND1) and cultivated as floating neurospheres. qRT-PCR analyses and MEA recordings were performed weekly from day 0 until 15 weeks *in vitro*. Cells were fixed for immunocytochemical staining after 28 days of differentiation. For MEA plating spheres were cut into 0.1 mm aggregates and 200 were seeded on PDL/laminin pre-coated MEA recording fields.

comparable amount of glutamatergic and GABAergic neurons, one would expect a strong increase in network activity after bicuculline exposure (Xiang et al., 2007; Mack et al., 2014) that we did not observe. In addition, the NMDAR and AMPAR antagonists, AP5 and NBQX, respectively, exhibited no effects on NN except for AP5 reducing spike frequency in the rNN which suggests the possible presence of NMDAR in rNN (Fig. 5A).

3.4. NN response to the shellfish toxin DA

To determine if the NN assay based on hiNPC differentiated in CINDA medium is a useful tool for acute neurotoxicity testing *in vitro*, we treated CINDA- as well as rNN with the shellfish toxin and glutamate analogue DA (Chandrasekaran et al., 2004; Watanabe et al., 2011; Vassallo et al., 2017), which is a model compound previously used in a multi-laboratory evaluation of MEA-based measurements of neural network activity for acute neurotoxicity testing (Vassallo et al., 2017). DA is an excitotoxicant which binds to postsynaptic glutamate receptors with a 100-fold higher affinity than glutamate, causing receptor over-activation, which leads to neuronal excitotoxicity, neuronal degeneration and ultimately cell death (Watanabe et al., 2011; Magdalini et al., 2019). For concentration-response analyses we used 24-well multiwell-MEAs (mwMEAs) instead of single-well MEAs as a medium throughput setup for compound testing. One well of a mwMEA contains 12 electrodes, compared to 59 electrodes in a single well MEA (Fig. 6A). The

distances between electrodes are 200 µm. Of the total of 72 and 96 wells measured with human and rat NN, respectively, 33 (45.8%) and 32 wells (44.5%) had 9–12 AE/well, 22 (30.6%) and 30 wells (31.3%) had 5–8 AE/well, 13 (18.1%) and 28 wells (29.2%) had 1–4 AE/well, and only 4 (5.6%) and 6 wells (6.3%) had no AE/well (Fig. 6B). Acute exposure to increasing concentrations of DA for 15 min increased spontaneous activity of hNN and rNN with significant effects only for the total burst count in rNN (Fig. 6C) but did not cause cytotoxicity in either of the networks up to 24 h after exposure (Fig. S5). Although not statistically quantifiable, the firing pattern visualized in the representative Spike Raster Plots (SRP) reveals changes in activity pattern in both species after treatment with 1 µM DA compared to baseline activity (Fig. 6D). Additional activity parameters exhibited no significant changes (Fig. S5).

3.5. Microarray analyses of CINDA-NN and a comparison to published *in vivo* data

To monitor differentiation and maturation processes of hNN on the transcriptome level, we analyzed mRNA expression profiles of hiPSC, proliferating hiNPC, and hiNPC-derived NN differentiated for 5, 14, and 28DIV in CINDA medium using Human PrimeViewArrays from Affymetrix. Microarray data was validated by qRT-PCR analyses for representative genes (Fig. S6). Only genes that were at least 2-fold significantly regulated ($p \leq 0.05$) were used for subsequent analyses.

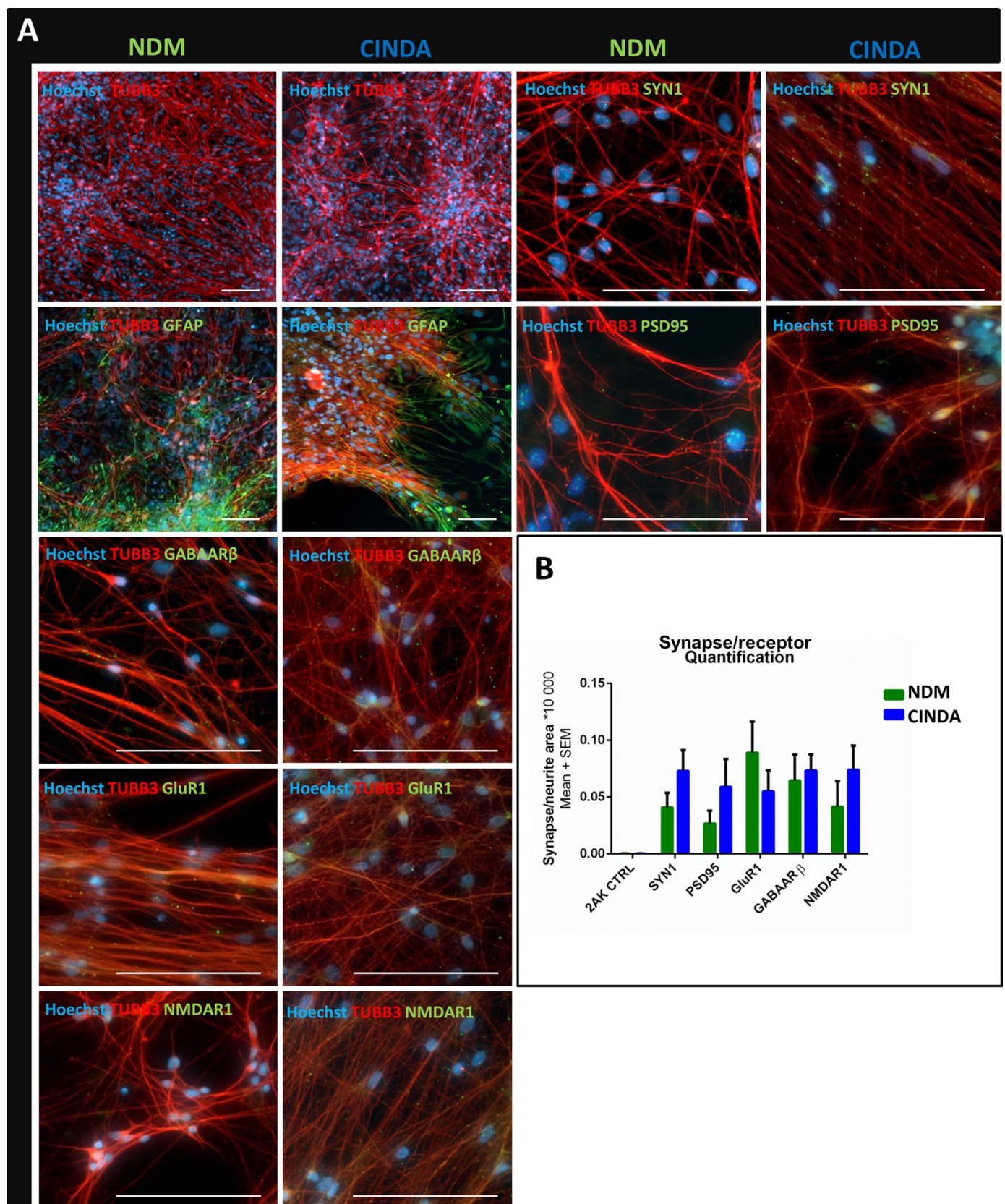


Fig. 2. Immunocytochemical staining of hNN. (A) Representative pictures of hNN differentiated with NDM or CINDA medium for 28 days: neurons (TUBB3; red), astrocytes (GFAP; green), pre- (SYN1) and post synapses (PSD95; green dots), GABA receptor (GABAAR β), glutamate receptor (GLUR1) and NMDA receptor (NMDAR1; green dots). Nuclei were stained with Hoechst. Scale bars are 100 μ m. (B) Quantifications of synapses/receptors (mean + SEM) as ratio to total neurite area ($n = 3-6$). (For interpretation of the references to color in this figure legend, the reader is referred to the web version of this article.)

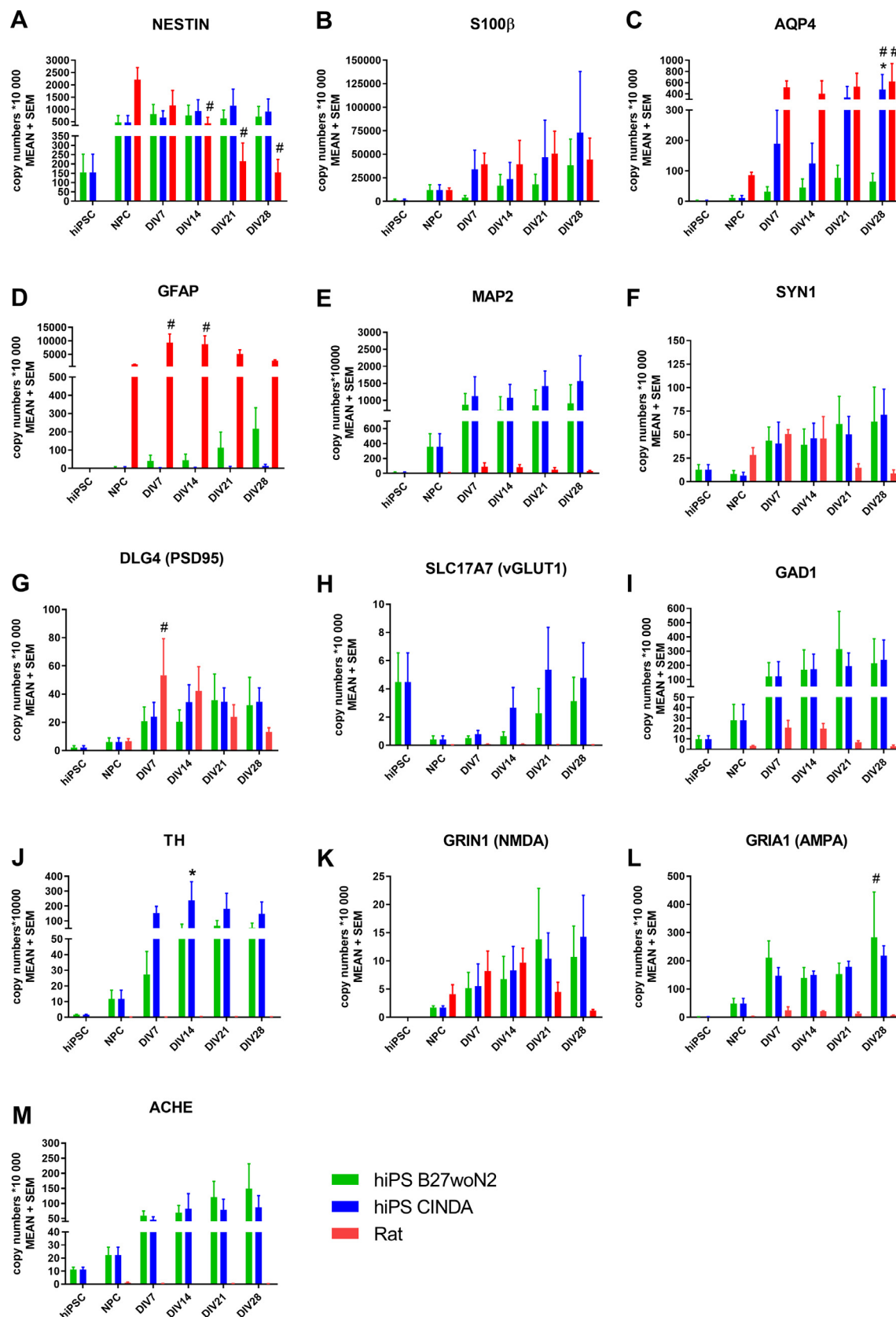


Fig. 3. mRNA expression profiles of hiPSC, hiNPC and hNN compared to rNPC and rNN. qRT-PCR analysis of different cell types for neural progenitor (*NESTIN*, *MAP2*), astrocyte (*S100 β* , *AQP4*, *GFAP*), synaptic (*SYN1*, *DLG4*) and neuronal subtype specific markers (*SLC17A7*, *ACHE*, *GRIA1*, *GRIN1*, *GAD1*, *TH*) differentiated for 28 DIV in NDM or CINDA medium. rNN serve as positive control. Data are presented as mean + SEM. *significant to NDM, #significant to NPC ($n = 3$, $p < 0.05$).

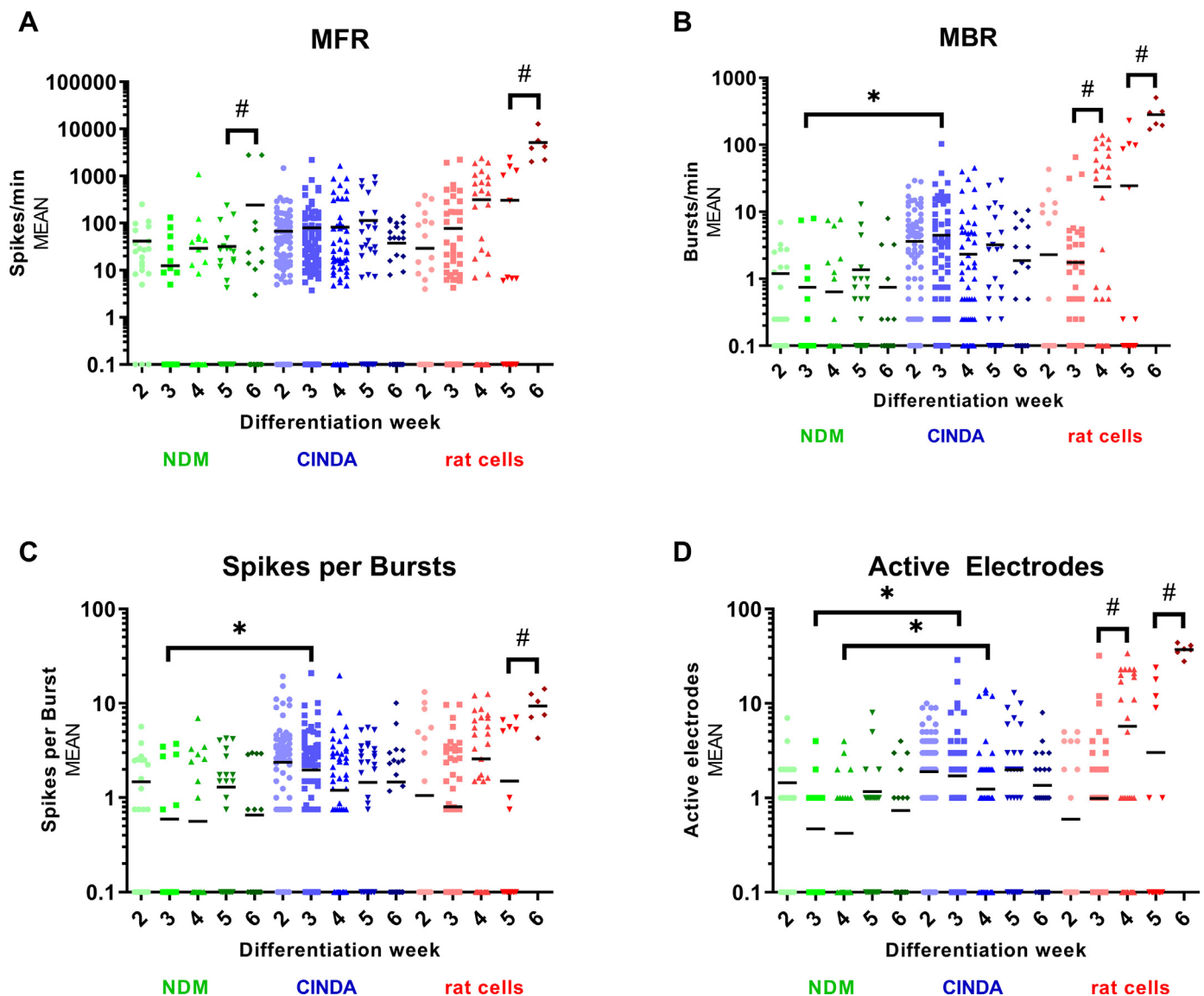


Fig. 4. Spontaneous electrical activity of hNN- and rNN on MEA. Scatter plots of hNN (NDM/CINDA) and rNN differentiated for six weeks on MEAs. Plotted are the (A) MFR, (B) MBR, (C) spikes per burst and (D) AEs, one dot represents the mean of one chip. Both hiNPC: $n = 40$ and rat: $n = 43$ at start of experiment. Black lines represent the mean of all data points. *Significant to NDM, #significant within condition ($p < 0.05$). Note: For a better visualization all values between 0 and 0.1 were manually set to 0.1 so that the data points appear on the X-axis.

Cluster- and principle component analyses (PCA) support the strong differentiation potential of hiPSC (turquoise) into proliferating hiNPC (green) and further neutrally differentiated hiNPC at DIV5 (blue), DIV14 (red) and DIV28 (purple) with very small replicate variations (Fig. 7A and B). In differentiating hiNPC a total of 2629 genes are differentially expressed (DEX) across the three time points (Fig. 7C). The number of DEX genes increased over differentiation time, from 1370 (DIV5) to 1793 (DIV14) and to 2368 (DIV28). The overlap of all conditions was 43.3% (1139 genes), indicating that these genes might be generally important during the transition from a proliferative neural progenitor cell to neural effector cells. This is supported by an overrepresentation of gene ontology (GO) biological processes related to cell proliferation (e.g. GO:0007049~cell cycle, GO:0000280~nuclear division or GO:0006260~DNA replication). In contrast, genes that are regulated between 5 and 14, 14 and 28 as well as 5 and 28 days, control processes related to neuronal differentiation and maturation (e.g. GO:0007399 ~ nervous system development, GO:0048699 ~ generation of neurons, GO:0099537 ~ trans-synaptic signaling; Appendix I). Overrepresentation analysis of GO biological processes of all regulated

genes (2629) summarize gene changes of proliferation-differentiation transition as well as neural differentiation and neuronal network maturation (Appendix II). These findings support the *in vitro* development of hNN consisting of neurons and astroglia cells, forming synapses to build a functional NN. To determine to which extent the gene changes observed *in vitro* are representative of the developing human brain *in vivo*, *in vitro* DEX genes (Ovs28DIV) were compared to published DEX genes of *in vivo* transcription profiles of the prefrontal cortex between post-conceptional week 6 (embryonic) and 12 (fetal; (Kang et al., 2011)). These timepoints were chosen based on a recent publication mapping developing brain organoids to *in vivo* fetal brain samples (Amiri et al., 2018). The comparison of *in vivo* vs. *in vitro* DEX genes revealed that from more than 2837 *in vivo* DEX genes, 868 (44.1% *in vivo* and 36.7% *in vitro*) are commonly regulated (Fig. 7D). DEX gene groups over-represented in these data sets were identified by an overrepresentation analysis (Appendix III). DEX genes within a selection of manually selected GO-terms including the neural/neuronal specific terms, i.e. neural proliferation (NP), astrocytic-, general glia cell- and neuronal differentiation, synapse formation/plasticity, glutamatergic

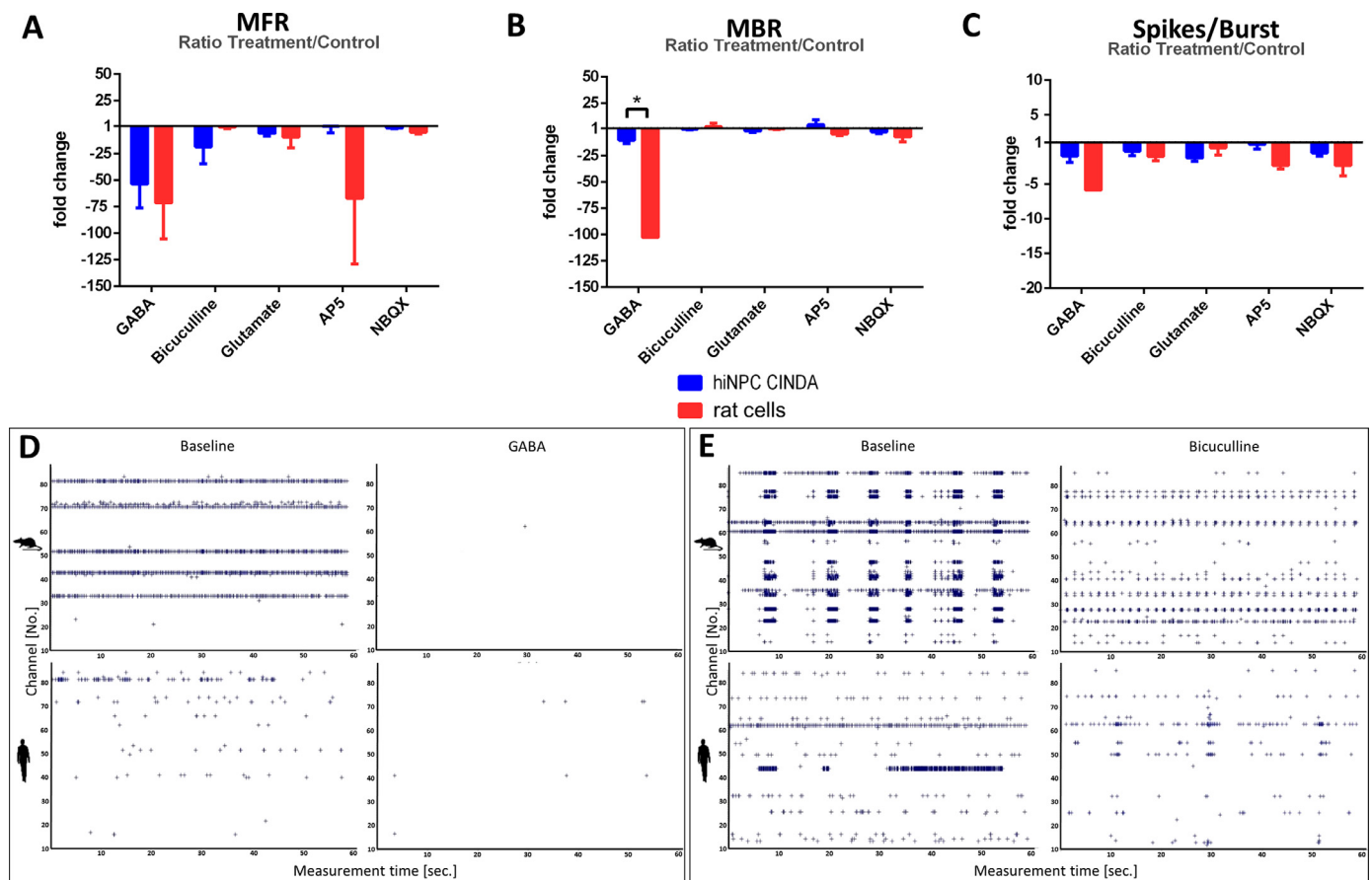


Fig. 5. Modifications of electrical activity by acute pharmacological treatment. Ratio of treatment/control of CINDA-NN and rNN treated with GABA [1 mM], bicuculline [10 μ M], glutamate [100 μ M], AP5 [20 μ M] and NBQX [10 μ M]. Results are depicted as A) MFR, B) MBR and C) Spikes/Burst as mean + SEM. hiNPC: $n = 7-10$, rNN: $n = 6-10$. D and E Representative 60 s SRP of hNN and rNN of baseline- and GABA (D) or bicuculline treatment (E). *Significant within condition ($p < 0.05$).

neurons, GABAergic neurons, and radial glia (RG) differentiation (Appendix III) were compared between the *in vitro* and *in vivo* data sets. The result indicates that *in vivo* more GO-terms are enriched, more genes are generally regulated in each GO term and respective genes are mostly stronger regulated *in vivo* than *in vitro*, yet transcriptomes of the *in vitro* cultures reveal well-defined cellular differentiation processes (Fig. 7E, Appendices II and III).

4. Discussion

Human hazard and risk assessment of potentially neurotoxic chemicals is based on *in vivo* animal experiments (Bal-Price et al., 2008). Those experiments are time and cost intensive and do not necessarily reflect the human situation because of inter-species variations (Leist and Hartung, 2013). Thus, alternative *in vitro* testing strategies using human-based material are of special interest for neurotoxicity testing (Coecke et al., 2006; Zuang et al., 2017). We previously established the neural induction of hiPSC to hiNPC, cultured as 3D neurospheres (Hofrichter et al., 2017) and now continued the work by characterizing differentiating hiNPC for their ability of NN formation. We composed the CINDA medium by adding agents to NDM, which support (i) synapse formation, (ii) maturation of different neuronal subtypes and (iii) spontaneous NN activity (Andres et al., 2008; Belinsky et al., 2013; Dutta et al., 2015; Leipzig et al., 2010; Zhu et al., 2012). Human cultures that differentiate over a time course of 28DIV into neurons and astrocytes express *NESTIN* during the whole differentiation time. Although *NESTIN* is down-regulated and replaced by neurofilaments and *GFAP* during neuro- or gliogenesis *in vivo*

(Michalczyk and Ziman, 2005), as well as in the differentiating rat cultures, it was reported by others that neurally differentiated hiNPC do not down-regulate *NESTIN* over time (Pistollato et al., 2014; Zagoura et al., 2017). In human stem cell-derived culture neurogenesis occurs before astrogenesis (Nat et al., 2007; Liu and Zhang, 2011; Yuan et al., 2011). Thus, the neuronal marker *MAP2* already plateaus after 7DIV with no differences between CINDA medium and NDM, while it takes until 21DIV for the astrocyte marker *AQP4* to reach maximum expression. CINDA-NN seem to favor astrocyte differentiation compared to NDM-NN as *AQP4* is significantly higher expressed in CINDA-NN compared to NDM-NN. In contrast, *gfap* expression already levels after 7DIV in rNN followed by a continuous up-regulation of *map2* over the 28DIV. rNN are not produced from iPSC-derived NPC, but are primary NPC prepared from rat postnatal day (PND) 1 pups. These resemble a later developmental phase which might explain the differences in timing (Baumann et al., 2014, Baumann et al., 2016, Masjosthusmann et al., 2018a). Compared to the rat, human NDM-NN express 25–100-fold less *GFAP* and CINDA-NN express little *GFAP* on mRNA level, however, the immunostaining suggests the presence of *GFAP* protein. One reason for this could be that astrocytes in hNN are protoplasmic, which express far less *GFAP* than fibrous astrocytes (Molofsky et al., 2012; Molofsky and Deneen, 2015). The significantly stronger *gfap* expression in rNN is likely due to the presence of radial glia in these cultures as suggested by their morphology. Molecular analyses reveal the presence of pre- (*SYN1*) and post-synaptic (*DLG4/PSD95*) structures as well as glutamate NMDA and AMPA receptors and the GABAA receptor in developing NN with no differences between NDM and CINDA medium. Despite receptor expression, glutamatergic

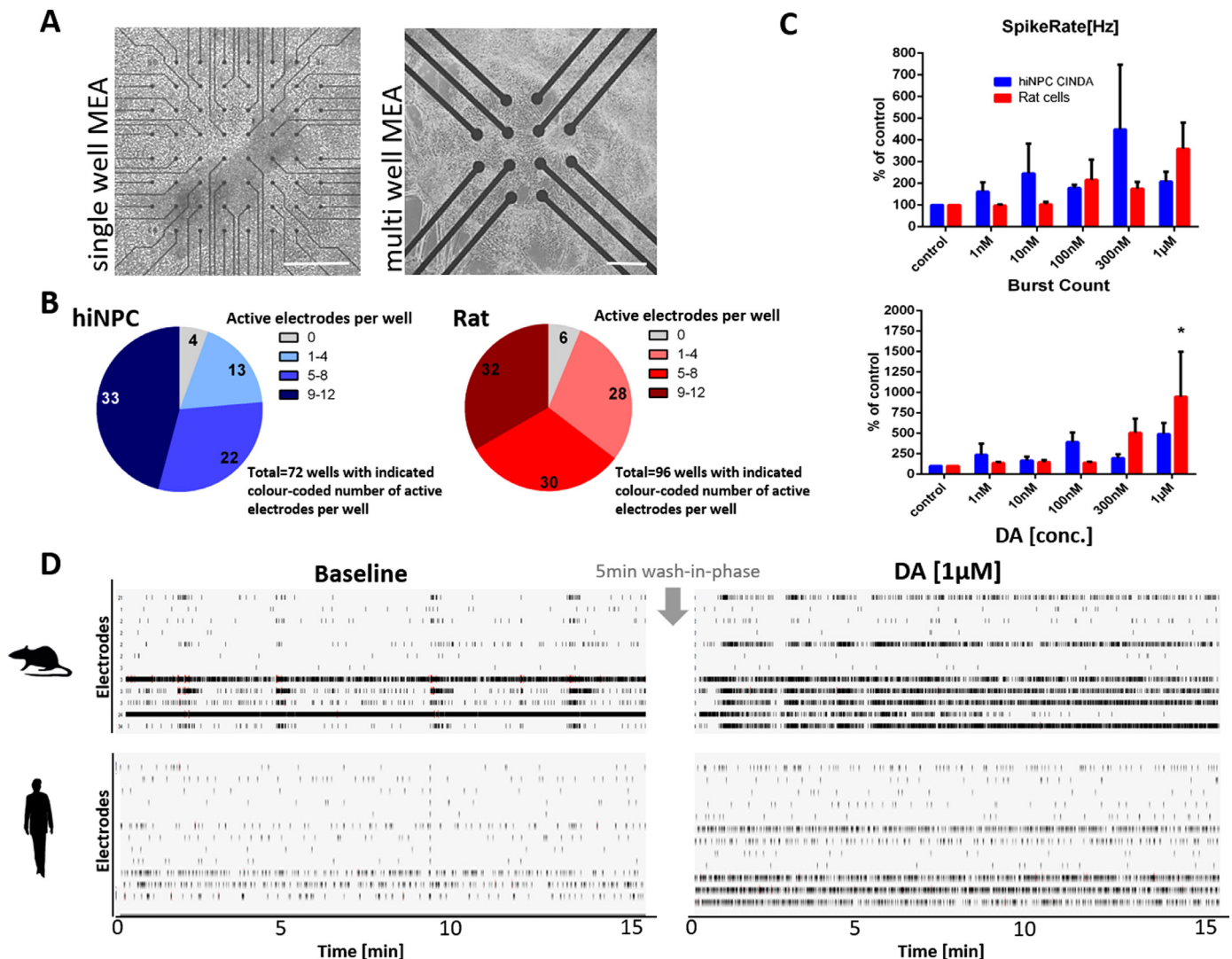


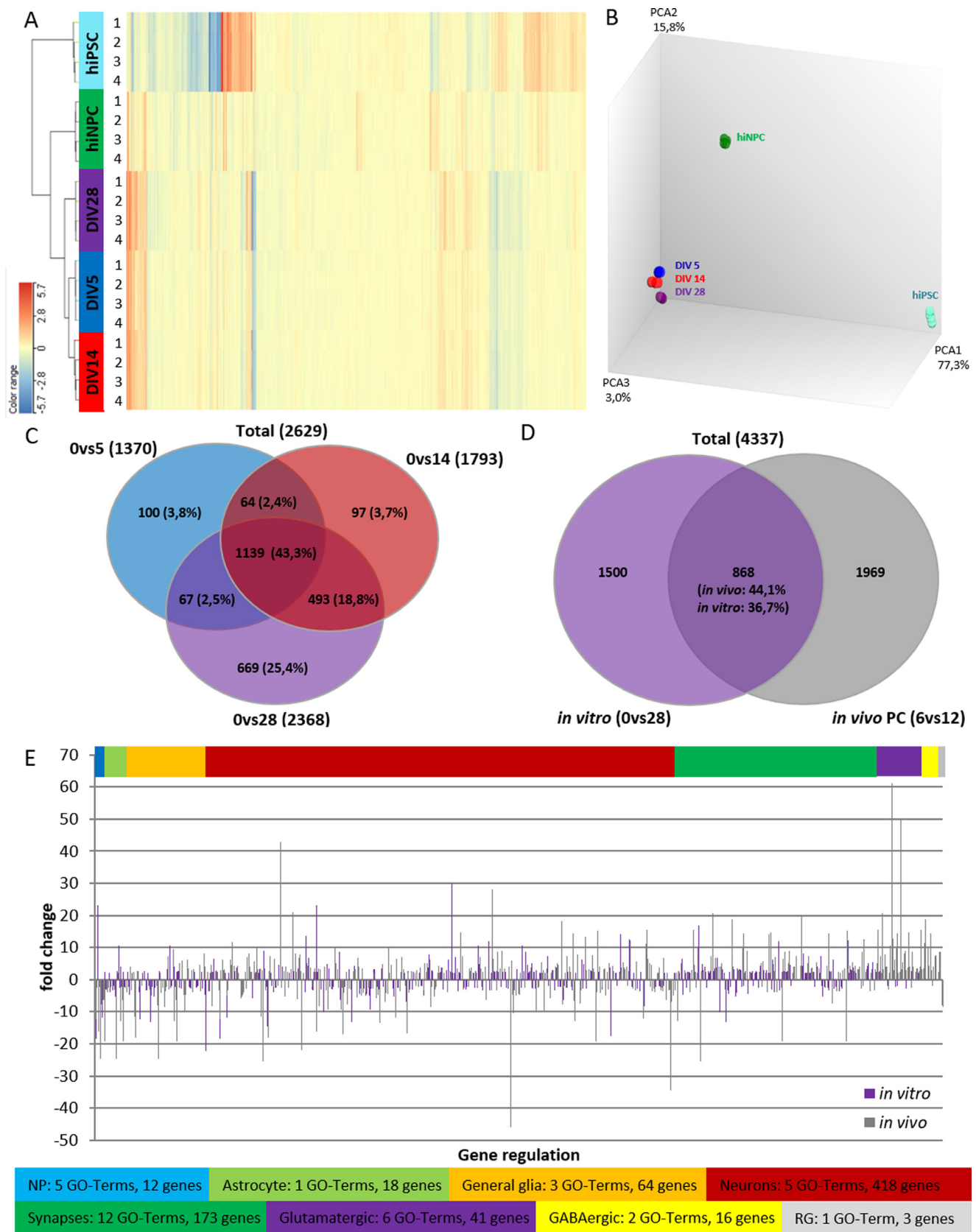
Fig. 6. Acute treatment of NN in mwMEAs with the shellfish toxin DA. (A) Representative phase-contrast images of hiNN on a singlewell- and multiwell-MEA recording field. (B) Pie-diagram of the all wells of hiNN (blue, 72 wells, measured on day 18, 20 and 22) and rNN (red, 96 wells, measured on day 20 and 22) with indication (color-code) of the numbers of AEs per well. (C) Acute treatment of hiNPC and rNN with DA. Mean + SEM of the spike rate [Hz] and the burst count (number of total bursts) are plotted in percent of solvent control for the acute exposure time of 15 min. *significant to control ($n = 3$, $p < 0.05$). (D) Representative 15 min SRP of 1 μ M DA of rNN and hiNN. (For interpretation of the references to color in this figure legend, the reader is referred to the web version of this article.)

neurons seem to be absent in the cultures and neurons mainly seem to be of GABAergic nature with presence of dopaminergic and cholinergic neurons. Here, only TH expression was significantly higher expressed in CINDA-NN on DIV14 compared to NDM-NN. Dopaminergic differentiation might be promoted by cAMP in the CINDA medium (Belinsky et al., 2013).

Only few groups have been analyzing electrical activity of hiPSC-derived neural cultures on MEAs (Toivonen et al., 2013; Odawara et al., 2014, 2016; Tukker et al., 2016; Hofrichter et al., 2017; Seidel et al., 2017; Tukker et al., 2018; Izsak et al., 2019; Shimba et al., 2019). Some studied spontaneous firing in hiPSC-derived pure neuronal cultures (Toivonen et al., 2013) or in co-cultures with human (Tukker et al., 2016, 2018) or rat astrocytes (Odawara et al., 2014; Seidel et al., 2017). Astrocytes support neuronal function like signal transmission and maturation, their presence should therefore be advantageous *in vitro* NN (Clarke and Barres, 2013). However, when studying hNN, the use of human instead of rat astrocytes is preferable (Oberheim et al., 2006; Tjarnlund-Wolf et al., 2014). The differentiation protocol used in this study yields hiPSC-derived neurons and astrocytes simultaneously. NN differentiated in two different media, CINDA or NDM, lead to astrocyte maturation and overall electrical network activity with a higher

number of AE, MBR and spikes/burst when cells were grown in CINDA medium. Bursting activity is associated with enhanced synapse formation and long-term potentiation of neuronal connections (Maeda et al., 1995; Lisman, 1997) indicating a certain degree of network maturity. rNN were more mature than hNN during week 2–6, indicated by the higher burst activities, possibly due to a faster development of this species (Semple et al., 2013).

To test the functionality of neuronal receptors, we treated hNN, grown in CINDA, and rNN with GABA or glutamate receptor agonists and antagonists. Network data indicates presence of functionally active GABAR that respond to GABA with NN inhibition in both species. In contrast, glutamate receptors seem to be non-functional, as the excitatory neurotransmitter glutamate did not increase spike frequency. The small decrease in MFR upon glutamate treatment might be due to astrocytic glutamate metabolism (Gegelashvili and Schousboe, 1998) to glutamine that is then synthesized to GABA by GABAergic neurons in the absence of glutamatergic neurons (Lujan et al., 2005; Walls et al., 2015). That glutamatergic neurons are non-functional is further supported by a bicuculline treatment: As GABAR inhibitor, bicuculline should increase the NN activity (Fukushima et al., 2016; Odawara et al., 2014, 2016), which is not observed in this study. Very low mRNA



(caption on next page)

expression of *SLC17A7* (vGLUT1) supports these functional findings. Antagonization of the glutamate receptors NMDA and AMPA with AP5 and NBQX, respectively, cause only small changes in hNN activity levels. Presence of their gene products *GRIN1* and *GRIA1* as well as their receptor proteins in combination with the functional data is indicative of not fully matured glutamate receptors. Similar results were

Fig. 7. Transcriptome analyses of hiPSC, hiNPC and hNN and overrepresentation analyses of GO biological processes compared to *in vivo* data. (A) Cluster analysis of hiPSC, hiNPC and hNN. Turquoise = hiPSCs; green = hiNPC; blue = hNN (DIV5); red = hNN (DIV14); violet = hNN (DIV28), 4 replicates each. In the heatmap blue genes are down-regulated, red genes are upregulated. The intensity of the colors serves as a measure of the strength of the regulation ($p \leq 0.05$). (B) PCA of gene expression as demonstrated in (A). (C) Venn-diagram of regulated genes. Plotted are all genes that are significantly ($p \leq 0.05$) up or down regulated by at least 2-fold between the following conditions: red = 0vs5DIV, blue = 0vs14DIV and green = 0vs28DIV. (D) Venn-diagram of regulated genes comparing *in vitro* to *in vivo*. Plotted are all genes that are significantly ($p \leq 0.05$) up or down regulated by at least 2-fold between the following conditions: violet: *in vitro* hiNPC (0vs28DIV) and gray: *in vivo* samples of human prefrontal cortex from week 6vs12 (Kang et al., 2011). (E) Comparative analyses of single gene expression (genes from (D)) annotated to the color-coded GO-terms, which are associated to neural and synaptic markers *in vitro* (violet, 0vs28DIV) and *in vivo* (gray, prefrontal cortex, week 6vs12, (Kang et al., 2011)). (For interpretation of the references to color in this figure legend, the reader is referred to the web version of this article.)

reported from Tang et al., 2013. Plating hiPSC-derived NPCs on laminin for patch-clamp analyses revealed much larger GABA receptor currents than glutamate receptor currents, while NMDA receptor currents were very low in the examined time span of 60DIV. This was similar to previous findings in rat embryonic neurons (Deng et al., 2007) making the authors suggest an evolutionarily conserved role of GABA during early neural development (Tang et al., 2013). However, rNN, which resemble a later developmental stage compared to hNN, seem to possess some functional NMDAR, as addition of AP5 strongly decreases network activity. In the future, the differentiation of hiNPC into also glutamatergic neurons might be achieved by addition of the neurotrophic factors BDNF and GDNF (Izsak et al., 2019) or retinoic acid (Zhang et al., 2013) to the CINDA medium.

It has been proposed that iPSC-derived cell models might be suitable alternative models for future *in vitro* toxicological testings (Jennings, 2015; Suter-Dick et al., 2015). Therefore, we adapted the NN to a 24-well plate MEA testing format that allows higher throughput testing than single well MEAs. Our data suggests that stability and reproducibility of the multi-well MEAs is higher compared to single well MEAs because the number of active chips and the percentage of AE is higher in multi-well compared to single well MEAs. We used the shellfish-toxin DA as a model compound for acute neurotoxicity testing (Vassallo et al., 2017), which causes neuronal excitotoxicity, neuronal degeneration and ultimately cell death (Magdalini et al., 2019; Watanabe et al., 2011). SRP of both analyzed species indicate pattern changes after acute DA exposure, yet only rNN display a significant alteration of the total burst count at 1 μ M. NN characterization suggests an immature hNN glutamate receptor system, while rNN seem to possess at least some functional NMDAR that probably mediate the DA effect on the burst count. In previous studies rNN from cortical cultures responded to an acute treatment of 500 nM DA with a decrease of network activity parameters (Hogberg et al., 2011; Wallace et al., 2015; Vassallo et al., 2017), suggesting cytotoxicity of neurons due to hyperstimulation. The higher sensitivity of these cultures is probably due to a higher maturity of primary rat neurons compared to rNN that were differentiated from NPC in this study. So far, no data on DA treatment of hNN *in vitro* is available. As recently shown, rNN grown on MEAs are well suited for screening large amounts of neurotoxic compounds. This is especially due to their low inter-experimental variability (Frank et al., 2017; Shafer et al., 2019).

To compare the hNN *in vitro* system to developing brains *in vivo*, we performed transcriptome analyses of hiPSC, hiNPC and further differentiated NN at 5, 14 and 28 DIV. Different *in vitro* differentiation stages clearly separate in the PCA analyses showing hiPSC differentiation potential on a global gene expression level. Similar results were published earlier e.g. for generating good manufacturing practice grade hiNPC for therapeutic purposes (Rosati et al., 2018) as well as for hiPSC-derived brain organoids (Amiri et al., 2018). The *in vitro-in vivo* comparison relates DEX genes between 0 and 28DIV with DEX genes between 6 and 12 weeks post conception from the previously published data of *in vivo* prefrontal cortex samples (Kang et al., 2011). Of the 2837 DEX genes during early brain development *in vivo*, 868 are also regulated *in vitro* indicating that as expected only a fraction of the neurodevelopmental processes that are regulated in the intact organ take place *in vitro*. However, enriched GO-terms of the *in vitro* cultures reveal presence of well-defined cellular differentiation processes.

5. Summary and conclusion

NN from hiNPC cultured as neurospheres consist of a co-culture of neurons and astrocytes. Synapse-specific proteins, neuronal subtype-specific receptors and enzymes are expressed and respective proteins are present. While GABAR are shown to be functional, glutamate related receptors seem to be absent or lack maturity, which is a limitation of this model. In contrast, at least the NMDAR seems to be functional in rNN that are also responsive to GABA. The neuronal maturation medium CINDA resulted in higher NN activity levels compared to NDM. Formation of NN in this work relied on spontaneous, self-organized hiNPC differentiation, maturation and synapse formation and is therefore highly variable. This is a critical hurdle for pharmacological or toxicological applications. Use of multi-well MEAs compared to single well MEAs seems to improve variability of MEA measurements, but more optimizing work is needed before this system is ready for testing application. Yet in the future GABAergic hNN grown in CINDA medium might be useful as part of an *in vitro* battery for assessing neurotoxicity.

CRediT authorship contribution statement

Laura Nimtz: Conceptualization, Methodology, Investigation, Writing - original draft. **Julia Hartmann:** Investigation, Writing - review & editing. **Julia Tigges:** Supervision, Writing - original draft. **Stefan Masjosthusmann:** Formal analysis, Writing - original draft. **Martin Schmuck:** Software. **Eike Keßel:** Software. **Stephan Theiss:** Software. **Karl Köhrer:** Data curation. **Patrick Petzsch:** Data curation. **James Adjaye:** Resources. **Claudia Wigmann:** Formal analysis. **Dagmar Wiecek:** Data curation. **Barbara Hildebrandt:** Data curation. **Farina Bendt:** Investigation. **Ulrike Hübenthal:** Investigation. **Gabriele Brockerhoff:** Investigation. **Ellen Fritsche:** Funding acquisition, Supervision, Project administration, Writing - review & editing.

Acknowledgments

This work was supported by the project CERST (Center for Alternatives to Animal Testing) of the Ministry for innovation, science and research of the State of North-Rhine Westphalia, Germany [file number 233-1.08.03.03-121972].

Disclosure of Potential Conflicts of Interest

None.

Supplementary materials

Supplementary material associated with this article can be found, in the online version, at doi:10.1016/j.scr.2020.101761.

References

- Alloisio, S., Nobile, M., Novellino, A., 2015. Multiparametric characterisation of neuronal network activity for *in vitro* agrochemical neurotoxicity assessment. *Neurotoxicology* 48, 152–165. <https://doi.org/10.1016/j.neuro.2015.03.013>.
- Andres, R.H., Ducray, A.D., Schlattner, U., et al., 2008. Functions and effects of creatine in the central nervous system. *Brain Res. Bull.* 76, 329–343. <https://doi.org/10.1016/j.bbr.2008.03.013>.

- brainresbull.2008.02.035.
- Amiri, A., Coppola, G., Scuderi, S., et al., 2018. Transcriptome and epigenome landscape of human cortical development modeled in organoids. *Science* 362, 6420. <https://doi.org/10.1126/science.aat6720>.
- Aschner, M., Ceccatelli, S., Daneshian, M., et al., 2017. Reference compounds for alternative test methods to indicate developmental neurotoxicity (DNT) potential of chemicals: example lists and criteria for their selection and use. *ALTEX* 34, 49–74. <https://doi.org/10.14573/altex.1604201>.
- Bal-Price, A.K., Sunol, C., Weiss, D.G., et al., 2008. Application of *in vitro* neurotoxicity testing for regulatory purposes: symposium iii summary and research needs. *Neurotoxicology* 29, 520–531. <https://doi.org/10.1016/j.neuro.2008.02.008>.
- Baumann, J., Gassmann, K., Fritsche, E., 2014. Comparative human and rat “Neurosphere assay” for developmental neurotoxicity testing. In: Costa, L.G., Davila, J.C., Lawrence, D.A., Reed, D.J. (Eds.), *Current Protocols in Toxicology*. John Wiley & Sons.
- Baumann, J., Gassmann, K., Masjosthusmann, S., et al., 2016. Comparative human and rat neurospheres reveal species differences in chemical effects on neurodevelopmental key events. *Arch. Toxicol.* 90, 1415–1427. <https://doi.org/10.1007/s00204-015-1568-8>.
- Belinsky, G.S., Sirois, C.L., Rich, M.T., et al., 2013. Dopamine receptors in human embryonic stem cell neurodifferentiation. *Stem Cells Dev.* 22, 1522–1540. <https://doi.org/10.1089/scd.2012.0150>.
- Brown, J.P., Hall, D., Frank, C.L., et al., 2016. Editor's highlight: evaluation of a microelectrode array-based assay for neural network ontogeny using training set chemicals. *Toxicol. Sci.: Off. J. Soc. Toxicol.* 154, 126–139. <https://doi.org/10.1093/toxsci/kfw147>.
- Chandrasekaran, A., Ponnambalam, G., Kaur, C., 2004. Domoic acid-induced neurotoxicity in the hippocampus of adult rats. *Neurotox. Res.* 6, 105–117. <https://doi.org/10.1007/bf03033213>.
- Clarke, L.E., Barres, B.A., 2013. Emerging roles of astrocytes in neural circuit development. *Nat. Rev. Neurosci.* 14, 311–321. <https://doi.org/10.1038/nrn3484>.
- Coecke, S., Eskes, C., Gartlon, J., et al., 2006. The value of alternative testing for neurotoxicity in the context of regulatory needs. *Environ. Toxicol. Pharmacol.* 21, 153–167. <https://doi.org/10.1016/j.etap.2005.07.006>.
- Costa, L.G., Giordano, G., Guizzetti, M., et al., 2008. Neurotoxicity of pesticides: a brief review. *Front. Biosci.* 13, 1240–1249. <https://doi.org/10.2741/2758>.
- Cotterill, E., Charlesworth, P., Thomas, C.W., et al., 2016. A comparison of computational methods for detecting bursts in neuronal spike trains and their application to human stem cell-derived neuronal networks. *J. Neurophysiol.* 116, 306–321. <https://doi.org/10.1152/jn.00093.2016>.
- Dach, K., Bendt, F., Huebenthal, U., et al., 2017. BDE-99 impairs differentiation of human and mouse NPCs into the oligodendroglial lineage by species-specific modes of action. *Sci. Rep.* 7. <https://doi.org/10.1038/srep44861>.
- Deng, L., Yao, J., Fang, G., et al., 2007. Sequential postsynaptic maturation governs the temporal order of GABAergic and glutamatergic synaptogenesis in rat embryonic cultures. *J. Neurosci.* 27, 10860–10869. <https://doi.org/10.1523/JNEUROSCI.2744-07.2007>.
- Dutta, A., Gautam, R., Chatterjee, S., et al., 2015. Ascorbate protects neurons against oxidative stress: a Raman microspectroscopic study. *ACS Chem. Neurosci.* 6, 1794–1801. <https://doi.org/10.1021/acschemneuro.5b00106>.
- EPA, U.S. 1998. Health Effects Guidelines OPPTS 870.6200, Neurotoxicity Screening Battery, vol. EPA 71.
- Frank, C.L., Brown, J.P., Wallace, K., et al., 2017. From the cover: developmental neurotoxins disrupt activity in cortical networks on microelectrode arrays: results of screening 86 compounds during neural network formation. *Toxicol. Sci.: Off. J. Soc. Toxicol.* 160, 121–135. <https://doi.org/10.1093/toxsci/kfx169>.
- Fritsche, E., Gassmann, K., Schreiber, T., 2011. Neurospheres as a model for developmental neurotoxicity testing. *Methods Mol. Biol.* 758, 99–114. https://doi.org/10.1007/978-1-61779-170-3_7.
- Fukushima, K., Miura, Y., Sawada, K., et al., 2016. Establishment of a human neuronal network assessment system by using a human neuron/astrocyte co-culture derived from fetal neural stem/progenitor cells. *J. Biomol. Screen.* 21, 54–64. <https://doi.org/10.1177/1087057115610055>.
- Gassmann, K., Abel, J., Bothe, H., Haarmann-Stemmann, T., Merk, H.F., Quasthoff, K.N., Rockel, T.D., Schreiber, T., Fritsche, E., 2010. Species-specific differential ahr expression protects human neural progenitor cells against developmental neurotoxicity of PAHs. *Environ. Health Perspect.* 118, 1571–1577. <https://doi.org/10.1289/ehp.0901545>.
- Gegelashvili, G., Schousboe, A., 1998. Cellular distribution and kinetic properties of high-affinity glutamate transporters. *Brain Res. Bull.* 45, 233–238. [https://doi.org/10.1016/s0361-9230\(97\)00417-6](https://doi.org/10.1016/s0361-9230(97)00417-6).
- Hofrichter, M., Nimtzt, L., Tigges, J., Kabiri, Y., et al., 2017. Comparative performance analysis of human iPSC-derived and primary neural progenitor cells (NPC) grown as neurospheres *in vitro*. *Stem Cell Res.* 25, 72–82. <https://doi.org/10.1016/j.scr.2017.10.013>.
- Hogberg, H.T., Sobanski, T., Novellino, A., et al., 2011. Application of micro-electrode arrays (MEAs) as an emerging technology for developmental neurotoxicity: evaluation of domoic acid-induced effects in primary cultures of rat cortical neurons. *Neurotoxicology* 32, 158–168. <https://doi.org/10.1016/j.neuro.2010.10.007>.
- Hyvärinen, Tanja, Hyysalo, Anu, Kapucu Emre, Fikret, et al., 2019. Functional characterization of human pluripotent stem cell-derived cortical networks differentiated on laminin-521 substrate: comparison to rat cortical cultures. *Nature Scientific Reports*. <https://doi.org/10.1038/s41598-019-53647-8>.
- Izsak, J., Seth, H., Andersson, M., et al., 2019. Robust generation of person-specific, synchronously active neuronal networks using purely isogenic human iPSC-3D neural aggregate cultures. *Front. Neurosci.* 13 (351). <https://doi.org/10.3389/fnins.2019.00351>.
- Jennings, P., 2015. “The future of *in vitro* toxicology. *Toxicol. In Vitro* 29, 1217–1221. <https://doi.org/10.1016/j.tiv.2014.08.011>.
- Johnstone, A.F., Gross, G.W., Weiss, D.G., et al., 2010. Microelectrode arrays: a physiologically based neurotoxicity testing platform for the 21st century. *Neurotoxicology* 31, 331–350. <https://doi.org/10.1016/j.neuro.2010.04.001>.
- Kang, H.J., Kawasawa, Y.I., Cheng, F., et al., 2011. Spatio-temporal transcriptome of the human brain. *Nature* 478, 483–489. <https://doi.org/10.1038/nature10523>.
- Kao, C.F., Chuang, C.Y., Chen, C.H., et al., 2008. Human pluripotent stem cells: current status and future perspectives. *Chin. J. Physiol.* 51, 214–225.
- Kasteel, E.E., Westerink, R.H., 2017. Comparison of the acute inhibitory effects of Tetrodotoxin (TTX) in rat and human neuronal networks for risk assessment purposes. *Toxicol. Lett.* 270, 12–16. <https://doi.org/10.1016/j.toxlet.2017.02.014>.
- Leipzig, N.D., Xu, C., Zahir, T., Shoichet, M.S., 2010. Functional immobilization of interferon-gamma induces neuronal differentiation of neural stem cells. *J. Biomed. Mater. Res. A* 93, 625–633. <https://doi.org/10.1002/jbm.a.32573>.
- Leist, M., Hartung, T., 2013. Inflammatory findings on species extrapolations: humans are definitely no 70-kg mice. *Arch. Toxicol.* 87, 563–567. <https://doi.org/10.1007/s00204-013-1038-0>.
- Lisman, J.E., 1997. Bursts as a unit of neural information: making unreliable synapses reliable. *Trends Neurosci.* 20, 38–43. [https://doi.org/10.1016/S0166-2236\(96\)10070-9](https://doi.org/10.1016/S0166-2236(96)10070-9).
- Liu, H., Zhang, S.C., 2011. Specification of neuronal and glial subtypes from human pluripotent stem cells. *Cell. Molec. Life Sci.* 68, 3995–4008. <https://doi.org/10.1007/s00018-011-0770-y>.
- Lujan, R., Shigemoto, R., Lopez-Bendito, G., 2005. Glutamate and GABA receptor signalling in the developing brain. *Neuroscience* 130, 567–580. <https://doi.org/10.1016/j.neuroscience.2004.09.042>.
- Mack, C.M., Lin, B.J., Turner, J.D., et al., 2014. Burst and principal components analyses of MEA data for 16 chemicals describe at least three effects classes. *Neurotoxicology* 40, 75–85. <https://doi.org/10.1016/j.neuro.2013.11.008>.
- Maeda, E., Robinson, H.P., Kawana, A., 1995. The mechanisms of generation and propagation of synchronized bursting in developing networks of cortical neurons. *J. Neurosci.* 15, 6834–6845. <https://doi.org/10.1523/JNEUROSCI.15-10-06834.1995>.
- Magdalini, S., Munn, S., Bal-Price, A., 2019. AOP: 48. Binding of Agonists to Ionotropic Glutamate Receptors in Adult Brain Causes Excitotoxicity that Mediates Neuronal Cell Death, Contributing to Learning and Memory Impairment. *AOPwiki.org*.
- Masjosthusmann, S., Barenys, M., Elgamal, M., et al., 2018a. Literature Review and Appraisal On Alternative Neurotoxicity Testing Methods, External Scientific Report, 10.2903/sp.efsa.2018.EN-1410.
- Masjosthusmann, S., Becker, D., Petzuch, B., et al., 2018b. A transcriptome comparison of time-matched developing human, mouse and rat neural progenitor cells reveals human uniqueness. *Toxicol. Appl. Pharmacol.* 354, 40–55. <https://doi.org/10.1016/j.taap.2018.05.009>.
- Matthews, R.A., 2008. Medical progress depends on animal models – doesn't it? *J. R. Soc. Med.* 101, 95–98. <https://doi.org/10.1258/jrsm.2007.070164>.
- Mayer, M., Arriazabalaga, O., Lieb, F., et al., 2018. Electrophysiological investigation of human embryonic stem cell derived neurospheres using a novel spike detection algorithm. *Biosens. Bioelectron.* 100, 462–468. <https://doi.org/10.1016/j.bios.2017.09.034>.
- McConnell, E.R., McClain, M.A., Ross, J., et al., 2012. Evaluation of multi-well microelectrode arrays for neurotoxicity screening using a chemical training set. *Neurotoxicology* 33, 1048–1057. <https://doi.org/10.1016/j.neuro.2012.05.001>.
- Michalczyk, K., Ziman, M., 2005. Nestin structure and predicted function in cellular cytoskeletal organisation. *Histol. Histopathol.* 20, 665–671. <https://doi.org/10.14670/HH-20.665>.
- Molofsky, A.V., Deneen, B., 2015. Astrocyte development: a guide for the perplexed. *Glia* 63, 1320–1329. <https://doi.org/10.1002/glia.22836>.
- Molofsky, A.V., Krenick, R., Ullian, E.M., et al., 2012. Astrocytes and disease: a neurodevelopmental perspective. *Genes Dev.* 26, 891–907. <https://doi.org/10.1101/gad.188326.112>.
- Napoli, Alessandro, Obeid, Iyad, 2016. Comparative Analysis of Human and Rodent Brain Primary Neuronal Culture Spontaneous Activity Using Micro-Electrode Array Technology. *Journal of Cellular Biochemistry* <https://doi.org/10.1002/jcb.25312>.
- Nat, R., Nilbratt, M., Narkilahti, S., et al., 2007. Neurogenic neuroepithelial and radial glial cells generated from six human embryonic stem cell lines in serum-free suspension and adherent cultures. *Glia* 55, 385–399. <https://doi.org/10.1002/glia.20463>.
- Oberheim, N.A., Wang, X., Goldman, S., et al., 2006. Astrocytic complexity distinguishes the human brain. *Trends Neurosci.* 29, 547–553. <https://doi.org/10.1016/j.tins.2006.08.004>.
- Odawara, A., Katoh, H., Matsuda, N., et al., 2016. Physiological maturation and drug responses of human induced pluripotent stem cell-derived cortical neuronal networks in long-term culture. *Sci. Rep.* 6, 26181. <https://doi.org/10.1038/srep26181>.
- Odawara, A., Saitoh, Y., Alhebshi, A.H., et al., 2014. Long-term electrophysiological activity and pharmacological response of a human induced pluripotent stem cell-derived neuron and astrocyte co-culture. *Biochem. Biophys. Res. Commun.* 443, 1176–1181. <https://doi.org/10.1016/j.bbrc.2013.12.142>.
- OECD, Test No. 424: Neurotoxicity Study in Rodents, 1997.
- Paavilainen, T., Pelkonen, A., Mäkinen, M.E., et al., 2018. Effect of prolonged differentiation on functional maturation of human pluripotent stem cell-derived neuronal cultures. *Stem Cell Res.* 27, 151–161. <https://doi.org/10.1016/j.scr.2018.01.018>.
- Pistollato, F., Canovas-Jorda, D., Zagoura, D., et al., 2017. Nrf2 pathway activation upon rotenone treatment in human iPSC-derived neural stem cells undergoing differentiation towards neurons and astrocytes. *Neurochem. Int.* 108, 457–471. <https://doi.org/10.1016/j.neuint.2017.06.006>.

- Pistollato, F., Louise, J., Scelfo, B., et al., 2014. Development of a pluripotent stem cell derived neuronal model to identify chemically induced pathway perturbations in relation to neurotoxicity: effects of CREB pathway inhibition. *Toxicol. Appl. Pharmacol.* 280, 378–388. <https://doi.org/10.1016/j.taap.2014.08.007>.
- Robinton, D.A., Daley, G.Q., 2012. The promise of induced pluripotent stem cells in research and therapy. *Nature* 41, 295–305. <https://doi.org/10.1038/nature10761>.
- Rosati, J., Ferrari, D., Altieri, F., et al., 2018. Establishment of stable iPSC-derived human neural stem cell lines suitable for cell therapies. *Cell Death Dis.* 9 (10), 937.
- Russell Jr., W.F., Kass, I., Heaton, A.D., et al., 1959. Combined drug treatment of tuberculosis. III. Clinical application of the principles of appropriate and adequate chemotherapy to the treatment of pulmonary tuberculosis. *J. Clin. Invest.* 38, 1366–1375. <https://doi.org/10.1172/JCI103912>.
- Seidel, D., Jahnke, H.G., Englich, B., et al., 2017. *In vitro* field potential monitoring on a multi-microelectrode array for the electrophysiological long-term screening of neural stem cell maturation. *Analyst* 142, 1929–1937. <https://doi.org/10.1039/c6an02713j>.
- Semple, B.D., Blomgren, K., Gimlin, K., et al., 2013. Brain development in rodents and humans: identifying benchmarks of maturation and vulnerability to injury across species. *Prog. Neurobiol.* 106–107, 1–16. <https://doi.org/10.1016/j.pneurobio.2013.04.001>.
- Shafer, T.J., Brown, J.P., Lynch, B., et al., 2019. Evaluation of chemical effects on network formation in cortical neurons grown on microelectrode arrays. *Toxicol. Sci.: Off. J. Soc. Toxicol.* 169, 436–455. <https://doi.org/10.1093/toxsci/kfz052>.
- Shimba, K., Sakai, K., Iida, S., et al., 2019. Long-term developmental process of the human cortex revealed *in vitro* by axon-targeted recording using a microtunnel-augmented microelectrode array. *IEEE Trans. Biomed. Eng.* 66, 2538–2545. <https://doi.org/10.1109/TBME.2019.2891310>.
- Singh, V.K., Kalsan, M., Kumar, N., et al., 2015. Induced pluripotent stem cells: applications in regenerative medicine, disease modeling, and drug discovery. *Front. Cell Dev. Biol.* 3 (2). <https://doi.org/10.3389/fcell.2015.00002>.
- Suter-Dick, L., Alves, P.M., Blaauboer, B.J., et al., 2015. Stem cell-derived systems in toxicology assessment. *Stem Cells Dev.* 24, 1284–1296. <https://doi.org/10.1089/scd.2014.0540>.
- Takahashi, K., Okita, K., Nakagawa, M., et al., 2007. Induction of pluripotent stem cells from fibroblast cultures. *Nat. Protoc.* 2, 3081–3089. <https://doi.org/10.1038/nprot.2007.418>.
- Tang, X., Zhou, L., Wagner, A.M., et al., 2013. Astroglial cells regulate the developmental timeline of human neurons differentiated from induced pluripotent stem cells. *Stem Cell Res.* 11 (2), 743–757. <https://doi.org/10.1016/j.scr.2013.05.002>.
- Tjarnlund-Wolf, A., Hultman, K., Blomstrand, F., et al., 2014. Species-Specific regulation of t-PA and PAI-1 gene expression in human and rat astrocytes. *Gene Regul. Syst. Biol.* 8, 113–118. <https://doi.org/10.4137/GRSB.S13387>.
- Toivonen, S., Ojala, M., Hyysalo, A., et al., 2013. Comparative analysis of targeted differentiation of human induced pluripotent stem cells (hiPSCs) and human embryonic stem cells reveals variability associated with incomplete transgene silencing in retrovirally derived hiPSC lines. *Stem Cells Transl. Med.* 2, 83–93. <https://doi.org/10.5966/sctm.2012-0047>.
- Tukker, A.M., Wijnolts, F.M.J., de Groot, A., et al., 2018. Human iPSC-derived neuronal models for *in vitro* neurotoxicity assessment. *Neurotoxicology* 67, 215–225. <https://doi.org/10.1016/j.neuro.2018.06.007>.
- Tukker, A.M., de Groot, M.W., Wijnolts, F.M., et al., 2016. Is the time right for *in vitro* neurotoxicity testing using human iPSC-derived neurons? *ALTEX* 33, 261–271. <https://doi.org/10.14573/altex.1510091>.
- Valdivia, P., Martin, M., LeFevre, W.R., et al., 2014. Multi-well microelectrode array recordings detect neuroactivity of ToxCast compounds. *Neurotoxicology* 44, 204–217. <https://doi.org/10.1016/j.neuro.2014.06.012>.
- Vassallo, A., Chiappalone, M., De Camargos Lopes, R., et al., 2017. A multi-laboratory evaluation of microelectrode array-based measurements of neural network activity for acute neurotoxicity testing. *Neurotoxicology* 60, 280–292. <https://doi.org/10.1016/j.neuro.2016.03.019>.
- Wagenaar, A., Daniel, Pine, Jerome, Potter M, Steve, 2006. An extremely rich repertoire of bursting patterns during the development of cortical cultures. *BMC Neuroscience* 7 (11) <https://doi.org/10.1186/1471-2202-7-11>.
- Wallace, K., Strickland, J.D., Valdivia, P., et al., 2015. A multiplexed assay for determination of neurotoxicant effects on spontaneous network activity and viability from microelectrode arrays. *Neurotoxicology* 49, 79–85. <https://doi.org/10.1016/j.neuro.2015.05.007>.
- Walls, A.B., Waagepetersen, H.S., Bak, L.K., et al., 2015. The glutamine-glutamate/GABA cycle: function, regional differences in glutamate and GABA production and effects of interference with GABA metabolism. *Neurochem. Res.* 40, 402–409. <https://doi.org/10.1007/s11064-014-1473-1>.
- Walter, K.M., Dach, K., Hayakawa, K., et al., 2019. Ontogenetic expression of thyroid hormone signaling genes: an *in vitro* and *in vivo* species comparison. *PLoS ONE* 14, e0221230. <https://doi.org/10.1371/journal.pone.0221230>.
- Wang, Y., Adjaye, J., 2011. A cyclic amp analog, 8-Br-cAMP, enhances the induction of pluripotency in human fibroblast cells. *Stem Cell Rev. Rep.* 7, 331–341. <https://doi.org/10.1007/s12015-010-9209-3>.
- Watanabe, K.H., Andersen, M.E., Basu, N., et al., 2011. Defining and modeling known adverse outcome pathways: domoic acid and neuronal signaling as a case study. *Environ. Toxicol. Chem.* 30, 9–21. <https://doi.org/10.1002/etc.373>.
- Xiang, G., Pan, L., Huang, L., et al., 2007. Microelectrode array-based system for neuropharmacological applications with cortical neurons cultured *in vitro*. *Biosens. Bioelectron.* 22, 2478–2484. <https://doi.org/10.1016/j.bios.2006.09.026>.
- Yuan, S.H., Martin, J., Elia, J., et al., 2011. Cell-surface marker signatures for the isolation of neural stem cells, glia and neurons derived from human pluripotent stem cells. *PLoS ONE* 6, e17540. <https://doi.org/10.1371/journal.pone.0017540>.
- Zagoura, D., Canovas-Jorda, D., Pistollato, F., et al., 2017. Evaluation of the rotenone-induced activation of the Nrf2 pathway in a neuronal model derived from human induced pluripotent stem cells. *Neurochem. Int.* 106, 62–73. <https://doi.org/10.1016/j.neuint.2016.09.004>.
- Zhang, Y., Pak, C., Han, Y., et al., 2013. Rapid single-step induction of functional neurons from human pluripotent stem cells. *Neuron* 78, 785–798. <https://doi.org/10.1016/j.neuron.2013.05.029>.
- Zhu, G., Sun, C., Liu, W., 2012. Effects of neurotrophin-3 on the differentiation of neural stem cells into neurons and oligodendrocytes. *Neural Regen. Res.* 7, 1483–1487. <https://doi.org/10.3969/j.issn.1673-5374.2012.19.006>.
- Zuang, V., Casati, S., Aschberger, K., et al., 2018. Standardisation of defined approaches for skin sensitisation testing to support regulatory use and international adoption: position of the international cooperation on alternative test methods. *Arch. Toxicol.* 92, 611–617. <https://doi.org/10.1007/s00204-017-2097-4>.
- Zuang, V., Barroso, J., Belz, S., et al., EURL ecvam status report on the development, validation and regulatory acceptance of alternative methods and approaches in Publications Office of the European Union, 2017, 10.2760/818599.

SUPPLEMENTARY MATERIAL

1. MATERIAL AND METHODS:

1.1. Compounds used

Table S1: Information about compounds, solvent and used concentrations

Compound	Supplier	Order number	CAS number	Purity	Solvent	Used concentrations
γ -Aminobutyric acid (GABA)	Sigma Aldrich (Saint Louis, USA)	A5835	56-12-2	$\geq 99\%$	deionized water	1 mM
L-Glutamic Acid	Sigma Aldrich (Saint Louis, USA)	49621	6106-04-3	$\geq 98.0\%$	deionized water	100 μ M
Domoic Acid (DA)	Sigma Aldrich (Saint Louis, USA)	D6152	14277-97-5	$\geq 90\%$	deionized water	1 nM, 10 nM, 100 nM, 300 nM, 1 μ M
NBQX disodium salt	Santa Cruz Biotechnologies (Texas, USA)	sc-222048	479347-86-9	$\geq 98\%$	deionized water	10 μ M
DL-AP5 sodium salt	Santa Cruz Biotechnologies (Texas, USA)	sc-201503	76326-31-3	$\geq 95\%$	deionized water	20 μ M
Bicuculline	Santa Cruz Biotechnologies (Texas, USA)	sc-202498	485-49-4	$\geq 98\%$	dimethyl sulfoxide (DMSO)	10 μ M

Stock solutions of each compound were prepared in the following solvents: deionized water (NBQX, AP5, Glutamic acid, GABA, DA), DMSO (Bicuculline). Stock solutions were diluted 1:1000 to gain a final concentration of the respective solvents of 0,1% [vol/vol].

1.2. Cell culture and neural induction

1.2.1. Neural induction medium (NIM):

- DMEM and Ham's F12 (3:1 ratio, Gibco, Invitrogen)
- 20 ng/mL human recombinant epidermal growth factor (EGF, Gibco, Invitrogen)
- 1:50 B27 supplement (50x Stock, Gibco, Invitrogen)
- 1:100 N2 Supplement (100x Stock, Gibco, Invitrogen)
- 1:100 Penicillin/Streptomycin (100x Stock, PAN-Biotech)
- 20% knockout serum replacement (KSR, Thermo Fisher Scientific)

- 10 μ M SB431542 (Merck, Germany)
- 0,5 μ M LDN-193189 (Sigma Aldrich, Germany).

1.2.2. Neural proliferation medium (NPM):

- DMEM and Ham's F12 (3:1 ratio, Gibco, Invitrogen)
- 20 ng/mL human recombinant epidermal growth factor (EGF, Gibco, Invitrogen)
- 1:50 B27 supplement (50x Stock, Gibco, Invitrogen)
- 1:100 Penicillin/Streptomycin (100x Stock, PAN-Biotech)
- for hiNPC: human recombinant FGF (20 ng/mL, R&D systems)
- for rat NPC: rat recombinant FGF (10 ng/ml, R&D systems)

1.3. Cultivation of primary human NPC

Human neural progenitor cells [hNPC, male, gestational week (GW) 16–18] isolated from whole brain were purchased from Lonza Verviers SPRL (CAT. #PT-2599; LOT NO.:0000277385; Verviers, Belgium). HNPC were cultured as described previously [Baumann, 2014]. Briefly, neurospheres were cultivated in neural proliferation medium (NPM, see 3.2.2) at 37°C with 5% CO₂. Half of the medium was replaced by fresh medium every two to three days and the cultures were passaged every week by mechanical chopping of the spheres using a tissue chopper (McIlwain Tissue Chopper, Vibratome).

1.4. Neuronal differentiation and Immunocytochemistry

1.4.1. Differentiation-medium (NDM):

- DMEM and Ham's F12 (3:1 ratio, Gibco, Invitrogen)
- 1:50 B27 supplement (50x Stock, Gibco, Invitrogen)
- 1:100 N2 Supplement (100x Stock, Gibco, Invitrogen)
- 1:100 Penicillin/Streptomycin (100x Stock, PAN-Biotech)

1.4.2. Differentiation-medium CINDA:

- DMEM and Ham's F12 (3:1 ratio, Gibco, Invitrogen)
- 1:50 B27 supplement (50x Stock, Gibco, Invitrogen)
- 1:100 N2 Supplement (100x Stock, Gibco, Invitrogen)
- 1:100 Penicillin/Streptomycin (100x Stock, PAN-Biotech)
- 5 mM creatine monohydrate (Sigma Aldrich, Germany)
- 100 U/ml Interferon- γ (PeproTech, Germany)
- 20 ng/ml neurotrophin-3 (PeproTech, Germany)
- 300 μ M dibutyryl-cAMP (Sigma Aldrich, Germany)
- 20 μ M ascorbic acid (Sigma Aldrich, Germany)

Five neurospheres with a diameter of 300 μ m were plated on PDL/laminin-coated slides in neural differentiation medium (NDM, see 3.4.1) or maturation-supporting CINDA medium (see 3.4.2). Plated spheres were cultured for 28 days and medium was changed once a week. Afterwards, cells were fixed with 4% PFA (Sigma Aldrich, Germany) for 30 min at 37 °C and washed with PBS. Cells were stained with primary antibodies for 1 h at 37 °C. After washing with PBS, cells were incubated with the respective secondary antibodies for 30 min at 37°C. Nuclei were stained with Hoechst33258 (Sigma Aldrich, Germany). Samples were analyzed

using a fluorescent microscope (Carl Zeiss, Germany) and the ZEN 2 Rel.4.8 software (Carl Zeiss, Germany). Each experiment was performed at least three times with three independent neural inductions.

Primary antibodies:

Table S2: Information about primary antibodies used for ICC staining.

Antibody	Used dilution	Cat. No., Company
mouse-anti- β (III)-Tubulin	1:100	T8660, Sigma Aldrich, Germany
rabbit-anti- β (III)-Tubulin	1:200	T2200, Sigma Aldrich, Germany
rabbit-anti-GFAP	1:100	G9269, Sigma Aldrich, Germany
rabbit-anti-PSD-95	1:100	ab76115, Abcam
mouse-anti-Synapsin1	1:100	106001, Synaptic Systems
rabbit-anti-glutamate-receptor 1	1:100	AB1504, Millipore
anti-mouse-GABA-A-receptor β	1:200	MAB341, Millipore
anti-mouse-NMDA-receptor 1	1:750	MAB363, Merck, Germany

Secondary antibodies:

Table S3: Information about secondary antibodies used for ICC staining.

Antibody	Used dilution	Cat. No., Company
anti-mouse-Alexa-546	1:100	A11030, Invitrogen, USA
anti-rabbit-Alexa488	1:100	A11008, Invitrogen, USA

1.5. Quantification

Quantification analyses of synapses and receptors were performed by analyzing the neurite mass in μm^2 and number of synapses (synapses/neurite area [μm^2]) using the Omnisphero software as previously described [Hofrichter, 2017]. In detail, to account for a brighter TUBB3 staining, structuring elements to eliminate uneven background were adjusted and thresholding of the resulting images was performed with the Otsu method. Here, algorithms for the segmentation of digital images generated binary images and allowed the recognition of pixels that either represent objects (e.g. neurites and synapses) or their environment. The Otsu method defines a threshold that determines classes in which the dispersion within the classes is as small as possible, but between the classes as large as possible. The quotient between the two variances is determined and a threshold value is calculated in which the quotient is as large as possible [Otsu, 1979].

For quantification analyses of synapses and receptors of hiNN, three independent experiments consisting of three neural inductions were performed. For each individual n a minimum of 6 images was analyzed for quantifications. Here, both the total number of synapses and the number and area of β (III)-tubulin positive neurites were calculated. Synapses that colocalize with neurites were analyzed using a script written in the Omnisphero software [Schmuck, 2017]. Therefore, the images of β (III)-tubulin stainings were first preprocessed using two different analyzing methods:

- i. foreground-pixels were removed using a non-flat structuring element (sphere) (<https://www.mathworks.com/help/images/ref/imopen.html>), which allows estimation of the uneven background. This background was then subtracted from the image.
- ii. an adaptive threshold method was used on the same images (<https://www.mathworks.com/matlabcentral/fileexchange/8647-local-adaptive-thresholding>).

The resulting binary image was used as a mask and compared to the image from (i) to extract background regions. After this, the image was provided with a fixed threshold calculated by the Isodata-(Iterative Self-Organizing Data Analysis) technique-algorithm [Ball, 1965]. In a second approach, the same image (background-corrected), was processed with different edge-detection algorithms [Canny, 1986; Lim, 1990; Parker, 2011]. This image was then added to the images resulting from the two-step adaptive thresholding and small holes were filled up using the fill function. Images of immunofluorescent staining of synapses (postsynaptic marker PSD95 and presynaptic marker SYN1) were also processed by removing the foreground pixels to estimate the background. Subsequently, an isodata threshold was applied to filter out large particles that were not considered to be synapses. In a final step, all synapses that were not on a binary component of the neurite image were removed. Finally, the area of the binary neurite components, as well as the number of synapse particles and the relevant density of these particles were calculated as particles per area (synapses / neurite area [μm^2]). The method described was applied not only to synapse staining, but also to the staining of various neuronal receptors (NMDAR1 as a marker for the NMDA receptor, GluR1 as a marker for the AMPA receptor, GABAAR β 1 as a marker for the GABA receptor) for the identification and quantification of the neuronal subtypes present in the culture.

1.6. Quantitative reverse-transcription PCR

Table S4: Sequences of primers used in qRT-PCR.

Gene:	Human Primer:	Rat Primer:
βACTIN	FW:5'-CAGGAAGTCCCTTGCCATCC-3' RV:5'-ACCAAAAGCCTTCATACATCTCA-3'	FW:5'-CAGGAAGTCCCTTGCCATCC-3' RV:5'-ACCAAAAGCCTTCATACATCTCA-3'
NESTIN	FW:5'-CCCCGTCGGTCTCTTTTCTC-3' RV:5'-TCGTCTGACCCACTGAGGAT-3'	FW:5'-GGATGGGACGAGGATCAAG-3' RV:5'-TGAGGACCAGGAATCCCCAT-3'
MAP2	FW:5'-TGCCTCAGAACAGACTGTCAC-3' RV:5'-AAGGCTCAGCTGTAGAGGGA-3'	FW:5'-CTGGAAGAAGCCTCGAAGATGG-3' RV:5'-TACTTGTGTCCGGCTGAGGA-3'
S100β	FW:5'-CACAAAGCTGAAGAAATCCGAAC-3' RV:5'-CACATTGCGCGTCTCCATC-3'	FW:5'-GCTTCTCTGTCTACCCTCCTA-3' RV:5'-CCCTCTCTCCCTGAATACTGAT-3'
AQP4	FW:5'-GGTGCCAGCATGAATCCC-3' RV:5'-TGGACAGAAGACATACTCATAAAGG-3'	FW:5'-CAATTATACCGGAGCCAGCAT-3' RV:5'-TCAGGACAGAAGACATACTCGT-3'
GFAP	FW:5'-GATCAACTCACCGCCAACAGC-3' RV:5'-CTCCTCCTCCAGCGACTCAATCT-3'	FW:5'-ACAGCAAAACAAGGCGCTGGC-3' RV:5'-TCTTGGAGCTTCTGCCTCAGGG-3'
SYN1	FW:5'-GTGCTGCTGGTCATCGAC-3' RV:5'-CCACAAGGTTGAGATCAGAGAA-3'	FW:5'-CAAACCACAGCTGGCTCAGAA-3' RV:5'-GGTCAGAGACTGGGATTTGTTGAG-3'
DLG4	FW:5'-CCAGAAGAGTACAGCCGATTC-3' RV:5'-CTTGGTCTTGTCGTAATCAAACAG-3'	FW:5'-ACCAAGAAATACCGCTACCAAG-3' RV:5'-TCACCTGCAACTCATATCCTG-3'
SLC17A7	FW:5'-CAGAAAGCCCAGTTCAGC-3' RV:5'-ACAATAGCAAAGCCGAAAACCTC-3'	FW:5'-CACTGCCTCACCTTGTCAT-3' RV:5'-TTCATCAGCTTTCGCACATTG-3'
GRIA1	FW:5'-CTTAATCGAGTTCTGCTACAAATCC-3' RV:5'-GTATGGCTTCGTTGATGGATTG-3'	FW:5'-CCACTACATCCTCGCCAATC-3' RV:5'-GTCACTTGTCTCCATTGCT-3'
GRIN1	FW:5'-CTCCTGGAAGATTCAGCTCAA-3' RV:5'-GTGGATGGCTAACTAGGATGG-3'	FW:5'-TCATCTCTAGCCAGGTCTACG-3' RV:5'-GATTCTGTAGAAGCCAGCTGT-3'
GAD1	FW:5'-GACCCCAATACCACTAACCTG-3' RV:5'-GCTGTTGGTCCTTTGCAAG-3'	FW:5'-CTCCAAGAACCTGCTTTCCT-3' RV:5'-TCAACCACCTCCAGTAAGAAC-3'

TH	FW:5'-TTCTCGCAGGACATTGGC-3' RV:5'-CTTACACAGCCCCGAAGTCC-3'	FW:5'-AGTACAAGCACGGTGAACCA-3' RV:5'-GATGCTGTCTCTCGGTAGC-3'
ACHE	FW:5'-ATGCGATACTGGGCCAAC-3' RV:5'-GTCCAGACTAACGTACTGCT-3'	FW:5'-TCAGGTTTCAGGCTCACGTAT-3' RV:5'-TCAGGTTTCAGGCTCACGTAT-3'
SLC6A4	FW:5'-GCTGTGTCTTGGTTCTATGGC-3' RV:5'-GGCTCATCAGAAAAGTCAAA-3'	FW:5'-TGCTCATCTTCACCGTAATCTAC-3' RV:5'-GGACAGAGAGGACAATGTATGG-3'
NOTCH1	FW:5'-GAAGTTCGGTTCGAGGAGC-3' RV:5'-ATGAAGTCGGAGATGACGGC-3'	
EGFR	FW:5'-ATCACCTGCACAGGACGGGA-3' RV:5'-GGACGGGATCTTAGGCCCATTCG-3'	
ID2	FW:5'-ACCCGATGAGCCTGCTATAC-3' RV:5'-GCTGACAATAGTGGGAT-3'	
CALB2	FW:5'-GGAAATATGGAAGCACTTTGACG-3' RV:5'-TCACTCTTTGACATCATGCCA-3'	
OLIG2	FW:5'-CCGATGACCTTTTTCTGCCG-3' RV:5'-CCACTGCCTCCTAGCTTGTC-3'	
DCX	FW:5'-GGATCCAGGAAGATCGGAAG-3' RV:5'-TTACGTTGACAGACCAGTTGG-3'	
DRD4	FW:5'-TGCTGCCGCTCTTCGTC-3' RV:5'-GAACCTGTCCACGCTGATG-3'	
GRIA4	FW:5'-CAGGGAATTGACATGGAGAGG-3' RV:5'-TTGTGTAATTGACTCTACGTCCA-3'	
STMN2	FW:5'-CGTCTGCACATCCCTACAATG-3' RV:5'-TGCTTCACTTCCATATCATCGT-3'	
GRM5	FW:5'-TGTGAGAAAGGCCAGATCAAG-3' RV:5'-TGCCTTGCATGTGTACTCATC-3'	
CHRM3	FW:5'-TCACGCTGGGAGCTGTA-3' RV:5'-AGCAAAACCTTATTGTACCTTAGC-3'	
GABBR1	FW:5'-CTGAGGTCTTCACTTCGACTC-3' RV:5'-AAAGTCCCACGATGATTCGG-3'	
GABRB3	FW:5'-AACCGCATGATCCGTCTTC-3' RV:5'-GCCATAGCTTTCAATTTCCAGA-3'	

1

2 **1.7. NN differentiated on microelectrode arrays (MEA)**

3 Statistical analyses of baseline activity parameters (MFR, MBR, spikes/burst and AE) were
4 done in R version 3.6.0 [R-CoreTeam, 2019]. In case of the hiNPC-derived neural networks
5 (NDM and CINDA), we modelled the activity of the networks (measured by spikes/min (MFR),
6 bursts/min (MBR), spikes/burst and number of active electrodes (AE)) using a mixed model
7 with random intercepts [Laird, 1982] to account for the repeated measurements of each
8 network. The fixed terms of the model include a common intercept, the week of measurement
9 (weeks 2 to 6), the condition and the interaction of week and medium. The model was fitted
10 using the R function package nlme [Pinheiro, 2019]. To test for differences between the media
11 for each week and between consecutive weeks for each medium, we used simultaneous
12 confidence intervals for general linear hypotheses controlling the family-wise error rate as
13 implemented in package multcomp [Hothorn, 2008]. In case of the rNN, we used a separate
14 mixed model with random intercepts for each network, where the fixed term only includes the
15 common intercept and the week of measurement. We tested for differences between
16 consecutive weeks using the methodology described above. To analyze long-term effects, we
17 applied the same procedure as described above but replaced the week of measurement in the
18 fixed term by a factor variable indicating short (weeks 1-6), medium (weeks 7- 11) and long
19 term (more than 11 weeks).

20 For the statistical analyses of all experiments also values from 0-0.1 were included.

21

22 **1.8. NN characterization with pharmacological treatments**

Data acquisition was managed with MC-Rack (Multichannelsystems, Germany). We performed 5 min of consecutive 1-min recordings (first minute was deleted subsequently). Raw data were generated using a sampling rate of 20-25 kHz on all electrodes using a band pass filter (100-3500Hz). For spike detection we used the SpaNnEr software (Results Medical GmbH, Duesseldorf, Germany) with a variable threshold spike detector of 6x standard deviation of the internal ground noise on each electrode. To be regarded as active each electrode must record ≥ 5 Spikes/min. A well was defined as active, if ≥ 3 active electrodes were calculated.

1.9. Cytotoxicity of acute treatment of NN in mwMEA with domoic acid (DA)

Data acquisition was managed with the Multiwell-Screen (Multichannelsystems, Germany). We performed 15 min baseline- and treatment-recordings. Raw data were generated using a sampling rate of 20 kHz on all electrodes using a band pass filter (300-3500 Hz). Spike detection of the MEA-multiwell-plates were performed with the Multiwell-Analyzer (Multichannelsystems, Germany) using an automatic threshold estimation of 500 ms baseline duration and rising/falling edge of 5x standard deviation of the noise level. For burst detection the Multiwell-Analyzer Burst Detector (Multichannelsystems, Germany) was used using a max. 100 ms interval to start/end a burst, a 20 ms interval between bursts with 10 ms duration of each burst. A burst was defined as a minimum of 3 spikes. Cytotoxicity was assessed using the Lactate-Dehydrogenase (LDH) Cytotoxicity Assay (G7891, Promega, Germany) according to manufacturer's instructions. Briefly, medium from control and treated hiNN and rNN was collected and incubated with the LDH solution for 2 h before fluorescence (540Ex/590Em) was measured using a multimode microplate reader (Tecan, Switzerland) and normalized to lysis control.

1.10. Affymetrix Microarray analysis

Data analyses on Affymetrix CEL files were conducted with GeneSpring GX software (Vers.12.5; Agilent Technologies) and Transcriptome Analysis Console (TAC; Vers. 4.0.1.36 Thermo Fisher Scientific). In GeneSpring, probes within each probe set were summarized by GeneSpring's ExonRMA16 algorithm after quantile normalization of probe-level signal intensities across all samples to reduce inter-array variability [Bolstad, 2003]. Input data pre-processing was concluded by baseline transformation to the median of all samples. After grouping of samples (for biological replicates each) according to their respective experimental condition, a given probe set had to be expressed above background (i.e., fluorescence signal of that probe set was detected within the 20th and 100th percentiles of the raw signal distribution of a given array) in all four replicates in at least one of five conditions to be further analyzed in pairwise comparisons. Differential gene expression was statistically determined by Moderated T-Test. The Resulting values were corrected for multiple testing by Bonferroni-correction. A p - value of ≤ 0.05 was considered significant. Hierarchical cluster analysis was performed with Euclidian similarity measures and Ward's linkage. The expression profile of single genes in the heatmap (Fig.7A) was prepared with the Multiple Experiment Viewer (MeV 4.9.0; [http://mev. tm4.org/](http://mev.tm4.org/)). In TAC the probes within each probe set were summarized by Robust Multichip Average (RMA) after quantile normalization of probe level signal intensities across all samples to reduce inter-array variability. For analysis, samples were grouped according to their respective experimental conditions (four replicates for each condition). For the generation of Venn diagrams (Fig. 7C, D) we compared all genes that were differentially expressed with a false discovery rate (FDR) of ≤ 0.05 and a two-fold change in expression. Duplicate probe sets were deleted so that each differentially expressed gene is represented as 1 probe set. We compared our *in vitro* transcription profiles to *in vivo* samples

that originate from homogenates of the prefrontal cortex postconceptional week (pcw) 6 (embryonic) and pcw 12, (fetal; Kang, 2011). These brain regions have been chosen, because they consist both of proliferating progenitor cells as well as differentiating and migrating neurons and glia cells [Silbereis, 2016]. *In vitro* and *in vivo* samples for the generation of Venn diagrams were evaluated with TAC as described above. Data evaluation of all other figures was performed in GeneSpring GX software. Overrepresentation analysis of GO biological processes was performed using the functional annotation tool DAVID Bioinformatics Resources 6.8 [Galperin and Cochrane, 2009; Huang, 2009].

1.11. Flow cytometry analysis

For flow cytometry analysis 50 hiNPC and primary hNPC neurospheres each with a diameter of 300µm were collected. Cells were singularized by incubation with Accutase (Invitrogen, USA) for 10 min at 37°C and 5% CO₂. Singularized cells were stained with Fixable viability dye eFluor® 506 (65-0866-14, ThermoFisher Scientific, USA) for 30min in the dark at 4°C. Afterwards, cells were fixed with 4% paraformaldehyde (PFA, Sigma Aldrich, Germany) for 30 min at 37°C and washed with PBS (Life Technologies, USA). Subsequently, cells were permeabilized with 0.1% Triton-X and blocked with 10% mouse serum (Sigma Aldrich, Germany) in PBS (Life Technologies, USA, 0.1% PBS-T) at room temperature for 15 min. Finally, cells were stained with anti-Nestin-Alexa647 (BD Bioscience, Germany) and either anti-PAX6-Alexa488 or anti-SOX2-Alexa488 (BD Bioscience, Germany) antibodies in 0.1% PBS-T supplemented with 10% mouse serum in the dark at 4°C for 60 min. Samples were analyzed using a BD FACS-Canto-II flow cytometer and the software FlowJo Version 10.5.3 (BD Biosciences, Germany).

Flow cytometry antibodies:

Table S5: Information about flow cytometry antibodies used.

Antibody	Used dilution	Cat. No., Company
Mouse-anti-nestin-Alexa647	1:50	560393, BD Biosciences, Germany
Mouse-anti PAX6-Alexa488	1:50	561664, BD Biosciences, Germany
Mouse-anti-SOX2-Alexa488	1:50	560301, BD Biosciences, Germany

2. REFERENCES

- Ball, G., Hall, D.** 1965, Isodata, a novel method of dataanalysis and pattern classification, Stanford Res. Inst. Tech. Rep.
- Baumann, J.B., M.; Gassmann, K.; Fritsche, E.,** Comparative Human and Rat “Neurosphere Assay” for Developmental Neurotoxicity Testing., in: L.G. Costa, J.C. Davila, D.A. Lawrence, D.J. Reed (Eds.) Current protocols in toxicology, John Wiley & Sons, 2014, pp. 12.21.11–12.21.24.
- Bolstad, B.M., Irizarry, R.A., Astrand, M., et al.** 2003, A comparison of normalization methods for high density oligonucleotide array data based on variance and bias., *Bioinformatics*, 19(2), 185-193.
- Canny, J.** 1986, A computational approach to edge detection, *IEEE Trans Pattern Anal Mach Intell*, 8 679-698.
- Galperin, M. Y., and Cochrane, G. R.** 2009, Nucleic acids research annual database issue and the NAR

- 1 online molecular biology database collection in 2009. *Nucleic Acids Res.* 37, 2–5.
2 doi:10.1093/nar/gkn942.
- 3 **Hofrichter, M., Nimtz, L., Tigges, J., Kabiri, Y., et al.** 2017, Comparative performance analysis of human
4 iPSC-derived and primary neural progenitor cells (NPC) grown as neurospheres in vitro, *Stem Cell Res*,
5 25 72-82, 10.1016/j.scr.2017.10.013.
- 6 **Hothorn, T., Bretz, F., Westfall, P.** 2008, Simultaneous inference in general parametric models, *Biom*
7 *J*, 50 346-363, 10.1002/bimj.200810425.
- 8 **Huang, D. W., Sherman, B. T., and Lempicki, R. A.** 2009, Systematic and integrative analysis of large
9 gene lists using DAVID bioinformatics resources. *Nat. Protoc.* 4, 44–57. doi:10.1038/nprot.2008.211.
- 10 **Kang, H.J., Kawasawa, Y.I., Cheng, F., et al.** 2011, Spatio-temporal transcriptome of the human brain,
11 *Nature*, 478 483-489, 10.1038/nature10523.
- 12 **Laird, N.M., Ware, J.H.** 1982, Random-effects models for longitudinal data, *Biometrics*, 38 963-974,
- 13 **Lim, J.** 1990, Two-dimensional signal and image processing, Englewood Cliffs, NJ, Prentice Hall, 710
- 14 **Otsu, N.** 1979, A Threshold Selection Method from Gray-Level Histograms, *IEEE Transactions on*
15 *Systems, Man, and Cybernetics*, 9:1 10.1109/TSMC.1979.4310076.
- 16 **Parker, J.R., Jim, R., Terzidis, K.** 2011, Algorithms for image processing and computer vision, Wiley
17 Pub.
- 18 **Pinheiro, J., Bates, D., DebRoy, S., et al.** 2019, nlme: Linear and Nonlinear Mixed Effects Models, R
19 package version 3.1-139.
- 20 **R-CoreTeam** 2019, R: A language and environment for statistical computing, R Foundation for
21 Statistical Computing, Vienna, Austria.
- 22 **Schmuck, M.R., Temme, T., Dach, K., et al.** 2017, Omnisphero: a high-content image analysis (HCA)
23 approach for phenotypic developmental neurotoxicity (DNT) screenings of organoid neurosphere
24 cultures in vitro, *Archives of toxicology*, 91 2017-2028, 10.1007/s00204-016-1852-2.
- 25 **Silbereis, J.C., Pochareddy, S., Zhu, Y., et al.** 2016, The Cellular and Molecular Landscapes of the
26 Developing Human Central Nervous System, *Neuron*, 89 248-268, 10.1016/j.neuron.2015.12.008.

Supplementary Figures:

Fig.S1: Representative Flow cytometry analyses of hiNPC and primary human NPC (hNPC, Hofrichter *et al.* 2017). (A) Gating strategy for hiNPC (IMR90) in comparison the ‘gold standard’, hNPC. Samples were gated according to size and granularity (left panel), single cells (no doublets, middle panel) and viability (right panel). (B) Flow cytometry analysis of unstained (left panel) and stained (right panel) samples for the neural markers PAX6 and Nestin as well as (C) SOX2 and Nestin. Samples were analyzed using a BD FACS Canto II and FlowJo software 10.5.3 (BD Biosciences, Germany). Number of analyzed cells =20 000.

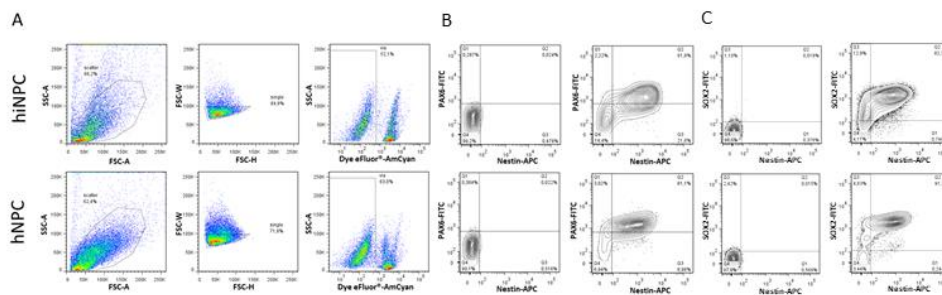


Fig.S2: Immunocytochemical stainings of rNN. Representative pictures of rNN differentiated in NDM for 28 days into TUBB3⁺ neurons (red) and GFAP⁺ astrocytes (green). Nuclei were stained with Hoechst. Scale bars = 100 μ m.

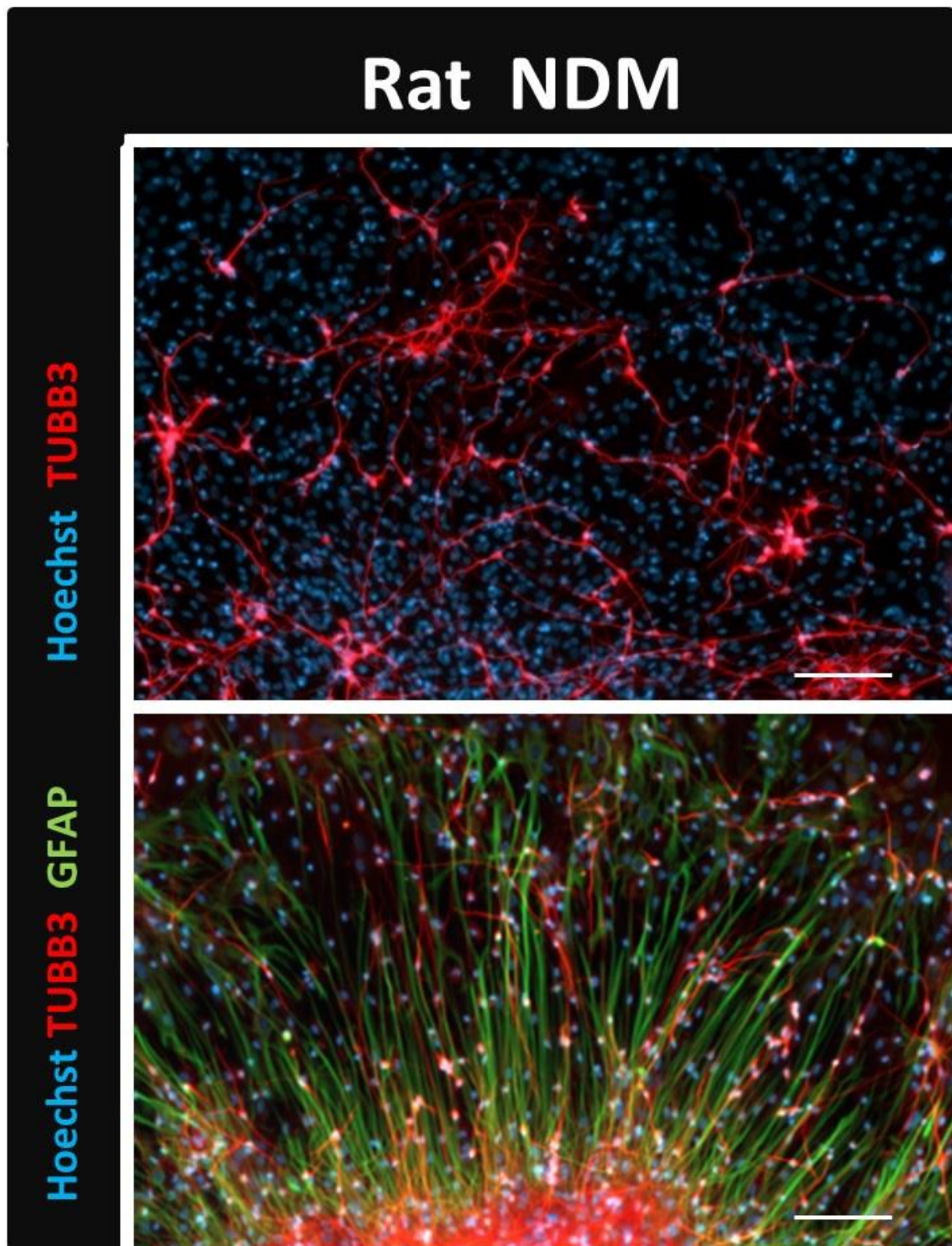


Fig.S3: mRNA expression profiles of hiPSC, hiNPC and hNN compared to rNPC and rNN. qRT-PCR analysis of the serotonergic transporter gene *SLC6A4* after 28 DIV in NDM or CINDA medium. Rat samples serve as a positive control. Data are presented as mean+SEM (n = 3).

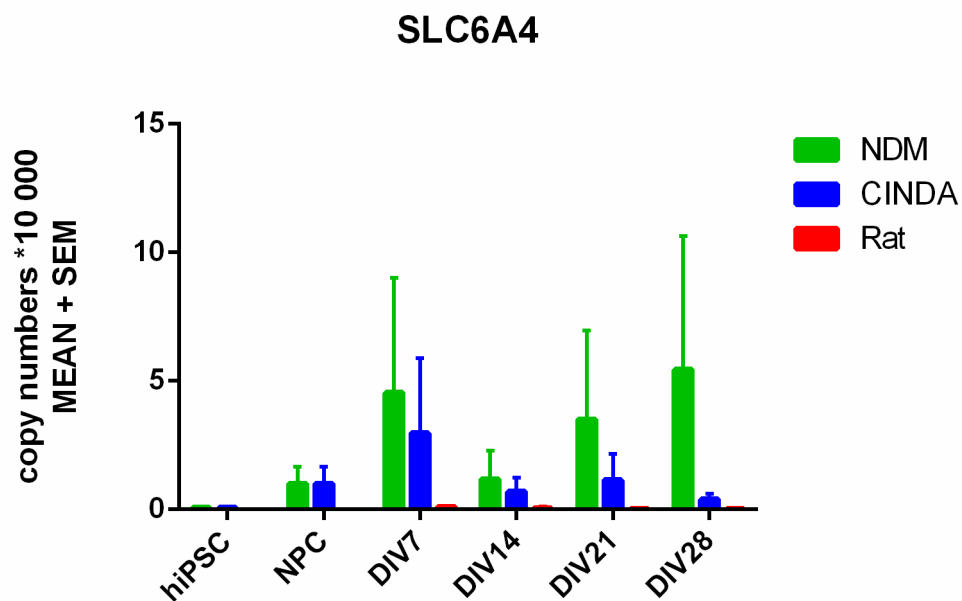


Fig.S4: Spontaneous electrical activity of hNN- and rNN. Shown are scatter plots of hNN (NDM/CINDA) and rNN differentiated for 15 weeks *in vitro* (WIV) on MEAs. Plotted are the **A)** mean firing rate (MFR), **B)** mean bursting rate (MBR), **C)** spikes per burst and **D)** active electrodes. One dot represents one chip (hiNPC: n=40, Rat: n=43 at start of experiment). Black lines represent the mean of all data points. *=significant to NDM, #=significant within condition ($p < 0.05$). Note: for a better visualization all values between 0 and 0.1 were manually set to 0.1 so that the data points appear on the X-axis.

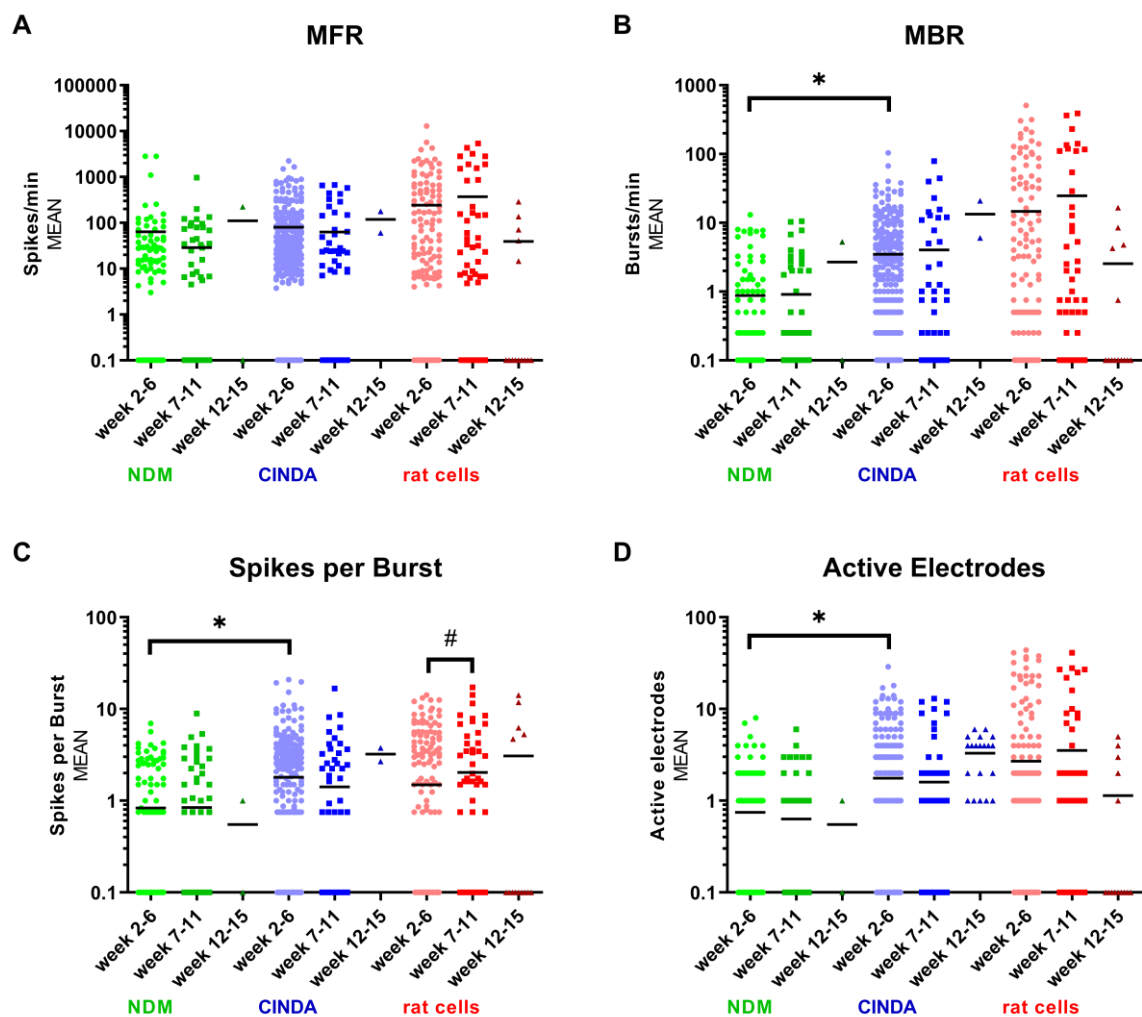


Fig.S5: Acute treatment of NN in mwMEA with the shellfish toxin domoic acid (DA). Acute treatment of hiNPC and rNN with DA. Mean+SEM of **A)** percentage of spikes per burst, **B)** mean Burst spike rate [Hz], **C)** mean burst duration are plotted in percent of solvent control for the acute exposure time of 15 min. Cytotoxicity of **D)** rNN and **E)** CINDA-NN was assessed using the Lactate-Dehydrogenase (LDH) Cytotoxicity Assay (Promega, Germany) and normalized to lysis control (hNN: n=3, rNN: n=3).

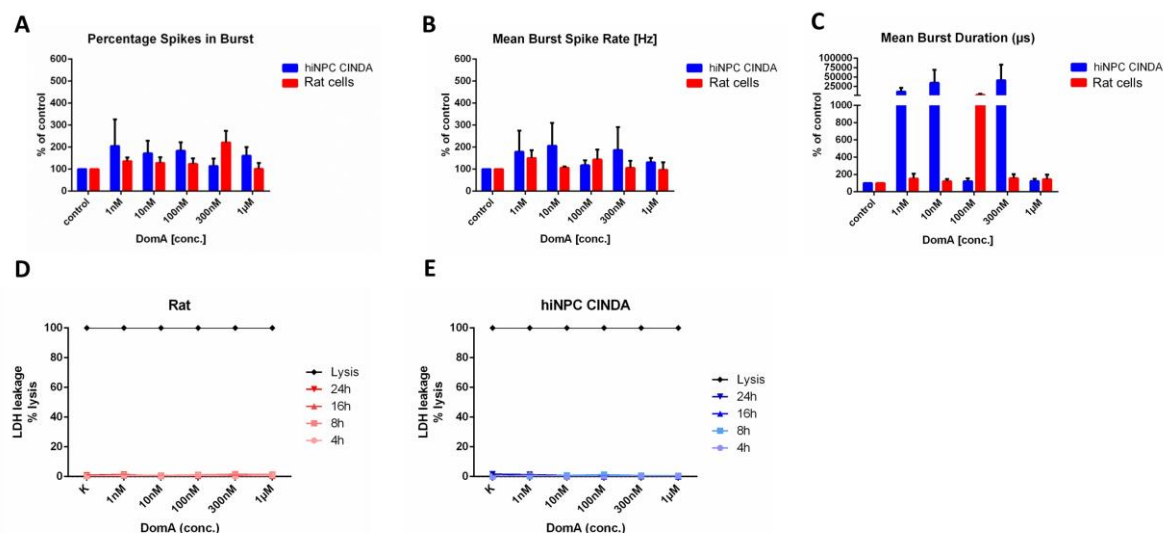
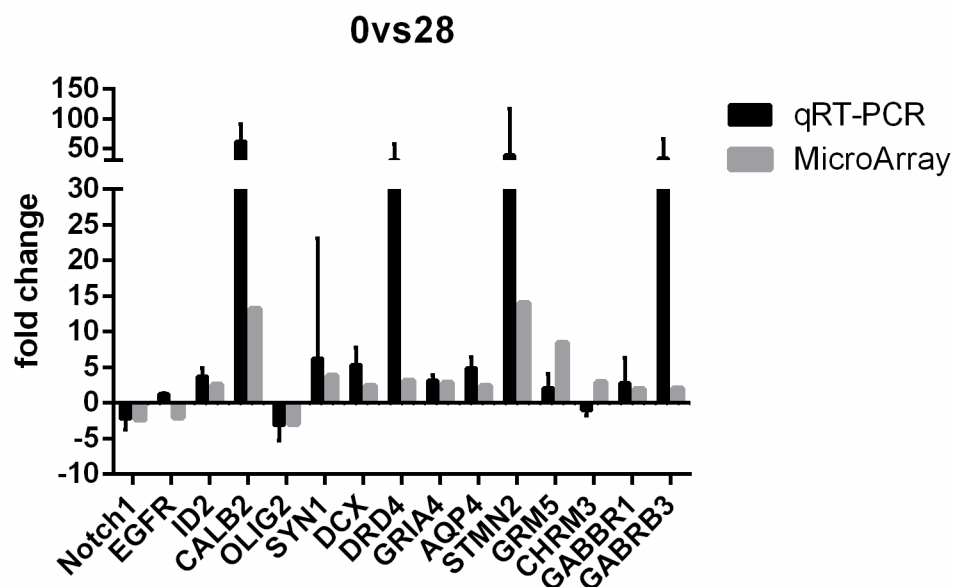


Fig.S6: Validation of microarray experiments by qRT-PCR. qRT-PCR analysis of mRNA samples from hiNPC (four replicates) that were used for transcriptional microarray analysis were compared to results of microarray analysis. Data is presented as mean+SEM fold change between 0 and 28 days (black: qRT-PCR, grey: microarray analysis).



Characterization and application of electrically active neuronal networks established from human induced pluripotent stem cell-derived neural progenitor cells for neurotoxicity evaluation

Laura Nimtz, **Julia Hartmann**, Julia Tigges, Stefan Masjosthusmann, Martin Schmuck, Eike Keßel, Stephan Theiss, Karl Köhrer, Patrick Petzsch, James Adjaye, Claudia Wigmann, Dagmar Wieczorek, Barbara Hildebrandt, Farina Bendt, Ulrike Hübenthal, Gabriele Brockerhoff, Ellen Fritsche

Fachzeitschrift/Buch: *Stem Cell Research*

Impact Factor: 2,02 (2020)

Beteiligung an der Publikation: 5 %

Schreiben und Überarbeitung des
Manuskripts für die Wiedereinreichung
(Resubmission)

Typ der Autorenschaft: Co-Autorenschaft

Status der Publikation: veröffentlicht am 10.März 2020

2.4 Measurement of Electrical Activity of differentiated Human iPSC-Derived Neurospheres recorded by Microelectrode Arrays (MEA)

Kristina Bartmann, **Julia Hartmann**, Julia Kapr, and Ellen Fritsche

Springer Protocols

Neurotoxizität wird durch eine Vielzahl von verschiedenen Chemikalien verursacht und betrifft alle Lebensphasen vom sich entwickelnden Kind bis zum älteren Menschen. Die Untersuchung auf Neurotoxizität beruht derzeit noch hauptsächlich auf Experimenten mit Versuchstieren, diese sind jedoch sehr ressourcenintensiv und die Speziesunterschiede führen zu Ergebnissen die nicht humanrelevant sind. Um diese Probleme zu überwinden, werden Alternativmethoden benötigt, die auf menschlichen Zellen basieren. Die Möglichkeit somatische Zellen in pluripotente Stammzellen zu induzieren, hat weitreichende Fortschritte im Bereich der *in vitro* Neurotoxizitätstestung begünstigt. HiPSCs können in Neurone und Astrozyten differenziert werden und elektrisch aktive Netzwerke bilden. Die spontane Netzwerkaktivität kann mittels MEAs gemessen und evaluiert werden. Dieses Kapitel beschreibt die neurale Induktion von hiPSCs in Neurosphären, welche aus hiNPCs bestehen, und ihre anschließende Differenzierung in funktionelle neurale Netzwerke auf MEAs. Die Messung der spontanen Netzwerkaktivität sowie die Auswertung der erhaltenen Daten werden beschrieben.



Measurement of Electrical Activity of Differentiated Human iPSC-Derived Neurospheres Recorded by Microelectrode Arrays (MEA)

Kristina Bartmann, Julia Hartmann, Julia Kapr, and Ellen Fritsche

Abstract

Neurotoxicity is caused by a large variety of compound classes and affects all life stages from the developing child to the elderly. Studying for neurotoxicity often involves animal models, which are very resource-intensive and bear the problem of species-differences. Thus, alternative human-based models are needed to overcome these issues. Over the last years, far-reaching advancements in the field of neurotoxicity were made possible by the ability to reprogram human somatic cells into induced pluripotent stem cells (hiPSC). These hiPSCs can be differentiated into neurons and astrocytes, which spontaneously form functional neuronal networks (NN) in vitro. Microelectrode arrays (MEA) are a valuable tool to assess the electrophysiology of such networks. This chapter explains the neural induction of hiPSCs to human neural progenitor cells (hiNPC) in the form of free-floating spheres and their subsequent differentiation into functional neurons on MEAs. The measurement of the electrical network activity, as well as the evaluation of the received data is described.

Key words Neurotoxicology, Neurotoxicity, Human induced pluripotent stem cells (hiPSC), Human induced neural progenitor cells (hiNPC), Microelectrode array (MEA), Neuronal network, Electrical activity

1 Introduction

Adverse effects on the peripheral or central nervous system caused by chemical, biological, or physical agents are referred to as neurotoxicity [1]. Substances such as metals (e.g., lead), industrial chemicals (e.g., acrylamide), pharmaceutical drugs (e.g., doxorubicin), pesticides (e.g., deltamethrin), and natural toxins (e.g., domoic acid) have been shown to cause neurotoxicity [1, 2]. They are often included in industrial, agricultural, and consumer products, which must then be registered and approved by the European Chemical Agency (ECHA) and the European Food Safety

Kristina Bartmann and Julia Hartmann are contributed equally to this chapter.

Authority (EFSA), prior to entering the European market. Depending on the production volume, different toxicity tests have to be conducted. Current neurotoxicity guideline studies [3, 4] that precede the approval of such products are performed in vivo and are thus highly resource-intensive with regard to time, money, and animals [5]. Additionally, animal and human interspecies variations greatly challenge the translation of the generated data, especially for the nervous system [6–8]. Therefore, we are in urgent need of animal-free alternatives that better mimic human nervous system physiology [9]. The ability to reprogram human somatic cells into induced pluripotent stem cells (hiPSC) [10] has extensively advanced the field of neurotoxicity evaluation [11–14].

The use of human cellular models gave rise to a very important component of hazard identification—the neurophysiological assessment. Cultured in vitro, hiPSCs are able to grow, migrate, and differentiate into functional neuronal networks (NN) [15–19]. Important tools to study the electrophysiology of such NN are microelectrode arrays (MEA). These integrated arrays of electrodes, photoetched into a glass slide or “chip”, allow the simultaneous extracellular recording of electrical activity from a large number of individual sites in one tissue [20]. So far, neurotoxicological testing with MEAs has mainly been performed with rodent NN [21–30]. However, the use of human in vitro cultures is preferred, because responses to test compounds might be affected by species differences in toxicodynamics [31–35]. For this reason, human cells are increasingly used to measure neurotoxicity on MEAs [36–40]. In this chapter, we describe the neural induction of hiPSCs to free-floating neural progenitor cells (hiNPC), their differentiation on poly-d-lysine (PDL)/laminin-coated MEAs and the subsequent formation and measurement of functional NN (Fig. 1) [15, 16].

2 Materials

All cell culture procedures need to be performed in a Class II Biological Safety Cabinet under sterile conditions. The cells are cultivated in an incubator at 37 °C and 5% CO₂.

2.1 Generation of Human Induced Neural Progenitor Cells (hiNPC)

2.1.1 Preparation of Neural Induction Medium (NIM)

Mix **DMEM** (high glucose, GlutaMAX™ Supplement, pyruvate, Thermofisher Scientific #31966-021) and **Ham's F12 Nutrient Mix** (GlutaMAX™ Supplement, Thermofisher Scientific #31765-027) 3:1 and add **1% Penicillin-Streptomycin** (10,000 U/mL, Thermofisher Scientific #15140-122), **2% B27™ supplement** (serum-free (50×), Thermofisher Scientific #17504-044), **0.2% Human recombinant epidermal growth factor** (EGF, Thermofisher Scientific #PHG0313), **1% N2 Supplement** (100×, Thermofisher Scientific #17502-048), **20% KnockOut™ Serum**

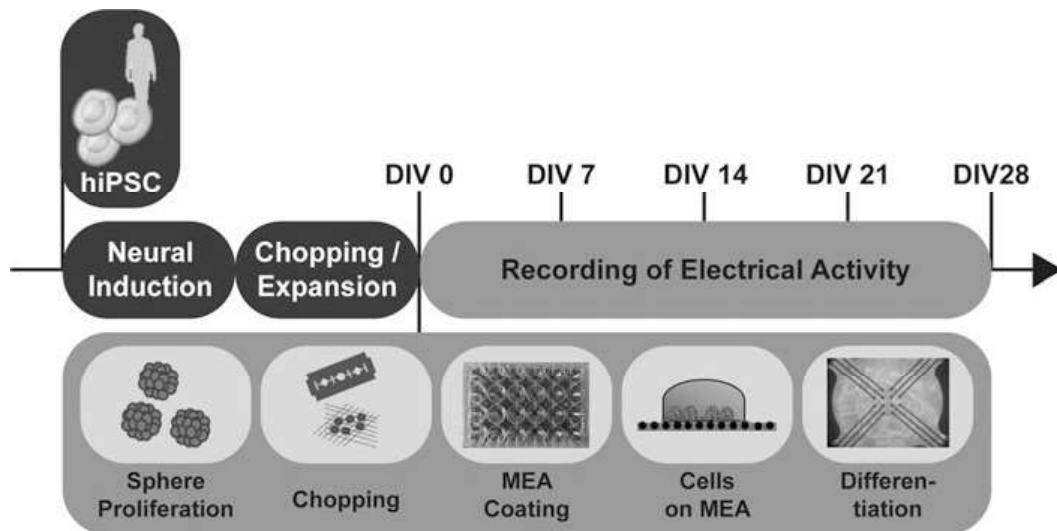


Fig. 1 Experimental setup (adapted from Nimtz et al. [15]). Human iPSCs were neurally induced to hiNPC and cultivated as free-floating 3D neurospheres. Neurospheres proliferate in neural proliferation medium (NPM) supplemented with basic fibroblast growth factor (FGF2) and epidermal growth factor (EGF). By mechanical passaging with a razorblade (chopping), neurospheres are cut into small pieces (100 μ m) and directly plated onto a PDL-Laminin-coated mwMEA plate. In CINDA the NN differentiate and can be cultured for multiple weeks. The electrical activity can be measured from day 7. *DIV*: days in vitro

Replacement (KSR, Thermofisher Scientific #10828-028), **10 μ M SB-431542 hydrate** (Sigma #S4317, dissolved at 10 mM in DMSO), and **0.5 μ M LDN-193189 hydrochloride** (Sigma #SML0559, dissolved at 500 μ M in ultrapure water).

The medium can be stored at 2–8 °C for at least 3 weeks. Warm it to 37 °C prior to use.

2.1.2 Preparation of Neural Proliferation Medium (NPM)

Mix **DMEM** (high glucose, GlutaMAX™ Supplement, pyruvate, Thermofisher Scientific #31966-021) and **Ham's F12 Nutrient Mix** (GlutaMAX™ Supplement, Thermofisher Scientific #31765-027) 3:1 and add **1% Penicillin-Streptomycin** (10,000 U/mL, Thermofisher Scientific #15140-122), **2% B27™ supplement** (serum-free (50 \times), Thermofisher Scientific #17504-044), and **0.2% human recombinant epidermal growth factor** (EGF, Thermofisher Scientific #PHG0313). Previously, EGF is dissolved at 10 μ g/mL in sterile PBS, containing 0.1% bovine serum albumin (BSA, Serva #11920) and 1 mM DL-Dithiothreitol solution (DTT, Sigma #646563-10 \times). EGF is stored at –20 °C.

The NPM, containing supplements, antibiotics, and growth factors, can be stored up to 2 weeks at 2–8 °C. Prior to use, warm it to 37 °C and add **basic human recombinant fibroblast growth factor** (FGF2, R&D Systems #233-FB) to a final concentration of **20 ng/mL**. FGF2 is dissolved at 10 μ g/mL in sterile PBS, containing 0.1% bovine serum albumin (BSA, Serva #11920) and 1 mM DL-Dithiothreitol solution (DTT, Sigma #646563-10 \times). The reconstituted FGF2 can be stored for a maximum of 3 months at –20 °C.

2.1.3 Preparation of Poly-HEMA Solution

Dissolve 1.2 g of Poly(2-hydroxyethyl methacrylate) (Poly-HEMA, Sigma-Aldrich #P3932) in 40 mL ethanol (94.8%) using a magnetic stirrer for 5–16 h (*see Note 1*).

2.1.4 Neural Induction

- iPSC (IMR90) clone (#4), WiCell (*see Note 2*).
- mTeSR1, Stemcell Technologies #05850.
- Corning® Matrigel® Growth Factor Reduced (GFR) Basement Membrane Matrix, Phenol Red-free, LDEV-free, Corning #356231.
- Y-27632 (Rock Inhibitor), Tocris #1254, diluted to 10 mM in ultrapure water.
- StemPro™ EZPassage™ Disposable Stem Cell Passaging Tool, Thermofisher Scientific #23181010.
- Corning® cell lifter, Merck #CLS3008.
- McIlwain tissue chopper, Mickle Laboratory Engineering Co. Ltd.
- NIM (*see Subheading 2.1.1*).
- NPM (*see Subheading 2.1.2*).
- Dulbecco's phosphate-buffered saline with CaCl₂ and MgCl₂ (DPBS, 1×, Gibco).
- Culture dish (Ø10 cm and Ø6 cm).

2.2 Multiwell Microelectrode Arrays (mwMEAs)

2.2.1 Preparation of Differentiation Medium—CINDA

Mix **DMEM** (high glucose, GlutaMAX™ Supplement, pyruvate, Thermofisher Scientific #31966-021) and **Ham's F12 Nutrient Mix** (GlutaMAX™ Supplement, Thermofisher Scientific #31765-027) 3:1 and add **1% Penicillin-Streptomycin** (10,000 U/mL, Thermofisher Scientific #15140-122), **2% B27™ supplement** (serum-free (50×), Thermofisher Scientific #17504-044), **1% N2 Supplement** (100×, Thermofisher Scientific #17502-048), **5 mM creatine monohydrate** (Sigma #C3630), **100 U/mL human recombinant interferon-γ** (IFN-γ, Peprotech #300-02), **20 ng/mL human recombinant neurotrophin-3** (Peprotech #450-03) and **20 μM L-Ascorbic acid** (Sigma #A5960).

Store the medium at 2–8 °C for up to 2 weeks. Warm the differentiation medium to 37 °C and add **300 μM N⁶,2'-O-Dibutyryl adenosine 3',5'-cyclic monophosphate sodium salt** (Dibutyryl cAMP, Sigma #D0260) prior to use (*see Note 3*).

2.2.2 Differentiation on Poly-D-Lysin/ Laminin-Coated 24-Multiwell MEAs

- 24-Well plate with PEDOT electrodes on glass (mw-MEA), Multichannelsystems #24W300/30G-288.
- Poly-D-lysine hydrobromide (PDL), Sigma #P0899.
- Laminin from Engelbreth-Holm-Swarm sarcoma basement membrane (Laminin, working solution: $c = 1$ mg/mL), Sigma #L2020 (*see Note 4*).

- Autoclaved ultrapure water.
- McIlwain tissue chopper, Mickle Laboratory Engineering Co. LTD.
- Dulbecco's phosphate-buffered saline with CaCl_2 and MgCl_2 (DPBS, $1\times$, Gibco).
- Counting Chamber Nageotte, Marienfeld #KHY3.1.

2.2.3 Devices and Software for mwMEA Recordings and Analysis

- Multiwell-MEA headstage, Multi Channel Systems MCS GmbH.
- Multiwell-Screen, Version 1.11.6.0, Multi Channel Systems MCS GmbH.
- Multiwell-Analyzer, Version 1.8.6.0, Multi Channel Systems MCS GmbH.

2.3 Lactate- Dehydrogenase Assay

- CytoTox-ONE Homogenous Membrane Integrity Assay Kit (#G7891, Promega; -20°C).
 - Substrate mix.
 - Assay buffer.
- Triton X-100 (10% in H_2O), Sigma-Aldrich #T8787.
- CINDA (*see* Subheading 2.2.1).
- 96-Well plate compatible with fluorometer.
- Fluorescence plate reader with excitation 530–570 nm and emission 580–620 nm filter pair.

3 Methods

All experiments need to be performed under sterile conditions.

3.1 Neural Induction of hiPSCs into Human Induced Neural Progenitor Cells (hiNPC)

During embryogenesis the human central nervous system develops from the ectoderm, one of the three germ layers that compose the entire body. These complex procedures can now be taken into a dish due to the unique technique of stem cell differentiation. In vitro, pluripotent stem cells, such as hiPSCs, can be directed to the ectodermal lineage by using neural induction media (NIM). The NIM used in this protocol is based on dual SMAD inhibition, and contains the small molecules LDN-193189 and SB431542 [15]. These factors inhibit TGF- β and SMAD signaling pathways and thereby prevent differentiation into non-neural ectodermal directions [41]. The neural induction is performed in Poly-HEMA-coated culture dishes to prevent cell adhesion to the dishes' surface and to ensure neurosphere formation. From day 7, 10 ng/mL FGF2 are added to the NIM. On day 21, the NPCs are

transferred to the NPM for further maintenance. With time, the neurospheres grow and need to be reduced in size by cutting into smaller pieces in order to avoid a necrotic sphere core (chopping; [42]). By using this method, neurospheres can be expanded and cultivated over several months. The number of possible passages depends on the cell line.

1. Add 1.5 mL Poly-HEMA solution to a 6 cm, or 3 mL to a 10 cm, culture dish and distribute the solution evenly across the surface. Let the solution evaporate overnight under sterile conditions or at least for 2 h (*see Note 5*).
2. The iPSC colonies are cultivated on Matrigel in a 6-well plate, with mTeSR1 medium. Assess the cell morphology under a microscope. If there are differentiated cells, mark the culture dish at the respective point and scratch off the cells with a pipette (*see Note 6*).
3. Add 10 μ M Y-27632 into the culture medium and swivel the plate in order to distribute it evenly.
4. Incubate the cells for 1 h at 37 °C and 5% CO₂.
5. After the incubation, discard the medium and wash each well with 1 mL pre-warmed DPBS.
6. Add 1 mL NIM with 10 μ M Y-27632 to the culture and cut the iPSC colonies into pieces by rolling them with StemPro™ EZPassage™ Disposable Stem Cell Passaging Tool once from top to bottom and once from left to right (*see Note 7*).
7. Scrape the resulting cell-clusters off the plate using a cell lifter. Use a microscope to make sure that uncut colonies are not lifted from the edge of the well.
8. Transfer the scratched colonies of each two wells to one 6 cm Poly-HEMA-coated culture dish and add 5 mL NIM including 10 μ M Y-27632 to each dish to reach a final volume of 7 mL.
9. After 2 days, move the culture dish in small circles to collect the formed neurospheres in the middle of the dish and replace 3.5 mL culture medium with the same volume NIM, without Y-27632.
10. Place the dishes into the incubator and carefully move the dish six times horizontally left and right as well as back and forth to distribute the spheres evenly and to avoid clumping.
11. Replace half of the medium every other day by following instructions 9 and 10.
12. Starting from day 7, add 10 ng/mL FGF2 to the NIM.
13. On day 21, collect all neurospheres by gathering them in the middle of the dish and transfer them into a 10 cm Poly-HEMA-coated culture dish. Further cultivate them in 20 mL NPM with 20 ng/mL FGF2.

14. Replace half of the media with fresh NPM every other day, by following instructions 9 and 10.
15. Neurospheres with a diameter of 0.7 mm or above are mechanically passaged with a razor blade (chopped). This is necessary approximately every 7 days.
16. For chopping, use the McIlwan tissue chopper and attach a sterilized razor blade onto the chopping arm. Make sure the razor blade is positioned correctly and screwed on tightly (*see Note 8*).
17. Adjust the chop distance to 0.25 mm.
18. Transfer neurospheres from the culture dish to the lid of a sterile 6 cm culture dish, with less medium as possible. Remove the supernatant medium, to prevent moving of neurospheres during the process.
19. Place the lid in the holder of the tissue chopper, move it to the start position, and start the device, by pressing “reset”.
20. Stop the tissue chopper when the razor blade reached the end of the dish lid, rotate the lid 90°, and repeat **step 19**.
21. Resuspend the chopped neurospheres in 1 mL NPM by carefully pipetting up and down. Equally distribute the cell suspension into two to three new Poly-HEMA-coated culture dishes (Ø 10 cm), each with 20 mL NPM.
22. Cultivate the cells in an incubator at 37 °C and 5% CO₂.

3.2 Recording Electrical Activity of Neural Networks with mwMEAs

By plating the neurospheres as a monolayer onto an extracellular matrix, here PDL and laminin, and cultivating them in neural differentiation medium, they differentiate into an electrically active NN. Laminin is one of the major integrin interaction factors and, besides facilitating cell adherence, it supports growth, survival, and functional development in iPSC-based neural cultures in vitro [43]. The differentiation medium CINDA contains additional maturation supporting factors (Creatine, Interferon- γ , Neurotrophin-3, Dibutyl cAMP and Ascorbic acid) that support neuronal maturation, synapse formation, and spontaneous NN activity [15]. This NN activity can be measured on MEAs, which simultaneously derive the membrane potential of numerous neurons via an electrode recording field. The here used 24-multiwell MEAs have an electrode field of 12 PEDOT-coated gold-electrodes plus four reference electrodes per well. Each electrode has a diameter of 30 μ m and an interelectrode distance of 300 μ m. The measured neuronal activity is detected and displayed as spikes and bursts, whereas each spike is derived from one action potential and several consecutive spikes are defined as one burst. Another measurable parameter is network bursts, which occur when the network matures over time and develops a synchronous bursting pattern.

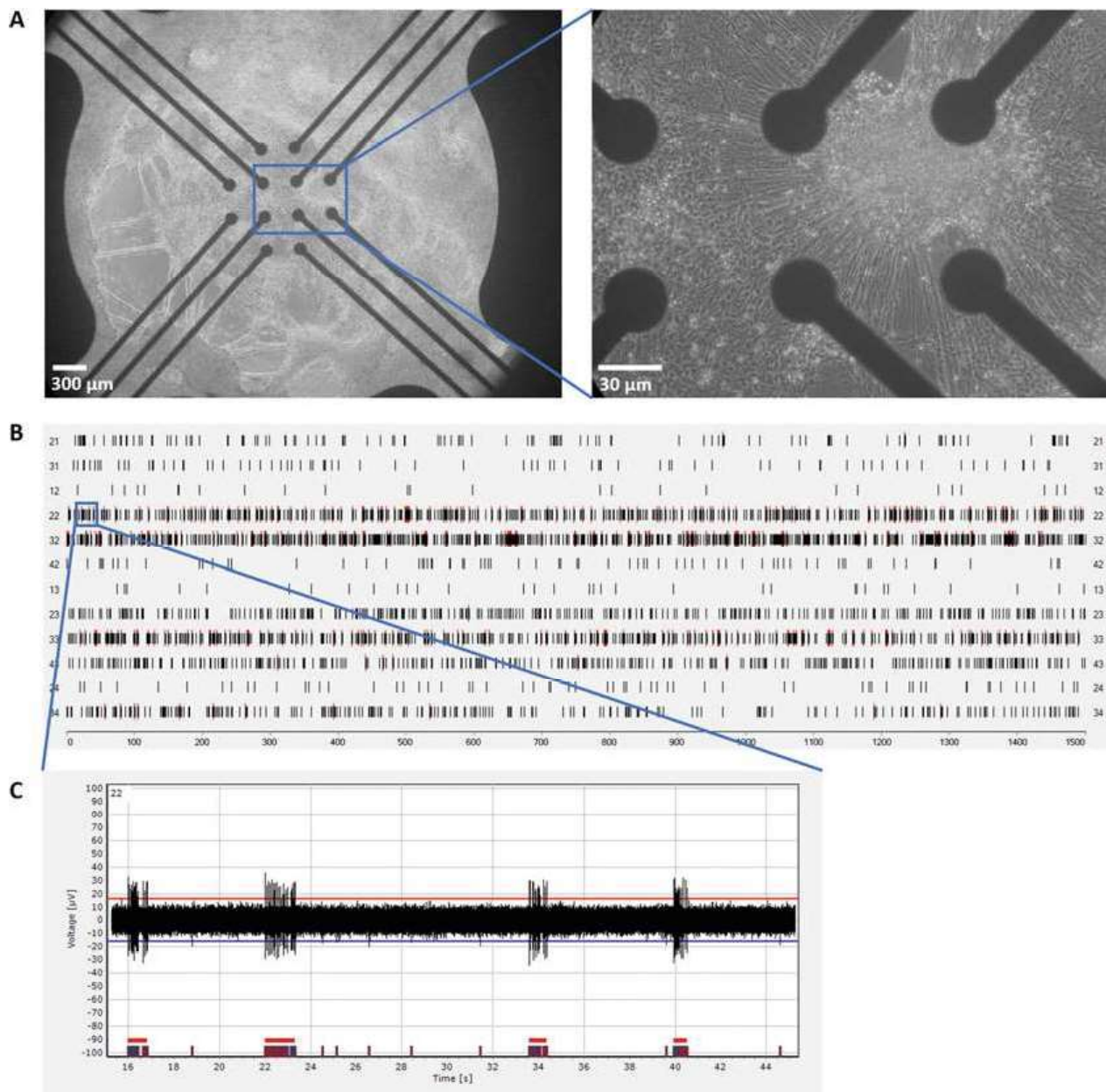


Fig. 2 Measurement of electrical NN activity on mwMEA. (a) Representative phase-contrast images of a human NN, differentiated on mwMEA electrodes for 12 days. (b) SRP of one well of a 24-mwMEA, after 10 days of differentiation. Each vertical black line represents a spike and each horizontal red bar represents a burst. (c) Spike train of the blue marked position in the SRP

During the measurement, the signals are shown as spike raster plots (SRP) and spike trains (Figs. 2 and 3). By setting certain values and thresholds, which have to be adapted for each network, the sensitivity of the measurement can be adjusted and the background noise can be filtered. The measurement data give information about spike count, spike rate [Hz], burst count, mean burst duration [μs], mean burst spike count, percentage of spikes in a burst, mean interburst interval [μs], and number of active electrodes, as well as the same information about network bursts. The combined data set allows a good characterization of the network activity and

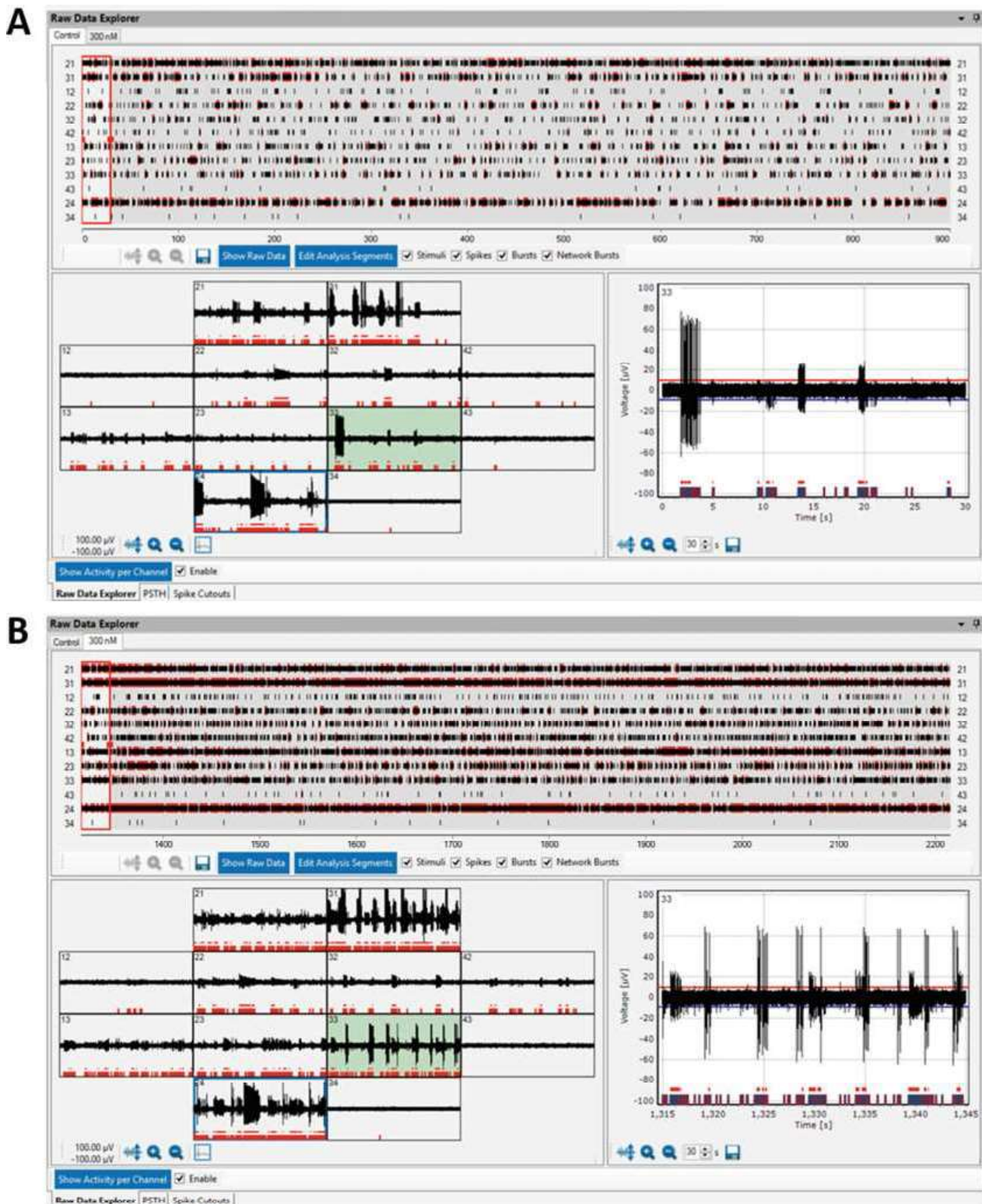


Fig. 3 Neuronal network activity before and during treatment with domoic acid. Domoic acid binds to glutamate receptors with a higher affinity than glutamate itself. This results in an overreaction that can lead to excitotoxicity and finally to cell death. The images show representative software screen shots after 10 DIV of the **a)** baseline activity and **b)** the activity during the treatment with 300 nM domoic acid (after wash-in-phase of 5 min). Each vertical black line represents a spike and each horizontal red line represents a burst. Software: Multiwell-Analyzer, Version 1.8.6.0, Multi Channel Systems MCS GmbH

its response to neurotoxic substance exposure. In order to define a valid experiment, the two parameters minimum spike rate/electrode and number of active electrodes/well need to be monitored. The limit values for these parameters can vary depending on the cell line used.

3.2.1 Differentiation on PDL/Laminin-Coated 24-Multiwell MEAs

1. Dilute PDL in sterile ultrapure water to reach a final concentration of 100 µg/mL and store working stocks at -20°C until use. Prior to coating, thaw the PDL solution at 37°C .
2. Add 100 µL PDL solution (100 µg/mL) to each well of a 24-mwMEA plate and incubate at least for 1 h at 37°C or for 48 h at 4°C .
3. Thaw laminin in the fridge ($4-8^{\circ}\text{C}$) to avoid gel formation and dilute the laminin with sterile ultrapure water 1:80 to obtain a final concentration of 12.5 ng/mL.
4. Aspirate the PDL solution and wash wells once with sterile ultrapure water.
5. Add 100 µL laminin (12.5 µg/mL) solution to each well and incubate at least for 1 h at 37°C (*see Note 9*).
6. Aspirate the laminin solution, wash the wells once with sterile ultrapure water, and directly use the coated plate.
7. Chop the neurospheres to a size of 0.1 mm (for details *see* Subheading 3.1, step 16–21).
8. Resuspend the cut spheres in 1 mL prewarmed CINDA.
9. Transfer 80 µL of the cut spheres suspension into a Nageotte counting chamber and count the sphere parts. Dilute the cut spheres solution if necessary to reach a maximum of 4000 sphere parts/mL.
10. Collect 200 sphere parts in up to 100 µL CINDA and carefully pipet them directly onto the electrodes of a mwMEA well. The solution should form a droplet on top of the electrodes. Allow the spheres to settle and adhere to the well surface, by incubating the droplet for 2 h at 37°C and 5% CO_2 .
11. Add 1 mL CINDA to each well and incubate the plate at 37°C and 5% CO_2 .
12. Feed the cells once a week, by replacing half of the medium in each well.
13. From day 7, measure the electrical activity twice a week as long as the neurons are electrically active (*see Note 10*). Preheat the mwMEA headstage to 37°C and gas the device with carbogen, before adding the mwMEA. For parameter settings *see* Table 1.
14. Let the mwMEA acclimatize for 15 min, before starting the 15 min baseline recording.

Table 1
Parameter settings for mwMEA measurement

Parameter	Setting
Sampling rate	20,000 Hz
Low-pass filter type	Butterworth
Low-pass-filter order	4
Low-pass filter cutoff frequency	3,500 Hz
High-pass filter type	Butterworth
High-pass-filter order	2
High-pass filter cutoff frequency	300 Hz

15. For acute toxicity measurements, stick to the following time schedule:
 - Baseline measurement: 15 min recording.
 - Wash-in-phase: add the substance and equilibrate for 5 min.
 - Treatment: 15 min recording.
 - Cytotoxicity analysis: remove the medium and transfer it into a new 24-well plate for cytotoxicity analysis (*see* Sub-heading 3.3 for further details).
 - Wash-out-phase: wash each well twice with CINDA to wash out the substance.
16. Further cultivate the cells in fresh CINDA medium at 37 °C and 5% CO₂.

3.2.2 Analysis of mwMEA Recordings

1. Load the .mwr file, which is automatically generated during recording, into the Multiwell-Analyzer Software.
2. Set the “Spike Detector Configuration” to an automatic threshold estimation of 500 ms baseline duration and rising/falling edge of 5× standard deviation (*see* **Note 11**).
3. For the “Burst Detector Configuration” choose the following settings (*see* **Note 12**):
 - Max. Interval to start burst: 100 ms.
 - Max. Interval to end burst: 100 ms.
 - Min. Interval between bursts: 20 ms.
 - Min. Duration of burst: 10 ms.
 - Min. Spike count in burst: 3.
4. To select active wells only, set the “Channel Selection Configuration” to a minimum of 5 spikes/minute (=0.083 Hz) for

each channel and a minimum of 3 active channels for each well [21].

5. Run the analysis.
6. Check each channel for artifacts and defective electrodes (*see Note 13*).
7. Export the analysis of all intact electrodes without artifacts as a .csv file.
8. Open the .csv file and copy the data into a software for statistical analysis and data plotting.

3.3 Assessment of Cytotoxicity via the Lactate-Dehydrogenase Assay

To ensure that the adverse effects are due to neurotoxicity and not cytotoxicity, we perform the Lactate-Dehydrogenase (LDH) Assay. The substrate mix contains lactate, NAD^+ , and resazurin. If the cell membrane is damaged, the cytosolic lactate dehydrogenase enzyme is released into the cell culture medium and can be quantified by subsequent enzymatic reactions. LDH first catalyzes the conversion of lactate to pyruvate, with a simultaneous reduction of NAD^+ to NADH. By oxidation of NADH to NAD^+ , the enzyme diaphorase reduces resazurin to resorufin, which can be measured with a fluorometer (excitation: 540 nm; emission: 590 nm). The amount of produced resorufin is thus proportional to the amount of released LDH. Cells with an intact membrane do not release LDH and therefore no fluorescence is measurable in the culture medium. Two controls are required to perform this assay: a 100% cell lysis control (LC) and a background control (BG; culture medium without cells). By lysing the cells of the LC with Triton X-100, the maximum amount of LDH present is determined.

1. Prepare the CytoTox-ONE Reagent as indicated in the supplier's manual and protect it from light (*see Note 14*).
2. For the LC, add 10% (v/v) Triton X-100 solution 1:5 to the desired number of wells (final concentration 2%).
3. Preincubate the LC for 30 min at 37 °C and 5% CO_2 .
4. Transfer the complete medium of each well into a new 24-well plate.
5. Transfer 50 μL medium of each well of interest of the 24-well plate into a 96-well plate, including the LC and the BG.
6. Add 50 μL CytoTox-ONE Reagent to each of the wells.
7. Incubate at room temperature for 2 h, protected from light.
8. Measure the fluorescence of the samples at an excitation wavelength of 540 nm and an emission wavelength of 590 nm in a plate reader (*see Note 15*).
9. Calculate the mean of all technical replicate measurements and normalize data by subtracting the mean of the BG from the mean of the different conditions.

10. Calculate the values of each condition as percent of the mean of the LC.
11. The results of at least three independent experiments are pooled, and mean, standard deviation (SD), and standard error of the mean (SEM) are calculated. Data analyses, statistical analyses, and data plotting are performed in GraphPad Prism, using OneWay ANOVA and Bonferroni's post hoc test.

4 Notes

1. The Poly-HEMA solution is stable for up to 2 months at 4 °C.
2. When using a different hiPSC line, the protocol may have to be adapted.
3. Dibutyl cAMP is sensitive to light and moisture. The CINDA medium should therefore not be exposed to light for more than 1 h.
4. The product concentration depends on the batch number and has to be adjusted to 1 mg/mL with autoclaved ultrapure water.
5. Poly-HEMA-coated dishes can be used for up to 3 months if stored sealed at room temperature and in the dark.
6. iPSCs are small and round in shape and have a high nucleus-to-cytoplasm ratio, with prominent nucleoli. Differentiating cells have a lower nucleus-to-cytoplasm ratio and the morphology differs visibly from the original round shape.
7. We banked our hiPSCs so that we can start each neural induction with a similar passage number. We use the cells starting from passage 3 post-thawing at the earliest and up to passage 10 post-thawing at the latest. This must be adapted for other cell lines.
8. Each side of a razor blade can be used three times.
9. PDL/Laminin-coated plates can be stored in the refrigerator (4–8 °C) for a maximum of 2 weeks prior to use.
10. During cell differentiation, the burst behavior changes and begins to synchronize as the network matures. For this reason, exposure to the same substance in different experiments should always be carried out in the same time frame.
11. This eliminates the detected background signals.
12. These settings need to be adapted to the specific cell signals and vary depending on the cell line.
13. An artifact can be caused by external influences and is visible as an exactly simultaneous signals on all electrodes. Furthermore,

artifacts and defective electrodes can be excluded by observing the spike signal that should resemble a waveform.

14. Aliquot unused CytoTox-ONE reagent and protect the reagent from light. Aliquots should be labeled with preparation date and reagent number and can be stored tightly capped at -20°C for 6–8 weeks.
15. If the plate reader measures from above, remove the lid of the plate before measurement.

References

1. Costa LG, Giordano G, Guizzetti M, Vitalone A (2008) Neurotoxicity of pesticides: a brief review. *Front Biosci* 13:1240–1249. <https://doi.org/10.2741/2758>
2. Massaro EJ (2002) *Handbook of neurotoxicology*. Humana Press, Totowa, NJ
3. OECD guideline for the testing of Chemicals (1997) Test no. 424: neurotoxicity study in rodents. In: *OECD guideline for the testing of chemicals*. OECD, Paris, pp 1–15
4. Forum RA (1998) Guidelines for neurotoxicity risk assessment
5. Bal-Price AK, Suñol C, Weiss DG et al (2008) Application of in vitro neurotoxicity testing for regulatory purposes: symposium III summary and research needs. *Neurotoxicology* 29:520–531. <https://doi.org/10.1016/j.neuro.2008.02.008>
6. Leist M, Hartung T (2013) Inflammatory findings on species extrapolations: humans are definitely no 70-kg mice. *Arch Toxicol* 87:563–567
7. Borrell V, Götz M (2014) Role of radial glial cells in cerebral cortex folding. *Curr Opin Neurobiol* 27:39–46
8. Toutain P-L, Ferran A, Bousquet-Melou A (2010) Species differences in pharmacokinetics and pharmacodynamics. In: *Comparative and Veterinary Pharmacology, Handbook of Experimental Pharmacology*, Springer, pp 19–48. https://doi.org/10.1007/978-3-642-10324-7_2
9. Masjosthusmann S, Barenys M, El-Gamal M et al (2018) Literature review and appraisal on alternative neurotoxicity testing methods. *EFSA Support Publ* 15:1–108. <https://doi.org/10.2903/sp.efsa.2018.cn-1410>
10. Takahashi K, Tanabe K, Ohnuki M et al (2007) Induction of pluripotent stem cells from adult human fibroblasts by defined factors. *Cell* 131:861–872. <https://doi.org/10.1016/j.cell.2007.11.019>
11. Pei Y, Peng J, Behl M et al (2016) Comparative neurotoxicity screening in human iPSC-derived neural stem cells, neurons and astrocytes. *Brain Res* 1638:57–73. <https://doi.org/10.1016/j.brainres.2015.07.048>
12. Barenys M, Fritsche E (2018) A historical perspective on the use of stem/progenitor cell-based in vitro methods for neurodevelopmental toxicity testing. *Toxicol Sci* 165:10–13. <https://doi.org/10.1093/toxsci/kfy170>
13. de Groot MWGDM, Westerink RHS, Dingemans MML (2013) Don't judge a neuron only by its cover: neuronal function in in vitro developmental neurotoxicity testing. *Toxicol Sci* 132:1–7. <https://doi.org/10.1093/toxsci/kfs269>
14. Tukker AM, De Groot MWGDM, Wijnolts FMJ et al (2016) Research article is the time right for in vitro neurotoxicity testing using human iPSC-derived neurons? *ALTEX* 33:261–271. <https://doi.org/10.14573/altex.1510091>
15. Nimtz L, Hartmann J, Tigges J et al (2020) Characterization and application of electrically active neuronal networks established from human induced pluripotent stem cell-derived neural progenitor cells for neurotoxicity evaluation. *Stem Cell Res* 45:101761. <https://doi.org/10.1016/j.scr.2020.101761>
16. Hofrichter M, Nimtz L, Tigges J et al (2017) Comparative performance analysis of human iPSC-derived and primary neural progenitor cells (NPC) grown as neurospheres in vitro. *Stem Cell Res* 25:72–82. <https://doi.org/10.1016/j.scr.2017.10.013>
17. Izsak J, Seth H, Andersson M et al (2019) Robust generation of person-specific, synchronously active neuronal networks using purely isogenic human iPSC-3D neural aggregate cultures. *Front Neurosci* 13. <https://doi.org/10.3389/fnins.2019.00351>

18. Hyvärinen T, Hyysalo A, Kapucu FE et al (2019) Functional characterization of human pluripotent stem cell-derived cortical networks differentiated on laminin-521 substrate: comparison to rat cortical cultures. *Sci Rep* 9:17125. <https://doi.org/10.1038/s41598-019-53647-8>
19. Pamies D, Barreras P, Block K et al (2017) A human brain microphysiological system derived from induced pluripotent stem cells to study neurological diseases and toxicity. *ALTEX* 34:362–376. <https://doi.org/10.14573/altext.1609122>
20. Johnstone AFM, Gross GW, Weiss DG et al (2010) Microelectrode arrays: a physiologically based neurotoxicity testing platform for the 21st century. *Neurotoxicology* 31:331–350
21. McConnell ER, McClain MA, Ross J et al (2012) Evaluation of multi-well microelectrode arrays for neurotoxicity screening using a chemical training set. *Neurotoxicology* 33:1048–1057. <https://doi.org/10.1016/j.neuro.2012.05.001>
22. Hogberg HT, Sobanski T, Novellino A et al (2011) Application of micro-electrode arrays (MEAs) as an emerging technology for developmental neurotoxicity: evaluation of domoic acid-induced effects in primary cultures of rat cortical neurons. *Neurotoxicology* 32:158–168. <https://doi.org/10.1016/j.neuro.2010.10.007>
23. Mack CM, Lin BJ, Turner JD et al (2014) Burst and principal components analyses of MEA data for 16 chemicals describe at least three effects classes. *Neurotoxicology* 40:75–85
24. Shafer TJ, Brown JP, Lynch B et al (2019) Evaluation of chemical effects on network formation in cortical neurons grown on micro-electrode arrays. *Toxicol Sci* 169:436–455. <https://doi.org/10.1093/toxsci/kfz052>
25. Alloisio S, Nobile M, Novellino A (2015) Multiparametric characterisation of neuronal network activity for in vitro agrochemical neurotoxicity assessment. *Neurotoxicology* 48:152–165. <https://doi.org/10.1016/j.neuro.2015.03.013>
26. Shafer TJ, Rijal SO, Gross GW (2008) Complete inhibition of spontaneous activity in neuronal networks in vitro by deltamethrin and permethrin. *Neurotoxicology* 29:203–212. <https://doi.org/10.1016/j.neuro.2008.01.002>
27. Defranchi E, Novellino A, Whelan M et al (2011) Feasibility assessment of micro-electrode chip assay as a method of detecting neurotoxicity in vitro. *Front Neuroeng* 4:1–12. <https://doi.org/10.3389/fneng.2011.00006>
28. Valdivia P, Martin M, LeFew WR et al (2014) Multi-well microelectrode array recordings detect neuroactivity of ToxCast compounds. *Neurotoxicology* 44:204–217. <https://doi.org/10.1016/j.neuro.2014.06.012>
29. Wallace K, Strickland JD, Valdivia P et al (2015) A multiplexed assay for determination of neurotoxicant effects on spontaneous network activity and viability from microelectrode arrays. *Neurotoxicology* 49:79–85. <https://doi.org/10.1016/j.neuro.2015.05.007>
30. Novellino A, Scelfo B, Palosaari T et al (2011) Development of micro-electrode array based tests for neurotoxicity: assessment of Interlaboratory reproducibility with neuroactive chemicals. *Front Neuroeng* 4:1–14. <https://doi.org/10.3389/fneng.2011.00004>
31. Gassmann K, Abel J, Bothe H et al (2010) Species-specific differential ahr expression protects human neural progenitor cells against developmental neurotoxicity of PAHs. *Environ Health Perspect* 118:1571–1577. <https://doi.org/10.1289/ehp.0901545>
32. Dach K, Bendt F, Huebenthal U et al (2017) BDE-99 impairs differentiation of human and mouse NPCs into the oligodendroglial lineage by species-specific modes of action. *Sci Rep* 7:1–11. <https://doi.org/10.1038/srep44861>
33. Masjosthusmann S, Becker D, Petzuch B et al (2018) A transcriptome comparison of time-matched developing human, mouse and rat neural progenitor cells reveals human uniqueness. *Toxicol Appl Pharmacol* 354:40–55. <https://doi.org/10.1016/j.taap.2018.05.009>
34. Oberheim NA, Takano T, Han X et al (2009) Uniquely hominid features of adult human astrocytes. *J Neurosci* 29:3276–3287. <https://doi.org/10.1523/JNEUROSCI.4707-08.2009>
35. Perreault M, Feng G, Will S et al (2013) Activation of TrkB with TAM-163 results in opposite effects on body weight in rodents and non-human primates. *PLoS One* 8:e62616. <https://doi.org/10.1371/journal.pone.0062616>
36. Tukker AM, Wijnolts FMJ, de Groot A, Westerink RHS (2018) Human iPSC-derived neuronal models for in vitro neurotoxicity assessment. *Neurotoxicology* 67:215–225. <https://doi.org/10.1016/j.neuro.2018.06.007>
37. Tukker AM, Wijnolts FMJ, de Groot A, Westerink RHS (2020) Applicability of hiPSC-derived neuronal co-cultures and rodent primary cortical cultures for in vitro seizure liability assessment. *Toxicol Sci*. <https://doi.org/10.1093/toxsci/kfaa136>

38. Tukker AM, Bouwman LMS, van Kleef RGDM et al (2020) Perfluorooctane sulfonate (PFOS) and perfluorooctanoate (PFOA) acutely affect human $\alpha 1\beta 2\gamma 2\text{L}$ GABAA receptor and spontaneous neuronal network function in vitro. *Sci Rep* 10. <https://doi.org/10.1038/s41598-020-62152-2>
39. Ylä-Outinen L, Heikkilä J, Skottman H et al (2010) Human cell-based micro electrode array platform for studying neurotoxicity. *Front Neuroeng* 3. <https://doi.org/10.3389/fneng.2010.00111>
40. Odawara A, Matsuda N, Ishibashi Y et al (2018) Toxicological evaluation of convulsant and anticonvulsant drugs in human induced pluripotent stem cell-derived cortical neuronal networks using an MEA system. *Sci Rep* 8:10416. <https://doi.org/10.1038/s41598-018-28835-7>
41. Qi Y, Zhang XJ, Renier N et al (2017) Combined small-molecule inhibition accelerates the derivation of functional cortical neurons from human pluripotent stem cells. *Nat Biotechnol* 35:154–163. <https://doi.org/10.1038/nbt.3777>
42. Svendsen CN, Ter Borg MG, Armstrong RJE et al (1998) A new method for the rapid and long term growth of human neural precursor cells. *J Neurosci Methods* 85:141–152. [https://doi.org/10.1016/S0165-0270\(98\)00126-5](https://doi.org/10.1016/S0165-0270(98)00126-5)
43. Farrukh A, Zhao S, del Campo A (2018) Microenvironments designed to support growth and function of neuronal cells. *Front Mater* 5:1–22. <https://doi.org/10.3389/fmats.2018.00062>

Measurement of Electrical Activity of differentiated Human iPSC-Derived Neurospheres recorded by Microelectrode Arrays (MEA)

Kristina Bartmann, **Julia Hartmann**, Julia Kapr, and Ellen Fritsche

Fachzeitschrift/Buch: *Springer Protocols*

Impact Factor: wird für Buchkapitel nicht berechnet

Beteiligung an der Publikation: 40 %

Schreiben der Kapitel „2 Materials“, „3 Methods“ und „4 Notes“ und das Erstellen der Abbildungen 2 und 3

Typ der Autorenschaft: Erstautorenschaft

Status der Publikation: veröffentlicht am 24.Juli 2021

2.5 Alginate-laminin hydrogel supports long-term neuronal activity in three-dimensional human induced pluripotent stem cell-derived neuronal networks

Julia Hartmann, Ines Lauria, Farina Bendt, Stephan Rütten, Katharina Koch, Andreas Blaeser, and Ellen Fritsche

Advanced Materials Interfaces

Für 3D neurale Kulturen werden langlebige Hydrogele benötigt, die über einen langen Differenzierungszeitraum bestehen bleiben und dadurch die Reifung der neuronalen Netzwerke (NN) ermöglichen. In dieser Studie wurden aus hiPSCs generierte neurale Progenitorzellen (hiNPCs), in Alginate mit oder ohne Zusatz des extrazellulären Matrixproteins L111 eingebettet und in NN differenziert. Wir haben die Hydrogele hinsichtlich Porosität, L111 Verteilung innerhalb des Gels, Viskosität und Zytokompatibilität mittels Laktat-Dehydrogenase (LDH)-Assay und CellTiter-Blue Assay gemessen. Die neurale Netzbildung wurde anhand von Zellmigration, Differenzierung und spontaner elektrischer Aktivität beurteilt. Die Zugabe von L111 zu Alginate erhöht die neurale Migration, die Differenzierung in Neurone und Astrozyten sowie die Synaptogenese. Die in Hydrogel eingebetteten NN waren bis zu 206 Tage elektrisch aktiv, wobei das L111 einen positiven Einfluss auf die elektrische Aktivität, die Netzbildung und die Synchronität im Vergleich zu den 2D Kontrollen und den Hydrogelkulturen ohne L111 gezeigt hat. Des Weiteren beschleunigt die Zugabe von L111 die Wiederherstellung der elektrischen Aktivität nach Blockierung der Natriumkanäle durch Tetrodotoxin (TTX). Aus diesen Gründen sind in Alginate-L111-Hydrogelen kultivierte hiPSC-basierte NN eine vielversprechende Methode für

zukünftige langfristige Anwendungen als Krankheitsmodell oder zur Beurteilung von Arzneimitteln oder Chemikalien.

Alginate-Laminin Hydrogel Supports Long-Term Neuronal Activity in 3D Human Induced Pluripotent Stem Cell-Derived Neuronal Networks

Julia Hartmann, Ines Lauria, Farina Bendt, Stephan Rütten, Katharina Koch, Andreas Blaeser, and Ellen Fritsche*

For 3D neural cultures durable hydrogels are required, which persist over a long differentiation period and thus enable the maturation of neuronal networks (NN). Here, 3D models based on human induced pluripotent stem cell-derived neural progenitor cells that are embedded in hydrogels of either pure alginate or alginate functionalized with the extracellular matrix protein laminin 111 (L111) are established. This study analyzes material characteristics such as porosity, L111 distribution and shear viscosity, cell compatibility of hydrogels by measuring viability and cytotoxicity, and neural function by monitoring cell migration, differentiation as well as NN formation and activity on multielectrode arrays. The addition of L111 increases neural migration and enhances differentiation into neurons and astrocytes as well as synaptogenesis in alginate hydrogels. NN formed in hydrogels are electrically active for up to 206 d and L111-supplementation further increases electrical activity, network maturation, and synchronicity compared to 2D controls and NN grown in pure alginate hydrogels. L111 addition to alginate gels further accelerates recovery of electrical activity after blockage of sodium channels with tetrodotoxin. In conclusion, NN grown in alginate-L111 hydrogel blends are promising models for future long-term applications in disease modeling, drug or chemical evaluation.

1. Introduction

Ethical concerns, high costs, and low testing throughput have questioned the applicability of animal models in biomedical research and initiated a transition to the use of alternative human-based in vitro models. Moreover, experimental research revealed the restricted predictive power of animal experiments for humans, especially concerning the brain.^[1] So far, 2D cell culture models have been the main alternative to animal experiments, because they are relatively easy to handle, established in several functional assays, and scalable to high-throughput applications.^[2] However, cells in 2D often elicit a nonphysiological cell morphology, there is a lack of tissue-specific structures and interactions as well as mechanical and biochemical stimuli that influence cell proliferation and differentiation.^[3,4] Due to their more adequate representation of human physiology, 3D in vitro models gained

J. Hartmann, I. Lauria, F. Bendt, K. Koch, E. Fritsche
IUF – Leibniz-Research Institute for Environmental Medicine
Auf'm Hennekamp 50, 40225 Duesseldorf, Germany
E-mail: ellen.fritsche@iuf-duesseldorf.de

S. Rütten
Electron Microscopy Facility
Institute of Pathology
RWTH Aachen University Hospital
Pauwelsstrasse 30, 52074 Aachen, Germany



The ORCID identification number(s) for the author(s) of this article can be found under <https://doi.org/10.1002/admi.202200580>.

© 2022 The Authors. Advanced Materials Interfaces published by Wiley-VCH GmbH. This is an open access article under the terms of the Creative Commons Attribution License, which permits use, distribution and reproduction in any medium, provided the original work is properly cited.

DOI: 10.1002/admi.202200580

A. Blaeser
Institute for BioMedical Printing Technology
Technical University of Darmstadt
64289 Darmstadt, Germany

A. Blaeser
Centre for Synthetic Biology
Technical University of Darmstadt
64289 Darmstadt, Germany

E. Fritsche
Medical Faculty
Heinrich-Heine-University
Universitätsstraße 1, 40225 Düsseldorf, Germany

increasing attention in biomedical research. They have been implicated as novel preclinical and toxicological test systems and are being developed for regenerative medicine. 3D models can be divided into nonengineered models such as neurospheres and organoids as well as engineered models containing scaffolds, which are composed of different materials with distinct mechanical properties.^[4–6] The addition of bioactive molecules to hydrogel blends, such as the extracellular matrix (ECM) component laminin 111 (L111), positively affected proliferation, migration, and differentiation of neural progenitor cells (NPCs) into neural cells and the elongation of neurons in vitro.^[7–13] In addition, interactions between laminin molecules and the hydrogel matrix influence the density, pore size, and stiffness of the gel.^[9]

Depending on the analysis method and brain region, the human brain has a shear modulus between 0.4 and 1.4 kPa, making it the softest tissue of the human body.^[14,15] Several in vitro studies on rodent and human cell models demonstrated that especially hydrogels with low elastic moduli favor neuronal differentiation and neurite outgrowth.^[16–19] Moreover, co-culture studies with neurons and astrocytes indicated that glial differentiation is supported by substantially higher elastic moduli than neuronal differentiation.^[20–23] Godbe et al. even demonstrated with human induced pluripotent stem cell (hiPSC)-derived neurons that dopaminergic neurons require a softer matrix (storage modulus of 0.05 kPa) than other beta-III tubulin (TUBB3)-positive neurons.^[24] These cell-type-specific requirements in vitro complicate the co-cultivation of various neuronal subtypes together with glial cells, which is essential for an adequate representation of physiological and functional neural networks (NN).^[25–28]

The electrophysiological analysis of NN is a key measure of neuronal function.^[29,30] For this purpose, microelectrode arrays (MEAs) have been established as a reliable method, e.g., for neurotoxicological research applications with good intra- and interlaboratory reproducibility.^[31,32] First established with rodent cells, in the last years, more and more laboratories successfully developed NN formation assays based on human cell sources such as human embryonic stem cells (ESCs) and, more recently, hiPSCs.^[33,34] Moreover, in an attempt to better represent human brain physiology, first electrophysiologically active scaffold-based 3D models have been developed.^[35–38] However, long-term MEA cultures of more than 35 d have not been performed in 3D hydrogels so far, which is too short for generating synchronized neuronal network activities.^[39,40]

For the first time, we established 3D models of hiPSC-derived neural progenitor cells (hiNPCs) in alginate hydrogels on MEAs and differentiated them into electrically active NN over an extended period of 206 d. We chose alginate as matrix material because it is biocompatible, its mechanical properties can be adjusted to match the elastic modulus of human brain tissue, and it is suitable for long-term culture.^[16,41–43] To increase the bioactivity of the matrix we further supplemented the hydrogel with L111 because it was reported to enhance neurite outgrowth and differentiation.^[7,44] We added L111 in different concentrations (0.0025%, 0.005%, and 0.01%) to the 1% alginate matrix and investigated effects on cell viability, migration as well as neuronal and glial differentiation. To assess the functionality

of the formed NN, we recorded the electrical activity for up to 206 d (> 6 months) by using MEAs and compared the performance to respective hiPSC-derived 2D neural cultures.

2. Results

2.1. Addition of L111 Influences Pore Formation and Viscosity Behavior of Alginate Hydrogel Blends

To characterize the microstructural and rheological properties of the different alginate hydrogels, pore formation, viscosity, and L111 distribution were examined. The microstructures of alginate and alginate–L111 hydrogel blends were analyzed using scanning electron microscopy (SEM). Pores were present in all hydrogel blends, yet their size decreased with increasing L111 concentration (**Figure 1A**). However, due to their high magnification, only microstructural characteristics and no larger pore structures can be examined. Rheological characterization revealed that increasing L111 concentrations gradually decrease the viscosities of uncrosslinked gels at shear rates between 0.1 and 1 s^{−1} (**Figure 1B**). The elevated flow consistency index (*K*) underlines this observation (**Table 1**). In addition, L111 supplementation was found to reduce the shear thinning behavior of the mixture as indicated by the increasing flow behavior index (*n*). The L111 distribution within the 1% A–0.01% L111 hydrogel blend was monitored by confocal laser scanning microscopy (CLSM). The fluorescence of the antibody-stained L111 and the reflection of alginate revealed aggregate formation of L111, however, these aggregates were evenly distributed throughout the whole hydrogel blend (**Figure 1C**).

2.2. Alginate Hydrogel Blends Are Suitable for Differentiation of hiNPCs

After ensuring that the alginate–L111 hydrogel blends form a homogenous matrix for the cells, we pursued two strategies to load the different hydrogels with hiNPCs. First, hiNPC neurospheres were embedded in alginate hydrogels to enable the formation of interconnected micro-tissues with high cell densities. Second, in view of a possible bioprinting application, singularized hiNPCs were embedded in hydrogels (**Figure 2A**). To examine the cytocompatibility of alginate and alginate–L111 hydrogel blends, cell viability, and cytotoxicity were measured. Cell viability of embedded hiNPC neurospheres and single cells was confirmed by Alamar Blue assay on days 1, 7, and 14 (**Figure 2B,D**). As controls, hiNPC neurospheres and single cells were seeded directly on poly-D-lysine (PDL)/L111 (2D) and embedded in Matrigel. The resorufin fluorescence of the 2D cultures measured on day 1 was set to 100%. The viability of embedded neurospheres in alginate hydrogels on day 1 was 47% (1% A), 48% (1% A–0.0025% L111), 43% (1% A–0.005% L111), and 41% (1% A–0.01% L111). A cultivation time of 14 d, however, increased cell viability up to 59% (1% A), 63% (1% A–0.0025% L111), 64% (1% A–0.005% L111), and 64% (1% A–0.01% L111). Viability of embedded singularized hiNPCs was 60% (1% A), 62% (1% A–0.0025% L111), 65% (1% A–0.005% L111),

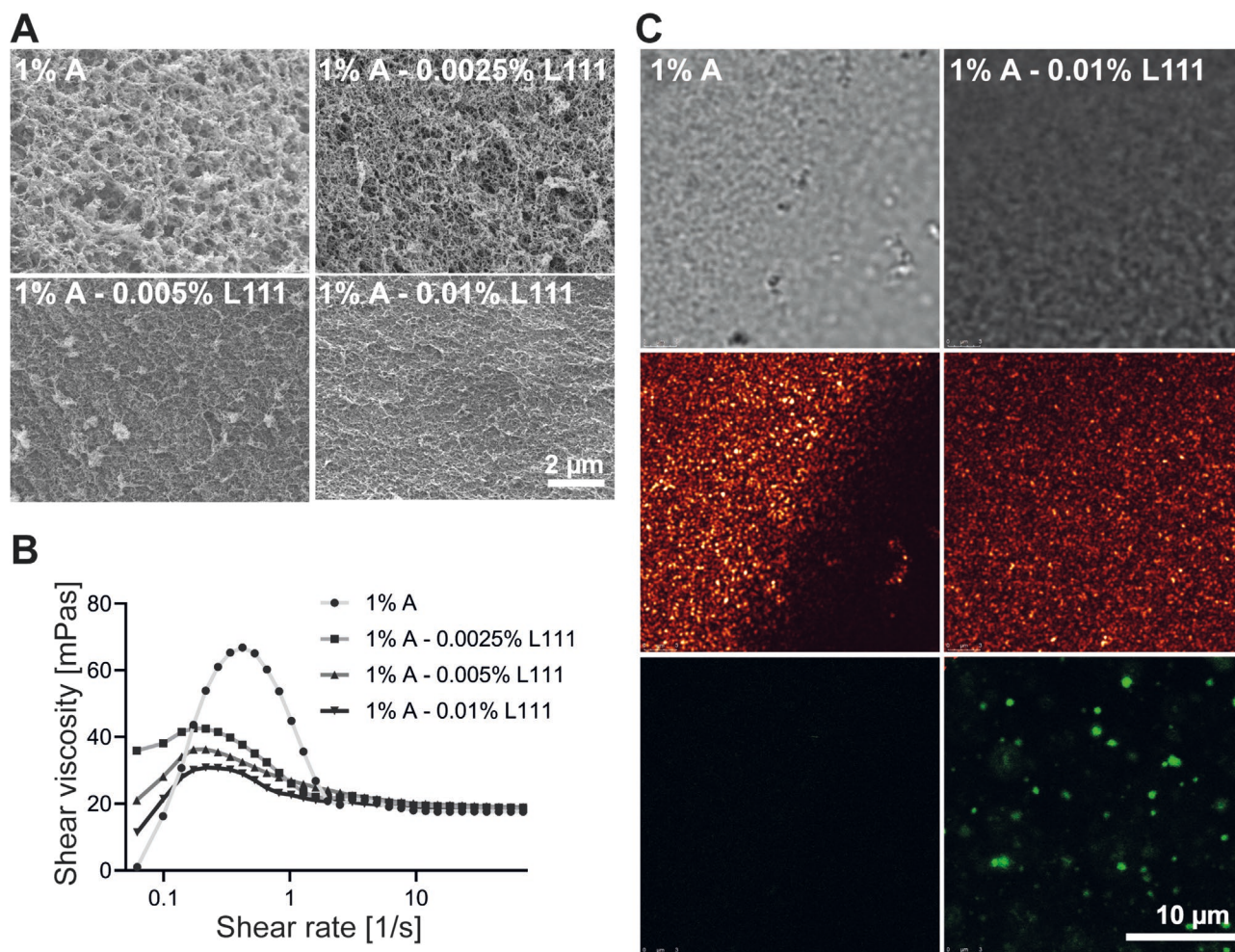


Figure 1. Material characterization of alginate and alginate–L111 hydrogel blends. A) SEM of freshly prepared hydrogels after fixation with glutaraldehyde. Samples were dehydrated in an ascending ethanol series followed by critical point drying in liquid CO_2 . B) Rheological characterization of pure (1% A) and L111 supplemented (0.0025%–0.01% L111) alginate solutions. Shear viscosity was measured using a rotary rheometer with a plate-cone setup and plotted as a logarithmic function of shear rate. C) Confocal laser scanning microscopy (CLSM) analysis of the hydrogel structure visualizes the L111 distribution. Hydrogels (1% A and 1% A–0.01% L111) were fixed with paraformaldehyde and incubated with antibodies against L111 (green dots, Alexa488). Pictures were taken in transmission (top row), reflection (middle), and fluorescence (bottom) mode. A, alginate; L111, laminin 111.

and 63% (1% A–0.01% L111) on day 1 and decreased to 32% (1% A), 39% (1% A–0.0025% L111), 37% (1% A–0.005% L111), and 39% (1% A–0.01% L111) on day 14. The relatively low viability was most likely not caused by impaired cell function, but due to insufficient diffusion of the resorufin during the Alamar Blue assay since the hydrogels exhibited higher fluorescence than the medium supernatant. Cytotoxicity of the hydrogels was

assessed by measuring lactate dehydrogenase (LDH) release on day 1 (Figure 2C,E). As a reference, the LDH leakage of lysed cells was set to 100%. Cytotoxicity in 1% alginate and 1% alginate–L111 hydrogel blends was comparably low for neurospheres and singularized hiNPCs and did not exceed 20% except for Matrigel-embedded hiNPCs (27%).

Table 1. Flow behavior (n) and flow consistency indexes (K) of native and L111-supplemented alginate.

	1% alginate + L111			
	0.0000%	0.0025%	0.005%	0.01%
n	0.82	0.92	0.92	0.96
K [mPa s]	45.07	25.31	25.22	21.09

2.3. Supplementation of Alginate Hydrogels with L111 Leads to the Fusion of Neurospheres

Both single cell (cells migrating out of the sphere core) and neurosphere motility (whole spheres merging within the hydrogels) were assessed with live-cell imaging during the first day of cultivation (Figure 3A,B; Videos S1 and S2, Figure S2, Supporting Information). Laminin presence determined initial cell and neurosphere motility. Single cells from neurospheres

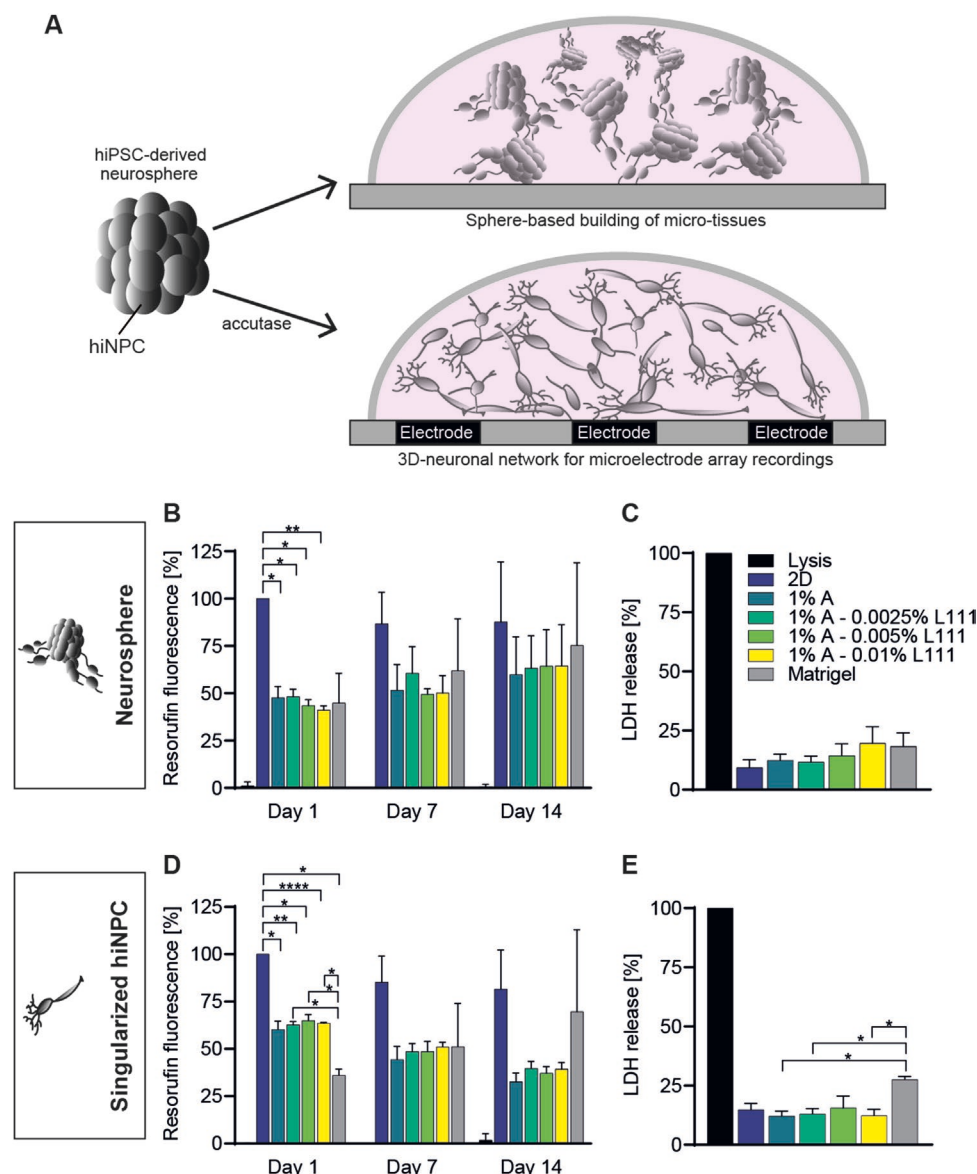


Figure 2. Cytocompatibility of pure alginate and alginate–L111 hydrogel blends. A) Experimental setup: Neurospheres were chopped to 0.1 mm and either embedded directly in alginate and alginate–L111 hydrogel blends or singularized with accutase before embedding. B,D) Viability of embedded hiNPC neurospheres and single cells, respectively. Resazurin reduction to resorufin was measured on days 1, 7, and 14. Data are shown as mean \pm SEM as percent of respective 2D cultures on day 1 ($n = 3$ with 4 technical replicates, $p \leq 0.05$). C,E) Cytotoxicity analyses by measuring LDH release on day 1 after cell-laden hydrogel preparation with hiNPC neurospheres and single cells, respectively. Shown are mean \pm SEM as percent of lysis control ($n = 3$ with 4 technical replicates, $p \leq 0.05$). A, alginate; L111, laminin 111.

embedded in 1% alginate without L111 were motile because they appeared in the space between the spheres, however, the spheres themselves showed no clear movement (Figure 3A). In contrast, 0.01% L111 supplementation to 1% alginate gels facilitated entire neurospheres to move towards each other and fusing within less than 2 h (Figure 3B). To visualize the interaction between neurospheres and hydrogel scaffold after longer embedding times, SEM was performed after 14 d of cultivation. Neurospheres were embedded and adhered to the alginate hydrogels regardless of the presence of L111. Pseudopodia or potential axonal or dendritic structures were also present in all hydrogel conditions (Figure 3B).

2.4. L111 Promotes Differentiation into GFAP-Positive Astrocytes

Previous studies showed that hiNPC neurospheres cultivated in 2D on PDL/L111 matrices or in 3D in ADA-GEL or Alginate/Gellan Gum/Laminin hydrogel blends differentiate into neurons and astrocytes.^[7,13,33] To assess the cell type composition within the pure alginate and alginate–L111 hydrogel models, we performed immunocytochemical staining and CLSM analyses of hiNPC neurospheres differentiated for 14 d in 1% alginate with and without 0.0025%, 0.005%, and 0.01% L111. Neurospheres in all hydrogel conditions expressed the neuronal markers TUBB3 and MAP2 (Figure 4A; Figures S3 and S6,

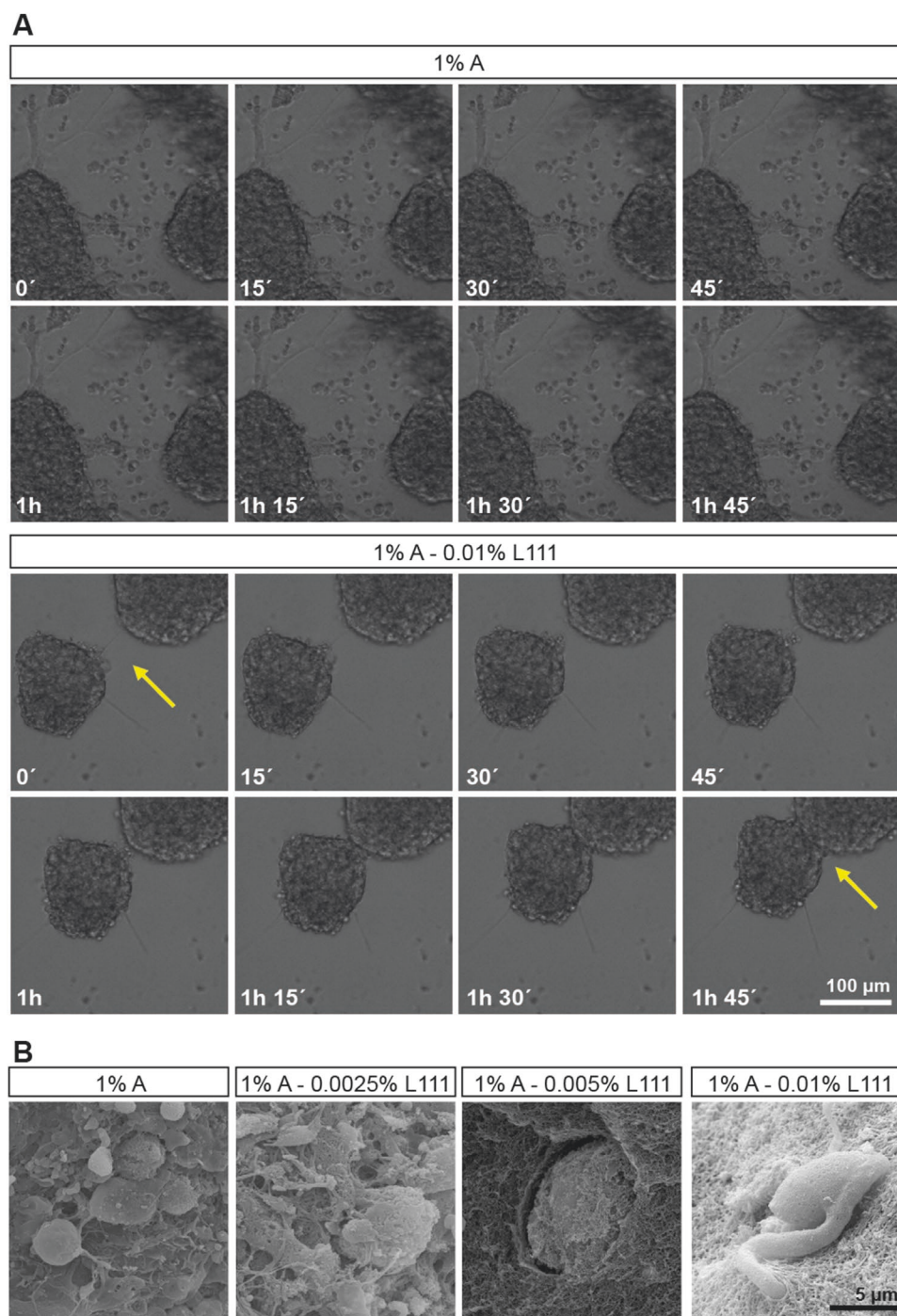


Figure 3. Motility of embedded neurospheres in pure or laminin L111-supplemented hydrogel blends. A) Live-cell bright field image analysis of neurospheres 24 h after embedding into 1% alginate and 1% alginate–0.01% L111 hydrogel blends. Cells detached from the spheres and built connecting paths in both hydrogels. Whole spheres only moved in alginate hydrogel blends supplemented with L111 (yellow arrow). Images show time-lapse pictures with an interval of 15 minutes between each. Representative original videos from the time period 24–42 h can be found in Videos S1 and S2 (Supporting Information). B) Scanning electron microscopy (SEM) of alginate hydrogels with embedded neurospheres after 14 d of differentiation. A, alginate; L111, laminin 111.

Supporting Information). However, L111 promoted neuronal outgrowth thus increasing connections between the individual spheres. Within these connecting strands, TUBB3- and MAP2-positive structures were clearly distinguishable from each other

(Figure 4A, enlargements 1 and 2). The astrocytic marker GFAP was expressed in all alginate hydrogels but most prominently in the blend containing the highest L111 concentration (1% alginate–0.01% L111, Figure 4B,C). This indicates a positive effect of

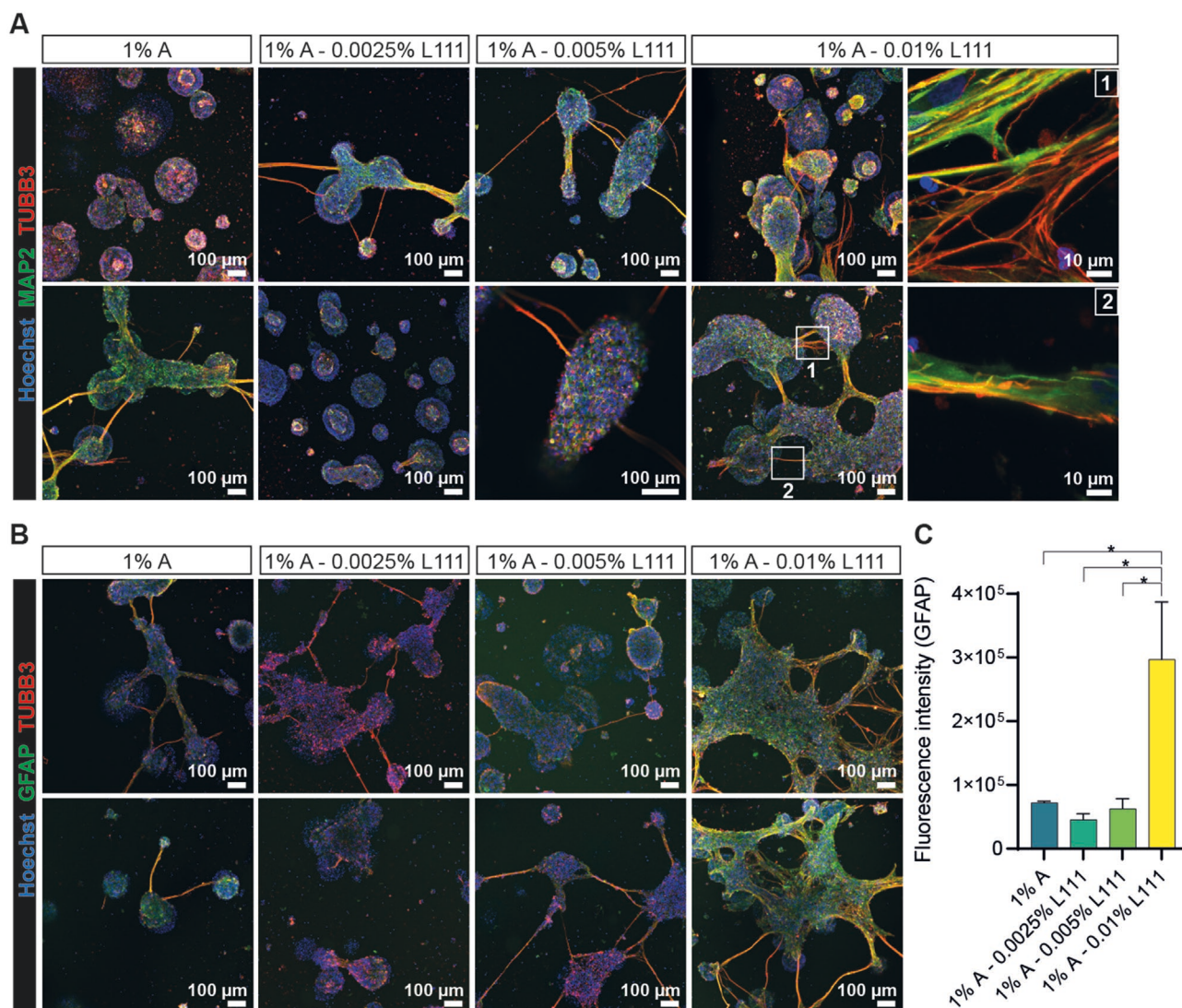


Figure 4. L111 supports neuronal outgrowth and astrocyte differentiation of hiNPC neurospheres cultured in 3D. Confocal laser scanning microscopy of immunostained neurospheres differentiated in alginate and alginate–L111 hydrogels for 14 d. Specimens were immunostained for TUBB3 (red, Alexa546) and A) MAP2 (green, Alexa488) or B) GFAP (green, Alexa488). Nuclei were counterstained with Hoechst (blue). Representative maximum intensity projections are shown. C) Quantification of GFAP fluorescence intensity. Shown are mean \pm SEM of two to three pictures with five ROI each ($p \leq 0.05$). A, alginate; L111, laminin 111.

L111 on glial differentiation. In contrast to TUBB3, which was mainly expressed within the interconnecting strands, GFAP-positive cells were also found within the spheres.

2.5. Differentiated Neurons Express Synaptic Proteins

As a prerequisite for electrically active neuronal networks, neurons must be connected via synapses for chemical signal transmission. Synapse formation of hiNPC-derived neurons in 3D alginate gels was analyzed by immunocytochemical stainings of the presynaptic marker synapsin 1 (SYN1) and the postsynaptic marker PSD95 after 14 d of differentiation. Both proteins were expressed in hiNPC-derived neurons in pure as well as in L111-supplemented alginate hydrogel blends with a higher abundance of SYN1 in the 1% A–0.01% L111 gel blends. While

SYN1 was mainly located at the neuronal strands between neurospheres, PSD95 was localized within the neurospheres for the pure alginate gels and additionally at neurite bundle interconnection points for the L111 supplemented hydrogels (Figure 5; Figure S4, Supporting Information).

2.6. L111 Promotes Alginate-Based 3D-NN Formation and Maturation

To investigate the functionality of the 3D-NN derived from hydrogel-embedded hiNPCs, electrical activity was measured using multiwell microelectrode arrays (mwMEAs, Figure 6; Figure S5, Supporting Information). For this purpose, singularized hiNPCs were embedded in 1% alginate (1% A) or 1% alginate–0.01% L111 (1% A–0.01% L111) gel blends. Human

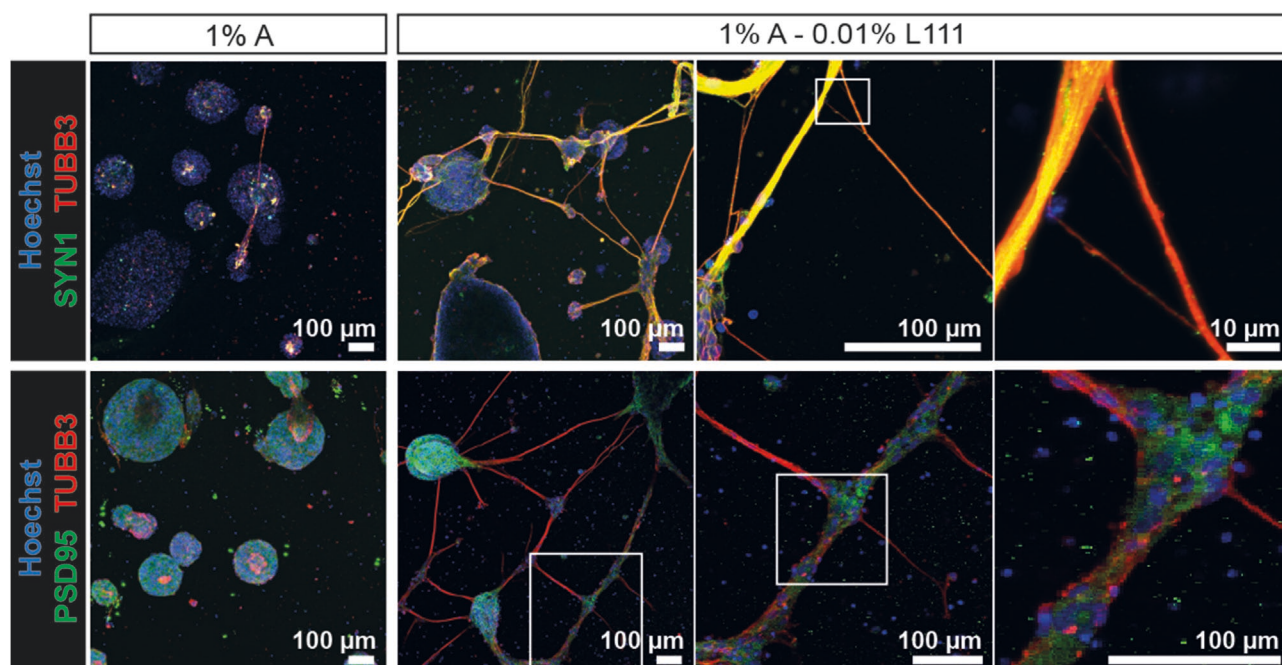


Figure 5. hiNPC-derived neurons differentiated in alginate hydrogels express both pre- and postsynaptic markers. Neurospheres were embedded into the indicated hydrogels, differentiated for 14 d, and immunostained for TUBB3 (red, Alexa546) and either synapsin 1 (SYN1, green, Alexa488) or PSD95 (green, Alexa488). The nuclei were counterstained with Hoechst (blue). Representative maximum intensity projections of z-stacks are shown. A, alginate; L111, laminin 111.

iNPCs cultivated in 2D on PDL/L111 served as controls. The 2D controls were performed with two different cell numbers: i) cell numbers comparable to our previously published data (2D, Nimtz et al., 2020), ii) same cell numbers as used for the hydrogels, which is ten times higher than 2D ($10 \times 2D$). NN formed under $10 \times 2D$ and 1% A–0.01% L111 conditions showed spontaneous electrical activity after 14 d of differentiation. While the adherent cells stayed active, the NN differentiated in 1% A–0.01% L111 were inactive for the following 10 d until they were active again on day 24. The NN formed under the other two conditions (2D and 1% A) were first electrically active on day 16. Both 2D controls (2D and $10 \times 2D$) had more active electrodes than the 3D-NN, especially during the first two months of culture. The 2D control stopped its spiking activity after 108 d because cells started to detach from the mwMEA surface. The remaining NN stayed active until differentiation day 178 ($10 \times 2D$), and 206 (1% A and 1% A–0.01% L111). For the first 5 months, the mean firing rates (MFR) were similar in all conditions, but the MFR of the 1% A–0.01% L111-NN increased steadily thereafter and exceeded the activity of the $10 \times 2D$ -NN and the 1% A-NN significantly after six months in culture. While the $10 \times 2D$ -NN exhibited higher burst rates than both 3D-NN during two and six months of cultivation, the extent of spikes contributing to a burst differed, which is a sign of a more mature network. More precisely, in the first 2 months, the $10 \times 2D$ -NN had significantly more spikes contributing to individual bursts, however, from month 4 on, both 3D-NN exhibited higher amounts of spikes contributing to bursts. Network bursts only occur in mature and synchronized NN. Their rate was highest in 1% A–0.01% L111 NN, while they were hardly present in the other conditions emphasizing

that this hydrogel blend provides optimal conditions for NN maturation.

2.7. L111 Supplementation of Alginate Hydrogels Allows Faster Recovery from Tetrodotoxin (TTX) Exposure

Next, we applied the voltage-gated sodium channel (VGSC) blocker TTX (0.5 and 1×10^{-6} M) to the matured networks ($10 \times 2D$, 3D–1% A, and 3D–1% A–0.01% L111) on day 128 for 30 min, followed by a washout for studying acute effects on the NN as well as their recovery. In NN grown in 2D ($10 \times 2D$) and in 3D–1% A hydrogels, the electrical activity (wMFR) was completely blocked with 0.5×10^{-6} M TTX, whereas for the 3D–1% A–0.01% L111 NN total blockage of the electrical activity required 1×10^{-6} M TTX (Figure 7). The NN activities were measured again after 1, 8, and 11 d after the washout to study recovery from the TTX treatment. The $10 \times 2D$ -NN were not active after 11 d (Figure 7), but regained activity 15 d after the TTX treatment and washout (Figure 6). Recovery of the 3D-NN was faster in comparison to 2D-NN with restored activity after 8 d. Supplementation of hydrogels with L111 accelerated the recovery even further, leading to first NN activity already after one day. Here, enhanced performance was observed regarding all four measured parameters regarding electrical activity (wMFR), burst behavior (burst rate, spikes in bursts), and network behavior (network burst rate, Figure 7A). It is to note that the baseline electrical activity of NN grown in 3D with L111 is much higher and more robust than without L111. Our data on TTX-treated NN indicate that the electrical activity measured using the MEA technology is based on VGSC activity.

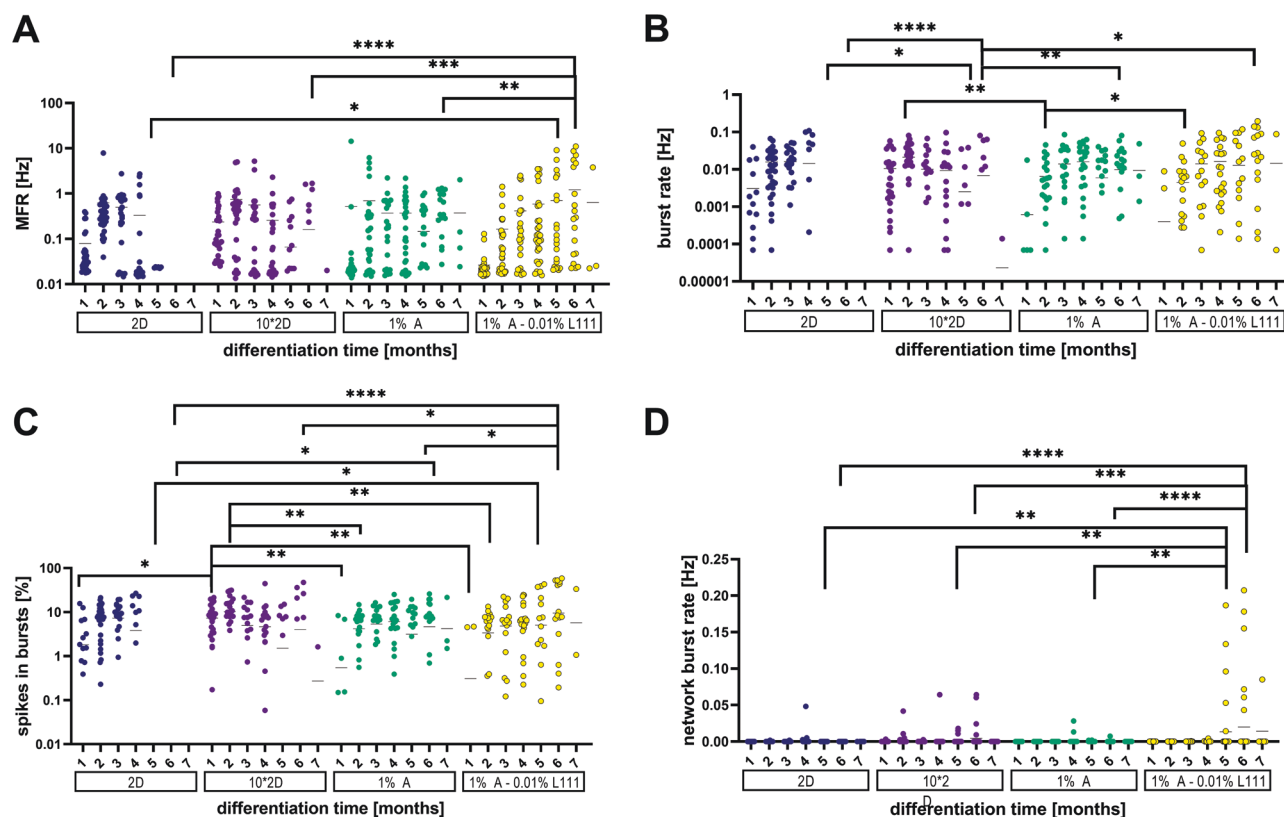


Figure 6. Alginate-L111 hydrogel blends facilitate long-term electrical activity and synchronicity of neuronal networks for over six months. Singularized hiNPCs were seeded directly (2D, 10*2D), or embedded in 1% alginate hydrogels without (1% A) or with L111 (1% A–0.01% L111) onto L111-coated mwMEAs. Cells were cultivated in differentiation medium for up to 206 d. The neural network activities were evaluated by comparing A) mean firing rate (MFR), B) burst rate, C) percentages of spikes contributing to a burst, and D) network burst rate. Each data point represents the mean of all electrodes of one well with $n = 24\text{--}36$ for each month (month 1–6) or $n = 6$ (month 7). A, alginate; L111, laminin 111; MFR, mean firing rate.

We observed that sodium transients measured as spikes are stronger when cells are grown in hydrogels in 3D compared to 2D and that 3D-NN have a shorter recovery time after VGSC blockage than 2D-NN, especially when L111 is added to the hydrogels. The synchronicity of the 3D-NN completely depended on L111 supplementation.

3. Discussion

Historically, in vitro cell models were based on 2D cultures grown on flat glass or plastic surfaces, which might be coated with ECM proteins to improve cell adhesion.^[45] However, recent studies indicate that an artificial 2D environment alters the cell's physiological properties.^[46] This understanding initiated the development of 3D cell cultivation techniques, which better resemble the physiological cell environment and enable complex cell–cell and cell–matrix interactions.^[45–47] For neural models, hydrogels with a low modulus of elasticity and high water content are ideal 3D matrices mimicking human brain tissue.^[4] Here, we demonstrate that alginate hydrogels supplemented with L111 facilitate the formation of electrically highly active and synchronous neuronal networks, which can be cultivated for up to 206 d in multiwell MEA plates.

L111 supplementation only caused minor microstructural and rheological alterations of the matrix material (Figure 1), slightly decreasing the pore network compared to native alginate, due to the increased polymer content present in the bulk volume. The decreasing flow consistency index (K) indicates a reduced zero shear viscosity of the alginate–L111 hydrogel blends. At the same time, the flow index (n) was trending toward 1 in the blend, which exhibited almost Newtonian flow behavior, compared to shear thinning, native alginate. Ultimately, the even distribution of fluorescence-labeled L111 (Figure 1C) underlines the successful and homogenous integration of the biopolymer with the surrounding polysaccharide matrix.

A prerequisite for the applicability of a hydrogel blend for 3D cell culture models is continuous cell survival after the embedding process. To determine, whether the alginate hydrogels fulfill this requirement of cytocompatibility for our hiNPCs single-cell and neurosphere cultures, cell viability and cytotoxicity were assessed over a time course of 14 d and compared to 2D cultures. While cytotoxicity was neither observed in the 2D nor the 3D cultures over a time course of 14 d, viability was reduced in the 3D compared to the 2D models. Most likely, this is due to insufficient diffusion of the assay reagents through the hydrogel and thus rather a technical issue than a result of reduced cytocompatibility. In line with that, alginate hydrogels

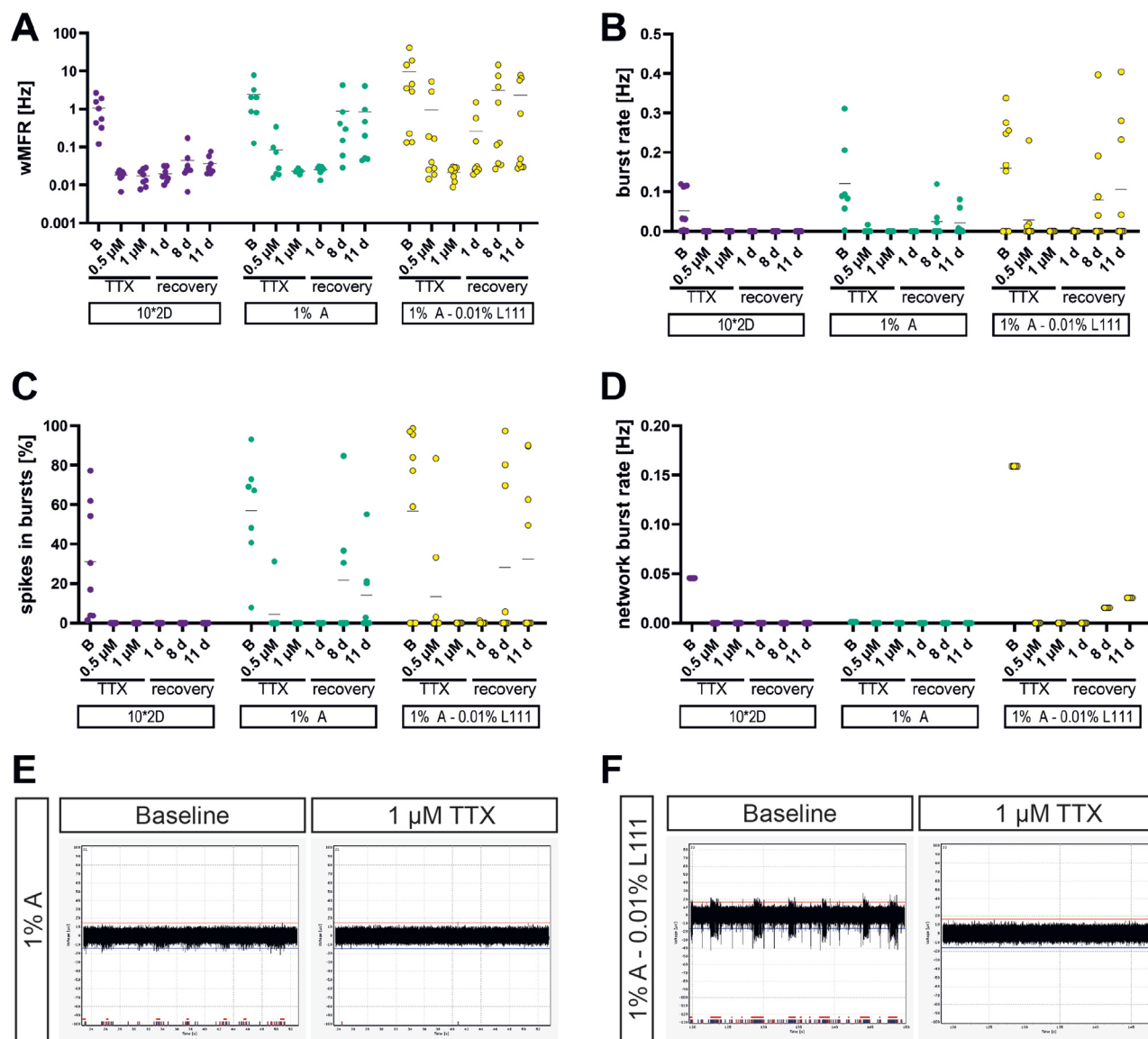


Figure 7. Hydrogel supplementation with L111 accelerates the recovery of NN activity after tetrodotoxin (TTX) treatment. TTX was applied to neuronal networks (NN) developed in 2D (10*2D), 1% alginate (1% A), and 1% alginate–0.01% L111 (1% A–0.01% L111) on differentiation day 128. A–D) min./max. box plots of the indicated measurement parameters upon TTX treatment and after recovery for the indicated days. Each dot represents one electrode. E+F) Representative spike trains of the NN electrical activity without treatment (baseline) and after treatment with 1×10^{-6} M TTX. A, alginate; B, Baseline; L111, laminin 111; TTX, Tetrodotoxin, wMFR, weighted mean firing rate.

are amongst the most frequently used 3D matrices and their biocompatibility has been confirmed in various studies.^[16,48,49] Since we observed optimal cell motility and functionality of the NN, we conclude that alginate-based hydrogels support the cultivation of the hiNPC-based cell models in 3D. The cells and spheres differentiated in Matrigel showed similar viability compared to the alginate blends, however, with much higher standard deviation. In addition, singularized cells grown in Matrigel showed significantly increased LDH release. For these reasons, as well as high batch-to-batch variability and unknown compositions of various growth factors and other proteins, the following experiments were only carried out with alginate hydrogels.^[50–52]

Functionalization of the 1% alginate hydrogels with L111 further promoted neurosphere motility and sphere fusion. We showed that time laps microscopy uniquely enables tracing of sphere movement and to the best of our knowledge, this is the first description of this phenomenon. We further hypothesize that the observed sphere movement is distinct from other cellular movements like neurite outgrowth and cell migration that can be observed in hiNPC cultures at later time points. Binding of the ECM protein laminin by cell membrane-associated integrins is crucial for cell migration and differentiation during brain development.^[53,54] Integrins are heterodimeric surface proteins consisting of a α and β subunit, whereas the $\alpha 3$, $\alpha 6$, $\alpha 7$, $\beta 1$, and $\beta 4$ subunits are responsible for laminin binding.^[11,55] We

recently demonstrated the significance of β 1-integrin-L111 interactions for the adhesion and migration of primary human NPCs.^[56–58] In addition, the beneficial effect of L111 regarding cell migration, neuronal and glial differentiation was shown with diverse neural cell models cultivated in 2D and 3D.^[9–11,59,60] Among L111, other laminin isoforms (e.g., L511 and L521) and short binding motifs of the laminin protein (e.g. IKVAV) promote cell viability, neural cell migration, and neuronal differentiation.^[8,61–66] Alginate–L111 blends further supported the differentiation of our hiNPC-derived neural cultures. Although all embedded hiNPCs differentiated into NN expressing neuronal (TUBB3), astrocytic (GFAP), pre- (SYN1), and postsynaptic (PSD95) markers, L111 clearly supported neuronal connectivity—represented by enhanced staining for TUBB3, SYN1, and PSD95—and astrocyte differentiation (GFAP). Further experiments have to clarify whether the enhanced glial differentiation is caused by the biological activity of L111 itself or by the altered microstructural, rheological, or viscoelastic properties of the blend. For instance, the microarchitecture, pore size, and relaxation behavior were shown to impact gene expression and thereby activate specific differentiation patterns.^[9,67,68]

The increased expression of the synaptic markers SYN1 and PSD95 observed in hiNPCs differentiated in L111-supplemented hydrogels endorsed us to further investigate NN functionality. Having future biofabrication applications in mind, e.g., 3D-bioprinting, a so-called bioink comprising single hiNPC within hydrogel blends was prepared.^[69,70] Alginate-embedded singularized cells developed into functional NN, which were active for at least 206 d. Whereas 2D culture-derived NN were functional after two weeks of differentiation and up to 95% electrodes were active per well, the 3D cultures took three to four weeks to develop with about half the number of active electrodes compared to 2D cultures. This is in line with observations made with hydrogel-embedded hESCs^[38] and can be explained by the direct contact of the 2D culture neuron monolayer with the electrodes, whereas in hydrogels, neurons are distributed in all three dimensions, which results in less cells with direct contact to the electrodes. Nevertheless, eventually also hydrogel-embedded hiNPCs had contact with sufficient numbers of electrodes and ultimately exhibited higher mean firing and burst rates than 2D cultured neural networks. L111 supplementation increased these two parameters even further, thus improving the functionality of the NN. Our observations are in line with studies on the 3D cultivation of rodent cells, which also showed increased mean firing and burst rates compared to respective 2D controls.^[35–37] Moreover, the addition of L111 to alginate hydrogels resulted in a more mature bursting pattern and a higher synchronicity of the networks, which can be explained by the laminin-dependent promotion of neuronal differentiation^[10,63] and synapse formation (present study). In rodent models, laminin improved synaptic activity since depletion or blocking of integrin β 1 impaired long-term potentiation.^[71–73] In our study, L111 supported glial differentiation into GFAP-positive astrocytes as well as expression of pre- and postsynaptic markers already after 14 d of differentiation. If the accelerated astroglia differentiation contributes to the maturation of neurons by regulating synaptogenesis (synapse formation, elimination, and function) as well as axonal growth and guidance,^[74–82] or if the enhanced neuronal maturation

is a direct consequence of the L111, merits further investigations. So far, recent 2D neural in vitro studies, where neurons co-cultivated with astrocytes are electrically more active and show a more mature bursting pattern than neurons grown in absence of astrocytes,^[26,83,84] promote the first hypothesis. Comparing the neuronal network activities achieved with our optimized alginate/L111 protocol to previously generated 2D in vitro hiPSC-derived NN reveals an up to ten times higher MFR.^[25,26,39,40,85] Only two other studies achieved comparable high MFR values with 2D cultivated hiPSC-derived NN,^[84,86] however, they used other cell lines, different cell culture media and protocols, and a different MEA recording system. To our knowledge, we are the first to study hiPSC-derived hydrogel-based 3D-NN on MEA. The here reported hiPSC-derived NN are well suited not only for studying neuronal network activity but also NN synchronicity, a crucial readout for neuronal network function.^[87–90] Most importantly, the consistent high electrical activity of the 3D models over a cultivation period of 206 d (30 weeks) is unique. So far, only two other studies reported comparable cultivation periods of 2D cultivated hiPSC-derived cerebral cortical neurons on MEAs (34 weeks)^[39] and 3D cultivated hiPSC-derived NN analyzed with calcium imaging (36 weeks).^[91] Long-term cultures will increase the applicability of in vitro NN in disease modeling and long-term low concentration exposure studies of drugs or toxins. In addition to planar MEAs, as used in our study, various 3D MEA models are currently being developed. Although they differ in their design, the aim is to measure electrical signals in the Z dimension and improve applicability for 3D hydrogel cultures.^[92–94]

To determine the involvement of VGSCs in the electrical activities recorded by the MEAs, we challenged matured NN with the sodium channel blocker TTX (0.5 and 1.0×10^{-6} M) on day 128 of differentiation. Independent of the culturing conditions, TTX completely blocked NN activity as observed previously in NN generated from rat cortical cells, neurons/astrocytes co-cultures (iCell), hESCs, hiPSCs, blood-derived induced NPCs (BD-iNPCs), and hESC-derived cerebral organoids.^[95–101] After washing out the TTX, we observed a particularly fast recovery of electrical activity in NN embedded in alginate with 0.01% (w/v) L111, which is a further advantage of L111 supplementation in hydrogels. In line with this, Gopalakrishna and co-workers reported a neuroprotective effect of soluble L111 and its peptide, YIGSR, in rat PC-12 cells.^[102] They hypothesized that binding to the 67 kDa laminin receptor (67LR) causes internalization of L111 and activation of adenylyl cyclase (AC), thus increasing intracellular cAMP concentrations. Whether L111 bound to alginate triggers a similar effect in differentiating hiNPCs remains to be investigated. Another explanation for the faster regeneration of the NN activity in presence of L111 might be the increased number of astrocytes in the 1% alginate–0.01% L111 hydrogel blends. Since it was shown, that rodent astrocytes prevent neuronal cell death upon TTX exposure by releasing neuroprotective factors,^[103–109] As these observations were derived from different cell systems concerning species and cell origin, it is only speculative if this mechanism is also responsible for the higher TTX resistance of neurons in hiNPC-derived alginate/L111 3D cultures. However, it is likely that the noncovalently incorporated L111 is no longer present after 128 d. This tends to support our second hypothesis, since

differentiation into astrocytes was initiated early in culture, as shown by immunocytochemistry after 14 d of differentiation.

Overall, our observations concerning the L111 supplementation of hydrogels support beneficial in vitro effects of this molecule reported in previous studies. For example, alginate/gellan gum/laminin hydrogel blends support differentiation and spontaneous calcium transient generation of hiNPC.^[13] The addition of laminin to methylcellulose hydrogel cultures enhanced migration of murine primary neurospheres^[10] and supplementation of alginate dialdehyde-gelatin (ADA-GEL) hydrogels with L111 increased the number of migrated hiNPC-derived neurospheres.^[7]

4. Conclusion

By functionalization of alginate hydrogels with the ECM protein L111, we were able to differentiate hiPSC-derived NPCs into multicellular tissue-like structures that generate highly functional NN, which are suitable for long-term studies. L111 not only promoted the migration of cells and expression of synaptic markers as a prerequisite for electrical activity, it further increased differentiation into astrocytes, thereby further indirectly supporting neuronal function. Electrophysiological analyses confirmed a matured neuronal bursting behavior, long-term activity and increased synchronicity of the networks formed in L111-supplemented alginate hydrogels, thus highlighting the higher degree of network maturation. Moreover, L111 accelerated the recovery of network activity after blockage of VGSC by TTX treatment. By refining 3D cultivation techniques for hiPSC-derived neural cells, we were able to contribute to the establishment of human-based in vitro methods according to the 3R principles.^[110] Application of such methods for long-term neural cultivation is manifold in biomedical science ranging from disease modeling to drug development and toxicity testing.

5. Experimental Section

Preparation of Hydrogels: Laminin-111 (L111, 0.1% w/v in Tris-buffered saline, #L2020, Sigma-Aldrich, St. Louis, MO) was added to 3% (w v⁻¹ in water) BlueDrop alginate (#BD-003, Black Drop Biodrucker GmbH, Aachen, Germany) and mixed with CINDA differentiation medium (see Table S1, Supporting Information) to obtain the desired final hydrogel blends of 1% alginate and 0–0.01% (w/v) L111 (1% A, 1% A–0.0025% L111, 1% A–0.005% L111, 1% A–0.01% L111). The volumes for preparing 50 μ L hydrogel are listed in Table S2 (Supporting Information). Scaffolds (50 μ L/well) were ionically crosslinked by the addition of 90×10^{-3} M CaCl₂ (#1023780500, Sigma-Aldrich, St. Louis, MO) for 5 min at room temperature (RT) and afterward washed twice with DPBS (#14040, ThermoFisher Scientific, Waltham, MA) (Figure S1, Supporting Information).

Rheological Characterization: The rheological behavior of uncrosslinked native and L111 supplemented alginate hydrogels was analyzed using a rotational rheometer (Kinexus Pro+, Malvern Instruments, UK). For each experiment, a sample volume of 1.2 mL was gently pipetted on the upper plate of the device. The opposing 4° cone-plate (PL6550905 SS, Malvern Instruments) was slowly lowered into the gel until a gap of 23.6 μ m between the tip of the cone and the plate was reached. Excessive gel rests or gas bubbles were trimmed using a silicone spatula. The shear viscosity was measured during a shear rate sweep ranging from 0.01

to 70 s⁻¹. The measurements were conducted at 37 °C (± 0.17 °C). Each experiment was repeated three times ($n = 3$). To illustrate the results, shear viscosity was plotted over the logarithmic function of the applied shear rate. Finally, the flow consistency and flow behavior indexes were calculated from the plotted curve as described previously.^[111]

Scanning Electron Microscopy: Hydrogel samples were washed with PBS (#L1825/L1835, Biochrom, Berlin, Germany) and fixed with 3% glutaraldehyde (#G5882, Sigma-Aldrich, St. Louis, MO) in PBS for 1 h at RT, and stored at 4 °C until drying. Dehydration was achieved by incubation of gels in ascending ethanol series followed by critical point drying in liquid CO₂. Prior to SEM imaging using the FEI-Philips XL30 ESEM FEG, a 12.5 nm palladium/gold (Science Services, Munich, Germany) film was deposited on the insulating surfaces using Leica EM SCD500 high vacuum sputter coater to avoid sample charging.

Cell Culture: All cells were maintained under humidified conditions at 37 °C and 5% CO₂. hiPSC culture and neural induction were performed as described earlier.^[33,112] In brief, hiPSCs were purchased (iPS(IMR90)-4; WiCell, Madison, USA) and cultivated on Matrigel-coated dishes (hESC-qualified matrix, LDEV-free, #354277, Corning, NY) in mTeSR1 medium (#05850, StemCell Technologies, Cologne, Germany). After preincubation with 10×10^{-6} M ROCK-inhibitor (Y-27632, #1254, Tocris Biosciences, Bristol, UK) in mTeSR1 medium for 1 h, hiPSC colonies were fragmented with a StemPro EZPassage tool (#23181010, ThermoFisher Scientific, Waltham, MA), transferred onto a poly(2-hydroxyethyl methacrylate)-coated dish (30 mg mL⁻¹, #P3932, Merck, Darmstadt, Germany) and cultured in neural induction medium (see Table S1, Supporting Information) supplemented with 10×10^{-6} M ROCK-inhibitor. Half of the medium was changed three times per week. Upon first medium change, ROCK inhibitor was omitted from the medium. Seven days after the start of the induction, 10 ng mL⁻¹ recombinant human FGF (#233-FB, R&D Systems, Minneapolis, MN) were added to the culture medium. Upon day 21, formed neurospheres (hiNPC, hiPSC-derived neural progenitor cells) were cultivated in proliferation medium (see Table S1, Supporting Information). Spheres were chopped approximately every week to 0.25 mm using a Mcllwain Tissue Chopper (Ted Pella, Redding, CA).

Preparation of Cell-Laden Hydrogels and Neural Differentiation: Either single cells or 0.1 mm freshly chopped spheres were embedded into alginate hydrogels at a density of 1×10^7 cells mL⁻¹ or 5000 spheres mL⁻¹. For 2D controls, surfaces were coated with PDL (17 μ g cm⁻² on a multiwell plate, 35 μ g cm⁻² on glass; #P0899) and L111 (2 μ g cm⁻² on a multiwell plate, 4.5 μ g cm⁻² on glass; #L2020, both Sigma-Aldrich, St. Louis, MO) and 500,000 cells or 500 freshly chopped spheres were seeded onto the coated surfaces. Single NPCs were generated by accutase treatment (#A1110501, ThermoFisher Scientific, Waltham, MA) of chopped 0.1 mm spheres. L111 (0.1% w/v in Tris-buffered saline) was added to 3% (w/v) alginate and vortexed. Single cells or sphere suspensions in CINDA differentiation medium were added to the hydrogel solution and carefully resuspended to mix all components and reach a final concentration of 1% (w/v) alginate and 0%, 0.0025%, 0.005%, or 0.01% L111 (e.g., 1% A–0.01% L111) and 1×10^7 cells mL⁻¹ or 5000 spheres mL⁻¹. The desired volumes for preparing 50 μ L hydrogel are listed in Table S2 (Supporting Information). The resulting hydrogel cell suspensions were added into wells of a 96-well plate (50 μ L/well) and ionically crosslinked by the addition of 90×10^{-3} M CaCl₂ for 5 min at RT. After repeated rinsing in DPBS (#14040, ThermoFisher Scientific, Waltham, MA), CINDA medium was added and the cell-laden hydrogels were cultivated at 37 °C and 5% CO₂ until analysis. Half of the medium was changed twice a week.

Cell Viability Assessment: Cell viability was measured by the ability of living cells to reduce resazurin to fluorescent resorufin using the CellTiter-Blue Assay (#G8080, Promega, Madison, WI) according to manufacturer's instructions. After 2 h incubation time the fluorescence was measured with the Tecan infinite M200 Pro reader (ex: 540 nm; em: 590 nm). For background correction, cell culture medium without cells was subtracted. The relative fluorescence unit (RFU) was calculated as percent of the 2D control on day 1. Three independent experiments with NPCs from two independent neural inductions were used.

Cytotoxicity Assessment: Cytotoxicity was assessed by measuring LDH release into the medium using the CytoTox-ONE Homogeneous Membrane Integrity assay (#G7890, Promega, Madison, WI). LDH release was determined by a coupled enzymatic reaction that results in the reduction of resazurin to resorufin. As control, cells were lysed by adding Triton-X-100 (#T8787, Sigma Aldrich) to the culture medium for 10 min at 37 °C and 5% CO₂ to reach a final concentration of 0.2% (v/v). The resorufin fluorescence was measured with the Tecan infinite M200 Pro reader (ex: 540 nm; em: 590 nm) and shown as percent of the lysis control. NPCs from two independent neural inductions were used for three independent experiments.

Live-Cell Imaging: Neurospheres were embedded and cultivated as described in the previous section in a 96-well plate (#89626, Ibidi, Gräfelting, Germany). Four samples per condition were analyzed using a high content screening microscope (EvoS FL Auto2, Life Technologies, Carlsbad, CA), focusing on selected embedded spheres to visualize movement of cells or spheres over a time period of 42 h in brightfield mode using the objective PL FL 4× LWD PH, 0.13 NA.

Confocal Laser Scanning Fluorescence Microscopy: To analyze L111 presence and distribution, CLSM (TCS SP8, Leica Microsystems, Wetzlar, Germany) using the objective HC PL APO CS2 63×/1.40 OIL was performed with excitation at 488 nm and emission at 525–700 nm. Hydrogels were fixed in 4% paraformaldehyde (#P6148, Sigma-Aldrich, St. Louis, MO) in DPBS at 37 °C for 2 h and washed three times with PBS. Samples were blocked with 1% BSA/PBS for 4 h at RT and then incubated with anti-L111 (1:1000, rabbit polyclonal, #ARG10736, Arigo Bio) overnight at 4 °C. Samples were rinsed three times with PBS for 20 min at RT and subsequently incubated with anti-rabbit-Alexa488 (1:500, goat, #R37116, Invitrogen) in 1% BSA/PBS overnight at 4 °C. Hydrogels were washed three times in PBS and stored in PBS at 4 °C until analysis. For immunostaining of neuronal networks, cell-laden hydrogels were rinsed in prewarmed DPBS and fixed in 4% (w/v) paraformaldehyde/DPBS at RT for 2 h. Samples were incubated overnight at 4 °C in anti-TUBB3 (1:200, rabbit polyclonal, Sigma Aldrich, #T2200), anti-gial fibrillary acidic protein (GFAP) (1:200, mouse monoclonal, Merck, #MAB3402), anti-microtubule-associated protein 2 (MAP2) (1:500, mouse monoclonal, Sigma, #M4403), anti-Synapsin 1 (SYN1) (1:100, monoclonal mouse, Synaptic Systems, #106011), or anti-postsynaptic density protein 95 (PSD95) antibody (1:100, rabbit monoclonal, Abcam, #ab76115) in 10% (v/v) goat serum (#G9023)/0.1% (v/v) Triton X-100 (#T8787, all Sigma-Aldrich, St. Louis, MO)/PBS. After washing with PBS three times for 2 h at RT, specimens were incubated overnight at 4 °C in anti-rabbit-Alexa546 (1:500, #A11010, Invitrogen), anti-mouse-Alexa488 (1:500, Thermo Fisher Scientific, #A11001), and 1% Hoechst (bisBenzimide H33258, Sigma Aldrich, #B1155) in 2% goat serum/PBS. Afterward, samples were washed three times with PBS at RT for 2 h and directly imaged by CLSM using the objectives HC PL FLUOTAR 5 × /0.15 DRY, HC PL APO CS2 10–/0.40 DRY, and HC PL APO CS2 20 × /0.75 DRY. Maximum intensity projections of recorded z-stacks were constructed using Fiji Image J 1.52p.^[113]

Quantification of Fluorescence Intensity: The expression of GFAP and MAP2 was analyzed using Fiji ImageJ (Version 1.53q). In each picture, five circular regions of interest (ROI) for background and for GFAP or MAP2 expression were measured. The corrected total cell fluorescence (CTCF) was calculated with following formula and as described earlier:^[114] CTCF = Integrated density – (Area of ROI × Mean fluorescence of background).

MEA Recordings and Analyses: Extracellular recordings of neuronal activity were performed using mwMEAs in a 24-well plate format with 12 electrodes/well (PEDOT on glass surface, 30 µm electrode diameter, 300 µm spacing; Multi Channel Systems/MCS, Reutlingen, Germany, #24W300/30G-288). mwMEAs were coated with PDL (15.41 µg cm⁻²) for 2 d at 4 °C, then washed with sterile water and layered with L111 (1.81 µg cm⁻²) for additional 2 d at 4 °C. Wells were rinsed once with DPBS and dried. Freshly chopped 0.1 mm neurospheres were accutase treated, and the cell suspension was prepared and incubated at 37 °C in CINDA differentiation medium (see Table S1, Supporting Information). For the 2D controls, 50 000 (2D) or 500 000 (10×2D) cells in 50 µL differentiation medium were pipetted as one single drop directly onto the electrode

field. In analogy, 50 µL hydrogels, 1% alginate, and 1% alginate–0.01% L111 (w/v) containing single cells at a density of 1×10^7 cells mL⁻¹, were placed onto the electrodes. Six wells were seeded with 2D and 10×2D controls or hydrogels/condition obtaining 72 recording channels/condition. CINDA medium (see Table S1, Supporting Information) was changed once a week and recording was performed once or twice each week for 30 min using the Multiwell-Screen (MCS) program, with only the last 20 min being analyzed. On days 127, 128, 149, and 177 the recording time was only 15 min. The recording was performed using a sampling rate of 20 000 kHz, second-order Butterworth high-pass filter of 300 Hz, and fourth-order Butterworth low-pass filter of 3500 Hz. Analysis was run on the software Multiwell-Analyzer 1.7.1.0 (MCS) using 300 Hz high-pass and 3500 Hz low-pass filters. Spike detection threshold was set to a signal amplitude of 10 segments at 500 ms ± 5 standard deviations and a channel was considered as active when at least 5 spikes min⁻¹ (= 0.0833 Hz) were detected. Bursts were defined when a minimum of four spikes occurred within a duration of 50 ms. Neuronal network activity was defined as at least three electrodes bursting synchronously. Pharmacological treatment was performed with 0.5 and 1×10^{-6} M TTX, Sigma, #T8024, CAS 4368-28-9) on day 128. Baseline, first concentration-response (0.5×10^{-6} M), and second concentration-response (1×10^{-6} M) of the compound were recorded for 15 min and the whole recording was analyzed as described earlier. Before each measurement, there was a waiting period of 15 min to allow the TTX to equilibrate. The MEA parameters, number of active electrodes, MFR, burst rate, percentage spikes in burst, and network burst rate were analyzed. The first parameters refer to individual electrodes, while the network burst parameter includes all electrodes of the well and allows statements about the synchronicity of the network and hence network quality and maturation. For analyzing the NN activity over time, all electrodes of one well, and for evaluating the TTX treatment only active electrodes with a higher firing activity than 0.0833 Hz during the baseline measurement were included.

Statistics, Graphics, and Software: Unless otherwise stated data evaluation and statistical analyses were performed in GraphPad Prism 8 for Windows (GraphPad, USA). Shown is the arithmetic mean of the acquired parameters of independent experiments ± standard error of the mean. Cytotoxicity, GFAP, and MAP2 quantification data were analyzed using one-way ANOVA and viability data were analyzed using two-way ANOVA. The significance cut-off was set to $p \leq 0.05$. Image analysis was performed using Fiji ImageJ.^[115] Plots and graphics were imported into Adobe Illustrator CC 2019 to generate vector graphic files.

Supporting Information

Supporting Information is available from the Wiley Online Library or from the author.

Acknowledgements

J.H., I.L., K.K., A.B., and E.F. contributed equally to this work. The CLSM and live-cell imaging was performed at the Imaging Facility of the Cologne Excellence Cluster of Aging Research (CECAD) with the excellent support of Christian Jüngst. The authors gratefully thank Jens Sicking and David Schneider, Bayer AG, for the CLSM L111 distribution analysis. This work was supported by the Bayer AG and CERST-NRW (Center for Alternatives to Animal Testing of the Ministry for Innovation, Science, and Research of the State of North-Rhine Westphalia, Germany, File No. 233-1.08.03.03-121972) (E.F.).

Conflict of Interest

The co-author Andreas Blaeser is also co-founder of the Black Drop Biodrucker GmbH and consults the company in biotechnological matters.

Data Availability Statement

The data that support the findings of this study are available from the corresponding author upon reasonable request.

Keywords

alginate hydrogel, electrical activity, hiPSC, laminin, long-term 3D culture, MEA, neuronal network, neurospheres

Received: July 25, 2022

Revised: November 22, 2022

Published online:

- [1] M. Paparella, S. H. Bennekou, A. Bal-Price, *Reprod. Toxicol.* **2020**, 96, 327.
- [2] B. Z. Schmidt, M. Lehmann, S. Gutbier, E. Nembo, S. Noel, L. Smirnova, A. Forsby, J. Hescheler, H. X. Avci, T. Hartung, M. Leist, J. Kobolák, A. Dinnyés, *Arch. Toxicol.* **2017**, 91, 1.
- [3] K. Duval, H. Grover, L. Han, Y. Mou, A. F. Pegoraro, J. Fredberg, Z. Chen, *Physiology* **2017**, 32, 266.
- [4] A. R. Murphy, A. Laslett, C. M. O'Brien, N. R. Cameron, *Acta Biomater.* **2017**, 54, 1.
- [5] P. Zhuang, A. X. Sun, J. An, C. K. Chua, S. Y. Chew, *Biomaterials* **2018**, 154, 113.
- [6] E. Fritsche, T. Haarmann-Stemmann, J. Kapr, S. Galanjuk, J. Hartmann, P. R. Mertens, A. A. M. Kämpfer, R. P. F. Schins, J. Tigges, K. Koch, *Small* **2020**, 17, 2006252.
- [7] T. Distler, I. Lauria, R. Detsch, C. M. Sauter, F. Bendt, J. Kapr, S. Rütten, A. R. Boccaccini, E. Fritsche, *Biomedicine* **2021**, 9, 261.
- [8] C. Hellwig, M. Barenys, J. Baumann, K. Gassmann, G. Kauer, L. Casanellas, G. Kauer, E. Fritsche, L. Casanellas, G. Kauer, E. Fritsche, *Toxicol. In Vitro* **2018**, 52, 106.
- [9] S. Ortinau, J. Schmich, S. Block, A. Liedmann, L. Jonas, D. G. Weiss, C. A. Helm, A. Rolf, M. J. Frech, *Biomed. Eng. Online* **2010**, 9, 70.
- [10] S. E. Stabenfeldt, G. Munglani, A. J. García, M. C. Laplace, *Tissue Eng., Part A* **2010**, 16, 3747.
- [11] L. A. Flanagan, L. M. Rebaza, S. Derzic, P. H. Schwartz, S. Edwin, E. S. Monuki, S. Edwin, *J. Neurosci. Res.* **2006**, 83, 845.
- [12] S. K. Powell, J. Rao, E. Roque, M. Nomizu, Y. Kuratomi, Y. Yamada, H. K. Kleinman, *J. Neurosci. Res.* **2000**, 61, 302.
- [13] J. Kapr, L. Petersilie, T. Distler, I. Lauria, F. Bendt, C. M. Sauter, A. R. Boccaccini, C. R. Rose, E. Fritsche, *Adv. Healthcare Mater.* **2021**, 10, 2100131.
- [14] S. Budday, G. Sommer, C. Birkel, C. Langkammer, J. Haybaeck, J. Kohnert, M. Bauer, F. Paulsen, P. Steinmann, E. Kuhl, G. A. Holzapfel, *Acta Biomater.* **2017**, 48, 319.
- [15] A. Gefen, S. S. Margulies, *J. Biomech.* **2004**, 37, 1339.
- [16] A. Banerjee, M. Arha, S. Choudhary, R. S. Ashton, S. R. Bhatia, D. V. Schaffer, R. S. Kane, S. Choudhary, R. S. Ashton, S. R. Bhatia, D. V. Schaffer, R. S. Kane, *Biomaterials* **2009**, 30, 4695.
- [17] S. Wu, R. Xu, B. Duan, P. Jiang, *J. Mater. Chem. B* **2017**, 5, 3870.
- [18] S. Ali, I. B. Wall, C. Mason, A. E. Pelling, F. S. Veraitch, *Acta Biomater.* **2015**, 25, 253.
- [19] N. D. Leipzig, M. S. Shoichet, *Biomaterials* **2009**, 30, 6867.
- [20] K. Saha, A. J. Keung, E. F. Irwin, Y. Li, L. Little, D. V. Schaffer, K. E. Healy, *Biophys. J.* **2008**, 95, 4426.
- [21] S. K. Seidlits, Z. Z. Khaing, R. R. Petersen, J. D. Nickels, J. E. Vanscoy, J. B. Shear, C. E. Schmidt, *Biomaterials* **2010**, 31, 3930.
- [22] P. C. Georges, W. J. Miller, D. F. Meaney, E. S. Sawyer, P. A. Janmey, *Biophys. J.* **2006**, 90, 3012.
- [23] X. Jiang, P. C. Georges, B. Li, Y. Du, M. K. Kutzinger, M. L. Previtera, N. A. Langrana, B. L. Firestein, *Open Neurosci. J.* **2007**, 1, 7.
- [24] J. M. Godbe, R. Freeman, L. F. Burbulla, J. Lewis, D. Krainc, S. I. Stupp, *ACS Biomater. Sci. Eng.* **2020**, 6, 1196.
- [25] A. M. Tukker, M. W. G. D. M. De Groot, F. M. J. Wijnolts, E. E. J. J. Kasteel, L. Hondebrink, R. H. S. S. Westerink, *ALTEX* **2016**, 33, 261.
- [26] A. M. Tukker, F. M. J. J. Wijnolts, A. de Groot, R. H. S. S. Westerink, A. De Groot, R. H. S. S. Westerink, A. de Groot, R. H. S. S. Westerink, *Neurotoxicology* **2018**, 67, 215.
- [27] T. Kayama, I. Suzuki, A. Odawara, T. Sasaki, Y. Ikegaya, *Biochem. Biophys. Res. Commun.* **2018**, 495, 1028.
- [28] E. Fritsche, J. Tigges, J. Hartmann, J. Kapr, M. M. Serafini, B. Viviani, in *Organotypic Models in Drug Development* (Eds: M. Schäfer-Korting, S. Stuchi Maria-Engler, R. Landsiedel), Handbook of Experimental Pharmacology, Vol. 265, Springer, Cham **2020**.
- [29] T. J. Shafer, in *In Vitro Neuronal Networks. Advances in Neurobiology* (M. Chiappalone, V. Pasquale, M. Frega), Vol. 22, Springer, Cham **2019**, https://doi.org/10.1007/978-3-030-11135-9_12.
- [30] E. van Vliet, L. Stoppini, M. Balestrino, C. Eskes, C. Griesinger, T. Sobanski, M. Whelan, T. Hartung, S. Coecke, *Neurotoxicology* **2007**, 28, 1136.
- [31] A. Vassallo, M. Chiappalone, R. De Camargos Lopes, B. Scelfo, A. Novellino, E. Defranchi, T. Palosaari, T. Weisschu, T. Ramirez, S. Martinoia, A. F. M. Johnstone, C. M. Mack, R. Landsiedel, M. Whelan, A. Bal-Price, T. J. Shafer, *Neurotoxicology* **2017**, 60, 280.
- [32] A. M. Tukker, R. G. D. M. van Kleef, F. M. J. Wijnolts, A. de Groot, R. H. S. Westerink, *ALTEX* **2019**, 178, 71.
- [33] L. Nimtz, J. Hartmann, J. Tigges, S. Masjosthusmann, M. Schmuck, E. Keßel, S. Theiss, K. Köhrer, P. Petzsch, J. Adjaye, C. Wigmann, D. Wiczorek, B. Hildebrandt, F. Bendt, U. Hübenthal, G. Brockerhoff, E. Fritsche, *Stem Cell Res.* **2020**, 45, 101761.
- [34] A. Pelkonen, C. Pistono, P. Klecki, M. Gómez-Budía, A. Dougalis, H. Konttinen, I. Stanová, I. Fagerlund, V. Leinonen, P. Korhonen, T. Malm, *Cells* **2021**, 11, 106.
- [35] J. L. Bourke, A. F. Quigley, S. Duchy, C. D. O'Connell, J. M. Crook, G. G. Wallace, M. J. Cook, R. M. I. Kapsa, *J. Tissue Eng. Regen. Med.* **2018**, 12, 490.
- [36] M. T. Tedesco, D. Di Lisa, P. Massobrio, N. Colistra, M. Pesce, T. Catelani, E. Dellacasa, R. Raiteri, S. Martinoia, L. Pastorino, *Biomaterials* **2018**, 156, 159.
- [37] M. Frega, M. Tedesco, P. Massobrio, M. Pesce, S. Martinoia, *Sci. Rep.* **2014**, 4, 1.
- [38] L. Ylä-Outinen, T. Joki, M. Varjola, H. Skottman, S. Narkilathi, *J. Tissue Eng. Regen. Med.* **2012**, 13, 512.
- [39] A. Odawara, H. Katoh, N. Matsuda, I. Suzuki, *Sci. Rep.* **2016**, 6, 26181.
- [40] T. Paavilainen, A. Pelkonen, M. E.-L. E. L. Mäkinen, M. Peltola, H. Huhtala, D. Fayuk, S. Narkilahti, S. Narkilathi, *Stem Cell Res.* **2018**, 27, 151.
- [41] G. Palazzolo, N. Brogiere, O. Cenciarelli, H. Dermutz, M. Zenobi-Wong, *Tissue Eng., Part A* **2015**, 21, 2177.
- [42] K. Y. Lee, D. J. Mooney, *Prog. Polym. Sci.* **2012**, 37, 106.
- [43] A. D. Augst, H. J. Kong, D. J. Mooney, *Macromol. Biosci.* **2006**, 6, 623.
- [44] H. Hayashi, M. Yamada, J. Kumai, N. Takagi, M. Nomizu, *Arch. Biochem. Biophys.* **2018**, 648, 53.
- [45] E. G. Z. Centeno, H. Cimarosti, A. Bithell, *Mol. Neurodegener.* **2018**, 13, 27.
- [46] S. P. Paşca, *Nature* **2018**, 553, 437.
- [47] K. M. Yamada, E. Cukierman, *Cell* **2007**, 130, 601.

- [48] M. Matyash, F. Despong, C. Ikonomidou, M. Gelinsky, *Tissue Eng., Part C* **2014**, 20, 401.
- [49] G. Palazzolo, M. Moroni, A. Soloperto, G. Aletti, G. Naldi, M. Vassalli, T. Nieuw, F. Difato, *Sci. Rep.* **2017**, 7, 8499.
- [50] N. C. Talbot, T. J. Caperna, *Cytotechnology* **2015**, 67, 873.
- [51] C. S. Hughes, L. M. Postovit, G. A. Lajoie, *Proteomics* **2010**, 10, 1886.
- [52] E. A. Aisenbrey, W. L. Murphy, *Nat. Rev. Mater.* **2020**, 5, 539.
- [53] C. S. Barros, S. J. Franco, U. Müller, *Cold Spring Harbor Perspect. Biol.* **2011**, 3, a005108.
- [54] J. D. Humphries, A. Byron, M. J. Humphries, *J. Cell Sci.* **2006**, 119, 3901.
- [55] R. Nishiuchi, J. Takagi, M. Hayashi, H. Ido, Y. Yagi, N. Sanzen, T. Tsuji, M. Yamada, K. Sekiguchi, *Matrix Biol.* **2006**, 25, 189.
- [56] A. Bal-Price, P. J. Lein, K. P. Keil, S. Sethi, T. Shafer, M. Barenys, E. Fritsche, M. Sachana, M. E. (Bette) Meek, *Neurotoxicology* **2017**, 59, 240.
- [57] M. Barenys, K. Gassmann, C. Baksmeier, S. Heinz, I. Reverte, M. Schmuck, T. Temme, F. Bendt, T. C. Zschauer, T. D. Rockel, K. Unfried, W. Wätjen, S. M. Sundaram, H. Heuer, M. T. Colomina, E. Fritsche, *Arch. Toxicol.* **2017**, 91, 827.
- [58] J. Klose, L. Li, M. Pahl, F. Bendt, U. Hübenthal, C. Jüngst, P. Petzsch, A. Schauss, F. Köhrer, P. C. Leung, C. C. Wang, K. Koch, J. Tigges, X. Fan, E. Fritsche, *Cell Biol. Toxicol.* **2022**, <https://doi.org/10.1007/s10565-022-09730-4>.
- [59] J. Arulmoli, H. J. Wright, D. T. T. Phan, U. Sheth, R. A. Que, G. A. Botten, M. Keating, E. L. Botvinick, M. M. Pathak, T. I. Zarembinski, D. S. Yanni, O. V. Razorenova, C. C. W. Hughes, L. A. Flanagan, *Acta Biomater.* **2016**, 43, 122.
- [60] Y. P. Lu, C. H. Yang, J. A. Yeh, F. H. Ho, Y. C. Ou, C. H. Chen, M. Y. Lin, K. S. Huang, *Int. J. Pharm.* **2014**, 463, 177.
- [61] X. Li, X. Liu, B. Josey, J. C. Chou, Y. Tan, N. Zhang, X. Wen, *Stem Cells Transl. Med.* **2014**, 3, 662.
- [62] G. A. Silva, C. Czeisler, K. L. Niece, E. Beniash, D. A. Harrington, J. A. Kessler, S. I. Stupp, *Science* **2004**, 303, 1352.
- [63] W. Sun, T. Iccitti, C. Migliaresi, A. Quattrone, S. Casarosa, A. Motta, *J. Tissue Eng. Regener. Med.* **2017**, 11, 1532.
- [64] R. Patel, M. Santhosh, J. K. Dash, R. Karpoomath, A. Jha, J. Kwak, M. Patel, J. H. Kim, *Polym. Adv. Technol.* **2019**, 30, 4.
- [65] A. Hyysalo, M. Ristola, M. E. L. Mäkinen, S. Häyrynen, M. Nykter, S. Narkilahti, *Stem Cell Res.* **2017**, 24, 118.
- [66] C. Åstrand, V. Chotteau, A. Falk, M. Hedhammar, *Biomater. Sci.* **2020**, 8, 2514.
- [67] A. J. Engler, S. Sen, H. L. Sweeney, D. E. Discher, *Cell* **2006**, 126, 677.
- [68] O. Chaudhuri, L. Gu, D. Klumpers, M. Darnell, S. A. Bencherif, J. C. Weaver, N. Huebsch, H. Lee, E. Lippens, G. N. Duda, D. J. Mooney, *Nat. Mater.* **2016**, 15, 326.
- [69] N. Ashammakhi, S. Ahadian, C. Xu, H. Montazerian, H. Ko, R. Nasiri, N. Barros, A. Khademhosseini, *Mater. Today Bio* **2019**, 1, 100008.
- [70] J. Groll, J. A. Burdick, D. W. Cho, B. Derby, M. Gelinsky, S. C. Heilshorn, T. Jüngst, J. Malda, V. A. Mironov, K. Nakayama, A. Ovsianikov, W. Sun, S. Takeuchi, J. J. Yoo, T. B. F. Woodfield, *Biofabrication* **2019**, 11, 013001.
- [71] Z. Huang, K. Shimazu, N. H. Woo, K. Zang, U. Müller, B. Lu, L. F. Reichardt, *J. Neurosci.* **2006**, 26, 11208.
- [72] C. S. Chan, E. J. Weeber, L. Zong, E. Fuchs, J. D. Sweatt, R. L. Davis, *J. Neurosci.* **2006**, 26, 223.
- [73] E. A. Kramár, B. Lin, C. S. Rex, C. M. Gall, G. Lynch, *Proc. Natl. Acad. Sci. USA* **2006**, 103, 5579.
- [74] I. D. Vainchtein, G. Chin, F. S. Cho, K. W. Kelley, J. G. Miller, E. C. Chien, S. A. Liddelow, P. T. Nguyen, H. Nakao-Inoue, L. C. Dorman, O. Akil, S. Joshita, B. A. Barres, J. T. Paz, A. B. Molofsky, A. V. Molofsky, *Science* **2018**, 359, 1269.
- [75] N. J. Allen, M. L. Bennett, L. C. Foo, G. X. Wang, C. Chakraborty, S. J. Smith, B. A. Barres, *Nature* **2012**, 486, 410.
- [76] I. Farhy-Tselnicker, A. C. M. van Casteren, A. Lee, V. T. Chang, A. R. Aricescu, N. J. Allen, *Neuron* **2017**, 96, 428.
- [77] G. Fossati, D. Pozzi, A. Canzi, F. Mirabella, S. Valentino, R. Morini, E. Ghirardini, F. Filipello, M. Moretti, C. Gotti, D. S. Annis, D. F. Mosher, C. Garlanda, B. Bottazzi, G. Tarabozzi, A. Mantovani, M. Matteoli, E. Menna, *EMBO J.* **2019**, 38, 99529.
- [78] E. Blanco-Suarez, T. F. Liu, A. Kopelevich, N. J. Allen, *Neuron* **2018**, 100, 1116.
- [79] J. Yang, H. Yang, Y. Liu, X. Li, L. Qin, H. Lou, S. Duan, H. Wang, *Elife* **2016**, 5, 15043.
- [80] M. A. Anderson, J. E. Burda, Y. Ren, Y. Ao, T. M. O'Shea, R. Kawaguchi, G. Coppola, B. S. Khakh, T. J. Deming, M. V. Sofroniew, *Nature* **2016**, 532, 195.
- [81] K. Kanemaru, Y. Okubo, K. Hirose, M. Iino, *J. Neurosci.* **2007**, 27, 8957.
- [82] H. Hama, C. Hara, K. Yamaguchi, A. Miyawaki, *Neuron* **2004**, 41, 405.
- [83] E. M. Ullian, S. K. Saperstein, K. S. Christopherson, B. A. Barres, *Science* **2001**, 291, 657.
- [84] A. Odawara, N. Matsuda, Y. Ishibashi, R. Yokoi, I. Suzuki, *Sci. Rep.* **2018**, 8, 10416.
- [85] T. Hyvärinen, A. Hyysalo, F. E. Kapucu, L. Aarnos, A. Vinogradov, S. J. Eglén, L. Ylä-Outinen, S. Narkilahti, *Sci. Rep.* **2019**, 9, 17125.
- [86] J. Izsak, H. Seth, M. Andersson, D. Vizlin-hodszic, S. Theiss, E. Hanse, H. Ågren, K. Funa, S. Illes, *Front. Neurosci.* **2019**, 13, 351.
- [87] M. Chiappalone, M. Bove, A. Vato, M. Tedesco, S. Martinoia, *Brain Res.* **2006**, 1093, 41.
- [88] S. Illes, W. Fleischer, M. Siebler, H. P. Hartung, M. Dihné, *Exp. Neurol.* **2007**, 207, 171.
- [89] P. Charlesworth, E. Cotterill, A. Morton, S. G. N. Grant, S. J. Eglén, *Neural Dev.* **2015**, 10, 1.
- [90] E. Cotterill, D. Hall, K. Wallace, W. R. Mundy, S. J. Eglén, T. J. Shafer, *J. Biomol. Screening* **2016**, 21, 510.
- [91] W. L. Cantley, C. Du, S. Lomoio, T. Depalma, E. Peirent, D. Kleinknecht, M. Hunter, M. D. Tang-Schomer, G. Tesco, D. L. Kaplan, D. Kleinknecht, M. Hunter, M. D. Tang-Schomer, G. Tesco, D. L. Kaplan, D. Kleinknecht, M. Hunter, M. D. Tang-Schomer, G. Tesco, D. L. Kaplan, *ACS Biomater. Sci. Eng.* **2018**, 4, 4278.
- [92] D. A. Soscia, D. Lam, A. C. Tooker, H. A. Enright, M. Triplett, P. Karande, S. K. G. Peters, A. P. Sales, E. K. Wheeler, N. O. Fischer, *Lab Chip* **2020**, 20, 901.
- [93] H. Shin, S. Jeong, J. H. Lee, W. Sun, N. Choi, I. J. Cho, *Nat. Commun.* **2021**, 12, 492.
- [94] Y. Liu, A. F. McGuire, H.-Y. Lou, T. L. Li, J. B.-H. Tok, B. Cui, Z. Bao, *Proc. Natl. Acad. Sci. USA* **2018**, 115, 11718.
- [95] V. Bane, M. Lehane, M. Dikshit, A. O'Riordan, A. Furey, *Toxins* **2014**, 6, 693.
- [96] E. E. J. Kasteel, R. H. S. Westerink, *Toxicol. Lett.* **2017**, 270, 12.
- [97] T. J. Heikkilä, L. Ylä-Outinen, J. M. A. Tanskanen, R. S. Lappalainen, H. Skottman, R. Suuronen, J. E. Mikkonen, J. A. K. Hyttinen, S. Narkilahti, *Exp. Neurol.* **2009**, 218, 109.
- [98] J. H. Lee, R. R. Mitchell, J. D. McNicol, Z. Shapovalova, S. Laronde, B. Tanasijevic, C. Milsom, F. Casado, A. Fiebig-Comyn, T. J. Collins, K. K. Singh, M. Bhatia, *Cell Rep.* **2015**, 11, 1367.
- [99] M. A. Lancaster, M. Renner, C. Martin, D. Wenzel, S. Bicknell, M. E. Hurler, T. Homfray, J. M. Penninger, P. Andrew, *Nature* **2013**, 501, 373.
- [100] N. Stanslowsky, A. Haase, U. Martin, M. Naujock, A. Leffler, R. Dengler, F. Wegner, *Stem Cell Res. Ther.* **2014**, 5, 35.
- [101] T. Sasaki, I. Suzuki, R. Yokoi, K. Sato, Y. Ikegaya, *Biochem. Biophys. Res. Commun.* **2019**, 513, 300.

- [102] R. Gopalakrishna, U. Gundimeda, S. Zhou, H. Bui, A. Davis, T. McNeill, W. Mack, *Biochem. Biophys. Res. Commun.* **2018**, 495, 230.
- [103] D. E. Brenneman, E. A. Neale, G. A. Foster, S. W. d'Autremont, G. L. Westbrook, *J. Cell Biol.* **1987**, 104, 1603.
- [104] M. Bassan, R. Zamostiano, A. Davidson, A. Pinhasov, E. Giladi, O. Perl, H. Bassan, C. Blat, G. Gibney, G. Glazner, D. E. Brenneman, I. Gozes, *J. Neurochem.* **1999**, 72, 1283.
- [105] D. E. Brenneman, I. Gozes, *J. Clin. Invest.* **1996**, 97, 2299.
- [106] I. Husson, C. M. Rangon, V. Lelièvre, A. P. Bemelmans, P. Sachs, J. Mallet, B. E. Kosofsky, P. Gressens, *Cereb. Cortex* **2005**, 15, 250.
- [107] W. A. Lagrèze, A. Pielen, R. Steingart, G. Schlunck, H. D. Hofmann, I. Gozes, M. Kirsch, *Invest. Ophthalmol. Visual Sci.* **2005**, 46, 933.
- [108] M. Reichenstein, M. Rehavi, A. Pinhasov, *J. Mol. Neurosci.* **2008**, 36, 330.
- [109] M. Zusev, I. Gozes, *Regul. Pept.* **2004**, 123, 33.
- [110] R. L. Russell, W. M. S. Burch, *The Principles of Humane Experimental Technique*, Methuen, London **1959**.
- [111] A. Blaaser, D. F. Duarte Campos, U. Puster, W. Richtering, M. M. Stevens, H. Fischer, *Adv. Healthcare Mater.* **2016**, 5, 326.
- [112] K. Bartmann, J. Hartmann, J. Kapr, E. Fritsche, Humana, New York **2021**, pp. 473–488.
- [113] J. Schindelin, I. Arganda-Carreras, E. Frise, V. Kaynig, M. Longair, T. Pietzsch, S. Preibisch, C. Rueden, S. Saalfeld, B. Schmid, J.-Y. Tinevez, D. J. White, V. Hartenstein, K. Eliceiri, P. Tomancak, A. Cardona, *Nat. Methods* **2012**, 9, 676.
- [114] J. L. Barbosa, S. R. Béla, M. F. Ricci, M. L. M. de Noviello, C. T. Cartelle, B. V. Pinheiro, R. W. A. de Vitor, R. M. E. Arantes, *Neurosci. Lett.* **2020**, 718, 134721.
- [115] C. A. Schneider, W. S. Rasband, K. W. Eliceiri, *Nat. Methods* **2012**, 9, 671.

Supporting Information

for *Adv. Mater. Interfaces*, DOI: 10.1002/admi.202200580

Alginate-Laminin Hydrogel Supports Long-Term
Neuronal Activity in 3D Human Induced Pluripotent Stem
Cell-Derived Neuronal Networks

*Julia Hartmann, Ines Lauria, Farina Bendt, Stephan
Rütten, Katharina Koch, Andreas Blaeser, and Ellen
Fritsche**

Supporting information for:

Alginate-laminin hydrogel supports long-term neuronal activity in three-dimensional human induced pluripotent stem cell-derived neuronal networks

Julia Hartmann[#], Ines Lauria[#], Farina Bendt, Stephan Rütten, Katharina Koch[#], Andreas Blaeser[#], and Ellen Fritsche^{#}*

[#] contributed equally

^{*} corresponding author

J. Hartmann, I. Lauria, F. Bendt, K. Koch, E. Fritsche
IUF - Leibniz Research Institute for Environmental Medicine
Auf'm Hennekamp 50
40225 Duesseldorf, Germany
E-Mail: Ellen.fritsche@iuf-duesseldorf.de

S. Rütten
Electron Microscopy Facility, Institute of Pathology
RWTH Aachen University Hospital
Pauwelsstrasse 30
52074 Aachen, Germany

A. Blaeser
Institute for BioMedical Printing Technology
Technical University of Darmstadt
64289 Darmstadt, Germany

A. Blaeser
Centre for Synthetic Biology
Technical University of Darmstadt
64289 Darmstadt, Germany

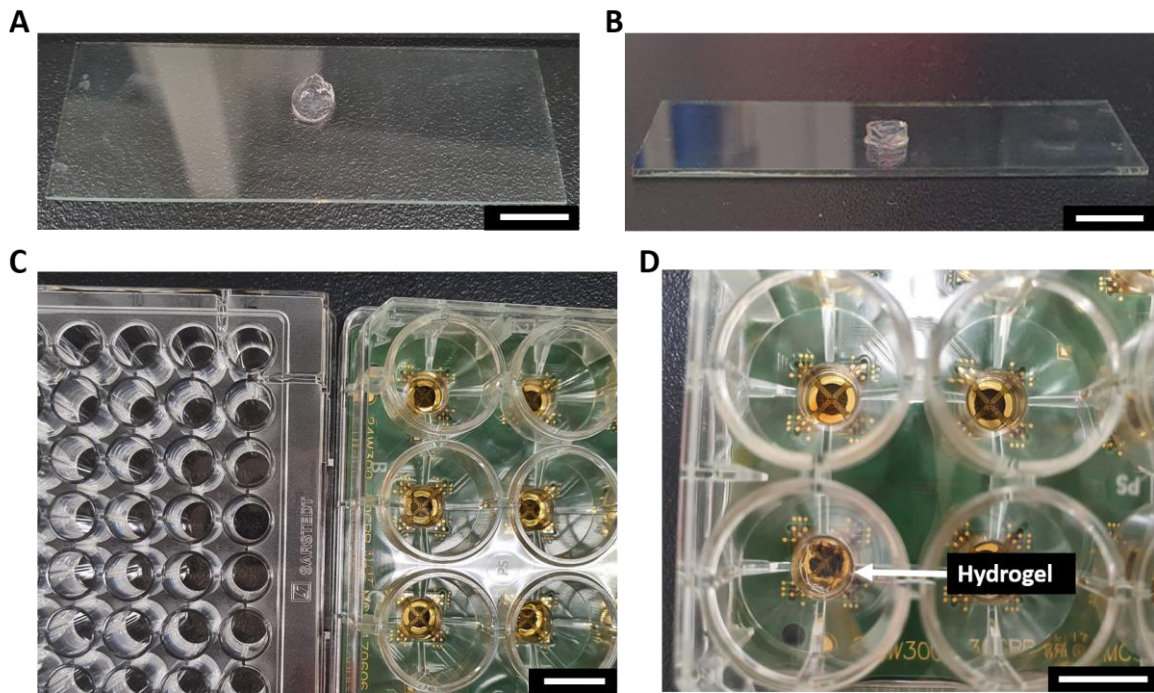
E. Fritsche
Medical Faculty
Heinrich-Heine-University
Universitätsstraße 1
40225 Düsseldorf, Germany

Supplementary Table 1. Cell culture media compositions.

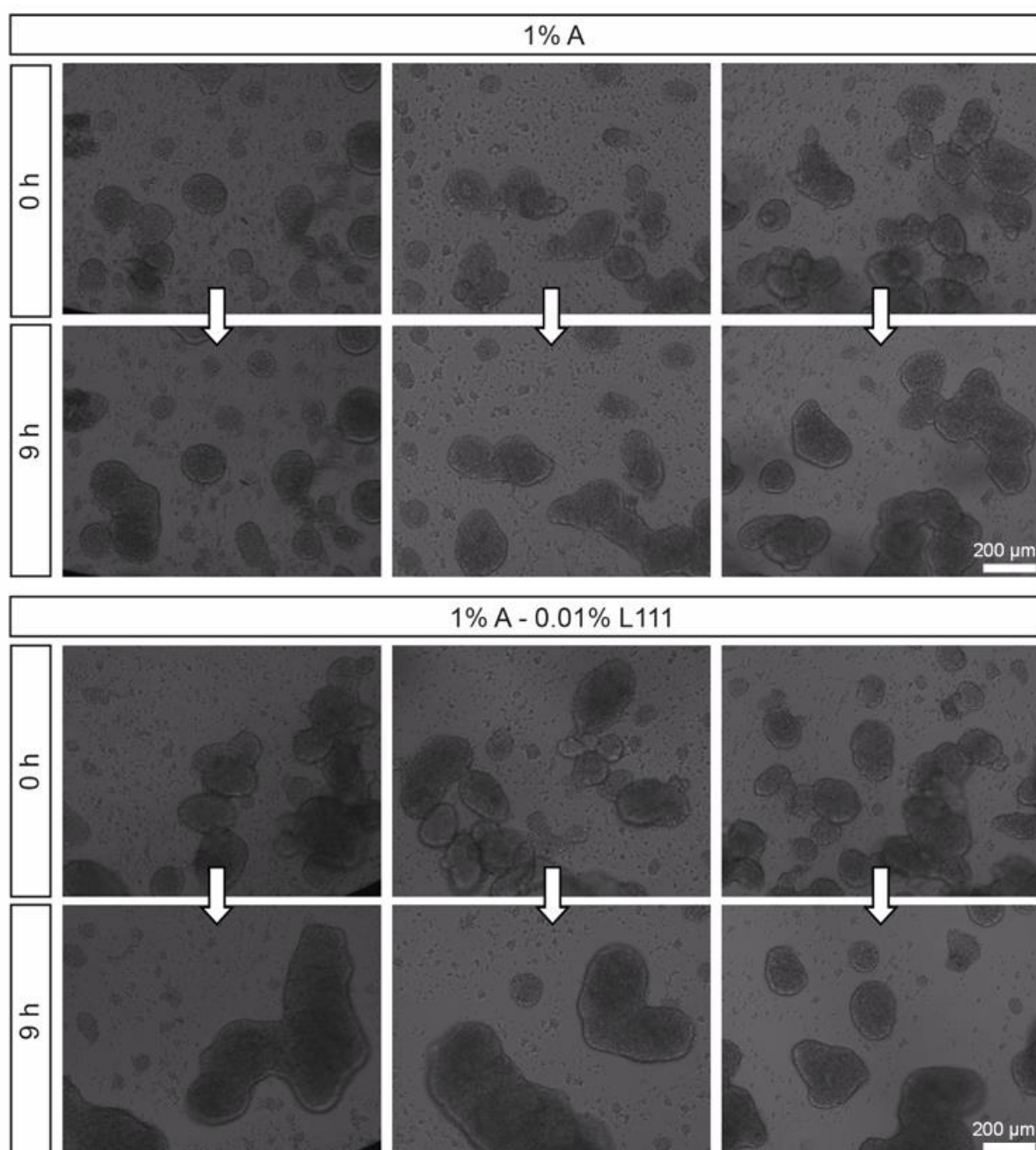
Neural induction medium	Proliferation medium	Differentiation medium CINDA
<p>Basic medium:</p> <p>DMEM high glucose/Ham's F12 (2:1 ratio, #31966-021/ #31765-027, ThermoFisher Scientific, Waltham USA),</p> <p>1 % Penicillin-Streptomycin (#15140-122, ThermoFisher Scientific, Waltham USA),</p> <p>2 % B27™ supplement (serum-free, 50x, #17504-044, ThermoFisher Scientific, Waltham USA)</p>		
<p>1 % N2 supplement (100x, #17502-048, ThermoFisher Scientific, Waltham USA),</p> <p>20% (v/v) KnockOut™ Serum Replacement (#10828-028, ThermoFisher Scientific, Waltham USA),</p> <p>0.2 % human recombinant epidermal growth factor (EGF, #PHG0313, ThermoFisher Scientific, Waltham USA),</p> <p>20 ng mL⁻¹ basic human recombinant fibroblast growth factor (FGF, # 233-FB, R&D Systems, Minneapolis USA).</p>	<p>0.2 % human recombinant epidermal growth factor (EGF, #PHG0313, ThermoFisher Scientific, Waltham USA),</p> <p>20 ng mL⁻¹ basic human recombinant fibroblast growth factor (FGF, # 233-FB, R&D Systems, Minneapolis USA).</p>	<p>1 % N2 supplement (100x, #17502-048, ThermoFisher Scientific, Waltham USA),</p> <p>5 mM creatine monohydrate (#C3630, Sigma-Aldrich, Taufkirchen Germany),</p> <p>100 U mL⁻¹ human recombinant interferon-γ (#300-02, Peprotech, Hamburg Germany),</p> <p>20 ng/mL human recombinant neurotrophin-3 (#450-03, Peprotech, Hamburg Germany),</p> <p>300 μM N⁶,2'-O-Dibutyryladenine 3',5'-cyclic monophosphate sodium salt (Dibutyryl cAMP, #D0260, Sigma-Aldrich, Taufkirchen Germany),</p> <p>20 μM L-ascorbic acid (#A5960, Sigma-Aldrich, Taufkirchen Germany).</p>

Supplementary Table 2. Volumes for preparing 50 μl alginate blends.

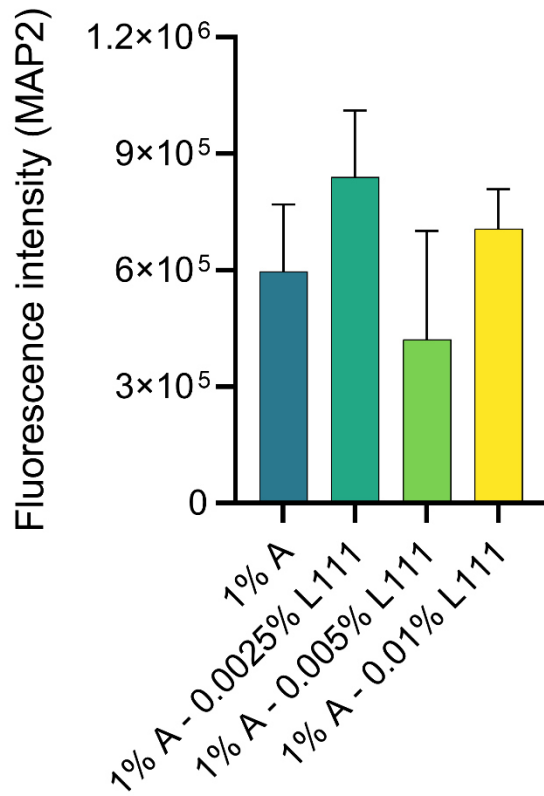
	1 % A	1 % A – 0.0025 % L111	1 % A + 0.005 % L111	1 % A – 0.01 % L111
Alginate (3 % w v⁻¹)	16,67 μl	16,67 μl	16,67 μl	16,67 μl
Laminin 111 (0.1 % w v⁻¹)	-	1.25 μl	2.5 μl	5 μl
Differentiation medium CINDA (with or without cells/spheres)	33.33 μl	32.08 μl	30.83 μl	28.33 μl



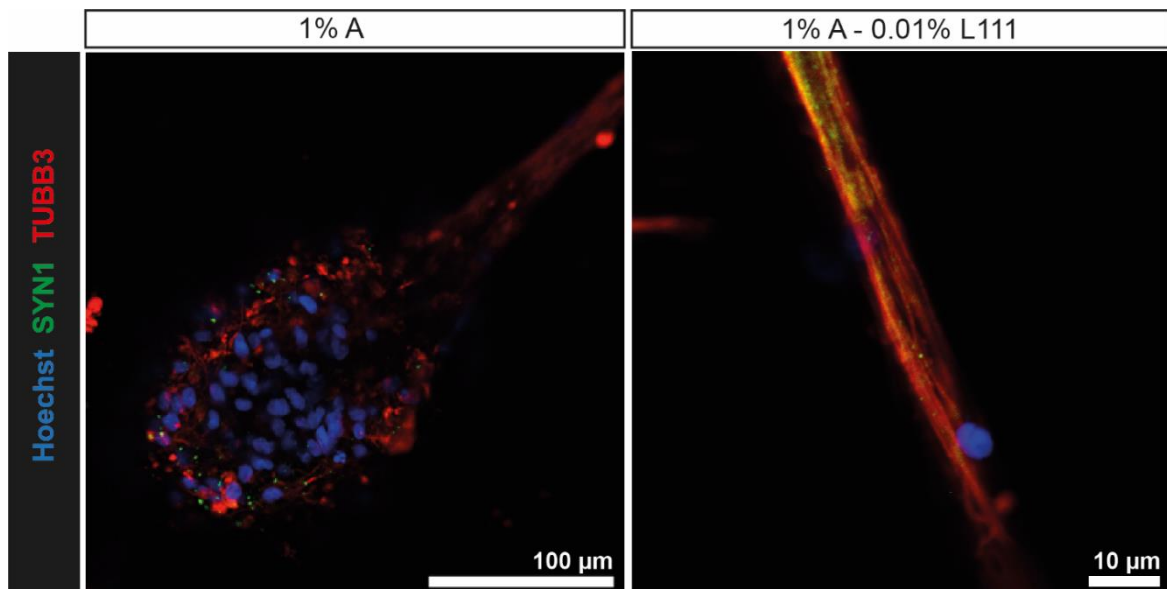
Supplementary Figure 1. Size and form of alginate hydrogels crosslinked in a 96-well plate. The hydrogel (1% alginate) was manufactured as described in the methods part. Briefly, 50 μ l alginate was added into one well of a 96-well plate and 5 min ionically crosslinked with CaCl_2 at RT. The CaCl_2 was removed and the hydrogel was washed twice with DPBS. (A, B) For better visualization of the prepared hydrogel, it was transferred to a microscopy slide. (C) The cultivation area of a 24-well MEA plate (0.32 cm^2) is similar to the area of a 96-well plate (0.29 cm^2). (D) The prepared hydrogel with a volume of 50 μ l covers the culture area of a 24-well MEA plate completely. Scale bar = 10 mm.



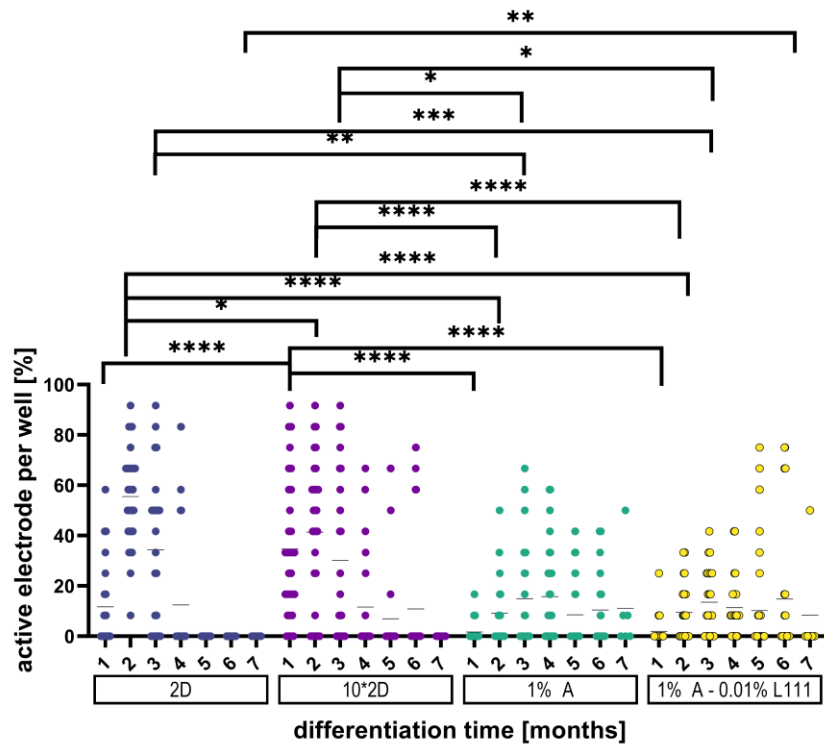
Supplementary Figure 2. Cell movement analyses of neurospheres embedded in pure alginate or alginate-L111 hydrogel blends. Time lapse video analysis in bright field to analyse cell movement and neurosphere fusion. Shown are representative images at the start of recording and after 9 h. A, alginate; L111, laminin 111.



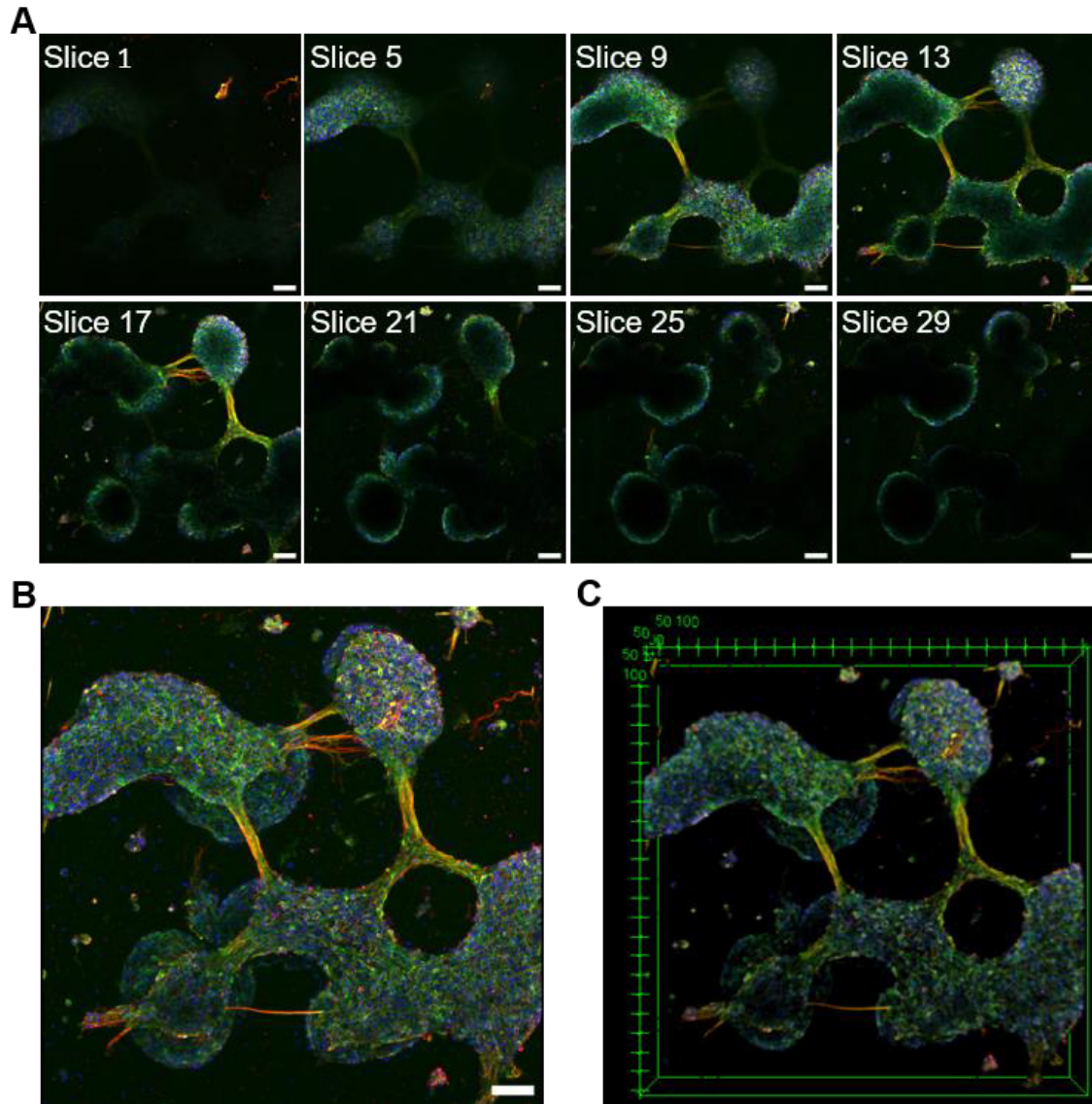
Supplementary figure 3: Quantification of MAP2 expression in different hydrogel blends. Shown is the fluorescence intensity as corrected total cell fluorescence as mean \pm SEM of 3 to 5 pictures with 5 ROI each. A, alginate; L111, laminin 111.



Supplementary Figure 3. Closeup of Synapsin 1 staining. CLSM of neurospheres embedded in alginate hydrogels without and with L111 and stained for tubulin- β -III (TUBB3, red, Alexa546) and Synapsin (SYN1, green, Alexa488) after 14 days of differentiation. Nuclei were counterstained with Hoechst (blue). A, alginate; L111, laminin 111.



Supplementary Figure 5. Active Electrodes during 7 months cultivation time. hiNPCs were singularized and seeded directly (2D, 10*2D), or embedded in alginate hydrogels without (1 % A) or with L111 (1 % A – 0.01 % L111) onto L111-coated mwMEAs. They were cultivated in differentiation medium for up to 206 days. Electrodes with a higher firing activity than 0.0833 Hz were considered as active. Each data point represents the percentage of active electrodes of one well with n=24-36 for each month (month 1 to 6) or n=6 (month 7). A, alginate; L111, laminin 111; MFR, mean firing rate.



Supplementary Figure 6. 3D view of neurospheres differentiated in 1 % A – 0.01 % L111. CLSM of neurospheres embedded in alginate hydrogel with 0.01 % L111 and stained against tubulin- β -III (TUBB3, red, Alexa546) and MAP2 (green, Alexa488) after 14 days of differentiation. Nuclei were counterstained with Hoechst (blue). (A) Every fourth slice of a z-stack of 31 slices and 155 μ m in total. (B) 3D Projection and (C) 3D view of all 31 slices generated with ImageJ. Scale bar = 100 μ m.

Alginate-laminin hydrogel supports long-term neuronal activity in three-dimensional human induced pluripotent stem cell-derived neuronal networks

Julia Hartmann, Ines Lauria, Farina Bendt, Stephan Rütten, Katharina Koch, Andreas Blaeser, and Ellen Fritsche

Fachzeitschrift/Buch: *Advanced Materials Interfaces*

Impact Factor: 6,398 (2021)

Beteiligung an der Publikation: 75 %

Planung, Durchführung und Auswertung der Experimente zur Untersuchung der Zellviabilität, Zytotoxizität, Materialcharakterisierung mittels Rasterelektronenmikroskop und Beweis der Gelierung. Auswertung der Immunzytochemie, der elektrischen Aktivität und der Behandlung mit TTX. Erstellen aller Abbildungen (außer Figure 1) und Schreiben des gesamten Manuskripts.

Typ der Autorenschaft: Erstautorenschaft

Status der Publikation: veröffentlicht am 09.Dezember 2022

2.6 Molecular and functional characterization of different BrainSphere models for use in neurotoxicity testing on microelectrode arrays

Julia Hartmann, Noah Henschel, Kristina Bartmann, Arif Dönmez, Gabriele Brockerhoff, Katharina Koch and Ellen Fritsche

Cells

Die derzeit akzeptierten Methoden in der Neurotoxizitätstestung (NT) beruhen auf Tierversuchen, allerdings verhindern hohe Kosten und ein geringer Durchsatz ihre Anwendung für eine große Anzahl von Chemikalien. Um diese Einschränkungen zu überwinden, werden derzeit *in vitro* Methoden entwickelt, die auf humanen Stammzellen basieren und einen höheren Testdurchsatz ermöglichen. Wir haben drei verschiedene Protokolle zur neuralen Induktion von hiPSCs in hiNPCs, welche alle auf der dualen SMAD-Inhibierung basieren, charakterisiert und zwei Medien für die anschließende Differenzierung in NN miteinander verglichen. Um eine gleichmäßige Verteilung der über das Kulturmedium bereitgestellten exogenen Faktoren zu gewährleisten, erfolgte die neurale Induktion als adhärente Kultur in 2D. Für die anschließende neurale Differenzierung wurden die hiNPCs als 3D BrainSpheres kultiviert, um die Bildung physiologischer Zell-Zell-Kontakte zu ermöglichen. Alle Induktionsprotokolle ergaben fast 100% NESTIN-positive hiNPCs, jedoch zeigten sie unterschiedliche Genexpressionsprofile und differenzierten in unterschiedlich viele Astrozyten und dopaminerge Neurone. Darüber hinaus zeigten die verschiedenen generierten BrainSpheres Unterschiede in der elektrischen Aktivität. Eine detaillierte funktionelle Charakterisierung mittels Sortierung der Spikeformen ermöglichte den Nachweis von verschiedenen neuronalen Subtypen wie GABAergen, glutamatergen,

dopaminergen, serotonergen und cholinergen Neuronen. Zur Anwendung einer solchen MEA-basierten Spike Sortierung in der Neurotoxizitätstestung wurde der humane Multineurotransmitterrezeptor Assay (*human multi-neurotransmitter receptor assay*, hMNR) vorgeschlagen. Die in dieser Studie etablierten Modelle sind vielversprechende Werkzeuge nicht nur in der Toxikologie, sondern auch in der Arzneimittelentwicklung und Krankheitsmodellierung.

Article

Molecular and Functional Characterization of Different BrainSphere Models for Use in Neurotoxicity Testing on Microelectrode Arrays

Julia Hartmann ¹ , Noah Henschel ¹, Kristina Bartmann ^{1,2}, Arif Dönmez ^{1,2}, Gabriele Brockerhoff ¹, Katharina Koch ^{1,2} and Ellen Fritsche ^{1,2,3,*} 

¹ IUF—Leibniz-Research Institute for Environmental Medicine, Auf'm Hennekamp 50, 40225 Duesseldorf, Germany

² DNTOX GmbH, Gurlittstraße 53, 40223 Düsseldorf, Germany

³ Medical Faculty, Heinrich-Heine-University, Universitätsstraße 1, 40225 Düsseldorf, Germany

* Correspondence: ellen.fritsche@iuf-duesseldorf.de

Abstract: The currently accepted methods for neurotoxicity (NT) testing rely on animal studies. However, high costs and low testing throughput hinder their application for large numbers of chemicals. To overcome these limitations, in vitro methods are currently being developed based on human-induced pluripotent stem cells (hiPSC) that allow higher testing throughput at lower costs. We applied six different protocols to generate 3D BrainSphere models for acute NT evaluation. These include three different media for 2D neural induction and two media for subsequent 3D differentiation resulting in self-organized, organotypic neuron/astrocyte microtissues. All induction protocols yielded nearly 100% *NESTIN*-positive hiPSC-derived neural progenitor cells (hiNPCs), though with different gene expression profiles concerning regional patterning. Moreover, gene expression and immunocytochemistry analyses revealed that the choice of media determines neural differentiation patterns. On the functional level, BrainSpheres exhibited different levels of electrical activity on microelectrode arrays (MEA). Spike sorting allowed BrainSphere functional characterization with the mixed cultures consisting of GABAergic, glutamatergic, dopaminergic, serotonergic, and cholinergic neurons. A test method for acute NT testing, the human multi-neurotransmitter receptor (hMNR) assay, was proposed to apply such MEA-based spike sorting. These models are promising tools not only in toxicology but also for drug development and disease modeling.

Keywords: hiPSCs; organoids; neural induction; neural differentiation; brain; in vitro; neural network; BrainSphere; multielectrode arrays (MEA); PARC



Citation: Hartmann, J.; Henschel, N.; Bartmann, K.; Dönmez, A.; Brockerhoff, G.; Koch, K.; Fritsche, E. Molecular and Functional Characterization of Different BrainSphere Models for Use in Neurotoxicity Testing on Microelectrode Arrays. *Cells* **2023**, *12*, 1270. <https://doi.org/10.3390/cells12091270>

Academic Editor: Patrice X. Petit

Received: 13 March 2023

Revised: 14 April 2023

Accepted: 25 April 2023

Published: 27 April 2023



Copyright: © 2023 by the authors. Licensee MDPI, Basel, Switzerland. This article is an open access article distributed under the terms and conditions of the Creative Commons Attribution (CC BY) license (<https://creativecommons.org/licenses/by/4.0/>).

1. Introduction

The currently accepted methods for neurotoxicity (NT) testing rely on animal studies. These are defined in the OECD test guidelines (TG) 418, 419, and 424 [1–3]. The drawbacks of these TG studies are their resource intensities regarding money and time, their high variability, their lack of mechanistic understanding, and their uncertainties due to species differences [4,5]. Such species specificities between humans and rodents decrease confidence in TG neurotoxicity testing as the human brain holds unique features [6,7]. The human uniqueness of the brain is also reflected in the high attrition rates in central nervous system-related drug development when moving from preclinical research to clinical drug applications in humans [8,9]. Species-specific differences in pharmacokinetics and pharmacodynamics are one reason for this poor human prognosis [10]. Moreover, there is a lack of human-relevant neural disease models that also contributes to the high drug attrition rate [11].

One of the main arguments for a paradigm change in human health risk assessment, however, is the low testing throughput that has been leading to a large number of untested

chemicals in our exposome [12]. There is international consensus that current testing needs cannot be satisfied by animal guideline studies. Hence, regulatory agencies, industry, and academia are currently promoting a change to mechanism-based new approach method (NAM)-based next-generation risk assessment (NGRA) [13–17]. NGRA aims at replacing apical endpoints measured in animals via broad biological coverage NAMs that establish a point-of-departure (POD) based on compounds' bioactivities, and comparison of those PODs with exposure measures or their predictions, e.g., via physiological-based kinetic modeling [18]. Uncertainties can be quantified using probability assessment [19]. NAMs should address both general cellular targets and targets specific to the function of the investigated organ system. Therefore, each method should be carefully examined for the presence or absence of biological processes in order to thereby characterize a suitable application domain (fit-for-purpose models) that is best defined by applying model substances or performing case studies [20,21]. Since *in vitro* systems cannot represent an entire organism, they should be contextualized, e.g., in an integrated approach for testing and assessment (IATA) [13].

Since the nervous system is a very complex organ, it can be disrupted via a plethora of modes-of-action (MoAs) involving amongst other neurotransmitter receptors and ion transporters [22]. In general, these MoA affect neuronal function and communication by inhibiting neurotransmitter synthesis or degradation, increasing or preventing neurotransmitter release, blocking neurotransmitter receptors, or interfering with the multiple ion channels [23–27]. Effects on neuronal function can be assessed by recording extracellular local field potentials of cultured neurons on microelectrode arrays (MEAs), thus providing functional readouts for neurotoxicity assessment [28]. Therefore, data on spike-, burst- and network synchronicity-related parameters are generated [29]. MEAs have already been successfully used for acute neurotoxicity studies with rodent cell cultures and genetically engineered human induced pluripotent stem cell (hiPSC)-derived neurons and human astrocytes [30–37]. Brain regions, neuronal subtypes, and individual neuronal units were not evaluated in these studies. However, this is of particular importance regarding disease modeling and drug screening, especially for diseases that only affect certain cell types, such as Parkinson's disease (PD, dopaminergic neurons), or brain regions, such as Huntington's disease (striatum) [38,39].

The reprogramming of somatic cells into hiPSCs [40,41] opened up new ways to generate self-organized human *in vitro* neural networks (NN) via ectodermal and further mixed culture (neuronal and glia) differentiation [42]. To date, a plethora of 2D and 3D neural induction and differentiation protocols are available that can be applied fit-for-purpose [43]. One promising way to neurally induce hiPSC in 2D and 3D cultures is dual SMAD inhibition, which induces neuroectodermal differentiation by altering bone morphogenic protein (BMP) and transforming growth factor beta (TGF β)1 signaling pathways [44–46]. Subsequent neural differentiation of hiPSC-derived neural progenitor cells (hiNPC) into neurons and glial cells *in vitro* is performed with different neurotrophic factors and deprivation of growth factors such as EGF [47–54]. Medium composition in the stem cell differentiation process is critical [55]. For example, we recently showed that the addition of creatine monohydrate, interferon- γ , neurotrophin-3, dibutyryl-cAMP, and ascorbic acid enhances neuronal electrical activity [56]. Two-dimensional protocols for neural induction and differentiation are highly efficient and reproducible due to the even distribution of the provided media supplements; however, they lack formation of a complex three-dimensional morphological architecture and cell–cell-contacts [45,57,58]. Brain organoid cultures overcome this drawback by containing morphological organization; however, they require long differentiation periods beginning from 1 up to 9 months and show high variability between specimens [59,60]. Spheroid cultures, such as BrainSpheres, allow more complex cytoarchitecture than monolayer cultures and form more cell–cell contacts than 2D cultures. Moreover, they need shorter differentiation times than organoids, are less variable and are hence suitable for medium-throughput testing in neurotoxicity studies, drug development, or disease modeling [56,57,61–68].

In this study, we compared the molecular and functional consequences of applying six different cell culture medium protocols for BrainSphere generation by gene and protein analyses as well as MEA recordings. As a reference for gene expression, 35-day differentiated SynFire cells (NeuCyte, Mountain View, CA, USA), which represent a mixed cell population of hiPSC-derived glutamatergic and GABAergic as well as primary human astrocytes, were used. In addition, we set up a MEA-based NAM for acute neurotoxicity testing by using spike sorting.

2. Materials and Methods

2.1. Cultivation of hiPSCs

To guarantee high-quality pluripotent cells, we banked our hiPSCs in a two-tiered process containing a fully characterized master cell bank (MCB) and a partially characterized working cell bank (WCB) as described in the work of Tigges et al., 2021 [69]. The characterization of the cells includes assays regarding cell morphology and identity, pluripotency, karyotype stability, antigen and gene expression, viability, mycoplasma contamination, and post-thaw recovery. In this work, the hiPSC line IMR90 (clone 4, WiCell, Madison, WI, USA) was used and cultivated under humidified conditions at 37 °C and 5% CO₂. The cells were grown on laminin (5 µg/mL, #LN521, Biolamina, Sundbyberg, Sweden)-coated 6-well plates in iPS-Brew XF medium (#130-104-368, Miltenyi Biotech, Bergisch Gladbach, Germany) supplemented with 1% Penicillin/Streptomycin (#P06-07100, PAN Biotech, Aidenbach, Germany). The medium was replaced on 6 out of 7 days per week, and on the 7th day, the cells received the double amount of medium (“double feed”). The hiPSC colonies were passaged with 0.5 mM EDTA (#15575020, Thermo Fisher Scientific, Waltham, MA, USA), performing ‘colony-splitting’.

2.2. Neural Induction of hiPSCs into Human-Induced Neural Progenitor Cells (hiNPCs)

For each neural induction protocol, hiPSC-colonies were dissolved using the Gentle Cell Dissociation Reagent (#100-0485, Stemcell Technologies, Vancouver, BC, Canada) for 10 min at 37 °C and 5% CO₂. After centrifugation (300× g, 10 min), the cell pellet was resuspended in the respective neural induction medium and the cells were seeded with a cell density of 2×10^6 cells per well and cultivated under humidified conditions at 37 °C and 5% CO₂. During the neural induction, the cells were fed on 6 out of 7 days per week, and on the 7th day, the cells were fed with twice the amount of medium.

2.2.1. 2D-NIM Protocol

The 2D-NIM protocol was adapted from our previously published 3D neural induction protocol (NIM; refs. [56,70]) and modified as followed to achieve a 2D culture. The neural induction medium consists of two parts DMEM (high glucose, #31966021, Invitrogen, Carlsbad, CA, USA) and one part Ham’s F12 Nutrient Mix (#31765027, Invitrogen, Carlsbad, CA, USA) supplemented with 1% Penicillin/Streptomycin (#P06-07100, PAN-Biotech, Aidenbach, Germany), 2% B-27™ supplement (50×, serum-free, #17504044, Invitrogen, Carlsbad, CA, USA), 1% N-2 supplement (100×, #17502048, Thermo Fisher Scientific, Waltham, MA, USA), 20 ng/mL recombinant human EGF (#PHG0313, Gibco, Grand Island, NY, USA), 20% Knockout Serum Replacement (#10828028, Thermo Fisher Scientific, Waltham, MA, USA), 10 µM SB-431542 (#S4317, Sigma-Aldrich, St. Louis, MO, USA), and 0.5 µM LDN-193189 hydrochloride (#SML0559, Sigma-Aldrich, St. Louis, MO, USA). After the above-described singularization, the hiPSCs were transferred to a polyethyleneimine (PEI, 0.1%; #181978, Sigma-Aldrich, St. Louis, MO, USA)-laminin (15 µg/mL; #LN521, Biolamina, Sundbyberg, Sweden)-coated 6-well plate and cultivated in 2D-NIM medium supplemented with 10 µM Y-27632 (only for the first 24 h after passaging; #HB2297, Hello Bio, Bristol, UK). On days 12 and 17, hiNPCs were passaged by enzymatic dissociation with Accutase (#07920, Stemcell Technologies, Vancouver, BC, Canada) for 10 min at 37 °C and 5% CO₂ and transferred to a new PEI-laminin-coated 6-well plate. From day 12, the cells were cultivated in neural progenitor medium based on 2D-NIM medium without

the dual SMAD inhibitors SB-431542 and LDN-193189 and supplemented with 20 ng/mL recombinant human basic FGF (#233-FB, R&D Systems, Wiesbaden, Germany) and 10 μ M Y-27632 (only for the first 24 h after passaging). On day 21, hiNPCs were singularized with Accutase and frozen in neural progenitor medium containing 10% dimethyl sulfoxide (DMSO, #A994.1, Carl-Roth, Karlsruhe, Germany) and 10 μ M Y-27632.

2.2.2. GNEIB Protocol

The GNEIB neural induction protocol published by Hyvärinen et al., 2019 and Shi et al., 2012 was applied with minor changes [46,48]: The hiPSC-colonies were singularized as described above and resuspended in GNEIB neural induction medium based in one part DMEM/F-12 (#31331028, Gibco, Grand Island, NY, USA) and one part Neurobasal™ medium (#21103049, Gibco, Grand Island, NY, USA) supplemented with 1% Penicillin/Streptomycin (#P06-07100, PAN-Biotech, Aidenbach, Germany), 1% B-27™ supplement (50 \times , serum-free, #17504044, Thermo Fisher Scientific, Waltham, MA, USA), 0.5% N-2 supplement (100 \times , #17502048, Thermo Fisher Scientific, Waltham, MA, USA), 0.5 mM GlutaMAX™ supplement (#35050061, Thermo Fisher Scientific, Waltham, MA, USA), 0.5% MEM non-essential amino acids (100 \times , #11140050, Thermo Fisher Scientific, Waltham, MA, USA), 2.5 μ g/mL insulin (#I9278, Sigma-Aldrich, St. Louis, MO, USA), 50 μ M beta-mercaptoethanol (#31350010, Thermo Fisher Scientific, Waltham, MA, USA), 10 μ M SB-431542 (#S4317, Sigma-Aldrich, St. Louis, MO, USA), and 100 nM LDN-193189 hydrochloride (#SML0559, Sigma-Aldrich, St. Louis, MO, USA). The cells were transferred onto a poly-L-ornithine (PLO, 100 μ g/mL; #P4957, Sigma-Aldrich, St. Louis, MO, USA)-laminin (15 μ g/mL; #LN521, Biolamina, Sundbyberg, Sweden)-coated 6-well plate and 10 μ M Y-27632 (#HB2297, Hello Bio, Bristol, UK) were added for the first 24 h. On days 12 and 17, hiNPCs were passaged with Accutase (#07920, Stemcell Technologies, Vancouver, BC, Canada) and transferred to a new PLO-laminin-coated plate. From day 12, the hiNPCs were cultivated in neural progenitor medium based on GNEIB medium without SB-431542 and LDN-193189, supplemented with 20 ng/mL recombinant human basic FGF (#233-FB, R&D Systems, Wiesbaden, Germany) and 10 μ M Y-27632 (only for the first 24 h after passaging). On day 21, hiNPCs were singularized with Accutase for 10 min at 37 °C and 5% CO₂ before they were frozen in neural progenitor medium supplemented with 10% dimethyl sulfoxide (DMSO, #A994.1, Carl-Roth, Karlsruhe, Germany) and 10 μ M Y-27632.

2.2.3. Stemdiff Protocol

The Stemdiff protocol was performed using the STEMdiff™ SMADi Neural Induction Kit (#08581, Stemcell Technologies, Vancouver, BC, Canada) according to the manufacturer's protocol with minor modifications. Briefly, the hiPSC colonies were singularized as described above and resuspended in STEMdiff™ Neural Induction Medium supplemented with STEMdiff™ SMADi Neural Induction Supplement and 1% Penicillin/Streptomycin (#P06-07100, PAN-Biotech, Aidenbach, Germany). The cells were transferred to a PLO (15 μ g/mL; #P4957, Sigma-Aldrich, St. Louis, MO, USA)-laminin (10 μ g/mL; #L2020, Sigma-Aldrich, St. Louis, MO, USA)-coated 6-well plate with 10 μ M Y-27632 (only for the first 24 h after passaging; #HB2297, Hello Bio, Bristol, UK). The cells were passaged on day 6 using Accutase (#07920, Stemcell Technologies, Vancouver, BC, Canada) and transferred to a new PLO-laminin-coated 6-well plate with a cell density of 1.5×10^6 cells per well. On day 12, the hiNPCs were singularized with Accutase and frozen in STEMdiff™ Neural Progenitor Freezing Medium (#05838, Stemcell Technologies, Vancouver, BC, Canada) containing 10 μ M Y-27632 (#HB2297, Hello Bio, Bristol, UK).

2.3. Thawing of hiNPCs

The vials of hiNPCs were quickly thawed in the palms of the hand and each vial containing 4×10^6 cells was directly diluted in 10 mL of the respective neural progenitor medium with 10 μ M Y-27632 (#HB2297, Hello Bio, Bristol, UK). After centrifugation (300 \times g, 5 min), the cell pellet was resuspended in the respective neural progenitor medium with

10 μ M Y-27632 (#HB2297, Hello Bio, Bristol, UK). The cells of one frozen cryovial were divided into three wells of a coated 6-well plate. The medium was replaced daily without the addition of Y-27632 (2D-NIM and GNEIB protocol) or with 10 μ M Y-27632 (Stemdiff protocol).

2.4. Formation of BrainSpheres

On day 4 after thawing, the hiNPCs were singularized with Accutase for 10 min at 37 °C and 5% CO₂ (#07920, Stemcell Technologies, Vancouver, BC, Canada) and centrifuged (300 \times g, 10 min). After the cell pellet was resuspended in the respective neural progenitor medium with 10 μ M Y-27632 (#HB2297, Hello Bio, Bristol, UK), 2×10^6 cells were transferred into one well of a new 6-well plate (#83.3920, Sarstedt, Nürmbrecht, Germany) in 4 mL medium. Sphere formation took place in a gyrical shaking incubator (#LT-XC, Kuhner Shaker GmbH, Basel, Switzerland) at 140 rpm, 12.5 mm diameter, 37 °C, 5% CO₂, and 85% humidity for 7 days. On day 7, to equalize the size of the hiNPC spheres, they were chopped to 250 μ m (McIlwain tissue chopper, Mickle Laboratory Engineering Co., Ltd., Guildford, UK) as described previously [71].

2.5. Neural Differentiation

For neural differentiation, the BrainSpheres were chopped to 250 μ m (McIlwain tissue chopper, Mickle Laboratory Engineering Co. LTD., Guildford, UK) and transferred to neural differentiation medium CINDA+ or Electro. CINDA+ consists of two parts DMEM (high glucose, #31966021, Invitrogen, Carlsbad, CA, USA) and one part Ham's F12 Nutrient Mix (#31765027, Invitrogen, Carlsbad, CA, USA) supplemented with 1% Penicillin/Streptomycin (#P06-07100, PAN-Biotech, Aidenbach, Germany), 2% B-27™ Plus supplement (#A3582801, Thermo Fisher Scientific, Waltham, MA, USA), 1% N-2 supplement (#17502048, Thermo Fisher Scientific, Waltham, MA, USA), 650 μ g/mL creatine monohydrate (#C3630, Sigma-Aldrich, St. Louis, MO, USA), 5 ng/mL human recombinant interferon- γ (IFN- γ , #300-02, Peprotech, Hamburg, Germany), 20 ng/mL human recombinant neurotrophin-3 (#450-03, Peprotech, Hamburg, Germany), 20 μ M L-ascorbic acid (A5960, Sigma-Aldrich, St. Louis, MO, USA), and 3 mM N6,2'-O-Dibutyryl adenosine 3',5'-cyclic monophosphate sodium salt (cAMP, #D0260, Sigma-Aldrich, St. Louis, MO, USA). The Electro medium consists of 1:1 DMEM/F-12 (#31331028, Gibco, Grand Island, NY, USA) and Neurobasal medium electro (#A14098-01, Gibco, Grand Island, NY, USA) supplemented with 1% Penicillin/Streptomycin (#P06-07100, PAN-Biotech, Aidenbach, Germany), 1% B-27 supplement electro (#A14097-01, Gibco, Grand Island, NY, USA), 0.5% N-2 supplement (100 \times , #17502048, Thermo Fisher Scientific, Waltham, MA, USA), 0.5 mM GlutaMAX™ supplement (#35050061, Thermo Fisher Scientific, Waltham, MA, USA), 0.5% MEM non-essential amino acids (100 \times , #11140050, Thermo Fisher Scientific, Waltham, MA, USA), 2.5 μ g/mL insulin (#I9278, Sigma-Aldrich, St. Louis, MO, USA), 50 μ M beta-mercaptoethanol (#31350010, Thermo Fisher Scientific, Waltham, MA, USA), 20 ng/mL recombinant human brain derived neurotrophic factor (BDNF, #450-02, Peprotech, Hamburg, Germany), 10 ng/mL recombinant human glial cell line-derived neurotrophic factor (GDNF, #212-GD-010, R&D Systems, Wiesbaden, Germany), 500 μ M cAMP (#D0260, Sigma-Aldrich, St. Louis, MO, USA) and 200 μ M L-ascorbic acid (#A5960, Sigma-Aldrich, St. Louis, MO, USA). The BrainSpheres were differentiated in a shaking incubator (#LT-XC, Kuhner Shaker GmbH, Basel, Switzerland) at 37 °C, 5% CO₂, 85% humidity, 140 rpm (12.5 mm diameter) for 1, 2, or 3 weeks, and half of the medium was replaced twice a week.

2.6. Neural Differentiation on Microelectrode Arrays (MEA)

To access the neuronal electrical activity, the BrainSpheres were plated on 96-well multielectrode arrays (MEA, #M768-tMEA-96B, Axion Biosystems, Atlanta, GA, USA) after 3 weeks, 2 weeks, 1 week, or without 3D differentiation under constant shaking in CINDA+ or Electro differentiation medium. The MEA was coated with specific matrices for each differently generated and differentiated BrainSphere (see Supplementary Table S1).

After coating with the respective matrix, one BrainSphere was placed in the middle of each well of the MEA, except for BrainSpheres generated with the GNEIB protocol and differentiated in Electro differentiation medium. Here, three BrainSpheres were placed per well as they were smaller in size. The BrainSpheres were fed twice per week by replacing half of the differentiation medium. Supplementary Figure S5B shows representative placements of the BrainSpheres on the MEAs after 3 weeks of 3D-differentiation and a further 3 weeks differentiated on the MEAs. The neuronal electrical activity was recorded twice per week, and BrainSpheres were acutely exposed to L-glutamate (50 μ M), DL-2-Amino-5-phosphonovaleric acid (AP5, 50 μ M), and NBQX disodium salt (NBQX, 50 μ M), bicuculline (3 and 10 μ M), picrotoxin (5, 10 and 20 μ M), haloperidol (1 and 10 μ M), carbaryl (5, 10, 20, 50, and 100 μ M), and buspirone hydrochloride (5, 10, 20, 50, and 100 μ M) after 2–6 weeks on the MEA. For the substance testing, the BrainSpheres were first exposed to the neurotransmitters glutamate (50 μ M) or GABA (10 μ M) before the antagonists AP5 (50 μ M) and NBQX (50 μ M) or bicuculline (10 μ M) were added. The substances were removed with a complete exchange of the medium and the neuronal networks were allowed to recover for 2 to 3 h. After another baseline recording, the test compounds trimethyltin chloride (TMT) and emamectin were consecutively added until the final concentration was reached. Detailed information such as CAS registry numbers (CASRN), suppliers, and solvents is available in Supplementary Table S2. The data for subtype characterization were derived from 3 different MEA plates with 8 wells per condition and 8 electrodes per well, resulting in 192 electrodes per condition. The data of the substance testing experiment with TMT, emamectin, and quinpirole were derived from one MEA plate with 8 wells per condition and subtype specification, resulting in 64 electrodes.

2.6.1. Recording and Data Analysis of MEA Neuronal Electrical Activity

Extracellular recording of the neuronal electrical activity was performed twice a week for 15 min (baseline and each tested compound concentration) at 37 °C and 5% CO₂ after the cells were allowed to equilibrate for 15 min in the Axion Maestro Pro system (Axion Biosystems, Atlanta, GA, USA). Data recording was operated by the Axion Integrated Studios (AxIS) navigator software (version 3.1.2, Axion Biosystems, Atlanta, GA, USA) with a sampling frequency of 12.5 kHz and a digital band-pass filter of 200–3000 Hz. Subsequent spike detection was performed using the method “adaptive threshold crossing” with a threshold of 6 root mean square (rms) noise on each electrode and a pre- and post-spike duration of 0.84 ms and 2.16 ms, respectively, and an electrode was defined as active with at least 2 spikes per min. Quantification of general electrical activity and neuronal network activity was performed with the Neural Metric Tool software (version 3.1.7, Axion Biosystems, Atlanta, GA, USA). If several spikes occur one after the other on the same electrode and meet certain criteria, they are referred to as a burst. For burst detection, the method “Inter-spike interval (ISI) threshold” was used with a minimum of five contributing spikes and a maximum ISI of 100 ms. If bursts occur simultaneously on several electrodes within a well, this is defined as a network burst. Network bursts were identified using the algorithm “envelope” with a threshold factor of 1.25, a minimal inter-burst interval (IBI) of 100 ms, at least 35% participating electrodes, and 75% burst inclusion. Parameters for neuronal activity (percentage of active electrodes and weighted mean firing rate (wMFR)) as well as for network maturation and synchronicity (burst frequency and network burst frequency) were analyzed.

2.6.2. Spike Sorting

For spike sorting, the AxIS generated .spk files of the baseline measurement and each corresponding treatment concentration were concatenated and converted into .nex files with a MATLAB (R2021b, R2022b, MathWorks, Natick, MA, USA) script. The generated .nex files were sorted with the neural spike sorting software Offline Sorter (OFS, version 4.4, Plexon, Dallas, TX, USA) using the automatic clustering T-Distribution EM method with 10 degrees of freedom (D.O.F) and 20 initial number of units. The sorted units were

exported as per-unit and per-waveform data giving information about the number of spikes per unit per baseline and substance concentration. For analysis, only units with at least 2 spikes/min during the baseline measurement were analyzed and they were considered responding units when the fold change to the baseline was at least ± 0.25 (increase or decrease).

2.7. Cytotoxicity Assessment

Cytotoxicity was assessed by measuring the lactate dehydrogenase (LDH) release from cells with damaged membranes using the CytoTox-ONE Homogeneous Membrane Integrity assay (#7891, Promega, Madison, WI, USA). For this, parallel to the substance testing on the MEA, one Brainphere was placed in the middle of each well of a coated 96-well plate (for coating see Supplementary Table S1) and differentiated in CINDA+ for 4 weeks. After acute treatment with the respective substance (15 min at 37 °C), 50 μ L medium from each well was transferred to a new 96-well plate and 50 μ L CytoTox-ONE reagent was added. As lysis control, neurospheres were treated with 10% Triton-X 100. The medium without spheres was used to correct for background fluorescence. Fluorescence was detected with the Tecan infinite M200 Pro reader (ex: 540 nm; em: 590 nm).

2.8. Cultivation of SynFire Cells

SynFire cells (SynFire Co-Culture Kit (MEA), #1010-7.5, NeuCyte, Mountain View, CA, USA) were cultivated according to the manufacturer's protocol and as described in detail in Bartmann et al.'s work (preprint) [72]. Briefly, the cells were thawed, resuspended in seeding medium, and seeded on PEI (0.1%, #181978, Sigma-Aldrich, St. Louis, MO, USA)-laminin (20 μ g/mL, #23017015, Thermo Fisher Scientific, Waltham, MA, USA)-coated 48-well MEA plates (#M768-KAP-48, Axion Biosystems, Atlanta, GA, USA) in a ratio of 140,000 glutamatergic neurons, 60,000 GABAergic neurons, and 70,000 astrocytes per well. On days 3 and 5, half of the medium was replaced with short-term medium. From day 7 onwards, the medium was gradually replaced with long-term medium and the cells were fed twice per week.

2.9. Flow Cytometry

Flow cytometry analyses were performed to confirm the success of the neural inductions. Therefore, hiNPCs were singularized with Accutase (#07920, Stemcell Technologies, Vancouver, BC, Canada) for 10 min at 37 °C and 5% CO₂ before they were stained with Fixable Viability Stain 510 (1:100, #564406, BD Horizon, Franklin Lakes, NJ, USA) for 15 min at room temperature (RT) in the dark. Afterwards, they were washed twice by centrifuging (500 \times g, 5min, RT) and resuspending in Stain Buffer (#554656, BD Pharmingen, Franklin Lakes, NJ, USA). Cells were fixed in Fixation Buffer (#554655, BD Cytotfix, Franklin Lakes, NJ, USA) for 20 min at RT in the dark, washed two times in DPBS (*w/o* Mg²⁺ and Cl²⁺, #12559069, Gibco, Grand Island, NY, USA) and then permeabilized in Perm Buffer III (#558050, BD Phosflow, Franklin Lakes, NJ, USA). After two additional washing steps in Stain buffer, the hiNPCs were stained with PerCP-Cy5.5 mouse anti-OCT3/4 (1:20, #51-9006267, BD Pharmingen, Franklin Lakes, NJ, USA), PE mouse anti-human PAX-6 (1:20, #561552, BD Pharmingen, Franklin Lakes, NJ, USA), Alexa Fluor 647 mouse anti-NESTIN (1:20, #560341, BD Pharmingen, Franklin Lakes, NJ, USA), and Alexa Fluor 488 mouse anti-KI-67 (1:20, #558616, BD Pharmingen, Franklin Lakes, NJ, USA) for 30 min at RT in the dark. To exclude unspecific staining, the isotype controls PerCP-Cy5.5 mouse IgG1, κ (1:10, #51-9006272, BD, Franklin Lakes, NJ, USA), PE mouse IgG2 α , κ (1:20, #558595, BD Phosflow, Franklin Lakes, NJ, USA), Alexa Fluor 647 mouse IgG1, κ (1:20, #557732, BD Pharmingen, Franklin Lakes, NJ, USA), and Alexa Fluor 488 mouse IgG1, κ (1:5, #557782, BD Phosflow, Franklin Lakes, NJ, USA) were used. Data acquisition of 20,000 cells per sample was performed with the BD FACSCanto II (BD, Bioscience, Franklin Lakes, NJ, USA). Dead cells, cell debris, and doublets were discarded during the gating and analyzing process

with FlowJo (version 10.8.1, Ashland, OR, USA). Flow cytometry analyses were performed with hiNPCs derived from 3–4 independent neural inductions of each protocol ($n = 3–4$).

2.10. Quantitative Polymerase Chain Reaction (qPCR)

For gene expression analyses, samples were collected at different time points indicated in Figure 1. Messenger RNA (mRNA) was isolated using the Rneasy Mini Kit (#74104, Qiagen, Hilden, Germany) and transcribed into cDNA using the QuantiTect Reverse Transcription Kit (#205311, Qiagen, Hilden, Germany). qPCR was performed in the Rotor-Gene Q Cyclor (#9001560, Qiagen, Hilden, Germany) using the QuantiFast SYBR Green PCR Kit (#204056, Qiagen, Hilden, Germany). For quantification, standard curves of all examined genes were generated for calculating copy numbers (CN) as described in Walter et al.'s work, 2019 [73]. All steps were performed according to the manufacturer's instructions and CN of the gene of interest were normalized to β -actin expression. Primer sequences are listed in Supplementary Table S3. The data were derived from three–four independent experiments, each performed with a different batch of hiNPCs.

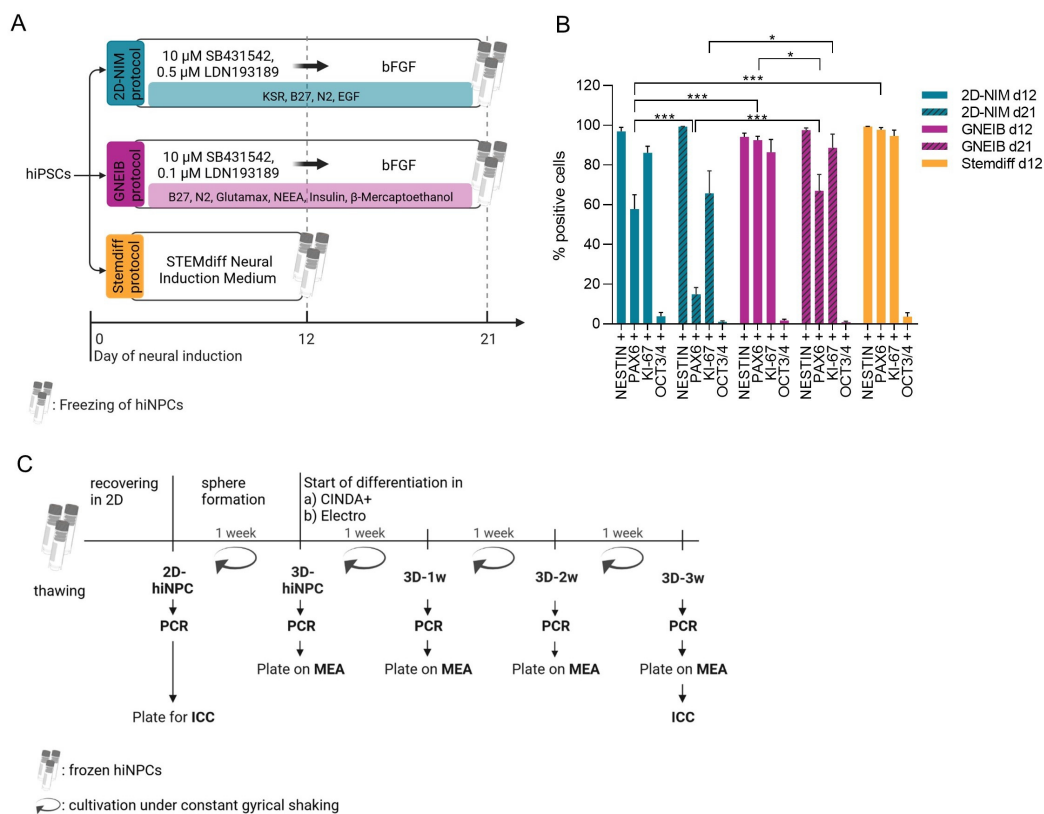


Figure 1. Schematic overview of experimental timeline and characterization of the human-induced neural progenitor cells (hiNPCs). **(A)** Overview of the three different neural induction protocols used. The hiPSC line IMR90 was neurally induced with the 2D-NIM, the GNEIB, and the Stemdiff protocol at least three times. The resulting hiNPCs were frozen on day 12 (Stemdiff protocol) or day 21 (2D-NIM and GNEIB protocol). **(B)** Flow cytometry analysis of hiNPCs on day 12 and day 21 of the neural induction. All induction protocols generated hiNPCs expressing the neural progenitor markers *NESTIN*, *PAX6*, and the proliferation marker *KI-67*, whereas the stemness marker *OCT3/4* was not expressed anymore. Data are represented as mean \pm SEM of $n = 3$ –4 independent experiments (* $p \leq 0.05$, *** $p \leq 0.001$). **(C)** Experimental setup of BrainSphere formation and differentiation. After thawing, the hiNPCs were cultivated in 2D to recover and proliferate. On day 4, they were transferred to a shaking incubator, formed BrainSpheres (3D), and were differentiated in CINDA+ or Electro medium for 1 week (3D-1w), 2 weeks (3D-2w), or 3 weeks (3D-3w). Characterization of gene expression (PCR), protein expression (ICC), and electrical activity (MEA) was performed at the indicated time points. ICC, immunocytochemistry; MEA, microelectrode array. Created with biorender.com.

2.11. Immunocytochemistry (ICC) of Adherent hiNPCs

On day 4 after thawing, hiNPCs were singularized with Accutase (10 min at 37 °C and 5% CO₂), and 20,000 cells were transferred into each chamber of a coated 8-chamber slide (#354118, BD Falcon, Franklin Lakes, NJ, USA) for another 3 days of cultivation before fixing with 4% paraformaldehyde (PFA, #P6148, Sigma-Aldrich, St. Louis, MO, USA) for 30 min at 37 °C. Unspecific binding sites were blocked by DPBS (*w/o* Mg²⁺ and Cl²⁺, #12559069, Gibco, Grand Island, NY, USA) containing 2% bovine serum albumin (BSA, #11920.04, Serva, Germany), 10% goat serum (GS, #G9023, Sigma-Aldrich, St. Louis, MO, USA), and 0.1% Triton X-100 (#T8787, Sigma-Aldrich, St. Louis, MO, USA) for 60 min at 37 °C. After the hiNPCs were washed twice with DPBS, they were incubated with antibodies against *NESTIN* (anti-*NESTIN* AF 647, 1:20, #560341, BD Pharmingen™, Heidelberg, Germany) and *KI-67* (anti-*KI-67* AF488, 1:20, #558616, BD Pharmingen™, Heidelberg, Germany) in DPBS containing 10% GS, 0.1% Triton X-100 and 1% Hoechst 34580 (#H21486, Thermo Fisher

Scientific, Waltham, MA, USA) for 60 min at 37 °C. After removal of the staining solution, cells were washed three times with DPBS before embedding with Aqua-Poly/Mount (#18606-20, Polysciences Inc., Warrington, PA, USA) and a cover glass. Images were acquired with the high content analysis (HCA) platform Cellinsight CX7 (Thermo Fisher Scientific, Waltham, MA, USA). Quantification of *NESTIN*- and *KI-67*-positive cells were performed using the HCS Studio Cellomics Scan software (version 6.6.1, Thermo Fisher Scientific, Waltham, MA, USA) and the protocol TargetActivation.V4. *KI-67*-positive cells were identified by setting an intensity threshold within the perimeter of the Hoechst-stained nuclei as *KI-67* is a nuclear protein. *NESTIN*-positive cells were identified by enlarging the perimeter of the detected nuclei to include cytoplasmatic *NESTIN* signals near the nucleus, without detecting the signal of neighboring cells.

2.12. ICC of BrainSpheres

After three weeks of differentiation under constant shaking, BrainSpheres were fixed with 4% PFA (#P6148, Sigma-Aldrich, St. Louis, MO, USA) for 60 min at room temperature (RT). Afterwards, they were washed twice with DPBS (*w/o* Mg^{2+} and Cl^{2+} , #12559069, Gibco, Grand Island, NY, USA) and unspecific binding sites were blocked with DPBS containing 10% GS (#G9023, Sigma-Aldrich, St. Louis, MO, USA) for 30 min at 4 °C. The blocking solution was removed and the first staining solution containing 2% GS, 0.1% Triton X-100 (#T8787, Sigma-Aldrich, St. Louis, MO, USA), and the primary antibodies against *TUBB3* (1:250, anti-*TUBB3*, Mouse IgG2b, #T8600, Sigma-Aldrich, St. Louis, MO, USA) and *S100B* (1:500, anti-*S100B*, rabbit IgG, #ab52642, Abcam, Cambridge, UK) or *MAP2* (1:1000 or anti-*MAP2*, mouse IgG1, #13-1500, Thermo Fisher Scientific, Waltham, MA, USA) and *TH* (1:250, anti-*TH*, rabbit IgG, #ab112, Abcam, Cambridge, UK) were added for 24 h at 4 °C. After the BrainSpheres had been washed twice with DPBS, the second staining solution containing 1% Hoechst 34580 (#H21486, Thermo Fisher Scientific, Waltham, MA, USA), 2% GS and the secondary antibodies (anti-mouse IgG, 1:500, AF488, #A10680, Thermo Fisher Scientific, Waltham, MA, USA; anti-rabbit IgG, 1:1000, AF546, #A11010, Thermo Fisher Scientific, Waltham, MA, USA) was added and incubated for 2 h at 4 °C. After washing twice with DPBS, the BrainSpheres were transferred to a microscopy slide, Aqua-Poly/Mount (#18606-20, Polysciences Inc., Warrington, PA, USA) was added, and they were covered with a cover glass. Image acquisition was performed with the confocal laser scanning system LSM 710 (Zeiss, Oberkochen, Germany) at the Center for Advanced Imaging (CAi) of the Heinrich-Heine-University in Düsseldorf.

2.13. Statistical Analysis

All statistical analyses were performed with GraphPad Prism (version 8.4.3, Boston, MA, USA). The MEA data were examined for significant differences between the SDs using the Brown–Forsythe test. If the SDs were not significantly different, one-way ANOVA followed by the post hoc Dunnett test were applied. If the SDs were significantly different, Brown–Forsythe and Welch ANOVA followed by the post hoc Games–Howell test were performed. Flow cytometry data were analyzed using a two-way-ANOVA followed by Tukey test for correction of multiple comparisons. qPCR data were analyzed in two ways. For media comparisons, an unpaired *t*-test with Welch’s correction was used. For comparison to the first time point (2D or 3D), one-way ANOVA and the post hoc test Dunnett were used. The calculated *p*-values for each comparison can be found in Supplementary Table S4.

3. Results

3.1. All Three Neural Induction Protocols Successfully Induce hiPSCs into the Neural Lineage

The hiPSC line IMR-90 (clone 4, WiCell, Madison, WI, USA) was quality-controlled and banked as described in Tigges et al.’s work 2021 [69]. From a full quality-controlled master cell bank (MCB), a quality-controlled working cell bank (WCB) was prepared to ensure equal starting material for all experiments. The quality controls included the microscopic assessment of colony and cell morphology, mycoplasma detection, STR genotyping,

caryotype analysis, protein expression of stem cell markers, viability assessment, gene expression analysis (only MCB), pluripotency assays (only MCB), and post-thaw recovery analysis. The data are shown in Tigges et al.'s work 2021 [69]. Three different neural induction protocols were compared for their capacity to generate human-induced neural progenitor cells (hiNPCs). Two of them were modified from previously published protocols (2D-NIM, [56]; GNEIB, [46,48]) and a third one was commercially available (Stemdiff). The hiPS cell line IMR90 was neurally induced as described in Figure 1A and characteristic molecular marker expression was analyzed using flow cytometry on day 12 (all three protocols) and day 21 (2D-NIM and GNEIB) of the protocol (Figure 1B). The stemness marker octamer-binding transcription factor 3/4 (OCT3/4) [40] was downregulated in all protocols to under 4% positive cells. After 12 days of neural induction, the neural progenitor cell marker *NESTIN* [74] was expressed in 97% (on day 21: 99%), 94% (on day 21: 98%), and 99% of hiNPCs generated with the 2D-NIM, GNEIB, and Stemdiff protocols, respectively. Expression of the neural progenitor marker *PAX6* [75] was unequal in the three protocols, i.e., in 93% and 98% of the cells generated with the GNEIB (day 12) and the Stemdiff protocol, respectively, but only in 58% of cells generated with the 2D-NIM (day 12) protocol. Additionally, the number of cells expressing *PAX6* decreased on day 21 for 2D-NIM (15%) and GNEIB (67%). The proliferation marker *KI-67* was expressed in 86% (2D-NIM), 87% (GNEIB), and 95% (Stemdiff) of the cells on day 12 and decreased to 66% (2D-NIM) and 67% (GNEIB) cells on day 21 of neural induction. After neural induction and FACS evaluation, the hiNPCs were frozen in liquid nitrogen to start each protocol with the same passage number and reduce inter-experimental variability. To ensure that the freezing process did not change molecular marker expression, we confirmed *NESTIN* and *KI-67* expression after thawing via immunocytochemistry (Supplementary Figure S1). For forming BrainSpheres in 3D, the adherent hiNPCs were cultivated under shaking conditions in 6-well plates according to Honegger et al. 1979 and Pamies et al., 2017 [57,76] using the two differentiation media, i.e., CINDA+ and Electro. These media were chosen for optimization of BrainSphere electrical activity. Their potential to support oligodendrocyte differentiation will be investigated in future studies. Spheres were characterized with regard to gene and protein expression, as well as neuronal network activity on MEAs in the proliferating state and after 1, 2 and 3 weeks of 3D differentiation (Figure 1C).

3.2. BrainSpheres Differ in Neural Marker Gene Expression Depending on the Applied Protocol

For characterizing BrainSpheres' brain region specificity, developmental stage, neural subtypes, neurotransmitter processing and astrocyte maturation gene expression analyses were performed via qPCR at different time points as indicated in Figure 1. As markers for different brain regions, the genes *FOXP1* (forkhead box G1, forebrain), *LMX1A* (LIM homeobox transcription factor 1 alpha, midbrain), *EN1* (engrailed homeobox 1, midbrain), and *HOXA2* (homeobox A2, hindbrain) were analyzed (Figure 2, Supplementary Table S4) [43,77]. The forebrain marker *FOXP1* was significantly higher expressed in BrainSpheres generated with the GNEIB protocol and almost not expressed in BrainSpheres generated with the 2D-NIM protocol. Although *FOXP1* expression in Stemdiff-derived BrainSpheres was the highest, its induction was not statistically significant due to high standard deviations. The midbrain marker *LMX1A* was highest expressed in BrainSpheres generated with the GNEIB protocol; however, this was not statistically significant. The midbrain marker *EN1* was higher expressed in BrainSpheres derived from the 2D-NIM and GNEIB protocols compared to BrainSpheres derived from the Stemdiff protocol, whose *EN1* expression decreased significantly during differentiation. The hindbrain marker *HOXA2* registered the highest expression in the early hiNPC stages of the 2D-NIM and GNEIB protocol, whereas the expression decreased significantly during three weeks of differentiation.

The genes *SLC12A2* (solute carrier family 12 member 2) and *SLC12A5* (solute carrier family 12 member 5) are encoding for the two ion transporters, i.e., $\text{Na}^+\text{-K}^+\text{-2Cl}^-$ cotransporter-1, (*NKCC1*) and $\text{K}^+\text{-Cl}^-$ cotransporter (*KCC2*), respectively, that are key in the postnatal shift from excitatory to inhibitory GABAergic neurons caused by a reduced

expression of *SLC12A2* and an increased expression of *SLC12A5* [78]. While *SLC12A2* expression did not decrease significantly, *SLC12A5* significantly increased in BrainSpheres derived from the 2D-NIM protocol; yet, with overall very low copy number expression. For comparison, mRNA expression from a fairly mature, 35 days differentiated neuron-glia mixed culture 2D network, i.e., the SynFire kit [72], was analyzed. *SLC12A2* copy number expression was much lower and *SLC12A5* copy number expression was much higher in the differentiated SynFire cells than in the BrainSpheres indicating prematurity of up to 3 weeks differentiated BrainSpheres independent of the applied protocol.

Expression of *MAP2* (microtubule associated protein 2), which encodes for a dendritic protein [79], significantly increased during BrainSphere differentiation generated with the 2D-NIM and GNEIB protocols. The pre-synaptic marker *SYN1* (synapsin 1) registered the highest expression in BrainSpheres generated with the 2D-NIM and the Stemdiff protocols and differentiated in CINDA+; however, this increase is not statistically significant as in 2D-NIM-BrainSpheres differentiated in Electro medium. The postsynaptic *DLG4* (discs large MAGUK scaffold protein 4) expression was abundant in all BrainSpheres even without differentiation and reached similar or even higher expression levels (Stemdiff Electro) than in 35-day differentiated SynFire cells during differentiation.

For analyzing the potential for BrainSphere glial differentiation, the genes *GFAP* (glial fibrillary acidic protein), *S100B* (S100 calcium binding protein B) and *AQP4* (aquaporin 4), which represent different stages of astrocyte maturation, were chosen [80]. *GFAP* was only expressed in BrainSpheres generated with the 2D-NIM protocol and differentiated in CINDA+ for at least 2 weeks. *S100B* was already expressed after one week of differentiation with significantly increased expression in BrainSpheres generated with the 2D-NIM (CINDA+) and the GNEIB protocol (both differentiation media), whereas both conditions differentiated in CINDA+ reached higher expression levels than the 35-day differentiated SynFire cells. *AQP4*, which denotes astrocytes with higher maturity, was hardly expressed in all BrainSpheres, yet highly expressed in SynFire cells.

Expression of genes encoding for the glutamate receptors *GRIA1* (glutamate ionotropic receptor AMPA type subunit 1) and *GRIN1* (glutamate ionotropic receptor NMDA type subunit 1) were only significantly increased during differentiation in BrainSpheres generated with the 2D-NIM protocol in both differentiation media; however, the *GRIA1* expression in Stemdiff BrainSpheres exceeded the expression of 35-day differentiated SynFire cells. The expression of *GABRA1* (gamma-aminobutyric acid type A receptor subunit alpha 1) increased during differentiation in BrainSpheres generated with the 2D-NIM and the Stemdiff protocols. The gene *DRD2* encoding for the dopamine receptor D2 was not significantly expressed; however, it registered higher expression levels in BrainSpheres generated with the GNEIB protocol. The genes *HTR1A* (5-hydroxytryptamine receptor 1A) and *CHRNA4* (cholinergic receptor nicotinic alpha 4 subunit), encoding for serotonin and choline receptors, respectively, were scarcely expressed in all conditions. All receptors were expressed in the SynFire cells.

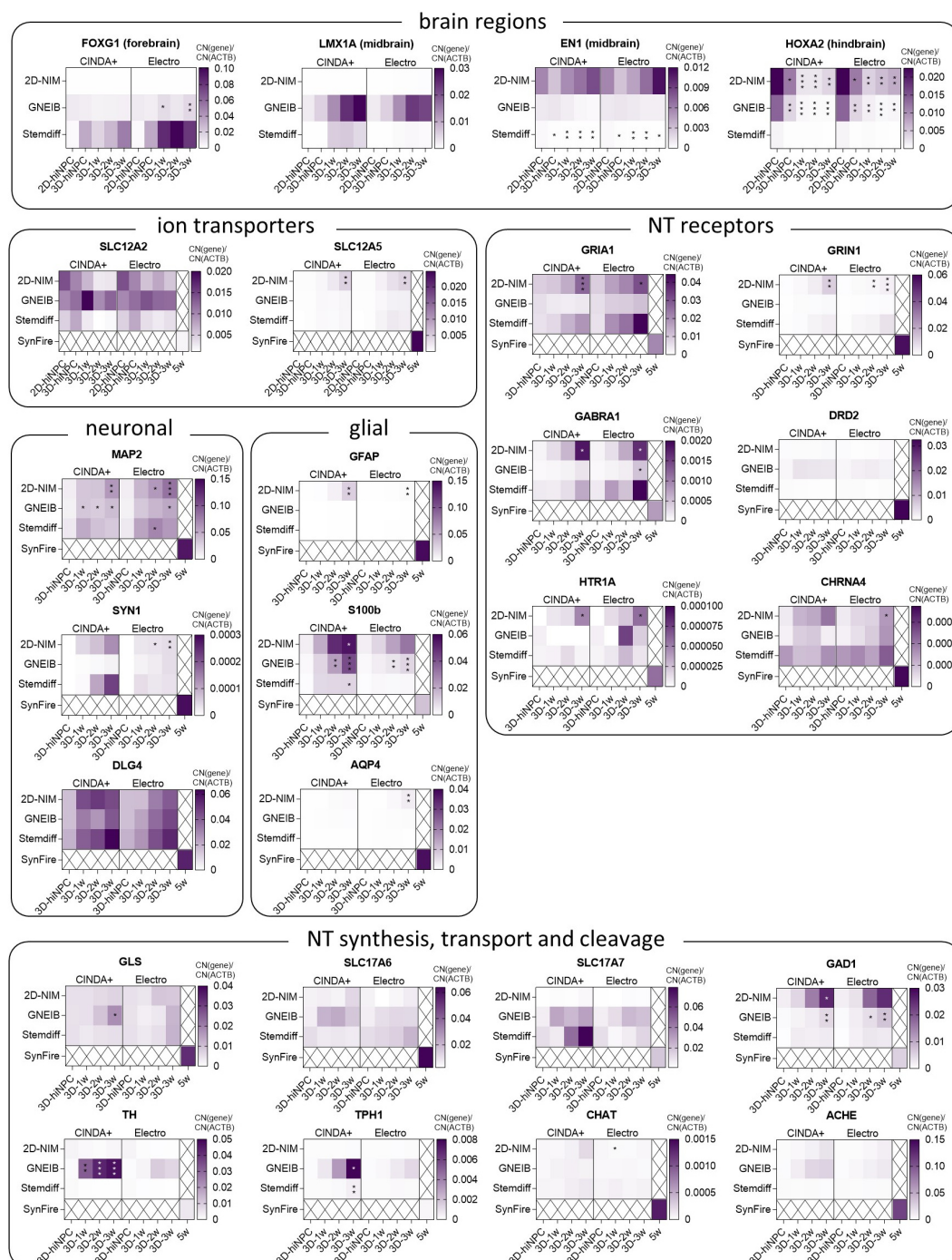


Figure 2. Expression profiles of genes distinguishing different brain regions (*FOXG1*, *LMX1A*, *EN1*, *HOXA2*), ion transporters defining the stage of the postnatal GABA shift (*SLC12A2*, *SLC12A5*), marker for neuronal (*MAP2*, *SYN1*, *DLG4*) and glial (*GFAP*, *S100B*, *AQP4*) cells, neurotransmitter (NT) receptors (*GRIA1*, *GRIN1*, *GABRA1*, *DRD2*, *HTR1A*, *CHRNA4*), NT synthesis enzymes (*GLS*, *GAD1*, *TH*, *TPH1*, *CHAT*), NT transporters (*SLC17A6*, *SLC17A7*), or NT cleavage enzymes (*ACHE*). Shown are the copy numbers (CN) of the genes normalized to CN of β -actin (*ACTB*). Data are represented as median of $n = 3$ –4 independent experiments with three technical replicates each (* $p \leq 0.05$, ** $p \leq 0.01$, *** $p \leq 0.001$). The p -values resulting from statistical analyses of the comparisons between undifferentiated hiNPCs (2D-hiNPC or 3D-hiNPC) and differentiated BrainSpheres (3D-1w to 3D-3w) and between the six different protocols are listed in Supplementary Table S4.

In addition to neurotransmitter receptors, synthesis and transport of neurotransmitters are also crucial for neural functioning. The enzyme glutaminase (*GLS*) is necessary for glutamate synthesis [81] and the encoding gene was already expressed in the undifferentiated BrainSpheres and increased significantly only in GNEIB-BrainSpheres during differentiation in CINDA+, whereas the gene for vesicular glutamate transporter 1 (*SLC17A7*) registered the highest expression levels in Stemdiff BrainSpheres after 2 and 3 weeks of differentiation in CINDA+; however, this was not statistically significant. The expression of vesicular glutamate transporter 2 (*SLC17A6*) did not strongly increase during differentiation. Glutamate decarboxylase 1 (*GAD1*), which catalyzes a critical step in GABA synthesis [82], registered the highest expression levels in BrainSpheres generated with the 2D-NIM protocol and the expression significantly increased during maturation. The highest expression levels of tyrosine hydroxylase (*TH*) and tryptophan hydroxylase 1 (*TPH1*) were found in GNEIB-BrainSpheres differentiated in CINDA+. The genes *CHAT* (choline acetyltransferase) and *ACHE* (acetylcholinesterase) were hardly expressed in all BrainSpheres but highly so in the SynFire cells. Additionally, *SLC17A7*, *GAD1*, *TH*, and *TPH1* registered higher expression levels in some BrainSpheres than in the 35-day differentiated SynFire cells.

3.3. Neural Induction and Differentiation Protocols Determine the Potential of BrainSpheres to Differentiate into Astrocytes and Dopaminergic Neurons

Immunofluorescence stainings of BrainSpheres differentiated for 3 weeks revealed their differentiation potentials into astrocytes (*S100B*) and dopaminergic neurons (*TH*). BrainSpheres neurally induced with the 2D-NIM protocol differentiated into an abundance of *S100B*-positive cells that formed a dense layer underneath the *TUBB3*-positive neurons, regardless of the differentiation medium used. In contrast, BrainSpheres derived from the other two neural induction protocols generated only a few or no cells of the astrocytic lineage (Figure 3A). Furthermore, BrainSpheres generated with the GNEIB protocol and differentiated in CINDA+ generated the most *TH*-positive dopaminergic neurons followed by BrainSpheres generated with the 2D-NIM protocol (CINDA+ and Electro) (Figure 3B). The other BrainSphere conditions showed no or only a few *TH*-positive neurons. Furthermore, the BrainSpheres had different sphere and neuron morphologies. Especially of note, GNEIB-BrainSpheres differentiated in Electro medium showed a more inhomogeneous distribution of neurons.

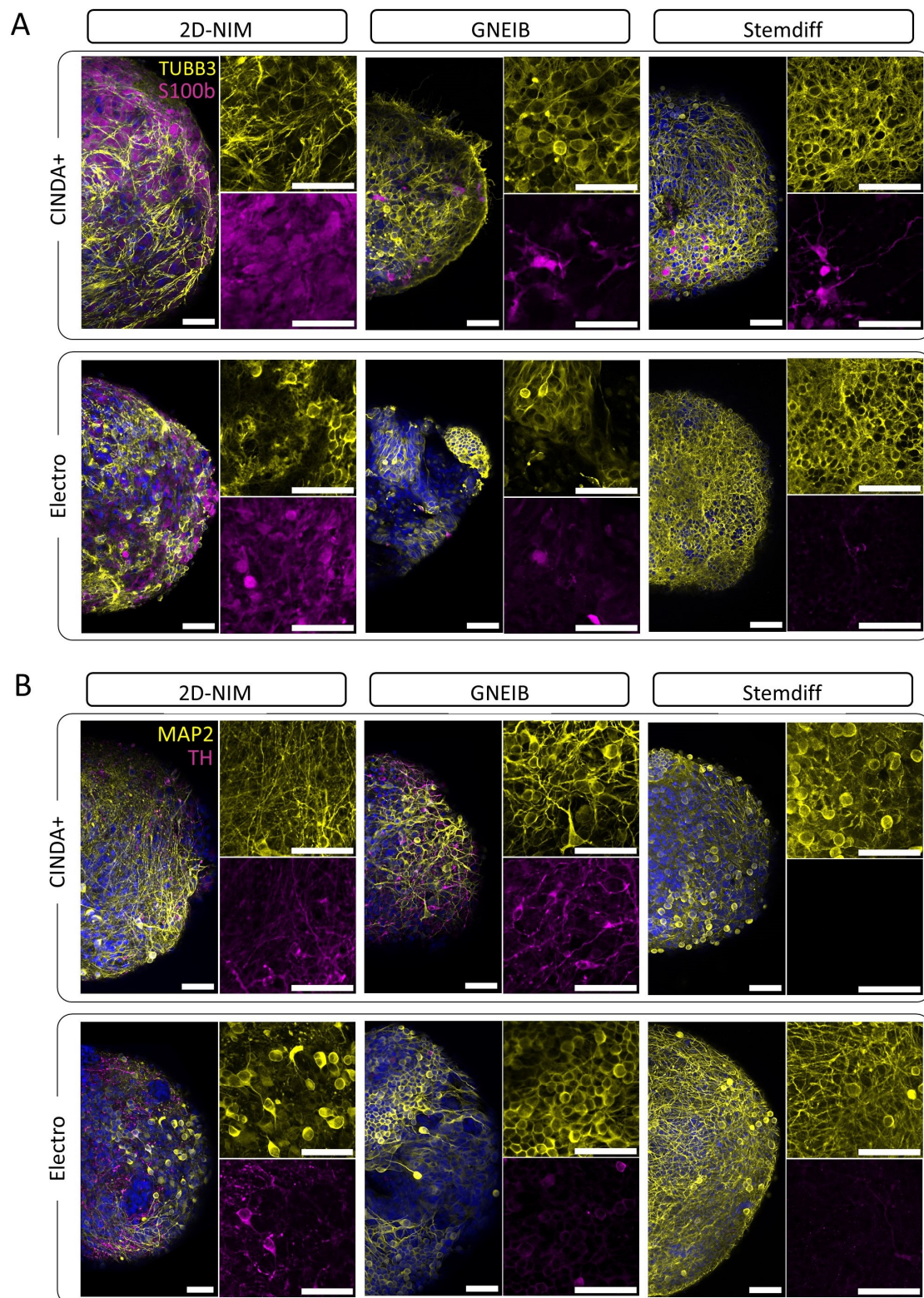


Figure 3. Immunocytochemical characterization of 3-week-differentiated BrainSpheres that were neurally induced with the 2D-NIM, GNEIB, or Stemdiff protocol before they were chopped to 250 μ m before being 3D differentiated in CINDA+ or Electro medium. The presence of (A) neurons (*TUBB3*, yellow) and the astrocytic lineage (*S100b*, magenta) or (B) neurons (*MAP2*, dendritic marker, yellow) and dopaminergic neurons (*TH*, magenta) were analyzed. Nuclei were counterstained with Hoechst 34580 (blue). Shown are representative images. Scale bar = 50 μ M.

3.4. Neural Induction and Differentiation Media Determine Neuronal Activity and Neural Network Function of BrainSpheres on MEAs

MEAs are powerful tools to evaluate the electrical activity of neuronal networks providing information on, e.g., the number of active electrodes, the rate of action potentials per electrode (weighted mean firing rate; wMFR), the clustering of spikes to bursts as a sign of neuronal maturation (burst frequency) and the neuronal network activity mirroring synchronous communication between different neurons within the neuronal network (network burst frequency). To evaluate and compare the functionality of the neural networks (NN), BrainSpheres were plated on MEAs either without or after 3D differentiation on a gyrical shaker for 1, 2, or 3 weeks, and the electrical activity was measured twice a week for 7 additional weeks. In general, the most active electrodes and the highest wMFR were observed after 3 weeks of 3D differentiation before plating BrainSpheres on the MEAs (Figure 4, Supplementary Figures S2–S4). Therefore, all of the following experiments were performed with this condition. The number of active electrodes is a valuable parameter as we observed that an inactive electrode does not necessarily indicate that neurons are not growing across the electrode; however, a non-electrically active cell may cover it (Supplementary Figure S5). The NN generated with the 2D-NIM induction protocol and 3D differentiated in CINDA+ medium showed the most active wells (83%) and electrodes (58%) with the highest wMFR of 6.86 Hz after 7 weeks on MEAs (Figure 4, Table 1). BrainSpheres derived from the GNEIB protocol differentiated in CINDA+ had the second most active wells (83%), electrodes (31%), and wMFR (6.30 Hz), but also had the highest variance with a standard error of mean (SEM) of 1.25 Hz. Both NN showed a similar mean burst frequency (2D-NIM: 0.31 Hz, GNEIB: 0.36 Hz) and an increasing activity over the course of 7 weeks on the MEAs. In contrast, NN derived from BrainSpheres either neurally induced with the 2D-NIM or GNEIB protocol and differentiated in Electro medium, or neurally induced with the Stemdiff protocol and differentiated in CINDA+ medium showed a decrease in the wMFR and burst frequency over the 7 weeks starting from 4 weeks on the MEAs. The NN derived from BrainSpheres neurally induced with the GNEIB protocol and differentiated in CINDA+ had the highest network burst frequency with 0.15 Hz. The percentages of spikes contributing to a network burst (network burst percentage) were similar for all conditions that generated network bursts after 7 weeks on MEA, but highest for the NN generated with the Stemdiff neural induction protocol and subsequent differentiation in Electro medium (48.02%, Table 1). In general, neural induction of hiPSCs using the 2D-NIM and GNEIB protocols followed by BrainSphere differentiation in CINDA+ for 3 weeks generated the most functional NNs with the most active electrodes and highest wMFR, burst frequencies and network burst frequencies, indicating that these protocols are favorable for the generation of mature NN from BrainSpheres.

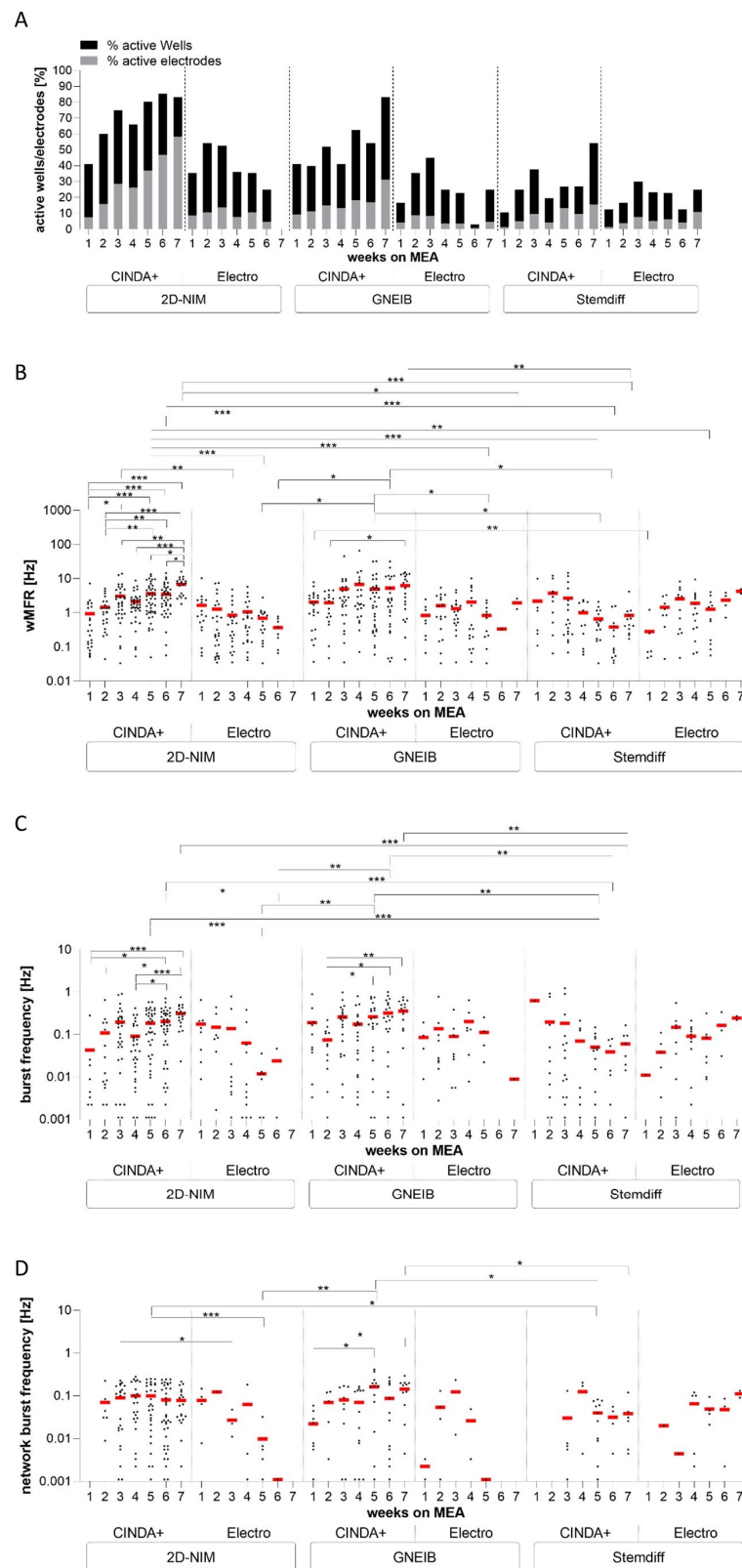


Figure 4. Comparison of electrical activity of 3-week 3D differentiated BrainSpheres for 7 weeks on microelectrode arrays (MEA). The neuronal functionality was measured twice per week and the parameters active wells and active electrodes (**A**), weighted mean firing rate (wMFR, (**B**)), burst frequency (**C**), and network burst frequency (**D**) were analyzed. Each dot represents the mean of one well containing eight electrodes and the black, grey (**A**), and red (**B–D**) bars represent the mean of all wells resulting from three independent MEA experiments each (* $p \leq 0.05$, ** $p \leq 0.01$, *** $p \leq 0.001$).

Table 1. Summary of MEA and spike sorting data of 3-week 3D differentiated BrainSpheres.

Mode	Parameter	2D-NIM		GNEIB		Stemdiff	
		CINDA+	Electro	CINDA+	Electro	CINDA+	Electro
General electrical activity after 7 weeks on MEA	Active Wells [%]	83	0	83	25	54	25
	Active electrodes [%]	58	0	31	5	16	11
	wMFR [Hz] (\pm SEM)	6.86 (± 0.82)	-	6.29 (± 1.25)	1.94 (± 0.65)	0.84 (± 0.29)	4.3 (± 0.63)
	mean burst frequency [Hz] (\pm SEM)	0.31 (± 0.04)	-	0.36 (± 0.06)	0.009 (± 0)	0.06 (± 0.02)	0.25 (± 0.03)
	mean network burst frequency [Hz] (\pm SEM)	0.08 (± 0.02)	-	0.15 (± 0.03)	-	0.04 (± 0.02)	0.11 (± 0.02)
	mean network burst percentage [%] (\pm SEM)	42.86 (± 5.04)	-	42.28 (± 6.32)	-	41.68 (± 14.39)	48.02 (± 3.13)
Glutamatergic response	units responding to 50 μ M glu with an increase (as % of unsorted units)	20	27	30	43	15	26
	mean fold change in responding units to 50 μ M glu with an increase (\pm SEM)	3.98 (± 1.12)	4.73 (± 2.28)	5.43 (± 2.18)	7.71 (± 2.23)	2.12 (± 0.42)	1.80 (± 0.20)
	units responding to 50 μ M glu with a decrease (as % of unsorted units)	57	54	37	27	77	52
	mean fold change in responding units to 50 μ M glu with a decrease (\pm SEM)	0.16 (± 0.03)	0.13 (± 0.06)	0.32 (± 0.05)	0.13 (± 0.05)	0.10 (± 0.03)	0.50 (± 0.06)
	units responding to 50 μ M glu and 50 μ M AP5/NBQX (as % of unsorted units)	9	12	16	40	15	26
	mean fold change in responding units to 50 μ M glu and 50 μ M AP5/NBQX (\pm SEM)	0.23 (± 0.08)	0.33 (± 0.18)	0.23 (± 0.05)	0.03 (± 0.01)	0.04 (± 0.02)	0.17 (± 0.07)
GABAergic response	units responding with an increase to 10 μ M bic (as % of unsorted units)	25	45	36	21	16	17
	mean fold change in responding units with an increase to 10 μ M bic (\pm SEM)	3.45 (± 0.60)	3.7 (± 0.85)	4.17 (± 0.99)	8.58 (± 6.48)	1.99 (± 0.20)	1.92 (± 0.2)
	units responding with a decrease to 10 μ M bic (as % of unsorted units)	46	29	35	48	59	33
	mean fold change in responding units with a decrease to 10 μ M bic (\pm SEM)	0.43 (± 0.02)	0.50 (± 0.07)	0.37 (± 0.04)	0.33 (± 0.08)	0.37 (± 0.04)	0.42 (± 0.09)
	units responding with an increase to 10 μ M ptx (as % of unsorted units)	28	62	30	27	28	45
	mean fold change in responding units with an increase to 10 μ M ptx (\pm SEM)	4.19 (± 1.81)	2.66 (± 0.36)	6.69 (± 2.05)	2.25 (± 0.35)	3.06 (± 0.89)	2.47 (± 0.59)
	units responding with a decrease to 10 μ M ptx (as % of unsorted units)	23	15	28	13	31	12
	mean fold change in responding units with a decrease to 10 μ M ptx (\pm SEM)	0.47 (± 0.04)	0.48 (± 0.11)	0.39 (± 0.04)	0.39 (± 0.07)	0.40 (± 0.08)	0.46 (± 0.07)
Dopaminergic response	units responding with an increase to 1 μ M halo (as % of unsorted units)	20	0	16	6	15	9
	mean fold change in responding units with an increase to 1 μ M halo (\pm SEM)	3.23 (± 0.53)	-	7.82 (± 1.88)	10.25 (± 0)	1.71 (± 0.26)	1.99 (± 0.44)
	units responding with a decrease to 1 μ M halo (as % of unsorted units)	57	85	65	89	73	47
	mean fold change in responding units with a decrease to 1 μ M halo (\pm SEM)	0.28 (± 0.02)	0.15 (± 0.05)	0.21 (± 0.02)	0.13 (± 0.04)	0.29 (± 0.04)	0.32 (± 0.06)
Serotonergic response	units responding with a decrease to 5 μ M bsp (as % of unsorted units)	26	88	52	29	63	38
	mean fold change in responding units to 5 μ M bsp (\pm SEM)	0.44 (± 0.02)	0.26 (± 0.07)	0.26 (± 0.03)	0.39 (± 0.10)	0.41 (± 0.06)	0.59 (± 0.05)
	units responding with an increase to 5 μ M bsp (as % of unsorted units)	31	13	23	14	8	15
	mean fold change in responding units with an increase to 5 μ M bsp (\pm SEM)	2.49 (± 0.24)	1.51 (± 0.26)	2.67 (± 0.47)	2.56 (± 0)	2.56 (± 1.17)	1.63 (± 0.06)

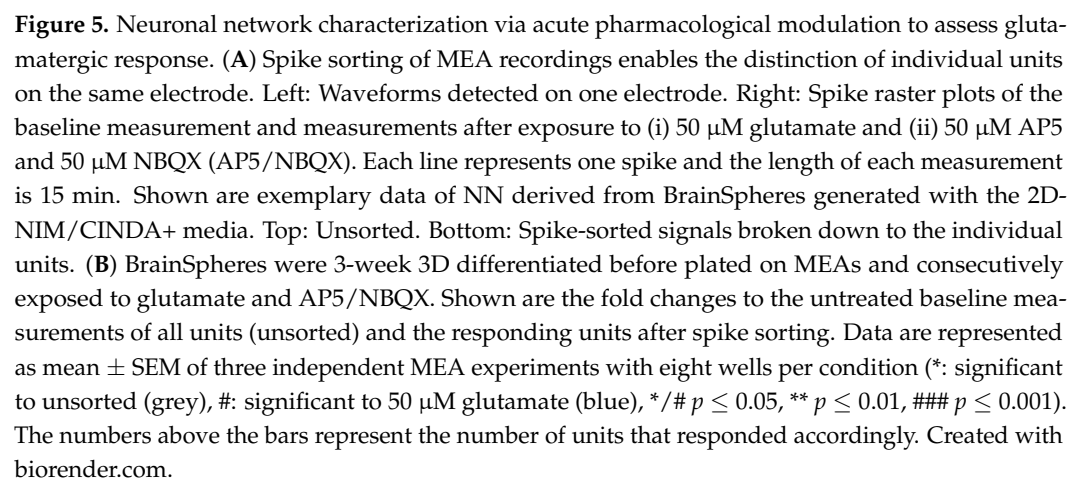
Table 1. Cont.

Mode	Parameter	2D-NIM		GNEIB		Stemdiff	
		CINDA+	Electro	CINDA+	Electro	CINDA+	Electro
Cholinergic response	units responding with a decrease to 5 μ M crb (as % of unsorted units)	22	33	30	33	11	13
	mean fold change in responding units with decreased wMFR to 5 μ M crb (\pm SEM)	0.47 (\pm 0.03)	0.10 (\pm0)	0.48 (\pm 0.04)	0.44 (\pm 0.05)	0.71 (\pm 0.03)	0.72 (\pm 0.01)
	units responding with an increase to 5 μ M crb (as % of unsorted units)	34	0	22	0	25	7
	mean fold change in responding units with increased wMFR to 5 μ M crb (\pm SEM)	2.14 (\pm 0.10)	-	2.11 (\pm 0.49)	-	2.35 (\pm0.33)	1.47 (\pm 0)

The culture conditions with the strongest responses to each treatment are highlighted in bold. wMFR, weighted mean firing rate; glu, glutamate; bic, bicuculline; ptb, picrotoxin; halo, haloperidol; bsp, buspirone hydrochloride; crb, carbaryl.

3.5. Neural Induction and Differentiation Media Determine BrainSpheres' Neuronal Subtype Differentiation

For characterization of the NN not only the general electrical activity is important but also the responses to specific pharmacological modulators which highly depends on the occurrence of different neuronal subtypes. Therefore, we addressed the presence of glutamatergic, GABAergic, dopaminergic, serotonergic, and cholinergic neurons in 3-week 3D differentiated BrainSpheres after 2 to 6 weeks on MEAs. Quantification of neuronal units' wMFR responding to pharmacological modulation was possible due to spike sorting with the software Offline Sorter (Figure 5A). This allowed the identification of specific responses of individual neurons within the integrated neuronal activities of single electrodes. Neural units reacting to the modulation with a change of at least $\pm 25\%$ in comparison to the baseline measurement were defined as responding (glutamatergic, GABAergic, dopaminergic, serotonergic, or cholinergic) units. The percentage of responding units, their fold-change to the untreated baseline measurement (colored), and the comparison to the fold-changes of the unsorted (grey) units were analyzed.



First, the glutamatergic response was measured by applying the neurotransmitter glutamate followed by the application of the two glutamate receptor antagonists AP5 (antagonizes NMDA receptors) and NBQX (blocks AMPA receptors) [83]. It is expected that glutamate increases the electrical activity as an excitatory neurotransmitter. Without spike sorting, glutamate-dependent increased electrical activity was only measured in NN derived from BrainSpheres differentiated with GNEIB/Electro media, whereas BrainSpheres derived from the other five protocols showed no clear positive response or even a decreased wMFR upon acute glutamate exposure (Figure 5B). After spike sorting, glutamate-responsive units from BrainSpheres produced with the 2D-NIM and GNEIB protocols produced the highest response to glutamate. Half of glutamate-responding neuronal units in 2D-NIM/CINDA+ and GNEIB/CINDA+ BrainSpheres also responded with a decline in the wMFR to subsequent glutamate receptor inhibition by AP5/NBQX. In contrast, wMFRs of all neuronal glutamate-responsive units from BrainSpheres produced with Stemdiff/CINDA+ and Stemdiff/Electro were inhibited by AP5/NBQX. However, the latter two protocols per se produced very few responding units with minor changes in the wMFR amplitude (Figure 5B, Table 1). In addition to the fold changes shown in Figure 5B, the raw values of the wMFR are presented in the supplementary material (Supplementary Figure S6).

To characterize the GABAergic response, the GABA receptor antagonists bicuculline and picrotoxin were applied. Bicuculline binds to GABA_A receptors, whereas picrotoxin targets GABA_A and GABA_C receptors [84,85]. It is expected that upon treatment with the GABA receptors antagonists, mature GABAergic neurons post the GABA switch respond with an increased activity, e.g., wMFR, while immature GABAergic neurons before the GABA switch respond with a decreased firing. Without spike sorting, none of the BrainSphere cultures derived from any of the six protocols produced changes in NN activity upon GABA receptor antagonism (Figure 6). After spike sorting, neuronal units of all BrainSphere protocols were identified that contained increased or decreased wMFR upon bicuculline and picrotoxin treatment; yet, most of the responses showed considerable variation in magnitude of responses and thus lacked statistical significance. Only NN from BrainSpheres generated with 2D-NIM/CINDA+, 2D-NIM/Electro, Stemdiff/CINDA+ and Stemdiff/Electro significantly increased the wMFR upon bicuculline treatment, with NN from 2D-NIM/Electro generated BrainSpheres being the least sensitive with the earliest response at 10 μ M. In response to picrotoxin only the BrainSpheres generated with 2D-NIM/CINDA+ (5 μ M) significantly induced the wMFR of NN. Neuronal units responding with an increased wMFR towards the GABA receptor antagonists ranged between 16% (Stemdiff/CINDA+) and 62% (2D-NIM/Electro) of all active neurons. However, the 2D-NIM/CINDA+ media generated the highest absolute number of positively responding neuronal units (Figure 6). In addition to the units reacting to the GABA antagonists with increased wMFR, some units responded with a decreased activity. This is in line with the low gene expression of *SLC12A5*, which encodes for the ion receptor KCC2 (Figure 2). KCC2 increases its expression after the postnatal GABA switch from excitatory to inhibitory GABAergic neurons. Therefore, without spike sorting, the pre-mature and the more mature GABA receptor containing units compensated each other and resulted in no visible response to the antagonists. BrainSpheres generated with 2D-NIM/CINDA+ media produced the highest absolute numbers of neuronal units responding with an inhibitory and decreased wMFR towards the GABA receptor antagonists. Regarding the Stemdiff neural induction differentiated in CINDA+, in relation to all firing units, 31% (picrotoxin) to 59% (bicuculline) of BrainSphere-derived units responded with a decrease in activity towards GABA receptor antagonism (Figure 6). The raw values of the wMFR after exposure to bicuculline and picrotoxin are shown in Supplementary Figures S7 and S8.

Inhibitory dopaminergic D2 receptors were addressed by applying the antagonist haloperidol to the cultures, which should increase the wMFR [86,87]. Without spike sorting, haloperidol enhanced the wMFR in GNEIB/CINDA+ (Figure 7). After spike sorting, all protocols derived units responding with an increased and decreased wMFR

after exposure to haloperidol, except for BrainSpheres from 2D-NIM/Electro media, which only resulted in units with decreased activity. Haloperidol decreased the wMFR of neuronal units in NN generated with 2D-NIM/CINDA+ and GNEIB/CINDA+ BrainSpheres most effectively with significant wMFR reductions at 1 μ M haloperidol in 57% and 65% of all neuronal units, respectively. In addition, NN generated with the GNEIB/CINDA+ protocol showed the strongest increased activity at 1 μ M. However, most BrainSphere neurons differentiated with 2D-NIM/CINDA+ media seem to express inhibitory D2 receptors as 20% of all recorded neuronal units responded to 1 μ M haloperidol with an increased activity (Figure 7). Rising haloperidol concentrations decrease the number of units responding with an increase in wMFR, while the number of units reacting with decreased wMFR enhances under the treatment. The raw wMFR values of the unsorted and the responding units after exposure to haloperidol are shown in Supplementary Figure S9 and Table 1.

Buspirone, which agonizes the inhibitory serotonin 5-HT_{1A} receptor, was applied to investigate the presence of serotonergic responses in the NN [88]. Without spike sorting, buspirone did not cause significant changes in neuronal activity in any of the BrainSpheres. However, after sorting, it decreased the wMFR of NN generated with 2D-NIM/CINDA+ and GNEIB/CINDA+ BrainSpheres most effectively with significant wMFR reductions at 5 μ M buspirone. In BrainSpheres produced using these protocols, 26% and 52% of all neuronal units responded to the compound with a decreased activity, respectively. BrainSpheres differentiated in Electro medium overall produced fewer serotonergic neurons than CINDA+ differentiated spheres with all neural induction protocols. However, with 88% of all units, neurons derived from BrainSphere generated with 2D-NIM/Electro media exhibited the highest percentage of neurons responding to buspirone with a decreased activity (Figure 8, Table 1). All protocols generated lower percentages of units responding with an increased wMFR to buspirone compared to a decreased activity except for BrainSpheres generated with 2D-NIM/CINDA+, where 31% of units responded with an increase. In addition to the fold change, the raw values of the wMFR are shown in Supplementary Figure S10.

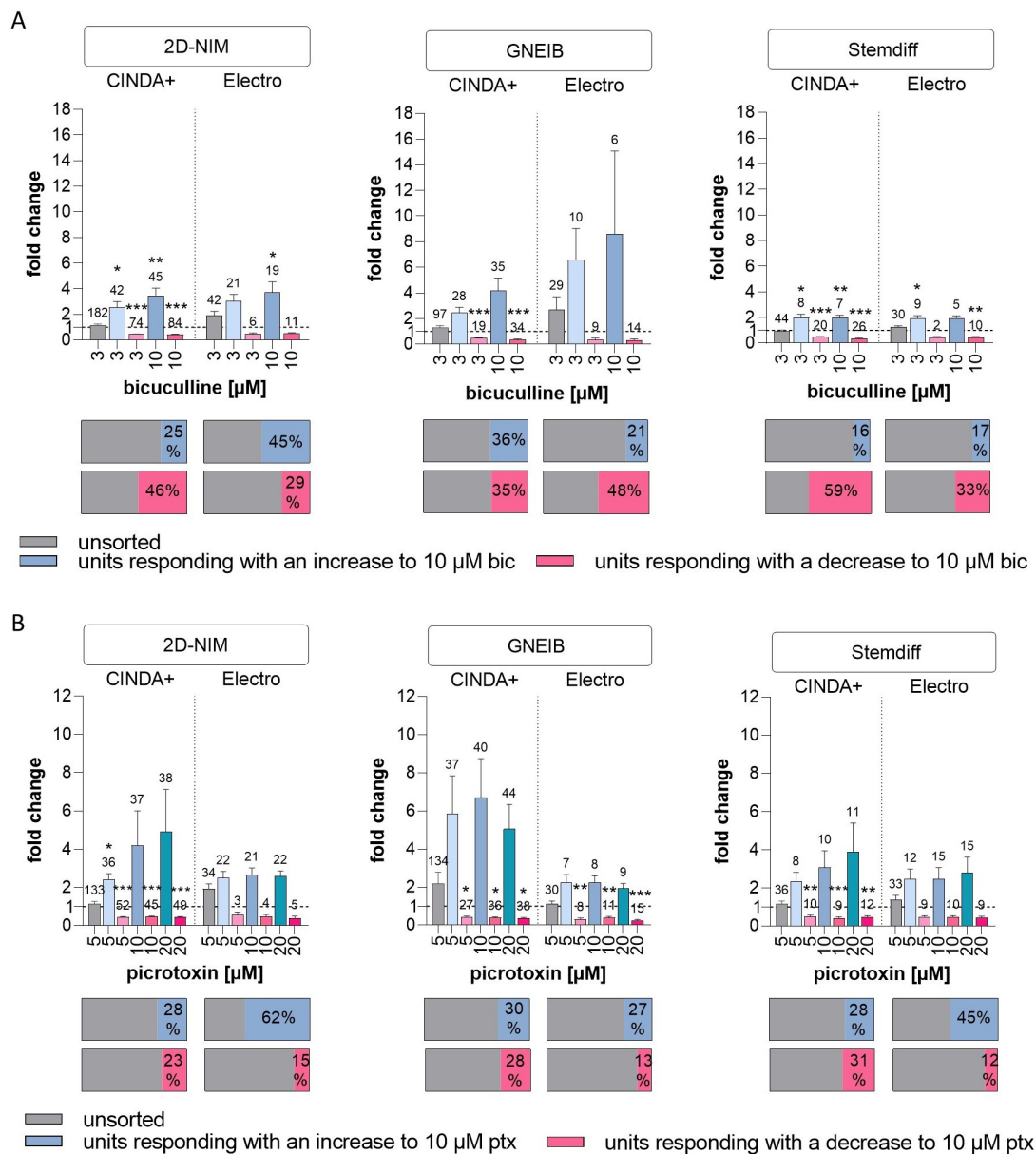


Figure 6. Neuronal network characterization via acute pharmacological modulation to assess GABAergic response. BrainSpheres were 3-week 3D differentiated before plated on MEA and consecutively exposed to (A) bicuculline (bic) or (B) picrotoxin (ptx). Shown are the fold changes to the untreated baseline measurements of all units (unsorted) and the sorted responding units (colored). Data are represented as mean \pm SEM of three independent MEA experiments with eight wells per condition (*: significant to unsorted, * $p \leq 0.05$, ** $p \leq 0.01$, *** $p \leq 0.001$). The numbers above the bars represent the number of units that responded accordingly.

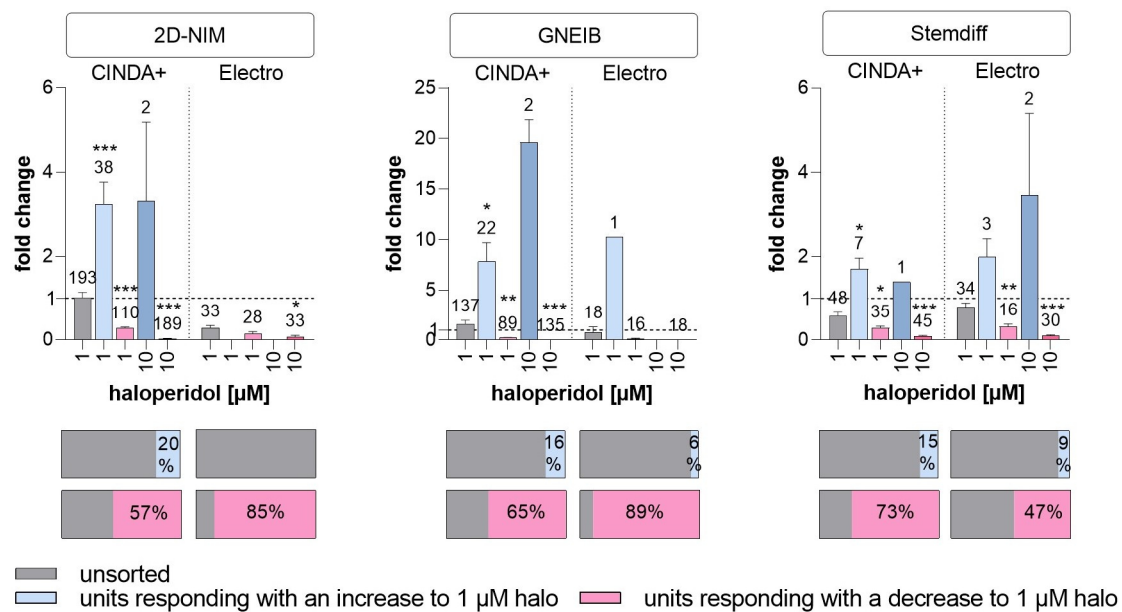


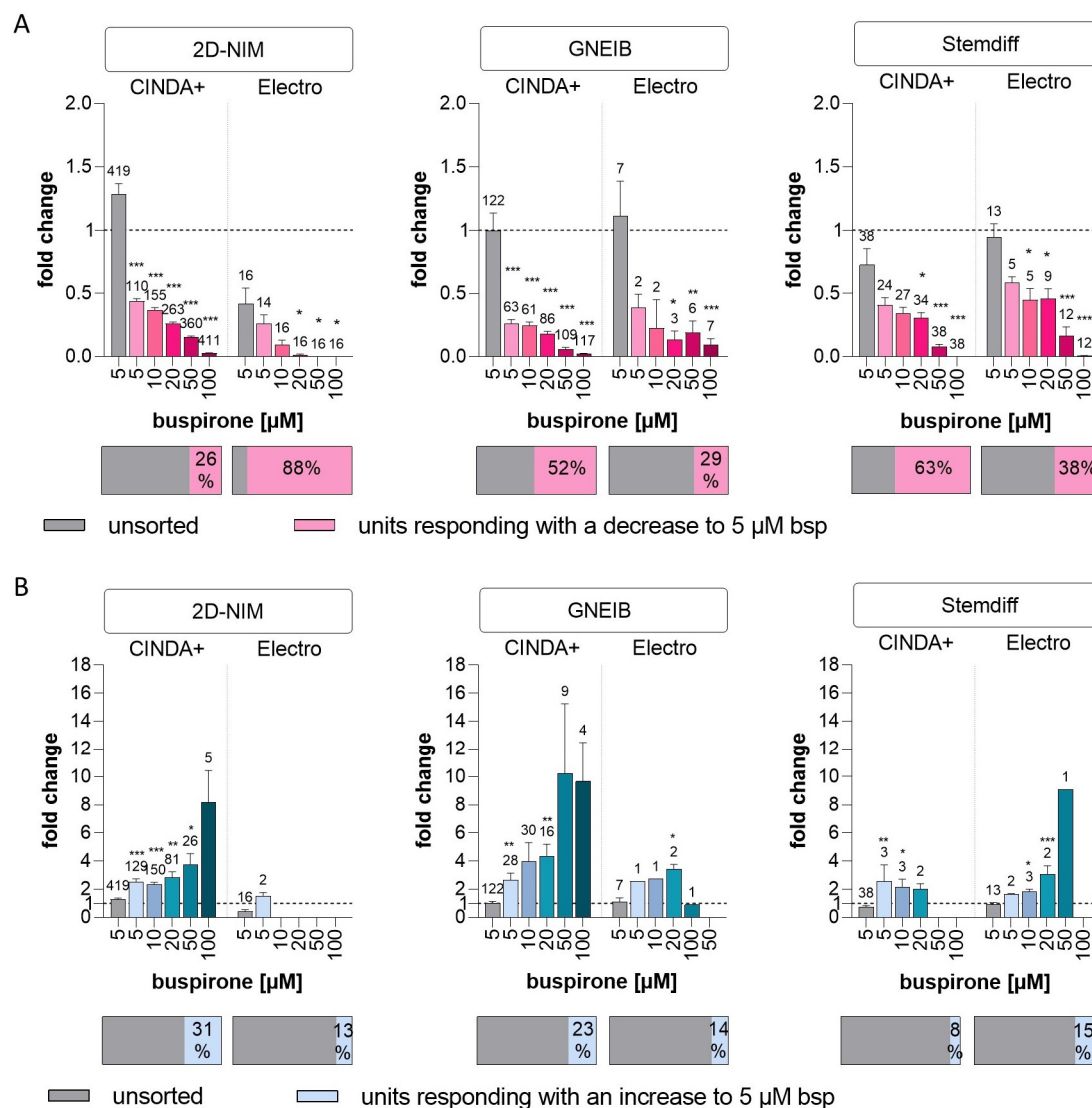
Figure 7. Neuronal network characterization via acute pharmacological modulation to assess dopaminergic responses. BrainSpheres were 3-week 3D differentiated before plated on MEAs and exposed to haloperidol (halo). Shown are the fold changes to the untreated baseline measurement of all units (unsorted, grey) and the responding units after sorting (colored). Data are represented as mean \pm SEM of three independent MEA experiments with eight wells per condition (*: significant to unsorted, * $p \leq 0.05$, ** $p \leq 0.01$, *** $p \leq 0.001$). The numbers above the bars represent the total number of units that respond accordingly.

Cholinergic signal transduction was modulated with the insecticide carbaryl, which inhibits the enzyme acetylcholinesterase (AChE) [89] and binds to nicotinic acetylcholine receptors (nAChR) [90]. While AChE blockage increases, binding to nAChR decreases cholinergic neuronal activity [91]. Without spike sorting, no significant change in wMFR was observed after exposure to 5 μ M carbaryl (Figure 9). After spike sorting, carbaryl decreased the wMFR in NN generated with 2D-NIM/CINDA+ and GNEIB/CINDA+ BrainSpheres most effectively with significant wMFR reductions at 5 μ M carbaryl and 22–30% of all neuronal units responding to the compound. Both Stemdiff/CINDA+ and Stemdiff/Electro protocols produced BrainSpheres with the lowest number of (11 and 13%, respectively) and least sensitive (50 and 10 μ M carbaryl, respectively) responding neuronal units (Figure 9A, Table 1). NN derived from BrainSpheres generated with the 2D-NIM/CINDA+ and GNEIB/CINDA+ protocols also exhibited the highest absolute number of neuronal units reacting with the highest increased activity in wMFR to carbaryl (Figure 9B). In addition, 2D-NIM BrainSpheres were overall the most sensitive to wMFR modulation in both directions, significantly responding at 5 μ M (Figure 9). Interestingly, rising carbaryl concentrations increased the number of neuronal units that responded with a decrease in wMFR, while the number of units reacting with enhanced wMFR decreased under the treatment. In addition to the fold change, the raw values of the wMFR are shown in Supplementary Figure S11.

3.6. Set-Up of a New NAM for Acute Neurotoxicity Testing Using MEAs and Spike Sorting, the Human Multi-Neurotransmitter Receptor (hMNR) Assay

With the well-characterized BrainSpheres, we propose the set-up of a test method as a NAM for acute neurotoxicity testing using MEAs and spike sorting. While general MEA activity can provide an overview of the general changes in NN activity, its resolution is not high enough to understand individual neuronal responses. Spike sorting in combination with neuronal subtype-specific model compounds seems to be a valuable solution for neuronal subtype identification in BrainSpheres on MEAs. To study if this system is

suitable for acute neurotoxicity assessment, we set up a standard operating procedure combining neuronal unit identification with consecutive compound testing (Figure 10A). With this setup, as a proof-of-concept, we measured the effects of two compounds, i.e., TMT, which enhances glutamate release, and emamectin, a GABA-receptor agonist [92,93], on glutamatergic and GABAergic neuronal units in differentiated BrainSpheres (Figure 10B). These compounds are the first substances of a chemical training set for the test method and were selected from the mode-of-action analyses in Masjosthusmann et al.'s work 2018 [22]. BrainSpheres generated with the 2D-NIM/CINDA+ protocol were used due to the resulting higher number of active electrodes and lower variance in comparison to the other protocols. Neural units reacting to neurotransmitter and antagonist with a change of at least $\pm 25\%$ in comparison to the baseline measurement were defined as responding glutamatergic or GABAergic units (Supplementary Figure S12A).



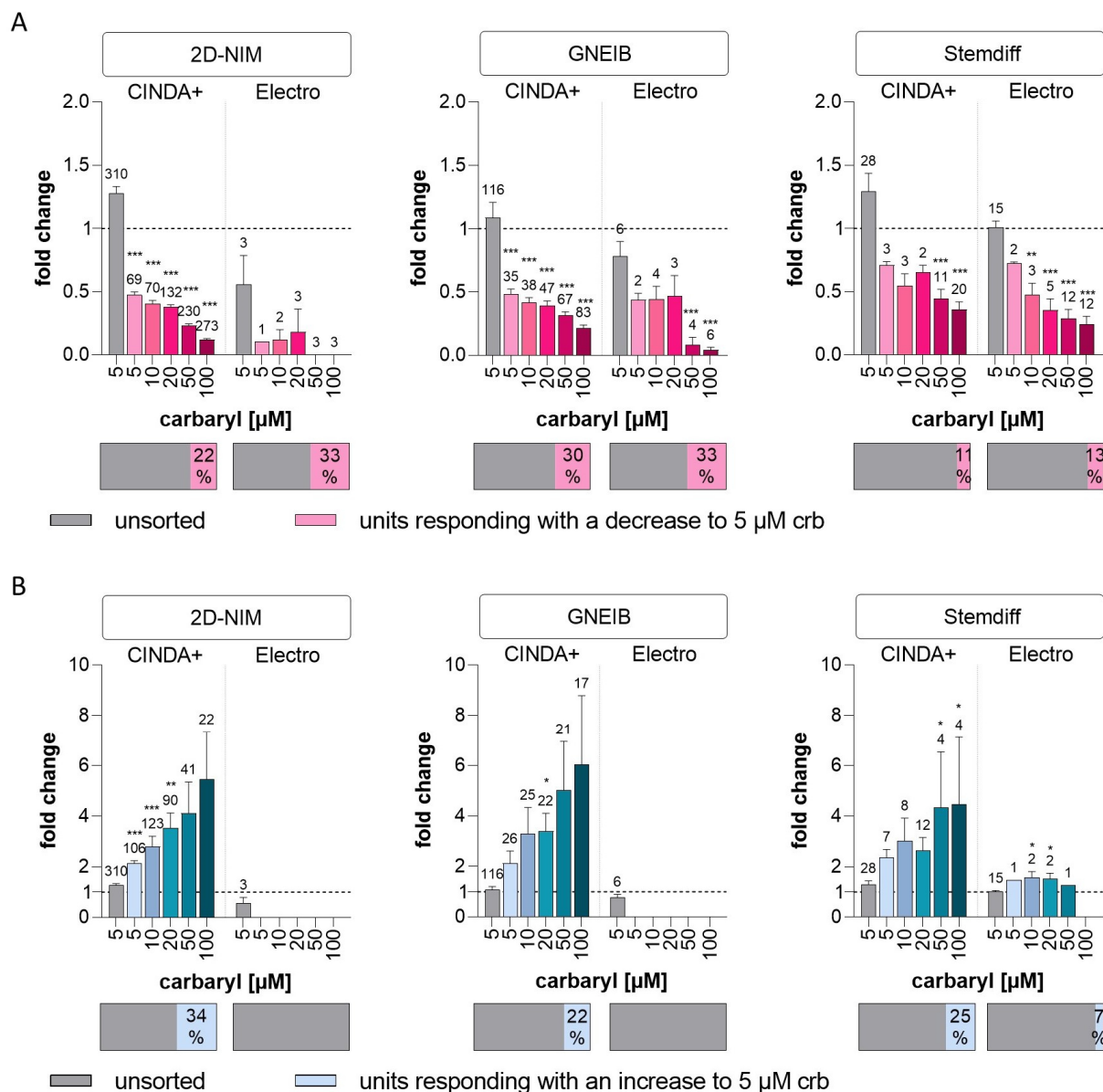
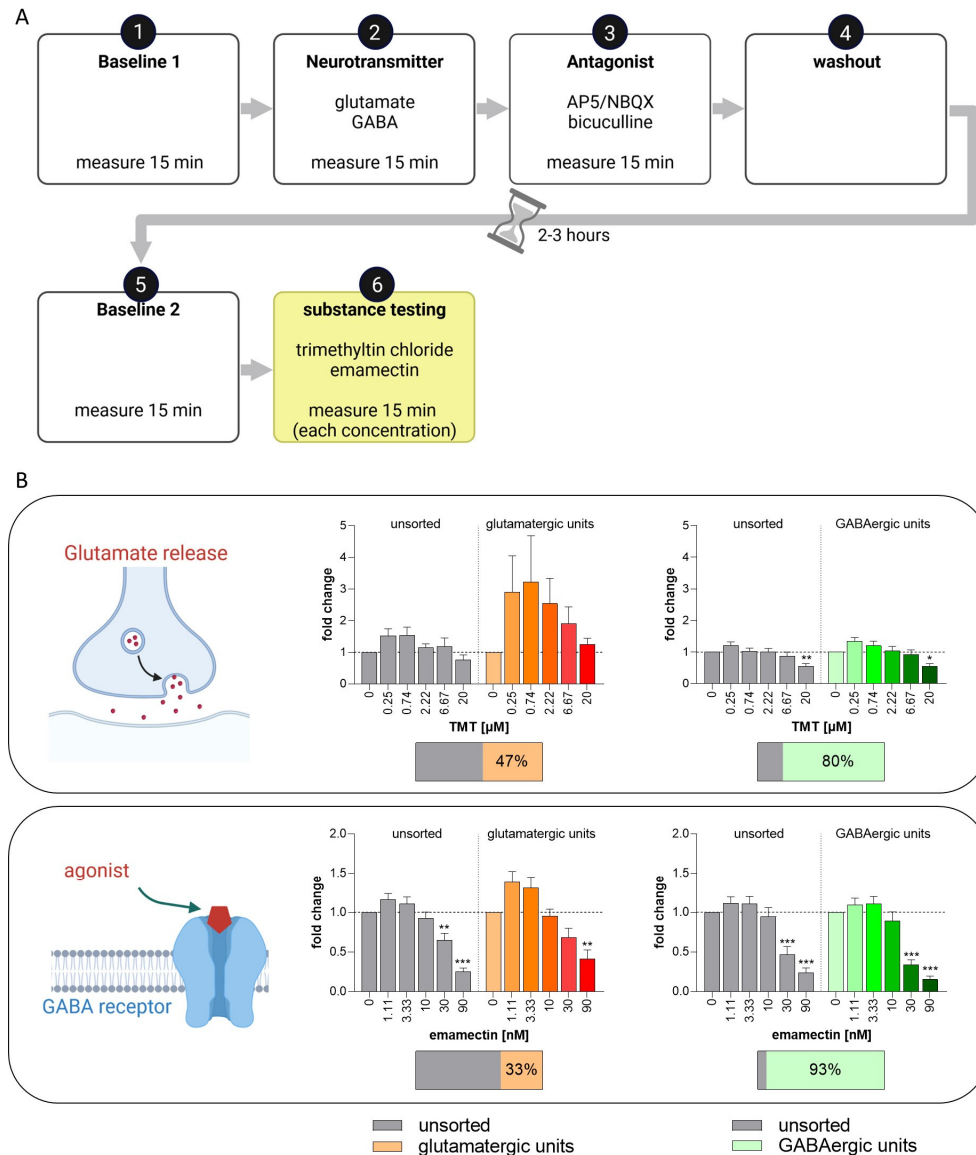


Figure 9. Neuronal network characterization via acute pharmacological modulation to assess cholinergic responses. BrainSpheres were 3-week 3D differentiated before plated on MEA and exposed to carbaryl (crb). (A) Decreased and (B) increased responses after exposure to crb were detected. Shown are the fold changes to the untreated baseline measurement of all units (unsorted, grey) and the responding units after sorting (colored). Data are represented as mean \pm SEM of three independent MEA experiments with eight wells per condition (*: significant to unsorted, * $p \leq 0.05$, ** $p \leq 0.01$, *** $p \leq 0.001$). The numbers above the bars represent the number of units that respond accordingly.

After exposure to TMT and respective spike sorting, TMT caused an increased wMFR in glutamatergic units in the sub-micromolar range with a decreasing effect starting at 2.22 μ M TMT (Figure 10B). This expected increasing effect in wMFR due to enhanced glutamate release by TMT [93] was not observed in the unsorted and GABAergic units. Additionally, the highest TMT concentration (20 μ M) also decreased the wMFR of the unsorted and the GABAergic units. Treatment with the GABA_A and GABA_C receptor agonist emamectin [92] decreased the wMFR of all unsorted and sorted units in a concentration-dependent manner. However, the effect was strongest in sorted GABAergic units with a reduction to a fold change of 0.34 at 30 nM (Figure 10B). That the emamectin effects can even be observed in the unsorted units can be explained by the high abundance of

GABAergic units in these particular BrainSpheres, with 80 to 95% of the units reacting to GABA and bicuculline.

Unspecific cytotoxic effects of the two test compounds were excluded by measuring LDH release (Supplementary Figure S12B).



4. Discussion

In recent years, industry, regulators, and academia have agreed on the need for NAMs to test chemicals with higher throughput, lower costs, and better predictivity for humans [13,15]. For this task, human cell systems designed for a specific purpose should preferably be used and combined with other in vitro and in silico methods to cover multiple endpoints [94,95]. Human in vitro models for acute neurotoxicity testing that examine neurotransmission mainly refer to effects of total neural networks by measuring spike-, burst-, and network-related parameters. While these parameters provide valuable information, they do not necessarily account for a large variety of neurotoxic MoA [31,37,96–100]. The low granularity of the classical MEA evaluation by studying integrated signals over single electrodes is accompanied by a high dependence on the NN composition. As hiPSC-derived NN are especially fairly variable [43], high uncertainty might be involved in using spontaneously formed NN from hiPSC for in vitro neurotoxicity studies. Therefore, we characterized mixed culture BrainSpheres [57] for setting up a multiplexed test method for acute neurotoxicity evaluation with the goal of adding multiple neurotoxicity MoA to the established parameters measured with MEAs. First, we characterized six different BrainSphere models resulting from three adherent neural induction protocols combined with two different media for subsequent differentiation. All neural induction protocols showed low variability and high efficiency by resulting in at least 97% cells expressing the neural progenitor marker *NESTIN* [45,74]. However, hiNPC generated with the 2D-NIM, yet not with the GNEIB protocol, contained less *KI-67* positive cells on day 21 of neural induction. This might be the consequence of asymmetrical cell division into proliferative and non-proliferative daughter cells [101]. *PAX6* controls various processes regarding the neuroectodermal fate in a concentration-dependent manner and, if absent, leads to asymmetric cell division and thus to neurogenesis [75,102,103]. Hence, the low *PAX6* expression in 2D-NIM hiNPCs could explain the decrease in proliferating cells and indicate a more developed state in comparison to the other two protocols.

After the successful neural induction, hiNPCs were frozen in liquid nitrogen. This allows each subsequent experiment to be performed with the same hiNPC passage number, reduces variability and saves time and money. We confirmed that this additional step does not alter the expression of *NESTIN* and *KI-67*.

Gene expression data at various differentiation times showed that BrainSpheres produced in different media differ in genes referring to distinct brain regions, synapse formation, astrocyte differentiation, receptors, and neuronal subtypes. Interestingly, the neural induction media influence gene expression more strongly than the differentiation media. Moreover, gene expression comparison to the SynFire neural cells, which are cell ratio-controlled, pre-differentiated excitatory and inhibitory neurons and astrocytes forming functional and highly synchronous neural networks over 35 days in culture, revealed that the BrainSpheres are still fairly immature after 3 weeks of differentiation (e.g., comparing *MAP2*, *SYN1*, *DLG4*, *AQP4* expression). This is supported by the low expression of the K^+ - Cl^- -co-transporter (*KCC2*, *SLC12A5*) we observed in BrainSpheres compared to the SynFire cells. The increase in *KCC2* expression together with the decrease in expression of the Na^+ - K^+ - $2Cl^-$ -co-transporter (*NKCC1*, *SLC21A2*) initiates the postnatal switch from excitatory to inhibitory GABA signaling [78]. The presence of mature and immature GABAergic neurons was also supported by the MEA measurements after exposure to the GABA antagonists bicuculline and picrotoxin, which resulted in both increases and decreases in wMFR. We observed very low expression of genes encoding for serotonin receptor (*HTR1A*), choline receptor (*CHRNA4*), and choline synthesis enzyme (*CHAT*); however, the MEA analysis revealed functional receptors. Previous studies showed that some neuronal subtype-specific markers were only expressed in mature neurons, which can take up to 16 weeks to achieve with hiPSC-derived NN [49,104]. Therefore, such gene expression data in mixed cultures have to be regarded with caution as gene expression measured is an integration of cellular expression and cell abundance in the cultures. Hence,

protein analyses using immunocytochemistry combined with functional studies, e.g., using MEAs, are needed for proper test system characterization.

Immunocytochemical stainings for different neuronal and astrocytic markers revealed different potentials of the distinct neural induction/differentiation protocols for differentiation into *S100B*-positive cells of the astrocyte lineage, with the 2D-NIM/CINDA+ and GNEIB/CINDA+ protocols being the most effective, while GNEIB/Electro and Stemdiff/Electro BrainSpheres only differentiated into very few or no *S100B* positive cells. These data were supported by the gene expression analyses. Astrocytes are essential for NN maturation and function since they play an important role in synaptogenesis, neuronal survival and outgrowth, phagocytosis, and NT uptake from the synaptic cleft [105,106]. However, spatiotemporal astrocyte marker expression has to be considered when analyzing astrocytes in vitro. Data from human in vivo investigations reveal that GFAP, a marker most commonly used in in vitro studies, should not be used as a general and sole astrocytic marker [80]. Therefore, immunocytochemical analyses supported by qPCR results using a panel of astrocytic lineage markers (e.g., GFAP, *S100B*, and AQP4) seem reasonable. Astrocyte presence is also important concerning the effects of chemicals, as neurons and astrocytes might react differently to toxic substances [107–109]. Moreover, astrocytes might be the mediators of neuronal toxicity [110,111] or even neuroprotective [112,113]. Hence, astrocytes' presence in mixed co-cultures is thought to enhance the applicability domain compared to pure cultures.

Not only do astrocytes and neurons respond differently to certain chemicals, but toxic effects on individual neuronal subtypes are also frequent causes of neurotoxicity [22,59,114]. Prominent examples are the pesticide rotenone, which acts specifically on dopaminergic neurons [115], or the acetylcholinesterase inhibitor parathion targeting cholinergic neurons [116]. In that regard, it might be of interest to generate fit-for-purpose BrainSpheres enabling the study of distinct neuronal subtypes depending on the scientific or regulatory question. Here, for example, ICC stainings revealed that BrainSpheres generated with the 2D-NIM (both differentiation media) or the GNEIB/CINDA+ protocols generated the highest numbers of *TH*-positive dopaminergic neurons, while in Stemdiff BrainSpheres, they were much fewer. However, besides cell type-specific marker expression, for a physiologically relevant neural test systems, the formation of a functional neuronal network and adequate responses to model compounds have to be demonstrated.

In addition to the mRNA and protein expression data, BrainSpheres were characterized for their performance on MEAs. Similar to the expression analyses, the applied induction and differentiation protocols determined the BrainSphere's activities on the MEAs. BrainSpheres induced in 2D-NIM and GNEIB media differentiated in CINDA+ showed the most active electrodes, the highest wMFRs, and the highest burst frequencies. The wMFR and bursting behavior depend on various factors, predominantly the presence of astrocytes and the ratio of excitatory to inhibitory neurons [31,32,34]. According to the expression data, these two protocols express the highest levels of the astrocytic lineage marker *S100B*. Hence, astrocyte presence might be responsible for the abundant firing activity of these BrainSpheres. In contrast to BrainSpheres neurally induced with the 2D-NIM and GNEIB media, BrainSpheres generated with Stemdiff medium displayed higher electrical activity when subsequently differentiated with the Electro medium. This indicates that the combination of neural induction and differentiation media highly influences NN functionality. To date, only the influence of different neural induction protocols or various differentiation conditions have been analyzed; however, a combination of both has not been examined so far [53,56,117,118].

While spike, burst, and network parameters provide important information on general network function, their level of granularity is not particularly high. Therefore, we applied the method of spike sorting to the MEA data [119]. Spike sorting enables the identification of single active neuronal 'units' within the signal of one MEA electrode using curve progression analyses. These units can be evaluated individually and hence quantified across multiple electrodes. We challenged the NN with model compounds targeting

glutamate, GABA, dopamine, serotonin and nACh receptors, as well as acetylcholine esterase to identify different neuronal subtype signalling.

Without spike sorting, glutamate did not significantly increase wMFR signals on MEAs. After spike sorting, neuronal units were identified that increased or decreased their activity. Neuronal response of increased activity was expected for an excitatory neurotransmitter. The opposite effect might be attributed to presynaptic metabotropic glutamate receptors (mGluR) that can act as a negative feedback loop and inhibit glutamate release [120–124] possibly in early developing neurons as a counterpart to immature excitatory GABAergic neurons [125]. Such opposite glutamate effects were observed earlier in other neural in vitro models [32,56].

Spike sorting of MEA activity after exposure to the GABA receptor antagonists bicuculline and picrotoxin revealed that all established NN contain both excitatory and inhibitory GABAergic neurons. This was not visible in the whole electrode recordings, since the two opposite reactions cancel each other out. Excitatory action of GABA is a physiological response before the GABA switch [78]. Hence, all NN also contain immature neurons that precede the GABA switch in addition to inhibitory GABAergic neurons. GABA_A and GABA_C receptors seem to mature differently as picrotoxin, which binds to GABA_A and GABA_C receptors [85], increases the increase/decrease ratios of neuronal units compared to bicuculline, which only interacts with GABA_A receptors [84], suggesting higher maturation states of GABA_A receptors. The gene expression for the two ion transporters *NKCC1* and *KCC2*, which marks the switch from pre-mature excitatory to mature inhibitory GABAergic neurons, supports these functional data.

All BrainSphere models also responded to haloperidol, buspirone, and carbaryl, by directly or indirectly acting on baseline transmission of dopaminergic, serotonergic, and cholinergic receptors, respectively. Overall, differentiation in CINDA+ seems to produce higher numbers of these neuronal subtypes compared to differentiation in Electro medium, possibly due to the higher number of active electrodes these CINDA+ BrainSpheres produce in total. Haloperidol and buspirone bind to dopaminergic and serotonergic receptors, respectively. Haloperidol is an antagonist for the inhibitory dopamine D2 receptor [86,87]; thus, we observe an increasing effect of this drug on the wMFR of neuronal units. Interestingly, all NN contained more units responding with a decreased electrical activity, which is in line with the results of previous in vitro studies that observed only inhibitory reactions after acute treatment [126–130]. Görtz and colleagues suggested that this effect may occur due to a direct blockage of ion channels [126], which explains the rising number of units responding with decreased activity at the highest haloperidol concentration. Buspirone's primary MoA is binding to presynaptic inhibitory 5-HT_{1A} receptors as an agonist [88], thus producing an inhibitory action as we observe for most units within the NN in vitro. Carbaryl inhibits the enzyme acetylcholine esterase, thereby leading to an accumulation of choline in the synaptic cleft [89]. However, the second MoA of this insecticide is binding to nACh receptors [90,91,131]. Interestingly, previous in vitro studies only showed decreased electrical activity after exposure to carbaryl [132–135]. In this study, all NN exhibit neuronal units that respond in both directions, thereby covering both MoA. This might be due to an abundance of nACh receptor expression independent of the cholinergic synapse on GABAergic neurons [136].

Finally, we used the BrainSpheres in combination with spike sorting for setting up a test method, the human multi-neurotransmitter receptor (hMNR) assay for acute neurotoxicity testing that aims at enlightening the neurotoxic MoA for unknown test compounds in the future. As a small proof-of-concept study, we exemplified the use of this test method by studying the effects of the compounds TMT and emamectin with previously-described MoA for glutamatergic and GABAergic neurons. The hMNR confirmed the two MoA of the test compounds: (1) the enhanced glutamatergic activity by TMT-induced glutamate release [93]; (2) the reduced GABAergic neurotransmission caused by the GABA_A and GABA_C agonist emamectin [92]. Long-term exposure studies showed that TMT also affects synaptic vesicle fusion and recycling [137,138]. This could be a possible explanation for

the wMFR reduction at higher TMT concentrations. Although the effect of emamectin was strongest in the GABAergic units, it was also observed in the unsorted and glutamatergic units. This is probably due to the high abundance of GABAergic units in these particular BrainSpheres, with 80 to 95% of the units reacting to GABA and bicuculline.

As this is a rather restricted case study, respective proof-of-concept studies for the applicability of the hMNR assay also have to be devised for the other neuronal subtypes. However, this small setup already demonstrates a high sensitivity for the two model compounds by detecting the compounds' effects in the nM range. In the end, we envision a test method setup that identifies all five different neurotransmitter receptors in the first identification phase followed by compound exposure with unknown substances. Spike sorting will identify compounds' MoA through this effort and hence deliver a neurotoxic MoA profile for each tested compound. The advantage of this system is that one analyzes neuronal units in a mixed neuronal/glia network context; however, information on the individual neuronal level is assessed.

Additional applications for acute substance testing in hiPSC-based BrainSpheres combined with spike sorting analyses are disease modeling and drug development. The pathophysiology of several neurological disorders such as Rett syndrome, autism spectrum disorders, schizophrenia, Down syndrome, and fragile X involves, amongst others, a disrupted GABA switch during brain development leading to an inhibitory/excitatory imbalance [139–142]. Moreover, they are suited as Parkinson's disease model and for untargeted disease modeling, revealing, to date, unstudied disease mechanisms and gene–environment interactions [62,143]. Another application can be envisioned in drug development for safety or efficacy evaluation, e.g., for seizure liability assessment [68,144–146]. In addition, interference of compounds with neurotransmitter systems might also be an indication of their developmental neurotoxicity (DNT) potential. Therefore, in the future, this test method might also be a valuable addition to the current DNT in vitro testing battery [147] as test methods for substances' effects on neuronal subtypes were identified as one gap in current NAM-based DNT evaluation [148].

5. Summary and Conclusions

Taken together, we generated six different BrainSphere models by combining 2D neural induction protocols with 3D differentiation methods and showed distinguished neural differentiation patterns, although all protocols were based on dual SMAD inhibition. This emphasizes the importance of thorough characterization of each cell model and highlights the difficulties in comparing studies that use different media compositions. The different gene and protein expressions regarding neural subtype and receptor expression were also reflected in the functionality of the BrainSpheres measured on MEAs. To overcome the mixed signals of different neuronal subtypes, we applied spike sorting, which allowed us to distinguish between glutamatergic, GABAergic, dopaminergic, serotonergic, and cholinergic responses. Finally, this led us to introduce the hMNR assay which has possible applications beyond acute neurotoxicity for DNT testing, including in the field of disease modeling and for safety and efficacy evaluation in drug development.

Supplementary Materials: The following supporting information can be downloaded at: <https://www.mdpi.com/article/10.3390/cells12091270/s1>, Figure S1: Immunocytochemistry staining of human induced neural progenitor cells (hiNPCs); Figure S2: Comparison of electrical activity of BrainSpheres (without 3D differentiation) for 7 weeks on microelectrode arrays (MEA); Figure S3: Comparison of electrical activity of 1 week 3D differentiated BrainSpheres for 7 weeks on MEA; Figure S4: Comparison of electrical activity of 2 weeks 3D differentiated BrainSpheres for 7 weeks on MEA; Figure S5: Spike raster plots (SRP) and microscopy images of 3 weeks 3D differentiated BrainSpheres differentiated for further 3 weeks on MEA; Figure S6: Modification of electrical activity by acute pharmacological modulation with glutamate and ap5/nbqx; Figure S7: Modification of electrical activity by acute pharmacological modulation with bicuculline; Figure S8: Modification of electrical activity by acute pharmacological modulation with picrotoxin; Figure S9: Modification of electrical activity by acute pharmacological modulation with haloperidol; Figure S10: Modification of electrical activity by acute pharmacological modulation with buspirone; Figure S11: Modification of electrical activity by acute pharmacological modulation with carbaryl; Figure S12: Specification of glutamatergic and GABAergic units for acute neurotoxicity testing; Table S1: Coatings used for neural differentiation of BrainSpheres generated with different neural induction protocols; Table S2: Information about used compounds and their solvents; Table S3: Primer sequences; Table S4: *p*-values resulting from statistical analyses of the gene expression data.

Author Contributions: Conceptualization, J.H., K.K. and E.F.; methodology, J.H. and E.F.; software, J.H. and A.D.; formal analysis, J.H., N.H. and A.D.; investigation, J.H., N.H., K.B. and G.B.; resources, E.F.; writing—original draft preparation, J.H.; writing—review and editing, J.H., K.K. and E.F.; visualization, J.H.; supervision, K.K. and E.F.; project administration, E.F.; funding acquisition, E.F. All authors have read and agreed to the published version of the manuscript.

Funding: This research was funded by the project CERST (Center for Alternatives to Animal Testing) of the Ministry for innovation, science and research of the State of North-Rhine Westphalia, Germany (file number 233-1.08.03.03-121972), the Danish Environmental Protection Agency (EPA) under the grant number MST-66-00205, and the Horizon Europe project PARC (Grant Agreement No 101057014). This work was supported by the European Union's Horizon 2020 Research and Innovation Program, under the Grant Agreement number 825759 of the ENDpoiNTs project.

Institutional Review Board Statement: Not applicable.

Informed Consent Statement: Not applicable.

Data Availability Statement: The data presented in this study are available upon request from the corresponding author.

Acknowledgments: We would like to acknowledge the Center for Advanced Imaging (CAi) at Heinrich Heine University Düsseldorf for providing access to the Zeiss LSM 710 (DFG-INST 208/539-1 FUGG). Figures 1A,C, 5A and 10 were created with BioRender.com.

Conflicts of Interest: K.B., A.D., K.K. and E.F. are shareholders of the company DNTOX which provides DNT-IVB assay services. The authors J.H., N.H. and G.B. declare no conflicts of interest. The funders had no role in the design of the study; in the collection, analyses, or interpretation of data; in the writing of the manuscript; or in the decision to publish the results.

References

1. OECD. *OECD Guideline for the Testing of Chemicals 419 Delayed Neurotoxicity of Organophosphorus Substances: 28-Day Repeated Dose Study*; OECD: Paris, France, 1995; pp. 1–7.
2. OECD. *OECD Guideline for the Testing of Chemicals 418 Delayed Neurotoxicity of Organophosphorus Substances Following Acute Exposure*; OECD: Paris, France, 1995; pp. 1–8.
3. OECD. *OECD guideline for the testing of Chemicals Test No. 424: Neurotoxicity Study in Rodents*. In *OECD Guideline for the Testing of Chemicals*; Section 4; OECD: Paris, France, 1997; pp. 1–15. ISBN 9789264071025.
4. Buschmann, J. The OECD Guidelines for the Testing of Chemicals and Pesticides. *Methods Mol. Biol.* **2013**, *947*, 37–56. [CrossRef]
5. Bal-Price, A.K.; Hogberg, H.T.; Buzanska, L.; Coecke, S. Relevance of in Vitro Neurotoxicity Testing for Regulatory Requirements: Challenges to Be Considered. *Neurotoxicol. Teratol.* **2010**, *32*, 36–41. [CrossRef] [PubMed]
6. Somel, M.; Liu, X.; Tang, L.; Yan, Z.; Hu, H.; Guo, S.; Jiang, X.; Zhang, X.; Xu, G.; Xie, G.; et al. MicroRNA-Driven Developmental Remodeling in the Brain Distinguishes Humans from Other Primates. *PLoS Biol.* **2011**, *9*, e1001214. [CrossRef] [PubMed]

7. Pollen, A.A.; Nowakowski, T.J.; Chen, J.; Retallack, H.; Sandoval-Espinosa, C.; Nicholas, C.R.; Shuga, J.; Liu, S.J.; Oldham, M.C.; Diaz, A.; et al. Molecular Identity of Human Outer Radial Glia during Cortical Development. *Cell* **2015**, *163*, 55–67. [\[CrossRef\]](#)
8. Waring, M.J.; Arrowsmith, J.; Leach, A.R.; Leeson, P.D.; Mandrell, S.; Owen, R.M.; Paireau, G.; Pennie, W.D.; Pickett, S.D.; Wang, J.; et al. An Analysis of the Attrition of Drug Candidates from Four Major Pharmaceutical Companies. *Nat. Rev. Drug Discov.* **2015**, *14*, 475–486. [\[CrossRef\]](#) [\[PubMed\]](#)
9. Mohs, R.C.; Greig, N.H. Drug Discovery and Development: Role of Basic Biological Research. *Alzheimer's Dement. Transl. Res. Clin. Interv.* **2017**, *3*, 651–657. [\[CrossRef\]](#) [\[PubMed\]](#)
10. Toutain, P.-L.; Ferran, A.; Bousquet-Melou, A. Species Differences in Pharmacokinetics and Pharmacodynamics. In *Handbook of Experimental Pharmacology*; Springer: Cham, Switzerland, 2010; pp. 19–48.
11. Marshall, L.J.; Bailey, J.; Cassotta, M.; Herrmann, K.; Pistollato, F. Poor Translatability of Biomedical Research Using Animals—A Narrative Review. *Altern. Lab. Anim.* **2023**, *51*, 102–135. [\[CrossRef\]](#) [\[PubMed\]](#)
12. Wang, Z.; Walker, G.W.; Muir, D.C.G.; Nagatani-Yoshida, K. Toward a Global Understanding of Chemical Pollution: A First Comprehensive Analysis of National and Regional Chemical Inventories. *Environ. Sci. Technol.* **2020**, *54*, 2575–2584. [\[CrossRef\]](#) [\[PubMed\]](#)
13. Pallocca, G.; Moné, M.J.; Kamp, H.; Luijten, M.; Van de Water, B.; Leist, M. Next-Generation Risk Assessment of Chemicals—Rolling out a Human-Centric Testing Strategy to Drive 3R Implementation: The RISK-HUNT3R Project Perspective. *ALTEX* **2022**, *39*, 419–426. [\[CrossRef\]](#)
14. Dent, M.P.; Vaillancourt, E.; Thomas, R.S.; Carmichael, P.L.; Ouedraogo, G.; Kojima, H.; Barroso, J.; Ansell, J.; Barton-Maclaren, T.S.; Bennekou, S.H.; et al. Paving the Way for Application of next Generation Risk Assessment to Safety Decision-Making for Cosmetic Ingredients. *Regul. Toxicol. Pharmacol.* **2021**, *125*, 105026. [\[CrossRef\]](#)
15. Krewski, D.; Andersen, M.E.; Tyshenko, M.G.; Krishnan, K.; Hartung, T.; Boekelheide, K.; Wambaugh, J.F.; Jones, D.; Whelan, M.; Thomas, R.; et al. *Toxicity Testing in the 21st Century: Progress in the Past Decade and Future Perspectives*; Springer Berlin/Heidelberg: Heidelberg, Germany, 2020; Volume 94, ISBN 0123456789.
16. Kavlock, R.J.; Bahaduri, T.; Barton-Maclaren, T.S.; Gwinn, M.R.; Rasenberg, M.; Thomas, R.S. Accelerating the Pace of Chemical Risk Assessment. *Chem. Res. Toxicol.* **2018**, *31*, 287–290. [\[CrossRef\]](#) [\[PubMed\]](#)
17. Vinken, M.; Benfenati, E.; Busquet, F.; Castell, J.; Clevert, D.A.; de Kok, T.M.; Dirven, H.; Fritsche, E.; Geris, L.; Gozalbes, R.; et al. Safer Chemicals Using Less Animals: Kick-off of the European ONTOX Project. *Toxicology* **2021**, *458*, 152846. [\[CrossRef\]](#) [\[PubMed\]](#)
18. Carmichael, P.L.; Baltazar, M.T.; Cable, S.; Cochrane, S.; Dent, M.; Li, H.; Middleton, A.; Muller, I.; Reynolds, G.; Westmoreland, C.; et al. Ready for Regulatory Use: NAMs and NGRA for Chemical Safety Assurance. *ALTEX* **2022**, *39*, 359–366. [\[CrossRef\]](#) [\[PubMed\]](#)
19. Maertens, A.; Golden, E.; Luechtefeld, T.H.; Hoffmann, S.; Tsaïoun, K.; Hartung, T. Probabilistic Risk Assessment—The Keystone for the Future of Toxicology. *ALTEX* **2022**, *39*, 3–29. [\[CrossRef\]](#)
20. Mahony, C.; Ashton, R.S.; Birk, B.; Boobis, A.R.; Cull, T.; Daston, G.P.; Ewart, L.; Knudsen, T.B.; Manou, I.; Maurer-Stroh, S.; et al. New Ideas for Non-Animal Approaches to Predict Repeated-Dose Systemic Toxicity: Report from an EPAA Blue Sky Workshop. *Regul. Toxicol. Pharmacol.* **2020**, *114*, 104668. [\[CrossRef\]](#) [\[PubMed\]](#)
21. van der Stel, W.; Carta, G.; Eakins, J.; Delp, J.; Suci, I.; Forsby, A.; Cedié-Ulloa, A.; Attoff, K.; Troger, F.; Kamp, H.; et al. New Approach Methods (NAMs) Supporting Read-Across: Two Neurotoxicity AOP-Based IATA Case Studies. *ALTEX* **2021**, *38*, 615–635. [\[CrossRef\]](#) [\[PubMed\]](#)
22. Masjosthusmann, S.; Barenys, M.; El-Gamal, M.; Geerts, L.; Gerosa, L.; Gorreja, A.; Kühne, B.; Marchetti, N.; Tigges, J.; Viviani, B.; et al. Literature Review and Appraisal on Alternative Neurotoxicity Testing Methods. *EFSA Support. Publ.* **2018**, *15*, 1410E. [\[CrossRef\]](#)
23. Harry, G.J.; Tiffany-Castiglioni, E. Evaluation of Neurotoxic Potential by Use of in Vitro Systems. *Expert Opin. Drug Metab. Toxicol.* **2005**, *1*, 701–713. [\[CrossRef\]](#)
24. Lisek, M.; Boczek, T.; Stragierowicz, J.; Wawrzyniak, J.; Guo, F.; Klimczak, M.; Kilanowicz, A.; Zylinska, L. Hexachloronaphthalene (HxCN) Impairs the Dopamine Pathway in an in Vitro Model of PC12 Cells. *Chemosphere* **2022**, *287*, 132284. [\[CrossRef\]](#)
25. Schultz, L.; Zurich, M.G.; Culot, M.; da Costa, A.; Landry, C.; Bellwon, P.; Kristl, T.; Hörmann, K.; Ruzek, S.; Aiche, S.; et al. Evaluation of Drug-Induced Neurotoxicity Based on Metabolomics, Proteomics and Electrical Activity Measurements in Complementary CNS in Vitro Models. *Toxicol. Vitro* **2015**, *30*, 138–165. [\[CrossRef\]](#) [\[PubMed\]](#)
26. Hausherr, V.; van Thriel, C.; Krug, A.; Leist, M.; Schöbel, N. Impairment of Glutamate Signaling in Mouse Central Nervous System Neurons in Vitro by Tri-Ortho-Cresyl Phosphate at Noncytotoxic Concentrations. *Toxicol. Sci.* **2014**, *142*, 274–284. [\[CrossRef\]](#) [\[PubMed\]](#)
27. Loser, D.; Schaefer, J.; Danker, T.; Möller, C.; Brüll, M.; Suci, I.; Ückert, A.K.; Klima, S.; Leist, M.; Kraushaar, U. Human Neuronal Signaling and Communication Assays to Assess Functional Neurotoxicity. *Arch. Toxicol.* **2021**, *95*, 229–252. [\[CrossRef\]](#) [\[PubMed\]](#)
28. Kosnik, M.B.; Strickland, J.D.; Marvel, S.W.; Wallis, D.J.; Wallace, K.; Richard, A.M.; Reif, D.M.; Shafer, T.J. Concentration–Response Evaluation of ToxCast Compounds for Multivariate Activity Patterns of Neural Network Function. *Arch. Toxicol.* **2020**, *94*, 469–484. [\[CrossRef\]](#) [\[PubMed\]](#)
29. Johnstone, A.F.M.; Gross, G.W.; Weiss, D.G.; Schroeder, O.H.-U.; Gramowski, A.; Shafer, T.J. Microelectrode Arrays: A Physiologically Based Neurotoxicity Testing Platform for the 21st Century. *Neurotoxicology* **2010**, *31*, 331–350. [\[CrossRef\]](#) [\[PubMed\]](#)

30. Vassallo, A.; Chiappalone, M.; De Camargos Lopes, R.; Scelfo, B.; Novellino, A.; Defranchi, E.; Palosaari, T.; Weisschu, T.; Ramirez, T.; Martinoia, S.; et al. A Multi-Laboratory Evaluation of Microelectrode Array-Based Measurements of Neural Network Activity for Acute Neurotoxicity Testing. *Neurotoxicology* **2017**, *60*, 280–292. [\[CrossRef\]](#)
31. Saavedra, L.; Wallace, K.; Freudenrich, T.F.; Mall, M.; Mundy, W.R.; Davila, J.; Shafer, T.J.; Wernig, M.; Haag, D. Comparison of Acute Effects of Neurotoxic Compounds on Network Activity in Human and Rodent Neural Cultures. *Toxicol. Sci.* **2021**, *180*, 295–312. [\[CrossRef\]](#) [\[PubMed\]](#)
32. Tukker, A.M.; De Groot, M.W.G.D.M.; Wijnolts, F.M.J.; Kasteel, E.E.J.J.; Hondebrink, L.; Westerink, R.H.S. Is the Time Right for in Vitro Neurotoxicity Testing Using Human iPSC-Derived Neurons? *ALTEX* **2016**, *33*, 261–271. [\[CrossRef\]](#) [\[PubMed\]](#)
33. Tukker, A.M.; van Kleef, R.G.D.M.; Wijnolts, F.M.J.; de Groot, A.; Westerink, R.H.S. Towards Animal-Free Neurotoxicity Screening: Applicability of HiPSC-Derived Neuronal Models for in Vitro Seizure Liability Assessment. *ALTEX* **2019**, *37*, 121–135. [\[CrossRef\]](#) [\[PubMed\]](#)
34. Tukker, A.M.; Wijnolts, F.M.J.J.; de Groot, A.; Westerink, R.H.S. Human iPSC-Derived Neuronal Models for in Vitro Neurotoxicity Assessment. *Neurotoxicology* **2018**, *67*, 215–225. [\[CrossRef\]](#)
35. Mack, C.M.; Lin, B.J.; Turner, J.D.; Johnstone, A.F.M.; Burgoon, L.D.; Shafer, T.J. Burst and Principal Components Analyses of MEA Data for 16 Chemicals Describe at Least Three Effects Classes. *Neurotoxicology* **2014**, *40*, 75–85. [\[CrossRef\]](#)
36. Brown, J.P.; Hall, D.; Frank, C.L.; Wallace, K.; Mundy, W.R.; Shafer, T.J. Editor's Highlight: Evaluation of a Microelectrode Array-Based Assay for Neural Network Ontogeny Using Training Set Chemicals. *Toxicol. Sci.* **2016**, *154*, 126–139. [\[CrossRef\]](#)
37. Tukker, A.M.; Wijnolts, F.M.J.; de Groot, A.; Westerink, R.H.S. Applicability of HiPSC-Derived Neuronal Cocultures and Rodent Primary Cortical Cultures for In Vitro Seizure Liability Assessment. *Toxicol. Sci.* **2020**, *178*, 71–87. [\[CrossRef\]](#) [\[PubMed\]](#)
38. Balestrino, R.; Schapira, A.H.V. Parkinson Disease. *Eur. J. Neurol.* **2020**, *27*, 27–42. [\[CrossRef\]](#) [\[PubMed\]](#)
39. Nopoulos, P.C. Huntington Disease: A Single-Gene Degenerative Disorder of the Striatum. *Dialogues Clin. Neurosci.* **2016**, *18*, 91–98. [\[CrossRef\]](#) [\[PubMed\]](#)
40. Takahashi, K.; Yamanaka, S. Induction of Pluripotent Stem Cells from Mouse Embryonic and Adult Fibroblast Cultures by Defined Factors. *Cell* **2006**, *126*, 663–676. [\[CrossRef\]](#)
41. Takahashi, K.; Tanabe, K.; Ohnuki, M.; Narita, M.; Ichisaka, T.; Tomoda, K.; Yamanaka, S. Induction of Pluripotent Stem Cells from Adult Human Fibroblasts by Defined Factors. *Cell* **2007**, *131*, 861–872. [\[CrossRef\]](#) [\[PubMed\]](#)
42. Shi, Y.; Inoue, H.; Wu, J.C.; Yamanaka, S. Induced Pluripotent Stem Cell Technology: A Decade of Progress. *Nat. Rev. Drug Discov.* **2017**, *16*, 115–130. [\[CrossRef\]](#)
43. Galiakberova, A.A.; Dashinimaev, E.B. Neural Stem Cells and Methods for Their Generation From Induced Pluripotent Stem Cells in Vitro. *Front. Cell Dev. Biol.* **2020**, *8*, 815. [\[CrossRef\]](#)
44. Li, W.; Sun, W.; Zhang, Y.; Wei, W.; Ambasudhan, R.; Xia, P.; Talantova, M.; Lin, T.; Kim, J.; Wang, X.; et al. Rapid Induction and Long-Term Self-Renewal of Primitive Neural Precursors from Human Embryonic Stem Cells by Small Molecule Inhibitors. *Proc. Natl. Acad. Sci. USA* **2011**, *108*, 8299–8304. [\[CrossRef\]](#)
45. Chambers, S.M.; Fasano, C.A.; Papapetrou, E.P.; Tomishima, M.; Sadelain, M.; Studer, L. Highly Efficient Neural Conversion of Human ES and IPS Cells by Dual Inhibition of SMAD Signaling. *Nat. Biotechnol.* **2009**, *27*, 275–280. [\[CrossRef\]](#)
46. Shi, Y.; Kirwan, P.; Smith, J.; Robinson, H.P.C.; Livesey, F.J. Human Cerebral Cortex Development from Pluripotent Stem Cells to Functional Excitatory Synapses. *Nat. Neurosci.* **2012**, *15*, 477–486. [\[CrossRef\]](#) [\[PubMed\]](#)
47. Izsak, J.; Seth, H.; Andersson, M.; Vizlin-hodzic, D.; Theiss, S.; Hanse, E.; Ågren, H.; Funa, K.; Illes, S. Robust Generation of Person-Specific, Synchronously Active Neuronal Networks Using Purely Isogenic Human iPSC-3D Neural Aggregate Cultures. *Front. Neurosci.* **2019**, *13*, 351. [\[CrossRef\]](#) [\[PubMed\]](#)
48. Hyvärinen, T.; Hyysalo, A.; Kapucu, F.E.; Aarnos, L.; Vinogradov, A.; Eglen, S.J.; Ylä-Outinen, L.; Narkilahti, S. Functional Characterization of Human Pluripotent Stem Cell-Derived Cortical Networks Differentiated on Laminin-521 Substrate: Comparison to Rat Cortical Cultures. *Sci. Rep.* **2019**, *9*, 17125. [\[CrossRef\]](#) [\[PubMed\]](#)
49. Paavilainen, T.; Pelkonen, A.; Mäkinen, M.E.; Peltola, M.; Huhtala, H.; Fayuk, D.; Narkilahti, S. Effect of Prolonged Differentiation on Functional Maturation of Human Pluripotent Stem Cell-Derived Neuronal Cultures. *Stem Cell Res.* **2018**, *27*, 151–161. [\[CrossRef\]](#)
50. Gunhanlar, N.; Shpak, G.; van der Kroeg, M.; Gouty-Colomer, L.A.; Munshi, S.T.; Lendemeijer, B.; Ghazvini, M.; Dupont, C.; Hoogendijk, W.J.G.; Gribnau, J.; et al. A Simplified Protocol for Differentiation of Electrophysiologically Mature Neuronal Networks from Human Induced Pluripotent Stem Cells. *Mol. Psychiatry* **2017**, *23*, 1336–1344. [\[CrossRef\]](#)
51. de Leeuw, V.C.; van Oostrom, C.T.M.; Wackers, P.F.K.; Pennings, J.L.A.; Hodemaekers, H.M.; Piersma, A.H.; Hessel, E.V.S. Neuronal Differentiation Pathways and Compound-Induced Developmental Neurotoxicity in the Human Neural Progenitor Cell Test (HNPT) Revealed by RNA-Seq. *Chemosphere* **2022**, *304*, 135298. [\[CrossRef\]](#)
52. Pistollato, F.; Canovas-Jorda, D.; Zagoura, D.; Price, A. Protocol for the Differentiation of Human Induced Pluripotent Stem Cells into Mixed Cultures of Neurons and Glia for Neurotoxicity Testing. *J. Vis. Exp.* **2017**, *2017*, 55702. [\[CrossRef\]](#)
53. Schenke, M.; Schjeide, B.M.; Püschel, G.P.; Seeger, B. Analysis of Motor Neurons Differentiated from Human Induced Pluripotent Stem Cells for the Use in Cell-Based Botulinum Neurotoxin Activity Assays. *Toxins* **2020**, *12*, 276. [\[CrossRef\]](#)
54. De Leeuw, V.C.; Van Oostrom, C.T.M.; Zwart, E.P.; Heusinkveld, H.J.; Hessel, E.V.S. Prolonged Differentiation of Neuron-Astrocyte Co-Cultures Results in Emergence of Dopaminergic Neurons. *Int. J. Mol. Sci.* **2023**, *24*, 3608. [\[CrossRef\]](#)

55. Suzuki, I.K.; Vanderhaeghen, P. Is This a Brain Which I See before Me? Modeling Human Neural Development with Pluripotent Stem Cells. *Development* **2015**, *142*, 3138–3150. [\[CrossRef\]](#)
56. Nimtz, L.; Hartmann, J.; Tigges, J.; Masjosthusmann, S.; Schmuck, M.; Keßel, E.; Theiss, S.; Köhrer, K.; Petzsch, P.; Adjaye, J.; et al. Characterization and Application of Electrically Active Neuronal Networks Established from Human Induced Pluripotent Stem Cell-Derived Neural Progenitor Cells for Neurotoxicity Evaluation. *Stem Cell Res.* **2020**, *45*, 101761. [\[CrossRef\]](#)
57. Pamies, D.; Barreras, P.; Block, K.; Makri, G.; Kumar, A.; Wiersma, D.; Smirnova, L.; Zhang, C.; Bressler, J.; Christian, K.M.; et al. A Human Brain Microphysiological System Derived from Induced Pluripotent Stem Cells to Study Neurological Diseases and Toxicity. *ALTEX* **2017**, *34*, 362–376. [\[CrossRef\]](#)
58. Pistollato, F.; Louisse, J.; Scelfo, B.; Mennecozzi, M.; Accordi, B.; Basso, G.; Gaspar, J.A.; Zagoura, D.; Barilari, M.; Palosaari, T.; et al. Development of a Pluripotent Stem Cell Derived Neuronal Model to Identify Chemically Induced Pathway Perturbations in Relation to Neurotoxicity: Effects of CREB Pathway Inhibition. *Toxicol. Appl. Pharmacol.* **2014**, *280*, 378–388. [\[CrossRef\]](#) [\[PubMed\]](#)
59. Fritsche, E.; Tigges, J.; Hartmann, J.; Kapr, J.; Serafini, M.M.; Viviani, B. Neural In Vitro Models for Studying Substances Acting on the Central Nervous System. In *Handbook of Experimental Pharmacology*; Springer: Cham, Switzerland, 2020. [\[CrossRef\]](#)
60. Logan, S.; Arzua, T.; Canfield, S.G.; Seminary, E.R.; Sison, S.L.; Ebert, A.D.; Bai, X. Studying Human Neurological Disorders Using Induced Pluripotent Stem Cells: From 2D Monolayer to 3D Organoid and Blood Brain Barrier Models. *Compr. Physiol.* **2019**, *9*, 565–611.
61. Abreu, C.M.; Gama, L.; Krasemann, S.; Chesnut, M.; Odwin-Dacosta, S.; Hogberg, H.T.; Hartung, T.; Pamies, D. Microglia Increase Inflammatory Responses in iPSC-Derived Human BrainSpheres. *Front. Microbiol.* **2018**, *9*, 2766. [\[CrossRef\]](#) [\[PubMed\]](#)
62. Pamies, D.; Wiersma, D.; Katt, M.E.; Zhao, L.; Burtcher, J.; Harris, G.; Smirnova, L.; Searson, P.C.; Hartung, T.; Hogberg, H.T. Human iPSC 3D Brain Model as a Tool to Study Chemical-Induced Dopaminergic Neuronal Toxicity. *Neurobiol. Dis.* **2022**, *169*, 105719. [\[CrossRef\]](#) [\[PubMed\]](#)
63. Pamies, D.; Block, K.; Lau, P.; Gribaldo, L.; Pardo, C.A.; Barreras, P.; Smirnova, L.; Wiersma, D.; Zhao, L.; Harris, G.; et al. Rotenone Exerts Developmental Neurotoxicity in a Human Brain Spheroid Model. *Toxicol. Appl. Pharmacol.* **2018**, *354*, 101–114. [\[CrossRef\]](#)
64. Nunes, C.; Gorczyca, G.; Mendoza-deGyves, E.; Ponti, J.; Bogni, A.; Carpi, D.; Bal-Price, A.; Pistollato, F. Upscaling Biological Complexity to Boost Neuronal and Oligodendroglia Maturation and Improve in Vitro Developmental Neurotoxicity (DNT) Evaluation. *Reprod. Toxicol.* **2022**, *110*, 124–140. [\[CrossRef\]](#)
65. Kobolak, J.; Teglas, A.; Bellak, T.; Janstova, Z.; Molnar, K.; Zana, M.; Bock, I.; Laszlo, L.; Dinnyes, A. Human Induced Pluripotent Stem Cell-Derived 3D-Neurospheres Are Suitable for Neurotoxicity Screening. *Cells* **2020**, *9*, 1122. [\[CrossRef\]](#)
66. Harris, G.; Hogberg, H.; Hartung, T.; Smirnova, L. 3D Differentiation of LUHMES Cell Line to Study Recovery and Delayed Neurotoxic Effects. *Curr. Protoc. Toxicol.* **2017**, *73*, 11–23. [\[CrossRef\]](#)
67. Smirnova, L.; Harris, G.; Delp, J.; Valadares, M.; Pamies, D.; Hogberg, H.T.; Waldmann, T.; Leist, M.; Hartung, T. A LUHMES 3D Dopaminergic Neuronal Model for Neurotoxicity Testing Allowing Long-Term Exposure and Cellular Resilience Analysis. *Arch. Toxicol.* **2016**, *90*, 2725–2743. [\[CrossRef\]](#) [\[PubMed\]](#)
68. Leite, P.E.C.; Pereira, M.R.; Harris, G.; Pamies, D.; Dos Santos, L.M.G.; Granjeiro, J.M.; Hogberg, H.T.; Hartung, T.; Smirnova, L. Suitability of 3D Human Brain Spheroid Models to Distinguish Toxic Effects of Gold and Poly-Lactic Acid Nanoparticles to Assess Biocompatibility for Brain Drug Delivery. *Part. Fibre Toxicol.* **2019**, *16*, 22. [\[CrossRef\]](#) [\[PubMed\]](#)
69. Tigges, J.; Bielec, K.; Brockerhoff, G.; Hildebrandt, B.; Hübenthal, U.; Kapr, J.; Koch, K.; Teichweide, N.; Wiczorek, D.; Rossi, A.; et al. Academic Application of Good Cell Culture Practice for Induced Pluripotent Stem Cells. *ALTEX* **2021**, *38*, 595–614. [\[CrossRef\]](#) [\[PubMed\]](#)
70. Bartmann, K.; Hartmann, J.; Kapr, J.; Fritsche, E. Measurement of Differentiated Human iPSC-Derived Neurospheres Recorded by Microelectrode Arrays (MEA). In *Experimental Neurotoxicology Methods*; Humana: New York, NY, USA, 2021; pp. 473–488. ISBN 978-1-0716-1637-6.
71. Koch, K.; Bartmann, K.; Hartmann, J.; Kapr, J.; Klose, J.; Kuchovská, E.; Pahl, M.; Schlüppmann, K.; Zühr, E.; Fritsche, E. Scientific Validation of Human Neurosphere Assays for Developmental Neurotoxicity Evaluation. *Front. Toxicol.* **2022**, *4*, 7. [\[CrossRef\]](#) [\[PubMed\]](#)
72. Bartmann, K.; Bendt, F.; Dönmez, A.; Haag, D.; Keßel, E.; Masjosthusmann, S.; Noel, C.; Wu, J.; Zhou, P.; Fritsche, E. A Human iPSC-Based in Vitro Neural Network Formation Assay to Investigate Neurodevelopmental Toxicity of Pesticides. *bioRxiv* **2023**, 1–41. [\[CrossRef\]](#)
73. Walter, K.M.; Dach, K.; Hayakawa, K.; Giersiefer, S.; Heuer, H.; Lein, P.J.; Fritsche, E. Ontogenetic Expression of Thyroid Hormone Signaling Genes: An in Vitro and in Vivo Species Comparison. *PLoS ONE* **2019**, *14*, e0221230. [\[CrossRef\]](#)
74. Park, D.; Xiang, A.P.; Mao, F.F.; Zhang, L.; Di, C.G.; Liu, X.M.; Shao, Y.; Ma, B.F.; Lee, J.H.; Ha, K.S.; et al. Nestin Is Required for the Proper Self-Renewal of Neural Stem Cells. *Stem Cells* **2010**, *28*, 2162–2171. [\[CrossRef\]](#)
75. Sansom, S.N.; Griffiths, D.S.; Faedo, A.; Kleinjan, D.J.; Ruan, Y.; Smith, J.; Van Heyningen, V.; Rubenstein, J.L.; Livesey, F.J. The Level of the Transcription Factor Pax6 Is Essential for Controlling the Balance between Neural Stem Cell Self-Renewal and Neurogenesis. *PLoS Genet.* **2009**, *5*, e1000511. [\[CrossRef\]](#)
76. Honegger, P.; Lenoir, D.; Favrod, P. Growth and Differentiation of Aggregating Fetal Brain Cells in a Serum-Free Defined Medium. *Nature* **1979**, *282*, 305–308. [\[CrossRef\]](#)
77. Tao, Y.; Zhang, S.C. Neural Subtype Specification from Human Pluripotent Stem Cells. *Cell Stem Cell* **2016**, *19*, 573–586. [\[CrossRef\]](#)

78. Leonzino, M.; Busnelli, M.; Antonucci, F.; Verderio, C.; Mazzanti, M.; Chini, B. The Timing of the Excitatory-to-Inhibitory GABA Switch Is Regulated by the Oxytocin Receptor via KCC2. *Cell Rep.* **2016**, *15*, 96–103. [\[CrossRef\]](#) [\[PubMed\]](#)
79. Maccioni, R.B.; Cambiazo, V. Role of Microtubule-Associated Proteins in the Control of Microtubule Assembly. *Physiol. Rev.* **1995**, *75*, 835–864. [\[CrossRef\]](#)
80. Holst, C.B.; Bröchner, C.B.; Vitting-Seerup, K.; Møllgård, K. Astroglialogenesis in Human Fetal Brain: Complex Spatiotemporal Immunoreactivity Patterns of GFAP, S100, AQP4 and YKL-40. *J. Anat.* **2019**, *235*, 590–615. [\[CrossRef\]](#)
81. Rowley, N.M.; Madsen, K.K.; Schousboe, A.; White, H.S. Glutamate and GABA Synthesis, Release, Transport and Metabolism as Targets for Seizure Control. *Neurochem. Int.* **2012**, *61*, 546–558. [\[CrossRef\]](#) [\[PubMed\]](#)
82. Walls, A.B.; Nilsen, L.H.; Eyjolfsson, E.M.; Vestergaard, H.T.; Hansen, S.L.; Schousboe, A.; Sonnewald, U.; Waagepetersen, H.S. GAD65 Is Essential for Synthesis of GABA Destined for Tonic Inhibition Regulating Epileptiform Activity. *J. Neurochem.* **2010**, *115*, 1398–1408. [\[CrossRef\]](#)
83. Niciu, M.J.; Kelmendi, B.; Sanacora, G. Overview of Glutamatergic Neurotransmission in the Nervous System. *Pharmacol. Biochem. Behav.* **2012**, *100*, 656–664. [\[CrossRef\]](#) [\[PubMed\]](#)
84. Bormann, J. The “ABC” of GABA Receptors. *Trends Pharmacol. Sci.* **2000**, *21*, 16–19. [\[CrossRef\]](#) [\[PubMed\]](#)
85. Popova, E. Ionotropic GABA Receptors and Distal Retinal ON and OFF Responses. *Scientifica* **2014**, *2014*, 149187. [\[CrossRef\]](#)
86. Fan, L.; Tan, L.; Chen, Z.; Qi, J.; Nie, F.; Luo, Z.; Cheng, J.; Wang, S. Haloperidol Bound D2 Dopamine Receptor Structure Inspired the Discovery of Subtype Selective Ligands. *Nat. Commun.* **2020**, *11*, 1074. [\[CrossRef\]](#)
87. Martel, J.C.; McArthur, S.G. Dopamine Receptor Subtypes, Physiology and Pharmacology: New Ligands and Concepts in Schizophrenia. *Front. Pharmacol.* **2020**, *11*, 1003. [\[CrossRef\]](#)
88. Sagarduy, A.; Llorente, J.; Miguelez, C.; Morera-Herreras, T.; Ruiz-Ortega, J.A.; Ugedo, L. Buspirone Requires the Intact Nigrostriatal Pathway to Reduce the Activity of the Subthalamic Nucleus via 5-HT1A Receptors. *Exp. Neurol.* **2016**, *277*, 35–45. [\[CrossRef\]](#) [\[PubMed\]](#)
89. Qujeq, D.; Roushan, T.; Norouzy, A.; Habibi-Rezaei, M.; Mehdinejad-Shani, M. Effects of Dichlorvos and Carbaryl on the Activity of Free and Immobilized Acetylcholinesterase. *Toxicol. Ind. Health* **2012**, *28*, 291–295. [\[CrossRef\]](#) [\[PubMed\]](#)
90. Smulders, C.J.G.M.; Bueters, T.J.H.; Van Kleef, R.G.D.M.; Vijverberg, H.P.M. Selective Effects of Carbamate Pesticides on Rat Neuronal Nicotinic Acetylcholine Receptors and Rat Brain Acetylcholinesterase. *Toxicol. Appl. Pharmacol.* **2003**, *193*, 139–146. [\[CrossRef\]](#) [\[PubMed\]](#)
91. Nagata, K.; Huang, C.S.; Song, J.H.; Narahashi, T. Direct Actions of Anticholinesterases on the Neuronal Nicotinic Acetylcholine Receptor Channels. *Brain Res.* **1997**, *769*, 211–218. [\[CrossRef\]](#) [\[PubMed\]](#)
92. Xu, X.; Sepich, C.; Lukas, R.J.; Zhu, G.; Chang, Y. Emamectin Is a Non-Selective Allosteric Activator of Nicotinic Acetylcholine Receptors and GABAA/C Receptors. *Biochem. Biophys. Res. Commun.* **2016**, *473*, 795–800. [\[CrossRef\]](#)
93. Patterson, T.A.; Eppler, B.; Dawson, R. Attenuation of Trimethyltin-Evoked Glutamate (GLU) Efflux from Rat Cortical and Hippocampal Slices. *Neurotoxicol. Teratol.* **1996**, *18*, 697–702. [\[CrossRef\]](#)
94. Bal-Price, A.K.; Suñol, C.; Weiss, D.G.; van Vliet, E.; Westerink, R.H.S.; Costa, L.G. Application of in Vitro Neurotoxicity Testing for Regulatory Purposes: Symposium III Summary and Research Needs. *Neurotoxicology* **2008**, *29*, 520–531. [\[CrossRef\]](#)
95. Coecke, S.; Eskes, C.; Gartlon, J.; Kinsner, A.; Price, A.; Van Vliet, E.; Prieto, P.; Boveri, M.; Bremer, S.; Adler, S.; et al. The Value of Alternative Testing for Neurotoxicity in the Context of Regulatory Needs. *Environ. Toxicol. Pharmacol.* **2006**, *21*, 153–167. [\[CrossRef\]](#)
96. Tate, K.; Kirk, B.; Tseng, A.; Ulfers, A.; Litwa, K. Effects of the Selective Serotonin Reuptake Inhibitor Fluoxetine on Developing Neural Circuits in a Model of the Human Fetal Cortex. *Int. J. Mol. Sci.* **2021**, *22*, 10457. [\[CrossRef\]](#)
97. Tukker, A.M.; Bouwman, L.M.S.; van Kleef, R.G.D.M.; Hendriks, H.S.; Legler, J.; Westerink, R.H.S. Perfluorooctane Sulfonate (PFOS) and Perfluorooctanoate (PFOA) Acutely Affect Human A1β2γ2L GABAA Receptor and Spontaneous Neuronal Network Function in Vitro. *Sci. Rep.* **2020**, *10*, 5311. [\[CrossRef\]](#)
98. Sirenko, O.; Parham, F.; Dea, S.; Sodhi, N.; Biesmans, S.; Mora-Castilla, S.; Ryan, K.; Behl, M.; Chandy, G.; Crittenden, C.; et al. Functional and Mechanistic Neurotoxicity Profiling Using Human iPSC-Derived Neural 3D Cultures. *Toxicol. Sci.* **2019**, *167*, 58–76. [\[CrossRef\]](#) [\[PubMed\]](#)
99. van Melis, L.V.J.; Heusinkveld, H.J.; Langendoen, C.; Peters, A.; Westerink, R.H.S. Organophosphate Insecticides Disturb Neuronal Network Development and Function via Non-AChE Mediated Mechanisms. *Neurotoxicology* **2022**, *94*, 35–45. [\[CrossRef\]](#) [\[PubMed\]](#)
100. Loser, D.; Grillberger, K.; Hinojosa, M.G.; Blum, J.; Haufe, Y.; Danker, T.; Johansson, Y.; Möller, C.; Nicke, A.; Bennekou, S.H.; et al. Acute Effects of the Imidacloprid Metabolite Desnitro-Imidacloprid on Human NACH Receptors Relevant for Neuronal Signaling. *Arch. Toxicol.* **2021**, *95*, 3695–3716. [\[CrossRef\]](#)
101. Kosodo, Y.; Röper, K.; Haubensak, W.; Marzesco, A.M.; Corbeil, D.; Huttner, W.B. Asymmetric Distribution of the Apical Plasma Membrane during Neurogenic Divisions of Mamalian Neuroepithelial Cells. *EMBO J.* **2004**, *23*, 2314–2324. [\[CrossRef\]](#) [\[PubMed\]](#)
102. Bayatti, N.; Sarma, S.; Shaw, C.; Eyre, J.A.; Vouyiouklis, D.A.; Lindsay, S.; Clowry, G.J. Progressive Loss of PAX6, TBR2, NEUROD and TBR1 mRNA Gradients Correlates with Translocation of EMX2 to the Cortical Plate during Human Cortical Development. *Eur. J. Neurosci.* **2008**, *28*, 1449–1456. [\[CrossRef\]](#)

103. Estivill-Torres, G.; Pearson, H.; van Heyningen, V.; Price, D.J.; Rashbass, P. Pax6 Is Required to Regulate the Cell Cycle and the Rate of Progression from Symmetrical to Asymmetrical Division in Mammalian Cortical Progenitors. *Development* **2002**, *129*, 455–466. [\[CrossRef\]](#)
104. Togo, K.; Fukusumi, H.; Shofuda, T.; Ohnishi, H.; Yamazaki, H.; Hayashi, M.K.; Kawasaki, N.; Takei, N.; Nakazawa, T.; Saito, Y.; et al. Postsynaptic Structure Formation of Human IPS Cell-Derived Neurons Takes Longer than Presynaptic Formation during Neural Differentiation in Vitro. *Mol. Brain* **2021**, *14*, 149. [\[CrossRef\]](#)
105. Reemst, K.; Noctor, S.C.; Lucassen, P.J.; Hol, E.M. The Indispensable Roles of Microglia and Astrocytes during Brain Development. *Front. Hum. Neurosci.* **2016**, *10*, 566. [\[CrossRef\]](#)
106. Mahmoud, S.; Gharagozloo, M.; Simard, C.; Gris, D. Astrocytes Maintain Glutamate Homeostasis in the CNS by Controlling the Balance between Glutamate Uptake and Release. *Cells* **2019**, *8*, 184. [\[CrossRef\]](#)
107. Oyanagi, K.; Tashiro, T.; Negishi, T. Cell-Type-Specific and Differentiation-Status-Dependent Variations in Cytotoxicity of Tributyltin in Cultured Rat Cerebral Neurons and Astrocytes. *J. Toxicol. Sci.* **2015**, *40*, 459–468. [\[CrossRef\]](#)
108. Laurenza, I.; Pallocca, G.; Mennecozzi, M.; Scelfo, B.; Pamies, D.; Bal-Price, A. A Human Pluripotent Carcinoma Stem Cell-Based Model for in Vitro Developmental Neurotoxicity Testing: Effects of Methylmercury, Lead and Aluminum Evaluated by Gene Expression Studies. *Int. J. Dev. Neurosci.* **2013**, *31*, 679–691. [\[CrossRef\]](#) [\[PubMed\]](#)
109. Pei, Y.; Peng, J.; Behl, M.; Sipes, N.S.; Shockley, K.R.; Rao, M.S.; Tice, R.R.; Zeng, X. Comparative Neurotoxicity Screening in Human iPSC-Derived Neural Stem Cells, Neurons and Astrocytes. *Brain Res.* **2016**, *1638*, 57–73. [\[CrossRef\]](#) [\[PubMed\]](#)
110. Wang, Y.; Zhao, F.; Liao, Y.; Jin, Y.; Sun, G. Effects of Arsenite in Astrocytes on Neuronal Signaling Transduction. *Toxicology* **2013**, *303*, 43–53. [\[CrossRef\]](#) [\[PubMed\]](#)
111. Guttenplan, K.A.; Weigel, M.K.; Prakash, P.; Wijewardhane, P.R.; Hasel, P.; Rufen-Blanchette, U.; Münch, A.E.; Blum, J.A.; Fine, J.; Neal, M.C.; et al. Neurotoxic Reactive Astrocytes Induce Cell Death via Saturated Lipids. *Nature* **2021**, *599*, 102–107. [\[CrossRef\]](#)
112. Stary, C.M.; Sun, X.; Giffard, R.G. Astrocytes Protect against Isoflurane Neurotoxicity by Buffering Pro-Brain-Derived Neurotrophic Factor. *Anesthesiology* **2015**, *123*, 810–819. [\[CrossRef\]](#)
113. Brüll, M.; Spreng, A.S.; Gutbier, S.; Loser, D.; Krebs, A.; Reich, M.; Kraushaar, U.; Britschgi, M.; Patsch, C.; Leist, M. Incorporation of Stem Cell-Derived Astrocytes into Neuronal Organoids to Allow Neuro-Glial Interactions in Toxicological Studies. *ALTEX* **2020**, *37*, 409–428. [\[CrossRef\]](#)
114. Crofton, K.M.; Bassan, A.; Behl, M.; Chushak, Y.G.; Fritsche, E.; Gearhart, J.M.; Marty, M.S.; Mumtaz, M.; Pavan, M.; Ruiz, P.; et al. Current Status and Future Directions for a Neurotoxicity Hazard Assessment Framework That Integrates in Silico Approaches. *Comput. Toxicol.* **2022**, *22*, 100223. [\[CrossRef\]](#)
115. Betarbet, R.; Sherer, T.B.; Mackenzie, G.; Garcia-osuna, M.; Panov, A.V.; Greenamyre, J.T. Chronic Systemic Pesticide Exposure Produces Pd Symptoms Betarbet. *Nat. Neurosci.* **2000**, *26*, 1301–1306. [\[CrossRef\]](#)
116. Jokanović, M. Neurotoxic Effects of Organophosphorus Pesticides and Possible Association with Neurodegenerative Diseases in Man: A Review. *Toxicology* **2018**, *410*, 125–131. [\[CrossRef\]](#)
117. Pauly, M.G.; Krajka, V.; Stengel, F.; Seibler, P.; Klein, C.; Capetian, P. Adherent vs. Free-Floating Neural Induction by Dual SMAD Inhibition for Neurosphere Cultures Derived from Human Induced Pluripotent Stem Cells. *Front. Cell Dev. Biol.* **2018**, *6*, 3. [\[CrossRef\]](#)
118. Nadadhur, A.G.; Leferink, P.S.; Holmes, D.; Hinz, L.; Cornelissen-Steijger, P.; Gasparotto, L.; Heine, V.M. Patterning Factors during Neural Progenitor Induction Determine Regional Identity and Differentiation Potential in Vitro. *Stem Cell Res.* **2018**, *32*, 25–34. [\[CrossRef\]](#) [\[PubMed\]](#)
119. McCready, F.P.; Gordillo-Sampedro, S.; Pradeepan, K.; Martinez-Trujillo, J.; Ellis, J. Multielectrode Arrays for Functional Phenotyping of Neurons from Induced Pluripotent Stem Cell Models of Neurodevelopmental Disorders. *Biology* **2022**, *11*, 316. [\[CrossRef\]](#) [\[PubMed\]](#)
120. Tanabe, Y.; Masu, M.; Ishii, T.; Shigemoto, R.; Nakanishi, S. A Family of Metabotropic Glutamate Receptors. *Neuron* **1992**, *8*, 169–179. [\[CrossRef\]](#) [\[PubMed\]](#)
121. Bodzeta, A.; Scheefhals, N.; MacGillavry, H.D. Membrane Trafficking and Positioning of mGluRs at Presynaptic and Postsynaptic Sites of Excitatory Synapses. *Neuropharmacology* **2021**, *200*, 108799. [\[CrossRef\]](#) [\[PubMed\]](#)
122. Panatier, A.; Poulain, D.A.; Oliet, S.H.R. Regulation of Transmitter Release by High-Affinity Group III mGluRs in the Supraoptic Nucleus of the Rat Hypothalamus. *Neuropharmacology* **2004**, *47*, 333–341. [\[CrossRef\]](#)
123. Mateo, Z.; Porter, J.T. Group II Metabotropic Glutamate Receptors Inhibit Glutamate Release at Thalamocortical Synapses in the Developing Somatosensory Cortex. *Neuroscience* **2007**, *146*, 1062–1072. [\[CrossRef\]](#)
124. Bocchio, M.; Lukacs, I.P.; Stacey, R.; Plaha, P.; Apostolopoulos, V.; Livermore, L.; Sen, A.; Ansorge, O.; Gillies, M.J.; Somogyi, P.; et al. Group II Metabotropic Glutamate Receptors Mediate Presynaptic Inhibition of Excitatory Transmission in Pyramidal Neurons of the Human Cerebral Cortex. *Front. Cell. Neurosci.* **2019**, *12*, 508. [\[CrossRef\]](#)
125. Van Den Pol, A.N.; Gao, X.B.; Patrylo, P.R.; Ghosh, P.K.; Obrietan, K. Glutamate Inhibits GABA Excitatory Activity in Developing Neurons. *J. Neurosci.* **1998**, *18*, 10749–10761. [\[CrossRef\]](#)
126. Görtz, P.; Henning, U.; Theiss, S.; Lange-Asschenfeldt, C. Effect Fingerprints of Antipsychotic Drugs on Neural Networks in Vitro. *J. Neural Transm.* **2019**, *126*, 1363–1371. [\[CrossRef\]](#)

127. Gemperle, A.Y.; Enz, A.; Pozza, M.F.; Lüthi, A.; Olpe, H.R. Effects of Clozapine, Haloperidol and Iloperidone on Neurotransmission and Synaptic Plasticity in Prefrontal Cortex and Their Accumulation in Brain Tissue: An in Vitro Study. *Neuroscience* **2003**, *117*, 681–695. [\[CrossRef\]](#)
128. Chen, W.; Zhu, F.; Guo, J.; Sheng, J.; Li, W.; Zhao, X.; Wang, G.; Li, K. Chronic Haloperidol Increases Voltage-Gated Na⁺ Currents in Mouse Cortical Neurons. *Biochem. Biophys. Res. Commun.* **2014**, *450*, 55–60. [\[CrossRef\]](#) [\[PubMed\]](#)
129. Dzyubenko, E.; Juckel, G.; Faissner, A. The Antipsychotic Drugs Olanzapine and Haloperidol Modify Network Connectivity and Spontaneous Activity of Neural Networks in Vitro. *Sci. Rep.* **2017**, *7*, 11609. [\[CrossRef\]](#) [\[PubMed\]](#)
130. Valdivia, P.; Martin, M.; LeFew, W.R.; Ross, J.; Houck, K.A.; Shafer, T.J. Multi-Well Microelectrode Array Recordings Detect Neuroactivity of ToxCast Compounds. *Neurotoxicology* **2014**, *44*, 204–217. [\[CrossRef\]](#) [\[PubMed\]](#)
131. Smulders, C.J.G.M.; Van Kleef, R.G.D.M.; de Groot, A.; Gotti, C.; Vijverberg, H.P.M. A Noncompetitive, Sequential Mechanism for Inhibition of Rat α 4 β 2 Neuronal Nicotinic Acetylcholine Receptors by Carbamate Pesticides. *Toxicol. Sci.* **2004**, *82*, 219–227. [\[CrossRef\]](#)
132. McConnell, E.R.; McClain, M.A.; Ross, J.; LeFew, W.R.; Shafer, T.J. Evaluation of Multi-Well Microelectrode Arrays for Neurotoxicity Screening Using a Chemical Training Set. *Neurotoxicology* **2012**, *33*, 1048–1057. [\[CrossRef\]](#)
133. Defranchi, E.; Novellino, A.; Whelan, M.; Vogel, S.; Ramirez, T.; van Ravenzwaay, B.; Landsiedel, R. Feasibility Assessment of Micro-Electrode Chip Assay as a Method of Detecting Neurotoxicity in Vitro. *Front. Neuroeng.* **2011**, *4*, 6. [\[CrossRef\]](#)
134. Alloisio, S.; Nobile, M.; Novellino, A. Multiparametric Characterisation of Neuronal Network Activity for in Vitro Agrochemical Neurotoxicity Assessment. *Neurotoxicology* **2015**, *48*, 152–165. [\[CrossRef\]](#)
135. Dingemans, M.M.L.; Schütte, M.G.; Wiersma, D.M.M.; de Groot, A.; van Kleef, R.G.D.M.; Wijnolts, F.M.J.; Westerink, R.H.S. Chronic 14-Day Exposure to Insecticides or Methylmercury Modulates Neuronal Activity in Primary Rat Cortical Cultures. *Neurotoxicology* **2016**, *57*, 194–202. [\[CrossRef\]](#)
136. Kocaturk, S.; Guven, E.B.; Shah, F.; Tepper, J.M.; Assous, M. Cholinergic Control of Striatal GABAergic Microcircuits. *Cell Rep.* **2022**, *41*, 111531. [\[CrossRef\]](#)
137. Schwartz, D.; González-Ruiz, V.; Walter, N.; Antinori, P.; Jeanneret, F.; Tonoli, D.; Boccard, J.; Zurich, M.G.; Rudaz, S.; Monnet-Tschudi, F.; et al. Protein Pathway Analysis to Study Development-Dependent Effects of Acute and Repeated Trimethyltin (TMT) Treatments in 3D Rat Brain Cell Cultures. *Toxicol. Vitro* **2019**, *60*, 281–292. [\[CrossRef\]](#)
138. Brock, T.O.; O’Callaghan, J.P. Quantitative Changes in the Synaptic Vesicle Proteins Synapsin I and P38 and the Astrocyte-Specific Protein Glial Fibrillary Acidic Protein Are Associated with Chemical-Induced Injury to the Rat Central Nervous System. *J. Neurosci.* **1987**, *7*, 931–942. [\[CrossRef\]](#)
139. Amin, H.; Marinaro, F.; Tonelli, D.D.P.; Berdondini, L. Developmental Excitatory-to-Inhibitory GABA-Polarity Switch Is Disrupted in 22q11.2 Deletion Syndrome: A Potential Target for Clinical Therapeutics. *Sci. Rep.* **2017**, *7*, 15752. [\[CrossRef\]](#) [\[PubMed\]](#)
140. Deidda, G.; Parrini, M.; Naskar, S.; Bozarth, I.F.; Contestabile, A.; Cancedda, L. Reversing Excitatory GABA A R Signaling Restores Synaptic Plasticity and Memory in a Mouse Model of Down Syndrome. *Nat. Med.* **2015**, *21*, 318–326. [\[CrossRef\]](#) [\[PubMed\]](#)
141. He, Q.; Nomura, T.; Xu, J.; Contractor, A. The Developmental Switch in GABA Polarity Is Delayed in Fragile X Mice. *J. Neurosci.* **2014**, *34*, 446–450. [\[CrossRef\]](#) [\[PubMed\]](#)
142. Braat, S.; Kooy, R.F. The GABAA Receptor as a Therapeutic Target for Neurodevelopmental Disorders. *Neuron* **2015**, *86*, 1119–1130. [\[CrossRef\]](#)
143. Modafferi, S.; Zhong, X.; Kleinsang, A.; Murata, Y.; Fagiani, F.; Pamies, D.; Hogberg, H.T.; Calabrese, V.; Lachman, H.; Hartung, T.; et al. Gene–Environment Interactions in Developmental Neurotoxicity: A Case Study of Synergy between Chlorpyrifos and Chd8 Knockout in Human Brainspheres. *Environ. Health Perspect.* **2021**, *129*, 077001. [\[CrossRef\]](#)
144. Zhong, X.; Harris, G.; Smirnova, L.; Zufferey, V.; Baldino Russo, F.; Baleeiro Beltrao Braga, P.C.; Chesnut, M.; Zurich, M.G.; Hogberg, H.T.; Hartung, T.; et al. Antidepressant Paroxetine Exerts Developmental Neurotoxicity in an iPSC-Derived 3D Human Brain Model. *Front. Cell. Neurosci.* **2020**, *14*, 25. [\[CrossRef\]](#)
145. Rockley, K.L.; Roberts, R.A.; Morton, M.J. Innovative Models for In Vitro Detection of Seizure. *Toxicol. Res.* **2019**, *8*, 784–788. [\[CrossRef\]](#)
146. Tukker, A.M.; Westerink, R.H.S. Novel Test Strategies for in Vitro Seizure Liability Assessment. *Expert Opin. Drug Metab. Toxicol.* **2021**, *17*, 923–936. [\[CrossRef\]](#)
147. Blum, J.; Masjosthusmann, S.; Bartmann, K.; Bendt, F.; Dolde, X.; Dönmez, A.; Förster, N.; Holzer, A.-K.; Hübenthal, U.; Keßel, H.E.; et al. Establishment of a Human Cell-Based in Vitro Battery to Assess Developmental Neurotoxicity Hazard of Chemicals. *Chemosphere* **2023**, *311*, 137035. [\[CrossRef\]](#)
148. Crofton, K.M.; Mundy, W.R. External Scientific Report on the Interpretation of Data from the Developmental Neurotoxicity In Vitro Testing Assays for Use in Integrated Approaches for Testing and Assessment. *EFSA Support. Publ.* **2021**, *18*, 6924E. [\[CrossRef\]](#)

Disclaimer/Publisher’s Note: The statements, opinions and data contained in all publications are solely those of the individual author(s) and contributor(s) and not of MDPI and/or the editor(s). MDPI and/or the editor(s) disclaim responsibility for any injury to people or property resulting from any ideas, methods, instructions or products referred to in the content.

1. Supplementary Tables

Supplementary Table S1. Coatings used for neural differentiation of BrainSpheres generated with different neural induction protocols.

Neural induction protocol	Differentiation medium	coating	Order number and supplier
2D-NIM	CINDA+	0.1 mg/mL PLO ¹ / 50 µg/mL laminin	PLO: #P4957, Sigma-Aldrich, St. Louis, MO, USA laminin: #LN521, Biolamina, Sundbyberg, Sweden
	Electro	0.1 % PEI ² / 50 µg/mL laminin	PEI: #181978, Sigma-Aldrich, St. Louis, MO, USA laminin: #LN521, Biolamina, Sundbyberg, Sweden
GNEIB	CINDA+	25 µg/mL laminin	laminin: #LN521, Biolamina, Sundbyberg, Sweden
	Electro	0.015 mg/mL PLO ¹ / 50 µg/mL laminin	PLO: #P4957, Sigma-Aldrich, St. Louis, MO, USA laminin: #LN521, Biolamina, Sundbyberg, Sweden
Stemdiff	CINDA+	50 µg/mL laminin	laminin: #LN521, Biolamina, Sundbyberg, Sweden
	Electro	0.1 mg/mL PLO ¹ / 50 µg/mL laminin	PLO: #P4957, Sigma-Aldrich, St. Louis, MO, USA laminin: #LN521, Biolamina, Sundbyberg, Sweden

¹PLO: poly-L-ornithine; ²PEI: polyethyleneimine

Supplementary Table S2. Information about used compounds and their solvents.

Compound	CASRN	Order number and supplier	solvent	effect
Bicuculline	485-49-4	#0130, Tocris, Bristol, UK	DMSO	GABA _A antagonist
Buspirone hydrochloride	33386-08-2	#HY-B1115, MedChemExpress, South Brunswick, NJ, USA	DMSO	5-HT _{1A} agonist
Carbaryl	63-25-2	#32055, Sigma-Aldrich, St. Louis, MO, USA	DMSO	inhibits acetylcholinesterase
DL-2-amino-5-phosphonovaleric acid (AP5)	76326-31-3	#SC-201503, Santa Cruz Biotechnology Inc., Dallas, TX, USA	H ₂ O	NMDA antagonist

Emamectin benzoate	155569-91-8	#31733, Merck, Darmstadt, Germany	DMSO	GABA _A and GABA _C agonist
Haloperidol	52-86-8	#HY-14538, MedChemExpress, South Brunswick, NJ, USA	DMSO	D2 antagonist
L-glutamate	6106-04-3	#49621, Sigma-Aldrich, St. Louis, MO, USA	H ₂ O	Neurotransmitter
NBQX disodium salt (NBQX)	479347-86-9	#SC-222048, Santa Cruz Biotechnology Inc., Dallas, TX, USA	DMSO	AMPA antagonist
Picrotoxin	124-87-8	#SC-202765, Santa Cruz Biotechnology Inc., Dallas, TX, USA	DMSO	GABA _A and GABA _C antagonist
Trimethyltin chloride (TMT)	1066-45-1	#146498, Merck, Darmstadt, Germany	H ₂ O	Increases glutamate release
γ -Aminobutyric acid (GABA)	56-12-2	#A5835, Sigma-Aldrich, St. Louis, MO, USA	H ₂ O	Neurotransmitter

Supplementary Table S3. Primer sequences.

Gene	Forward primer sequence (5' → 3')	Reverse primer sequence (5' → 3')
ACHE	GTCCAGACTAACGTACTGCT	ATGCGATACTGGGCCAAC
ACTB	CAGGAAGTCCCTTGCCATCC	ACCAAAAGCCTTCATACATCTCA
AQP4	TGGACAGAAGACATACTCATAAAGG	GGTGCCAGCATGAATCCC
CHAT	GCCCATAGTATTGCTTCATGC	ACCAGCTGAGGTTTGCAG
CHRNA4	CTCGCGGGCTCTAGATG	CCACAGGAGAAGACGAACC
DLG4	CCAGAAGAGTACAGCCGATTCT	CTTGGTCTTGTCGTAATCAAACAG
DRD2	ACGGCGAGCATCCTGAACTT	GCCGGGTTGGCAATGATGCA
EN1	CTGGGTGTACTGCACACGTTAT	TACTCGCTCTCGTCTTTGTCTT
FOXG1	TCCATCCGCCACAATCTGTC	CCCAGCGAGTTCTGAGTCAA
GABRA1	ACAACACTTACGCTCCAACA	TTTCGGGCTTGACCTCTTTAG
GAD1	GACCCCAATACCACTAACCTG	GCTGTTGGTCTTTGCAAG
GFAP	CACTGTGAGGCAGAAGCTC	CCTCCAGCGACTCAATCTTC
GLS	CAGTTCCAAGATCATTAACAGCA	CGATTGTGGGGTGTGTCT
GRIA1	CTTAATCGAGTTCTGCTACAAATCC	GTATGGCTTCGTTGATGGATTG
GRIN1	CTCCTGGAAGATTGAGCTCAA	GTGGATGGCTAACTAGGATGG
HOXA2	CACCACGTCTACGGGCAAGAAC	AGCTGCTGATGCTGACTTCTGA
HTR1A	TGTCGCTTCTCACAACCTCTC	CTTCTCCTCTTTCTCTCTGCTC
LMX1A	CGGGTCATCTTGACAGGTTT	CAGAAGCAGCTCAGGTGGTA
MAP2	TGCCTCAGAACAGACTGTCAC	AAGGCTCAGCTGTAGAGGGA
S100B	CACATTCGCCGTCTCCATC	CACAAGCTGAAGAAATCCGAAC
SLC12A2	ACAAAGTTGAGGAAGAGGATGGC	CCTGATCTGCCGGTATGTCTTGG
SLC12A5	CCGATGACAATTACCCATGGA	CTGTCTACATCAGCTCCGTTG
SLC17A6	CCTCTACCCTAAATATGCTAATTCCA	TTGCTCCATATCCCATGACAT
SLC17A7	CAGAAAGCCCAGTTCAGC	ACAATAGCAAAGCCGAAACTC
SYN1	GTGCTGCTGGTCATCGAC	CCACAAGGTTGAGATCAGAGAA
TH	GGTCTCTAGATGGTGGATTTTG	TGCTAAACCTGCTCTTCTCC
TPH1	TGTCTCACATATTGAGTGCAGT	CCACAATTGGAAGATGTCTCC

	A	B	C	D	E	F	G	H	I	J	K
	gene	comparison			2D-NIM CINDA+	2D-NIM Electro	GNEIB CINDA+	GNEIB Electro	Stemdiff CINDA+	Stemdiff Electro	legend
1											
2	FOXG1	2D	vs.	3D	0,9085	0,8234	0,9943	0,9745	0,9801	0,9978	≤ 0,075
3				3D-1w	0,9971	0,992	0,9724	0,017	0,7683	0,8949	≤ 0,05
4				3D-2w	0,9985	0,9992	>0,9999	0,3716	0,8477	0,3798	≤ 0,01
5				3D-3w	>0,9999	0,9999	0,9998	0,0032	0,9234	0,4432	≤ 0,001
6	LMX1A	2D	vs.	3D	0,9986	0,9985	0,9972	0,9966	>0,9999	>0,9999	
7				3D-1w	0,841	0,8492	0,733	0,7318	0,3885	0,9998	
8				3D-2w	0,4581	0,5646	0,183	0,2276	0,1988	0,9777	
9				3D-3w	0,999	0,8508	0,0508	0,1159	0,3263	0,3139	
10	EN1	2D	vs.	3D	0,7124	0,6649	0,9993	0,9997	0,0163	0,0176	
11				3D-1w	0,9537	0,8693	0,9998	0,9968	0,008	0,0074	
12				3D-2w	0,9861	0,9918	0,6417	0,9739	0,0074	0,0085	
13				3D-3w	0,9604	0,8133	0,4242	0,9706	0,0076	0,0113	
14	HOXA2	2D	vs.	3D	0,0111	0,0208	0,0049	0,0055	0,3286	0,2558	
15				3D-1w	0,0006	0,0018	0,0006	0,0012	0,4368	0,2087	
16				3D-2w	0,0006	0,0034	0,0005	0,0009	0,1311	0,1206	
17				3D-3w	0,0011	0,0055	0,0006	0,0011	0,1024	0,0804	
18	SLC12A2	2D	vs.	3D	0,9649	0,9706	0,9584	0,9907	0,6926	0,995	
19				3D-1w	0,3011	0,2782	0,6535	0,7932	0,9648	>0,9999	
20				3D-2w	0,214	0,4348	0,8121	0,8353	0,7855	0,9383	
21				3D-3w	0,1233	0,3784	0,5131	0,5024	0,906	0,6484	
22	SLC12A5	2D	vs.	3D	>0,9999	>0,9999	>0,9999	>0,9999	0,9999	0,9999	
23				3D-1w	0,6468	0,6998	0,7279	0,8426	0,9384	0,8253	
24				3D-2w	0,0724	0,1397	0,6688	0,233	0,7777	0,2745	
25				3D-3w	0,0028	0,0021	0,1317	0,1242	0,3928	0,2496	
26	MAP2	3D	vs.	3D-1w	0,3432	0,2087	0,0184	0,2745	0,4753	0,1347	
27				3D-2w	0,0917	0,0126	0,0274	0,0733	0,292	0,0227	
28				3D-3w	0,0052	0,0006	0,0107	0,0482	0,4586	0,0811	
29				3D-1w	0,9902	0,8829	>0,9999	>0,9999	>0,9999	0,9326	
30	GFAP	3D	vs.	3D-2w	0,2129	0,1719	0,712	0,9706	0,9986	0,9024	
31				3D-3w	0,0067	0,0013	0,1623	0,1197	0,3103	0,0883	
32				3D-1w	>0,9999	0,2743	0,7274	0,4212	>0,9999	0,6352	
33	SYN1	3D	vs.	3D-2w	0,9318	0,0344	0,5502	0,3389	0,996	0,5024	
34				3D-3w	0,3427	0,0087	0,1568	0,1967	0,254	0,2165	

	A	B	C	D	E	F	G	H	I	J	K
1	gene	comparison			2D-NIM CINDA+	2D-NIM Electro	GNEIB CINDA+	GNEIB Electro	Stemdiff CINDA+	Stemdiff Electro	legend
35	DRD2	3D	vs.	3D-1w	0,9002	0,9791	0,0547	0,1691	0,9342	0,9871	
36				3D-2w	0,6218	0,9772	0,1256	0,214	0,8719	0,902	
37				3D-3w	0,8165	0,9882	0,3368	0,3211	0,9403	0,6766	
38	GABRA1	3D	vs.	3D-1w	0,9453	0,8227	0,89	>0.9999	0,9977	0,7664	
39				3D-2w	0,5603	0,4059	0,9954	0,8445	0,7559	0,5774	
40				3D-3w	0,0399	0,024	0,1417	0,0467	0,315	0,0852	
41	GRIA1	3D	vs.	3D-1w	>0.9999	0,7465	0,6425	0,8869	0,9696	0,7773	
42				3D-2w	0,1513	0,3257	0,3275	0,7132	0,6674	0,3948	
43				3D-3w	<0,0001	0,0316	0,9941	0,595	0,2814	0,0677	
44	DLG4	3D	vs.	3D-1w	0,9844	0,6375	0,8345	0,8022	0,9508	0,7698	
45				3D-2w	0,8235	0,9199	0,8225	0,9714	0,8509	0,8489	
46				3D-3w	0,5179	0,9875	0,6626	0,9812	0,7425	0,8505	
47	GRIN1	3D	vs.	3D-1w	0,6971	0,2945	0,6288	0,6952	0,9774	0,7598	
48				3D-2w	0,0709	0,0075	0,4285	0,2053	0,583	0,2056	
49				3D-3w	0,0024	<0,0001	0,1006	0,1014	0,3554	0,0611	
50	GAD1	3D	vs.	3D-1w	0,7971	0,9579	0,184	0,7619	0,8649	0,7943	
51				3D-2w	0,1774	0,2603	0,1051	0,0307	0,6434	0,3845	
52				3D-3w	0,023	0,0855	0,001	0,0029	0,4966	0,1619	
53	S100b	3D	vs.	3D-1w	0,6053	0,7505	0,1063	0,0946	0,3935	0,9447	
54				3D-2w	0,1818	0,3265	0,0052	0,0095	0,0915	0,8807	
55				3D-3w	0,0338	0,0789	0,0002	0,0004	0,0354	0,3487	
56	AQP4	3D	vs.	3D-1w	>0.9999	0,996	0,4973	0,6063	0,9995	0,8336	
57				3D-2w	0,9723	0,5207	0,2078	0,2454	0,7759	0,6125	
58				3D-3w	0,1782	0,0024	0,2021	0,1575	0,181	0,3784	
59	GLS	3D	vs.	3D-1w	0,9975	0,8933	0,9841	0,8821	>0.9999	0,979	
60				3D-2w	0,568	0,4245	0,3916	0,9994	0,9573	0,9595	
61				3D-3w	0,5674	0,2172	0,0111	0,3972	0,8806	0,5963	
62	TH	3D	vs.	3D-1w	0,6926	0,7843	0,0091	0,6568	0,9977	0,9771	
63				3D-2w	0,695	0,6931	0,0003	0,0984	0,995	0,9993	
64				3D-3w	0,832	0,9992	0,0003	0,0536	0,9525	0,9979	
65	ACHE	3D	vs.	3D-1w	0,9012	0,9338	0,3322	0,9075	0,9859	0,9914	
66				3D-2w	0,6174	0,6915	0,0727	0,4573	0,7097	0,72	
67				3D-3w	0,3285	0,2655	0,0507	0,3233	0,5947	0,6549	

	A	B	C	D	E	F	G	H	I	J	K
1	gene	comparison			2D-NIM CINDA+	2D-NIM Electro	GNEIB CINDA+	GNEIB Electro	Stemdiff CINDA+	Stemdiff Electro	legend
68	CHRNA4	3D	vs.	3D-1w	0,552	0,8397	0,7072	0,8066	0,9878	0,9996	
69				3D-2w	0,4335	0,8632	0,6003	0,8254	0,9916	0,9147	
70				3D-3w	0,0951	0,0436	0,9867	0,7507	0,8038	0,9384	
71	CHAT	3D	vs.	3D-1w	0,578	0,0488	0,9139	0,9997	0,9963	0,9817	
72				3D-2w	0,5784	0,1584	0,9266	0,959	0,635	0,8894	
73				3D-3w	0,0555	0,9805	0,9994	0,9659	0,5796	0,9913	
74	HTR1A	3D	vs.	3D-1w	0,9403	0,4453	0,7454	0,8735	0,5935	0,9999	
75				3D-2w	0,4443	0,2537	0,9897	0,706	0,6944	0,8326	
76				3D-3w	0,0222	0,0316	0,957	0,9476	0,6272	0,9636	
77	TPH1	3D	vs.	3D-1w	0,9867	0,9811	0,994	0,9773	0,6251	0,7427	
78				3D-2w	0,3754	0,7683	0,1518	0,4015	0,2204	0,0755	
79				3D-3w	0,9035	0,444	0,0399	0,0856	0,0047	0,392	
80	SLC17A6	3D	vs.	3D-1w	0,9432	>0.9999	0,2624	0,9113	0,9939	>0.9999	
81				3D-2w	0,8353	0,9965	0,1996	0,5766	0,848	0,994	
82				3D-3w	0,4013	0,4368	0,1732	0,3549	0,7187	0,564	
83	SLC17A7	3D	vs.	3D-1w	0,8912	0,9352	0,215	0,6334	0,9988	0,9804	
84				3D-2w	0,5879	0,6364	0,1704	0,2132	0,5176	0,9179	
85				3D-3w	0,7083	0,8872	0,4251	0,393	0,1069	0,5632	

	A	B	C	D	E	F	G	H	I	J	K	L
1	gene	time point	2D-NIM CINDA+	2D-NIM CINDA+	2D-NIM CINDA+	2D-NIM CINDA+	2D-NIM CINDA+	2D-NIM Electro	2D-NIM Electro	2D-NIM Electro	2D-NIM Electro	GNEIB CINDA+
2			2D-NIM CINDA+	2D-NIM CINDA+	2D-NIM CINDA+	2D-NIM CINDA+	2D-NIM CINDA+	2D-NIM Electro	2D-NIM Electro	2D-NIM Electro	2D-NIM Electro	GNEIB CINDA+
3			vs.									
4	FOXG1	2D	2D-NIM Electro	GNEIB CINDA+	GNEIB Electro	Stemdiff CINDA+	Stemdiff Electro	GNEIB CINDA+	GNEIB Electro	Stemdiff CINDA+	Stemdiff Electro	GNEIB Electro
5		3D	/	0,0768	0,0768	0,3992	0,3992	0,0768	0,0768	0,3992	0,3992	/
6		3D-1w	/	0,0134	0,0134	0,0669	0,0669	0,0134	0,0134	0,0669	0,0669	/
7		3D-2w	0,9908	0,1434	0,0092	0,3479	0,1789	0,1438	0,0098	0,3479	0,1789	0,2358
8		3D-3w	0,9351	0,0684	<0,0001	0,2897	0,2353	0,0693	0,0003	0,2895	0,2352	0,2247
9	LMX1A	2D	0,8825	0,046	0,0041	0,1868	0,2708	0,0473	0,0045	0,187	0,2709	0,0077
10		3D	/	0,1773	0,1773	0,3761	0,3761	0,1773	0,1773	0,3761	0,3761	/
11		3D-1w	/	0,23	0,23	0,399	0,399	0,23	0,23	0,399	0,399	/
12		3D-2w	0,9808	0,6342	0,658	0,7648	0,4633	0,6006	0,6222	0,7763	0,457	0,9337
13		3D-3w	0,921	0,6285	0,7021	0,6559	0,5145	0,522	0,5818	0,7014	0,5292	0,8594
14	EN1	2D	0,5254	0,1148	0,199	0,405	0,4763	0,1637	0,3077	0,8167	0,7674	0,7271
15		3D	/	0,0731	0,0731	0,0639	0,0639	0,0731	0,0731	0,0639	0,0639	/
16		3D-1w	/	0,0965	0,0965	0,0423	0,0423	0,0965	0,0965	0,0423	0,0423	/
17		3D-2w	0,8288	0,1528	0,1536	0,1106	0,1104	0,1305	0,1336	0,0915	0,0912	0,8938
18		3D-3w	0,54	0,1305	0,1413	0,1096	0,1096	0,115	0,1215	0,1014	0,1015	0,4695
19	HOXA2	2D	0,8747	0,2047	0,2385	0,1902	0,1906	0,127	0,1471	0,118	0,1182	0,2131
20		3D	/	0,094	0,094	0,0396	0,0396	0,094	0,094	0,0396	0,0396	/
21		3D-1w	/	0,0813	0,0813	0,0346	0,0346	0,0813	0,0813	0,0346	0,0346	/
22		3D-2w	0,6589	0,1668	0,2979	0,1428	0,1381	0,1744	0,2551	0,1567	0,1518	0,2216
23		3D-3w	0,3516	0,1451	0,2382	0,1256	0,1306	0,1872	0,2208	0,1771	0,1796	0,2237
24	SLC12A2	2D	0,5315	0,1739	0,2287	0,1529	0,1544	0,1717	0,202	0,1583	0,1593	0,2643
25		3D	/	0,6033	0,6033	0,1927	0,1927	0,6033	0,6033	0,1927	0,1927	/
26		3D-1w	/	0,5574	0,5574	0,4936	0,4936	0,5574	0,5574	0,4936	0,4936	/
27		3D-2w	0,8206	0,1236	0,2723	0,4495	0,961	0,1182	0,2609	0,5265	0,8936	0,8709
28		3D-3w	0,6124	0,2241	0,2537	0,4661	0,5388	0,2723	0,2917	0,2539	0,6523	0,7977
29	SLC12A5	2D	0,3977	0,2019	0,2682	0,9683	0,452	0,2466	0,306	0,4124	0,5412	0,7517
30		3D	/	0,2449	0,2449	0,0622	0,0622	0,2449	0,2449	0,0622	0,0622	/
31		3D-1w	/	0,5866	0,5866	0,9606	0,9606	0,5866	0,5866	0,9606	0,9606	/
32		3D-2w	0,9767	0,6198	0,4821	0,7813	0,6473	0,6379	0,4976	0,7697	0,6333	0,8651

	A	B	C	D	E	F	G	H	I	J	K	L
1												
2	gene	time point	2D-NIM CINDA+	2D-NIM CINDA+	2D-NIM CINDA+	2D-NIM CINDA+	2D-NIM CINDA+	2D-NIM Electro	2D-NIM Electro	2D-NIM Electro	2D-NIM Electro	GNEIB CINDA+
3												
4			2D-NIM Electro	GNEIB CINDA+	GNEIB Electro	Stemdiff CINDA+	Stemdiff Electro	GNEIB CINDA+	GNEIB Electro	Stemdiff CINDA+	Stemdiff Electro	GNEIB Electro
33		3D-2w	0,8268	0,1278	0,4003	0,9626	0,6481	0,2131	0,5438	0,9598	0,5829	0,4977
34		3D-3w	0,8247	0,189	0,2037	0,9698	0,8615	0,1483	0,1593	0,8932	0,7596	0,9275
35		3D	/	0,797	0,797	0,4239	0,4239	0,797	0,797	0,4239	0,4239	/
36	MAP2	3D-1w	0,8901	0,8044	0,9192	0,3081	0,1822	0,9437	0,9845	0,3533	0,238	0,9349
37		3D-2w	0,5525	0,5018	0,9515	0,6082	0,3763	0,1487	0,5907	0,8463	0,5987	0,4539
38		3D-3w	0,5412	0,1438	0,3603	0,6643	0,5259	0,0534	0,1467	0,4616	0,2311	0,4831
39		3D	/	0,3207	0,3207	0,3358	0,3358	0,3207	0,3207	0,3358	0,3358	/
40	GFAP	3D-1w	0,2961	0,2294	0,2294	0,23	0,2294	0,2224	0,2224	0,2253	0,2224	
41		3D-2w	0,242	0,2191	0,2189	0,2227	0,2185	0,1785	0,1757	0,2251	0,1718	0,7687
42		3D-3w	0,0847	0,0731	0,0733	0,0751	0,0728	0,0449	0,0448	0,9791	0,044	0,6066
43		3D	/	0,391	0,391	0,6593	0,6593	0,391	0,391	0,6593	0,6593	/
44	SYN1	3D-1w	0,3967	0,3674	0,4022	0,3932	0,4332	0,4074	0,8904	0,9479	0,3971	0,4108
45		3D-2w	0,4217	0,4153	0,4187	0,4402	0,4226	0,2116	0,6166	0,4039	0,9084	0,5732
46		3D-3w	0,4205	0,4186	0,4192	0,5113	0,4215	0,2666	0,5229	0,4017	0,8149	0,7447
47		3D	/	0,7872	0,7872	0,3636	0,3636	0,7872	0,7872	0,3636	0,3636	/
48	DRD2	3D-1w	0,587	0,4821	0,8974	0,5092	0,4832	0,1533	0,346	0,7718	0,6736	0,2761
49		3D-2w	0,5102	0,9941	0,656	0,4809	0,4806	0,1251	0,3635	0,8413	0,8378	0,2541
50		3D-3w	0,4778	0,9974	0,681	0,4287	0,5056	0,0888	0,323	0,7414	0,9192	0,2919
51		3D	/	0,9505	0,9505	0,367	0,367	0,9505	0,9505	0,367	0,367	/
52	GABRA1	3D-1w	0,8917	0,2483	0,2698	0,5192	0,8685	0,2993	0,3193	0,5172	0,9946	0,2229
53		3D-2w	0,8993	0,2391	0,2551	0,6525	0,5977	0,2044	0,2206	0,7102	0,641	0,2812
54		3D-3w	0,7511	0,1798	0,195	0,3958	0,3933	0,1353	0,1499	0,4751	0,4462	0,326
55		3D	/	0,142	0,142	0,1156	0,1156	0,142	0,142	0,1156	0,1156	/
56	GRIA1	3D-1w	0,2003	0,0038	0,2376	0,8331	0,2548	0,0473	0,0871	0,2889	0,7538	0,1376
57		3D-2w	0,4819	0,0122	0,1293	0,9503	0,208	0,0774	0,1411	0,7294	0,4379	0,1993
58		3D-3w	0,982	0,0006	0,012	0,7626	0,5668	0,0711	0,0895	0,7833	0,569	0,3793
59		3D	/	0,9483	0,9483	0,6865	0,6865	0,9483	0,9483	0,6865	0,6865	/
60		3D-1w	0,35	0,5871	0,3787	0,6696	0,4248	0,4189	0,2073	0,3936	0,2559	0,429

	A	B	C	D	E	F	G	H	I	J	K	L
1										comparison		
2	gene	time point	2D-NIM CINDA+	2D-NIM CINDA+	2D-NIM CINDA+	2D-NIM CINDA+	2D-NIM CINDA+	2D-NIM Electro	2D-NIM Electro	2D-NIM Electro	2D-NIM Electro	GNEIB CINDA+
3												
4			2D-NIM Electro	GNEIB CINDA+	GNEIB Electro	Stemdiff CINDA+	Stemdiff Electro	GNEIB CINDA+	GNEIB Electro	Stemdiff CINDA+	Stemdiff Electro	GNEIB Electro
61	GRIN1	3D-2w	0,4277	0,7996	0,4436	0,8481	0,4484	0,4493	0,6181	0,4376	0,3032	0,4596
62		3D-3w	0,4327	0,8803	0,433	0,9899	0,4332	0,4373	0,9812	0,4378	0,9858	0,4375
63		3D	/	0,0125	0,0125	0,1315	0,1315	0,0125	0,0125	0,1315	0,1315	/
64	GRIN1	3D-1w	0,2557	0,4339	0,1579	0,8266	0,6478	0,6478	0,1808	0,4475	0,2701	0,3338
65		3D-2w	0,1495	0,1386	0,103	0,6981	0,4587	0,9722	0,1772	0,4244	0,3128	0,4442
66		3D-3w	0,1124	0,0881	0,0677	0,8686	0,2381	0,8706	0,0198	0,4678	0,5048	0,3472
67	GAD1	3D	/	0,2838	0,2838	0,2509	0,2509	0,2838	0,2838	0,2509	0,2509	/
68		3D-1w	0,7268	0,318	0,2887	0,9767	0,3034	0,3616	0,3132	0,8188	0,337	0,6634
69		3D-2w	0,96	0,0582	0,0656	0,6844	0,0504	0,1444	0,1758	0,6832	0,1517	0,2146
70	S100b	3D-3w	0,8628	0,1585	0,1743	0,5166	0,1479	0,242	0,2677	0,6346	0,232	0,4227
71		3D	/	0,2221	0,2221	0,195	0,195	0,2221	0,2221	0,195	0,195	/
72		3D-1w	0,6717	0,4113	0,1546	0,1994	0,1313	0,7338	0,2924	0,3881	0,2394	0,304
73	AQP4	3D-2w	0,5381	0,3553	0,1161	0,1513	0,0954	0,7799	0,1855	0,2811	0,1436	0,0549
74		3D-3w	0,5389	0,4633	0,1356	0,1573	0,1126	0,9213	0,1433	0,1858	0,1075	0,0002
75		3D	/	0,3645	0,3645	0,9137	0,9137	0,3645	0,3645	0,9137	0,9137	/
76	GLS	3D-1w	0,6345	0,2825	0,2057	0,3715	0,5035	0,3812	0,2905	0,3805	0,9128	0,9428
77		3D-2w	0,7626	0,7561	0,8899	0,2349	0,35	0,4488	0,6351	0,0715	0,1083	0,8697
78		3D-3w	0,871	0,3884	0,4077	0,3449	0,363	0,1175	0,1261	0,0941	0,0968	0,5822
79	TH	3D	/	0,9994	0,9994	0,9487	0,9487	0,9994	0,9994	0,9487	0,9487	/
80		3D-1w	0,5177	0,5966	0,4519	0,8517	0,5791	0,7628	0,8316	0,6865	0,8712	0,5943
81		3D-2w	0,612	0,6663	0,4521	0,5434	0,5238	0,6986	0,4293	0,7692	0,6883	0,2991
82	AQP4	3D-3w	0,6214	0,7959	0,6274	0,5294	0,6284	0,219	0,9899	0,7378	0,9605	0,2442
83		3D	/	0,007	0,007	0,0433	0,0433	0,007	0,007	0,0433	0,0433	/
84		3D-1w	0,5703	0,9157	0,4715	0,4257	0,4195	0,1224	0,6272	0,4608	0,4409	0,0107
85	AQP4	3D-2w	0,6058	0,489	0,5596	0,4282	0,4293	0,0556	0,8776	0,4474	0,4507	0,0506
86		3D-3w	0,4675	0,2671	0,6334	0,4149	0,4195	0,0005	0,2166	0,4905	0,5303	0,001
87		3D	/	0,9405	0,9405	0,852	0,852	0,9405	0,9405	0,852	0,852	/
88	AQP4	3D-1w	0,5602	0,8232	0,6563	0,4787	0,4261	0,5306	0,806	0,7779	0,5895	0,7101

	A	B	C	D	E	F	G	H	I	J	K	L
1										comparison		
2	gene	time point	2D-NIM CINDA+	2D-NIM CINDA+	2D-NIM CINDA+	2D-NIM CINDA+	2D-NIM CINDA+	2D-NIM Electro	2D-NIM Electro	2D-NIM Electro	2D-NIM Electro	GNEIB CINDA+
3												
4			2D-NIM Electro	GNEIB CINDA+	GNEIB Electro	Stemdiff CINDA+	Stemdiff Electro	GNEIB CINDA+	GNEIB Electro	Stemdiff CINDA+	Stemdiff Electro	GNEIB Electro
89	ACME	3D-2w	0,5324	0,7347	0,734	0,5213	0,4246	0,4658	0,6408	0,9561	0,5811	0,9678
90		3D-3w	0,546	0,5692	0,6072	0,4405	0,3649	0,8917	0,8735	0,7035	0,4266	0,9425
91		3D	/	0,5268	0,5268	0,1337	0,1337	0,5268	0,5268	0,1337	0,1337	/
92		3D-1w	0,3541	0,5459	0,7821	0,7645	0,5319	0,4454	0,5431	0,4022	0,3024	0,6617
93	CHRNA4	3D-2w	0,3693	0,5435	0,8534	0,5719	0,4822	0,4292	0,4601	0,3925	0,3445	0,5949
94		3D-3w	0,7	0,6444	0,7664	0,6132	0,684	0,844	0,9348	0,521	0,5234	0,8058
95		3D	/	0,5099	0,5099	0,3819	0,3819	0,5099	0,5099	0,3819	0,3819	/
96	CHAT	3D-1w	0,3605	0,8972	0,7308	0,9728	0,7961	0,3754	0,3216	0,3558	0,0396	0,6662
97		3D-2w	0,2359	0,8653	0,4113	0,5062	0,9248	0,2395	0,1644	0,3778	0,2831	0,3814
98		3D-3w	0,0178	0,0493	0,0218	0,6685	0,1278	0,2706	0,5955	0,384	0,5026	0,5436
99	HTR1A	3D	/	0,3637	0,3637	0,3883	0,3883	0,3637	0,3637	0,3883	0,3883	/
100		3D-1w	0,325	0,192	0,4546	0,8303	0,4277	0,1904	0,5259	0,3	0,4694	0,4226
101		3D-2w	0,5535	0,5992	0,3437	0,6406	0,1954	0,7352	0,385	0,9105	0,9849	0,4987
102		3D-3w	0,7764	0,4296	0,6138	0,2528	0,6611	0,2897	0,6816	0,1362	0,7193	0,4299
103	TPH1	3D	/	0,1642	0,1642	0,5506	0,5506	0,1642	0,1642	0,5506	0,5506	/
104		3D-1w	0,71	0,88	0,5542	0,4852	0,4591	0,6366	0,4922	0,459	0,446	0,1171
105		3D-2w	0,9529	0,7396	0,5039	0,4392	0,4365	0,6743	0,5113	0,4397	0,4367	0,2183
106		3D-3w	0,533	0,1719	0,9055	0,5208	0,4357	0,7876	0,5134	0,4454	0,4265	0,169
107	SCL17A6	3D	/	0,8909	0,8909	0,0698	0,0698	0,8909	0,8909	0,0698	0,0698	/
108		3D-1w	0,4876	0,722	0,7768	0,7538	0,6194	0,115	0,4578	0,4313	0,5426	0,3386
109		3D-2w	0,4871	0,9522	0,8794	0,851	0,5733	0,164	0,3422	0,4589	0,6219	0,7286
110		3D-3w	0,6047	0,6829	0,6776	0,6346	0,5375	0,7984	0,8492	0,9501	0,8594	0,9683
111	SLC17A7	3D	/	0,2464	0,2464	0,0578	0,0578	0,2464	0,2464	0,0578	0,0578	/
112		3D-1w	0,5546	0,3434	0,861	0,6662	0,5181	0,1534	0,2513	0,661	0,872	0,3433
113		3D-2w	0,5567	0,7109	0,9573	0,8527	0,8499	0,2567	0,2799	0,2293	0,5607	0,6663
114		3D-3w	0,4933	0,7814	0,9753	0,3925	0,7747	0,0703	0,2056	0,195	0,41	0,6607

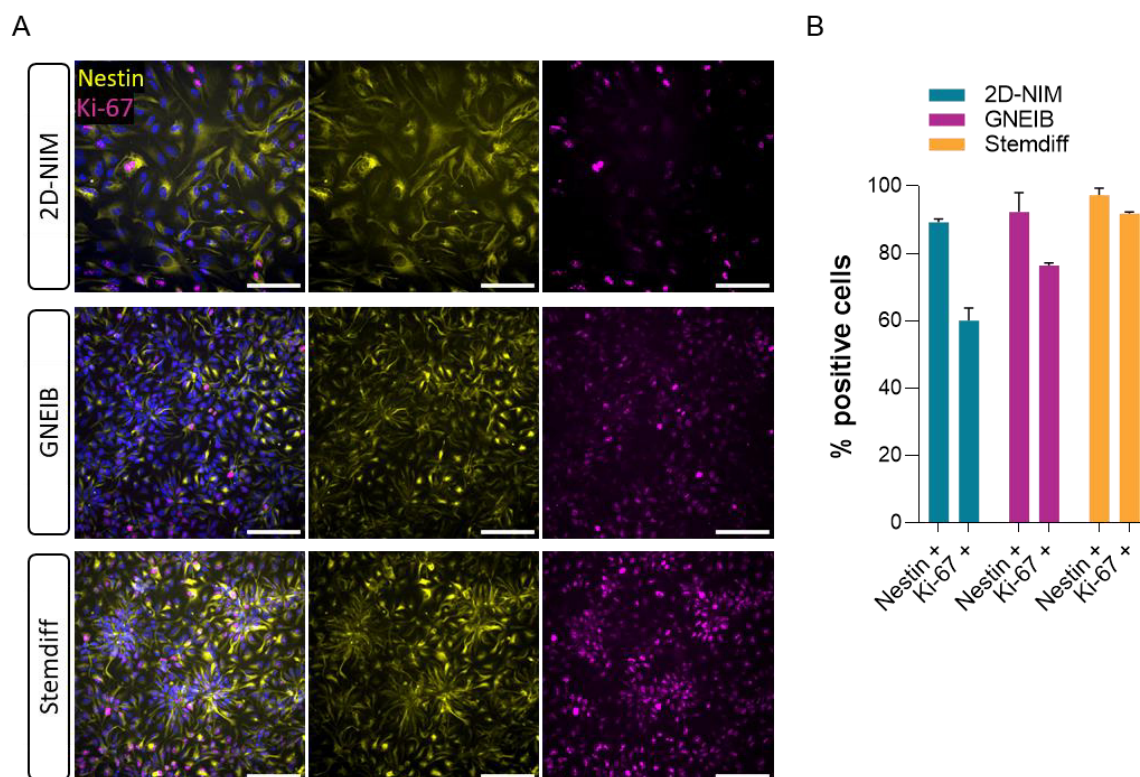
	M	N	O	P	Q	R
1						
2	GNEIB CINDA+	GNEIB CINDA+	GNEIB Electro	GNEIB Electro	Stemdiff CINDA+	
3						
4	Stemdiff CINDA+	Stemdiff Electro	Stemdiff CINDA+	Stemdiff Electro	Stemdiff Electro	legend
5	0,5914	0,5914	0,5914	0,5914	/	≤ 0,075
6	0,1229	0,1229	0,1229	0,1229	/	≤ 0,05
7	0,4167	0,2185	0,474	0,2559	0,8256	≤ 0,01
8	0,3494	0,2542	0,3835	0,2641	0,4147	≤ 0,001
9	0,2408	0,2916	0,3651	0,3262	0,4333	
10	0,1691	0,1691	0,1691	0,1691	/	
11	0,0553	0,0553	0,0553	0,0553	/	
12	0,254	0,1281	0,1999	0,0875	0,2414	
13	0,2471	0,1857	0,2043	0,1405	0,4493	
14	0,1385	0,3022	0,2517	0,4901	0,6385	
15	0,2163	0,2163	0,2163	0,2163	/	
16	0,009	0,009	0,009	0,009	/	
17	0,153	0,1515	0,0375	0,0371	0,4979	
18	0,0731	0,0733	0,0987	0,099	0,8042	
19	0,0867	0,0889	0,1187	0,1203	0,5783	
20	0,0692	0,0692	0,0692	0,0692	/	
21	0,0329	0,0329	0,0329	0,0329	/	
22	0,5562	0,2982	0,1421	0,1243	0,7239	
23	0,211	0,3133	0,1443	0,1617	0,5912	
24	0,1793	0,1968	0,1487	0,1538	0,6269	
25	0,2596	0,2596	0,2596	0,2596	/	
26	0,2771	0,2771	0,2771	0,2771	/	
27	0,1037	0,117	0,2366	0,268	0,5749	
28	0,1803	0,5696	0,2158	0,4781	0,4232	
29	0,199	0,7412	0,2667	0,5881	0,4498	
30	0,1489	0,1489	0,1489	0,1489	/	
31	0,6955	0,6955	0,6955	0,6955	/	
32	0,5998	0,4445	0,5472	0,3862	0,9432	

	M	N	O	P	Q	R
1						
2	GNEIB CINDA+	GNEIB CINDA+	GNEIB Electro	GNEIB Electro	Stemdiff CINDA+	
3						
4	Stemdiff CINDA+	Stemdiff Electro	Stemdiff CINDA+	Stemdiff Electro	Stemdiff Electro	legend
33	0,5508	0,2969	0,7375	0,4133	0,7035	
34	0,5966	0,5313	0,6156	0,5559	0,938	
35	0,3353	0,3353	0,3353	0,3353	/	
36	0,351	0,1919	0,3677	0,282	0,9533	
37	0,4009	0,2066	0,6319	0,3964	0,8498	
38	0,7017	0,3341	0,9428	0,7623	0,9305	
39	0,6584	0,6584	0,6584	0,6584	/	
40	0,4226		0,4226		0,4226	
41	0,4713	0,4298	0,4456	0,5504	0,4117	
42	0,4268	0,3679	0,436	0,3286	0,4181	
43	0,391	0,391	0,391	0,391	/	
44	0,6434	0,1706	0,8793	0,5221	0,53	
45	0,288	0,3391	0,3429	0,6239	0,4257	
46	0,3923	0,5051	0,3954	0,6039	0,4065	
47	0,0303	0,0303	0,0303	0,0303	/	
48	0,1366	0,1348	0,1469	0,11	0,8552	
49	0,1025	0,1023	0,2194	0,2093	0,9985	
50	0,0671	0,1637	0,227	0,499	0,7315	
51	0,379	0,379	0,379	0,379	/	
52	0,3158	0,1613	0,3676	0,1755	0,3649	
53	0,3427	0,2462	0,3735	0,2745	0,9658	
54	0,3685	0,1977	0,4248	0,2357	0,9345	
55	0,8003	0,8003	0,8003	0,8003	/	
56	0,3284	0,0928	0,7381	0,1513	0,2579	
57	0,2668	0,0624	0,4791	0,0827	0,376	
58	0,3368	0,2239	0,4246	0,2557	0,4964	
59	0,7316	0,7316	0,7316	0,7316	/	
60	0,8053	0,4439	0,4083	0,4607	0,4305	

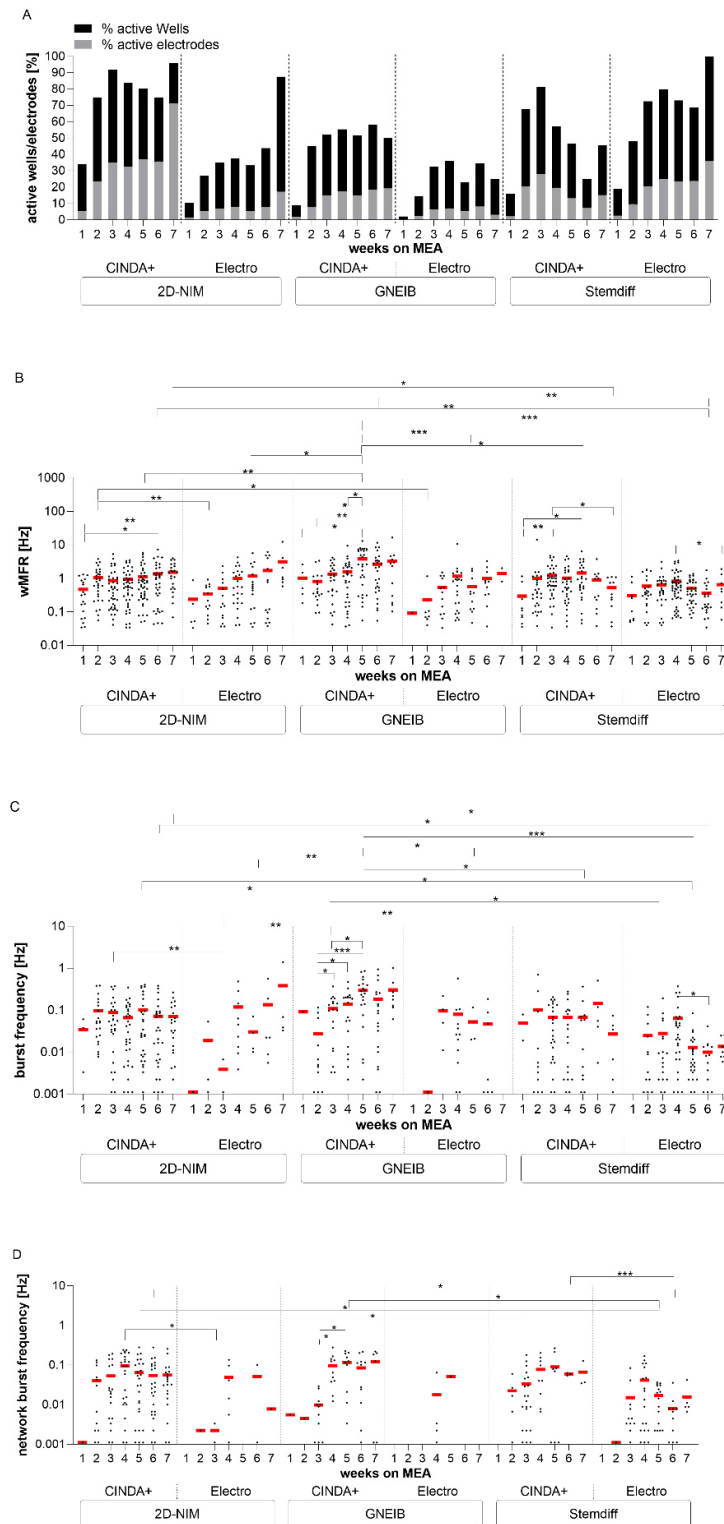
	M	N	O	P	Q	R
1						
2	GNEIB CINDA+	GNEIB CINDA+	GNEIB Electro	GNEIB Electro	Stemdiff CINDA+	
3						
4	Stemdiff CINDA+	Stemdiff Electro	Stemdiff CINDA+	Stemdiff Electro	Stemdiff Electro	legend
61	0,9403	0,4627	0,4492	0,8867	0,4527	
62	0,8904	0,4377	0,4381	0,9938	0,4383	
63	0,0598	0,0598	0,0598	0,0598	/	
64	0,5405	0,6379	0,3558	0,1243	0,6603	
65	0,4226	0,3215	0,3783	0,1857	0,5505	
66	0,4563	0,4845	0,3838	0,2321	0,5662	
67	0,7691	0,7691	0,7691	0,7691	/	
68	0,4823	0,8527	0,4485	0,7835	0,4659	
69	0,4557	0,6367	0,5414	0,5512	0,4888	
70	0,5329	0,877	0,5895	0,5436	0,5189	
71	0,3485	0,3485	0,3485	0,3485	/	
72	0,4597	0,2287	0,2667	0,2477	0,0866	
73	0,0985	0,0325	0,2307	0,0684	0,0956	
74	0,0487	0,0018	0,4439	0,2244	0,2122	
75	0,2701	0,2701	0,2701	0,2701	/	
76	0,2268	0,4046	0,1648	0,3092	0,2758	
77	0,2199	0,4013	0,261	0,4048	0,4332	
78	0,0657	0,4909	0,1248	0,3272	0,5769	
79	0,9463	0,9463	0,9463	0,9463	/	
80	0,7816	0,9222	0,608	0,7176	0,7549	
81	0,6184	0,5223	0,7461	0,7661	0,9579	
82	0,2209	0,2974	0,769	0,9712	0,8226	
83	0,7487	0,7487	0,7487	0,7487	/	
84	0,0155	0,017	0,3011	0,2502	0,7155	
85	0,044	0,044	0,1409	0,1416	0,945	
86	0,0038	0,003	0,1057	0,1064	0,8225	
87	0,775	0,775	0,775	0,775	/	
88	0,3666	0,2802	0,6044	0,463	0,7401	

	M	N	O	P	Q	R
1						
2	GNEIB CINDA+	GNEIB CINDA+	GNEIB Electro	GNEIB Electro	Stemdiff CINDA+	
3						
4	Stemdiff CINDA+	Stemdiff Electro	Stemdiff CINDA+	Stemdiff Electro	Stemdiff Electro	legend
89	0,4751	0,1794	0,6254	0,4216	0,6737	
90	0,5214	0,1155	0,6122	0,3928	0,6631	
91	0,2241	0,2241	0,2241	0,2241	/	
92	0,6138	0,7177	0,9336	0,868	0,7416	
93	0,8179	0,9258	0,6648	0,5566	0,8642	
94	0,4822	0,4828	0,538	0,5543	0,8164	
95	0,8692	0,8692	0,8692	0,8692	/	
96	0,9224	0,7176	0,7075	0,8421	0,769	
97	0,5324	0,801	0,4215	0,4902	0,4936	
98	0,4507	0,9375	0,4089	0,7184	0,4436	
99	0,511	0,511	0,511	0,511	/	
100	0,074	0,4082	0,4502	0,7597	0,425	
101	0,7032	0,734	0,3748	0,3862	0,8686	
102	0,8033	0,497	0,3887	0,9842	0,4584	
103	0,4911	0,4911	0,4911	0,4911	/	
104	0,0674	0,0678	0,4718	0,2888	0,6603	
105	0,187	0,1857	0,2388	0,2249	0,5206	
106	0,1426	0,1345	0,3252	0,2325	0,0626	
107	0,2785	0,2785	0,2785	0,2785	/	
108	0,2927	0,1756	0,9671	0,6969	0,6906	
109	0,7153	0,2338	0,9508	0,4661	0,5872	
110	0,8674	0,5601	0,9069	0,6806	0,8128	
111	0,3371	0,3371	0,3371	0,3371	/	
112	0,1803	0,1517	0,3465	0,2229	0,4885	
113	0,7886	0,5026	0,8392	0,7303	0,6093	
114	0,4382	0,9076	0,3556	0,762	0,594	

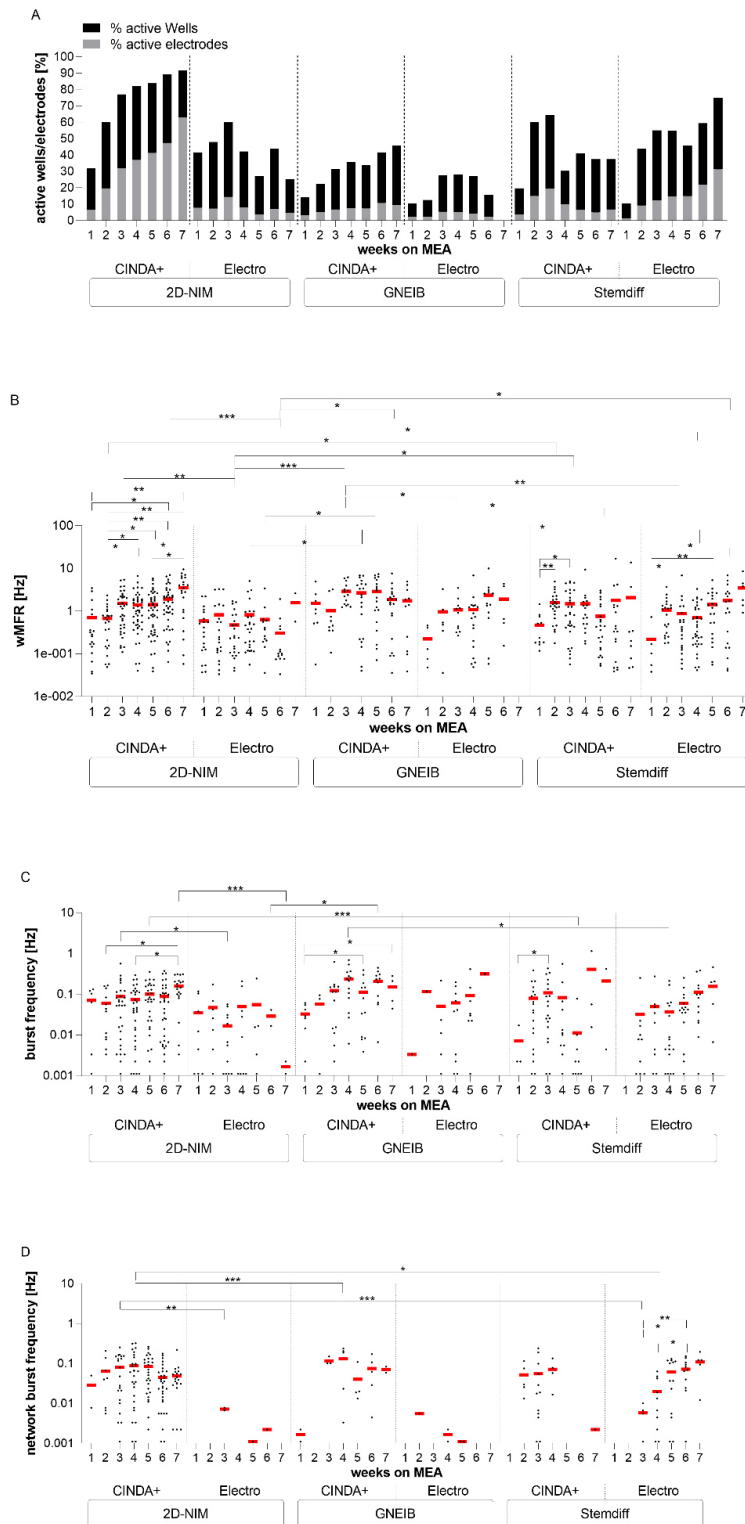
1. Supplementary Figures



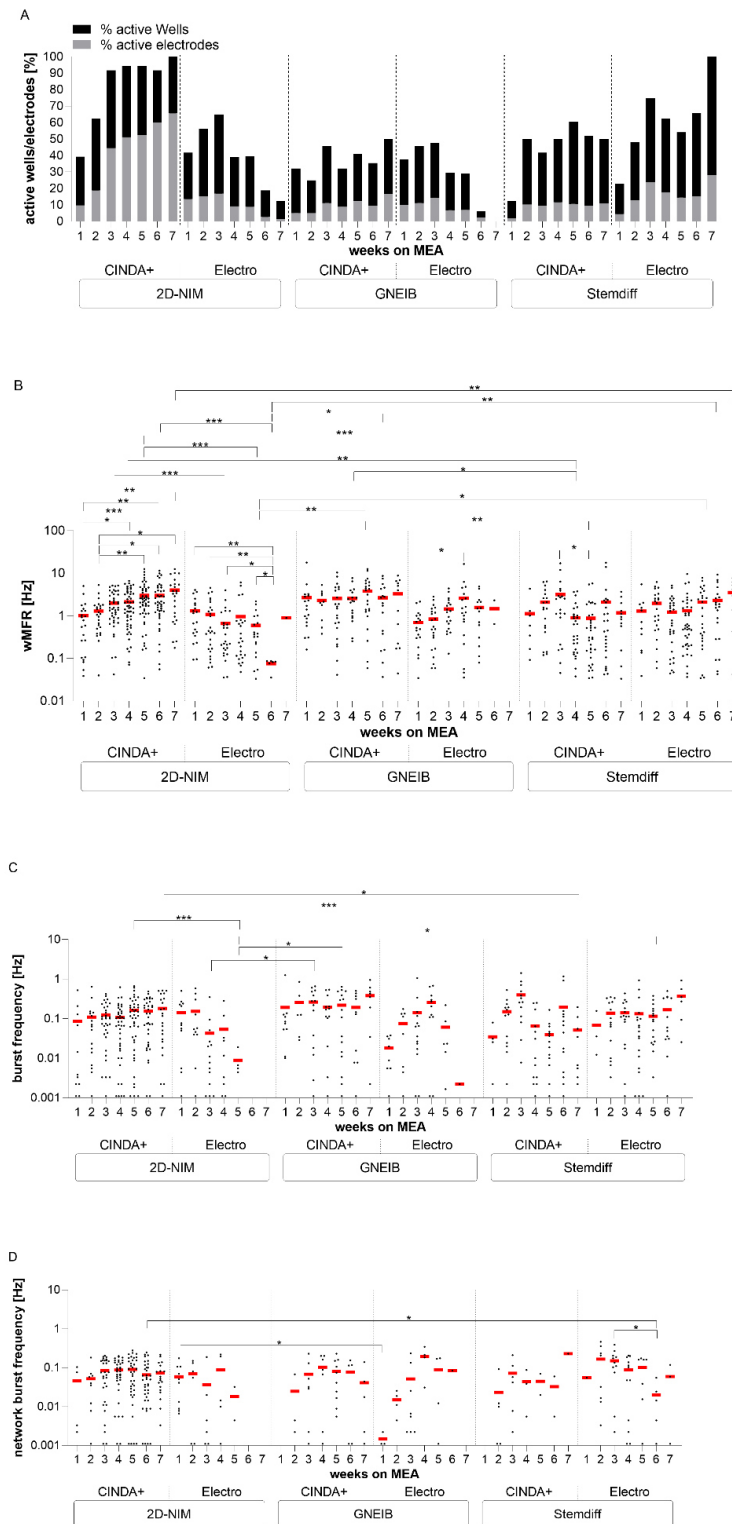
Supplementary Figure S1. Immunocytochemistry staining of human induced neural progenitor cells (hiNPCs). A) After thawing the hiNPCs were replated onto microscopy slides and stained for the neural progenitor marker nestin (yellow) and the proliferation marker Ki-67 (magenta). The nuclei were counterstained with Hoechst 34580 (blue). Representative images are shown. Scale bar = 100 μ m. B) Quantification of hiNPCs stained for the NPC marker nestin or the proliferation marker Ki-67. Data are represented as mean \pm SEM of two independent experiments.



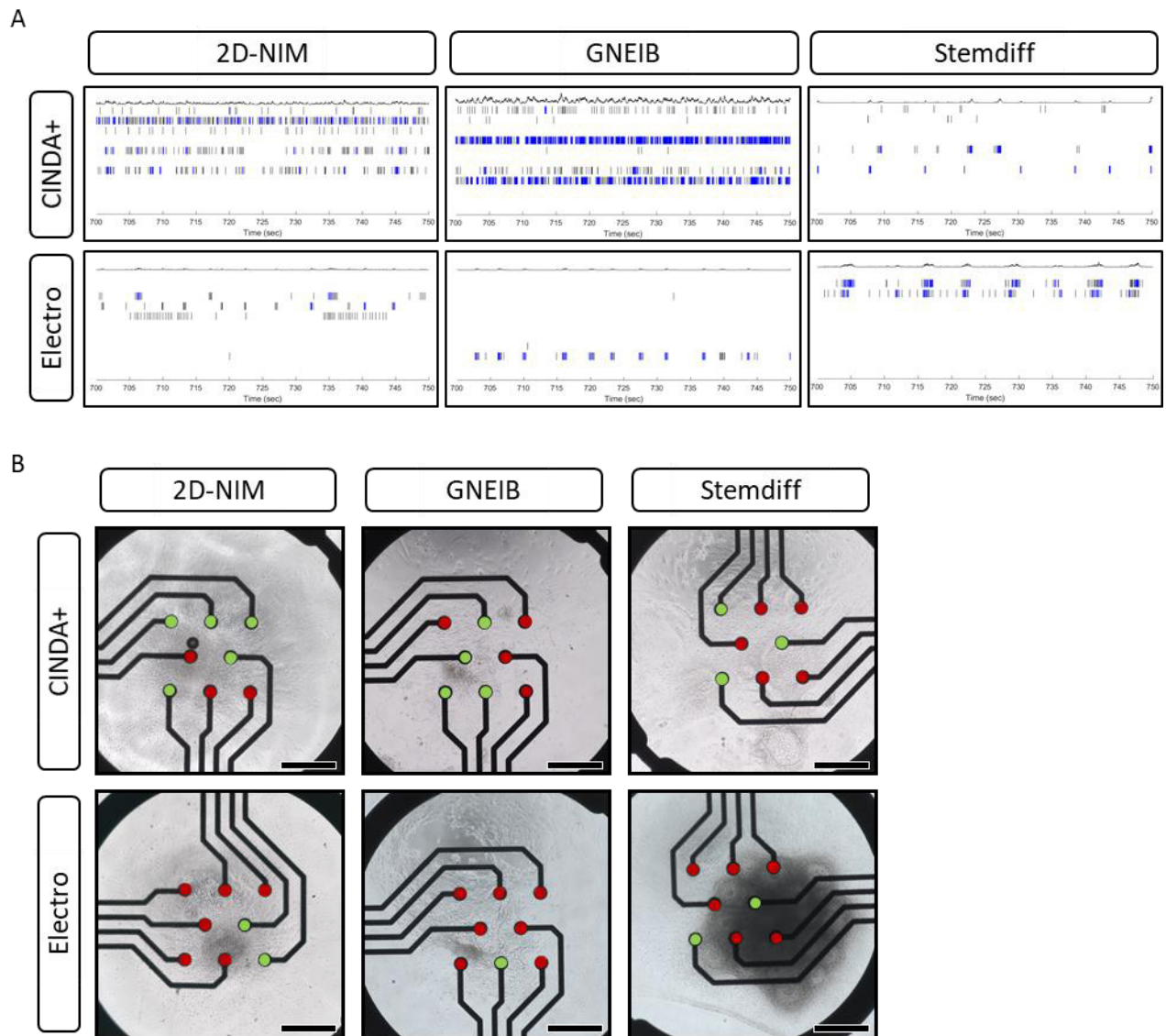
Supplementary Figure S2. Comparison of electrical activity of BrainSpheres (without 3D differentiation) for 7 weeks on microelectrode arrays (MEA). The neuronal functionality was measured twice per week and the parameters active wells and active electrodes (A), weighted mean firing rate (wMFR, B), burst frequency (C), and network burst frequency (D) were analyzed. Each dot represents the mean of one well containing 8 electrodes and the red bar represents the mean of all wells resulting from three independent MEA experiments each ($p \leq 0.05$).



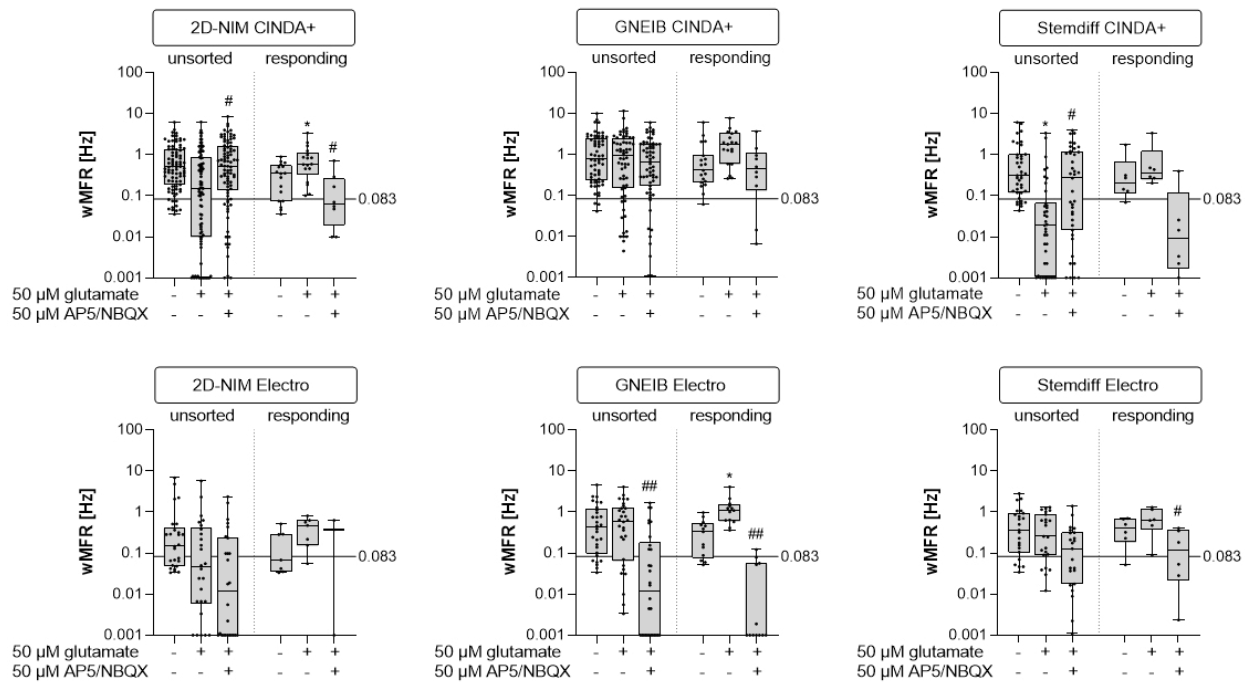
Supplementary Figure S3. Comparison of electrical activity of 1 week 3D differentiated BrainSpheres for 7 weeks on microelectrode arrays (MEA). The neuronal functionality was measured twice per week and the parameters active wells and active electrodes (A), weighted mean firing rate (wMFR, B), burst frequency (C), and network burst frequency (D) were analyzed. Each dot represents the mean of one well containing 8 electrodes and the red bar represents the mean of all wells resulting from three independent MEA experiments each ($p \leq 0.05$).



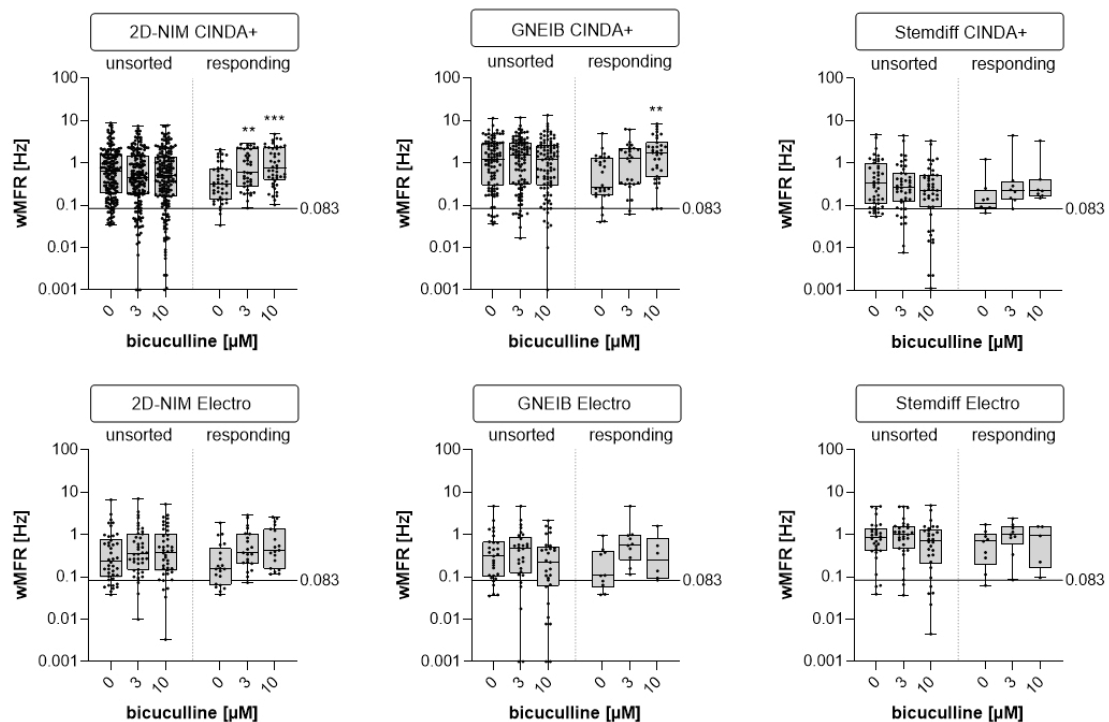
Supplementary Figure S4. Comparison of electrical activity of 2 weeks 3D differentiated BrainSpheres for 7 weeks on microelectrode arrays (MEA). The neuronal functionality was measured twice per week and the parameters active wells and active electrodes (A), weighted mean firing rate (wMFR, B), burst frequency (C), and network burst frequency (D) were analyzed. Each dot represents the mean of one well containing 8 electrodes and the red bar represents the mean of all wells resulting from three independent MEA experiments each ($p \leq 0.05$)



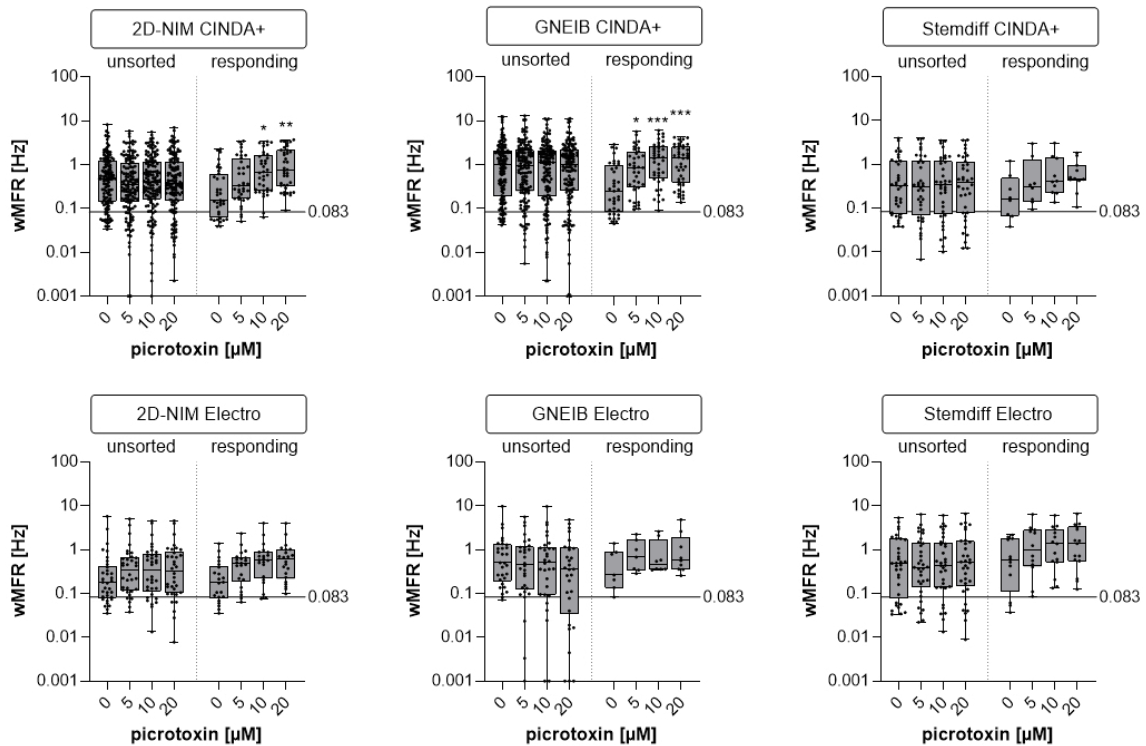
Supplementary Figure S5. Spike raster plots (SRP) and microscopy images of 3 weeks 3D differentiated BrainSpheres differentiated for further 3 weeks on microelectrode arrays (MEA). A) Representative 50 seconds spike raster plots of the respective networks. Spikes are shown as black bars and bursts are shown as blue bars. B) Exemplary microscopy pictures show the position of the BrainSpheres in the wells and the cells growing over the electrodes. Active Electrodes are marked with a green dot and inactive electrodes are marked with a red dot. Scale bar = 200 μm .



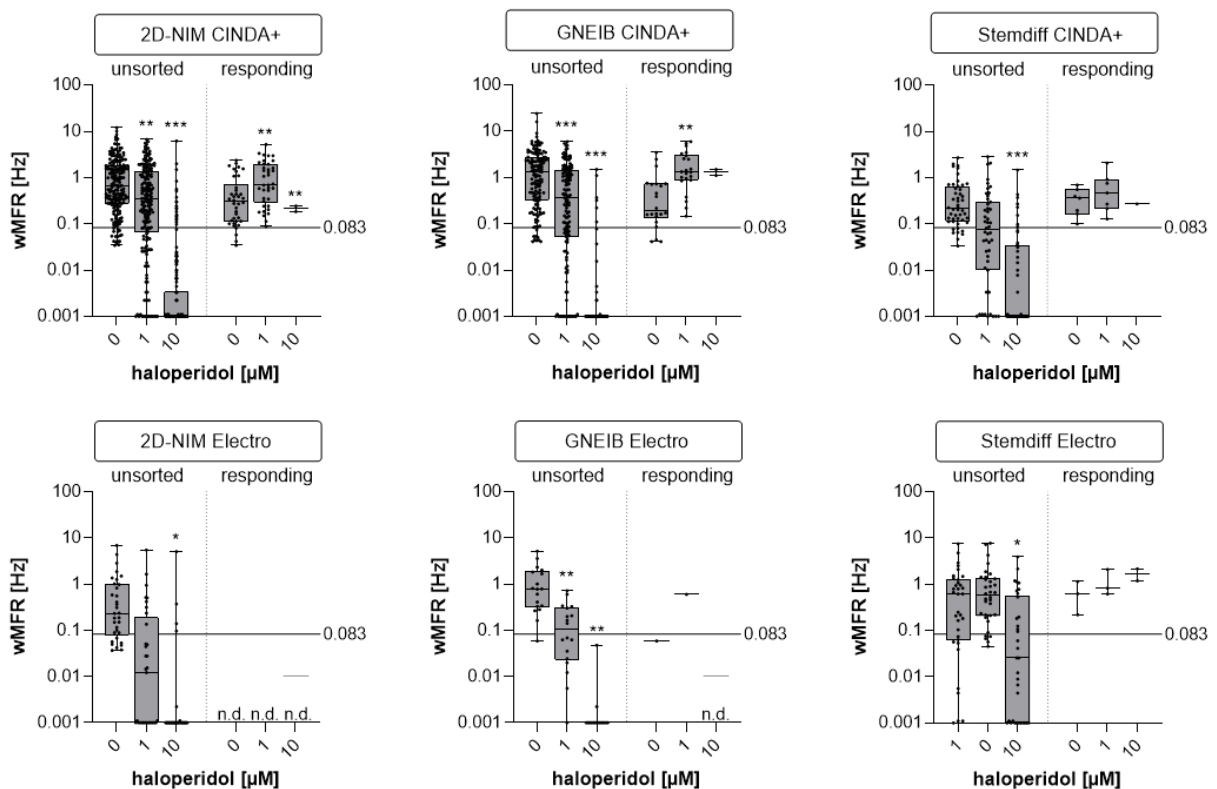
Supplementary Figure S6. Modification of electrical activity by acute pharmacological modulation with glutamate and ap5/nbqx. BrainSpheres were 3 weeks 3D differentiated before plated on MEA and exposed to glutamate (glu) and ap5/nbqx. Shown are the weighted mean firing rate (wMFR) of the untreated baseline measurement and after exposure to glu and ap5/nbqx of all units (unsorted) in comparison to the responding units (responding). Data are shown as box-whisker plots of three independent MEA experiments with 8 wells per condition (* $p \leq 0.05$, ** $p \leq 0.01$, *** $p \leq 0.001$). Each dot represents one unit.



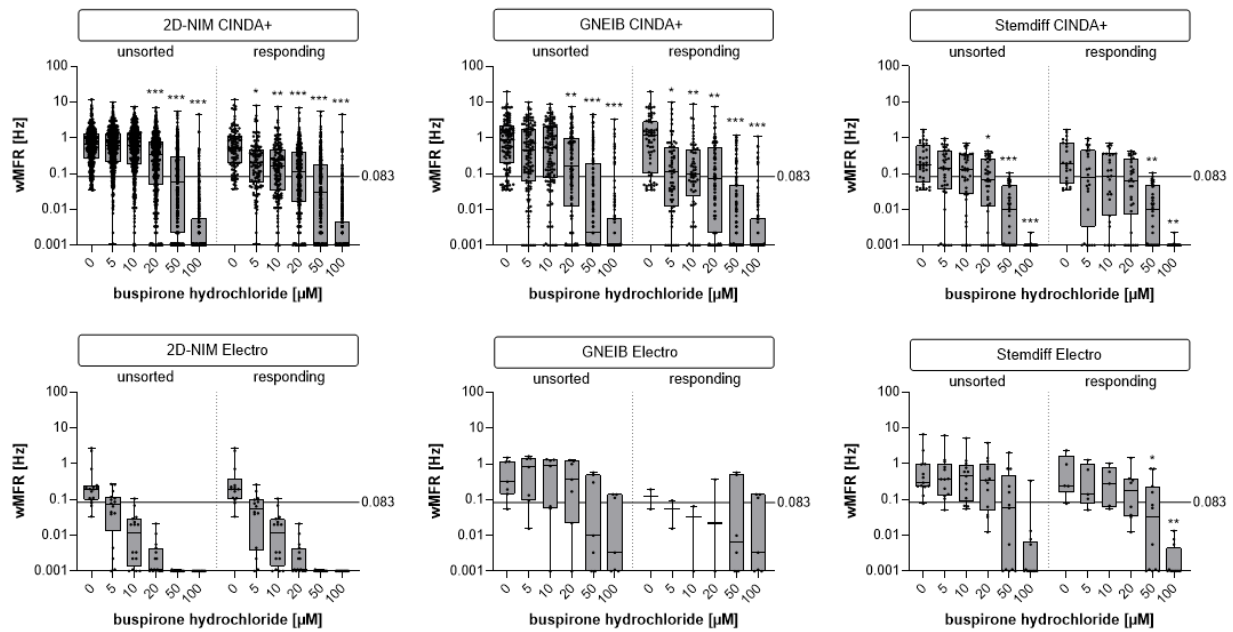
Supplementary Figure S7. Modification of electrical activity by acute pharmacological modulation with bicuculline. BrainSpheres were 3 weeks 3D differentiated before plated on MEA and exposed to bicuculline. Shown are the weighted mean firing rate (wMFR) of the untreated baseline measurement and after exposure to bicuculline of all units (unsorted) in comparison to the responding units (responding). Data are shown as box-whisker plots of three independent MEA experiments with 8 wells per condition (*: significant to the lowest concentration, * $p \leq 0.05$, ** $p \leq 0.01$, *** $p \leq 0.001$). Each dot represents one unit.



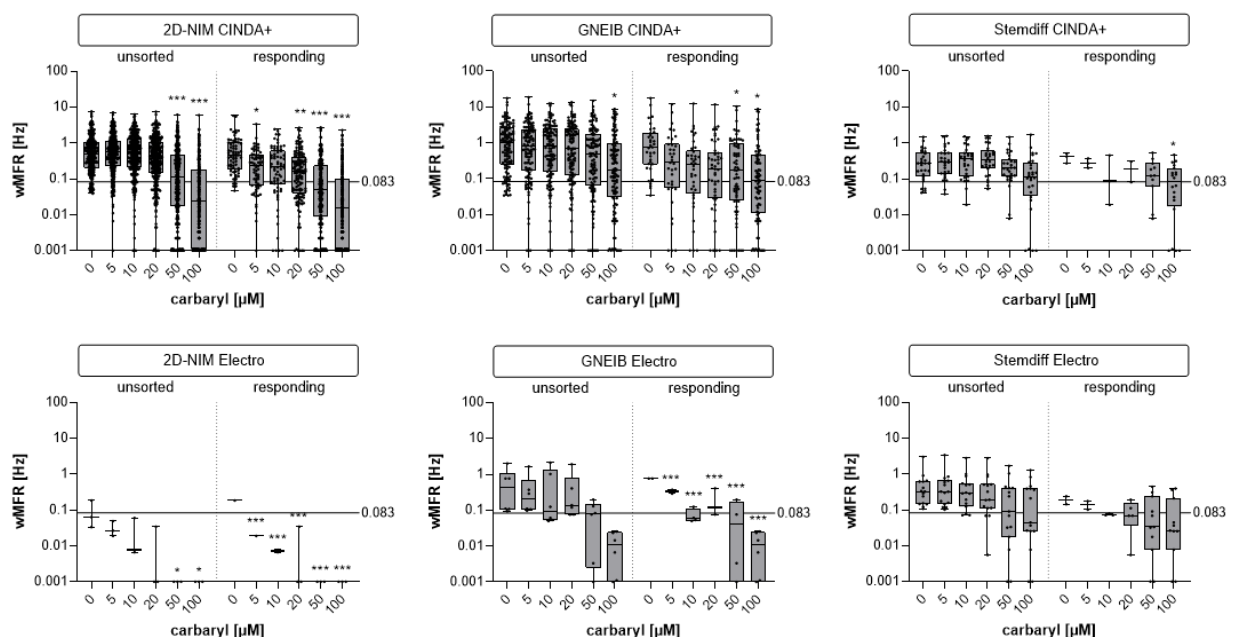
Supplementary Figure S8. Modification of electrical activity by acute pharmacological modulation with picrotoxin. BrainSpheres were 3 weeks 3D differentiated before plated on MEA and exposed to picrotoxin. Shown are the weighted mean firing rate (wMFR) of the untreated baseline measurement and after exposure to picrotoxin of all units (unsorted) in comparison to the responding units (responding). Data are shown as box-whisker plots of three independent MEA experiments with 8 wells per condition (*: significant to the lowest concentration, * $p \leq 0.05$, ** $p \leq 0.01$, *** $p \leq 0.001$). Each dot represents one unit.



Supplementary Figure S9. Modification of electrical activity by acute pharmacological modulation with haloperidol. BrainSpheres were 3 weeks 3D differentiated before plated on MEAs and exposed to haloperidol. Shown are the weighted mean firing rate (wMFR) of the untreated baseline measurements and after exposure to haloperidol of all units (unsorted) in comparison to the responding units (responding). Data are shown as box-whisker plots of three independent MEA experiments with 8 wells per condition (*: significant to the lowest concentration, $p \leq 0.05$, $**p \leq 0.01$, $***p \leq 0.001$). Each dot represents one unit.

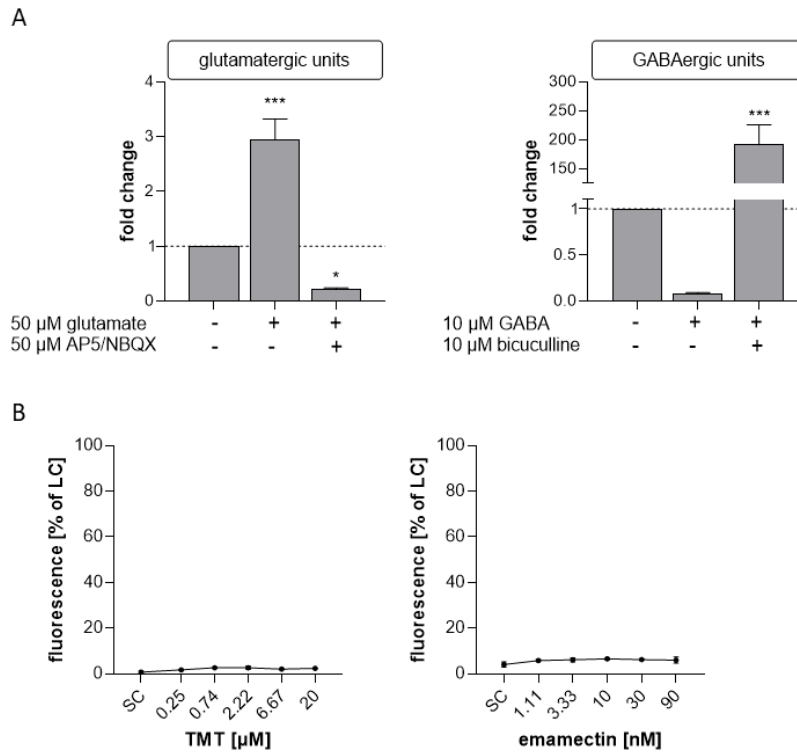


Supplementary Figure S10. Modification of electrical activity by acute pharmacological modulation with buspirone. BrainSpheres were 3 weeks 3D differentiated before plated on MEA and exposed to buspirone. Shown are the weighted mean firing rate (wMFR) of the untreated baseline measurement and after exposure to buspirone of all units (unsorted) in comparison to the responding units (responding). Data are shown as box-whisker plots of three independent MEA experiments with 8 wells per condition (*: significant to the lowest concentration, $p \leq 0.05$, $**p \leq 0.01$, $***p \leq 0.001$). Each dot represents one unit.



Supplementary Figure S11. Modification of electrical activity by acute pharmacological modulation with carbaryl. BrainSpheres were 3 weeks 3D differentiated before plated on MEAs and exposed to carbaryl. Shown are the weighted mean firing rate (wMFR)

of the untreated baseline measurement and after exposure to carbaryl of all units (unsorted) in comparison to the sorted responding units (sorted). Data are shown as box-whisker plots of three independent MEA experiments with 8 wells per condition (*: significant to the lowest concentration, $p \leq 0.05$, $**p \leq 0.01$, $***p \leq 0.001$). Each dot represents one unit.



Supplementary Figure S12. Specification of glutamatergic and GABAergic units for acute neurotoxicity testing. A) Response of neural units to glutamate and AP5/NBQX (left) or GABA and bicuculline (right). Shown are the fold changes of the wMFR to the untreated baseline measurement. Data are represented as mean \pm SEM of 24 wells with 8 electrodes each. (*: significant to the lowest concentration, $*p \leq 0.05$, $**p \leq 0.01$, $***p \leq 0.001$). B) Cytotoxicity assessment after acute exposure to the training compounds TMT and emamectin. Shown are the % of the LC as mean \pm SEM of 3 technical replicates. TMT, trimethyltin chloride; SC, solvent control; LC, lysis control.

Molecular and functional characterization of different BrainSphere models for use in neurotoxicity testing on microelectrode arrays

Julia Hartmann, Noah Henschel, Kristina Bartmann, Arif Dönmez, Gabriele Brockerhoff, Katharina Koch and Ellen Fritsche

Fachzeitschrift/Buch: *Cells*

Impact Factor: 7,666 (2021)

Beteiligung an der Publikation: 85 %

Planung, Durchführung und Auswertung aller Experimente, außer der immunzytochemischen Färbung der adhärennten neuronalen Vorläuferzellen (hier nur Planung). Erstellen aller Abbildungen und Schreiben des gesamten Manuskripts.

Typ der Autorenschaft: Erstautorenschaft

Status der Publikation: veröffentlicht am 27. April 2023

3 Diskussion

3.1 Alternativmethoden – von der Notwendigkeit bis zur derzeitigen Anwendung

Die toxikologische Risikobewertung ist von großer Bedeutung für unsere Gesundheit, da wir vielen Toxinen täglich ausgesetzt sind. Sie begegnen uns beispielsweise in Form von Pestiziden, Reinigungsmitteln, Lebensmittelzusätzen, Kosmetika, Metallen und synthetisch hergestellten Chemikalien (Massaro 2002; Grandjean and Landrigan 2006). Neurotoxine beeinträchtigen das Nervensystem und führen zu adversen Effekten, die wichtige biologische Prozesse beeinträchtigen und somit zu strukturellen und funktionellen Veränderungen bis hin zu neuralem Zelltod führen können (Fritsche et al. 2020b). In den letzten Jahrzehnten basierte die Risikobewertung bezüglich des neurotoxischen Potentials hauptsächlich auf Ergebnissen aus Tierversuchen, die durch die Prüfrichtlinien TG418, TG419 und TG424 der OECD vorgegeben sind (OECD 1995b, a, 1997). Doch, auch wenn Tierversuche in der Vergangenheit einen wesentlichen Beitrag zu unserem medizinischen und toxikologischen Verständnis beigetragen haben, wird ihr Nutzen mittlerweile hinterfragt. Einer der Gründe, die zum Umdenken geführt haben, ist die hohe Ausfallrate bei der Entwicklung neuer Medikamente. Etwa 75 bis 85 % der entwickelten Medikamente scheitern aufgrund von fehlender Wirksamkeit und/oder mangelnder Sicherheit im Menschen (Arrowsmith and Miller 2013; Harrison 2016; Fritsche et al. 2020b). Zu den möglichen Gründen zählen eine schlechte Charakterisierung der verwendeten Tiermodelle, unzureichende Qualität der *in vivo* Studien und speziesspezifische Unterschiede bezüglich Anatomie, Physiologie und Immunologie (Leist and Hartung 2013; Couzin-Frankel 2013; Perrin 2014; Weinhart et al. 2019). Die speziesspezifischen Unterschiede sind vielseitig und beziehen sich im Gehirn beispielsweise auf die Mikroarchitektur des Gehirns, die Morphologie von Astrozyten, das Verhältnis von neuronalen Subzelltypen, Rezeptoraffinitäten und die Genexpression von Neurotransmitterrezeptoren, Zelladhäsionsmolekülen und Elementen der extrazellulären Matrix (*extracellular matrix*, ECM) (DeFelipe et al. 2002; Oberheim et al. 2009; Schmidt et al. 2010; Gassmann et al. 2010; Dach et al. 2017;

Hodge et al. 2019; Klose et al. 2020). Zusätzlich geben die vorgeschriebenen Tierversuche keinen Aufschluss über die mechanistische Wirkungsweise eines Toxins (Lanzoni et al. 2019; Fritsche et al. 2020a). Aus diesen Gründen und dem sehr hohen Ressourcenverbrauch von Tierversuchen, kam es zu Beginn des Jahrhunderts zum Aufruf eines Paradigmenwechsels in der Toxizitätstestung, von der apikalen Endpunktevaluierung im Tier hin zu einer auf Mechanismen basierenden Erfassung von Toxizitäten (National Research Council 2007; Collins et al. 2008; Magurany et al. 2023).

Die sogenannte „Risikobewertung der nächsten Generation“ (*Next generation risk assessment*, NGRA) stützt sich auf mechanistisch relevante, und möglichst human-basierte *in vitro* Assays und *in silico* Ansätze (Krewski et al. 2020). Dafür werden unter anderem zelluläre Modelle benötigt, die eine Vielzahl an organ- und zelltypspezifischen Endpunkten abbilden, um die Wirkungsweise vieler verschiedener Toxine bestimmen zu können (Fritsche et al. 2020a). Dabei sollte bei der Wahl des *in vitro* Kultivierungssystems der Anwendungskontext und die Forschungsziele berücksichtigt werden und wenn erforderlich, eine Kombination aus verschiedenen Kultivierungstechniken verwendet werden. Um die *in vitro* erzeugten Daten in reale Expositionsbedingungen, mit denen eine Risiko- und Gefahrenbewertung durchgeführt werden kann, umzurechnen, müssen Zellmodelle mit Pharmako- und Toxikokinetik sowie computergestützter Modellierung kombiniert werden. Zusätzlich sollten Absorptions- und Verteilungsprozesse untersucht werden, da sich durch Verdunstung oder Bindung des Toxins an die Oberfläche des Kultivierungsgefäßes und die Beschichtung die biologische Verfügbarkeit verringern kann (Paini et al. 2019; Li et al. 2021). Eine Möglichkeit, die Ergebnisse aus den verschiedenen *in vitro* und *in silico* Ansätzen zu verbinden und in einen systemischen Kontext zu bringen, bietet das *Adverse Outcome Pathway* (AOP)-Konzept. Es dient der Darstellung von zusammenhängenden Ereignissen und startet mit einem initialen molekularen Ereignis, welches über ein oder mehrere Schlüsselereignisse in einem adversen Effekt resultiert (Sachana et al. 2021).

Die Akzeptanz von Alternativmethoden hängt von verschiedenen Faktoren ab, wie zum Beispiel dem Zweck der Prüfmethode, der Verwendung, der Anwendbarkeit und den nationalen Rechtsvorschriften (Eskes and Whelan 2016). Für die ersten beiden Punkte, müssen Alternativmethoden sorgfältig charakterisiert und einer oder mehreren Anwendungsdomänen klar zugeordnet werden. Dies ist beispielsweise durch Fallstudien oder Belastung des Zellmodells mit bekannten und gut studierten Modellsubstanzen möglich, die klar definierte und reproduzierbare adverse Effekte auslösen (Kavlock et al. 2018; Mahony et al. 2020; van der Stel et al. 2021). Schließlich muss durch eine Validierung bestätigt werden, dass die Methode alle definierten Anforderungen erfüllt und für den vorgesehenen Einsatz geeignet ist. Aus diesem Grund wurde das europäische Zentrum für die Validierung von Alternativmethoden (*European Centre for the Validation of Alternative Methods*, ECVAM) gegründet und die OECD Leitlinie Nr. 34 für eine international gültige Validierungsstrategie veröffentlicht (OECD 2005; Eskes and Whelan 2016). Diese Validierungsrichtlinie ist derzeit unter Revision, um sie den veränderten Gegebenheiten in der Nutzung von Alternativmethoden anzupassen. Während die regulatorische Anwendung von Alternativmethoden in Europa durch die Gesetzgebung noch stark begrenzt ist, verabschiedeten die USA im Dezember 2022 das FDA Modernisierungsgesetz 2.0 (engl. *FDA Modernization Act 2.0*), welches die Benutzung von Alternativmethoden in der präklinischen Medikamententestung ermöglicht. Zu den erlaubten Alternativmethoden in diesem Gesetz gehören zellbasierte Assays, Organ-on-a-Chip Methoden, mikrophysiologische Systeme, Computermodelle und andere biologisch-basierte Testmethoden wie 3D Bioprinting (Westmoreland et al. 2022; Adashi et al. 2023).

3.2 Die Eignung verschiedener Kultivierungstechniken für den Einsatz in der Neurotoxizitätstestung

Die Kultivierungstechniken für die Erzeugung von neuronalen Netzwerken *in vitro* sind vielfältig und reichen von Monolayer- über Suspensionskulturen bis hin zu

Hydrogelkulturen. Ihre Eignung für den Einsatz in der Neurotoxizitätstestung hängt von vielen Faktoren ab und erfordert ein tiefes Verständnis des Testsystems, der Applikationsdomäne und der untersuchten Endpunkte. Das Wissen über die Vor- und Nachteile, Aussagefähigkeit und Grenzen des Zellsystems, der Kultivierungsmethode und der analytischen Messmethoden sind bei der Etablierung von neuen Methoden essenziell (Schmidt et al. 2017).

Der erste wichtige Punkt bei der Entwicklung eines Zellmodells ist die Wahl der Zelllinie, da es große Unterschiede zwischen Tumor-, immortalisierten, primären und Stammzelllinien gibt. Tumorzelllinien teilen sich unbegrenzt und können über eine sehr lange Zeit kultiviert werden, aber sie sind im Vergleich zu gesunden Zellen stark artifiziell und stellen nicht den gesunden physiologischen Zustand dar. Primäre Zelllinien sind aufgrund ihrer Herkunft nur limitiert verfügbar, stammen häufig von verschiedenen Spendern ab und sind nicht unbegrenzt teilbar. Stammzellen dagegen sind unbegrenzt teilbar, können gezielt differenziert werden und die menschliche Zellphysiologie gut abbilden (Fabbri et al. 2023). Es muss jedoch nachgewiesen werden, dass die Stammzellen reproduzierbar in die spezifizierten Zelltypen differenziert werden können. Für eine mangelnde Reproduzierbarkeit gibt es verschiedene Gründe und sie kann beispielsweise durch Optimierung der Reprogrammierung, kurzzeitige Kultivierung unter hypoxischen Bedingungen, Anpassung der Kultivierungsmethode, Verwendung der gleichen Zellpassage sowie Nutzung von Zellbanken verbessert werden (Yoshida et al. 2009; Pamies et al. 2017a; Tigges et al. 2021). Die in dieser Dissertation verwendeten Stammzellen wurden in einem zweistufigen Bankingprozess eingefroren und auf Morphologie, Mykoplasmen, Identität, Stabilität des Karyotyps, Genexpression, Pluripotenz und Viabilität getestet (Tigges et al. 2021). Zusätzlich wurden die hiPSCs nach dem Auftauen maximal fünfmal passagiert und täglich morphologisch begutachtet. Ein weiterer kritischer Aspekt von hiPSCs ist, dass das epigenetische Gedächtnis des Ursprungsgewebes während der Reprogrammierung bestehen bleiben kann. Inwieweit dies das Potential zur gerichteten Differenzierung beeinflusst, ist ein aktuelles Forschungsgebiet (Kim et al. 2010; Scesa et al. 2021). Zudem gibt es einen neuen Ansatz für die

Reprogrammierung bei der das epigenetische Gedächtnis vollständig gelöscht wird (Buckberry et al. 2023).

Die Wahl der Kultivierungstechnik ist die nächste wichtige Entscheidung bei der Entwicklung von Alternativmethoden. Die Kultivierung in 2D ist verhältnismäßig einfach in der Handhabung, benötigt kein spezielles Equipment und ermöglicht homogene Zellkulturen. Da es eine seit Jahrzehnten etablierte Technik ist, existieren viele verschiedene Assays zur Analyse von spezifischen Endpunkten in 2D, die für Hochdurchsatzstudien geeignet sind (Centeno et al. 2018). In Manuskript 2.1 (Fritsche et al. 2020b) wurden 2D Modelle, die auf von hiPSCs-abgeleiteten Neuronen basieren und bereits für das Screening in der *in vitro* Neurotoxizitätstestung eingesetzt wurden, diskutiert. Zu den am häufigsten untersuchten Endpunkten in 2D Kulturen zählen Messungen der Zytotoxizität, elektrischen Aktivität, Zellzahl, Neuritenlänge und Apoptose (Malik et al. 2014; Rana et al. 2017; Snyder et al. 2018; Tukker et al. 2020a, c; Saavedra et al. 2021; Kang et al. 2022; Zhai et al. 2023). Einige Modelle wurden bereits in einem 384 Well Format durchgeführt und ermöglichen somit einen hohen Screening-Durchsatz (Sherman and Bang 2018; Stacey et al. 2018). Die 2D-Kultivierung ermöglicht zudem eine gleichmäßige Exposition der Zellen gegenüber dem Kulturmedium und der zu testenden Substanz, wodurch eine höhere Reproduzierbarkeit möglich ist (Centeno et al. 2018; Logan et al. 2019). Neben den Vorteilen weist eine adhärente Kultivierung aber auch Grenzen auf. Hierzu zählen eine artifizielle Zellmorphologie aufgrund der harten Kulturoberfläche und eine fehlende Komplexität in der Zellorganisation, wodurch interzelluläre Kontakte und Interaktionen begrenzt sind. Neurale 3D Kultivierungstechniken ermöglichen eine komplexere Zellarchitektur mit mehr Zell-Zell-Kontakten und stellen somit eine Alternative dar, die der physiologischeren Situation angepasster ist (Paşca 2018; Logan et al. 2019). Die Eignung von Neurosphären, welche aus primären Gewebezellen gewonnen werden, für die Verwendung in neurotoxikologischen Studien wurde bereits mehrfach gezeigt (Barenys et al. 2017; Klose et al. 2022a, b; Koch et al. 2022). In den letzten Jahren wurde diese Kultivierungstechnik für hiPSCs weiterentwickelt, so dass diese entweder als NPC-Neurosphären oder differenzierte BrainSpheres für toxikologische *in vitro*

Studien eingesetzt wurden (Pamies et al. 2017b, 2022; Abreu et al. 2018; Leite et al. 2019; Sirenko et al. 2019; Kobolak et al. 2020).

Die Zellmodelle, die im Zuge dieser Dissertation entwickelt und veröffentlicht wurden, wurden während ihrer Kultivierungsdauer auf verschiedene Weisen kultiviert. In Manuskript 2.3 (Nimtz et al. 2020) wurden die hiPSCs in einer Sphärenkultur in hiNPCs differenziert und anschließend als Neurosphären in Proliferationskultur gehalten, bevor sie adhärent auf beschichteten Kulturoberflächen in Neurone und Astrozyten differenziert wurden. Die Neurone waren elektrisch aktiv und haben verschiedene subtypspezifische Rezeptoren und Proteine exprimiert. Die Neurosphären wiesen allerdings eine recht hohe Variabilität auf. Dies zeigte sich zum einen darin, dass nicht jede Induktion in hiNPCs resultierte und zum anderen an einer unterschiedlich starken elektrischen Aktivität zwischen den einzelnen Batches und Neurosphären. Des Weiteren wurden glutamaterge N-Methyl-D-Aspartat (NMDA)- und α -Amino-3-Hydroxy-5-Methyl-4-Isoxazol-Propionsäure (AMPA)-Rezeptoren zwar nachgewiesen, aber die Neurone zeigten bei Antagonisierung der Rezeptoren keine Änderung der elektrischen Aktivität. Der Grund hierfür könnte einerseits in einer fehlenden oder unreifen Zellfunktion oder andererseits in der Art der Auswertung begründet sein, wodurch die elektrischen Aktivitäten der anderen neuronalen Zelltypen die Reaktion der glutamatergen Neurone überlagern. Dies könnte mit der *Spike Sorting*-Methode, die in Manuskript 2.6 (Hartmann et al. 2023) etabliert wurde, überprüft werden. Aufgrund der oben erwähnten höheren Reproduzierbarkeit von 2D Kulturen, wurden die hiPSCs in Manuskript 2.6 (Hartmann et al. 2023) adhärent in hiNPCs induziert und alle drei Induktionsprotokolle wiesen eine hohe Effizienz mit sehr geringen Varianzen auf. Das intermediäre Filamentprotein NESTIN, welches spezifisch in NPCs exprimiert wird (Park et al. 2010), wurde von mindestens 97 % der Zellen exprimiert. Nach einer kurzen Expansionsphase in 2D wurden die hiNPCs in einen Schüttelinkubator überführt und direkt nach der Sphärenbildung in Differenzierungsmedium zu BrainSpheres differenziert. Aufgrund verschiedener Kulturmedien wurden unter gleichen Kultivierungsbedingungen sechs verschiedene BrainSphere-Modelle miteinander verglichen. Durch die adhärente Induktion zeigten die BrainSpheres eine höhere Reproduzierbarkeit, aber es wurden deutliche

Unterschiede zwischen den verschiedenen Modellen festgestellt. Sie unterschieden sich hinsichtlich der Differenzierung in neuronale Subtypen und Astrozyten und der Stärke der elektrischen Aktivität. Der Einfluss des Kulturmediums, oder spezifischer einzelner Zusätze zum Kulturmedium, auf die neurale Differenzierung wurde auch in anderen Studien beobachtet. Dies stellt den Nutzen generischer Induktions- und Differenzierungsmedien in Frage und unterstreicht gleichzeitig die Bedeutung von sorgfältig für die spezifische Anwendung ausgewählter Medien (Nadadhur et al. 2018; Nimtz et al. 2020).

Imredy et al. untersuchten den Unterschied zwischen 2D und 3D Kultivierungsmethoden unter Verwendung des gleichen neuronalen Differenzierungsmediums und stellten Unterschiede in der Sensitivität und Spezifität der Assays fest. Als mögliche Gründe wurden unterschiedliche Differenzierungszeiten von etwa 85 Tagen für die Neurosphären und 23 Tagen für die 2D-Kulturen, sowie die unterschiedliche prozentuale Zusammensetzung von glutamatergen und GABAergen Neuronen und Astrozyten diskutiert (Imredy et al. 2023). Für einen direkten Vergleich sollten sich die Kultivierungsmethoden in Bezug auf die Kultivierungsdauer und die Zelltypzusammensetzung jedoch nicht unterscheiden, da sowohl unterschiedliche neuronale Subtypen als auch unterschiedliche Zellstadien verschiedene adverse Effekte aufweisen können (Masjosthusmann et al. 2018; Fritsche et al. 2020b). Slavin et al. haben 2D und 3D Kulturen zu verschiedenen Differenzierungszeitpunkten mit antiviralen Medikamenten belastet, von denen einige nur bei den 2D kultivierten und andere nur bei den als Neurosphären kultivierten Modellen zu einer Änderung in der funktionellen Calciumaktivität führten. Dabei wurden beide Modelle mit dem gleichen Medium und gleich lang differenziert und unterschieden sich zu Beginn der Kultivierung nicht in ihrer Zusammensetzung an neuronalen Subtypen (Slavin et al. 2021). Ob sich dies während der Differenzierungszeit von 8 Wochen verändert hat, wurde nicht untersucht. Eine weitere 2D-3D-Vergleichsstudie zeigt, dass Gene, die mit neuraler Differenzierung assoziiert sind, in Neurosphären stärker als in 2D kultivierten Zellen exprimiert werden und Neurosphären somit zum gleichen Zeitpunkt einen höheren Grad an Differenzierung erreichen (Nunes et al. 2022). Diese Beispiele verdeutlichen, dass der Endpunkt, an dem die Toxizität *in vitro* gemessen wird, für

jedes Zellmodell spezifisch ermittelt werden sollte. Zudem sollte durch eine zielgerichtete Charakterisierung die molekulare Ausstattung und das Entwicklungsstadium der Zellen klar definiert werden.

Eine weitere Möglichkeit der 3D neuronalen Netzbildung *in vitro* bietet die Einbettung in Hydrogele. In Manuskript 2.5 (Hartmann et al. 2022) wurde gezeigt, dass sich diese Kultivierungsart insbesondere für sehr lange Kultivierungszeiten von bis zu 7 Monaten eignet, so dass sie auch für Langzeitbelastungsstudien eingesetzt werden kann. Durch die Poren des Hydrogels wird der Austausch von Sauerstoff und Nährstoffen bis ins Innere des Gels ermöglicht, wodurch die Zellen keinem Versorgungsgradienten ausgesetzt sind, wie dies bei Organoiden und zu großen BrainSpheres der Fall ist (Murphy et al. 2017). Allerdings liegt die Schwierigkeit dieser Technik darin, einen geeigneten Assay für die Toxizitätsbestimmung zu finden. In Manuskript 2.5 (Hartmann et al. 2022) wurde gezeigt, dass vermeintlich simple Viabilitätsassays nur begrenzt eingesetzt werden können, da der Farbstoff nicht ungehindert durch das Hydrogel diffundieren kann. Dieser Aspekt muss auch bei toxikologischen Studien berücksichtigt werden. Diffusionsstudien mit dem entsprechenden Toxin und dem Hydrogel müssen zeigen, dass das Toxin ungehindert durch das Gel diffundieren kann und die eingebetteten Zellen mit der richtigen Konzentration exponiert werden. Bisher gibt es nur wenige Studien, in denen diese Kultivierungstechnik für (Entwicklungs-) Neurotoxikologische Studien eingesetzt wurde (Hellwig et al. 2018; Kang et al. 2021).

Die mögliche Anwendung von Organoiden in der Neurotoxizitätstestung wurde in den Manuskripten 2.1 (Fritsche et al. 2020b) und 2.2 (Fritsche et al. 2020a) diskutiert. Organoide bilden die verschiedenen kortikalen Schichten sowie spezifische Gehirnregionen ab und ermöglichen dadurch die Untersuchung adverser Effekte auf die Zytoarchitektur des Gehirns (Qian et al. 2016, 2018; Bagley et al. 2017; Lancaster et al. 2017; Quadrato et al. 2017). Einer der derzeitigen Anwendungsbereiche von Organoiden ist die Verwendung als Krankheitsmodell und die Untersuchung potenzieller Medikamente gegen beispielsweise durch das Zika-Virus ausgelöste Mikrozephalie oder Alzheimer (Watanabe et al. 2017; Zhou et al. 2017; Park et al.

2021). Die Schwierigkeiten dieser Kultivierungstechnik liegen in der hohen Heterogenität und Batch-zu-Batch Variabilität, insbesondere bei Modellen mit ungerichteter Selbstorganisation (Logan et al. 2019; Fan et al. 2022). Für toxikologische Screenings wurde sie bisher noch nicht eingesetzt.

3.3 Zusammensetzung des neuronalen *in vitro* Netzwerks im Kontext der toxikologischen Aussagekraft

Das menschliche Gehirn besteht aus einer Vielzahl an Zellen, die miteinander kommunizieren, um ein funktionierendes Netzwerk zu bilden. Jeder Zelltyp besitzt dabei eine andere molekulare Ausstattung und erfüllt eine spezifische Funktion. Somit zeigen Neurone, Astrozyten, Oligodendrozyten und Mikrogliazellen, sowie die neuronalen Subtypen untereinander, unterschiedliche adverse Effekte (Malik et al. 2014; Oyanagi et al. 2015; Pei et al. 2016; Masjosthusmann et al. 2018; Fritsche et al. 2020b; Crofton et al. 2022). Die Zusammensetzung des neuronalen Netzwerks (NN) ist daher ein wichtiger Faktor und es ist davon auszugehen, dass der toxikologische Anwendungsbereich durch eine Mischkultur aus verschiedenen neuronalen Zelltypen im Gegensatz zu einer Monokultur erweitert wird.

Die *in vitro* Modelle aus den Manuskripten 2.3 (Nimtz et al. 2020) und 2.6 (Hartmann et al. 2023) wurden auf molekularer und funktionaler Ebene auf neuronale Subtypen (GABAerge, glutamaterge, dopaminerge, serotonerge und cholinerge Neurone) und Astrozyten charakterisiert. Die Modelle wurden auf spezifische Enzyme für die Neurotransmittersynthese, exemplarische Rezeptoren und Änderung der elektrischen Aktivität unter Belastung spezifischer Modulatoren untersucht. Die Ergebnisse aus Manuskript 2.3 (Nimtz et al. 2020) verdeutlichen dabei, dass eine Charakterisierung auf ausschließlich molekularer Ebene nicht ausreichend ist. Hier konnte die Expression der glutamatergen NMDA- und AMPA-Rezeptor mittels PCR auf genetischer Ebene und mittels Immunzytochemie auf Proteinebene nachgewiesen werden, aber nicht auf funktioneller Ebene mittels Antagonisierung und Messung der

elektrischen Aktivität. Infolgedessen zeigte eine Belastung mit dem Neurotoxin Domoinsäure, welches spezifisch an den AMPA-Rezeptor bindet und bei hohen Konzentrationen zu exzitatorischem Zelltod führen sollte (Giordano et al. 2007), nicht zu einer erhöhten elektrischen Aktivität. Die verschiedenen BrainSphere-Modelle, die in Manuskript 2.6 (Hartmann et al. 2023) veröffentlicht wurden, weisen ebenfalls deutliche Unterschiede in den untersuchten neuronalen Subtypen auf. Beispielsweise variiert die Anzahl der Units, die auf Belastung mit Glutamat mit einer Zunahme der neuronalen Aktivität reagieren, zwischen den BrainSpheres von 15 % bis 43 %. Ohne *Spike Sorting*-Methode, die im nächsten Abschnitt ausführlicher diskutiert wird, wäre diese Änderung der elektrischen Aktivität bei den meisten BrainSphere-Modellen nicht auswertbar gewesen. Dies verdeutlicht, dass Zellmodell, Assay und Auswertung immer gemeinsam betrachtet werden sollten. Ein weiteres Beispiel für Zelltypspezifische Toxizität liefert das Pestizid Rotenon. Es schädigt bevorzugt dopaminerge Neurone, die in der *Substantia nigra* ansässig sind. Neueste Forschungsergebnisse haben gezeigt, dass die Expression des vesikulären Glutamattransporters 2 (*vesicular glutamate transporter 2*, VGLUT2) zu einer Resilienz gegenüber Rotenon beiträgt und die Expression dieses Rezeptors in dopaminergen Neuronen je nach Gehirnregion variiert (Betarbet et al. 2000; Buck et al. 2021). Daher ist es wichtig, *in vitro* Zellmodelle nicht nur auf verschiedene Zelltypen und ihre Proteinexpression zu charakterisieren, sondern auch, wie in Manuskript 2.6 (Hartmann et al. 2023), ihre Zugehörigkeit bezüglich der Gehirnregion zu bestimmen. Zusätzlich sollte bei der Entwicklung von *in vitro* Modellen beachtet werden, dass sich die neuronale Zusammensetzung zwischen den Gehirnregionen unterscheidet, so dass je nach Anwendungskontext das passende Modell angewendet wird („*fit for purpose*“) (Nadadhur et al. 2018; Nunes et al. 2022).

Neben den neuronalen Subtypen sind Gliazellen ebenfalls von großer Bedeutung. Sie spielen eine entscheidende Rolle in der Vermittlung von Neurotoxizität, indem sie situationsabhängig entweder neuroprotektiv oder neurotoxisch wirken (Wang et al. 2013; Stary et al. 2015; Brüll et al. 2020; Guttenplan et al. 2021). Zusätzlich übernehmen sie eine wichtige Funktion bei dem Neuritenauswuchs, der Synaptogenese, sowie der Freisetzung und Aufnahme von Neurotransmittern und sind

für die Reifung und Funktion von neuronalen Netzwerken unerlässlich (Reemst et al. 2016; Allen and Lyons 2018; Mahmoud et al. 2019). In Manuskript 2.5 (Hartmann et al. 2022) konnte die Differenzierung in Astrozyten durch die Zugabe von Laminin 111 (L111) verstärkt werden. Dies führte sowohl zu einer höheren elektrischen Aktivität mit einer stärkeren Netzwerkaktivität als auch zu einer schnelleren Rehabilitation der elektrischen Aktivität nach Zugabe des Natriumionenkanalblockers Tetrodotoxin (TTX). Ob die schnellere Rehabilitation auf die neuroprotektive Wirkung des L111 oder die Ausschüttung neuroprotektiver Faktoren durch Astrozyten zurückzuführen ist, muss in Folgestudien abschließend geklärt werden. Es ist jedoch wahrscheinlicher, dass die Astrozyten diesen starken Effekt begünstigen, da nach einer Kultivierungszeit von 128 Tagen nicht mehr genügend L111 vorhanden ist. In Manuskript 2.6 (Hartmann et al. 2023) stellten wir ebenfalls eine höhere elektrische Aktivität in den beiden BrainSphere-Modellen fest, bei denen mittels Immunzytochemie die meisten Astrozyten nachgewiesen wurden. Dies ist in Übereinstimmung mit anderen Studien, die den Einfluss von Neuronen-Astrozyten-Co-Kulturen auf die elektrische Aktivität untersuchten (Tukker et al. 2018; Odawara et al. 2018). Dieser Effekt kann durch den positiven Einfluss von Astrozyten auf die neuronale Netzwerkreifung und Synapsenbildung erklärt werden (Allen and Lyons 2018). Um die Zahl der Astrozyten *in vitro* zu kontrollieren beziehungsweise zu erhöhen, gibt es verschiedene Ansätze. Eine verlängerte Kultivierungszeit ermöglicht den Wechsel von Neurogenese zu Gliogenese und somit eine vermehrte Differenzierung in Astrozyten (Lappalainen et al. 2010; Paavilainen et al. 2018). Dies wurde auch in den hiNPCs, die im Zuge dieser Dissertation kultiviert wurden, beobachtet. Aus diesem Grund ist es wichtig, dass Experimente immer mit einer klar definierten Zellpassage durchgeführt werden. Außerdem kann die Differenzierung in Astrozyten durch spezifische Zusätze zum Kulturmedien angeregt werden, wie beispielsweise Fibroblasten Wachstumsfaktor 8 (*fibroblast growth factor 8*, FGF-8), Retinsäure (RA), Sonic hedgehog (SHH), Leukämiehemmender Faktor (*leukemia inhibitory factor*, LIF), ziliärer neurotropher Faktor (*ciliary neurotrophic factor*, CNTF), Knochenmorphogenetische Protein 2 (*bone morphogenetic protein 2*, BMP2), EGF oder Heregulin (Krencik et al. 2011; Shaltouki et al. 2013; Tao and Zhang 2016; Byun et al. 2020). Das Induktionsmedium, welches in Manuskript 2.6 (Hartmann et al. 2023) zu den meisten Astrozyten führte beinhaltet

im Gegensatz zu den anderen Induktionsmedien den Wachstumsfaktor EGF. Es wurde gezeigt, dass der EGF-Rezeptor (EGFR) an der Gliogenese und der Expression von Glia-spezifischen Proteinen beteiligt ist (Shen et al. 2001; Fu et al. 2021). Abhängig von den verwendeten Medienzusätzen und deren Verhältnis unterscheiden sich zudem der Phänotyp und die regionale Spezifikation der Astrozyten (Ben Haim and Rowitch 2016; Suga et al. 2019). Eine geringe Genexpression des sauren Gliafaserproteins (*glial fibrillary acidic protein*, GFAP) in Manuskript 2.3 (Nimtz et al. 2020) lässt vermuten, dass das CINDA-Medium die Differenzierung in protoplasmatische statt in faserförmige Astrozyten begünstigt (Molofsky et al. 2012). In zukünftigen Studien sollte daher je nach Anwendungsziel eine detailliertere Charakterisierung der Astrozyten in Erwägung gezogen werden.

In Manuskript 2.1 (Fritsche et al. 2020b) wurde die Bedeutung von Mikroglia diskutiert, die in unseren Modellen abundant sind. Sie stellen die Immunzellen des Gehirns dar und in ihrem aktivierten Zustand können sie sowohl pro- als auch anti-inflammatorische Faktoren ausschütten und beschädigtes Gewebe phagozytieren (Arcuri et al. 2017). Aus toxikologischer Sicht sind Mikroglia bedeutend, da sie nach Exposition gegenüber einem Toxin in einen überaktiven Zustand übergehen und cytotoxische Faktoren freisetzen, die Neurotoxizität vermitteln (Block et al. 2007). Zu den Toxinen, deren Neurotoxizität über Mikroglia vermittelt oder verstärkt werden, zählen beispielsweise Alkohol und Mangan (Tjalkens et al. 2017; Henriques et al. 2018). Da Mikroglia nicht aus dem Neuroektoderm entstammen, müssen sie *in vitro* separat induziert werden. Die *in vitro* Differenzierung von hiPSC in Mikroglia dauert je nach Protokoll etwa 30 bis 70 Tage und erfordert verschiedene Medienzusätze (Fritsche et al. 2020b). Um die Aussagekraft von neuronalen *in vitro* Netzwerken zu erweitern, gibt es bereits erste erfolgreiche Versuche Mikroglia in 3D Organoide und Sphären zu integrieren und gemeinsam mit Neuronen und Astrozyten zu kultivieren (Ormel et al. 2018; Brüll et al. 2020). Eine weitere wichtige Zellpopulation sind Oligodendrozyten, die in den hier erwähnten Manuskripten nicht analysiert wurden. Sie versorgen Axone mit Metaboliten und umhüllen sie mit Myelin, um eine saltatorische Erregungsleitung zu ermöglichen. (Saab and Nave 2017; Stadelmann et al. 2019). Eine genauere Charakterisierung in diese Richtung wäre eine geeignete Folgestudie.

Mögliche Markergene oder -lipide für den Nachweis von Oligodendrozyten sind Oligodendrozytentranskriptionsfaktor 2 (*oligodendrocyte transcription factor 2*, OLIG2), Myelinbasisprotein (*myelin basic protein*, MBP) und O4 (Ehrlich et al. 2017; Pamies et al. 2017b; García-León et al. 2020).

3.4 Auswertung von Mikroelektrodenarrays (MEAs) in der Neurotoxizitätstestung (NT)

Viele Neurotoxine beeinträchtigen die neuronale Kommunikation, indem sie beispielsweise Neurotransmitter, Neurotransmitterrezeptoren, die synaptische Vesikelaufnahme oder Ionenkanäle beeinflussen (Spencer and Lein 2014; Costa 2017). Eine Störung dieser interzellulären neuronalen Kommunikation kann *in vitro* mittels Mikroelektrodenarrays (MEA) untersucht werden, da diese Technologie die Aufzeichnung extrazellulärer Aktionspotentiale (EAP) in Echtzeit und auf nicht invasive Weise ermöglicht (Johnstone et al. 2010; Shafer 2019; Shafer et al. 2019). Die Analyse der gemessenen EAPs liefert wichtige Informationen über die allgemeine elektrische Aktivität, die Differenzierung und die Netzwerkaktivität (Cotterill et al. 2016). Einzelne EAPs, auch Spikes genannt, kodieren Informationen, die sowohl von internen als auch externen Quellen stammen können. Zusätzlich können Aktionspotentiale in frühen neuronalen Entwicklungsstadien auch spontan und ohne synaptische Aktivität entstehen, daher sollte eine tatsächliche synaptische Aktivität mit spezifischen pharmakologischen Agonisten und Antagonisten bestätigt werden. Je nach Stimulus, Hirnregion und Zelltyp können Spikes regelmäßig oder unregelmäßig auftreten und zeitliche Muster, sogenannte Bursts, abbilden. Dabei ist die Kodierung von Bursts system- und kontextabhängig. Netzwerkbursts entstehen, wenn Neurone miteinander kommunizieren und synchron verschaltet sind. Sie sind somit ein Zeichen für die Reife eines Netzwerks (Bradford and McNutt 2015; Zeldenrust et al. 2018).

Um Spikes, Bursts und Netzwerkbursts zu analysieren, bieten aktuelle MEA-Systeme viele verschiedene Parameter für die Auswertung an (Shafer 2019; Bartmann et al.

2023). Einige der Parameter, die auch in den Arbeiten dieser Dissertation verwendet wurden, sind die Anzahl aktiver Elektroden, gewichtete Feuerrate (*weighted mean firing rate*, wMFR), Burstfrequenz, Spikes pro Burst und Netzworkeburstfrequenz. Für eine aussagekräftige Auswertung müssen die Analyseparameter und Grenzwerte für die Spike- und Burstdetektion sorgfältig ausgewählt und für jedes Zellmodell und die Umgebung empirisch ermittelt werden. Hierzu zählen die Mindestanzahl an Spikes in Hertz (Hz) für die Definition einer aktiven Elektrode, die Mindestanzahl an Spikes pro Burst und der Abstand der einzelnen Spikes für die Definition eines Bursts, sowie die Mindestanzahl an Elektroden mit einem zur gleichen Zeit stattfindenden Burst für die Definition eines Netzworkebursts. Die MEA-Technologie und die oben erwähnten Analyseparameter wurden bereits erfolgreich für Neurotoxizitätsstudien mit Zellkulturen von Nagetieren und hiPSCs, die in Neurone und menschliche Astrozyten differenzieren, eingesetzt (Mack et al. 2014; Brown et al. 2016; Vassallo et al. 2017; Tukker et al. 2018, 2020b, c; Saavedra et al. 2021). Bei Vergleichsstudien zwischen mehreren Laboren konnte zudem eine hohe Sensitivität und Spezifität als auch Reproduzierbarkeit nachgewiesen werden, wenn murine primäre Zellen verwendet wurden (Novellino et al. 2011; McConnell et al. 2012; Valdivia et al. 2014). Wichtig bei einem Vergleich verschiedener Studien ist dabei die Verwendung des gleichen MEA-Systems und Plattenformats, da unterschiedliche Elektrodendichten, Kulturoberflächen und Analyseparameter, sowohl die Sensitivität als auch Spezifität des Assays beeinflussen (Zhai et al. 2023).

Die Stärke der Netzworkeaktivität ist ebenfalls von mehreren Einflussfaktoren abhängig. Hierzu zählen beispielsweise das Verhältnis von exzitatorischen zu inhibitorischen Neuronen, Co-Kultur mit Astrozyten, Zelldichte und Zellreife (Biffi et al. 2013; Tukker et al. 2018, 2020b; Saavedra et al. 2021; Hartmann et al. 2023; Parodi et al. 2023). Ein unausgewogenes Verhältnis von inhibitorischen GABAergen zu exzitatorischen glutamatergen Neuronen führt nicht nur zu einer unterschiedlichen elektrischen Aktivität, sondern kann auch zu einer Überlagerung der Signale des dominanten Zelltyps gegenüber des weniger vorherrschenden Zelltyps führen. Dies kann sich in einer fehlenden Reaktion auf Neurotransmitter (Manuskript 2.6 – Hartmann et al. 2023) oder einer falschen Reaktion auf Neurotoxine wie Domoinsäure (Manuskript 2.3 –

Nimt et al. 2020) zeigen. In Manuskript 2.6 konnten mit der oben erwähnten Analyse­methode nur in einem von sechs Zell­modellen glutamaterge Neurone nachgewiesen werden. Aus diesem Grund wurde die *Spike Sorting*-Methode auf die MEA-Daten angewandt. Diese Methode nutzt aus, dass die Wellenform eines Aktionspotentials je nach Zelltyp, Zellmorphologie, Anzahl der Ionenkanäle und Entfernung zur Elektrode variiert. Anhand von Kurvenver­laufsanalysen können einzelne aktive neuronale Einheiten (engl. *units*) innerhalb des Signals einer MEA-Elektrode erkannt, voneinander getrennt und anschließend individuell ausgewertet werden (Bean 2007; Rey et al. 2015; Pas et al. 2018). Die *Spike Sorting*-Methode wurde bereits erfolgreich für die Charakterisierung individueller Zelltypen angewandt (Mannal et al. 2021; Ronchi et al. 2021). Für die Sortierung der einzelnen Wellenformen gibt es verschiedene Algorithmen die eingesetzt werden können. Wie bei den Spike- und Burstparametern ist auch hier empirisch zu ermitteln, welcher Algorithmus für das jeweilige Zellsystem am besten geeignet ist (Sukiban et al. 2019). Ebenfalls sollte darauf geachtet werden, dass die Höhe der Amplitude sich unter dem Einfluss porenbildender und lytischer Toxine verringern kann (Negri et al. 2020). Auf die Zellmodelle in Manuskript 2.6 (Hartmann et al. 2023) wurde aus diesem Grund der Algorithmus „automatische Clusterbildung T-Verteilung EM-Methode“ (engl. *automatic clustering T-Distribution EM method*) mit zehn Freiheitsgraden und einer initialen Nummer von 20 Einheiten angewandt. Um die sortierten Einheiten einem spezifischen neuronalen Subtyp zuzuordnen, wurden die neuronalen Netzwerke zunächst mit Neurotransmit­tern und anschließend mit spezifischen Antagonisten oder Agonisten belastet. Unter der jeweiligen Belastung wurde die Änderung der wMFR gemessen und es wurden die Einheiten identifiziert, die auf den Neurotransmitter und den Antagonisten mit einer Änderung von mindestens $\pm 0,25$ reagierten. Diese Einheiten wurden als reagierende Einheiten (engl. *responding units*) bezeichnet. Anschließend wurde die Stärke der Änderung der wMFR aller reagierenden Einheiten und der prozentuale Anteil an reagierenden Einheiten ausgewertet. Mithilfe des *Spike Sortings* wurden in allen sechs BrainSphere-Modellen aus Manuskript 2.6 glutamaterge, GABAerge, dopaminerge, cholinerge und serotonerge Neurone nachgewiesen (Hartmann et al. 2023). Für zukünftige Studien wäre eine Erweiterung der Methode

sinnvoll, so dass auch das Burstverhalten einzelner neuronaler Einheiten ausgewertet werden kann.

Des Weiteren wurde im Zuge dieser Dissertation der humane Multineurotransmitterrezeptor Assay (*human multi-neurotransmitter receptor assay*, hMNR) entwickelt (Manuskript 2.6 - Hartmann et al. 2023). Der Assay basiert auf der *Spike Sorting*-Methode und besteht aus mehreren Belastungsphasen. In der ersten Phase wird das NN nach einer Basismessung zuerst mit dem Neurotransmitter und anschließend mit dem passenden Antagonisten belastet. Die Zuordnung zu reagierenden Einheiten erfolgt nach dem oben beschriebenen Prinzip. In der zweiten Phase wird das NN mit der unbekannten Testsubstanz belastet. Aufgrund der vorherigen Zuordnung der Einheiten kann sowohl der Effekt auf das ganze Netzwerk als auch der Effekt auf spezifische neuronale Zelltypen untersucht werden. Der Vorteil besteht darin, dass neuronale Einheiten in einer gemischten Co-Kultur aus Neuronen und Gliazellen kultiviert werden, aber trotzdem auf der individuellen neuronalen Ebene ausgewertet werden können. In einer kleinen *Proof-of-Concept*-Studie mit den zwei Testsubstanzen Trimethylzinnchlorid (*trimethyltin chloride*, TMT) und Emamectin wurde der Einsatz des Assays für glutamaterge und GABAerge Neurone bestätigt. Weitere Studien müssen die Anwendbarkeit des hMNR für weitere neuronale Subtypen bestätigen. Nachdem die Applikationsdomäne ausreichend definiert wurde, sollte die Aussagefähigkeit des Assays unter Verwendung von Testsubstanzen bestimmt werden. Positive Testsubstanzen, mit klar definierten und reproduzierbaren adversen Effekten, werden verwendet, um die Relevanz und die Sensitivität eines bestimmten Endpunktes eines Assays zu verifizieren. Negative Testsubstanzen, die nachweislich keine Neurotoxizität verursachen, werden zur Bestimmung der Spezifität benötigt (Crofton et al. 2011; Mundy et al. 2015). Um eine zuverlässige Aussage über die Sensitivität und Spezifität treffen zu können, sollten idealerweise mindestens 100 Chemikalien verwendet werden (Sachana et al. 2019).

4 Zusammenfassung

Neurotoxizität (NT) kann durch eine große Bandbreite an Chemikalien verursacht werden, denen wir täglich ausgesetzt sind. Dabei werden ihre adversen Effekte über eine Vielzahl an unterschiedlichen Wirkmechanismen transportiert, die schließlich zu einer Störung der neuronalen Funktion führen. Die derzeitige regulatorische Testung von Substanzen auf NT erfolgt mit Tierversuchen, doch deren hohe Kosten und geringer Testdurchsatz erschweren die Testung einer großen Anzahl an Chemikalien. Darüber hinaus verhindern teils gravierende Artenunterschiede die Übertragbarkeit auf den Menschen. Um die Datenlücke zu schließen und speziesspezifische Unterschiede zu umgehen, werden alternative, humanrelevante *in vitro* Methoden benötigt, welche auf menschlichen Stammzellen basieren, reproduzierbar und sorgfältig charakterisiert sind. Solche Modelle für die pharmakologische und toxikologische Anwendung zu entwickeln war das Ziel dieser Dissertation. Zunächst beschreiben die beiden Übersichtsartikel (Manuskript 2.1 und 2.2) den Einsatz von auf humanen induzierten pluripotenten Stammzellen (hiPSC)-basierten neuronalen *in vitro* Kulturen in der heutigen und zukünftigen Toxizitätstestung sowie in der Krankheitsmodellierung. Der Fokus von Manuskript 2.1 (Fritsche et al. 2020b) liegt auf zweidimensionalen (2D) Zellkulturen bestehend aus Neuronen und Gliazellen, die *in vitro* Differenzierung in Mikroglia, sowie dreidimensionale (3D) Organoid – und Hydrogelkulturen. Manuskript 2.2 (Fritsche et al. 2020a) behandelt die neusten Kultivierungstechniken, Organ-on-a-chip Methoden und Genome Editing. Die vier Originalarbeiten beschäftigen sich mit der Entwicklung oder Verbesserung von auf hiPSC basierenden neuronalen Zellmodellen. In Manuskript 2.3 (Nimtz et al. 2020) wurden humane neurale Netzwerke (hNN) aus hiPSCs differenziert und deren Funktion durch den Zusatz reifungsfördernder Faktoren verbessert. Dieses Protokoll wurde in Manuskript 2.4 (Bartmann et al. 2021) aufgegriffen und im Hinblick auf das Zellsystem und die Datenauswertung verbessert. Manuskript 2.5 (Hartmann et al. 2022) zeigte anhand von auf Alginathydrogelen basierenden 3D neuronalen Netzwerken, dass Laminin 111 (L111) die neurale Entwicklung inklusive der neuronalen Netzwerkreifung deutlich verbessert. In der letzten Publikation dieser Arbeit, Manuskript 2.6 (Hartmann et al. 2023), wurden reproduzierbare BrainSpheres aus 2D und 3D Kultivierungstechniken entwickelt und

die Methode des *Spike Sortings* etabliert, wodurch die Entwicklung des humanen Multineurotransmitterrezeptor Assays (hMNR) möglich war.

5 Summary

Neurotoxicity (NT) is caused by a wide range of chemicals to which we are exposed daily. Their adverse effects are transported via a variety of different mechanisms of action which ultimately lead to a disruption of neural function. Current regulatory testing of substances for NT is conducted using animal experiments, but their high costs and low throughput make it difficult to test a large number of chemicals. In addition, sometimes serious species differences prevent transferability to humans. In order to close the data gap and circumvent species-specific differences, alternative, human-relevant *in vitro* methods are needed that are based on human stem cells, are reproducible and carefully characterized. The aim of this dissertation was to develop such models for pharmacological and toxicological application. The two review articles (manuscripts 2.1 and 2.2) describe the use of human induced pluripotent stem cell (hiPSC)-based neural *in vitro* cultures in current and future toxicity testing and disease modeling. The focus of manuscript 2.1 (Fritsche et al. 2020b) is on two-dimensional (2D) cell cultures consisting of neurons and glial cells, *in vitro* differentiation into microglia, and three-dimensional (3D) organoid and hydrogel cultures. Manuscript 2.2 (Fritsche et al. 2020a) deals with the latest cultivation techniques, organ-on-a-chip methods, and genome editing. The four original papers deal with the development or improvement of hiPSC-based neural cell models. In manuscript 2.3 (Nimtz et al. 2020), human neural networks (hNN) were differentiated from hiPSC and their function was enhanced by the addition of maturation-promoting factors. This protocol was taken up in manuscript 2.4 (Bartmann et al. 2021) and improved regarding the cell system and data evaluation. Manuscript 2.5 (Hartmann et al. 2022) used alginate hydrogel-based 3D neural networks to show that laminin 111 (L111) significantly enhances neural development, including neural network maturation. In the last publication of this work, manuscript 2.6 (Hartmann et al. 2023), reproducible BrainSpheres were developed from 2D and 3D cultivation techniques and the spike sorting method was established, which enabled the development of the human multi-neurotransmitter receptor assay (hMNR).

Abkürzungsverzeichnis

2D	zweidimensional
3D	dreidimensional
ADP	Adenosindiphosphat
ALK	Aktivin Rezeptor-ähnliche Kinase (engl. <i>activin receptor-like kinases</i>)
AMPA	α -Amino-3-Hydroxy-5-Methyl-4-Isoxazol-Propionsäure
AOP	<i>Adverse Outcome Pathway</i>
AP	Aktionspotential
ATP	Adenosintriphosphat
BDNF	Gehirn-abstammender neurotropher Faktor (engl. <i>brain-derived neurotrophic factor</i>)
BMP 2, BMP4	Knochenmorphogenetisches Protein 2, 4 (engl. <i>bone morphogenetic protein 2, 4</i>)
cAMP	zyklisches Adenosinmonophosphat (engl. <i>cyclic adenosine monophosphate</i>)
C-MYC	zelluläres Myelozytomatose-Onkogen (engl. <i>cellular myelocytomatosis oncogene</i>) zelluläres
EAP	Extrazelluläres Aktionspotential
ECM	Extrazelluläre Matrix (engl. <i>extracellular matrix</i>)
ECVAM	europäisches Zentrum für die Validierung von Alternativmethoden (engl. <i>European Centre for the Validation of Alternative Methods</i>)
EGF	epidermaler Wachstumsfaktor (engl. <i>epidermal growth factor</i>)
EGFR	EGF-Rezeptor
EPSP	exzitatorisches postsynaptisches Potential (engl. <i>excitatory postsynaptic potential</i>)
ESC	Embryonale Stammzellen (engl. <i>embryonic stem cells</i>)
FGF-2, FGF-8	Fibroblasten Wachstumsfaktor 2, 8 (engl. <i>fibroblast growth factor 2, 8</i>)

Abkürzungsverzeichnis

GABA	γ -Aminobuttersäure (engl. <i>gamma-aminobutyric acid</i>)
GDNF	Gliazellen abstammenden neurotrophen Faktor (engl. <i>glial cell line-derived neurotrophic factor</i>)
GFAP	saures Gliafaserprotein (engl. <i>glial fibrillary acidic protein</i>)
GFRA1	GDNF Familienrezeptor α 1
hESC	Humane embryonale Stammzelle
hiNPC	HiPSC-abgeleitete neurale Progenitorzelle
hiPSC	Humane induzierte pluripotente Stammzelle (engl. <i>human induced pluripotent stem cell</i>)
hMNR	humaner Multineurotransmitterrezeptor Assay (engl. <i>human multi-neurotransmitter receptor assay</i>)
hNN	Humane neurale Netzwerke
Hz	Hertz; SI-Einheit der Frequenz
iPSC	Induzierte pluripotente Stammzelle (engl. <i>induced pluripotent stem cell</i>)
IPSP	inhibitorisches postsynaptisches Potential (engl. <i>inhibitory postsynaptic potential</i>)
JNK	c-Jun N-terminale Kinasen
KLF4	Krüppel-ähnlicher Faktor 4 (engl. <i>krüppel-like factor 4</i>)
L111	Laminin 111
LDH	Laktat-Dehydrogenase
LIF	Leukämiehemmender Faktor (engl. <i>leukemia inhibitory factor</i>)
LIN28	abnormale Zellabstammung 28 (engl. <i>cell lineage abnormal 28</i>)
MBP	Myelinbasisprotein (engl. <i>myelin basic protein</i>)
MEA	Mikroelektroden Array (engl. <i>microelectrode array</i>)
NAM	Alternativmethoden (engl. <i>new approach methods</i>)
NANOG	Homöoboxprotein NANOG (engl. <i>NANOG homeobox</i>)

NCAM	neurales Zelladhäsionsmolekül (engl. <i>neural cell adhesion molecule</i>)
NF1A, NF1B	nuklearer Faktor 1 A, B (engl. <i>nuclear factor 1 A, B</i>)
NGRA	Risikobewertung der nächsten Generation (engl. <i>next generation risk assessment</i>)
NMDA	N-Methyl-D-Aspartat
NN	Neurale Netzwerke
NPC	Neurale Progenitorzelle (engl. <i>neural progenitor cell</i>)
NT	Neurotoxizität
NT-3	Neurotrophin-3
OCT3/4	Oktamer-bindender Transkriptionsfaktor-3/4 (engl. <i>octamer-binding transcription factor-3/4</i>)
OECD	Organisation für wirtschaftliche Zusammenarbeit und Entwicklung (engl. <i>Organisation for Economic Co-operation and Development</i>)
OLIG2	Oligodendrozytentranskriptionsfaktor 2 (engl. <i>oligodendrocyte transcription factor 2</i>)
PAX6	gepaartes Box-Protein 6 (engl. <i>paired box protein 6</i>)
RA	Retinsäure (engl. <i>retinoic acid</i>)
REACH	Registrierung, Evaluierung und Autorisierung von Chemikalien (engl. <i>registration, evaluation and authorization of chemicals</i>)
rNN	Neurale Netzwerke aus primären Rattenzellen
ROS	Reaktive Sauerstoffspezies (engl. <i>reactive oxygen species</i>)
SHH	Sonic hedgehog
SOX1, SOX2, SOX9	Geschlechtsbestimmende Region Y-Box 1, 2, 9 (engl. <i>sex determining region Y-box 1, 2, 9</i>)
SRP	Spikerasterplot
STAT1	Signalüberträger und Aktivator der Transkription 1 (engl. <i>signal transducer and activator of transcription 1</i>)
TF	Transkriptionsfaktor

Abkürzungsverzeichnis

TG	Prüfrichtlinien (engl. <i>test guidelines</i>)
TGF- β	transformierender Wachstumsfaktor- β (engl. <i>transforming growth factor-β</i>)
TMT	Trimethylzinnchlorid (engl. <i>trimethyltin chloride</i>)
TRK	Tropomyosinrezeptorkinasen
TTX	Tetrodotoxin
VGLUT2	vesikulärer Glutamattransporter 2 (engl. <i>vesicular glutamate transporter 2</i>)
wMFR	gewichtete Feuerrate (engl. <i>weighted mean firing rate</i>)
ZNS	Zentrales Nervensystem

Literaturverzeichnis

- Abbas M, Moradi F, Hu W, et al (2021) Vertebrate cell culture as an experimental approach – limitations and solutions. *Comp Biochem Physiol B Biochem Mol Biol* 254. <https://doi.org/10.1016/j.cbpb.2021.110570>
- Abreu CM, Gama L, Krasemann S, et al (2018) Microglia Increase Inflammatory Responses in iPSC-Derived Human BrainSpheres. *Front Microbiol* 9:1–12. <https://doi.org/10.3389/fmicb.2018.02766>
- Adashi EY, O'Mahony DP, Cohen IG (2023) The FDA Modernization Act 2.0: Drug Testing in Animals is Rendered Optional. *Am J Med* 136:853–854. <https://doi.org/10.1016/j.amjmed.2023.03.033>
- Adrian ED (1936) The spread of activity in the cerebral cortex. *J Physiol* 88:127–161. <https://doi.org/10.1113/jphysiol.1936.sp003427>
- Alépée N (2014) State-of-the-art of 3D cultures (organs-on-a-chip) in safety testing and pathophysiology. *ALTEX* 31:441–477. <https://doi.org/10.14573/altex1406111>
- Allen NJ, Lyons DA (2018) Glia as architects of central nervous system formation and function. *Science* (1979) 362:181–185. <https://doi.org/10.1126/science.aat0473>
- Andres RH, Ducray AD, Schlattner U, et al (2008) Functions and effects of creatine in the central nervous system. *Brain Res Bull* 76:329–343. <https://doi.org/10.1016/j.brainresbull.2008.02.035>
- Arcuri C, Mecca C, Bianchi R, et al (2017) The Pathophysiological Role of Microglia in Dynamic Surveillance, Phagocytosis and Structural Remodeling of the Developing CNS. *Front Mol Neurosci* 10. <https://doi.org/10.3389/fnmol.2017.00191>
- Arrowsmith J, Miller P (2013) Phase II and Phase III attrition rates 2011–2012. *Nat Rev Drug Discov* 12:569. <https://doi.org/10.1038/nrd4090>

- Aumailley M (2013) The laminin family. *Cell Adh Migr* 7:48–55. <https://doi.org/10.4161/cam.22826>
- Azevedo FAC, Carvalho LRB, Grinberg LT, et al (2009) Equal numbers of neuronal and nonneuronal cells make the human brain an isometrically scaled-up primate brain. *Journal of Comparative Neurology* 513:532–541. <https://doi.org/10.1002/cne.21974>
- Bagley JA, Reumann D, Bian S, et al (2017) Fused cerebral organoids model interactions between brain regions. *Nat Methods* 14:743–751. <https://doi.org/10.1038/nmeth.4304>
- Bain G, Kitchens D, Yao M, et al (1995) Embryonic Stem Cells Express Neuronal Properties in Vitro. *Dev Biol* 168:342–357. <https://doi.org/10.1006/dbio.1995.1085>
- Bal-Price AK, Hogberg HT, Buzanska L, Coecke S (2010) Relevance of in vitro neurotoxicity testing for regulatory requirements: Challenges to be considered. *Neurotoxicol Teratol* 32:36–41. <https://doi.org/10.1016/j.ntt.2008.12.003>
- Barak S, Ahmadiantehrani S, Logrip ML, Ron D (2019) GDNF and alcohol use disorder. *Addiction Biology* 24:335–343. <https://doi.org/10.1111/adb.12628>
- Barenys M, Gassmann K, Baksmeier C, et al (2017) Epigallocatechin gallate (EGCG) inhibits adhesion and migration of neural progenitor cells in vitro. *Arch Toxicol* 91:827–837. <https://doi.org/10.1007/s00204-016-1709-8>
- Barnett MW, Larkman PM (2007) The action potential. *Pract Neurol* 7:192–7
- Bartmann K, Bendt F, Dönmez A, et al (2023) A human iPSC-based in vitro neural network formation assay to investigate neurodevelopmental toxicity of pesticides. *ALTEX* 452–470. <https://doi.org/10.14573/altex.2206031>
- Bartmann K, Hartmann J, Kapr J, Fritsche E (2021) Measurement of Electrical Activity of Differentiated Human iPSC-Derived Neurospheres Recorded by Microelectrode Arrays (MEA). *Humana*, New York, NY, pp 473–488

- Bean BP (2007) The action potential in mammalian central neurons. *Nat Rev Neurosci* 8:451–465. <https://doi.org/10.1038/nrn2148>
- Belinsky GS, Sirois CL, Rich MT, et al (2013) Dopamine receptors in human embryonic stem cell neurodifferentiation. *Stem Cells Dev* 22:1522–1540. <https://doi.org/10.1089/scd.2012.0150>
- Ben Haim L, Rowitch DH (2016) Functional diversity of astrocytes in neural circuit regulation. *Nat Rev Neurosci* 18:31–41. <https://doi.org/10.1038/nrn.2016.159>
- Benito-Kwiecinski S, Lancaster MA (2020) Brain organoids: Human neurodevelopment in a dish. *Cold Spring Harb Perspect Biol* 12:1–18. <https://doi.org/10.1101/cshperspect.a035709>
- Betarbet R, Sherer TB, MacKenzie G, et al (2000) Chronic systemic pesticide exposure reproduces features of Parkinson's disease. *Nat Neurosci* 3:1301–1306. <https://doi.org/10.1038/81834>
- Biffi E, Regalia G, Menegon A, et al (2013) The Influence of Neuronal Density and Maturation on Network Activity of Hippocampal Cell Cultures: A Methodological Study. *PLoS One* 8:e83899. <https://doi.org/10.1371/journal.pone.0083899>
- Block ML, Zecca L, Hong J-S (2007) Microglia-mediated neurotoxicity: uncovering the molecular mechanisms. *Nat Rev Neurosci* 8:57–69. <https://doi.org/10.1038/nrn2038>
- Bottenstein JE, Skaper SD, Varon SS, Sato GH (1980) Selective survival of neurons from chick embryo sensory ganglionic dissociates utilizing serum-free supplemented medium. *Exp Cell Res* 125:183–190. [https://doi.org/10.1016/0014-4827\(80\)90202-5](https://doi.org/10.1016/0014-4827(80)90202-5)
- Bourin M (2018) The GABAA receptor and benzodiazepine acceptor site. *SOJ Pharm Pharm Sci* 5:1–5. <https://doi.org/10.15226/2374-6866/5/2/00176>

- Bradford AB, McNutt PM (2015) Importance of being Nernst: Synaptic activity and functional relevance in stem cell-derived neurons. *World J Stem Cells* 7:899. <https://doi.org/10.4252/wjsc.v7.i6.899>
- Brannen CL, Sugaya K (2000) In vitro differentiation of multipotent human neural progenitors in serum-free medium. *Neuroreport* 11:1123–1128. <https://doi.org/10.1097/00001756-200004070-00042>
- Brewer GJ (1995) Serum-free B27/neurobasal medium supports differentiated growth of neurons from the striatum, substantia nigra, septum, cerebral cortex, cerebellum, and dentate gyrus. *J Neurosci Res* 42:674–683. <https://doi.org/10.1002/jnr.490420510>
- Brewer GJ, Torricelli JR, Evege EK, Price PJ (1993) Optimized survival of hippocampal neurons in B27-supplemented neurobasal™, a new serum-free medium combination. *J Neurosci Res* 35:567–576. <https://doi.org/10.1002/jnr.490350513>
- Brown JP, Hall D, Frank CL, et al (2016) Evaluation of a Microelectrode Array-Based Assay for Neural Network Ontogeny Using Training Set Chemicals. *Toxicological Sciences* 154:126–139. <https://doi.org/10.1093/toxsci/kfw147>
- Brüll M, Spreng AS, Gutbier S, et al (2020) Incorporation of stem cell-derived astrocytes into neuronal organoids to allow neuro-glial interactions in toxicological studies. *ALTEX* 37:409–428. <https://doi.org/10.14573/altex.1911111>
- Buck SA, de Miranda BR, Logan RW, et al (2021) VGLUT2 is a determinant of dopamine neuron resilience in a rotenone model of dopamine neurodegeneration. *Journal of Neuroscience* 41:4937–4947. <https://doi.org/10.1523/JNEUROSCI.2770-20.2021>
- Buckberry S, Liu X, Poppe D, et al (2023) Transient naive reprogramming corrects hiPS cells functionally and epigenetically. *Nature* 620:863–872. <https://doi.org/10.1038/s41586-023-06424-7>

- Budday S, Steinmann P, Kuhl E (2015) Physical biology of human brain development. *Front Cell Neurosci* 9:1–17. <https://doi.org/10.3389/fncel.2015.00257>
- Buschmann J (2013) The OECD guidelines for the testing of chemicals and pesticides. *Methods in Molecular Biology* 947:37–56. https://doi.org/10.1007/978-1-62703-131-8_4
- Byun JS, Lee CO, Oh M, et al (2020) Rapid differentiation of astrocytes from human embryonic stem cells. *Neurosci Lett* 716. <https://doi.org/10.1016/j.neulet.2019.134681>
- Cantor RS (2018) Path to the Desensitized State of Ligand-Gated Ion Channels: Why Are Inhibitory and Excitatory Receptors Different? *Journal of Physical Chemistry B* 122:5368–5374. <https://doi.org/10.1021/acs.jpcb.7b10961>
- Cebolla B, Fernández-Pérez A, Perea G, et al (2008) DREAM mediates cAMP-dependent, Ca²⁺-induced stimulation of GFAP gene expression and regulates cortical astrogliogenesis. *Journal of Neuroscience* 28:6703–6713. <https://doi.org/10.1523/JNEUROSCI.0215-08.2008>
- Centeno EGZ, Cimarosti H, Bithell A (2018) 2D versus 3D human induced pluripotent stem cell-derived cultures for neurodegenerative disease modelling. *Mol Neurodegener* 13:1–15. <https://doi.org/10.1186/s13024-018-0258-4>
- Chambers SM, Fasano CA, Papapetrou EP, et al (2009) Highly efficient neural conversion of human ES and iPS cells by dual inhibition of SMAD signaling. *Nat Biotechnol* 27:275–280. <https://doi.org/10.1038/nbt.1529>
- Chandrasekaran A, Avci HX, Ochalek A, et al (2017) Comparison of 2D and 3D neural induction methods for the generation of neural progenitor cells from human induced pluripotent stem cells. *Stem Cell Res* 25:139–151. <https://doi.org/10.1016/j.scr.2017.10.010>

- Chen C-Y, Chou F-S, Wang P-S (2019) Live-cell Migration Assays to Study Motility of Neural and Glial (Oligodendrocyte) Progenitor Cells. *Bio Protoc* 9:1–11. <https://doi.org/10.21769/bioprotoc.3275>
- Coecke S, Eskes C, Gartlon J, et al (2006) The value of alternative testing for neurotoxicity in the context of regulatory needs. *Environ Toxicol Pharmacol* 21:153–167. <https://doi.org/10.1016/j.etap.2005.07.006>
- Collins FS, Gray GM, Bucher JR (2008) Transforming environmental health protection. *Science* (1979) 319:906–907. <https://doi.org/10.1126/science.1154619>
- Costa LG (2017) Overview of Neurotoxicology. *Curr Protoc Toxicol* 74:11.1.1-11.1.11. <https://doi.org/10.1002/cptx.36>
- Cotterill E, Eglen SJ (2019) Burst Detection Methods. *Adv Neurobiol* 22:185–206. https://doi.org/10.1007/978-3-030-11135-9_8
- Cotterill E, Hall D, Wallace K, et al (2016) Characterization of early cortical neural network development in multiwell microelectrode array plates. *J Biomol Screen* 21:510–519. <https://doi.org/10.1177/1087057116640520>
- Couzin-Frankel J (2013) When Mice Mislead. *Science* (1979) 342:922–925. <https://doi.org/10.1126/science.342.6161.922>
- Crofton KM, Bassan A, Behl M, et al (2022) Current status and future directions for a neurotoxicity hazard assessment framework that integrates in silico approaches. *Computational Toxicology* 22. <https://doi.org/10.1016/j.comtox.2022.100223>
- Crofton KM, Mundy WR, Lein PJ, et al (2011) Developmental neurotoxicity testing: Recommendations for developing alternative methods for the screening and prioritization of chemicals. *ALTEX* 28:9–15. <https://doi.org/10.14573/altex.2011.1.009>

- Csobonyeiova M, Polak S, Zamborsky R, Danisovic L (2019) Recent progress in the regeneration of spinal cord injuries by induced pluripotent stem cells. *Int J Mol Sci* 20. <https://doi.org/10.3390/ijms20153838>
- Curti S, O'Brien J (2016) Characteristics and plasticity of electrical synaptic transmission. *BMC Cell Biol* 17:13. <https://doi.org/10.1186/s12860-016-0091-y>
- Dach K, Bendt F, Huebenthal U, et al (2017) BDE-99 impairs differentiation of human and mouse NPCs into the oligodendroglial lineage by species-specific modes of action. *Sci Rep* 7:1–11. <https://doi.org/10.1038/srep44861>
- de Leeuw VC, van Oostrom CTM, Wackers PFK, et al (2022) Neuronal differentiation pathways and compound-induced developmental neurotoxicity in the human neural progenitor cell test (hNPT) revealed by RNA-seq. *Chemosphere* 304:135298. <https://doi.org/10.1016/j.chemosphere.2022.135298>
- DeFelipe J, Alonso-Nanclares L, Arellano JI (2002) Microstructure of the neocortex: Comparative aspects. *J Neurocytol* 31:299–316. <https://doi.org/10.1023/A:1024130211265>
- Deiters Otto, Schultze MJS (1865) *Untersuchungen über Gehirn und Rückenmark des Menschen und der Säugethiere*. Vieweg, Braunschweig
- Dent MP, Vaillancourt E, Thomas RS, et al (2021) Paving the way for application of next generation risk assessment to safety decision-making for cosmetic ingredients. *Regulatory Toxicology and Pharmacology* 125:105026. <https://doi.org/10.1016/j.yrtph.2021.105026>
- Derynck R, Zhang YE (2003) Smad-dependent and Smad-independent pathways in TGF- β family signalling. *Nature* 425:577–584. <https://doi.org/10.1038/nature02006>
- Dutta A, Gautam R, Chatterjee S, et al (2015) Ascorbate Protects Neurons against Oxidative Stress: A Raman Microspectroscopic Study. *ACS Chem Neurosci* 6:1794–1801. <https://doi.org/10.1021/acscchemneuro.5b00106>

- Duval K, Grover H, Han L, et al (2017) Modeling Physiological Events in 2D vs. 3D Cell Culture. *Physiology* 32:266–277. <https://doi.org/10.1152/physiol.00036.2016>
- Egorov A V., Draguhn A (2013) Development of coherent neuronal activity patterns in mammalian cortical networks: Common principles and local heterogeneity. *Mech Dev* 130:412–423. <https://doi.org/10.1016/j.mod.2012.09.006>
- Ehrlich M, Mozafari S, Glatza M, et al (2017) Rapid and efficient generation of oligodendrocytes from human induced pluripotent stem cells using transcription factors. <https://doi.org/10.1073/pnas.1614412114>
- Eskes C, Whelan M (2016) *Validation of Alternative Methods for Toxicity Testing*. Springer International Publishing, Cham
- Fabbri R, Cacopardo L, Ahluwalia A, Magliaro C (2023) Advanced 3D Models of Human Brain Tissue Using Neural Cell Lines: State-of-the-Art and Future Prospects. *Cells* 12:1181. <https://doi.org/10.3390/cells12081181>
- Fan P, Wang Y, Xu M, et al (2022) The Application of Brain Organoids in Assessing Neural Toxicity. *Front Mol Neurosci* 15. <https://doi.org/10.3389/fnmol.2022.799397>
- Flanagan LA, Rebaza LM, Derzic S, et al (2006) Regulation of human neural precursor cells by laminin and integrins. *J Neurosci Res* 83:845–856. <https://doi.org/10.1002/jnr.20778>
- Fritsche E, Haarmann-Stemmann T, Kapr J, et al (2020a) Stem Cells for Next Level Toxicity Testing in the 21st Century. *Small* 2006252:1–31. <https://doi.org/10.1002/sml.202006252>
- Fritsche E, Tigges J, Hartmann J, et al (2020b) Neural In Vitro Models for Studying Substances Acting on the Central Nervous System. https://doi.org/10.1007/164_2020_367

- Fu Y, Yang M, Yu H, et al (2021) Heterogeneity of glial progenitor cells during the neurogenesis-to-gliogenesis switch in the developing human cerebral cortex. *Cell Rep* 34:108788. <https://doi.org/10.1016/j.celrep.2021.108788>
- Galiakberova AA, Dashinimaev EB (2020) Neural Stem Cells and Methods for Their Generation From Induced Pluripotent Stem Cells in vitro. *Front Cell Dev Biol* 8. <https://doi.org/10.3389/fcell.2020.00815>
- Ganguly C, Chakrabarti S (2020) A Discrete Time Framework for Spike Transfer Process in a Cortical Neuron with Asynchronous EPSP, IPSP, and Variable Threshold. *IEEE Transactions on Neural Systems and Rehabilitation Engineering* 28:772–781. <https://doi.org/10.1109/TNSRE.2020.2975203>
- García-León JA, García-Díaz B, Eggermont K, et al (2020) Generation of oligodendrocytes and establishment of an all-human myelinating platform from human pluripotent stem cells. *Nat Protoc* 15:3716–3744. <https://doi.org/10.1038/s41596-020-0395-4>
- Gassmann K, Abel J, Bothe H, et al (2010) Species-specific differential ahr expression protects human neural progenitor cells against developmental neurotoxicity of PAHs. *Environ Health Perspect* 118:1571–1577. <https://doi.org/10.1289/ehp.0901545>
- Giordano G, White CC, Mohar I, et al (2007) Glutathione levels modulate domoic acid-induced apoptosis in mouse cerebellar granule cells. *Toxicological Sciences* 100:433–444. <https://doi.org/10.1093/toxsci/kfm236>
- Goodwani S, Saternos H, Alasmari F, Sari Y (2017) Metabotropic and ionotropic glutamate receptors as potential targets for the treatment of alcohol use disorder. *Neurosci Biobehav Rev* 77:14–31. <https://doi.org/10.1016/j.neubiorev.2017.02.024>
- Goudet C, Magnaghi V, Landry M, et al (2009) Metabotropic receptors for glutamate and GABA in pain. *Brain Res Rev* 60:43–56. <https://doi.org/10.1016/j.brainresrev.2008.12.007>

- Grandjean P, Landrigan P (2006) Developmental neurotoxicity of industrial chemicals. *Lancet* 368:2167–2178. [https://doi.org/10.1016/S0140-6736\(06\)69665-7](https://doi.org/10.1016/S0140-6736(06)69665-7)
- Gritti A, Parati E, Cova L, et al (1996) Multipotential stem cells from the adult mouse brain proliferate and self-renew in response to basic fibroblast growth factor. *The Journal of Neuroscience* 16:1091–1100. <https://doi.org/10.1523/JNEUROSCI.16-03-01091.1996>
- Gross GW, Rieske E, Kreutzberg GW, Meyer A (1977) A new fixed-array multi-microelectrode system designed for long-term monitoring of extracellular single unit neuronal activity in vitro. *Neurosci Lett* 6:101–105. [https://doi.org/10.1016/0304-3940\(77\)90003-9](https://doi.org/10.1016/0304-3940(77)90003-9)
- Gross GW, Williams AN, Lucas JH (1982) Recording of spontaneous activity with photoetched microelectrode surfaces from mouse spinal neurons in culture. *J Neurosci Methods* 5:13–22. [https://doi.org/10.1016/0165-0270\(82\)90046-2](https://doi.org/10.1016/0165-0270(82)90046-2)
- Gunhanlar N, Shpak G, van der Kroeg M, et al (2017) A simplified protocol for differentiation of electrophysiologically mature neuronal networks from human induced pluripotent stem cells. *Mol Psychiatry* 23:1336–1344. <https://doi.org/10.1038/mp.2017.56>
- Guttenplan KA, Weigel MK, Prakash P, et al (2021) Neurotoxic reactive astrocytes induce cell death via saturated lipids. *Nature* 599:102–107. <https://doi.org/10.1038/s41586-021-03960-y>
- Hansen KB, Yi F, Perszyk RE, et al (2018) Structure, function, and allosteric modulation of NMDA receptors. *Journal of General Physiology* 150:1081–1105. <https://doi.org/10.1085/jgp.201812032>
- Harrison RK (2016) Phase II and phase III failures: 2013-2015. *Nat Rev Drug Discov* 15:817–818. <https://doi.org/10.1038/nrd.2016.184>

- Hartmann J, Henschel N, Bartmann K, et al (2023) Molecular and Functional Characterization of Different BrainSphere Models for Use in Neurotoxicity Testing on Microelectrode Arrays. *Cells* 12. <https://doi.org/10.3390/cells12091270>
- Hartmann J, Lauria I, Bendt F, et al (2022) Alginate-Laminin Hydrogel Supports Long-Term Neuronal Activity in 3D Human Induced Pluripotent Stem Cell-Derived Neuronal Networks. *Adv Mater Interfaces* 10. <https://doi.org/10.1002/admi.202200580>
- Hellwig C, Barenys M, Baumann J, et al (2018) Culture of human neurospheres in 3D scaffolds for developmental neurotoxicity testing. *Toxicology in Vitro* 52:106–115. <https://doi.org/10.1016/j.tiv.2018.06.002>
- Henriques JF, Portugal CC, Canedo T, et al (2018) Microglia and alcohol meet at the crossroads: Microglia as critical modulators of alcohol neurotoxicity. *Toxicol Lett* 283:21–31. <https://doi.org/10.1016/j.toxlet.2017.11.002>
- Hernández-Echeagaray E (2020) Neurotrophin-3 modulates synaptic transmission. In: *Vitamins and Hormones*, 1st edn. Elsevier Inc., pp 71–89
- Hodge RD, Bakken TE, Miller JA, et al (2019) Conserved cell types with divergent features in human versus mouse cortex. *Nature* 573:61–68. <https://doi.org/10.1038/s41586-019-1506-7>
- Hodgkin AL, Huxley AF (1939) Action Potentials Recorded from Inside a Nerve Fibre. *Nature* 144:710–711. <https://doi.org/10.1038/144710a0>
- Hofrichter M, Nimtz L, Tigges J, et al (2017) Comparative performance analysis of human iPSC-derived and primary neural progenitor cells (NPC) grown as neurospheres in vitro. *Stem Cell Res* 25:72–82. <https://doi.org/10.1016/j.scr.2017.10.013>
- Hopkins AM, DeSimone E, Chwalek K, Kaplan DL (2015) 3D in vitro modeling of the central nervous system. *Prog Neurobiol* 125:1–25. <https://doi.org/10.1016/j.pneurobio.2014.11.003>

- Horbelt D, Boergermann JH, Chaikuad A, et al (2015) Small molecules dorsomorphin and LDN-193189 inhibit myostatin/GDF8 signaling and promote functional myoblast differentiation. *Journal of Biological Chemistry* 290:3390–3404. <https://doi.org/10.1074/jbc.M114.604397>
- Humphries JD, Byron A, Humphries MJ (2006) Integrin ligands at a glance. *J Cell Sci* 119:3901–3903. <https://doi.org/10.1242/jcs.03098>
- Hyman SE (2005) Neurotransmitters. *Current Biology* 15:R154–R158. <https://doi.org/10.1016/j.cub.2005.02.037>
- Hyvärinen T, Hyysalo A, Kapucu FE, et al (2019) Functional characterization of human pluripotent stem cell-derived cortical networks differentiated on laminin-521 substrate: comparison to rat cortical cultures. *Sci Rep* 9:1–15. <https://doi.org/10.1038/s41598-019-53647-8>
- Hyysalo A, Ristola M, Mäkinen MEL, et al (2017) Laminin $\alpha 5$ substrates promote survival, network formation and functional development of human pluripotent stem cell-derived neurons in vitro. *Stem Cell Res* 24:118–127. <https://doi.org/10.1016/j.scr.2017.09.002>
- Ibáñez CF, Paratcha G, Ledda F (2020) RET-independent signaling by GDNF ligands and GFR α receptors. *Cell Tissue Res* 382:71–82. <https://doi.org/10.1007/s00441-020-03261-2>
- Imredy JP, Roussignol G, Clouse H, et al (2023) Comparative assessment of Ca²⁺ oscillations in 2- and 3-dimensional hiPSC derived and isolated cortical neuronal networks. *J Pharmacol Toxicol Methods*. <https://doi.org/10.1016/j.vascn.2023.107281>
- Inman GJ, Nicolás FJ, Callahan JF, et al (2002) SB-431542 is a potent and specific inhibitor of transforming growth factor- β superfamily type I activin receptor-like kinase (ALK) receptors ALK4, ALK5, and ALK7. *Mol Pharmacol* 62:65–74. <https://doi.org/10.1124/mol.62.1.65>

- Irala D, Bonafina A, Fontanet PA, et al (2016) The GDNF-GFR α 1 complex promotes the development of hippocampal dendritic arbors and spines via NCAM. *Development (Cambridge)* 143:4224–4235. <https://doi.org/10.1242/dev.140350>
- Itsykson P, Ilouz N, Turetsky T, et al (2005) Derivation of neural precursors from human embryonic stem cells in the presence of noggin. *Molecular and Cellular Neuroscience* 30:24–36. <https://doi.org/10.1016/j.mcn.2005.05.004>
- Izsak J, Seth H, Andersson M, et al (2019) Robust Generation of Person-Specific, Synchronously Active Neuronal Networks Using Purely Isogenic Human iPSC-3D Neural Aggregate Cultures. *Front Neurosci* 13. <https://doi.org/10.3389/fnins.2019.00351>
- Johnstone AFM, Gross GW, Weiss DG, et al (2010) Microelectrode arrays: A physiologically based neurotoxicity testing platform for the 21st century. *Neurotoxicology* 31:331–350. <https://doi.org/10.1016/J.NEURO.2010.04.001>
- Kang K ree, Kim CY, Kim J, et al (2022) Establishment of Neurotoxicity Assessment Using Microelectrode Array (MEA) with hiPSC-Derived Neurons and Evaluation of New Psychoactive Substances (NPS). *Int J Stem Cells* 15:258–269. <https://doi.org/10.15283/ijsc21217>
- Kang SY, Joshi P, Lee MY (2021) High-Throughput Screening of Compound Neurotoxicity Using 3D-Cultured Neural Stem Cells on a 384-Pillar Plate. *Curr Protoc* 1. <https://doi.org/10.1002/cpz1.107>
- Kanton S, Boyle MJ, He Z, et al (2019) Organoid single-cell genomic atlas uncovers human-specific features of brain development. *Nature* 574:418–422. <https://doi.org/10.1038/s41586-019-1654-9>
- Kapucu FE, Tanskanen JMA, Mikkonen JE, et al (2012) Burst analysis tool for developing neuronal networks exhibiting highly varying action potential dynamics. *Front Comput Neurosci* 6:1–14. <https://doi.org/10.3389/fncom.2012.00038>

- Kavlock RJ, Bahadori T, Barton-Maclaren TS, et al (2018) Accelerating the Pace of Chemical Risk Assessment. *Chem Res Toxicol* 31:287–290. <https://doi.org/10.1021/acs.chemrestox.7b00339>
- Kim K, Doi A, Wen B, et al (2010) Epigenetic memory in induced pluripotent stem cells. *Nature* 467:285–290. <https://doi.org/10.1038/nature09342>
- Kim SJ, Son TG, Kim K, et al (2007) Interferon- γ promotes differentiation of neural progenitor cells via the JNK pathway. *Neurochem Res* 32:1399–1406. <https://doi.org/10.1007/s11064-007-9323-z>
- Klose J, Li L, Pahl M, et al (2022a) Application of the adverse outcome pathway concept for investigating developmental neurotoxicity potential of Chinese herbal medicines by using human neural progenitor cells in vitro. *Cell Biol Toxicol*. <https://doi.org/10.1007/s10565-022-09730-4>
- Klose J, Pahl M, Bartmann K, et al (2022b) Neurodevelopmental toxicity assessment of flame retardants using a human DNT in vitro testing battery. *Cell Biol Toxicol* 38:781–807. <https://doi.org/10.1007/s10565-021-09603-2>
- Klose J, Tigges J, Masjosthusmann S, et al (2020) TBBPA targets converging key events of human oligodendrocyte development resulting in two novel AOPs. *ALTEX* 38:215–234. <https://doi.org/10.14573/altex.2007201>
- Kobolak J, Teglas A, Bellak T, et al (2020) Human Induced Pluripotent Stem Cell-Derived 3D-Neurospheres are Suitable for Neurotoxicity Screening. *Cells* 9. <https://doi.org/10.3390/cells9051122>
- Koch K, Bartmann K, Hartmann J, et al (2022) Scientific Validation of Human Neurosphere Assays for Developmental Neurotoxicity Evaluation. *Frontiers in Toxicology* 4:1–26. <https://doi.org/10.3389/ftox.2022.816370>
- Krencik R, Weick JP, Liu Y, et al (2011) Specification of transplantable astroglial subtypes from human pluripotent stem cells. *Nat Biotechnol* 29:528–534. <https://doi.org/10.1038/nbt.1877>

- Krewski D, Andersen ME, Tyshenko MG, et al (2020) Toxicity testing in the 21st century: progress in the past decade and future perspectives. *Arch Toxicol* 94:1–58. <https://doi.org/10.1007/s00204-019-02613-4>
- Kuhn HG, Winkler J, Kempermann G, et al (1997) Epidermal Growth Factor and Fibroblast Growth Factor-2 Have Different Effects on Neural Progenitors in the Adult Rat Brain. *The Journal of Neuroscience* 17:5820–5829. <https://doi.org/10.1523/JNEUROSCI.17-15-05820.1997>
- Lake BB, Ai R, Kaeser GE, et al (2016) Neuronal subtypes and diversity revealed by single-nucleus RNA sequencing of the human brain. *Science* (1979) 352:1586–1590. <https://doi.org/10.1126/science.aaf1204>
- Lancaster MA, Corsini NS, Wolfinger S, et al (2017) Guided self-organization and cortical plate formation in human brain organoids. *Nat Biotechnol* 35:659–666. <https://doi.org/10.1038/nbt.3906>
- Lancaster MA, Renner M, Martin C, et al (2013) Cerebral organoids model human brain development and microcephaly. *Nature* 501. <https://doi.org/10.1038/nature12517>
- Lanzoni A, Castoldi AF, Kass GEN, et al (2019) Advancing human health risk assessment. *EFSA Journal* 17. <https://doi.org/10.2903/j.efsa.2019.e170712>
- Lappalainen RS, Salomäki M, Ylä-Outinen L, et al (2010) Similarly derived and cultured hESC lines show variation in their developmental potential towards neuronal cells in long-term culture. *Regenerative Med* 5:749–762. <https://doi.org/10.2217/rme.10.58>
- Legradi JB, Di Paolo C, Kraak MHS, et al (2018) An ecotoxicological view on neurotoxicity assessment. *Environ Sci Eur* 30:1–34. <https://doi.org/10.1186/s12302-018-0173-x>

- Leipzig ND, Xu C, Zahir T, Shoichet MS (2010) Functional immobilization of interferon-gamma induces neuronal differentiation of neural stem cells. *J Biomed Mater Res A* 93:625–633. <https://doi.org/10.1002/jbm.a.32573>
- Leist M, Hartung T (2013) Inflammatory findings on species extrapolations: Humans are definitely no 70-kg mice¹. *Arch Toxicol* 87:563–567. <https://doi.org/10.1007/s00204-013-1038-0>
- Leite PEC, Pereira MR, Harris G, et al (2019) Suitability of 3D human brain spheroid models to distinguish toxic effects of gold and poly-lactic acid nanoparticles to assess biocompatibility for brain drug delivery. *Part Fibre Toxicol* 16:1–20. <https://doi.org/10.1186/s12989-019-0307-3>
- Li H, Yuan H, Middleton A, et al (2021) Next generation risk assessment (NGRA): Bridging in vitro points-of-departure to human safety assessment using physiologically-based kinetic (PBK) modelling – A case study of doxorubicin with dose metrics considerations. *Toxicology in Vitro* 74:105171. <https://doi.org/10.1016/j.tiv.2021.105171>
- Lilja J, Ivaska J (2018) Integrin activity in neuronal connectivity. *J Cell Sci* 131:jcs212803. <https://doi.org/10.1242/jcs.212803>
- Liu BC, Liu FY, Gao XY, et al (2021) Global transcriptional analyses of the wnt-induced development of neural stem cells from human pluripotent stem cells. *Int J Mol Sci* 22. <https://doi.org/10.3390/ijms22147473>
- Logan S, Arzua T, Canfield SG, et al (2019) Studying Human Neurological Disorders Using Induced Pluripotent Stem Cells: From 2D Monolayer to 3D Organoid and Blood Brain Barrier Models. *Compr Physiol* 9:565–611. <https://doi.org/10.1002/cphy.c180025>
- Ma J, Ma C, Li J, et al (2020) Extracellular Matrix Proteins Involved in Alzheimer's Disease. *Chemistry - A European Journal* 26:12101–12110. <https://doi.org/10.1002/chem.202000782>

- Ma W, Tavakoli T, Derby E, et al (2008) Cell-extracellular matrix interactions regulate neural differentiation of human embryonic stem cells. *BMC Dev Biol* 8:1–13. <https://doi.org/10.1186/1471-213X-8-90>
- Mack CM, Lin BJ, Turner JD, et al (2014) Burst and principal components analyses of MEA data for 16 chemicals describe at least three effects classes. *Neurotoxicology* 40:75–85. <https://doi.org/10.1016/j.neuro.2013.11.008>
- Magurany KA, Chang X, Clewell R, et al (2023) A pragmatic framework for the application of new approach methodologies in one health toxicological risk assessment. *Toxicological Sciences* 192:155–177. <https://doi.org/10.1093/toxsci/kfad012>
- Mahmoud S, Gharagozloo M, Simard C, Gris D (2019) Astrocytes Maintain Glutamate Homeostasis in the CNS by Controlling the Balance between Glutamate Uptake and Release. *Cells* 8:184. <https://doi.org/10.3390/cells8020184>
- Mahony C, Ashton RS, Birk B, et al (2020) New ideas for non-animal approaches to predict repeated-dose systemic toxicity: Report from an EPAA Blue Sky Workshop. *Regulatory Toxicology and Pharmacology* 114:104668. <https://doi.org/10.1016/j.yrtph.2020.104668>
- Malik N, Efthymiou AG, Mather K, et al (2014) Compounds with species and cell type specific toxicity identified in a 2000 compound drug screen of neural stem cells and rat mixed cortical neurons. *Neurotoxicology* 45:192–200. <https://doi.org/10.1016/j.neuro.2014.10.007>
- Mannal N, Kleiner K, Fauler M, et al (2021) Multi-Electrode Array Analysis Identifies Complex Dopamine Responses and Glucose Sensing Properties of Substantia Nigra Neurons in Mouse Brain Slices. *Front Synaptic Neurosci* 13:1–19. <https://doi.org/10.3389/fnsyn.2021.635050>
- Mark MD, Storm DR (1997) Coupling of epidermal growth factor (EGF) with the antiproliferative activity of cAMP induces neuronal differentiation. *Journal of Biological Chemistry* 272:17238–17244. <https://doi.org/10.1074/jbc.272.27.17238>

- Masjosthusmann S, Barenys M, El-Gamal M, et al (2018) Literature review and appraisal on alternative neurotoxicity testing methods. *EFSA Supporting Publications* 15:1–108. <https://doi.org/10.2903/sp.efsa.2018.en-1410>
- Massaro EJ (2002) *Handbook of Neurotoxicology*. Humana Press, New Jersey
- McConnell ER, McClain MA, Ross J, et al (2012) Evaluation of multi-well microelectrode arrays for neurotoxicity screening using a chemical training set. *Neurotoxicology* 33:1048–1057. <https://doi.org/10.1016/j.neuro.2012.05.001>
- Molofsky A V., Krenick R, Ullian E, et al (2012) Astrocytes and disease: a neurodevelopmental perspective. *Genes Dev* 26:891–907. <https://doi.org/10.1101/gad.188326.112>
- Moors M, Rockel TD, Abel J, et al (2009) Human neurospheres as three-dimensional cellular systems for developmental neurotoxicity testing. *Environ Health Perspect* 117:1131–1138. <https://doi.org/10.1289/ehp.0800207>
- Moretti M, Fraga DB, Rodrigues ALS (2017) Ascorbic Acid to Manage Psychiatric Disorders. *CNS Drugs* 31:571–583. <https://doi.org/10.1007/s40263-017-0446-8>
- Mundy WR, Padilla S, Breier JM, et al (2015) Expanding the test set: Chemicals with potential to disrupt mammalian brain development. *Neurotoxicol Teratol* 52:25–35. <https://doi.org/10.1016/j.ntt.2015.10.001>
- Murphy AR, Laslett A, O'Brien CM, Cameron NR (2017) Scaffolds for 3D in vitro culture of neural lineage cells. *Acta Biomater* 54:1–20. <https://doi.org/10.1016/j.actbio.2017.02.046>
- Nadadhur AG, Leferink PS, Holmes D, et al (2018) Patterning factors during neural progenitor induction determine regional identity and differentiation potential in vitro. *Stem Cell Res* 32:25–34. <https://doi.org/10.1016/j.scr.2018.08.017>
- National Research Council (2007) *Toxicity Testing in the 21st Century*. National Academies Press, Washington, D.C.

- Neely MD, Litt MJ, Tidball AM, et al (2012) DMH1, a highly selective small molecule BMP inhibitor promotes neurogenesis of hiPSCs: Comparison of PAX6 and SOX1 expression during neural induction. *ACS Chem Neurosci* 3:482–491. <https://doi.org/10.1021/cn300029t>
- Negri J, Menon V, Young-Pearse TL (2020) Assessment of spontaneous neuronal activity In vitro using multi-well multi-electrode arrays: Implications for assay development. *eNeuro* 7:1–27. <https://doi.org/10.1523/ENEURO.0080-19.2019>
- Nimtz L, Hartmann J, Tigges J, et al (2020) Characterization and application of electrically active neuronal networks established from human induced pluripotent stem cell-derived neural progenitor cells for neurotoxicity evaluation. *Stem Cell Res* 45:101761. <https://doi.org/10.1016/j.scr.2020.101761>
- Nishiuchi R, Takagi J, Hayashi M, et al (2006) Ligand-binding specificities of laminin-binding integrins: A comprehensive survey of laminin-integrin interactions using recombinant $\alpha 3\beta 1$, $\alpha 6\beta 1$, $\alpha 7\beta 1$ and $\alpha 6\beta 4$ integrins. *Matrix Biology* 25:189–197. <https://doi.org/10.1016/j.matbio.2005.12.001>
- Novellino A, Scelfo B, Palosaari T, et al (2011) Development of micro-electrode array based tests for neurotoxicity: Assessment of interlaboratory reproducibility with neuroactive chemicals. *Front Neuroeng* 4:1–14. <https://doi.org/10.3389/fneng.2011.00004>
- Nunes C, Gorczyca G, Mendoza-deGyves E, et al (2022) Upscaling biological complexity to boost neuronal and oligodendroglia maturation and improve in vitro developmental neurotoxicity (DNT) evaluation. *Reproductive Toxicology* 110:124–140. <https://doi.org/10.1016/j.reprotox.2022.03.017>
- Oberheim NA, Takano T, Han X, et al (2009) Uniquely hominid features of adult human astrocytes. *Journal of Neuroscience* 29:3276–3287. <https://doi.org/10.1523/JNEUROSCI.4707-08.2009>
- Odawara A, Matsuda N, Ishibashi Y, et al (2018) Toxicological evaluation of convulsant and anticonvulsant drugs in human induced pluripotent stem cell-derived cortical

neuronal networks using an MEA system. *Sci Rep* 8:10416.
<https://doi.org/10.1038/s41598-018-28835-7>

OECD (1995a) Test No. 418: Delayed Neurotoxicity of Organophosphorus Substances Following Acute Exposure. 1–8. <https://doi.org/10.1787/9789264070905-en>

OECD (1995b) Test No. 419: Delayed Neurotoxicity of Organophosphorus Substances: 28-day Repeated Dose Study. 1–7.
<https://doi.org/10.1787/9789264070929-en>

OECD (1997) Test No. 424: Neurotoxicity Study in Rodents. 1–15.
<https://doi.org/10.1787/9789264071025-en>

OECD (2005) Guidance Document on the Validation and International Acceptance of New or Updated Test Methods for Hazard Assessment. 1–96.
<https://doi.org/10.1787/e1f1244b-en>

Ormel PR, Vieira de Sá R, van Bodegraven EJ, et al (2018) Microglia innately develop within cerebral organoids. *Nat Commun* 9. <https://doi.org/10.1038/s41467-018-06684-2>

O'Rourke NA, Weiler NC, Micheva KD, Smith SJ (2012) Deep molecular diversity of mammalian synapses: Why it matters and how to measure it. *Nat Rev Neurosci* 13:365–379. <https://doi.org/10.1038/nrn3170>

Ortinou S, Schmich J, Block S, et al (2010) Effect of 3D-scaffold formation on differentiation and survival in human neural progenitor cells. *Biomed Eng Online* 9:1–18. <https://doi.org/10.1186/1475-925X-9-70>

Ou K, Hosseinkhani H (2014) Development of 3D in Vitro Technology for Medical Applications. *Int J Mol Sci* 15:17938–17962.
<https://doi.org/10.3390/ijms151017938>

Oyanagi K, Tashiro T, Negishi T (2015) Cell-type-specific and differentiation-status-dependent variations in cytotoxicity of tributyltin in cultured rat cerebral neurons

- and astrocytes. *Journal of Toxicological Sciences* 40:459–468. <https://doi.org/10.2131/jts.40.459>
- Paavilainen T, Pelkonen A, Mäkinen ME-LELL, et al (2018) Effect of prolonged differentiation on functional maturation of human pluripotent stem cell-derived neuronal cultures. *Stem Cell Res* 27:151–161. <https://doi.org/10.1016/j.scr.2018.01.018>
- Paini A, Leonard JA, Joossens E, et al (2019) Next generation physiologically based kinetic (NG-PBK) models in support of regulatory decision making. *Comput Toxicol* 9:61–72. <https://doi.org/10.1016/j.comtox.2018.11.002>
- Pallocca G, Moné MJ, Kamp H, et al (2022) Next-generation risk assessment of chemicals - Rolling out a human-centric testing strategy to drive 3R implementation: The RISK-HUNT3R project perspective. *ALTEX* 39:1–7. <https://doi.org/10.14573/altex.2204051>
- Pamies D, Bal-Price A, Simeonov A, et al (2017a) Good cell culture practice for stem cells & stem-cell-derived models. *ALTEX* 34:95–132. <https://doi.org/10.14573/altex.1607121>
- Pamies D, Barreras P, Block K, et al (2017b) A human brain microphysiological system derived from induced pluripotent stem cells to study neurological diseases and toxicity. *ALTEX* 34:362–376. <https://doi.org/10.14573/altex.1609122>
- Pamies D, Wiersma D, Katt ME, et al (2022) Human iPSC 3D brain model as a tool to study chemical-induced dopaminergic neuronal toxicity. *Neurobiol Dis* 169:105719. <https://doi.org/10.1016/j.nbd.2022.105719>
- Park D, Xiang AP, Mao FF, et al (2010) Nestin is required for the proper self-renewal of neural stem cells. *Stem Cells* 28:2162–2171. <https://doi.org/10.1002/stem.541>
- Park H, Poo MM (2013) Neurotrophin regulation of neural circuit development and function. *Nat Rev Neurosci* 14:7–23. <https://doi.org/10.1038/nrn3379>

- Park JC, Jang SY, Lee D, et al (2021) A logical network-based drug-screening platform for Alzheimer's disease representing pathological features of human brain organoids. *Nat Commun* 12. <https://doi.org/10.1038/s41467-020-20440-5>
- Park KS (2011) TGF-beta family signaling in embryonic stem cells. *Int J Stem Cells* 4:18–23. <https://doi.org/10.15283/ijsc.2011.4.1.18>
- Parodi G, Brofiga M, Pastore VP, et al (2023) Deepening the role of excitation/inhibition balance in human iPSCs-derived neuronal networks coupled to MEAs during long-term development. *J Neural Eng* 20. <https://doi.org/10.1088/1741-2552/acf78b>
- Pas J, Pitsalidis C, Koutsouras DA, et al (2018) Neurospheres on Patterned PEDOT:PSS Microelectrode Arrays Enhance Electrophysiology Recordings. *Adv Biosyst* 2:1–11. <https://doi.org/10.1002/adbi.201700164>
- Paşca AM, Sloan SA, Clarke LE, et al (2015) Functional cortical neurons and astrocytes from human pluripotent stem cells in 3D culture. *Nat Methods* 12:671–678. <https://doi.org/10.1038/nmeth.3415>
- Paşca SP (2018) The rise of three-dimensional human brain cultures. *Nature* 553:437–445. <https://doi.org/10.1038/nature25032>
- Pauly MG, Krajka V, Stengel F, et al (2018) Adherent vs. Free-Floating Neural Induction by Dual SMAD Inhibition for Neurosphere Cultures Derived from Human Induced Pluripotent Stem Cells. *Front Cell Dev Biol* 6. <https://doi.org/10.3389/fcell.2018.00003>
- Pedersen F, de Bruijn J, Munn S, van Leeuwen K (2003) Assessment of additional testing needs under REACH. European Commission Joint Research Centre
- Pei Y, Peng J, Behl M, et al (2016) Comparative neurotoxicity screening in human iPSC-derived neural stem cells, neurons and astrocytes. *Brain Res* 1638:57–73. <https://doi.org/10.1016/j.brainres.2015.07.048>

- Pelkonen A, Pistono C, Klecki P, et al (2021) Functional Characterization of Human Pluripotent Stem Cell-Derived Models of the Brain with Microelectrode Arrays. *Cells* 11:106. <https://doi.org/10.3390/cells11010106>
- Peng H, Xie P, Liu L, et al (2021) Morphological diversity of single neurons in molecularly defined cell types. *Nature* 598:174–181. <https://doi.org/10.1038/s41586-021-03941-1>
- Pereira L, Medina R, Baena M, et al (2015) IFN gamma regulates proliferation and neuronal differentiation by STAT1 in adult SVZ niche. *Front Cell Neurosci* 9:1–10. <https://doi.org/10.3389/fncel.2015.00270>
- Perrin S (2014) Preclinical research: Make mouse studies work. *Nature* 507:423–425. <https://doi.org/10.1038/507423a>
- Piper DR, Mujtaba T, Rao MS, Lucero MT (2000) Immunocytochemical and Physiological Characterization of a Population of Cultured Human Neural Precursors. *J Neurophysiol* 84:534–548. <https://doi.org/10.1152/jn.2000.84.1.534>
- Pistollato F, Canovas-Jorda D, Zagoura D, Price A (2017) Protocol for the differentiation of human induced pluripotent stem cells into mixed cultures of neurons and glia for neurotoxicity testing. *Journal of Visualized Experiments* 2017:1–14. <https://doi.org/10.3791/55702>
- Pistollato F, Louisse J, Scelfo B, et al (2014) Development of a pluripotent stem cell derived neuronal model to identify chemically induced pathway perturbations in relation to neurotoxicity: Effects of CREB pathway inhibition. *Toxicol Appl Pharmacol* 280:378–388. <https://doi.org/10.1016/j.taap.2014.08.007>
- Popova NK, Ilchibaeva T V., Naumenko VS (2017) Neurotrophic factors (BDNF and GDNF) and the serotonergic system of the brain. *Biochemistry (Moscow)* 82:308–317. <https://doi.org/10.1134/S0006297917030099>

- Qi Y, Zhang XJ, Renier N, et al (2017) Combined small-molecule inhibition accelerates the derivation of functional cortical neurons from human pluripotent stem cells. *Nat Biotechnol* 35:154–163. <https://doi.org/10.1038/nbt.3777>
- Qian X, Jacob F, Song MM, et al (2018) Generation of human brain region – specific organoids using a miniaturized spinning bioreactor. *Nat Protoc* 13:565–580. <https://doi.org/10.1038/nprot.2017.152>
- Qian X, Nguyen HN, Song MM, et al (2016) Brain-Region-Specific Organoids Using Mini-bioreactors for Modeling ZIKV Exposure. *Cell* 165:1238–1254. <https://doi.org/10.1016/j.cell.2016.04.032>
- Quadrato G, Nguyen T, Macosko EZ, et al (2017) Cell diversity and network dynamics in photosensitive human brain organoids. *Nature* 545:48–53. <https://doi.org/10.1038/nature22047>
- Rana P, Luerman G, Hess D, et al (2017) Utilization of iPSC-derived human neurons for high-throughput drug-induced peripheral neuropathy screening. *Toxicology in Vitro* 45:111–118. <https://doi.org/10.1016/j.tiv.2017.08.014>
- Reemst K, Noctor SC, Lucassen PJ, Hol EM (2016) The indispensable roles of microglia and astrocytes during brain development. *Front Hum Neurosci* 10:1–28. <https://doi.org/10.3389/fnhum.2016.00566>
- Rey HG, Pedreira C, Quiñan Quiroga R (2015) Past, present and future of spike sorting techniques. *Brain Res Bull* 119:106–117. <https://doi.org/10.1016/j.brainresbull.2015.04.007>
- Reynolds BA, Weiss S (1996) Clonal and Population Analyses Demonstrate That an EGF-Responsive Mammalian Embryonic CNS Precursor Is a Stem Cell. *Dev Biol* 175:1–13. <https://doi.org/10.1006/dbio.1996.0090>
- Ronchi S, Buccino AP, Prack G, et al (2021) Electrophysiological Phenotype Characterization of Human iPSC-Derived Neuronal Cell Lines by Means of High-

-
- Density Microelectrode Arrays. Adv Biol 5:1–16.
<https://doi.org/10.1002/adbi.202000223>
- Rovida C, Busquet F, Leist M, Hartung T (2023) REACH Out-Numbered! The Future of REACH and Animal Numbers. ALTEX 40:367–388.
<https://doi.org/10.14573/altex.2307121>
- Rowley NM, Madsen KK, Schousboe A, Steve White H (2012) Glutamate and GABA synthesis, release, transport and metabolism as targets for seizure control. Neurochem Int 61:546–558. <https://doi.org/10.1016/j.neuint.2012.02.013>
- Saab AS, Nave KA (2017) Myelin dynamics: protecting and shaping neuronal functions. Curr Opin Neurobiol 47:104–112.
<https://doi.org/10.1016/j.conb.2017.09.013>
- Saavedra L, Wallace K, Freudenrich TF, et al (2021) Comparison of acute effects of neurotoxic compounds on network activity in human and rodent neural cultures. Toxicological Sciences 180:295–312. <https://doi.org/10.1093/toxsci/kfab008>
- Sachana M, Bal-Price A, Crofton KM, et al (2019) International regulatory and scientific effort for improved developmental neurotoxicity testing. Toxicological Sciences 167:172–189. <https://doi.org/10.1093/toxsci/kfy211>
- Sachana M, Willett C, Pistollato F, Bal-Price A (2021) The potential of mechanistic information organised within the AOP framework to increase regulatory uptake of the developmental neurotoxicity (DNT) in vitro battery of assays. Reproductive Toxicology 103:159–170. <https://doi.org/10.1016/j.reprotox.2021.06.006>
- Scesa G, Adami R, Bottai D (2021) iPSC Preparation and Epigenetic Memory: Does the Tissue Origin Matter? Cells 10:1470. <https://doi.org/10.3390/cells10061470>
- Schenke M, Schjeide BM, Püschel GP, Seeger B (2020) Analysis of motor neurons differentiated from human induced pluripotent stem cells for the use in cell-based botulinum neurotoxin activity assays. Toxins (Basel) 12:1–20.
<https://doi.org/10.3390/toxins12050276>
-

- Schmidt BZ, Lehmann M, Gutbier S, et al (2017) In vitro acute and developmental neurotoxicity screening: an overview of cellular platforms and high-throughput technical possibilities. *Arch Toxicol* 91:1–33. <https://doi.org/10.1007/s00204-016-1805-9>
- Schmidt M, Raghavan B, Müller V, et al (2010) Crucial role for human Toll-like receptor 4 in the development of contact allergy to nickel. *Nat Immunol* 11:814–819. <https://doi.org/10.1038/ni.1919>
- Shafer TJ (2019) Application of Microelectrode Array Approaches to Neurotoxicity Testing and Screening. In: *Advances in Neurobiology*. pp 275–297
- Shafer TJ, Brown JP, Lynch B, et al (2019) Evaluation of Chemical Effects on Network Formation in Cortical Neurons Grown on Microelectrode Arrays. *Society of Toxicology 2019* 169:436–455. <https://doi.org/10.1093/toxsci/kfz052>
- Shaltouki A, Peng J, Liu Q, et al (2013) Efficient generation of astrocytes from human pluripotent stem cells in defined conditions. *Stem Cells* 31:941–952. <https://doi.org/10.1002/stem.1334>
- Shelly M, Lim BK, Cancedda L, et al (2010) Local and Long-Range Reciprocal Regulation of cAMP and cGMP in Axon/Dendrite Formation. *Science* (1979) 327:547–552. <https://doi.org/10.1126/science.1179735>
- Shen Y-M, Meltzer H, Saljooque F, Sang U H (2001) Stimulation of the Epidermal Growth Factor Receptor Induces Glial-Specific Protein Expression in the Human DAOY Neuroectodermal Cell Line. *Dev Neurosci* 23:84–90. <https://doi.org/10.1159/000048699>
- Sherman SP, Bang AG (2018) High-throughput screen for compounds that modulate neurite growth of human induced pluripotent stem cell-derived neurons. *Dis Model Mech* 11. <https://doi.org/10.1242/dmm.031906>

- Shi Y, Inoue H, Wu JC, Yamanaka S (2017) Induced pluripotent stem cell technology: a decade of progress. *Nat Rev Drug Discov* 16:115–130. <https://doi.org/10.1038/nrd.2016.245>
- Shi Y, Kirwan P, Livesey FJ (2012) Directed differentiation of human pluripotent stem cells to cerebral cortex neurons and neural networks. *Nat Protoc* 7:1836–1846. <https://doi.org/10.1038/nprot.2012.116>
- Shinoda Y, Sadakata T, Yagishita K, et al (2019) Aspects of excitatory/inhibitory synapses in multiple brain regions are correlated with levels of brain-derived neurotrophic factor/neurotrophin-3. *Biochem Biophys Res Commun* 509:429–434. <https://doi.org/10.1016/j.bbrc.2018.12.100>
- Sirenko O, Parham F, Dea S, et al (2019) Functional and mechanistic neurotoxicity profiling using human iPSC-Derived neural 3D cultures. *Toxicological Sciences* 167:249–257. <https://doi.org/10.1093/toxsci/kfy218>
- Slavin I, Dea S, Arunkumar P, et al (2021) Human iPSC-derived 2D and 3D platforms for rapidly assessing developmental, functional, and terminal toxicities in neural cells. *Int J Mol Sci* 22:1–15. <https://doi.org/10.3390/ijms22041908>
- Smirnova L, Harris G, Delp J, et al (2016) A LUHMES 3D dopaminergic neuronal model for neurotoxicity testing allowing long-term exposure and cellular resilience analysis. *Arch Toxicol* 90:2725–2743. <https://doi.org/10.1007/s00204-015-1637-z>
- Snyder C, Yu L, Ngo T, et al (2018) In vitro assessment of chemotherapy-induced neuronal toxicity. *Toxicology in Vitro* 50:109–123. <https://doi.org/10.1016/j.tiv.2018.02.004>
- Spencer PS, Lein PJ (2014) Neurotoxicity. *Encyclopedia of Toxicology: Third Edition* 489–500. <https://doi.org/10.1016/B978-0-12-386454-3.00169-X>
- Stabenfeldt SE, Munglani G, García AJ, Laplaca MC (2010) Biomimetic microenvironment modulates neural stem cell survival, migration, and

differentiation. Tissue Eng Part A 16:3747–3758.
<https://doi.org/10.1089/ten.tea.2009.0837>

Stacey P, Wassermann AM, Kammonen L, et al (2018) Plate-Based Phenotypic Screening for Pain Using Human iPSC-Derived Sensory Neurons. *SLAS Discovery* 23:585–596. <https://doi.org/10.1177/2472555218764678>

Stadelmann C, Timmler S, Barrantes-Freer A, Simons M (2019) Myelin in the central nervous system: Structure, function, and pathology. *Physiol Rev* 99:1381–1431. <https://doi.org/10.1152/physrev.00031.2018>

Stary CM, Sun X, Giffard RG (2015) Astrocytes Protect against Isoflurane Neurotoxicity by Buffering pro-brain–derived Neurotrophic Factor. *Anesthesiology* 123:810–819. <https://doi.org/10.1097/ALN.0000000000000824>

Suga M, Kondo T, Inoue H (2019) Modeling Neurological Disorders with Human Pluripotent Stem Cell-Derived Astrocytes. *Int J Mol Sci* 20:3862. <https://doi.org/10.3390/ijms20163862>

Sukiban J, Voges N, Dembek TA, et al (2019) Evaluation of Spike Sorting Algorithms: Application to Human Subthalamic Nucleus Recordings and Simulations. *Neuroscience* 414:168–185. <https://doi.org/10.1016/j.neuroscience.2019.07.005>

Surmacz B, Fox H, Gutteridge A, et al (2012) Directing differentiation of human embryonic stem cells toward anterior neural ectoderm using small molecules. *Stem Cells* 30:1875–1884. <https://doi.org/10.1002/stem.1166>

Suzuki IK, Vanderhaeghen P (2015) Is this a brain which i see before me? Modeling human neural development with pluripotent stem cells. *Development (Cambridge)* 142:3138–3150. <https://doi.org/10.1242/dev.120568>

Takahashi K, Tanabe K, Ohnuki M, et al (2007) Induction of Pluripotent Stem Cells from Adult Human Fibroblasts by Defined Factors. *Cell* 131:861–872. <https://doi.org/10.1016/j.cell.2007.11.019>

- Takahashi K, Yamanaka S (2006) Induction of Pluripotent Stem Cells from Mouse Embryonic and Adult Fibroblast Cultures by Defined Factors. *Cell* 126:663–676. <https://doi.org/10.1016/j.cell.2006.07.024>
- Tao Y, Zhang SC (2016) Neural Subtype Specification from Human Pluripotent Stem Cells. *Cell Stem Cell* 19:573–586. <https://doi.org/10.1016/j.stem.2016.10.015>
- Taylor K (2018) Ten years of reach - an animal protection perspective. *ATLA Alternatives to Laboratory Animals* 46:347–373. <https://doi.org/10.1177/026119291804600610>
- Thomas CAJ, Springer PA, Loeb G, et al (1972) A miniature microelectrode array to monitor the bioelectric activity of cultured cells. *Exp Cell Res* 74:61–66. [https://doi.org/10.1016/0014-4827\(72\)90481-8](https://doi.org/10.1016/0014-4827(72)90481-8)
- Thomson JA, Itskovitz-Eldor J, Shapiro SS, et al (1998) Embryonic stem cell lines derived from human blastocysts. *Science* (1979) 282:1145–1147. <https://doi.org/10.1126/science.282.5391.1145>
- Tigges J, Bielec K, Brockerhoff G, et al (2021) Academic application of Good Cell Culture Practice for induced pluripotent stem cells. *ALTEX* 1–19. <https://doi.org/10.14573/altex.2101221>
- Tjalkens RB, Popichak KA, Kirkley KA (2017) Inflammatory Activation of Microglia and Astrocytes in Manganese Neurotoxicity. In: *Advances in Neurobiology*. Springer New York LLC, pp 159–181
- Tukker AM, Bouwman LMS, van Kleef RGDM, et al (2020a) Perfluorooctane sulfonate (PFOS) and perfluorooctanoate (PFOA) acutely affect human $\alpha 1\beta 2\gamma 2L$ GABAA receptor and spontaneous neuronal network function in vitro. *Sci Rep* 10:1–14. <https://doi.org/10.1038/s41598-020-62152-2>
- Tukker AM, van Kleef RGDM, Wijnolts FMJ, et al (2020b) Towards animal-free neurotoxicity screening: Applicability of hiPSC-derived neuronal models for in vitro

seizure liability assessment. ALTEX 37:121–135.
<https://doi.org/10.14573/altex.1907121>

Tukker AM, Wijnolts FMJJ, de Groot A, et al (2018) Human iPSC-derived neuronal models for in vitro neurotoxicity assessment. *Neurotoxicology* 67:215–225.
<https://doi.org/10.1016/j.neuro.2018.06.007>

Tukker AM, Wijnolts FMJJ, de Groot A, Westerink RHSS (2020c) Applicability of hiPSC-Derived Neuronal Cocultures and Rodent Primary Cortical Cultures for In Vitro Seizure Liability Assessment. *Toxicological Sciences* 178:71–87.
<https://doi.org/10.1093/toxsci/kfaa136>

Valdivia P, Martin M, LeFew WR, et al (2014) Multi-well microelectrode array recordings detect neuroactivity of ToxCast compounds. *Neurotoxicology* 44:204–217. <https://doi.org/10.1016/j.neuro.2014.06.012>

van der Jagt K, Munn S, Torslov J, de Bruijn J (2004) Alternative Approaches Can Reduce the Use of Test Animals under REACH. European Commission Joint Research Centre

van der Stel W, Carta G, Eakins J, et al (2021) New Approach Methods (NAMs) Supporting Read-Across: Two Neurotoxicity AOP-based IATA Case Studies. *ALTEX* 38:615–635. <https://doi.org/10.14573/altex.2103051>

Vassallo A, Chiappalone M, De Camargos Lopes R, et al (2017) A multi-laboratory evaluation of microelectrode array-based measurements of neural network activity for acute neurotoxicity testing. *Neurotoxicology* 60:280–292.
<https://doi.org/10.1016/j.neuro.2016.03.019>

Verkhatsky A, Rose CR (2020) Na⁺-dependent transporters: The backbone of astroglial homeostatic function. *Cell Calcium* 85:102136.
<https://doi.org/10.1016/j.ceca.2019.102136>

von Bartheld CS, Bahney J, Herculano-Houzel S (2016) The search for true numbers of neurons and glial cells in the human brain: A review of 150 years of cell

- counting. Journal of Comparative Neurology 524:3865–3895.
<https://doi.org/10.1002/cne.24040>
- Wang Y, Zhao F, Liao Y, et al (2013) Effects of arsenite in astrocytes on neuronal signaling transduction. Toxicology 303:43–53.
<https://doi.org/10.1016/j.tox.2012.10.024>
- Watanabe M, Buth JE, Vishlaghi N, et al (2017) Self-Organized Cerebral Organoids with Human-Specific Features Predict Effective Drugs to Combat Zika Virus Infection. Cell Rep 21:517–532. <https://doi.org/10.1016/j.celrep.2017.09.047>
- Weigert C (1895) Beiträge zur Kenntnis der normalen menschlichen Neuroglia. Festschrift zum fünfzigjährigen Jubiläum des ärztlichen Vereins zu Frankfurt a M
- Weinhart M, Hocke A, Hippenstiel S, et al (2019) 3D organ models — Revolution in pharmacological research? Pharmacol Res 139:446–451.
<https://doi.org/10.1016/j.phrs.2018.11.002>
- Weis S, Büttner A (2018) Neurotoxicology and drug-related disorders. Handb Clin Neurol 145:181–192. <https://doi.org/10.1016/B978-0-12-802395-2.00014-6>
- Wen Z, Nguyen HN, Guo Z, et al (2014) Synaptic dysregulation in a human iPS cell model of mental disorders. Nature 515:414–418.
<https://doi.org/10.1038/nature13716>
- Westmoreland C, Bender HJ, Doe JE, et al (2022) Use of New Approach Methodologies (NAMs) in regulatory decisions for chemical safety: Report from an EPAA Deep Dive Workshop. Regulatory Toxicology and Pharmacology 135:105261. <https://doi.org/10.1016/j.yrtph.2022.105261>
- Wong G, Goldshmit Y, Turnley AM (2004) Interferon- γ but not TNF α promotes neuronal differentiation and neurite outgrowth of murine adult neural stem cells. Exp Neurol 187:171–177. <https://doi.org/10.1016/j.expneurol.2004.01.009>

- Wright-Jin EC, Gutmann DH (2019) Microglia as Dynamic Cellular Mediators of Brain Function. *Trends Mol Med* 25:967–979. <https://doi.org/10.1016/j.molmed.2019.08.013>
- Yamada M, Sekiguchi K (2015) Molecular Basis of Laminin–Integrin Interactions. In: *Current Topics in Membranes*. Elsevier Ltd, pp 197–229
- Yoshida Y, Takahashi K, Okita K, et al (2009) Hypoxia Enhances the Generation of Induced Pluripotent Stem Cells. *Cell Stem Cell* 5:237–241. <https://doi.org/10.1016/j.stem.2009.08.001>
- Yu J, Vodyanik MA, Smuga-Otto K, et al (2007) Induced pluripotent stem cell lines derived from human somatic cells. *Science* (1979) 318:1917–1920. <https://doi.org/10.1126/science.1151526>
- Zahir T, Chen YF, MacDonald JF, et al (2009) Neural stem/progenitor cells differentiate in vitro to neurons by the combined action of dibutyl cAMP and interferon- γ . *Stem Cells Dev* 18:1423–1432. <https://doi.org/10.1089/scd.2008.0412>
- Zakrzewski W, Dobrzyński M, Szymonowicz M, Rybak Z (2019) Stem cells: past, present, and future. *Stem Cell Res Ther* 10:68. <https://doi.org/10.1186/s13287-019-1165-5>
- Zeldenrust F, Wadman WJ, Englitz B (2018) Neural coding with bursts—Current state and future perspectives. *Front Comput Neurosci* 12:1–14. <https://doi.org/10.3389/fncom.2018.00048>
- Zeng H, Sanes JR (2017) Neuronal cell-type classification: Challenges, opportunities and the path forward. *Nat Rev Neurosci* 18:530–546. <https://doi.org/10.1038/nrn.2017.85>
- Zhai J, Traebert M, Zimmermann K, et al (2023) Comparative study for the IMI2-NeuroDeRisk project on microelectrode arrays to derisk drug-induced seizure liability. *J Pharmacol Toxicol Methods*. <https://doi.org/10.1016/j.vascn.2023.107297>

- Zhou T, Tan L, Cederquist GY, et al (2017) High-Content Screening in hPSC-Neural Progenitors Identifies Drug Candidates that Inhibit Zika Virus Infection in Fetal-like Organoids and Adult Brain. *Cell Stem Cell* 21:274-283.e5. <https://doi.org/10.1016/j.stem.2017.06.017>
- Zhuang P, Sun AX, An J, et al (2018) 3D neural tissue models: From spheroids to bioprinting. *Biomaterials* 154:113–133. <https://doi.org/10.1016/j.biomaterials.2017.10.002>
- Zimmerman LB, De Jesús-Escobar JM, Harland RM (1996) The Spemann organizer signal noggin binds and inactivates bone morphogenetic protein 4. *Cell* 86:599–606. [https://doi.org/10.1016/S0092-8674\(00\)80133-6](https://doi.org/10.1016/S0092-8674(00)80133-6)

Danksagung

In diesem Abschnitt möchte ich mich bei allen bedanken, die meine Promotion ermöglicht haben und mich während dieser Zeit unterstützt haben.

Zuerst möchte ich mich bei Prof. Dr. Ellen Fritsche für die Möglichkeit der Promotion an diesem interessanten Thema und die umfassende Betreuung bedanken. Bedanken möchte ich mich auch für die Ermöglichung der vielen Konferenzteilnahmen und internationalen Erfahrungen, die mich sehr bereichert haben.

Bei Frau Prof. Dr. Rose bedanke ich mich für die fakultätsübergreifende Betreuung und Übernahme der Mentorenschaft durch die meine Dissertation ermöglicht wurde.

Ein weiterer Dank geht an meine Betreuerin Dr. Katharina Koch für die fachliche und mentale Unterstützung. Danke für die bereichernden Diskussionen der Daten, sowie das Korrekturlesen der vielen Schriftstücke.

Vielen Dank auch an die derzeitigen und ehemaligen Kollegen der AG Fritsche für die nette und immer hilfsbereite Arbeitsatmosphäre. Mit euch haben die Konferenzen inklusive „After Show“-Partys besonders Spaß gemacht. Nicht zu vergessen unsere sportlichen und kreativen Tätigkeiten, sowie die Spieleabende.

Eidesstattliche Erklärung

Ich versichere an Eides Statt, dass die Dissertation von mir selbständig und ohne unzulässige fremde Hilfe unter Beachtung der „Grundsätze zur Sicherung guter wissenschaftlicher Praxis an der Heinrich-Heine-Universität Düsseldorf“ erstellt worden ist.

Düsseldorf, 27.11.2024

Ort, Datum

A handwritten signature in blue ink, appearing to read 'Julia Ha...', written over a horizontal line.

Unterschrift